Modern Aspects of Electrochemistry 61

Philippe Vernoux
Constantinos G. Vayenas *Editors*

Recent Advances in Electrochemical Promotion of Catalysis

Springer

Modern Aspects of Electrochemistry

Volume 61

This well-respected series commenced publication in the early 1950s. Over the years it has earned an excellent reputation by offering high quality reviews of current research into all areas of electrochemistry and electrochemical engineering and their applications. The international magazine Chemistry & Industry notes that this series "deserves a place in electrochemistry libraries and should prove useful to electrochemists and related workers." Starting with Number 43 in the series, two features have been introduced:

- Each volume is thematic and focuses on a new development in the field or reviews a well-established area that is regaining interest.
- Each volume is guest-edited. As in the past, all chapters are topical reviews.

Subjects covered in recent volumes include:

1. Modeling and Numerical Simulations
2. Progress in Corrosion Science and Engineering
3. Electrodeposition: Theory and Practice
4. Electrocatalysis: Theory and Experiments
5. Interfacial Phenomena in Fuel Cell Electrocatalysis
6. Diagnostics and Modeling of Polymer Electrolyte Fuel Cells
7. Applications of Electrochemistry and Nanotechnology in Biology and Medicine

Philippe Vernoux • Constantinos G. Vayenas
Editors

Recent Advances in Electrochemical Promotion of Catalysis

Springer

Editors
Philippe Vernoux
Université de Lyon
Institut de Recherches sur la Catalyse et l'Environnement de Lyon, UMR 5256, CNRS, Université Claude Bernard Lyon 1
Villeurbanne, France

Constantinos G. Vayenas
Department of Chemical Engineering
University of Patras
Patras, Greece

ISSN 0076-9924 ISSN 2197-7941 (electronic)
Modern Aspects of Electrochemistry
ISBN 978-3-031-13892-8 ISBN 978-3-031-13893-5 (eBook)
https://doi.org/10.1007/978-3-031-13893-5

This Springer imprint is published by the registered company Springer Nature Switzerland AG
The registered company address is: Gewerbestrasse 11, 6330 Cham, Switzerland

To our parents, our wives Susanne and Valérie, and our children Anne, George-Philippe, Lucie, Paul, and Thibault.

Preface

Twenty years have passed since the book entitled *Electrochemical Activation of Catalysis: Promotion, Electrochemical Promotion and Metal-Support Interactions*, authorized by C.G. Vayenas, S. Bebelis, C. Pliangos, S. Brosda, and D. Tsiplakides, and prologized in the foreword by the famous Professor John O' M. Bockris, was published by Kluwer Academic/Plenum Publishers.

That book established the basic phenomenology of the electrochemical promotion of catalysis (EPOC) by reviewing more than 70 catalytic reactions which had been already electropromoted at the time. The rules of electrochemical, but also of chemical, promotion were also derived and discussed, and it was established that promotion, electrochemical promotion, and metal-support interactions are fundamentally equivalent and only operationally different.

The present volume reviews the scientific advances of the last two decades in the EPOC field, starting from its story, the quest for its understanding, and effort towards practical applications. A major practical application stemming from the open EPOC literature has been in the correct choice of supports and promoters to optimize practical catalyst performance. The extent of this informational spillover is hard to quantify, but we have learned from very good colleagues and friends in the NAE of the USA and from industrial partners that catalyst manufacturers, for example, for ethylene epoxidation and emission control catalysts, were following for years with great interest the open EPOC literature on this reaction and were making their, at least initial, promoter screening and selection by using this literature as a valuable guideline. Some of these aspects are discussed in Chap. 2 of the present book by one of the world's top EPOC experts on ethylene epoxidation, Professor Symeon Bebelis. Professor Elena Baranova at Ottawa University, along with her co-workers Arash Fellah Jahromi and Christopher Panaritis, has exhaustively reviewed the intensive research effort to tailor electro-promoted metal nanoparticles (Chap. 3). This chapter highlights the variety of methods used to prepare mono- and bimetallic- nanoparticles and promising results recently obtained on transition metals. The mechanism and potential applications of the self-sustained electrochemical promotion concept are also fully discussed. In the course of this phenomenon, a

major discovery was made by Professor Ioannis Yentekakis at the Technical University of Crete at Chania. He found that the spontaneously formed effective-double layer ($[O^{\delta-}, {}^{\delta+}]$) on the catalyst particles, resulting from the thermally driven oxygen back-spillover from high OSC (oxygen storage capacity) supports, can strongly increase the thermal resistance of metallic nanoparticles (Chap. 4). This is a very important theoretical and practical finding which will be almost certainly fully utilized by the catalyst manufacturing industry.

The use of EPOC to face very important environmental challenges is described subsequently by the second chapter of Professor Ioannis Yentekakis (Chap. 5), coauthored with Professors Philippe Vernoux and Angel Caravaca, for emission control catalysts, and also in Chap. 6, co-authored by Christos Chatzilias, Eftychia Martino, Dimitrios Zagoraios, Professors Kyriakou and Katsaounis on the electropromotion of CO_2 valorization catalysts.

Two important applications of EPOC related to H_2 production and to ammonia synthesis are discussed in the chapters by Doctor Ruiz-Lopez, Professor Fernando Dorado, and Professor Antonio de Lucas-Consuegra (H_2 production, Chap. 7) and Anastasios Vouros, Ioannis Garagounis, and Professor Stoukides (NH_3 synthesis, Chap. 8).

In the last chapter of the book, Professors Angel Caravaca, Jesus Gonzalez-Cobos, Vasilis Kyriakou, and Philippe Vernoux provide a thorough and realistic in-depth discussion on the prospects towards large-scale application of EPOC.

Patras, Greece — Constantinos G. Vayenas

Villeurbanne, France — Philippe Vernoux

Contents

Contributors

Elena A. Baranova Department of Chemical and Biological Engineering, Centre for Catalysis Research and Innovation (CCRI), University of Ottawa, Ottawa, ON, Canada

Symeon Bebelis Department of Chemical Engineering, University of Patras, Patras, Greece

Angel Caravaca Departamento de Ingeniería Mecánica, Universidad Politécnica de Madrid, Madrid, Spain

Christos Chatzilias Department of Chemical Engineering, University of Patras, Patras, Greece

Antonio de Lucas-Consuegra Department of Chemical Engineering, School of Chemical Sciences and Technologies, University of Castilla-La Mancha, Ciudad Real, Spain

Fernando Dorado Department of Chemical Engineering, School of Chemical Sciences and Technologies, University of Castilla-La Mancha, Ciudad Real, Spain

Arash Fellah Jahromi Department of Chemical and Biological Engineering, Centre for Catalysis Research and Innovation (CCRI), University of Ottawa, Ottawa, ON, Canada

Ioannis Garagounis Chemical Engineering Department, Aristotle University of Thessaloniki & Center for Research and Technology Hellas, Thessaloniki, Greece

Jesus González-Cobos Université de Lyon, Institut de Recherches sur la Catalyse et l'Environnement de Lyon, CNRS, UMR 5256, Université Claude Bernard Lyon 1, Villeurbanne, France

Alexandros Katsaounis Department of Chemical Engineering, University of Patras, Patras, Greece

Georgios Kyriakou Department of Chemical Engineering, University of Patras, Patras, Greece

Vasilis Kyriakou Engineering and Technology Institute Groningen (ENTEG), University of Groningen, AG, Groningen, The Netherlands

Eftychia Martino Department of Chemical Engineering, University of Patras, Patras, Greece

Christopher Panaritis Department of Chemical and Biological Engineering, Centre for Catalysis Research and Innovation (CCRI), University of Ottawa, Ottawa, ON, Canada

Estela Ruiz-López Department of Chemical Engineering, School of Chemical Sciences and Technologies, University of Castilla-La Mancha, Ciudad Real, Spain

Michael Stoukides Chemical Engineering Department, Aristotle University of Thessaloniki & Center for Research and Technology Hellas, Thessaloniki, Greece

Constantinos G. Vayenas Department of Chemical Engineering, University of Patras, Patras, Greece

Philippe Vernoux Université de Lyon, Institut de Recherches sur la Catalyse et l'Environnement de Lyon, CNRS, UMR 5256, Université Claude Bernard Lyon 1, Villeurbanne, France

Anastasios Vourros Chemical Engineering Department, Aristotle University of Thessaloniki & Center for Research and Technology Hellas, Thessaloniki, Greece

Ioannis V. Yentekakis Laboratory of Physical Chemistry & Chemical Processes, School of Chemical & Environmental Engineering, Technical University of Crete (TUC), Chania, Greece

Dimitrios Zagoraios Department of Chemical Engineering, University of Patras, Patras, Greece

Part I
EPOC: Story and Fundamentals

Chapter 1
Presentation, Story, and Mechanistic Understanding of Electrochemical Promotion of Catalysis

Constantinos G. Vayenas and Philippe Vernoux

Abstract The electrochemical promotion of catalysis (EPOC) or non-Faradaic electrochemical promotion of catalysis (NEMCA effect) is a phenomenon observed as a reversible change in catalytic rate (i.e., no net charge transfer rate) of a chemical reaction occurring on a catalyst film (or supported dispersed catalyst) deposited on an ionically conducting or mixed electronically-ionically conducting solid electrolyte support upon the application of electrical potential between the catalyst and a second conductive film deposited on the solid electrolyte support. This chapter relates the discovery of the concept at the end of the 1970s and briefly describes the research efforts to unravel its physicochemical origin over the following 40 years.

Keywords NEMCA · EPOC · Discovery · Story · Mechanism

1.1 EPOC Discovery

EPOC is a phenomenon, discovered, rather unexpectedly, by Michael Stoukides and Costas (Constantinos) Vayenas at MIT in Spring 1978. Inspired by the use of solid electrolyte galvanic cells, for thermodynamic measurements [1, 2], for electrolysis of gases such as NO [3, 4], for cogeneration of electricity and chemicals [5], or for in situ measuring the activity of oxygen on working catalysts [6], assistant professor Costas Vayenas and his PhD student Mike Stoukides decided to explore if the rate and selectivity of ethylene epoxidation on Ag catalyst films deposited on yttria-stabilized-zirconia (YSZ), an oxygen ionic conductor, could be enhanced via

C. G. Vayenas (✉)
Department of Chemical Engineering, University of Patras, Patras, Greece
e-mail: cat@chemeng.upatras.gr

P. Vernoux
Université de Lyon, Institut de Recherches sur la Catalyse et l'Environnement de Lyon, UMR 5256, CNRS, Université Claude Bernard Lyon 1, Villeurbanne, France
e-mail: philippe.vernoux@ircelyon.univ-lyon1.fr

P. Vernoux, C. G. Vayenas (eds.), *Recent Advances in Electrochemical Promotion of Catalysis*, Modern Aspects of Electrochemistry 61,
https://doi.org/10.1007/978-3-031-13893-5_1

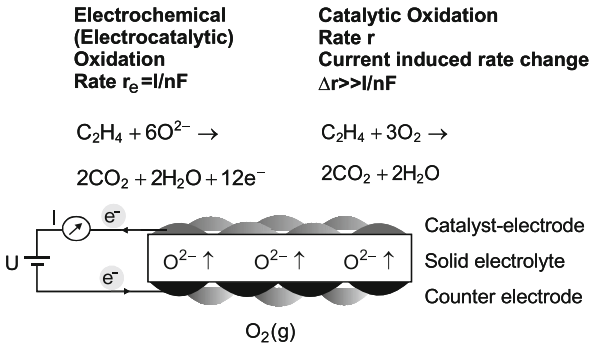

Fig. 1.1 Experimental setup used in NEMCA experiments. (Reprinted from ref. [38] with permission from Elsevier)

application of positive potentials between the porous Ag catalyst electrode and a counter Ag electrode deposited on the opposite side of the YSZ disc (Fig. 1.1).

A few days before the first experiments, Professor Vladimir Ponec from Prague, a prominent catalysis researcher at that time, was visiting MIT and giving a seminar after which Costas described to him the plan: "We will use a potentiostat to apply a potential between the catalyst and a reference electrode during ethylene epoxidation, and we will thus change the work function of the catalyst in order to see what effect this will have on catalytic rate and selectivity."

Professor Ponec said, "You will change the Fermi level but not the work function of the film!", and then he added, "And thus there will probably be no effect on the catalytic rate." "We shall see," Costas said.

As it turns out, Professor Ponec was right about the Fermi level change, but this does not imply a change in a catalytic (no net charge transfer) rate. But, as it turns out, the work function of the catalyst film is also changing, due to electrochemically controlled ion migration (spillover) on the catalyst surface, and this modifies the catalyst surface work function and thus modifies the catalytic rate. This electrochemically induced ion migration to the catalyst surface was not easy to anticipate those days, and this made all the difference, thus making EPOC an interesting and important field between catalysis and electrochemistry. The day for the first crucial experiments had finally arrived (Figs. 1.2 and 1.3).

In these first experiments, the porous Ag catalyst electrode had a thickness of the order of 10 μm. Figure 1.2 displays some of the first transient ethylene epoxidation and deep oxidation experiments. One sees that negative current application (i.e., O^{2-} removal from the Ag catalyst) causes a decrease both in epoxidation rate (r_1) and in the deep (complete) oxidation rate (r_2). The selectivity, S, defined as $r_1/(r_1 + r_2)$ decreases. The same figure shows that positive potential application, i.e., O^{2-} supply to the catalyst, causes both r_1 and r_2 to increase. The selectivity, S, increases. Consequently, the selectivity to ethylene oxide can be reversibly varied between 40 and 60% as shown in Fig. 1.2. The increase in the epoxidation rate r_1 is significantly larger (Fig. 1.3), typically a factor of 50, than the electrochemical rate, $I/4F$, denoted G_{O_2}, of supply to O_2 to the catalyst surface. As also shown in Figs. 1.3 and 1.4 which refer to Ag [7] and Pt [8] catalyst films respectively, the time

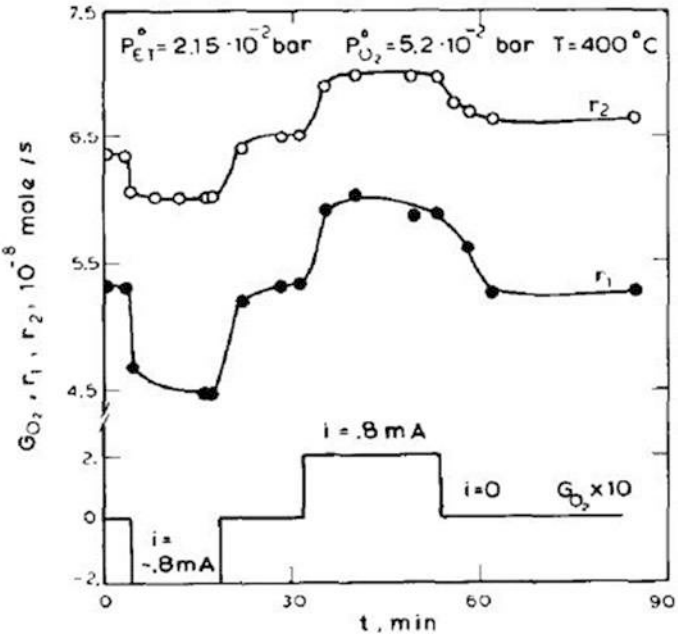

Fig. 1.2 Effect of electrochemical oxygen pumping on the rate of ethylene epoxidation r_1 and deep oxidation r_2. Comparison with the rate of oxygen transport through the electrolyte $G_{O_2} = i/4F$. (Reprinted with permission from Elsevier [7])

constant τ of the catalytic rate transients upon constant current imposition is of the order of several min. As it turns out, they are generally of the order of:

$$\tau = \frac{2FN}{I} \tag{1.1}$$

where N is the catalyst surface area in mol of metal and F is Faraday's constant. This is the time required for the migrating spillover O^{2-} species supplied at a rate $I/2F$ to occupy a surface with N sites.

It was with excitement that Stoukides and Vayenas obtained the results of Fig. 1.3. The rate of epoxidation could be enhanced by ~30%, and the rate of CO_2 production was also enhanced by ~15% or so; therefore, selectivity to ethylene oxide was enhanced. The effect was small, but it became obvious that other reactions and other conditions would exist where the effect would be much bigger. The big and unexpected surprise was that the increase in catalytic rate, Δr, was much larger than that anticipated from the law of Faraday, i.e., $I/2F$. The faradaic efficiency, Λ, could be defined from

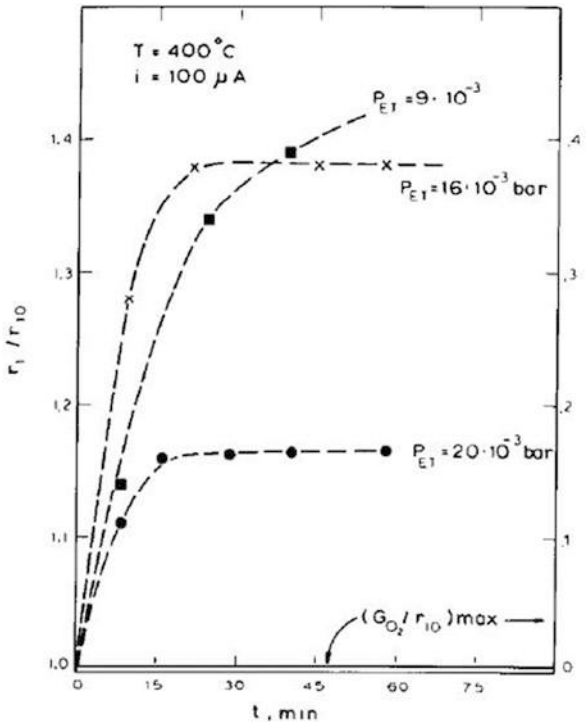

Fig. 1.3 Transient behavior of the rate of ethylene epoxidation r_1 when a constant current $I = 100$ μA is applied at I = 0. The P_{O_2} values were $13.5.10^{-2}$, 10.10^{-2}, and 6.10^{-2} bar, and P_{ET} was equal to 9.10^{-3}, 16.10^{-3}, and 20.10^{-3} bar. (Reprinted with permission from Elsevier [7])

$$\Lambda = \frac{\Delta r}{(I/2F)} \tag{1.2}$$

and Λ value up to 400 was measured already in the first study [7]. The new phenomenon was termed non-Faradaic electrochemical modification of catalytic activity (NEMCA effect). Figure 1.5 shows that Λ values up to $2{\cdot}10^5$ have been measured during ethylene oxidation on Pt [8, 9]. Figure 1.6 depicts the effect of gaseous composition on the electrochemical promotion of C_2H_4 oxidation on Pt. The effect is more pronounced at high O_2/C_2H_4 ratios, i.e., under oxidizing conditions and also when the Pt catalyst film surface has been re-oxidized.

1.2 EPOC Story

It took 7 years for the next NEMCA papers to be prepared and published [8–11], since family reasons had caused Costas Vayenas to return to Greece and start a new laboratory at the University of Patras. He was again quite lucky there to have some truly outstanding new PhD students of the same level as Mike Stoukides. These were Yannis Yentekakis [12–17], Symeon Bebelis [8, 9, 13, 14, 16], Stelios Neophytides

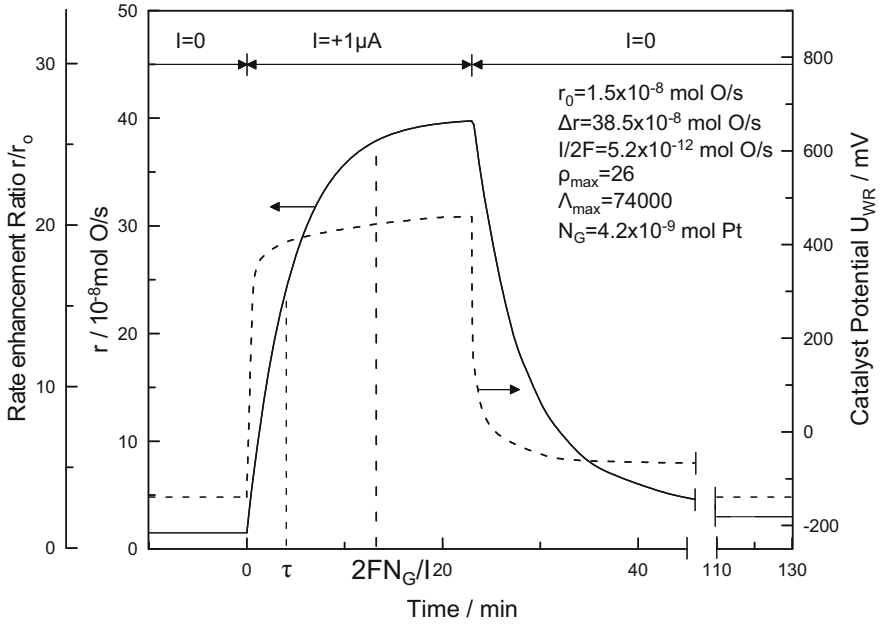

Fig. 1.4 NEMCA: Rate and catalyst potential response to step changes in applied current during ethylene oxidation on Pt [8, 9]; $T = 370$ °C, $p_{O2} = 4.6$ kPa, $p_{C2H4} = 0.36$ kPa. The experimental (τ) and computed ($2FN_G/I$) rate relaxation time constants are indicated on the figure. See text for discussion. $r_0 = 1.5 \cdot 10^{-8}$ mol O/s, $\Delta r = 38.5 \cdot 10^{-8}$ mol O/s, $I/2F = 5.2 \cdot 10^{-12}$ mol O/s, $\rho_{max} = 26$, $\Lambda_{max} = 74{,}000$, $N_G = 4.2 \cdot 10^{-9}$ mol Pt. (Reprinted from ref. [38] with permission from Elsevier)

[8, 13, 16, 22, 25], Panagiotis Tsiakaras [14, 18–20], and Marina Despotopoulou [21] followed by Costas Pliangos [10, 16, 23, 24, 37, 38], Susanne Brosda [37, 39], Yi Jiang [16, 17, 26, 27], Christos Karavasilis [28, 40, 56], Eleni Karasali [14, 29], Maria Makri [30–32], D. Archonta [33, 34, 46], K. Yiokari [35], D. Tsiplakides [22, 25, 33, 36, 38, 41, 42], Costas Koutsodontis [42, 43, 48], Alex Katsaounis [42–44, 48], Michalis Tsampas [45], Stamatios Souentie [49, 50], Fenia Sapountzi [45, 51], Ioannis Constantinou [47], and others. The work of these students, together with the equally spectacular work of Professor Lambert and his collaborators at Cambridge [11, 15], produced a series of papers with outstanding results which showed that the NEMCA effect is a general phenomenon *connecting electrochemistry and catalysis* and is not limited to any group of catalytic reactions or conducting catalyst phases [16]. Some examples of these papers are shown in Figs. 1.7, 1.8, and 1.10. The loneliness of NEMCA disappeared when, in addition to Richard Lambert, some equally prominent physical chemistry leaders of the time, i.e., Gary Haller and Louis Hegedus in catalysis and Christos Comninellis in electrochemistry, realized its importance and when John Pritchard, who reviewed the first paper of the Patras group in *Nature* [9], coined on that occasion the term electrochemical promotion of catalysis (EPOC) in a short and very important paper in the same issue of *Nature*

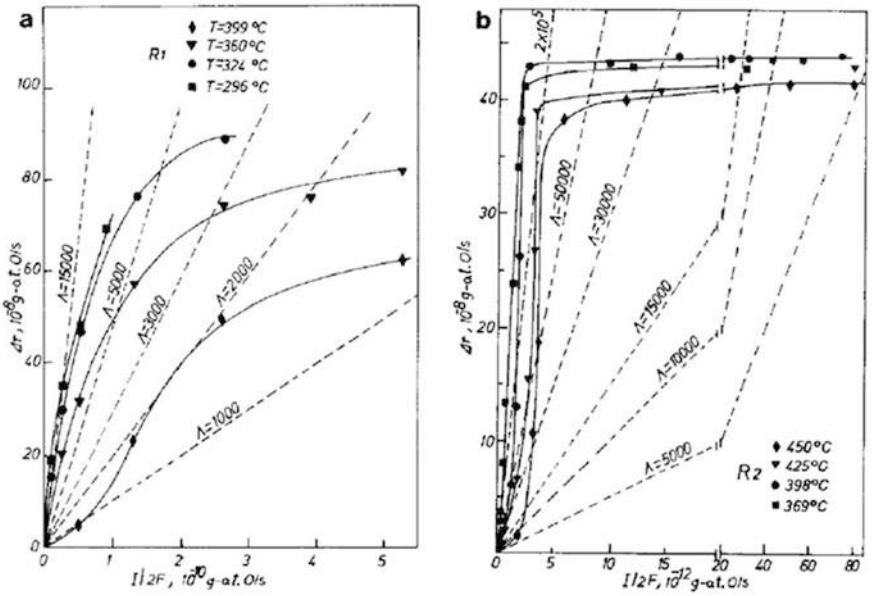

Fig. 1.5 Steady-state effect of applied current on the rate of C_2H_4 oxidation on Pt [8, 9]. Broken lines are constant enhancement factor lines. (**a**) Catalyst *R*1, $P_{ET} = 0.4 \times 10^{-2}$ bar, $P_{O_2} = 4.8 \times 10^{-2}$ bar. (**b**) Catalyst *R*2, $P_{ET} = 0.4 \times 10^{-2}$ bar, $P_{O_2} = 6.4 \times 10^{-2}$ bar. (Reprinted from ref. [8] with permission from Elsevier)

[52]. The term EPOC gradually replaced its synonymous term NEMCA effect after the group of Philippe Vernoux in France started producing some new contributions from 2002 [53, 54, 55] (Fig. 1.9 and 1.10).

At the same time, Fritz Kalhammer, former student of Schwab and vice president of Research for EPRI in the USA, became a prominent EPOC enthusiast and, as a result, EPRI in California, as well as BASF in Germany, provided stable funding for NEMCA research for many years. In year 2008, Philippe Vernoux and the EPOC scientific community organized a series of training schools and the first EPOC Conference on the Oleron Island in France with more than 100 participants coming from the United Kingdom (Metcalfe group), Switzerland (Comninellis and Harbich groups), Spain (Valverde and de Lucas-Consuegra group), Greece (Tsiplakides and Vayenas groups), France (Siebert, Billard, Guizard, and Vernoux groups), Germany (Anastasijevic group), and many other countries. By that time EPOC researchers produced some very exciting results bridging classical heterogeneous catalysis with electrochemistry (both solid and aqueous [22]) and with surface science published in a special issue in *Catalysis Today* (2009, Volume 146, Issues 3–4, pages 265–386 edited by Comninellis C, Vayenas CG and Vernoux P) and summarized in a review in 2013 [57].

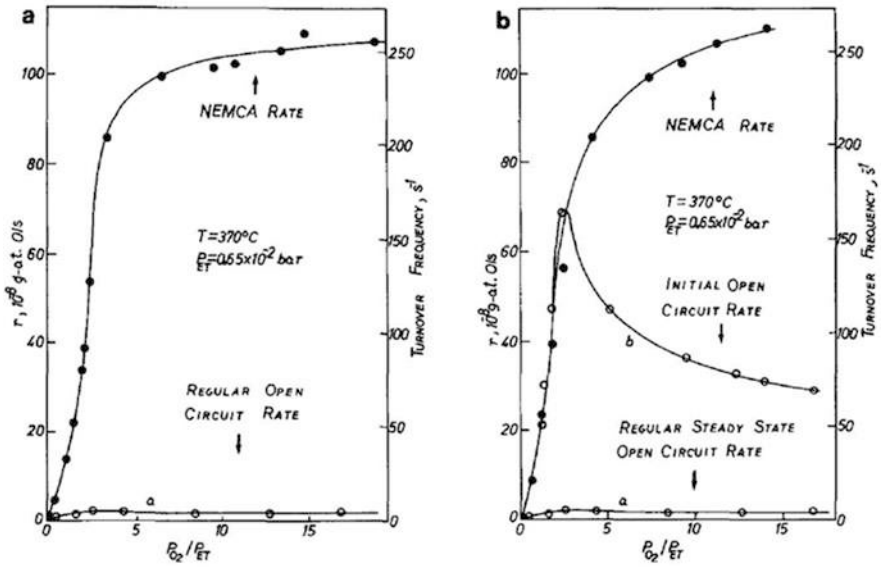

Fig. 1.6 Effect of gaseous composition on regular (open-circuit) and NEMCA-induced reaction rate ($V_{WR} = 1\ V$). Catalyst *R*2 [8]. (**a**) Preoxidized surface; (**b**) prereduced surface. (Reprinted from ref. [8] with permission from Elsevier)

1.3 The Quest for Understanding EPOC

Since its discovery, various spectroscopic, microscopic, electrochemical, and surface techniques were performed to unravel the EPOC physicochemical origin. Most of them were focused on Pt/YSZ catalysts, where a Pt film was interfaced on a dense YSZ membrane because the more pronounced NEMCA effects were observed on this system. Furthermore, Pt coatings are relatively thermally (sintering) and chemically (oxidation) stable in comparison to other metals such as Pd, Rh, Ag, or transition metals. However, recent efforts to investigate other systems such as Ni- or Ru-based catalysts have been done in the last decade and will be described in other chapters. O_2 temperature-programmed desorption (TPD) [63–68], XPS [58, 69, 70], cyclic voltammetry [71], photoemission electron spectroscopy (PEEM), [72] and STM [30] merge to the conclusion that ions from the ionically conducting supports can provide, via electrical potential application, spillover ions ($O^{\delta-}$, $Na^{\delta+}$, etc.) which establish an effective double layer on the gas-exposed catalyst surface. This double layer formed via spillover ions affects the work function of the catalyst surface and thus affects the binding energies of coadsorbed reactants, intermediates, and products. This process is called "sacrificial promoter" mechanism because spillover ionic species can react with the oxidizable reactant and then have a finite lifetime on the surface. This lifetime directly impacts the magnitude of the Faradaic efficiency: the higher the lifetime of the ionic promoters, the higher the NEMCA effect. This is, of course, only valid if the chemical reaction is

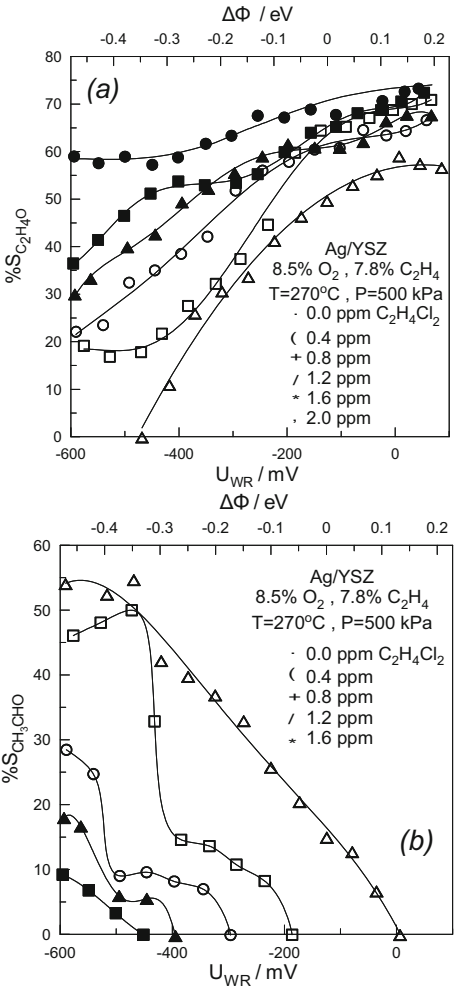

Fig. 1.7 Effect of Ag/YSZ catalyst potential, work function, and feed partial pressure of dichloroethane on the selectivity to ethylene oxide (**a**) and to acetaldehyde (**b**). $T = 270$ °C, $P = 500$ kPa, 8.5% O_2, 7.8% C_2H_4. (Reprinted from ref. [56] with permission from Elsevier)

under kinetic control conditions without any mass transfer or equilibrium limitations. The "sacrificial promoter" model provided the means to rationalize and even predict the experimental catalytic rate time constants via a simple equation [22, 59]. The theoretical work of Pacchioni and Illas [60] was also extremely valuable, as well as the STM work of Makri [30] and Archonta [33].

Isotopical labeling experiments, using labeled $^{18}O_2$, were also crucial to *operando* distinguish the oxygen species coming from the solid electrolyte (such as YSZ) with those from the gas phase [66, 67, 74]. Figure 1.9 gives the example of the propane oxidation which has been operated on Pt/YSZ in the presence of $^{18}O_2$ in the gas phase. At 350 °C, the application of a positive current density ($j = 43$ μA. cm^{-2}) was found to enhance the propane conversion from 8.4% up to 55%, leading to a Faradaic efficiency of 20. The predominant product of the reaction is $C^{18}O_2$,

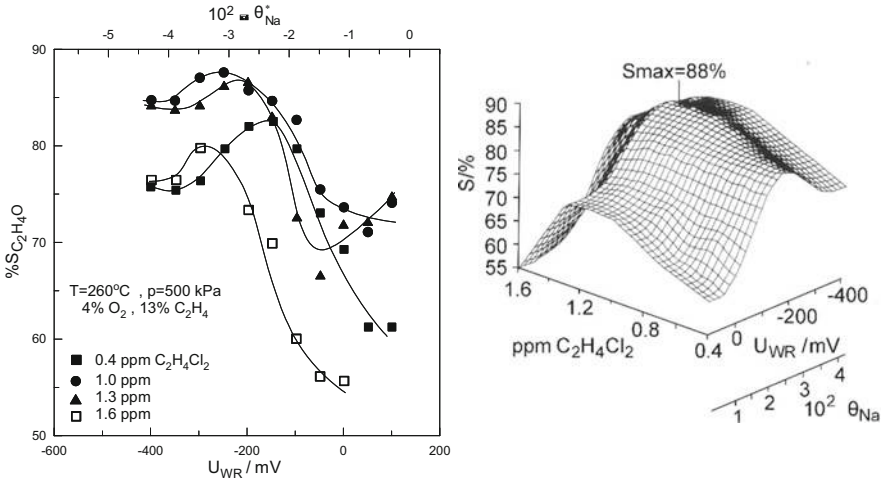

Fig. 1.8 Ethylene epoxidation on Ag/β″-Al_2O_3. Steady-state effect of catalyst potential on the selectivity to ethylene oxide at various levels of gas-phase dichloroethane (**a**) and three-dimensional representation of the effect of dichloroethane concentration, catalyst potential, and corresponding Na coverage on the selectivity to ethylene oxide (**b**). (Reprinted from ref. [40] with permission from Elsevier)

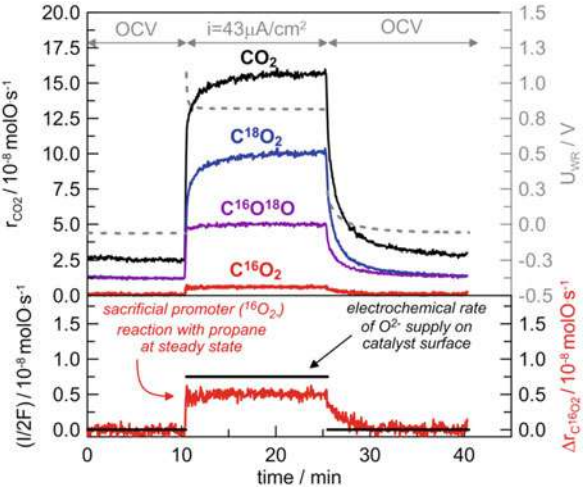

Fig. 1.9 Impact of a positive polarization ($J = 43$ μA/cm^2) on the overall CO_2 production and on CO_2 isotopomer distribution during propane combustion on Pt/YSZ (bottom). Comparison between the electrochemical rate of O^{2-} supplied onto the catalyst surface and the rate increase of $C^{16}O_2$ production. T = 350 °C. $C_3H_8/^{18}O_2$: 1000 ppm/2.5%. Overall flow: 2.4 L/h. (Reprinted from ref. [74] with the permission of Elsevier)

confirming that the backspillover of $^{16}O^{2-}$ species promotes the reaction of propane with gaseous oxygen ($^{18}O_2$). It is interesting to note that the enhancement in the rate of $C^{16}O_2$ formation almost coincides with the rate ($I/2F$) of O^{2-} supply to the catalyst ($\Lambda C^{16}O_2 = 1$). These results are in good agreement with the sacrificial promoter mechanism as they validate that $^{16}O^{2-}$ ionic species act as promoting agents and weakly participate to the reaction. More recently [75], density functional

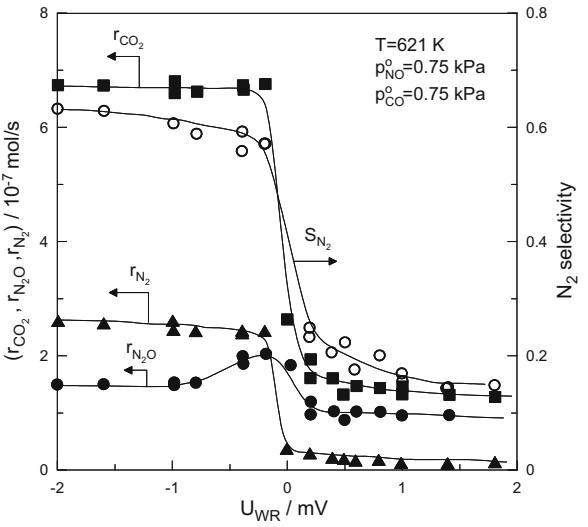

Fig. 1.10 Effect of catalyst potential on the rates of formation of CO_2, N_2, and N_2O and on the selectivity to N_2 during NO reduction by CO on Pt/β''-Al_2O_3. (Reprinted from ref. [11] with permission from Elsevier)

theory (DFT) was used to unravel the impact of applied potentials on the catalytic activity of RuO_2 deposited on YSZ for the ethylene oxidation at 350 °C. Increase in the ethylene conversion with a non-Faradaic manner was experimentally observed both for positive and negative polarizations. DFT modeling has explained these electrochemical activations by the strengthening of the ethylene adsorption on RuO_2 upon positive potentials, also facilitating the cleave of the C-C bond, and by the promotion of the oxygen chemisorption for negative polarizations. These conclusions are in accordance with the oxygen ion backspillover mechanism. This latter has also been analyzed by thermodynamic calculations [76] which have confirmed its validity but after considering some additional specific conditions such as the application of small potentials, low lateral interactions between surface ions (low ion coverage), and a fast surface diffusion of the ionic species.

Catalytic reactions were thus also soon directly grouped in four categories on the basis of the sign of the rate change observed upon positive potential applications: nucleophilic (or electrophobic), electrophilic, volcano-type, and inverted-volcano type [37, 39, 57, 77] (Fig. 1.11). Simple analytical expressions were derived describing the rate vs work function dependence in excellent agreement with experiment [37, 39, 57]. It was soon realized that the same rules also applied to classical ex situ promotion and to the phenomenon of metal-support interactions (MSI) [37, 39, 57] and that therefore promotion, electrochemical promotion, and metal-support interactions are fundamentally identical phenomena and only operationally different. For instance, Fig. 1.12 depicts the electrochemical promotion of Rh films [10] and the chemical promotion by changing the support of supported dispersed Rh catalysts. The two effects are similar and show that TiO_2 (4% WO_3) is the best catalyst support for this reaction on Rh [38].

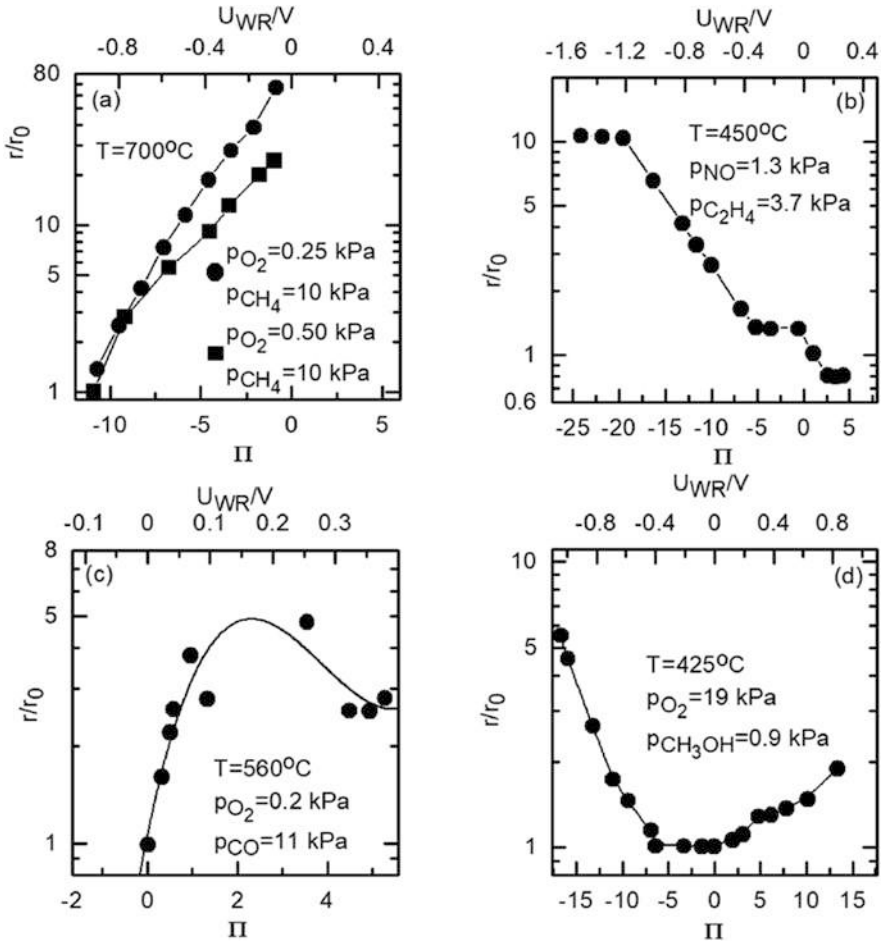

Fig. 1.11 Examples for the four types of global electrochemical promotion behavior: (**a**) electrophobic, (**b**) electrophilic, (**c**) volcano type, (**d**) inverted-volcano type. (**a**) Effect of catalyst potential and work function change (vs $I = 0$) for high, (20:1) and (40:1), CH_4 to O_2 feed ratios, Pt/YSZ; (**b**) effect of catalyst potential on the rate enhancement ratio for the rate of NO reduction by C_2H_4 consumption on Pt/YSZ; (**c**) NEMCA-generated volcano plots during CO oxidation on Pt/YSZ; (**d**) Effect of dimensionless catalyst potential on the rate constant of H_2CO formation, Pt/YSZ. $\Pi = FU_{WR}/RT$ ($=\Delta\Phi/k_bT$). (Reprinted from ref. [77] with the permission of Elsevier)

Simple expressions were also derived for the time constants of galvanostatic, i.e., fixed applied current, rate transients, and the first multichannel and multiplate EPOC units were designed and built [61]. At the same time, aqueous NEMCA was demonstrated with Pt catalyst electrodes in aqueous alkaline solutions [22].

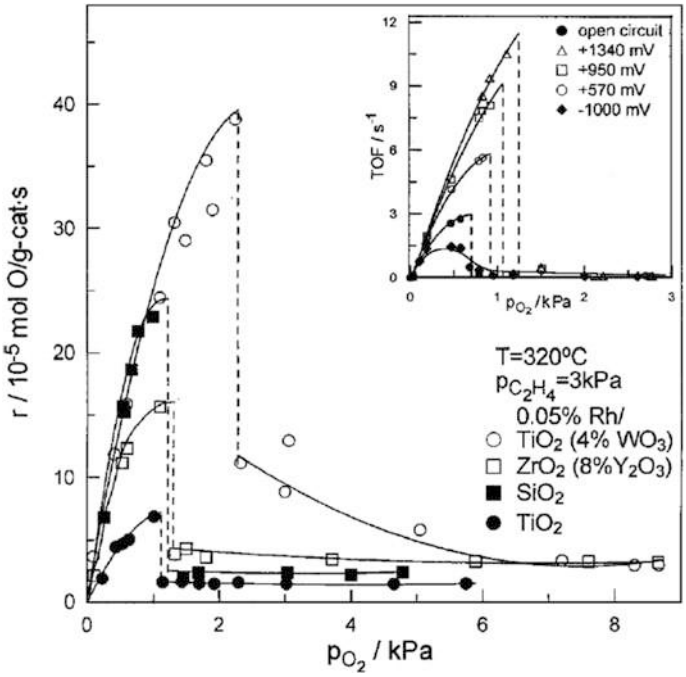

Fig. 1.12 Effect of p_{O2} on the rate of C_2H_4 oxidation on Rh supported on four supports of increasing Φ [10]. Rh loading 0.05 wt%. Inset: electrochemical promotion of a Rh catalyst film deposited on YSZ: effect of potentiostatically imposed catalyst potential U_{WR} on the TOF dependence on p_{O_2} at fixed p_{C2H4}. (Reprinted with permission from Elsevier [38])

1.4 EPOC Current Research Efforts

Two main directions are currently investigated: First, the design and testing of larger, simpler, and more efficient multiplate electropromoted units, and second, electrochemical promotion of nanodispersed catalysts. The latter is more difficult, since the particles of fully supported nanodispersed catalysts are already, at least partially, promoted via ion migration from the support to the nanoparticle surface. Such EPOC transients are often quite complex, exhibiting spikes of the type shown in Fig. 1.13. The successful interpretation of such transients and concomitating electropromotion of such catalysts remains both challenging and promising and could lead to practical applications. The nanostructure of nanodispersed EPOC catalysts is a scientific issue as the mobility of both electrons and ions is required to achieve significant electrochemical enhancements of catalytic rates. Different strategies of nano-architectures have been recently proposed to combine a high mixed electronic and ionic conductivity with a good thermal stability of the active nanoparticles like nanoporous electrodes, metal, or metal oxide nanoparticles finely dispersed on either electron conductor matrix or mixed ion-electron conductor matrix. Nevertheless, in situ and *operando* investigations, such as synchrotron or spectroscopic techniques, are still

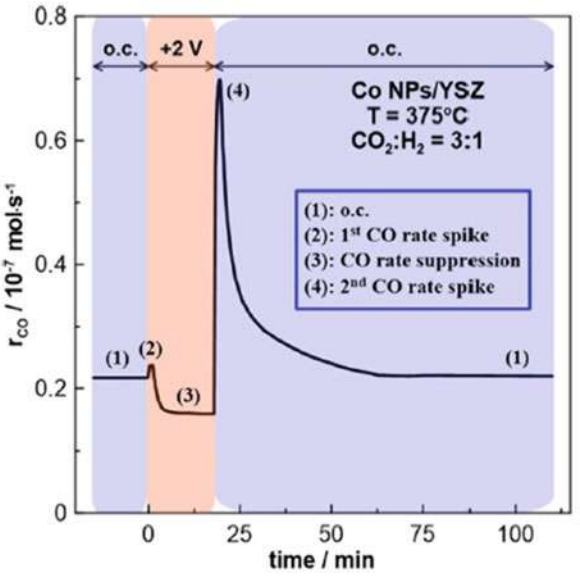

Fig. 1.13 Transient effect of constant applied positive (±2 V) potential on the catalytic rate of CO formation on the Co NPs/YSZ film. Regions where different rate responses are taking place are noted. (Reprinted from ref. [62] with the permission of the American Chemical Society)

missing on dispersed electropromoted catalysts to determine if the sacrificial promoter mechanism, demonstrated on continuous films, is also valid.

The polarization mode is also a research field to explore aiming to optimize non-Faradaic effects. Up to date, a constant potential or current in a static mode is commonly used to polarize the catalyst. However, in 2021, C. Wei Lim et al. [78] have demonstrated that the application of dynamic potentials can enhance with the non-Faradaic manner the ethylene hydrogenation rate on a Pd/C electrode at 60 °C in a liquid electrochemical cell although a conventional static polarization has no effect. Optimized polarization modes were achieved for potential oscillations between a low value (−0.25 V_{NHE}) and high value (0.55 V_{NHE}) with a frequency of around 0.1 Hz.

1.5 Conclusions

Electrochemical promotion of catalysis is related to the electrochemically supply of ionic species on the catalyst surface and the concomitant modifications of the electronic and chemisorptive properties of the catalyst. The lifetime of these ionic promoters on the surface is the key parameter that governs the EPOC magnitude. Since the discovery of EPOC, most of the studies focused on solid/gas interfaces in a temperature range (200–600 °C), where the ionic conductivity of solid electrolytes is high enough, and mainly involved platinum group metals (PGM) as catalysts for many different reactions. On these systems, the sacrificial promoter mechanism, based on the establishment of a neutral double layer at the gas/solid interface upon

the polarization of the catalyst/electrolyte interface, is now well established, and rules have been proposed to predict the impact of the electric field on the catalytic activity. Many research efforts are still needed to the development of EPOC reactors and electropromoted nanodispersed catalysts. We strongly believe that EPOC can play a vital role in the energy transition, the first consequence of which being the intensive electrification of processes.

References

1. Wagner C (1970) Adsorbed atomic species as intermediates in heterogeneous catalysis. Adv Catal 21:323–381. https://doi.org/10.1016/S0360-0564(08)60567-2
2. Vayenas CG, Saltsburg HM (1979) Chemistry at catalyst surfaces: the oxidation of SO_2 on noble metals. J Catal 57:296–314. https://doi.org/10.1016/0021-9517(79)90033-2
3. Pancharatnam S, Huggins RA, Mason DM (1975) Catalytic decomposition of nitric oxide on zirconia by electrolytic removal of oxygen. J Electrochem Soc 122(7):869–875. https://doi.org/10.1149/1.2134364
4. Gür TM, Huggins RA (1979) Decomposition of nitric oxide on zirconia in a solid-state electrochemical cell. J Electrochem Soc 126(6):1067–1075. https://doi.org/10.1149/1.2129175
5. Vayenas CG, Farr RD (1980) Cogeneration of electric energy and nitric oxide. Science 208: 593–595. https://doi.org/10.1126/science.208.4444.593
6. Stoukides M, Vayenas CG (1981) Solid electrolyte-aided study of the ethylene oxidation on polycrystalline silver. J Catal 69:18–31. https://doi.org/10.1016/0021-9517(83)90116-1
7. Stoukides M, Vayenas CG (1981) The effect of electrochemical oxygen pumping on the rate and selectivity of ethylene oxidation on polycrystalline silver. J Catal 70(1):137–146. https://doi.org/10.1016/0021-9517(81)90323-7
8. Bebelis S, Vayenas CG (1989) Non-faradaic electrochemical modification of catalytic activity: 1. The case of Ethylene Oxidation on Pt. J Catal 118:125–146. https://doi.org/10.1016/0021-9517(89)90306-0
9. Vayenas CG, Bebelis S, Ladas S (1990) Dependence of catalytic rates on catalyst work function. Nature 343(6259):625–627. https://doi.org/10.1038/343625a0
10. Pliangos C, Yentekakis IV, Verykios XE, Vayenas CG (1995) Non-faradaic electrochemical modification of catalytic activity: 8. Rh-catalyzed C_2H_4 oxidation. J Catalysis 154:124–136. https://doi.org/10.1006/jcat.1995.1154
11. Palermo A, Lambert RM, Harkness IR, Yentekakis IV, Marina OA, Vayenas CG (1996) Electrochemical promotion by Na of the platinum-catalyzed reaction between CO and NO. J Catal 161(1):471–479. https://doi.org/10.1006/jcat.1996.0206
12. Yentekakis IV, Vayenas CG (1988) The effect of electrochemical oxygen pumping on the steady-state and oscillatory behavior of CO oxidation on polycrystalline Pt. J Catalogue 111(1): 170–188. https://doi.org/10.1016/0021-9517(88)90075-9
13. Vayenas CG, Bebelis S, Neophytides S, Yentekakis IV (1989) Non-faradaic electrochemical modification of catalytic activity in solid electrolyte cells. Applied Physics (A) 49:95–103. https://doi.org/10.1007/BF00615471
14. Vayenas CG, Bebelis S, Yentekakis IV, Tsiakaras P, Karasali H, Karavasilis CH (1991) Solid electrolytes for in situ promotion of catalyst surfaces: the NEMCA effect. ISSI Letters 2:5–7
15. Yentekakis IV, Moggridge G, Vayenas CG, Lambert RM (1994) In situ controlled promotion of catalyst surfaces via NEMCA: the effect of Na on the Pt-catalyzed CO oxidation. J Catal 146(1): 292–305. https://doi.org/10.1016/0021-9517(94)90033-7
16. Vayenas CG, Ladas S, Bebelis S, Yentekakis IV, Neophytides S, Yi J, Karavasilis CH, Pliangos C (1994) Electrochemical promotion in catalysis: non-faradaic electrochemical modification of

catalytic activity. Electrochim Acta 39(11/12):1849–1855. https://doi.org/10.1016/0013-4686(94)85174-3
17. Jiang Y, Yentekakis IV, Vayenas CG (1994) Methane to ethylene with 85% yield in a gas-recycle electrocatalytic reactor-separator. Science 264:1563–1566. https://doi.org/10.1126/science.264.5165.1563
18. Vayenas CG, Bebelis S, Yentekakis IV, Tsiakaras P, Karasali H (1990) Non-faradaic electrochemical modification of catalytic activity. Reversible promotion of platinum metals catalyst. Plat Met Rev 34(3):122–130
19. Seimanides S, Tsiakaras P, Verykios XE, Vayenas CG (1991) Oxidative coupling of methane over Yttria-doped zirconia solid electrolyte. Appl Catalysis 68:41–53. https://doi.org/10.1016/S0166-9834(00)84092-0
20. Tsiakaras P, Vayenas CG (1993) Non-faradaic electrochemical modification of catalytic activity: VII. The case of methane oxidation on Pt. J Catal 140(1):53–70. https://doi.org/10.1006/jcat.1993.1068
21. Vayenas CG, Bebelis S, Despotopoulou M (1991) Non-faradaic electrochemical modification of catalytic activity: 4. The use of β″-Al2O3 as the solid electrolyte. J Catal 128:415–435. https://doi.org/10.1016/0021-9517(91)90300-S
22. Neophytides S, Tsiplakides D, Jaksic M, Stonehart P, Vayenas CG (1994) Electrochemical enhancement of a catalytic reaction in aqueous solution. Nature 370:45–47. https://doi.org/10.1038/370045a0
23. Pliangos C, Yentekakis IV, Ladas S, Vayenas CG (1996) Non-faradaic electrochemical modification of catalytic activity: 9. Ethylene oxidation on Pt deposited on TiO_2. J Catalysis 159:189–203. https://doi.org/10.1006/jcat.1996.0078
24. Papadakis VG, Pliangos CA, Yentekakis IV, Verykios XE, Vayenas CG (1996) Development of high performance, Pd-based, three way catalysts. Catal Today 29:71–75. https://doi.org/10.1016/0920-5861(95)00268-5
25. Tsiplakides D, Neophytides SG, Enea O, Jaksic MM, Vayenas CG (1997) Non-faradaic electrochemical modification of catalytic activity (NEMCA) of Pt black electrodes deposited on Nafion 117 solid polymer electrolyte. J Electrochem Soc 144(6):2072–2088. https://doi.org/10.1149/1.1837744
26. Vayenas CG, Bebelis S, Yentekakis IV, Karavasilis CH, Yi J (1994) Non-faradaic electrochemical modification of catalytic activity: solid electrolytes as active catalyst supports. Solid State Ionics 72:321–327. https://doi.org/10.1016/0167-2738(94)90167-8
27. Yi J, Yentekakis IV, Vayenas CG (1994) Potential-programmed reduction: a new technique for investigating chemisorption on catalysts supported on solid electrolytes. J Catalysis 148:240–251. https://doi.org/10.1006/jcat.1994.1205
28. Karavassilis CH, Bebelis S, Vayenas CG (1996) In situ controlled promotion of catalyst surfaces via NEMCA: the effect of Na on the Ag-catalyzed ethylene epoxidation in the presence of chlorine moderators. J Catal 160:205–213. https://doi.org/10.1006/jcat.1996.0139
29. Vayenas CG, Bebelis S, Yentekakis IV, Tsiakaras P, Karasali H, Karavasilis CH (1991) Catalytic and Electrocatalytic reactions in solid electrolyte cells: the NEMCA effect. Mater Sci Forum 76:141–148. https://doi.org/10.4028/www.scientific.net/MSF.76.141
30. Makri M, Vayenas CG, Bebelis S, Besocke KH, Cavalca C (1996) Atomic resolution STM imaging of electrochemically controlled reversible promoter dosing of catalysts. Surf Sci 369(1–3):351–359. https://doi.org/10.1016/S0039-6028(96)00911-9
31. Makri M, Vayenas CG, Bebelis S, Besocke KH, Cavalca C (1996) Atomic resolution scanning tunneling microscopy imaging of Pt electrodes intefaced with β″-Al_2O_3. Ionics 2:248–253. https://doi.org/10.1007/BF02376030
32. Makri M, Buekenhoudt A, Luyten J, Vayenas CG (1996) Non-faradaic electrochemical modification of the catalytic activity of Pt using a $CaZr_{0.9}In_{0.1}O_{3-a}$ proton conductor. Ionics 2:282–288. https://doi.org/10.1007/BF02376035

33. Vayenas CG, Archonta D, Tsiplakides D (2003) Scanning tunneling microscopy observation of the origin of electrochemical promotion and metal–support interactions. J Electroanal Chem 554-555:301–306. https://doi.org/10.1016/S0022-0728(03)00240-7
34. Tsiplakides D, Balomenou S, Katsaounis A, Archonta D, Koutsodontis C, Vayenas CG (2005) Electrochemical promotion of catalysis: mechanistic investigations and monolithic electropromoted reactors. Catal Today 100:133–144. https://doi.org/10.1016/j.cattod.2004.12.015
35. Yiokari CG, Pitselis GE, Polydoros DG, Katsaounis AD, Vayenas CG (2000) High-pressure electrochemical promotion of ammonia synthesis over an industrial iron catalyst. J Phys Chem A 104:10600–10602. https://doi.org/10.1021/jp002236v
36. Tsiplakides D, Vayenas CG (2001) Electrode work function and absolute potential scale in solid-state electrochemistry. J Electrochem Soc 148(5):E189–E202. https://doi.org/10.1149/1.1362547
37. Vayenas CG, Brosda S, Pliangos C (2001) Rules and mathematical modeling of electrochemical and chemical promotion: 1. Reaction classification and promotional rules. J Catal 203(2):329–350. https://doi.org/10.1006/jcat.2001.3348
38. Nicole J, Tsiplakides D, Pliangos C, Verykios XE, Comninellis C, Vayenas CG (2001) Electrochemical promotion and metal-support interactions. J Catal 204:23–34. https://doi.org/10.1006/jcat.2001.3360
39. Brosda S, Vayenas CG (2002) Rules and mathematical modeling of electrochemical and classical promotion 2. Modeling J Catal 208(1):38–53. https://doi.org/10.1006/jcat.2002.3549
40. Karavasilis C, Bebelis S, Vayenas CG (1996) In situ controlled promotion of catalyst surfaces via NEMCA: the effect of Na on the Ag-catalyzed ethylene epoxidation in the presence of chlorine moderators. J Catal 160:205–213. https://doi.org/10.1006/jcat.1996.0139
41. Tsiplakides D, Vayenas CG (2002) The absolute potential scale in solid state electrochemistry. Solid State Ionics 152-153:625–639. https://doi.org/10.1016/S0167-2738(02)00396-X
42. Koutsodontis C, Katsaounis A, Figueroa JC, Cavalca C, Pereira CJ, Vayenas CG (2006) The effect of catalyst film thickness on the magnitude of the electrochemical promotion of catalytic reactions. Top Catal 38(1–3):157–167. https://doi.org/10.1007/s11244-006-0081-y
43. Koutsodontis C, Katsaounis A, Figueroa JC, Cavalca C, Pereira CJ, Vayenas CG (2006) The effect of catalyst film thickness on the electrochemical promotion of ethylene oxidation on Pt. Top Catal 39(1–2):97–100. https://doi.org/10.1007/s11244-006-0042-5
44. Vayenas CG, Tsampas MN, Katsaounis A (2007) First principles analytical prediction of the conductivity of Nafion membranes. Electrochim Acta 52:2244–2256. https://doi.org/10.1016/j.electacta.2006.03.109
45. Sapountzi F, Tsampas MN, Vayenas CG (2007) Electrocatalysis and electrochemical promotion of CO oxidation in PEM fuel cells: the role of oxygen crossover. Top Catal 44(3):461–468. https://doi.org/10.1007/s11244-006-0138-y
46. Tsiplakides D, Archonta D, Vayenas CG (2007) Absolute potential measurements in solid and aqueous electrochemistry using two Kelvin probes and their implications for the electrochemical promotion of catalysis. Top Catal 44(3):469–479. https://doi.org/10.1007/s11244-006-0139-x
47. Constantinou I, Archonta D, Brosda S, Lepage M, Sakamoto Y, Vayenas CG (2007) Electrochemical promotion of NO reduction by C_3H_6 on Rh catalyst-electrode films supported on YSZ and on dispersed Rh/YSZ catalysts. J Catal 251:400–409. https://doi.org/10.1016/j.jcat.2007.07.034
48. Vayenas CG, Koutsodontis CG (2008) Non-faradaic electrochemical activation of catalysis. J. Chem. Phys 128:Article ID: 182506. (13 pages). https://doi.org/10.1063/1.2824944
49. Souentie S, Hammad A, Vayenas CG (2009) Steady-state multiplicity phenomena during the electrochemical promotion of NO reduction by C_2H_4 in presence of O_2 on thin Rh and Pt catalyst-electrodes in a monolithic electropromoted reactor. Catal Today 146(3–4):285–292. https://doi.org/10.1016/j.cattod.2009.04.020

50. Souentie S, Lizarraga L, Papaioannou EI, Vayenas CG, Vernoux P (2010) Permanent electrochemical promotion of C_3H_8 oxidation over thin sputtered Pt films. Electrochem Commun 12: 1133–1135. https://doi.org/10.1016/j.elecom.2010.06.002
51. Papaioannou EI, Souentie S, Sapountzi FM, Hammad A, Labou D, Brosda S, Vayenas CG (2010) The role of TiO_2 layers deposited on YSZ on the electrochemical promotion of C_2H_4 oxidation on Pt. J Appl Electrochem 40:1859–1865. https://doi.org/10.1007/s10800-010-0107-9
52. Pritchard J (1990) Electrochemical promotion. Nature 343:592–593. https://doi.org/10.1038/343592a0
53. Tsampas MN, Sapountzi FM, Vernoux P (2015) Applications of yttria stabilized zirconia (YSZ) in catalysis. Cat Sci Technol 5:4884–4900. https://doi.org/10.1039/c5cy00739a
54. Vernoux P, Gaillard F, Bultel L, Siebert E, Primet M (2002) Electrochemical promotion of propane and propene oxidation on Pt/YSZ. J Catal 205:412–421. https://doi.org/10.1006/jcat.2002.3573
55. Vernoux P, Gaillard F, Lopez C, Siebert E (2003) Coupling catalysis to electrochemistry: a solution to selective reduction of nitrogen oxides in lean burn exhausts ? J Catal 217:203–208. https://doi.org/10.1016/S0021-9517(03)00052-6
56. Karavasilis C, Bebelis S, Vayenas CG (1996) Non-faradaic electrochemical modification of catalytic activity: X. ethylene epoxidation on Ag deposited on stabilized ZrO2 in the presence of chlorine moderators. J Catal 160:190–204. https://doi.org/10.1006/jcat.1996.0138
57. Vernoux P, Lizarraga L, Tsampas MN, Sapountzi FM, De Lucas-Consuegra A, Valverde JL, Souentie S, Vayenas CG, Tsiplakides D, Balomenou S, Baranova EA (2013) Ionically conducting ceramics as active catalyst supports. Chem Rev 113:8192–8260. https://doi.org/10.1021/cr4000336
58. Vayenas CG, Lambert RM, Ladas S, Bebelis S, Neophytides S, Tikhov MS, Filkin NC, Makri M, Tsiplakides D, Cavalca C, Besocke K (1997) Direct STM, XPS and TPD observation of spillover phenomena over mm distances on metal catalyst films interfaced with solid electrolytes. Stud Surf Sci Catal 112:39–47. https://doi.org/10.1016/S0167-2991(97)80822-1
59. Ladas S, Kennou S, Bebelis S, Vayenas CG (1993) Origin of non-faradaic electrochemical modification of catalytic activity. J Phys Chem 97(35):8845. https://doi.org/10.1021/j100137a004
60. Pacchioni G, Illas F, Neophytides S, Vayenas CG (1996) Quantum-chemical study of electrochemical promotion in catalysis. J Phys Chem 100(41):16653–16661. https://doi.org/10.1021/jp9612386
61. Balomenou S, Tsiplakides D, Katsaounis A, Thiemann-Handler S, Cramer B, Foti G, Vayenas CG (2004) Novel monolithic electrochemically promoted catalytic reactor for environmentally important reactions. Appl Catal B 52(3):181–196. https://doi.org/10.1016/j.apcatb.2004.04.007
62. Zagoraios D, Tsatsos S, Kennou S, Vayenas CG, Kyriakou G, Katsaounis A (2020) Tuning the RWGS reaction via EPOC and in situ electro-oxidation of cobalt nanoparticles. ACS Catal 10: 14916–14927. https://doi.org/10.1021/acscatal.0c04133
63. Neophytides SG, Vayenas CG (1995) TPD and cyclic voltammetric investigation of the origin of electrochemical promotion in catalysis. J Phys Chem 99(47):17063–17067. https://doi.org/10.1021/j100047a001
64. Neophytides SG, Tsiplakides D, Vayenas CG (1998) Temperature-programmed desorption of oxygen from Pt films interfaced with Y2O3-doped ZrO2. J Catal 178(2):414–428. https://doi.org/10.1006/jcat.1998.2155
65. Tsiplakides D, Vayenas CG (1999) Temperature programmed desorption of oxygen from Ag films interfaced with Y2O3-doped ZrO2. J Catal 185:237–251. https://doi.org/10.1006/jcat.1999.2522
66. Katsaounis A, Nikopoulou Z, Verykios XE, Vayenas CG (2004) Comparative isotope-aided investigation of electrochemical promotion and metal–support interactions 1. 18O2 TPD of electropromoted Pt films deposited on YSZ and of dispersed Pt/YSZ catalysts. J Catal 222(1): 192–206. https://doi.org/10.1016/j.jcat.2003.10.010

67. Katsaounis A, Nikopoulou Z, Verykios XE, Vayenas CC (2004) Comparative isotope-aided investigation of electrochemical promotion and metal-support interactions 2. CO oxidation by 18O2 on electropromoted Pt films deposited on YSZ and on nanodispersed Pt/YSZ catalysts. J Catal 226(1):197–209. https://doi.org/10.1016/j.jcat.2004.05.009
68. Li X, Gaillard F, Vernoux P (2007) Investigations under real operating conditions of the electrochemical promotion by O2 temperature programmed desorption measurements. Top Catal 44(3):391–398. https://doi.org/10.1007/s11244-006-0131-5
69. Ladas S, Kennou S, Bebelis S, Vayenas CG (1993) Origin of non-faradaic electrochemical modification of catalytic activity. J Phys Chem 97(35):8845–8848. https://doi.org/10.1021/j100137a004
70. Espinós JP, Rico VJ, González-Cobos J, Sánchez-Valencia JR, Pérez-Dieste V, Escudero C, de Lucas-Consuegra A, González-Elipe AR (2018) In situ monitoring of the phenomenon of electrochemical promotion of catalysis. J Catal 358:27–34. https://doi.org/10.1016/j.jcat.2017.11.027
71. Yi J, Kaloyannis A, Vayenas CG (1993) High temperature cyclic voltammetry of Pt catalyst-electrodes in solid electrolyte cells. Electrochim Acta 38:2533. https://doi.org/10.1016/0013-4686(93)80149-T
72. Poppe J, Völkening S, Schaak A, Schütz E, Janek J, Imbihl R (1999) Electrochemical promotion of catalytic CO oxidation on Pt/YSZ catalysts under low pressure conditions. Phys Chem Chem Phys 1:5241. https://doi.org/10.1039/A905094I
73. Vayenas CG, Bebelis S, Pliangos C, Brosda S, Tsiplakides D (2001) Electrochemical activation of catalysis. Kluwer Academic/Plenum Publishers, New York
74. Tsampas MN, Sapountzi FM, Boréave A, Vernoux P (2013) Isotopical labeling mechanistic studies of electrochemical promotion of propane combustion on Pt/YSZ. Electrochem Commun 26:13–16. https://doi.org/10.1016/j.elecom.2012.09.043
75. Hajar YM, Treps L, Michel C, Baranova EA, Steinmann SN (2019) Theoretical insight into the origin of the electrochemical promotion of ethylene oxidation on ruthenium oxide. Cat Sci Technol 9(21):5915–5926. https://doi.org/10.1039/C9CY01421G
76. Metcalfe IS (2001) Electrochemical promotion of catalysis: I: thermodynamic considerations. J Catal 199:247. https://doi.org/10.1006/jcat.2001.3164
77. Brosda S, Vayenas CG, Wei J (2006) Rules of chemical promotion. Appl Catal B 68:109–124. https://doi.org/10.1016/j.apcatb.2006.07.021
78. Wei Lim C, Hulsey MJ, Yan N (2021) Non-faradaic promotion of ethylene hydrogenation under oscillating potentials. JACS Au 1:536–542. https://doi.org/10.1021/jacsau.1c00044

Chapter 2
Electrochemical Promotion of Catalysis: From Discovery to Fundamentals to Applications

Symeon Bebelis

Abstract Electrochemical promotion of catalysis (EPOC) is an electrochemically induced catalytic effect which corresponds to in situ reversible modification of the catalytic behavior of metal or metal oxide catalyst-electrodes deposited on solid electrolytes or mixed ionic-electronic conductors (MIEC) upon polarization of the electrode/electrolyte or MIEC interface. This work highlights the key landmarks in EPOC starting from its discovery. Firstly, a brief history of the experimental work that resulted in the rather unexpected discovery of EPOC when using as catalysts metal film electrodes deposited on $ZrO_2(Y_2O_3)$, an O^{2-} conductor, is presented. Secondly, the efforts towards validation of the general nature of EPOC, by investigating this phenomenon in a very large number of combinations of electrolytes or MIEC, electrodes, and catalytic reactions, are briefly described in chronological order. A short reference is then made to the experimental and theoretical works that led to understanding of the mechanistic origin of EPOC and its functional equivalence to metal-support interactions. The focus is then shifted to current activities and efforts towards developing configurations for practical applications of EPOC, with emphasis on bipolar designs, monolithic electropromoted reactors, EPOC with nanodispersed catalysts, and wireless self-driven and self-sustained EPOC systems.

Keywords Electrochemical promotion of catalysis (EPOC) · Electrochemical activation of catalysis · Non-faradaic electrochemical modification of catalytic activity (NEMCA) · Spillover-backspillover · Ionic promoters · Solid ionic and mixed conductors

S. Bebelis (✉)
Department of Chemical Engineering, University of Patras, Patras, Greece
e-mail: simeon@chemeng.upatras.gr

P. Vernoux, C. G. Vayenas (eds.), *Recent Advances in Electrochemical Promotion of Catalysis*, Modern Aspects of Electrochemistry 61,
https://doi.org/10.1007/978-3-031-13893-5_2

2.1 Introduction

The terms electrochemical promotion of catalysis (EPOC) or non-faradaic electrochemical modification of catalytic activity (NEMCA) both refer interchangeably to an electrochemically induced catalytic effect which corresponds to in situ or *in operando* reversible modification of the activity and selectivity of catalysts interfaced to solid electrolytes or mixed ionic-electronic conductors (MIEC), upon polarization of the catalyst/solid electrolyte or MIEC interface [1, 2]. This effect was first observed by M. Stoukides and C.G. Vayenas in 1981, as detailed in Chap. 1, in the reaction of ethylene oxidation on Ag deposited on yttria-stabilized zirconia or $ZrO_2(Y_2O_3)$, an O^{2-} conducting solid electrolyte [3], who reported polarization-induced non-faradaic changes in the catalytic rates of CO_2 and C_2H_4O production as well as in selectivity to C_2H_4O. However, this behavior was then attributed to peculiarity of the specific catalytic system and was explained by a kinetic model which was based on the hypothesis of formation of surface silver oxide, more active than reduced silver, on sites adjacent to chemisorbed oxygen [3]. It was some years later, in 1988, when C. G. Vayenas and his coworkers reported results showing conclusively that EPOC, then referred to as NEMCA effect, is a general effect in heterogeneous catalysis, which they attributed to electrochemically induced change in catalyst work function [4].

The distinguishing feature of EPOC is that the induced catalytic rate change $\Delta r = r - r_o$ upon catalyst polarization (via current or potential application), where r and r_o denote the observed reaction rates under closed- circuit (current $I \neq 0$) and open-circuit ($I = 0$) conditions, is higher, even by orders of magnitude, than the electrocatalytic rate dictated by Faraday's law, which is equal to the rate of ion transport through the electrolyte. The electrocatalytic rate is equal to $I/(nF)$, where I denotes the applied current, n denotes the number of exchanged electrons in the charge transfer reaction at the catalyst-electrode/solid electrolyte or MIEC interface (e.g., $n = 2$ for an O^{2-} conductor), and F is Faraday's constant. Thus, under EPOC conditions the absolute value of the enhancement factor or faradaic efficiency, Λ, of the process, defined from [1, 4],

$$\Lambda \equiv \frac{\Delta r}{\left(\frac{I}{nF}\right)} \tag{2.1}$$

is larger than 1 ($|\Lambda| > 1$), which can be explained only by induced changes in the catalytic properties of the electrode. Another important parameter for quantifying the EPOC effect is the rate enhancement ratio, ρ, defined from [1, 4]

$$\rho \equiv \frac{r}{r_o} = \frac{r_o + \Delta r}{r_o} \tag{2.2}$$

as the ratio of the catalytic rates in the presence and absence of polarization.

EPOC has been reported for a large number of catalytic reactions, involving various combinations of metal or metal oxide catalysts and solid electrolytes or MIEC as active catalyst supports, whereas it has been also demonstrated for catalytic reactions in aqueous electrolytes and inorganic melts. Work on EPOC prior to 2001 is summarized in a book [1] whereas more recent progress in several book chapters and review articles [2, 5–15]. This chapter concerns a historical tracing of the progress in research related to EPOC, describing briefly the important steps from its discovery to the fundamental understanding of its origin and the exploration of the underlying rules and principles, as well as its relation to other catalytic effects, and, finally, the key steps towards technological applications.

2.2 The Discovery of EPOC: An Electrochemically Induced Catalytic Effect

2.2.1 EPOC with O^{2-} Conductors

In 1981, M. Stoukides and C.G. Vayenas were the first to report that the catalytic activity and selectivity of a silver catalyst-porous electrode deposited on ZrO_2 (8 mol % Y_2O_3) solid electrolyte in a two-electrode asymmetric set-up (Fig. 2.1) could be significantly affected by polarization of the Ag electrode under conditions of ethylene epoxidation [3]. Specifically, they observed that electrochemical pumping of O^{2-} to the Ag catalyst via positive current application, under oxidative conditions, could induce reversible increases in both the rates of ethylene oxide and CO_2 production which exceeded by up to ca. 400 times (for the C_2H_4O production rate) the ion pumping rate and were accompanied by an increase in selectivity to ethylene

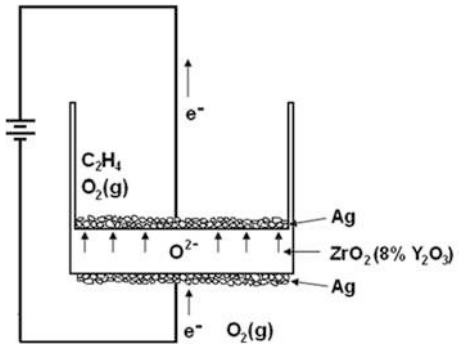

Fig. 2.1 Schematic diagram of the solid electrolyte cell reactor for the first EPOC experiments. The Ag catalyst-electrode film (working electrode) was deposited on the inner bottom side of a ZrO_2(8 mol% Y_2O_3) tube and was exposed to the reaction mixture. A similar Ag film deposited on the outside bottom side of the tube and exposed to ambient air served as the counter electrode. (Reprinted from ref. [3], with permission from Elsevier)

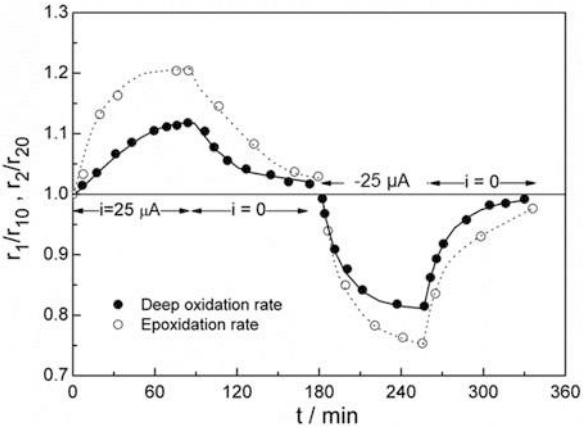

Fig. 2.2 Transient effect of electrochemical oxygen pumping during C_2H_4 epoxidation on Ag interfaced to ZrO_2(8 mol %Y_2O_3); r_1, rate of epoxidation; r_2, rate of CO_2 formation. Conditions: $P_{C_2H_4} = 1.6$ kPa, $P_{O_2} = 9.5$ kPa, $T = 400$ °C. Open-circuit rates: $r_{10} = 7.6 \times 10^{-8}$ mol/s, $r_{2,0} = 8.9 \times 10^{-8}$ mol/s. O^{2-} pumping rate: $G_{O^{2-}} = i/2F = 1.3 \times 10^{-10}$ mol/s. (Reprinted with permission from ref. [16]. Copyright (1982) American Chemical Society)

oxide (by more than 20%) [3, 16]. The opposite effect, i.e., a decrease in catalytic rates and in selectivity to C_2H_4O, was observed upon negative current application [3, 16]. A typical example of this behavior is shown in Fig. 2.2 [16]. The non-faradaic increase of the rates upon O^{2-} pumping to the Ag catalyst, corresponding to enhancement ratio ρ values up to 3 [16] and faradaic efficiency Λ values up to 400 [3], was attributed by the two authors to peculiarity of the specific catalytic system and was explained by a kinetic model which was based on the hypothesis of formation of a surface silver oxide, more active than reduced silver, on sites adjacent to chemisorbed oxygen [3]. However, a decade later it became clear that the observed changes in catalytic activity and selectivity were manifestation of the EPOC effect in this important catalytic system [17].

A qualitatively identical effect of O^{2-} pumping on rates and selectivity, considered in consistence with the surface silver oxide model, was reported in 1984 by Stoukides and Vayenas [18] for the reaction of propylene epoxidation on porous Ag interfaced to ZrO_2 (8 mol% Y_2O_3) in a similar two-electrode asymmetric set-up (Fig. 2.1). O^{2-} pumping to the Ag catalyst resulted in increase of both the epoxidation rate (by up to 45%) and deep oxidation rate (by up to 11%) and in a concomitant increase of selectivity to C_3H_6O (by more than 30%), which however did not exceed 4% [18]. Enhancement in the total rate of C_3H_6 consumption exceeding the O^{2-} pumping rate by more than two orders of magnitude was reported [18].

In 1988, the electrochemical promotion effect was reported for the first time by C. G. Vayenas and his coworkers as a general effect in heterogeneous catalysis, having been observed until then for a number of different reactions on porous Pt and Ag catalyst-electrodes (5–10 μm thick) interfaced to ZrO_2 (8 mol% Y_2O_3) or YSZ [4]. The term "non-faradaic electrochemical modification of catalytic activity"

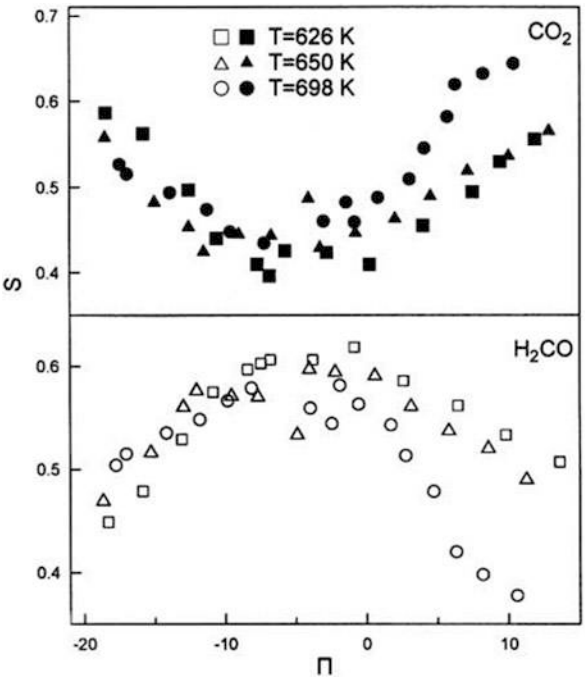

Fig. 2.3 Methanol oxidation on Pt/YSZ: Effect of dimensionless catalyst potential $\Pi \equiv F\,U_{WR}/RT$ on the selectivity to CO_2 and H_2CO; $P_{CH_3OH} = 0.9$ kPa, $P_{O_2} = 19$ kPa. (Reprinted from ref. [21], with permission from Elsevier)

(acronym NEMCA) was also introduced to describe it [4]. Specifically, electrochemical promotion had been observed in C_2H_4 epoxidation on Ag/YSZ [3, 16], in C_3H_6 epoxidation on Ag/YSZ [18], in C_2H_4 combustion on Pt/YSZ [4, 19], in CO oxidation on Pt/YSZ [4, 20], in CH_3OH oxidation to CO_2 and H_2CO on Pt/YSZ [4, 21], and in CH_3OH dehydrogenation to H_2CO and decomposition to CO and H_2 on Ag/YSZ [4, 22], with faradaic efficiency absolute values up to 3×10^5 [19], rate enhancement ratios up to 55 [19], and significant changes in selectivity [4, 21, 22] and in oscillatory behavior [20], where appropriate. Results from these studies, published from 1988 to 1991, are shown in Figs. 1.5 and 1.6 of Chap. 1 for C_2H_4 oxidation on Pt/YSZ [19] and in Fig. 2.3 for methanol oxidation on Pt/YSZ [21], respectively.

With the exception of C_2H_4 and C_3H_6 epoxidation on Ag/YSZ, the aforementioned studies were performed in a three electrode set-up [19] where two porous metal (Pt or Ag) films were deposited on the outer bottom side of the YSZ tube (Fig. 2.1), exposed to ambient air and serving as counter and reference electrode, respectively. This allowed for measurement of the catalyst-working electrode (W) potential U_{WR} with respect to the reference electrode (R) and for its association with the observed rate change. Interestingly, over specific U_{WR} range for each reaction, the catalytic rate, r, was found to depend exponentially on $\Delta U_{WR} = U_{WR} - U_{WR}^*$ according to the equation

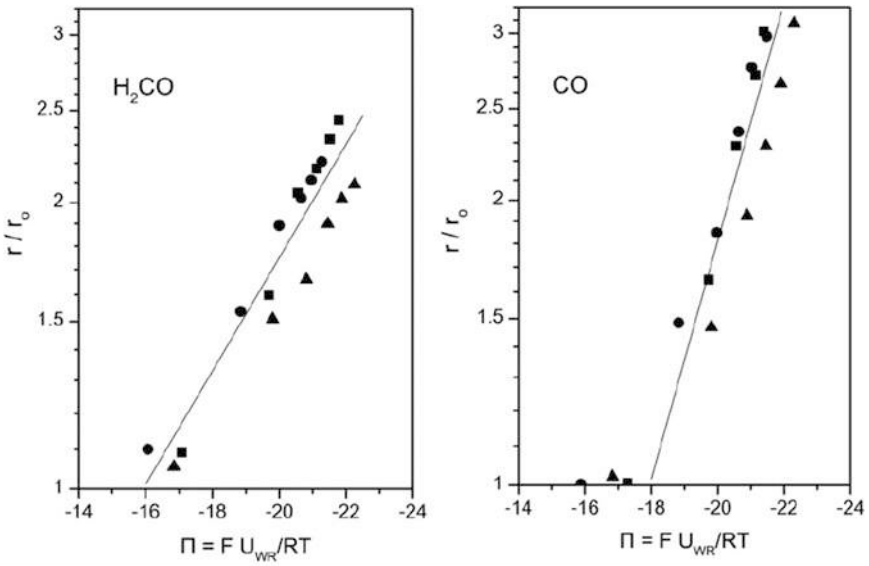

Fig. 2.4 CH_3OH dehydrogenation and decomposition on Ag/YSZ: Effect of dimensionless catalyst-electrode potential $\Pi \equiv FU_{WR}/RT$ on the formation rates of H_2CO and CO. P_{CH_3OH} = 5 kPa. ▲: $T = 620$ °C, ■: $T = 643$ °C, ●: $T = 663$ °C. (Reprinted (adapted) from ref. [22], with permission from Elsevier)

$$ln\left(\frac{r}{r_o}\right) = \frac{\alpha F \Delta U_{WR}}{RT} \tag{2.3}$$

where r_o is the open-circuit rate (current $I = 0$), F is the Faraday's constant, R is the universal gas constant, T is the absolute temperature, and α and U_{WR}* are reaction and catalyst specific constants, with $|\alpha|$ ranging typically from 0.1 to 1.0 [19, 21–23]. Reactions for which $\alpha > 0$, i.e., exhibiting rate increase by O^{2-} pumping to the catalyst ($I > 0$, $\Delta U_{WR} > 0$, $\Lambda > 0$), were termed electrophobic and reactions for which $\alpha < 0$, i.e., exhibiting rate increase upon O^{2-} removal from the catalyst ($I < 0$, $\Delta U_{WR} < 0$, $\Lambda < 0$), were termed electrophilic [1, 22]. An example of electrophilic behavior is shown in Fig. 2.4 for H_2CO and CO formation by CH_3OH dehydrogenation and decomposition on Ag/YSZ [22]. For dimensional catalyst potential $\Pi \equiv FU_{WR}/RT$ values below −16 for H_2CO and − 18 for CO, the corresponding formation rates increase exponentially with decreasing Π, in agreement with Eq. (2.3), with α values equal to −0.14 and − 0.30, respectively.

In the first EPOC studies with O^{2-} electrolyte where EPOC is reported as a general effect in heterogeneous catalysis [4, 19, 21, 22], the observed non-faradaic rate changes as well as the selectivity changes upon polarization were attributed to work function change $\Delta\Phi$ of the gas-exposed catalyst-electrode surface due to electrochemical adsorption of partially charged oxygen species $O^{\delta-}$ created at the gas-metal-solid electrolyte three-phase boundaries (tpd) and then migrating

(backspillovering) onto the catalyst surface. The first indication of this electrochemically controlled migration of oxygen promoting species came out from the observation that the catalytic rate relaxation time constant, τ, during galvanostatic transients (imposition of constant current I), i.e., the time required to reach 63% of the final rate change at steady state, was on the order of the time required to form a monolayer of $O^{\delta-}$ species on the catalyst surface when O^{2-} are supplied at the metal-gas-electrolyte three-phase boundaries (tpb) at a rate $I/(2F)$, as dictated by Faraday's law, i.e.,

$$\tau \approx \frac{N_G}{(I/2F)} \tag{2.4}$$

where N_G is the independently measured catalyst surface area, expressed as reactive oxygen uptake (in mol O) [3, 16, 18, 20–22]. The concomitantly induced work function change $\Delta\Phi$ was predicted theoretically on the basis of the spatial uniformity of the Fermi level throughout the conductive electrode and the consideration that the Volta potential (Ψ) difference at the electrode/gas interface is equal to zero ($\Delta\Psi = 0$), because of the presence of an overall neutral double layer at the metal-gas interface formed by the electrochemically adsorbed species paired with their compensating image charges in the metal, i.e., $[O^{\delta-} - \delta^+]$ for O^{2-} conductors [19, 21, 22]. Specifically, it was predicted that a change ΔU_{WR} in the (ohmic-drop free) catalyst-electrode (working electrode W) potential vs. the reference electrode (R) induces a change $\Delta\Phi$ in the work function of the gas-exposed catalyst-electrode surface, given by the equation (e: electron charge) [19, 21, 22]

$$\Delta\Phi = e\Delta U_{WR} \tag{2.5}$$

However, this theoretical prediction needed experimental validation.

This validation came after 1 year, in 1990, when C. G. Vayenas and his collaborators used the Kelvin probe vibrating condenser method to measure in situ the work function of a Pt catalyst-electrode interfaced to YSZ, both under open- and closed-circuit conditions [24]. These measurements (Fig. 2.5) showed conclusively that Eq. (2.5) describes the relation between the change ΔU_{WR} in catalyst-electrode potential, caused either by polarization or by variation of the gaseous composition, and the induced change $\Delta\Phi$ in the work function of the gas-exposed catalyst-electrode surface. Eq. (2.5), which was also confirmed experimentally for Pt catalyst-electrodes interfaced to β''-Al_2O_3 [25, 26], a Na^+ conductor, allows to write Eq. (2.3) as:

$$\ln\left(\frac{r}{r_o}\right) = \frac{\alpha\,(\Phi - \Phi^*)}{k_b T} \tag{2.6}$$

where $\Phi^* \equiv e\,U_{WR}^*$ and k_b is Boltzmann constant.

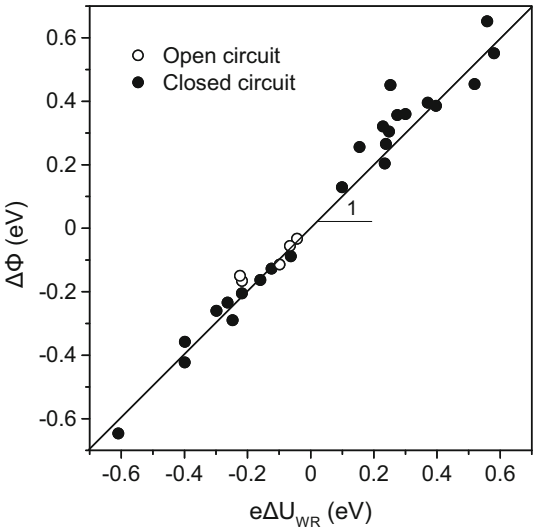

Fig. 2.5 Effect of change in ohmic-drop-free catalyst potential U_{WR} on the work function Φ of the gas-exposed catalyst-electrode surface; Pt catalyst film deposited on ZrO_2(8 mol% Y_2O_3) solid electrolyte; $T = 300$ °C. *Filled symbols:* Closed-circuit operation with the Pt catalyst exposed to air. *Open symbols:* Open-circuit operation with the Pt catalyst exposed to air, C_2H_4/O_2/He and NH_3/O_2/He mixtures. The straight line of slope unity corresponds to Eq. (2.5). (Reprinted from ref. [24], with permission from Springer Nature)

According to Eq. (2.6), electrophobic ($\alpha > 0$) and electrophilic ($\alpha < 0$) reactions are accelerated respectively by an increase or decrease in the catalyst work function, Φ, and by the concomitant decrease or increase in the availability of electrons from the catalyst for chemisorptive bond formation [22]. Equation (2.6) implies that catalytic rates depend exponentially on catalyst work function, which in many EPOC studies, with O^{2-} and cationic conductors, has been found to hold over wide ranges of experimental conditions and work function (typically 0.2–0.8 eV) on the basis of the corresponding catalyst potential change [1, 8, 13, 14, 19, 21, 22, 26–30]. More generally, it directly attributes the induced changes in catalytic activity and selectivity under EPOC conditions to changes in the catalyst-electrode work function, which alter the chemisorptive bond strengths and surface coverages of the adsorbed reacting species.

From a practical perspective, Eq. (2.5) shows that the work function of metal catalysts interfaced to solid electrolytes can be varied at will to influence their catalytic properties in desirable directions. Moreover, on the basis of Eq. (2.5), it can be anticipated [31] that in solid electrolyte cells the potential difference U_{WR} reflects the difference in the actual, adsorption and spillover modified, work functions Φ_W and Φ_R of the working and reference electrodes, respectively, i.e.,

$$eU_{WR} = \Phi_W - \Phi_R \tag{2.7}$$

Equation (2.7) shows that solid electrolyte cells can be used as work function probes for their gas-exposed electrode surfaces. Moreover, it allows establishment of an experimentally accessible absolute electrode potential scale in solid-state electrochemistry [32]. In 2001, Eq. (2.7) was experimentally validated by Tsiplakides and

Vayenas [32] in YSZ cells with various combinations of porous Pt, Ag, and Au working and reference electrodes exposed to O_2-He, O_2-H_2, and H_2-He mixtures, above 600 K and typically over 0.8 to 1 V wide U_{WR} ranges, using two Kelvin probes to measure Φ_W and Φ_R in situ and practically at the same time.

Up to 2001, electrochemical promotion with $ZrO_2(Y_2O_3)$ (or YSZ) as well as with mixed oxygen ion-electronic conductors (TiO_2, CeO_2, TiO_2-doped YSZ) had been studied in a large number of catalytic reactions using a variety of porous metal and metal oxide catalyst-electrodes (Pt, Rh, Pd, Ag, Ag-Au, Au, Ni, IrO_2, RuO_2) [1, 23, 31, 33]. These reactions included not only oxidation of CO, deep oxidation of light hydrocarbons (CH_4, C_2H_4, C_2H_6, C_3H_6) and CH_3OH, and epoxidation of C_2H_4 and C_3H_6 but also NO reduction (by C_2H_4 and by CO or C_3H_6, in the presence of O_2), N_2O reduction by CO, hydrogenation of CO and CO_2, CH_3OH dehydrogenation and decomposition, H_2S decomposition, and CH_4 steam reforming, corroborating the general nature of EPOC [1, 23, 31, 33]. Rate enhancement ratios ρ up to 150 [34] and faradaic efficiencies Λ up to 3×10^5 [19] were reported. CH_4 steam reforming on Ni-YSZ and Ni-YSZ cermet/YSZ [35] was the first EPOC study where non-noble metal catalyst-electrodes were used. Concerning the r vs. U_{WR} or, equivalently, r vs. Φ behavior over the entire experimentally accessible range (global behavior), four types of behavior were observed depending on the catalytic system and the experimental conditions: purely electrophobic behavior ($\partial r/\partial U_{WR} > 0$, $\partial r/\partial \Phi > 0$), as in C_2H_4 oxidation on Pt/YSZ [19]; purely electrophilic behavior ($\partial r/\partial U_{WR} < 0$, $\partial r/\partial \Phi < 0$), as in NO reduction by C_2H_4 on Pt/YSZ [36]; volcano-type behavior, i.e., a maximum in the reaction rate r with varying catalyst potential U_{WR} or work function Φ, as in CO oxidation on Pt/YSZ (under reducing conditions) [20]; and inverted volcano-type behavior, i.e., a minimum in r with varying U_{WR} or Φ, as in NO reduction by C_3H_6 on Rh/YSZ in the presence of excess O_2 [34].

An interesting aspect of EPOC discovered in 1997 by Comninellis and coworkers in the reaction of C_2H_4 oxidation on IrO_2/YSZ [37] is the "permanent NEMCA" or "permanent EPOC" (P-EPOC) effect, i.e., the remaining rate enhancement after current interruption following prolonged anodic polarization of the catalyst-electrode. Permanent EPOC, which is potentially important for practical applications (e.g., utilizing EPOC during catalyst preparation), has been observed also in C_2H_4 combustion on RuO_2/YSZ [38] and Pt/YSZ [39] and in NO reduction by C_3H_6 [34, 40, 41] or CO [41] in the presence of O_2 on Rh/YSZ. Permanent EPOC with YSZ has been explained by storage of promoting oxygen species at the catalyst-electrode/YSZ interface and subsequent migration towards the catalyst/gas interface after positive current interruption, through the catalyst-YSZ-gas three-phase boundaries [39, 42].

2.2.2 EPOC with Cationic Conductors and Aqueous Electrolytes

Studies concerning the discovery of EPOC and its first report as a general, electrochemically induced, catalytic effect were carried out using YSZ, an O^{2-} conducting solid electrolyte. In 1991 C.G. Vayenas and his coworkers reported for the first time EPOC using a Na^+ conductor, in the reaction of ethylene complete oxidation on Pt interfaced to β''-Al_2O_3 solid electrolyte in a fuel cell type reactor (β''-Al_2O_3 tube) [26]. An important conclusion of this study was that the observed EPOC features were the same as those for ethylene complete oxidation on Pt/YSZ, in particular the exhibited electrophobic behavior and the exponential dependence of rate on catalyst potential (Eq. 2.3) [26], which supported the explanation of the EPOC effect on the basis of an electrochemically induced alteration of the catalyst surface work function, as given by Eq. (2.5) [19]. Also, the fact that a very small sodium coverage, equal to 0.015, was found sufficient to cause a pronounced 70% decrease in the rate of ethylene oxidation provided strong evidence for "long-range" electronic interactions, ruling out any interpretation of EPOC based on geometric factors [26]. The main features observed in this work were confirmed some years later by Harkness et al. [43] who studied the same system in a single pellet reactor [44] and over a wider range of conditions, in parallel with kinetic and spectroscopic experiments with Pt(111)/Na model catalysts. In this type of reactor, the Pt catalyst-working electrode and two inert Au reference and counter electrodes were deposited on the opposite sides of a β''-Al_2O_3 disk, all exposed to the reaction mixture. Besides the application of a different reactor type, a new aspect of their work was the observation of a volcano-type behavior (a maximum in the ethylene combustion rate) with decreasing catalyst potential U_{WR} (increasing sodium coverage), corresponding to a very sharp cutoff of the rate below sufficiently negative values of U_{WR} which was attributed to extensive blocking of the Pt surface with sodium surface compound (s) and to strongly enhanced competitive adsorption of oxygen. Moreover, over the same range of sodium coverages, they observed agreement between the kinetic behavior of the electropromoted Pt catalyst and that of the Pt(111)/Na model catalyst, providing strong evidence for the role of sodium as the key promoting species under conditions of EPOC with Na^+ conducting solid electrolytes.

From 1991 to 2003, EPOC using alkali ion conductors, specifically β''-Al_2O_3, K-β''-alumina and NASICON ($Na_3Zr_2Si_2PO_{12}$), was studied by the groups of C. G. Vayenas in Patras, R.M. Lambert in Cambridge, and G. Haller in Yale in many other reactions [1], including complete and partial oxidations (C_2H_4 oxidation on Pt/NASICON [45]; CO oxidation on Pt/β''-Al_2O_3 [46]; C_2H_4 epoxidation on Ag/β''-Al_2O_3 [47]); NO reduction on Pt/β''-Al_2O_3 by C_2H_4 [48], CO [49], H_2 [50], or C_3H_6 [51], on Rh/β''-Al_2O_3 by CO [52, 53] or C_3H_6 [52, 54], and on Cu/β''-Al_2O_3 by CO [55]; hydrocarbon hydrogenations (C_6H_6 hydrogenation on Pt/β''-Al_2O_3 [56] and selective C_2H_2 hydrogenation on Pd/β''-Al_2O_3 [57], Pt/β''-Al_2O_3 [58], and Pt/K-β''-alumina [59]); CO_2 hydrogenation on Pd/β''-Al_2O_3 [28, 60]; and Fischer-Tropsch synthesis on Ru/β''-Al_2O_3 [14, 61] and Rh/K-β''-alumina [62]. The results of these

studies confirmed that EPOC is not restricted to O^{2-} conductors and to oxidation reactions but can be also induced with alkali ion conductors in many reaction types providing a means of in situ controlled alkali promotion with numerous potential applications. Since 2003, a large number of important new contributions to EPOC with alkaline conductors have appeared, as summarized in recent reviews [5, 7, 63, 64], including the electrochemically assisted NO_x storage/reduction on porous Pt/K-β-Al_2O_3 [65] under negative/positive polarization, respectively. EPOC with alkaline conductors for emissions control catalysis is fully described in Chap. 4. We can also mention the K^+-promoted (negative polarization) H_2 production by CH_3OH steam reforming on nanocolumnar Ni films deposited on K-β-Al_2O_3 and its simultaneous reversible storage in the presence of potassium species, mainly via spillover of H atoms from Ni onto graphene oxide (GO) produced in situ via electropromoted methanol decomposition [66]. This study is detailed in Chap. 9.

An attractive feature of using an alkali ion conductor for electrochemical promotion is that the coverage of alkali electrochemically introduced onto the gas-exposed catalyst surface can be accurately measured coulometrically. This allows easy comparison with classical promotion studies and evaluation of the promotion index PI_i, which is an important phenomenological parameter for quantification of the promoting or poisoning effect of a given species i (e.g., Na^+) co-adsorbed on a catalytic surface during a reaction. The promotion index PI_i is defined from:

$$PI_i \equiv \frac{(r - r_o)/r_o}{\Delta\theta_i} \tag{2.8}$$

where r_o is the catalytic reaction rate in the absence of species i and $r - r_o$ is the induced rate change by a change $\Delta\theta_i$ in the coverage θ_i of the promoting (or poisoning) species i. For the aforementioned reactions, promotion index values up to 6000 have been reported for the sodium species supplied electrochemically onto the catalyst surface [1]. An example of electrochemical promotion using a Na^+ conductor is shown in Fig. 2.6 for ethylene epoxidation on Ag/β″-Al_2O_3 in the presence of 1,2-$C_2H_4Cl_2$ as moderator, studied in a single pellet reactor [47]. Negative current application, i.e., Na^+ pumping to the Ag catalyst-electrode, resulted in enhancement of the ethylene epoxidation rate without affecting the ethylene combustion rate and, concomitantly, in substantial increase of the selectivity to C_2H_4O. The latter reached a maximum value of 88% for a sodium coverage of 0.03 and 1 ppm of 1,2-$C_2H_4Cl_2$ in the gas phase. The strong promotional effect of the electrochemically supplied Na species is reflected in the high values, up to 40, of the promotion index PI_{Na}.

Proton conductors are another class of solid electrolytes which has been used to induce electrochemical promotion of catalyst-electrodes [1, 11]. In 1990 Politova, Sobyanin, and Belyaev in Novosibirsk reported reversible non-faradaic rate changes in the reaction of ethylene hydrogenation on Ni interfaced to $CsHSO_4$, a H^+ conducting solid electrolyte, upon electrochemical H^+ pumping to or from the catalyst surface, corresponding to electrophobic EPOC behavior with enhancement factor ρ and faradaic efficiency $|\Lambda|$ values up to ca. 2 and 300, respectively [67]. This

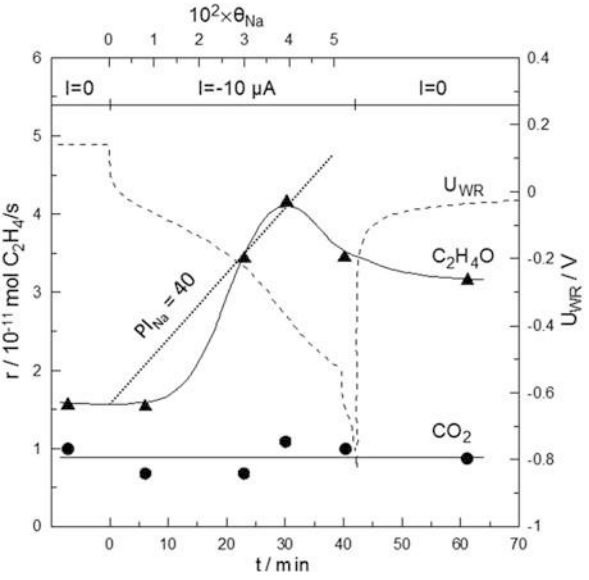

Fig. 2.6 C_2H_4 epoxidation on Ag/β″-Al_2O_3: Transient effect of a negative applied current (Na^+ supply to the catalyst-electrode) and corresponding sodium coverage on the rates of C_2H_4O (▲) and CO_2 (●) formation and on catalyst potential U_{WR}. The dotted line is constant promotion index line. $T = 260$ °C, total pressure $P = 5$ atm, $P_{O_2} =$ 17.5 kPa, $P_{C_2H_4} = 49$ kPa, 0.6 ppm 1,2-$C_2H_4Cl_2$. (Reprinted (adapted) from ref. [47], with permission from Elsevier)

work was the first EPOC study using a proton conductor and also the first EPOC study of a hydrogenation reaction. In the same decade, from 1993 to 2000, EPOC was studied in several other reactions using a variety of H^+ conductors. In 1993, M. Stoukides and his coworkers studied for the first time the non-oxidative coupling of methane to ethane and ethylene on Ag interfaced to $SrCe_{0.95}Yb_{0.05}O_3$ in a one-chamber cell [68]. The reaction exhibited electrophobic behavior with ρ values up to 8 and total selectivity to C_2 hydrocarbons near 100%; however, no faradaic efficiency values were reported. The first report of the use of a proton conductor for electrochemical promotion of an oxidation reaction appeared in 1996 by Makri et al. [30] who investigated the effect of electrochemical pumping of H^+ on the rate of ethylene combustion on Pt interfaced to $CaZr_{0.9}In_{0.1}O_{3-\delta}$, a solid electrolyte with predominantly proton conductivity over the temperature range 380–450 °C that was used in this study. Electrophilic EPOC behavior was observed, corresponding to reversible increase of the rate of C_2H_4 combustion by up to 500% upon proton supply to the catalyst-electrode film (negative current application) and to faradaic efficiency $|\Lambda|$ values up to 2×10^4.

In 2000, Yiokari et al. [69] demonstrated for the first time electrochemical promotion under high pressure (50 atm) and using a dispersed industrial non-precious metal catalyst. Specifically, they achieved up to 1300% non-faradaic ($|\Lambda| = 6$) enhancement of the rate of NH_3 synthesis on a state-of-the-art iron-based industrial catalyst (BASF S6-10RED) by depositing it on proton conductor $CaIn_{0.1}Zr_{0.9}O_{3-\delta}$ pellets, using a mixture of catalyst powder and commercial Fe paste, and electrochemically pumping H^+ to its surface. This work was also the first demonstration of scale-up of an EPOC reactor as a multi-pellet configuration (twenty-four $CaIn_{0.1}Zr_{0.9}O_{3-\delta}$ pellets) was used (Fig. 2.7). Some years later

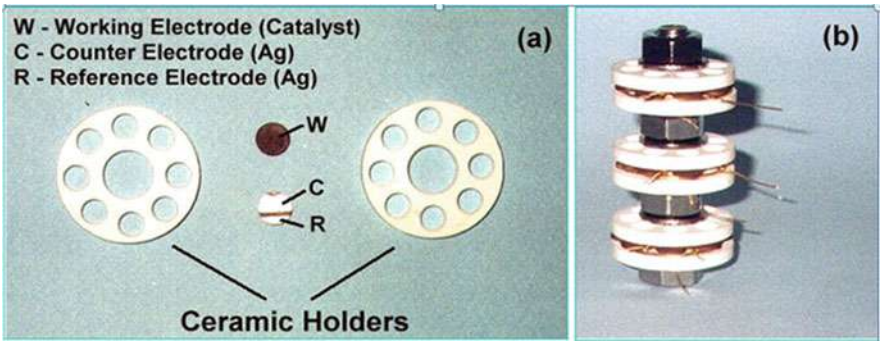

Fig. 2.7 Multi-pellet EPOC reactor for NH_3 synthesis at high pressure: (**a**) Machinable ceramic holders and two $CaIn_{0.1}Zr_{0.9}O_{3-\delta}$ pellets showing the location of the electrodes. (**b**) Twenty-four pellet unit. (Reprinted with permission from ref. [69]. Copyright (2000) American Chemical Society)

Stoukides and coworkers [70] also reported a similar weak EPOC effect ($|\Lambda|$ and rate enhancement ratio ρ less than 3 and 2, respectively) for NH_3 synthesis on an industrial Fe-based catalyst-electrode interfaced to the H^+ conductor $SrZr_{0.95}Y_{0.05}O_{3-\delta}$ at 450–700 °C and atmospheric pressure. Recent advances on the electrochemical promotion of ammonia synthesis are reviewed in Chap. 8.

The use of a solid polymer proton conductor in EPOC was reported for the first time in 1997 by Tsiplakides et al. [71] who studied the oxidation of H_2 by O_2 at room temperature on a Pt black catalyst-electrode deposited on Nafion 117 membrane, with the other side of the membrane being in contact with a 0.1 M KOH aqueous solution with a Pt wire counter electrode immersed in it. It was observed that positive current application reversibly increased the rate of H_2 oxidation by up to a factor of 20, whereas the induced rate increase was up to 300 times larger than the electrochemical rate of H_2 oxidation, implying change in the chemisorptive bond strength of adsorbed reactants with changing catalyst potential and work function (Eq. 2.5). Smotkin and coworkers, also using Nafion as solid electrolyte, demonstrated in 1997 for the first time electrochemical promotion for a unimolecular and non-redox catalytic reaction, specifically for the isomerization of 1-butene on a high surface area Pd/C cathode deposited on Nafion 117 in a membrane electrode assembly (MEA) with an essentially nonpolarizable Pt black/H_2 counter electrode [72]. Under galvanic cell operation at 70 °C, the rates of *cis*- and *trans*-2-butene formation increased dramatically, prior to a significant increase in butane formation by 1-butene hydrogenation, passing through a maximum at a cell voltage of 0.16 V and 0.1 V, respectively (Fig. 2.8). The enhancement factor ρ values at these maxima were approximately 38 and 46, respectively, whereas the absolute value of the faradaic efficiency for both isomers was approximately 28, denoting a strong non-faradaic electrophilic behavior. A mechanistic study of this electropromoted isomerization revealed that it is an acid-catalyzed reaction at the Pd surface facilitated by the superacidic Nafion electrolyte [73].

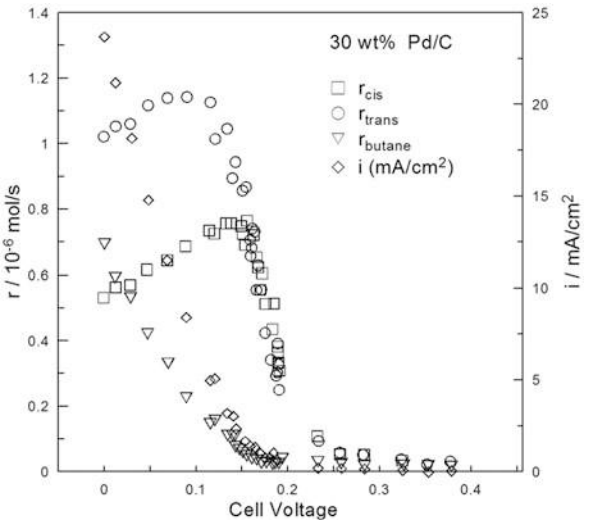

Fig. 2.8 Isomerization of 1-butene on Pd/C interfaced to Nafion 117: Effect of cell voltage on the rates of *cis*- and *trans*-2-butene and butane formation. $T = 70$ °C. (Reprinted (adapted) with permission from ref. [72]. Copyright (1997) American Chemical Society)

An interesting EPOC study with Pb^{2+} ion conductor appeared in 2002, when Lambert and coworkers reported the first demonstration of the use of electrochemical promotion to in situ control, in a reversible and reproducible manner, the composition and catalytic performance of bimetallic surface Pt/Pb alloy for hydrogenation of acetylene, via interfacing a porous Pt film with a Pb-β″-Al_2O_3 electrolyte (a Pb^{2+} conductor) and electrochemically pumping of Pb^{2+} to the Pt film [74, 75]. Increase in selectivity to ethylene from 20% on pure Pt to 85% on a ∼ 26% Pb alloy surface formed via Pb^{2+} pumping was observed, accompanied by a decrease in C_2H_2 conversion, which was attributed to weakening of the ethylene and acetylene chemisorptive bonds.

In 1993 Anastasijevic et al. [76] were first to report a non-faradaic effect in aqueous electrochemistry, specifically a current efficiency above 100% for H_2 evolution during HCHO oxidation on Cu and Ag electrodes in 0.1 M KOH solution. In 1994, Neophytides et al. [77] reported electrochemical promotion for H_2 oxidation on a graphite-supported Pt electrode immersed in 0.1 M KOH solution and, some years later, on a Pt black electrode [78], obtaining identical results. The Pt/graphite or Pt black working electrode was deposited on a Teflon-frit through which the reactant mixture was sparged, while a Pt counter electrode was positioned in a separate compartment. Figure 2.9 shows a characteristic galvanostatic transient obtained with the Pt/graphite electrode. As seen in the figure, the observed rate changes in H_2 and O_2 consumption are reversible and non-faradaic, corresponding, for $I = 15$ mA, to faradaic efficiencies equal to ca. 7 and 5, respectively, while the rate relaxation time constant is on the order of $2FN_G/I$, as in EPOC studies with O^{2-} conductors (Eq. 2.4). Application of positive overpotentials in this system, i.e., OH^- supply to the Pt electrode, increased the rate of H_2 oxidation by up to 500% in a non-faradaic manner with faradaic efficiencies up to 100 [77, 78]. Qualitatively similar results were obtained using a 0.1 M LiOH solution. Similarly to

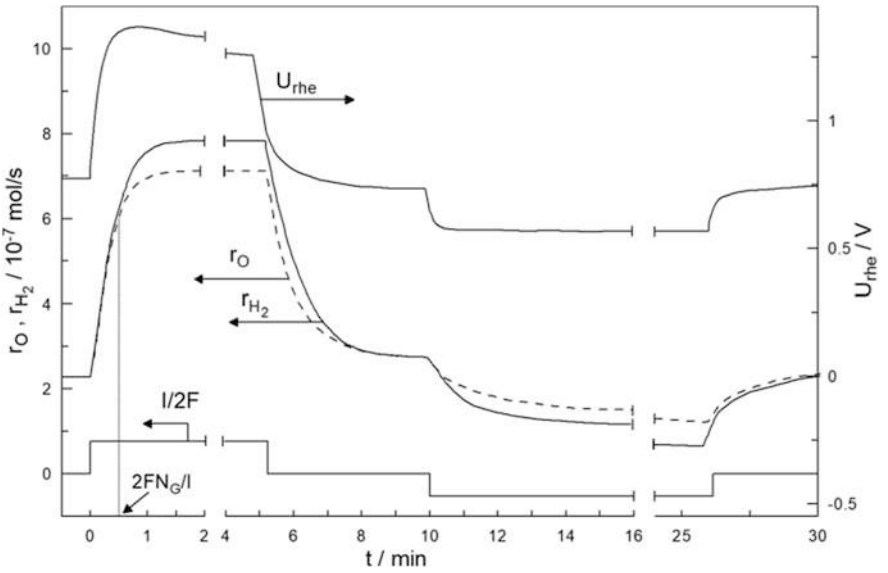

Fig. 2.9 EPOC in H_2 oxidation on Pt/graphite in 0.1 M KOH: Transient effect of applied positive and negative current I (15 mA and − 10 mA) on the rates of consumption of oxygen (r_O, mol O/s) and hydrogen (r_{H_2}, mol H_2/s); $P_{H_2} = 0.75$ kPa, $P_{O_2} = 1.06$ kPa, gas flow rate $F_v = 280$ cm^3/min at STP. Total Pt surface area $N_G = 3.0 \times 10^{-6}$ mol Pt. (Reprinted from ref. [77] with permission from Springer Nature)

electrochemical promotion with solid electrolytes, the observed EPOC behavior was attributed to polarization-induced changes in the work function of the Pt surface and to concomitant changes in the coverages and binding strengths of dissociatively chemisorbed oxygen and hydrogen [1, 77, 78].

2.3 The Physicochemical Origin of EPOC: Rules of Promotion

Since the early 1990s, EPOC had been conclusively associated with polarization-induced changes of the catalyst-electrodes, and Eq. (2.5) had been experimentally validated for oxygen and sodium ion conductors [24–26]; however, a detailed understanding of the EPOC effect at the molecular level was missing. Starting essentially from 1993, a large number of surface science, catalytic and electrochemical techniques, as well as theoretical calculations and thermodynamic considerations, mentioned in early and recent reviews [1, 2, 6, 8, 13, 14, 79–81], were employed to determine the physicochemical origin of electrochemical promotion, in particular as it concerns the nature of the promoting species and the catalyst surface state under electrochemical promotion conditions.

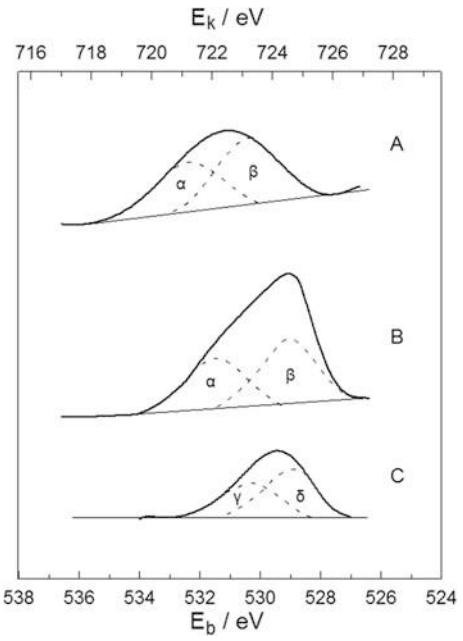

Fig. 2.10 Effect of electrochemical O^{2-} pumping on the O 1 s spectrum of Pt/YSZ. XPS spectra at 673 K: (**A**) open-circuit conditions; (**B**) constant overpotential $\Delta U_{WR} = 1.2$ V (steady state current $I = 40$ μA); (**C**) O 1 s difference spectrum. (Reprinted with permission from ref. [82]. Copyright (1993) American Chemical Society)

In 1993, X-ray photoelectron spectroscopy (XPS) was employed for the first time to study the effect of polarization on Pt catalyst-electrode films interfaced with YSZ [82]. Backspillover of oxygen species from the solid electrolyte onto the Pt surface upon electrochemical oxygen pumping to the catalyst was evidenced by an almost 60% increase in the total O1s spectrum area compared to that under open-circuit, which was accompanied by a shift of the peak maximum to lower binding energy by ca. 1.8 eV (Fig. 2.10). The difference O1s spectrum revealed that two distinct oxygen species existed on the Pt surface following oxygen pumping, specifically chemisorbed atomic oxygen, at a binding energy of 530.4 eV (peak γ), and a more anionic oxygen species, at a binding energy of 528.8 eV (peak δ). The latter oxygen species, which was less reactive than normally chemisorbed oxygen under the reducing UHV conditions, was identified as the promoter oxygen species responsible for electrochemical promotion of catalytic oxidations using O^{2-} solid electrolytes [1, 82].

In 1995, Neophytides and Vayenas used for the first time temperature-programmed desorption (TPD) under high-vacuum conditions to investigate the state of adsorbed oxygen on Pt catalyst-electrode films interfaced to YSZ as a function of catalyst potential [83]. A more detailed TPD study of the same system followed 3 years later by Neophytides et al. [84]. As shown in Fig. 2.11, gaseous oxygen adsorption ($t = 0$) resulted in a single adsorption state, while mixed gaseous-electrochemical oxygen adsorption via subsequent electrochemical supply of O^{2-} for various times (t = 125–3900 s) led to two distinct adsorbed oxygen states, specifically a weakly bonded state, shifted to lower peak desorption temperature

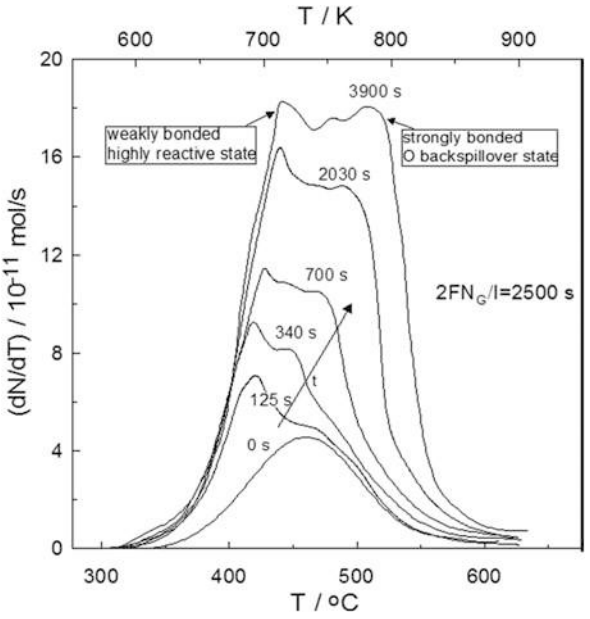

Fig. 2.11 Oxygen TPD spectra after gaseous oxygen adsorption on Pt/YSZ at 673 K and $P_{O_2} = 4 \times 10^{-6}$ Torr (oxygen exposure equal to 7.2 kilolangmuirs) followed by electrochemical O^{2-} supply ($I = 15$ μA) for various time periods; heating rate: 1 K/s. (Reprinted (adapted) with permission from ref. [83], copyright (1995) American Chemical Society and from ref. [84], copyright (1998) Elsevier)

T_p (by ca. 50 K) compared to that for oxygen adsorption from the gas phase only ($T_p \approx 738$ K), and a strongly bonded state (T_p from 743 to 773 K) gradually developing with increasing time of current application. Considering that the time required for complete development of the strongly bonded oxygen state and the relaxation time for the catalytic rate to reach its promoted state during galvanostatic transients in EPOC experiments were both comparable to $2FN_G/I$ (Eq. 2.4), equal to 2500 s, the conclusion drawn was that the strongly bonded oxygen state corresponds to partially charged ionic oxygen species created on the catalyst surface upon electrochemical pumping of O^{2-} to the catalyst-electrode, which forces normally chemisorbed oxygen to a more weakly bonded and more reactive adsorption state acting as "sacrificial promoter" as it is also consumed reacting with the oxidizable species present (e.g., C_2H_4, CO), at a rate $I/(2F)$ at steady state [83, 84]. In this context, the faradaic efficiency Λ (Eq. (2.1)) can be considered to express at steady state the ratio of the turnover frequencies TOF_r and TOF_p for the electrochemically promoted reaction and for the consumption of the sacrificial promoting species, respectively, or, equivalently, the ratio of the average lifetimes τ_p and τ_r of the promoting species and of the adsorbed gas-supplied reactants on the catalyst surface, the former estimated from the time decay of the reaction rate upon current interruption [1, 13].

The aforementioned XPS [82] and TPD [83, 84] studies of the Pt/YSZ system provided for the first time evidence for creation of a strongly bonded oxygen state on the Pt catalyst surface upon positive polarization, which does not form via adsorption from the gas phase and can act as a sacrificial promoting species in catalytic oxidations under EPOC conditions by weakening the binding strength of the more

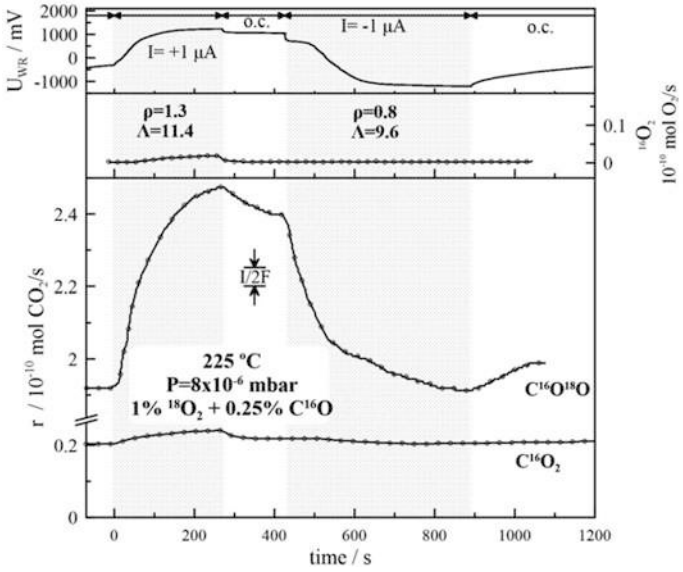

Fig. 2.12 CO oxidation by $^{18}O_2$ on Pt /YSZ: Low-temperature ($T = 225$ °C) galvanostatic transient ($P_{18}O_2 = 8 \times 10^{-8}$ mbar, $P_{C^{16}O} = 2.5 \times 10^{-8}$ mbar) leading to non-faradaic behavior; see text for discussion. (Reprinted from ref. [86], with permission from Elsevier)

reactive normally adsorbed oxygen. Since these first studies and up to 2001 the electrochemically induced creation of promoting oxygen species on metal catalyst-electrodes and the sacrificial promoter mechanism of EPOC with O^{2-} conductors had been corroborated by the results of many spectroscopic (including XPS, ultra-violet photoelectron spectroscopy (UPS), photoemission electron spectroscopy, and surface enhanced Raman spectroscopy) and electrochemical (AC impedance, cyclic voltammetry, potential programmed reduction) techniques [1]. Direct confirmation of the sacrificial promoter mechanism came in 2004 by Katsaounis et al. [85, 86] who studied under high-vacuum conditions both the adsorption of $^{18}O_2$ [85] and the oxidation of CO by $^{18}O_2$ [86] on electropromoted catalyst-electrode Pt films interfaced to YSZ. Their results showed clearly that under anodic polarization ^{16}O from the YSZ lattice migrates onto the Pt catalyst surface, acting there as a sacrificial promoter since the $^{16}O^{\delta-}$ species both react with CO and promote the catalytic reaction between CO and adsorbed ^{18}O from the gas phase. This is illustrated in Fig. 2.12 [86], which shows that upon positive ($I = +1$ μA) or negative ($I = -1$ μA) current application the induced increase or decrease, respectively, of the rate of $C^{16}O_2$ is very small and (sub)faradaic $\left(\Delta r_{C^{16}O_2}/(I/(2F)) < 1\right)$, whereas the corresponding increase or decrease of the rate of $C^{16}O^{18}O$ formation is much larger and non-faradaic, i.e., at steady state $|\Delta r_{C^{16}O^{18}O}|$ is ca. 11.4 and 9.6 times larger than the rate $|I|/(2F)$ of supply or removal, respectively, of O^{2-} to or from the Pt catalyst.

In 2007, P. Vernoux and his coworkers validated the sacrificial promoter mechanism of EPOC with O^{2-} conductors under real operating conditions, by performing

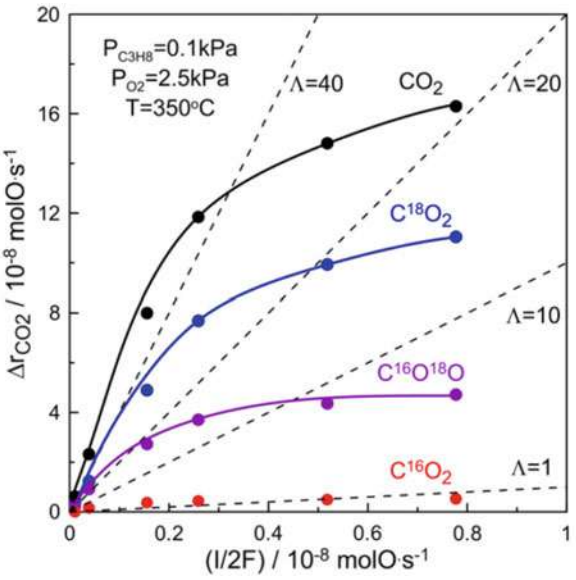

Fig. 2.13 Propane combustion on Pt/YSZ: Effect of electrochemical rate of O^{2-} supply on the CO_2 production rate increase. Dashed lines correspond to constant faradaic efficiency values. $P_{C_3H_8} = 0.1$ kPa, $P_{O_2} = 2.5$ kPa, $T = 350$ °C. (Reprinted from ref. [88], with permission from Elsevier)

O_2-TPD in the Pt/YSZ system under atmospheric pressure in the presence and absence of propane in the gas phase [87]. In continuation of this work, isotopic labeling experiments were performed by Tsampas et al. [88, 89] to *operando* investigate EPOC in the reaction of propane combustion on Pt/YSZ under atmospheric pressure and distinguish the role of oxygen species originating from the gas phase and from the YSZ solid electrolyte. In agreement with the sacrificial promoter model, application of positive polarization resulted in pronounced electropromotion (faradaic efficiency Λ up to 35) of the reaction of propane with gaseous O_2 ($C^{18}O_2$ production) and to significant surface oxygen exchange at the gas-Pt-YSZ boundaries generating active oxygen species, as evidenced by the production of $C^{16}O^{18}O$ which was also promoted but to a lesser extent, whereas production of $C^{16}O_2$ via (sub)faradaic electrochemical oxidation of propane by O^{2-} was also observed (Fig. 2.13) [88, 89].

The origin of EPOC when using alkali ionic conductors and the nature of the promoting alkali surface phases have been investigated by a large number of catalytic, spectroscopic, and surface imaging techniques [1, 6]. In 1995 and 1996 Lambert and coworkers combined for the first time kinetic and spectroscopic (postreaction XPS, Auger electron spectroscopy (AES), and TPD) data obtained with a Na-dosed Pt(111) single crystal and electrochemical promotion data for the reactions of ethylene combustion [43] and NO reduction by ethylene [48] on Pt films supported on β''-Al_2O_3. The observed agreement in the kinetic behavior of the Pt (111)/Na model catalyst with that of the electropromoted Pt film catalyst over the same range of sodium coverages provided strong evidence that reversible sodium backspillover is the origin of EPOC with Na^+ conductors. Moreover, postreaction XP and Auger spectra showed that the chemical state of the promoting sodium

depends on reaction conditions. From 1996 to 2003, Lambert and coworkers performed in situ and ex situ XPS, UPS, AES, and X-ray absorption near edge spectroscopy (XANES) studies on Pt/β″-Al_2O_3 [1, 51, 90], Rh/β″-Al_2O_3 [52, 54], Cu/β″-Al_2O_3 [55, 91], Pt/K-β″-Al_2O_3 [59], and Rh/K-β″-Al_2O_3 [62] under conditions simulating EPOC or after EPOC experiments (postreaction). These studies, which are summarized in a recent review [6], further confirmed that electrochemical promotion with alkali ion conductors is due to reversible backspillover of alkali species from the solid electrolyte to the catalyst-electrode. Moreover, they showed that the surface chemical state of the electrochemically pumped alkali is the same as that for alkali adsorbed on the surface via vacuum deposition and that under reaction conditions the alkali promoter is present as surface compounds with submonolayer coverage and with nature dependent on the composition of the reactive gas phase (e.g., as a mixture of $NaNO_2$ and $NaNO_3$ in NO reduction by propene or as Na_2CO_3 in propane oxidation on Pt/β″-Al_2O_3 [14]). Lambert and coworkers have also reported a linear correlation between catalyst potential U_{WR} and catalyst work function Φ in the Rh/β″-Al_2O_3 [14, 53] and Cu/β″-Al_2O_3 [91] systems over an extended range of catalyst potential ($\Delta U_{WR} \sim 2$ V and 0.9 V, respectively) and submonolayer sodium coverages, by determining the work function of Rh and Cu via UPS (secondary electron cutoff method). After 2003, ex situ (postreaction) SEM/EDX, XRD, XPS, and FTIR analyses as well as cyclic voltammetry have been also employed by the groups of P. Vernoux, J. L. Valverde, and A. de Lucas Consuegra to study the nature and arrangement of the potassium promoter phases present on the catalyst surface under EPOC conditions in the reactions of low-temperature propene oxidation on Pt/K-β-Al_2O_3 [92] and partial oxidation of methanol on Pt/K-β-Al_2O_3 [93] and Cu/K-β-Al_2O_3 [94].

In 1996, Vayenas and coworkers used successfully scanning tunneling microscopy (STM) to follow the polarization-induced reversible migration of sodium across macroscopic (on the order of mm) distances from a β″-Al_2O_3 pellet to the surface of a Pt(111) single crystal deposited on it and exposed to air [95], also achieving for the first time imaging of an electropromoted catalyst-electrode surface with atomic-level resolution. They observed that electrochemical pumping of sodium to the Pt(111) surface caused, at low sodium coverages (less than 0.05), the creation of a Pt(111)-(12 × 12)-Na adlayer (interatomic distance of 33.2 Å) which was present over atomically huge domains of the Pt(111) surface, overlapping the well-known Pt(111)-(2 × 2)-O adlattice (interatomic distance of 5.6 Å) formed by oxygen adsorbed from the gas phase. The Pt(111)-(12 × 12)-Na adlayer disappeared upon reversal of the direction of sodium pumping, leaving the Pt (111)-(2 × 2)-O adlattice intact. Some years later, an STM study of an air-exposed Pt(111) single crystal interfaced to an YSZ pellet similarly demonstrated the reversible migration of promoting oxygen species upon polarization, i.e., under conditions simulating EPOC, which formed a (12 × 12)-O adlattice coexisting with the underlying (2 × 2)-overlayer of the normally chemisorbed oxygen from the gas phase [96]. On a distance scale larger than that in STM studies, scanning photoelectron microscopy (SPEM) has been used by Lambert and coworkers to image the spatial distribution and time dependence of electro-pumped alkali at the surface of

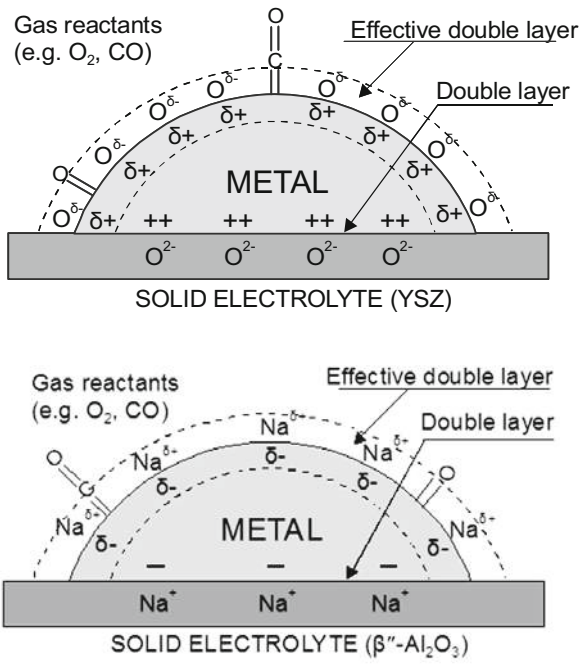

Fig. 2.14 Schematic representation of a metal electrode deposited on an O^{2-}conducting *(top)* and on a Na^{+}-conducting *(bottom)* solid electrolyte, showing the location of the metal-electrolyte double layer and of the effective double layer created at the metal-gas interface due to potential-controlled ion migration (backspillover). It is also depicted the interaction between the effective double layer and the adsorbed reactants during CO oxidation. (Reprinted from ref. [13], with the permission of AIP Publishing)

polycrystalline Cu interfaced to β''-Al_2O_3 [91] and at the surface of polycrystalline Pt interfaced either to β''-Al_2O_3 [14] or to K-β''-Al_2O_3 [59]. In all cases a practically uniform spatial distribution of the alkali was observed, with its surface concentration increasing with decreasing potential of the Pt or Cu electrode.

All the experimental techniques and theoretical studies that have been used to investigate the physicochemical origin of electrochemical promotion [1, 2, 6, 8, 13, 14, 79–81], mostly with O^{2-} and alkali ion conductors, have confirmed that EPOC is due to the electrochemically controlled introduction of partially charged promoting species from the solid electrolyte (or mixed ionic-electronic conductor) support to the gas-exposed catalyst-electrode surface. These electrocatalytically created species, accompanied by their compensating (image) charges in the electrode, form an overall neutral double layer on the catalyst/gas interface, as shown schematically in Fig. 2.14. The presence of this effective double layer, whose density and field strength in it vary with varying catalyst potential, affects the electronic properties (work function) of the catalyst surface and concomitantly its chemisorptive properties, thus inducing pronounced and reversible alterations in catalytic rates and selectivity. It is noted that although the nature of the promoting species under EPOC conditions has been extensively studied for O^{2-} and alkali ion conductors, establishing the sacrificial promoter mechanism [1, 13] in the former case, much less is known about the promoting species formed on the catalyst-electrode surface in EPOC with H^{+} conducting electrolytes, in particular in oxidation reactions. In this case it has been proposed that adsorbed hydroxyl species formed by association of

the migrating protons with chemisorbed atomic oxygen act as sacrificial promoters [1, 97].

In 2001, a systematic and meticulous search of the electrochemical promotion literature allowed Vayenas and coworkers to classify reactions in four types (electrophobic, electrophilic, volcano, and inverted volcano-type reactions, as defined in Sect. 2.2.1) on the basis of the rate versus catalyst potential or work function behavior and, moreover, establish simple and rigorous rules which permit prediction of the electrochemical promotion behavior on the basis of the reaction kinetics under unpromoted conditions or the chemisorptive bond strengths of the electron donor (D) and electron acceptor (A) reactants on the unpromoted catalyst [1, 98]. These rules were extended also to chemical promotion [1, 98] which was validated some years later using the chemical (classical) promotion literature [99]. The four global promotional rules (R1 to R4), which predict the rate r vs. catalyst potential U_{WR} or work function Φ behavior over the entire experimentally accessible range (typically, over 1.5 to 2 eV for Φ), are summarized schematically in Fig. 2.15 [100]. Vayenas and Brosda [100] showed that these four promotional rules can be combined in a single generalized rule which states that the r vs. Φ dependence always traces the rate vs. electron donor (D) reactant partial pressure dependence. Vayenas and coworkers also demonstrated that the electrostatic interaction between the electric field in the effective double layer and the adsorbate dipoles leads to Frumkin-type electrochemical isotherms, consistent with the experimentally observed in TPD studies linear changes of heats of adsorption with catalyst work function [1, 98], and to generalized Langmuir-Hinshelwood kinetics which successfully model the kinetics of promoted catalytic reactions, in good semiquantitative agreement with experiment, also mathematically describing the rules of promotion [1, 101].

The validity of the aforementioned rules of promotion and modelling of promoted catalytic kinetics for both electrochemical promotion, where the promoter level on the catalyst surface is varied in situ by varying catalyst potential, and for chemical (classical) promotion, where the promoters are typically added ex situ in the course of catalyst preparation, underlines their functional similarity and only operational differences [1, 99] which had become evident already from the first studies of the origin of EPOC, in particular those with alkali ion conductors. However, the in situ controllable reversible promotion and the ability to create and continuously replenish short-lived but extremely effective promoter species, such as $O^{\delta-}$, that are not available in classical promotion are distinct features of EPOC and important operational advantages [1, 102], highlighting its practical usefulness.

In 2001 it was also shown that EPOC with O^{2-} conductors is functionally equivalent with metal-support interaction (MSI) promotional phenomena in dispersed nanocrystalline metal (Pt, Rh) or metal-type conducting oxide (IrO_2) catalysts supported on porous O^{2-} conducting (e.g., YSZ) or mixed ionic-electronic conducting (e.g., WO_3-doped TiO_2) supports [1, 103]. In both cases backspillover of oxygen ions to the catalyst surface is the dominant promoting mechanism; thus EPOC can be considered an electrically controlled MSI [1, 102, 103]. The common underlying principle is shown schematically in Fig. 2.16. In conclusion,

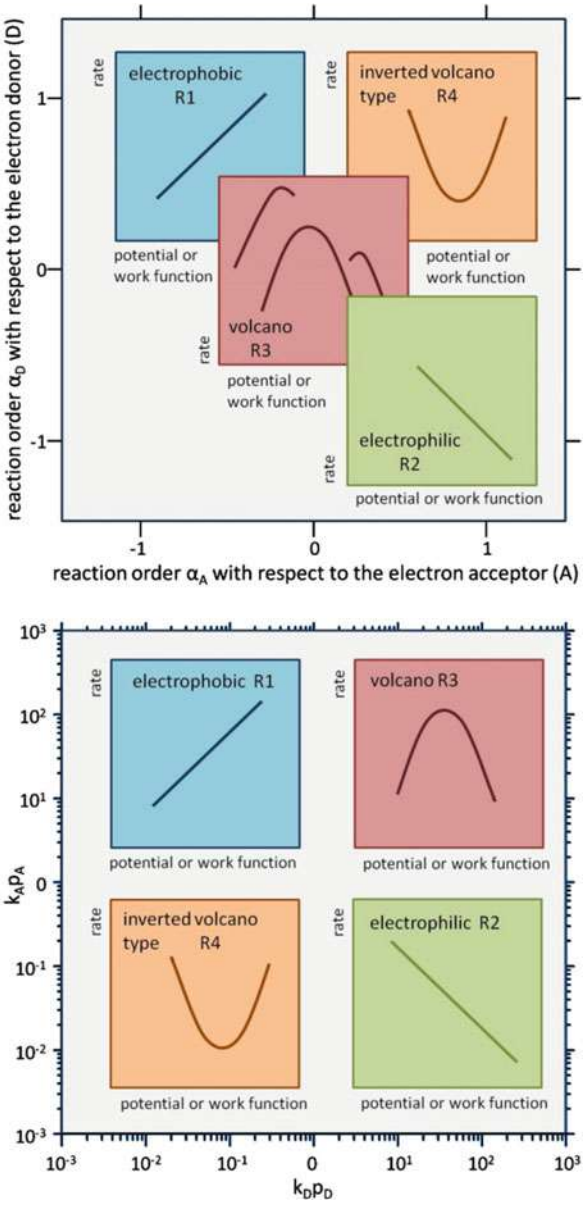

Fig. 2.15 Effect of the reaction orders α_A and α_D with respect to the electron acceptor, A, and electron donor, D, reactant *(top)* and effect of the magnitude of adsorption equilibrium constants k_D and k_A and corresponding partial pressures p_D and p_A of the electron donor and electron acceptor reactant, respectively, *(bottom)* on the observed rate dependence on catalyst potential or work function: electrophobic (/), electrophilic (\), volcano (∩), and inverted volcano (∪) dependence and range of validity of the corresponding four global promotional rules R1, R2, R3, and R4. (Reprinted from ref. [100], with permission from Springer Nature)

electrochemical promotion, promotion, and MSI on ionic and mixed conducting supports are all three facets of the same phenomenon and are due to the interaction of the adsorbed reacting species with the effective double layer formed by promoting species at the gas-exposed catalyst surface [1, 102].

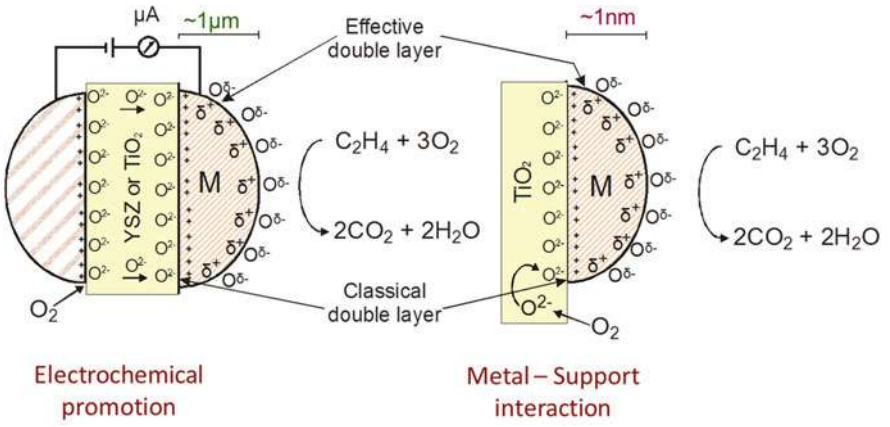

Fig. 2.16 Schematic of a metal grain (~μm) in a metal catalyst film deposited on YSZ or TiO_2 under EPOC conditions *(left)* and of a metal nanoparticle (~nm) deposited on a porous TiO_2 support *(right)*, showing the locations of the classical double layers formed at the metal-support interface and of the effective double layers formed at the metal-gas interface. (Reprinted (adapted) with from ref. [103], with permission from Elsevier)

2.4 From Fundamentals to Applications

Since its discovery, EPOC has been studied in more than 80 catalytic reactions (including oxidation, hydrogenation, and dehydrogenation, NO_x reduction and storage, decomposition, isomerization, and reforming reactions) using a variety of metal (mostly noble metal) or metal-type oxide catalysts supported on many different ionic or mixed ionic-electronic conductors, as summarized in a number of early and recent reviews [1, 2, 7, 8, 11]. EPOC has also been reported in a few catalytic systems with aqueous electrolytes [1, 76–78, 104, 105] and inorganic melts [1, 106], including a very recent study of methanol electrolysis with methanol–KOH solution introduced in both the anode and cathode, where the observed over-faradaic H_2 production was attributed to electrochemical promotion of the catalytic methanol decomposition at the Pd/C cathode by K^+ ions supplied from the liquid electrolyte under electrolysis conditions [107]. Over the years, there has been a gradual shift of the interest from EPOC studies of model reactions (originally oxidation reactions of C_2H_4 and CO), mainly aiming to elucidation of the origin and molecular-scale mechanism of this effect, to EPOC studies of reactions of environmental and industrial importance, such as selective catalytic reduction (SCR) of NO_x, H_2 production by catalytic reforming or partial oxidation, and CO_2 hydrogenation [1, 2, 7, 8, 11, 108–112]. In particular, electrochemical promotion of CO_2 hydrogenation has attracted increased interest in recent years aiming to management and mitigation of CO_2 emissions [2, 28, 29, 109–111, 113–118]. Recently, there is also growing interest for electrochemical promotion of non-noble transition metal [2, 66, 94, 109, 118–121] and metal oxide [122, 123] catalysts, driven by the need to develop sustainable and commercially viable processes, with the research efforts focused on H_2 production

[66, 94, 119, 120], CO_2 hydrogenation to hydrocarbons and other organics [118, 121], reverse water gas shift (RWGS) reaction [109, 122], and gas phase Brønsted acid-catalyzed reactions [123]. Theoretical modelling of EPOC using quantum mechanical calculations, which started in 1996 by Pacchioni et al. [124] and continued later by Leiva et at. [125], has also drawn increased interest recently, in particular by Steinmann, Baranova, and coworkers who have used density functional theory (DFT) calculations and ab initio atomistic thermodynamics to study the origin of EPOC in C_2H_4 oxidation on RuO_2/YSZ [79] and in CH_4 oxidation on Pt/YSZ [126].

Besides its fundamental scientific importance, EPOC has a great potential for practical utilization, although its commercial application is still missing for several technical and economic reasons [1, 2, 5, 8, 12, 13, 127]. The main technical obstacles for practical utilization of EPOC have been (a) the very low dispersion (less than ca. 0.01%) of the porous metal films (0.1–5 μm typical thickness) and (b) the lack of compact, efficient, and cheap reactor designs allowing electropromotion of the catalyst with a minimum number of electrical connections [2, 11–13]. Efforts to address these issues and foster practical applications of EPOC have started since the mid-90s with contributions by different groups, as summarized in recent reviews [2, 5, 8, 12, 128] and concisely described below.

2.4.1 EPOC via Polarization in Bipolar Configuration

In 1997 Marwood and Vayenas demonstrated EPOC in C_2H_4 combustion on a Pt stripe catalyst deposited on YSZ between two Au electrodes in a bipolar configuration where the Pt catalyst was electronically isolated, i.e., not used as an electrode, and polarization was applied between the two catalytically inert terminal Au electrodes [129]. Although the maximum rate enhancement ratio obtained in this bipolar configuration was a factor of 2 smaller than that obtained in the conventional monopolar configuration, which was attributed to current bypass and nonuniform distribution of the work function in the bipolar Pt electrode, it was clearly shown for the first time that EPOC can be induced without direct electrical connection to the catalyst [129]. Some years later the same idea was successfully extended to multistripe and multi-dot bipolar Pt catalysts [130]. In 1999, Comninellis and coworkers used a bipolar configuration to demonstrate for the first time EPOC of C_2H_4 combustion on RuO_2 catalyst deposited (by thermal decomposition of $RuCl_3 \cdot xH_2O$) on the inside of the channels (2 mm ID) of a cylindrical YSZ monolith (2.2 cm dia. × 1 cm height, 37 channels) in a plug flow reactor assembly, reporting enhancement factor and faradaic efficiency values up to 1.5 and 90, respectively, even for high (36%) open-circuit C_2H_4 conversions [131]. A schematic of this bipolar design is shown in Fig. 2.17a [132].

In 2010 bipolar configurations were used for the first time to electropromote isolated metal nanoparticles [133–135]. Comninellis and coworkers demonstrated EPOC of CO oxidation (under high vacuum) on isolated Pt nanoparticles (60 nm)

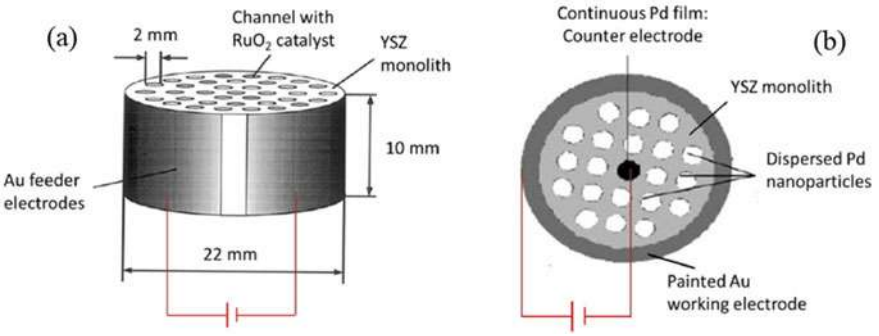

Fig. 2.17 Monolithic (multiple-channel) bipolar configurations for EPOC in ethylene combustion on RuO_2 deposited on YSZ (**a**) and in methane combustion on Pd isolated particles deposited on YSZ (**b**). (Reprinted (adapted) from refs. [132, 135], with permission from Elsevier)

sputter-deposited on a rectangular YSZ pellet by applying in plane polarization between two Au electrodes in a bipolar configuration [133, 134]. They also used for the first time isotopic $^{18}O_2$ as oxidant to accurately quantify EPOC in a bipolar system of non-percolated nanoparticles [134]. Vernoux and coworkers reported non-faradaic inhibiting effect on the rate of CH_4 combustion on isolated Pd nanoparticles deposited (by electroless deposition) on the inner surface of an YSZ honeycomb cylindrical monolith (3.2 cm dia. × 3.2 cm height, with ca. 600 channels 1 mm × 1 mm), upon applying polarization between a continuous Pd film deposited in the center channel and a Au film painted on the outer surface of the monolith (Fig. 2.17b) [135]. Such monolithic bipolar designs are in principle promising as it concerns scale-up of EPOC reactors; however, there are several technical issues to be addressed, including the current bypass [132] and the limited thermal stability of the metal nanoparticles as they are not deposited on a porous substrate [2].

2.4.2 Monolithic Electropromoted Reactors (MEPR)

A big step towards practical application of EPOC was the development of the monolithic electropromoted reactor (MEPR), whose successful operation was demonstrated for the first time in 2004 in the reactions of C_2H_4 combustion and NO_x reduction by C_2H_4 in the presence of O_2, on Pt and Rh catalysts [136]. The MEP reactor can be considered as a hybrid between a planar solid oxide fuel cell (SOFC) and a monolithic honeycomb reactor [12, 136]. A schematic and a picture of the MEPR are shown in Fig. 2.18. The reactor consists of several (typically >10) parallel solid electrolyte plates (flat or ribbed) positioned in properly carved grooves on the opposite internal surfaces of a ceramic casing. Thin (ca. 20–40 nm) porous catalyst films are sputter-deposited on both sides of the plates, exposed to the same reaction mixture. Suitably painted metal films on the surfaces of the grooves create two

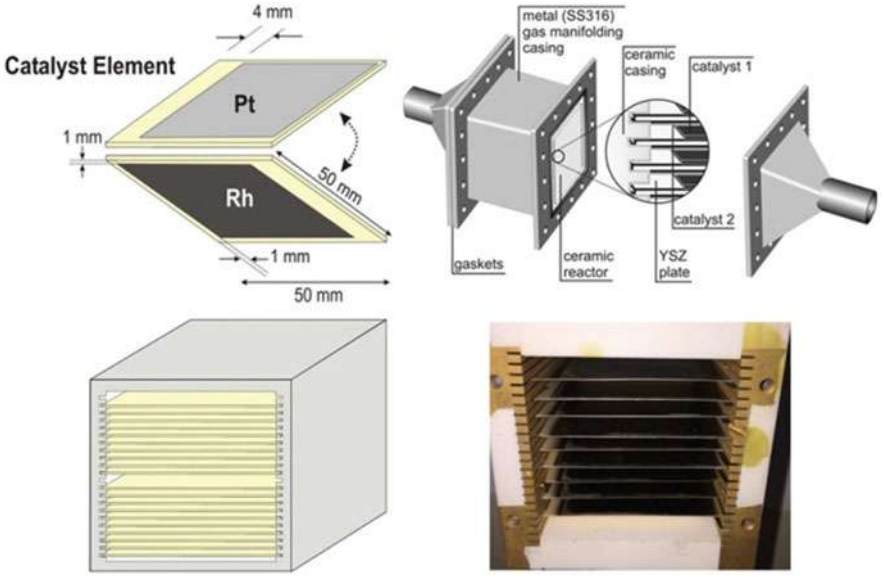

Fig. 2.18 Schematic and picture of the monolithic electropromoted reactor (MEPR). (Adapted from refs. [136, 137], with permission from Elsevier)

current collectors, the one providing electrical contact among all catalyst films on the top sides of the plates and the other among all catalyst films on the bottom sides of them. The entire assembly is enclosed in a properly designed stainless steel gas manifolding casing.

The MEP reactor is a simple, compact, and efficient reactor for practical utilization of EPOC. It requires only two external electrical connections to polarize simultaneously the catalyst films on all plates (with opposite polarity the two films on the two sides of each plate) and one of the plates can be used as a gas sensor element, there is only a single gas stream to and from the reactor, as in classical catalytic reactors, it is easily assembled and dismantled, permitting easy replacement of the solid electrolyte plates whenever necessary, and it exhibits very good thermal and mechanical stability, which allows its use in harsh environments [12, 136]. Equally important, the use of thin sputtered metal electrodes with metal dispersions higher than 10%, i.e., comparable with those of supported commercial catalysts, allows overcoming a major economic obstacle for practical utilization of EPOC which is the very low dispersion (less than 0.01%) and hence the poor metal utilization of the typically 0.1–5 μm-thick catalyst films used in EPOC studies [12, 136]. However, the thermal stability of the sputtered thin metal films may be low for practical long-term operation [2]. Since 2004, MEP reactors with YSZ electrolyte have been successfully implemented for EPOC of C_2H_4 combustion [136, 138] and NO reduction by C_2H_4 in the presence of O_2 on Pt and Rh [112, 136], including testing with simulated and real exhaust gas of a diesel engine [139], SO_2 oxidation on Pt [140], CO_2 hydrogenation on Rh, Pt, and Cu [118], and,

more recently, CO_2 hydrogenation on Ru [137, 141], at high hourly space velocities in all cases (up to ca. 3×10^4 h^{-1}[140]).

2.4.3 *Electrochemical Promotion of Highly Dispersed Catalysts*

The electrochemical promotion of a highly dispersed metal catalyst was first reported in 1998 by Marwood and Vayenas [142] in the reaction of C_2H_4 combustion on finely dispersed Pt (dispersion higher than ca. 20%) in a porous Au film electrode deposited on YSZ electrolyte. This finding pointed the way to practical applications of EPOC as supported highly dispersed metal catalysts exhibit efficient metal utilization, which is particularly important in case of noble metal catalysts, and improved thermal stability. Since this first demonstration of EPOC with highly dispersed catalysts, two main approaches have been followed in this direction, specifically dispersion of the catalytically active phase in an electronically or ionically conducting matrix and dispersion of the catalytically active phase in a mixed ionic-electronic conductive matrix, as concisely described below. Relevant work up to 2017 is summarized in recent reviews [2, 8].

2.4.3.1 Electrochemical Promotion of Metal Nanoparticles Dispersed in an Ionically or Electronically Conducting Matrix

In these EPOC systems, the ionically or electronically conducting matrix with the dispersed metal nanoparticles is deposited as film on a dense solid electrolyte element. Metal nanoparticles dispersed in an ionic conductor can also be deposited on a porous interlayer metal film supported on the dense solid electrolyte. The ionic promoting species are electrocatalytically created at the boundary between the gas phase, the solid electrolyte, and the electronically conductive phase and then migrate (backspillover) to the catalytic sites. The main drawback of this design is the difficulty of the ionic species to backspillover via the conductive support from the solid electrolyte to the catalytic active sites at the surface of the nanoparticles. The particular approach has been recently applied in the following catalytic systems:

- *CO_2 hydrogenation (to CH_4 and CO) on Ni- and Ru-impregnated carbon nanofibers (CNFs) deposited on dense YSZ*, in various configurations [143]. Negative polarization resulted in weak enhancement of the CO_2 consumption rate and, for the Ni-based catalyst, of the selectivity to CH_4, whereas the rate enhancement ratio for CH_4 (electrophilic behavior) was up to 3. The observed weak electropromotion was attributed to the limited transport of O^{2-} along the CNF support.
- *H_2 production from CH_3OH* via *partial oxidation and steam reforming on Pt nanoparticles dispersed on a diamond-like carbon (DLC) matrix deposited on*

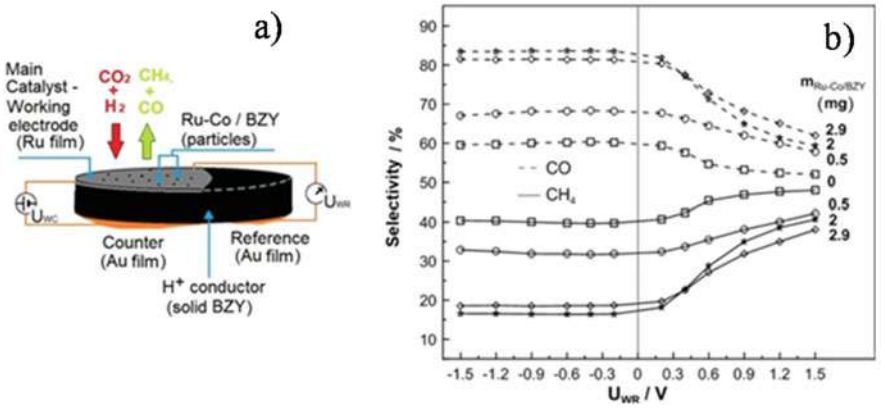

Fig. 2.19 CO_2 hydrogenation on Ru-Co nanodispersed in BZY powder and deposited on a Ru film supported on a dense BZY disk: (**a**) Schematic of the BZY support disk and of the three electrodes. (**b**) Effect of catalyst potential U_{WR} and dispersed Ru-Co/BZY catalyst loading, $m_{Ru\text{-}Co/BZY}$, on the selectivity to CH_4 and CO. $P_{H_2} = 7$ kPa, $T = 450$ °C, total flowrate $F_t = 200$ cm^3/min. (Reprinted (adapted) from ref. [111], with permission from Elsevier)

dense K-β-Al_2O_3 [144]. Electrochemical pumping of potassium ions to the catalyst resulted in increase of the H_2 production rate up to 2.5 and 3.4 times in partial oxidation and in steam reforming of CH_3OH, respectively, under optimal coverage of the potassium promoter.

- *CH_4 combustion on Pd dispersed (up to 27% dispersion) on a porous interlayer YSZ film deposited on dense YSZ* [145], aiming to a more intimate contact between YSZ and the palladium phases under reaction conditions. Electrophobic electrochemical promotion with faradaic efficiencies ranging from 8 to 61, depending on the CH_4/O_2 ratio, was reported. It is noted that CH_4 combustion has been also studied on Pd dispersed on a porous interlayer CeO_2 film deposited on dense YSZ [146]. This system exhibited high catalytic activity but no electropromotion was achieved.
- *CO_2 hydrogenation (to CH_4 and CO) on nanodispersed Ru-Co in BZY which was deposited on a porous interlayer Ru film supported on dense BZY ($BaZr_{0.85}Y_{0.15}O_3$ + 1 wt.% NiO) proton conductor* (Fig. 2.19a) [111]. This was the first study exploring the similarities between EPOC and MSI for the case of a H^+ conducting support (BZY) and the first EPOC study of a dispersed Ru-Co catalyst. Anodic polarization (proton removal from the catalyst) resulted in reversible non-faradaic increase of the methanation rate (electrophobic behavior), with faradaic efficiency values up to 65, and in parallel decrease of the CO production rate (electrophilic behavior). The selectivity to CH_4 varied between 16% and 41% with varying catalyst potential and dispersed Ru-Co/BZY loading (Fig. 2.19b). An important conclusion of this study was that both the Ru film and the Ru-Co nanoparticles were electropromoted, which implied that the polarization-imposed work function change on the Ru film is also imposed to a large extent on the metal nanoparticles of the dispersed Ru-Co/BZY catalyst.

- *CO_2 hydrogenation (to CH_4 and CO) on nanodispersed Ru in YSZ (2 wt.% Ru/YSZ) which was deposited on a porous interlayer Ru film supported on dense YSZ* [147]. Small non-faradaic enhancement of the CH_4 production rate with parallel decrease in the CO production rate was observed upon positive polarization (O^{2-} pumping to the catalyst). The weak electrochemical promotion was attributed to the fact that the catalyst was in a promoted state due to thermally induced backspillover of O^{2-} from the YSZ support.

2.4.3.2 Electrochemical Promotion of Metal Nanoparticles Dispersed in a Mixed Ionic-Electronic Conducting Matrix

The idea behind this approach is that mobility of both electrons and ions in the catalytic layer can yield significant electrochemical promotion of the dispersed catalytic nanoparticles [2]. The particular approach has been recently applied in the following catalytic systems, adopting different strategies:

- *H_2 production from steam reforming, partial oxidation, and autothermal steam reforming of CH_4, at 500 °C, on a composite electrode Pt-Pt/YSZ electrode deposited on a dense Na-β-Al_2O_3 electrolyte disk*, using an ink prepared by mixing a commercial Pt paste with powder of a dispersed 3 wt. % Pt on YSZ catalyst [148]. Positive polarization resulted in increase of H_2 production, as chemisorption of CH_x species was enhanced, but also to deactivation due to carbon deposition. However, in situ regeneration of the catalytic activity was possible, in particular under autothermal reforming conditions, by applying negative polarization, i.e., by supplying Na^+ to the catalyst, due to the induced increase in the coverage of H_2O and oxygen (electron acceptors) responsible for the deposited carbon removal. This behavior, which is shown in Fig. 2.20, demonstrated the possibility of cyclic operation between electropromoted H_2 production from CH_4 at relatively low temperature (500 °C) and in situ regeneration of the catalyst, under fixed reaction conditions.
- *Propane combustion on Pt nanoparticles (3–20 nm) dispersed (~15% dispersion) on a porous LSCF/GDC ($La_{0.6}Sr_{0.4}Co_{0.2}Fe_{0.8}O_{3-\delta}$/$Ce_{0.9}Gd_{0.1}O_{1.95}$) film (7.5 μm thick) deposited on dense GDC* [149]. Electrophobic EPOC behavior was observed corresponding to increase of propane conversion up to 38% and apparent faradaic efficiency up to 85. This study demonstrated the ability to electropromote metal nanoparticles dispersed in a porous mixed ionic-electronic conducting (MIEC) electrode (LSCF/GDC), its ionic conductivity ensuring the transport of the ionic oxygen promoting species from the solid electrolyte (GDC) to the nanoparticles.
- *C_2H_4 combustion on Ru nanoparticles (1.1 nm) dispersed on CeO_2 (a mixed electronic – O^{2-}conductor) with the 1 wt.% Ru/CeO_2 electrode deposited on dense YSZ,* using a suspension of Ru/CeO_2 powder in ethanol [150]. Electrophilic EPOC behavior was observed with up to 2.5 times increase in the catalytic rate and absolute values of faradaic efficiency up to 96. The increase of the C_2H_4

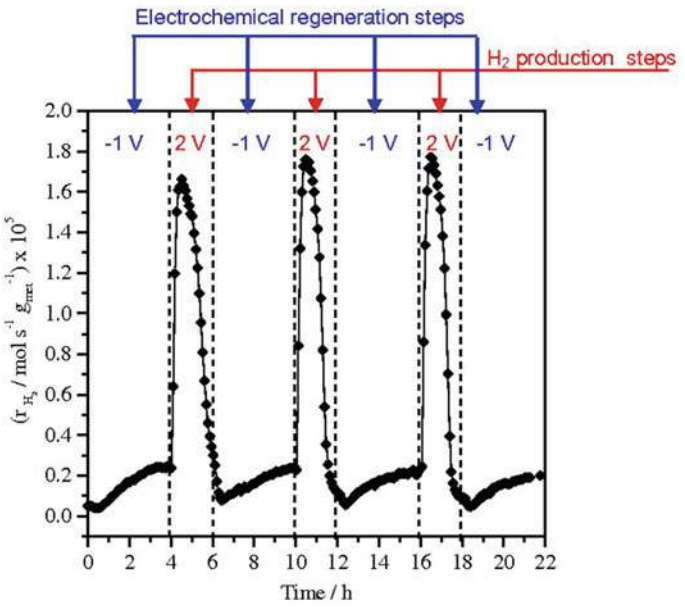

Fig. 2.20 Autothermal steam reforming of CH_4 on a composite Pt-Pt/YSZ electrode deposited on Na-β-Al_2O_3: Influence of the applied cell potential (two-electrode set-up) on H_2 production rate during the reproducibility experiment. $T = 500$ °C. Feed composition: $CH_4/H_2O/O_2$: 1%/4%/0.2% in N_2. Total flow rate: $F_t = 6$ L/h. (Reprinted (adapted) from ref. [148], with permission from Elsevier)

combustion rate with negative polarization was associated with partial reduction of CeO_2 and with formation of a stronger metal-support interaction (MSI) between the Ru nanoparticles and the partially reduced CeO_{2-x}, i.e., with in situ electrochemical enhancement of the MSI effect.

- *Selective partial oxidation of methanol on Au nanoparticles (2–10 nm) dispersed in an ultrafine grained YSZ matrix, with the composite Au/YSZ catalyst-electrode deposited on dense K-β-Al_2O_3* [151]. The Au/YSZ catalyst film, which was highly selective towards $HCOOCH_3$ formation and stable under reaction conditions, was prepared by reactive co-sputtering of Au and Zr-Y targets. This novel preparation method resulted in Au nanoparticles confined in the YSZ matrix but in contact with the reacting mixture [2, 151]. At 280 °C, electrochemical pumping of K^+ ions to the catalyst (negative polarization) resulted in enhancement of the H_2 and $HCOOCH_3$ rates by more than 9 and 5 times, respectively (electrophilic EPOC behavior), for a potassium coverage of ca. 0.5, which demonstrated the suitability of the employed configuration for electropromotion by potassium of a highly dispersed Au catalyst.
- *CH_4 combustion on nanodispersed Pd supported on porous Co_3O_4 (5 wt.% Pd/Co_3O_4) with the Pd/Co_3O_4 electrode deposited on dense YSZ* [152]. This was the first EPOC study where the catalyst consisted of metal nanoparticles

supported on a semiconductor (i.e., Co_3O_4), the latter acting both as an electronic conductor and as a pathway for the oxygen ions to reach the Pd nanoparticles. Positive current application under reducing conditions resulted in increase of the CO_2 production rate by up to 2.5 times, with faradaic efficiency up to 80.

- *CO_2 hydrogenation (to CH_4 and, mainly, to CO) on nanodispersed Ru (0.7–1 nm) supported on porous Co_3O_4 (2 wt.% Ru/Co_3O_4) with the Ru/Co_3O_4 catalyst-electrode deposited on dense BZY ($BaZr_{0.85}Y_{0.15}O_3$ + 1 wt.% NiO) proton conductor* [110]. Weak electrophilic EPOC behavior of the CO production rate was observed under oxidizing conditions. The low rate enhancement ratios were explained considering that the catalyst was already in a promoted state due to enhanced MSI effect ("wireless" EPOC) [103].

2.4.4 Wireless Self-Driven and Self-Sustained Electrochemical Promotion

In 1993, Cavalca et al. [153], in their study of electrochemical promotion of CH_3OH oxidation on Pt/YSZ in a single chamber flow reactor, demonstrated for the first time that it is possible to induce electrochemical promotion in an oxidation reaction applying not an external polarization but utilizing the potential difference between the active Pt catalyst-electrode and a more inert Au counter electrode, which results from the reaction-induced lower oxygen activity on the Pt catalyst. The observed electrophobic self-driven "wireless" electrochemical promotion (wireless NEMCA), realized by short-circuiting the Pt catalyst and the Ag counter electrode, was explained by the continuous supply of promoting ionic oxygen species from the YSZ support to the Pt surface, while the spent O^{2-} were continuously replenished by oxygen from the gas phase.

Almost 15 years later, the concept of wireless EPOC was realized by Poulidi et al. in C_2H_4 combustion over a porous Pt catalyst film deposited on one side of a dense pellet of a mixed ionic-electronic conductor (MIEC) in a dual chamber reactor consisting of the reaction side and a sweep side where a second Pt electrode deposited on the other side of the MIEC pellet was exposed to a sweep gas [154, 155]. In this configuration, the driving force for migration of the promoting species is the chemical potential difference across the MIEC generated by using an appropriate sweep gas, while the mixed conductivity eliminates the need for an external circuit by internally short-circuiting the system. Both $La_{0.6}Sr_{0.4}Co_{0.2}Fe_{0.8}O_{3-\delta}$ (a mixed oxygen ion-electronic conductor) [154, 156] and $Sr_{0.97}Ce_{0.9}Yb_{0.1}O_{3-\delta}$ (a mixed protonic-electronic conductor) [155] have been used as MIEC supports, while moderate rate increases, compared to symmetric operation, were induced via exposure of the Pt electrode in the sweep side to an O_2 and a H_2 atmosphere, respectively. Wireless electrochemical promotion in a similar dual chamber set-up was reported recently for CO oxidation on Pt supported on $BaCe_{0.6}Zr_{0.2}Y_{0.2}O_{3-\delta}$, a mixed protonic-electronic conductor at temperatures up to

650 °C, with a maximum rate increase of 10% observed upon introduction of H_2/He flow in the sweep side [157]. Wireless EPOC has been also investigated in C_2H_4 combustion over Pt supported on a $La_{0.6}Sr_{0.4}Co_{0.2}Fe_{0.8}O_{3-\delta}$ hollow fiber, where the use of this effect for in situ regeneration of the Pt catalyst was demonstrated [158].

A more recent and more promising concept for practical application of EPOC is the self-sustained electrochemical promotion (SSEP) of the catalytic activity of metal nanoparticles dispersed on ionic (O^{2-} conducting) or MIEC supports, due to migration of ionic oxygen species from the support to the surface of the nanoparticles without applying any external polarization, even at temperatures lower than 200 °C [2, 8, 128]. The self-sustained EPOC mechanism is based on the functional similarity of EPOC and metal-support interactions (MSI) [1, 81, 102, 103], merging EPOC and MSI at the nanometric scale [8]. As summarized in recent reviews [2, 5, 8, 80, 128], the self-sustained EPOC has been studied in several catalytic systems, including propane [159, 160], toluene [161], and CO [162, 163] oxidation on Pt nanoparticles dispersed on YSZ, ethylene combustion on Pt and Ru nanoparticles dispersed on YSZ and samarium-doped ceria (SDC) [164], and ethylene combustion on Pt, PtSn, Ru, and Ir nanoparticles dispersed on CeO_2 in the presence and absence of oxygen in the feed [165, 166]. These studies have elucidated the role of the ionic species in the support on the catalytic mechanism and on the promotion of the dispersed nanoparticles. Migration of ionic species from the support (backspillover) may be self-induced thermally [2, 8, 159, 163, 164] and/or by differences in the work function between the support and the metal, which affects their interaction [2, 165, 166]. In general, the driving force for migration will depend on the ionic conductivity and oxygen storage capacity of the support (e.g., for CeO_2), the temperature, and the metal-support interface at the nanoscale [2, 8, 128, 166]. It is also noted that in the absence of O_2 in the gas phase, Pt nanoparticles dispersed on YSZ or MIEC (SDC and CeO_2) have been found much more active for CO and C_2H_4 combustion than Pt nanoparticles dispersed on supports not exhibiting ionic conductivity (e.g., Al_2O_3) [128, 164, 167]. To explain this behavior, which was observed for nanoparticles less than 5 nm implying the necessity of strong interaction with the support, Baranova and coworkers proposed the mechanism of nano-galvanic cells, according to which Pt/YSZ or Pt/MIEC interfaces act as local nano-galvanic cells where CO and C_2H_4 are electrochemically oxidized by O^{2-} from the oxide support, which is reduced [167]. Thermally induced backspillover of oxygen ions to metal nanoparticles and creation of an effective double layer, accompanied by trapping of diffusing atomic metal species by the resulting surface oxygen vacancies, has been also proposed to explain the increased resistance to sintering of Ir [168] and Rh [169] nanoparticles dispersed on supports with high oxygen ion lability.

Self-sustained electrochemical promotion catalysts can also be synthesized by combining in the catalyst composition microparticles or nanoparticles of two materials with different catalytic and electrocatalytic properties which act as cathodes and anodes of microscopic galvanic cells formed if the two materials are dispersed either on a MIEC conductor or on a pure ionic conductor with an electronic conductor also added for the transfer of electrons [2]. When such a catalyst based on a mixed

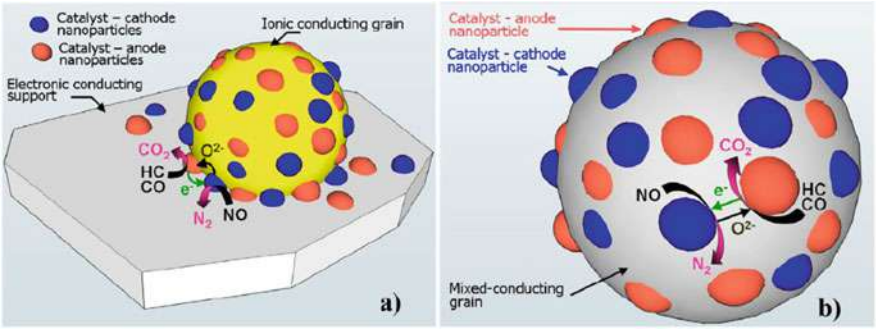

Fig. 2.21 Schematic illustration of the electrochemically-assisted NSR catalysts, with the metal nanoparticles dispersed (**a**) on an O^{2-} ion conducting support (e.g., YSZ) deposited on an electronic conductor (e.g., N-doped SiC-DPF) and (**b**) on a mixed conducting (ionic and electronic) support (e.g., GDC). (Reprinted from ref. [172], with permission from Elsevier)

oxygen ion-electron conductor is used in an oxidation reaction, oxygen species generated at the cathodes of the microscopic galvanic cells via reduction of gas phase oxygen are transferred to the anodes to promote, as sacrificial promoters, the catalytic oxidation reaction on their surface, while in parallel electrons are transferred from the anodes to the cathodes. Based on this concept, Zhou and coworkers have synthesized SSEP catalysts composed of $La_{0.9}Sr_{0.1}MnO_3$ as cathode, Ni-Cu-CeO_2 as anode, YSZ as oxygen ion conductor, and Cu or Ni-Cu as electron conductor [170, 171]. These SSEP catalysts demonstrated improved performance for partial oxidation reforming (POXR) of n-$C_{15}H_{32}$ at 450–650 °C [170] and CH_4 at 350–650 °C [171], compared both to commercial catalysts and to catalysts lacking one or more of the components of the SSEP catalyst. More recently, Vernoux and coworkers used the same concept to develop NO_x storage/reduction (NSR) catalysts which exhibited improved NO_x removal efficiency in synthetic diesel exhaust gas conditions [2, 172]. The NSR catalysts were developed by dispersing Pt and Rh nanoparticles on YSZ or gadolinium doped ceria (GDC) nanoparticles, to form nanometric electrodes (Pt anode and Rh cathode nano-electrodes), and then wash-coating the powder in the porosity of N-doped (electron conducting) and non-doped (insulating) SiC mini-DPFs (diesel particulate filters), respectively. A schematic illustration of these novel electrochemically assisted catalysts is shown in Fig. 2.21. The best performance was obtained with the GDC (mixed oxygen ion-electron conductor) as support of the metallic nanoparticles, whereas the reaction products analysis revealed that electrocatalytic reactions can occur on the nano-electrodes alongside the catalytic reactions.

2.5 Conclusions

After more than 40 years, electrochemical promotion of catalysis (EPOC) remains the focus of intensive research, which highlights the scientific importance of this effect and its potential for practical applications. The physicochemical origin of EPOC has been validated via application of numerous techniques and experimental approaches, in particular for O^{2-} and alkali ion conductors. Nevertheless, there are open research questions yet to be explored. The functional similarity of electrochemical promotion, classical promotion, and metal-support interactions has been conclusively established. Rules of promotion applying both to EPOC and classical catalysis have been derived, which allow promoter selection based on unpromoted kinetics. Current research in EPOC focuses on catalytic systems of technological and environmental importance, such as CO_2 hydrogenation to value-added products or H_2 production by reforming with simultaneous reversible storage, where EPOC could offer a competitive advantage, mainly aiming to electrochemical promotion of non-noble metals and nanodispersed metal/metal oxide catalysts. Development and scale-up of electropromoted reactors remains a priority, following two main directions: (a) improvement of MEPR design (durability, useful lifetime, electrolyte and stack cost minimization, scale-up) and use of nanodispersed catalysts, and (b) development of novel catalytic systems based on self-sustained EPOC. Coupling EPOC with electrolysis is also of strategic future importance as it can potentially reduce the electrolysis cost improving electrochemical technologies that are mature enough and easy to scale up.

References

1. Vayenas CG, Bebelis S, Pliangos C, Brosda S, Tsiplakides D (2001) Electrochemical activation of catalysis. Kluwer Academic/Plenum Publishers, New York
2. Vernoux P (2017) Recent advances in electrochemical promotion of catalysis. In: Spivey J, Han Y-F (eds) Catalysis. The Royal Society of Chemistry, London, pp 29–59
3. Stoukides M, Vayenas CG (1981) The effect of electrochemical oxygen pumping on the rate and selectivity of ethylene oxidation on polycrystalline silver. J Catal 70(1):137–146. https://doi.org/10.1016/0021-9517(81)90323-7
4. Vayenas CG, Bebelis S, Neophytides S (1988) Non-faradaic electrochemical modification of catalytic activity. J Phys Chem 92(18):5083–5085. https://doi.org/10.1021/j100329a007
5. Caravaca A, González-Cobos J, Vernoux P (2020) A discussion on the unique features of electrochemical promotion of catalysis (EPOC): are we in the right path towards commercial implementation? Catalysts 10(11):1276 (29 pages). https://doi.org/10.3390/catal10111276
6. González-Cobos J, de Lucas-Consuegra A (2016) A review of surface analysis techniques for the investigation of the phenomenon of electrochemical promotion of catalysis with alkaline ionic conductors. Catalysts 6(1):15 (13 pages). https://doi.org/10.3390/catal6010015
7. de Lucas-Consuegra A (2014) New trends of alkali promotion in heterogeneous catalysis: electrochemical promotion with alkaline ionic conductors. Catal Surv Asia 19(1):25–37. https://doi.org/10.1007/s10563-014-9179-6

8. Vernoux P, Lizarraga L, Tsampas MN, Sapountzi FM, De Lucas-Consuegra A, Valverde J-L, Souentie S, Vayenas CG, Tsiplakides D, Balomenou S, Baranova EA (2013) Ionically conducting ceramics as active catalyst supports. Chem Rev 113(10):8192–8260. https://doi.org/10.1021/cr4000336
9. Tang X, Xu X, Yi H, Chen C, Wang C (2013) Recent developments of electrochemical promotion of catalysis in the techniques of DeNOx. Sci World J:Article ID 463160 (13 pages). https://doi.org/10.1155/2013/463160
10. Vayenas CG (2011) Bridging electrochemistry and heterogeneous catalysis. J Solid State Electrochem 15(7–8):1425–1435. https://doi.org/10.1007/s10008-011-1336-5
11. Katsaounis A (2009) Recent developments and trends in the electrochemical promotion of catalysis (EPOC). J Appl Electrochem 40(5):885–902. https://doi.org/10.1007/s10800-009-9938-7
12. Tsiplakides D, Balomenou S (2009) Milestones and perspectives in electrochemically promoted catalysis. Catal Today 146(3–4):312–318. https://doi.org/10.1016/j.cattod.2009.05.015
13. Vayenas CG, Koutsodontis CG (2008) Non-faradaic electrochemical activation of catalysis. J. Chem. Phys 128:Article ID: 182506. (13 pages). https://doi.org/10.1063/1.2824944
14. Lambert RM (2003) Electrochemical and chemical promotion by alkalis with metal films and nanoparticles. In: Wieckowski A, Savinova ER, Vayenas CG (eds) Catalysis and electrocatalysis at nanoparticles surfaces, Ch. 16. Marcel Dekker, Inc., New York, pp 583–611
15. Vayenas CG, Katsaounis A, Brosda S, Hammad A (2008) Electrochemical modification of catalytic activity. In: Ertl G, Knözinger H, Schüth F, Weitkamp J (eds) Handbook of heterogeneous catalysis. Wiley-VCH, Weinheim, pp 1905–1935
16. Stoukides M, Vayenas CG (1982) Transient and steady-state vapor phase electrocatalytic ethylene epoxidation. In: Bell AT, Hegedus LL (eds) Catalysis under transient conditions. ACS Symp. Series 178(8), American Chemical Society, Washington, DC, pp 181–208. https://doi.org/10.1021/bk-1982-0178.ch008
17. Bebelis S, Vayenas CG (1992) Non-faradaic electrochemical modification of catalytic activity: 6. The epoxidation of ethylene on Ag/ZrO_2 (8mol%Y_2O_3). J Catal 138(2):588–610. https://doi.org/10.1016/0021-9517(92)90309-6
18. Stoukides M, Vayenas CG (1984) Electrocatalytic rate enhancement of propylene epoxidation on porous silver electrodes using a zirconia oxygen pump. J Electrochem Soc 131(4):839–845. https://doi.org/10.1149/1.2115710
19. Bebelis S, Vayenas CG (1989) Non-faradaic electrochemical modification of catalytic activity: 1. The case of ethylene oxidation on Pt. J Catal 118(1):125–146. https://doi.org/10.1016/0021-9517(89)90306-0
20. Yentekakis IV, Vayenas CG (1988) The effect of electrochemical oxygen pumping on the steady-state and oscillatory behavior of CO oxidation on polycrystalline Pt. J Catal 111(1):170–188. https://doi.org/10.1016/0021-9517(88)90075-9
21. Vayenas CG, Neophytides S (1991) Non-faradaic electrochemical modification of catalytic activity: III. The case of methanol oxidation on Pt. J Catal 127(2):645–664. https://doi.org/10.1016/0021-9517(91)90189-B
22. Neophytides S, Vayenas CG (1989) Non-faradaic electrochemical modification of catalytic activity: 2. The case of methanol dehydrogenation and decomposition on Ag. J Catal 118:147–163. https://doi.org/10.1016/0021-9517(89)90307-2
23. Vayenas CG, Bebelis S, Yentekakis IV, Lintz H-G (1992) Non-faradaic electrochemical modification of catalytic activity: a status report. Catal Today 11(3):303–438. https://doi.org/10.1016/0920-5861(92)80002-5
24. Vayenas CG, Bebelis S, Ladas S (1990) Dependence of catalytic rates on catalyst work function. Nature 343(6259):625–627. https://doi.org/10.1038/343625a0
25. Ladas S, Bebelis S, Vayenas CG (1991) Work function measurements on catalyst films subject to in situ electrochemical promotion. Surf Sci 251-252:1062–1068. https://doi.org/10.1016/0039-6028(91)91151-M

26. Vayenas CG, Bebelis S, Despotopoulou M (1991) Non-faradaic electrochemical modification of catalytic activity: 4. The use of β''-Al_2O_3 as the solid electrolyte. J Catal 128(2):415–435. https://doi.org/10.1016/0021-9517(91)90300-S
27. Tsiakaras P, Vayenas CG (1993) Non-faradaic electrochemical modification of catalytic activity: VII. The case of methane oxidation on Pt. J Catal 140(1):53–70. https://doi.org/10.1006/jcat.1993.1068
28. Bebelis S, Karasali H, Vayenas CG (2008) Electrochemical promotion of the CO_2 hydrogenation on Pd/YSZ and Pd/β''-Al_2O_3 catalyst-electrodes. Solid State Ionics 179(27–32):1391–1395. https://doi.org/10.1016/j.ssi.2008.02.043
29. Bebelis S, Karasali H, Vayenas CG (2008) Electrochemical promotion of CO_2 hydrogenation on Rh/YSZ electrodes. J Appl Electrochem 38(8):1127–1133. https://doi.org/10.1007/s10800-008-9574-7
30. Makri M, Buekenhoudt A, Luyten J, Vayenas CG (1996) Non-faradaic electrochemical modification of the catalytic activity of Pt using a $CaZr_{0.9}In_{0.1}O_{3-\alpha}$ proton conductor. Ionics 2:282–288. https://doi.org/10.1007/BF02376035
31. Vayenas CG, Jaksic MM, Bebelis SI, Neophytides SG (1996) The electrochemical activation of catalytic reactions. In: Bockris JO'M, Conway BE, White RE (eds) Modern aspects of electrochemistry. Springer, Boston, pp 57–202
32. Tsiplakides D, Vayenas CG (2001) Electrode work function and absolute potential scale in solid-state electrochemistry. J Electrochem Soc 148(5):E189–E202. https://doi.org/10.1149/1.1362547
33. Vayenas CG, Neophytides SG (1996) Electrochemical activation of catalysis: In situ controlled promotion of catalyst surfaces. In: Spivey JJ (ed) Catalysis, vol 12. The Royal Society of Chemistry, Cambridge, pp 199–253
34. Pliangos C, Raptis C, Badas T, Vayenas CG (2000) Electrochemical promotion of NO reduction by C_3H_6 on Rh/YSZ catalyst-electrodes. Solid State Ionics 136-137:767–773. https://doi.org/10.1016/S0167-2738(00)00549-X
35. Yentekakis IV, Jiang Y, Neophytides S, Bebelis S, Vayenas CG (1995) Catalysis, electrocatalysis and electrochemical promotion of the steam reforming of methane over Ni film and Ni-YSZ cermet anodes. Ionics 1:491–498. https://doi.org/10.1007/BF02375296
36. Marwood M, Kaloyannis A, Vayenas CG (1996) Electrochemical promotion of the NO reduction by C_2H_4 on Pt/YSZ and by CO on Pd/YSZ. Ionics 2:302–311. https://doi.org/10.1007/BF02376038
37. Nicole J, Tsiplakides D, Wodiunig S, Comninellis C (1997) Activation of catalyst for gas-phase combustion by electrochemical pretreatment. J Electrochem Soc 144(12):L312–L314. https://doi.org/10.1149/1.1838143
38. Wodiunig S, Patsis V, Comninellis C (2000) Electrochemical promotion of RuO_2-catalysts for the gas phase combustion of C_2H_4. Solid State Ionics 136-137:813–817. https://doi.org/10.1016/S0167-2738(00)00505-1
39. Falgairette C, Jaccoud A, Fóti G, Comninellis C (2008) The phenomenon of "permanent" electrochemical promotion of catalysis (P-EPOC). J Appl Electrochem 38(8):1075–1082. https://doi.org/10.1007/s10800-008-9554-y
40. Fóti G, Lavanchy O, Comninellis C (2000) Electrochemical promotion of Rh catalyst in gas-phase reduction of NO by propylene. J Appl Electrochem 30:1223–1228. https://doi.org/10.1023/A:1026505829359
41. Pliangos C, Raptis C, Badas T, Vayenas CG (2000) Electrochemical promotion of NO reduction by C_3H_6 and CO on Rh/YSZ catalyst - electrodes. Ionics 6:119–126. https://doi.org/10.1007/BF02375555
42. Souentie S, Xia C, Falgairette C, Li YD, Comninellis C (2010) Investigation of the "permanent" electrochemical promotion of catalysis (P-EPOC) by electrochemical mass spectrometry (EMS) measurements. Electrochem Commun 12(2):323–326. https://doi.org/10.1016/j.elecom.2009.12.031

43. Harkness IR, Hardacre C, Lambert RM, Yentekakis IV, Vayenas CG (1996) Ethylene oxidation over platinum: In situ electrochemically controlled promotion using Na–β″ alumina and studies with a Pt(111)/Na model catalyst. J Catal 160(1):19–26. https://doi.org/10.1006/jcat.1996.0119
44. Yentekakis IV, Bebelis S (1992) Study of the NEMCA effect in a single-pellet catalytic reactor. J Catal 137(1):278–283. https://doi.org/10.1016/0021-9517(92)90157-D
45. Petrolekas PD, Brosda S, Vayenas CG (1998) Electrochemical promotion of Pt catalyst electrodes deposited on $Na_3Zr_2Si_2PO_{12}$ during ethylene oxidation. Electrochem Soc 145(5): 1469–1477. https://doi.org/10.1149/1.1838506
46. Yentekakis IV, Moggridge G, Vayenas CG, Lambert RM (1994) In situ controlled promotion of catalyst surfaces via NEMCA: the effect of Na on the Pt-catalyzed CO oxidation. J Catal 146(1):292–305. https://doi.org/10.1016/0021-9517(94)90033-7
47. Karavasilis C, Bebelis S, Vayenas CG (1996) In situ controlled promotion of catalyst surfaces via NEMCA: the effect of Na on the Ag-catalyzed ethylene epoxidation in the presence of chlorine moderators. J Catal 160(2):205–213. https://doi.org/10.1006/jcat.1996.0139
48. Harkness IR, Lambert RM (1995) Electrochemical promotion of the NO + ethylene reaction over platinum. J Catal 152(1):211–214. https://doi.org/10.1006/jcat.1995.1075
49. Palermo A, Lambert RM, Harkness IR, Yentekakis IV, Marina O, Vayenas CG (1996) Electrochemical promotion by Na of the platinum-catalyzed reaction between CO and NO. J Catal 161(1):471–479. https://doi.org/10.1006/jcat.1996.0206
50. Marina OA, Yentekakis IV, Vayenas CG, Palermo A, Lambert RM (1997) In situ controlled promotion of catalyst surfaces via NEMCA: the effect of Na on the Pt-catalyzed NO reduction by H_2. J Catal 166(2):218–228. https://doi.org/10.1006/jcat.1997.1551
51. Yentekakis IV, Palermo A, Filkin NC, Tikhov MS, Lambert RM (1997) In situ electrochemical promotion by sodium of the platinum-catalyzed reduction of NO by propene. J Phys Chem B 101(19):3759–3768. https://doi.org/10.1021/jp963052c
52. Williams FJ, Palermo A, Tikhov MS, Lambert RM (2001) Mechanism of alkali promotion in heterogeneous catalysis under realistic conditions: application of electron spectroscopy and electrochemical promotion to the reduction of NO by CO and by propene over rhodium. Surf Sci 482-485(Part 1):177–182. https://doi.org/10.1016/S0039-6028(00)01040-2
53. Williams FJ, Palermo A, Tikhov MS, Lambert RM (2000) Electrochemical promotion by sodium of the rhodium-catalyzed NO + CO reaction. J Phys Chem B 104(50):11883–11890. https://doi.org/10.1021/jp001689x
54. Williams FJ, Palermo A, Tikhov MS, Lambert RM (2001) Electrochemical promotion by sodium of the rhodium-catalyzed reduction of NO by propene: kinetics and spectroscopy. J Phys Chem B 105(7):1381–1388. https://doi.org/10.1021/jp003269d
55. Lambert RM, Williams F, Palermo A, Tikhov MS (2000) Modelling alkali promotion in heterogeneous catalysis: in situ electrochemical control of catalytic reactions. Top Catal 13: 91–98. https://doi.org/10.1023/A:1009076720641
56. Cavalca CA, Haller GL (1998) Solid electrolytes as active catalyst supports: electrochemical modification of benzene hydrogenation activity on Pt/β″(Na)Al_2O_3. J Catal 177(2):389–395. https://doi.org/10.1006/jcat.1998.2060
57. Giannikos A, Petrolekas P, Pliangos C, Frenzel A, Vayenas CG, Pütter H (1998) Electrochemical promotion of Pd for the hydrogenation of C_2H_2. Ionics 4:161–169. https://doi.org/10.1007/BF02375941
58. Tracey S, Palermo A, Vazquez JPH, Lambert RM (1998) In situ electrochemical promotion by sodium of the selective hydrogenation of acetylene over platinum. J Catal 179(1):231–240. https://doi.org/10.1006/jcat.1998.2179
59. Williams FJ, Palermo A, Tracey S, Tikhov MS, Lambert RM (2002) Electrochemical promotion by potassium of the selective hydrogenation of acetylene on platinum: reaction studies and XP spectroscopy. J Phys Chem B 106(22):5668–5672. https://doi.org/10.1021/jp0203954
60. Karasali H (1994) PhD thesis, Department of Chemical Engineering. University of Patras, Greece

61. Williams FJ, Lambert RM (2000) A study of sodium promotion in Fischer–Tropsch synthesis: electrochemical control of a ruthenium model catalyst. Catal Lett 70:9–14. https://doi.org/10.1023/A:1019023418300
62. Urquhart AJ, Keel JM, Williams FJ, Lambert RM (2003) Electrochemical promotion by potassium of rhodium-catalyzed Fischer-Tropsch synthesis: XP spectroscopy and reaction studies. J Phys Chem B 107(38):10591–10597. https://doi.org/10.1021/jp035436q
63. González-Cobos J, Valverde JL, de Lucas-Consuegra A (2017) Electrochemical vs. chemical promotion in the H_2 production catalytic reactions. Int J Hydrog Energy 42(19):13712–13723. https://doi.org/10.1016/j.ijhydene.2017.03.085
64. Yentekakis IV, Vernoux P, Goula G, Caravaca A (2019) Electropositive promotion by alkalis or alkaline earths of Pt-group metals in emissions control catalysis: a status report. Catalysts 9(2):157 (74 pages). https://doi.org/10.3390/catal9020157
65. de Lucas-Consuegra A, Caravaca A, Sánchez P, Dorado F, Valverde JL (2008) A new improvement of catalysis by solid-state electrochemistry: an electrochemically assisted NOx storage/reduction catalyst. J Catal 259(1):54–65. https://doi.org/10.1016/j.jcat.2008.07.008
66. González-Cobos J, Rico VJ, González-Elipe AR, Valverde JL, de Lucas-Consuegra A (2016) Electrocatalytic system for the simultaneous hydrogen production and storage from methanol. ACS Catal 6(3):1942–1951. https://doi.org/10.1021/acscatal.5b02844
67. Politova TI, Sobyanin VA, Belyaev VD (1990) Ethylene hydrogenation in electrochemical-cell with solid proton-conducting electrolyte. React Kinet Catal Lett 41(2):321–326. https://doi.org/10.1007/BF02097888
68. Chiang PC, Eng D, Stoukides M (1993) Solid electrolyte aided direct coupling of methane. J Catal 139(2):683–687. https://doi.org/10.1006/jcat.1993.1060
69. Yiokari CG, Pitselis GE, Polydoros DG, Katsaounis AD, Vayenas CG (2000) High pressure electrochemical promotion of ammonia synthesis over an industrial iron catalyst. J Phys Chem A 104(46):10600–10602. https://doi.org/10.1021/jp002236v
70. Ouzounidou M, Skodra A, Kokkofitis C, Stoukides M (2007) Catalytic and electrocatalytic synthesis of NH_3 in a H^+ conducting cell by using an industrial Fe catalyst. Solid State Ionics 178(1–2):153–159. https://doi.org/10.1016/j.ssi.2006.11.019
71. Tsiplakides D, Neophytides SG, Enea O, Jaksic MM, Vayenas CG (1997) Non-faradaic electrochemical modification of catalytic activity (NEMCA) of Pt black electrodes deposited on Nafion 117 solid polymer electrolyte. J Electrochem Soc 144(6):2072–2088. https://doi.org/10.1149/1.1837744
72. Ploense L, Salazar M, Gurau B, Smotkin ES (1997) Proton spillover promoted isomerization of n-butylenes on Pt-black cathodes/Nafion 117. J Am Chem Soc 119(47):11550–11551. https://doi.org/10.1021/ja9728841
73. Ploense L, Salazar M, Gurau B, Smotkin ES (2000) Spectroscopic study of NEMCA promoted alkene isomerizations at PEM fuel cell Pd-Nafion cathodes. Solid State Ionics 136-137:713–720. https://doi.org/10.1016/S0167-2738(00)00567-1
74. Williams FJ, Palermo A, Holgado HP, Lambert RM (2002) First demonstration of in situ electrochemical control of the composition and performance of an alloy catalyst during reaction. J Catal 210(2):237–240. https://doi.org/10.1006/jcat.2002.3713
75. Palermo A, Williams FJ, Lambert RM (2002) In situ control of the composition and performance of a bimetallic alloy catalyst: the selective hydrogenation of acetylene over Pt/Pb. J Phys Chem B 106(39):10215–10219. https://doi.org/10.1021/jp021296t
76. Anastasijevic NA, Baltruschat H, Heitbaum J (1993) On the hydrogen evolution during the electrochemical oxidation of aldehydes at Ib metals. Electrochim Acta 38(8):1067–1072. https://doi.org/10.1016/0013-4686(93)80214-K
77. Neophytides S, Tsiplakides D, Stonehart P, Jaksic M, Vayenas CG (1994) Electrochemical enhancement of a catalytic reaction in aqueous solution. Nature 370:45–47. https://doi.org/10.1038/370045a0

78. Neophytides S, Tsiplakides D, Stonehart P, Jaksic M, Vayenas CG (1996) Non-faradaic electrochemical modification of the catalytic activity of Pt for H_2 oxidation in aqueous alkaline media. J Phys Chem 100(35):14803–14814. https://doi.org/10.1021/jp960971u
79. Hajar YM, Treps L, Michel C, Baranova EA, Steinmann SN (2019) Theoretical insight into the origin of the electrochemical promotion of ethylene oxidation on ruthenium oxide. Cat Sci Technol 9(21):5915–5926. https://doi.org/10.1039/C9CY01421G
80. Tsampas MN, Sapountzi FM, Vernoux P (2015) Applications of yttria stabilized zirconia (YSZ) in catalysis. Cat Sci Technol 5(11):4884–4900. https://doi.org/10.1039/C5CY00739A
81. Vayenas CG (2013) Promotion, electrochemical promotion and metal–support interactions: their common features. Catal Letters 143(11):1085–1097. https://doi.org/10.1007/s10562-013-1128-x
82. Ladas S, Kennou S, Bebelis S, Vayenas CG (1993) Origin of non-faradaic electrochemical modification of catalytic activity. J Phys Chem 97(35):8845–8848. https://doi.org/10.1021/j100137a004
83. Neophytides SG, Vayenas CG (1995) TPD and cyclic voltammetric investigation of the origin of electrochemical promotion in catalysis. J Phys Chem 99(47):17063–17067. https://doi.org/10.1021/j100047a001
84. Neophytides SG, Tsiplakides D, Vayenas CG (1998) Temperature-programmed desorption of oxygen from Pt films interfaced with Y_2O_3-doped ZrO_2. J Catal 178(2):414–428. https://doi.org/10.1006/jcat.1998.2155
85. Katsaounis A, Nikopoulou Z, Verykios XE, Vayenas CG (2004) Comparative isotope-aided investigation of electrochemical promotion and metal–support interactions 1. $^{18}O_2$ TPD of electropromoted Pt films deposited on YSZ and of dispersed Pt/YSZ catalysts. J Catal 222(1):192–206. https://doi.org/10.1016/j.jcat.2003.10.010
86. Katsaounis A, Nikopoulou Z, Verykios XE, Vayenas CC (2004) Comparative isotope-aided investigation of electrochemical promotion and metal-support interactions 2. CO oxidation by $^{18}O_2$ on electropromoted Pt films deposited on YSZ and on nanodispersed Pt/YSZ catalysts. J Catal 226(1):197–209. https://doi.org/10.1016/j.jcat.2004.05.009
87. Li X, Gaillard F, Vernoux P (2007) Investigations under real operating conditions of the electrochemical promotion by O_2 temperature programmed desorption measurements. Top Catal 44(3):391–398. https://doi.org/10.1007/s11244-006-0131-5
88. Tsampas MN, Sapountzi FM, Boréave A, Vernoux P (2013) Isotopical labeling mechanistic studies of electrochemical promotion of propane combustion on Pt/YSZ. Electrochem Commun 26:13–16. https://doi.org/10.1016/j.elecom.2012.09.043
89. Tsampas MN, Sapountzi FM, Boréave A, Vernoux P (2014) Investigation of the electrochemical promotion of catalysis origins on electrochemical catalysts with oxygen ion conductive supports: isotopic labeling mechanistic studies. Solid State Ionics 262:257–261. https://doi.org/10.1016/j.ssi.2014.01.008
90. Filkin NC, Tikhov MS, Palermo A, Lambert RM (1999) A kinetic and spectroscopic study of the in situ electrochemical promotion by sodium of the platinum-catalyzed combustion of propene. J Phys Chem A 103(15):2680–2687. https://doi.org/10.1021/jp984186o
91. Williams FJ, Palermo A, Tikhov MS, Lambert RM (2000) The origin of electrochemical promotion in heterogeneous catalysis: photoelectron spectroscopy of solid state electrochemical cells. J Phys Chem B 104(3):615–621. https://doi.org/10.1021/jp993037i
92. de Lucas-Consuegra A, Dorado F, Valverde JL, Karoum R, Vernoux P (2007) Low-temperature propene combustion over Pt/K-βAl_2O_3 electrochemical catalyst: characterization, catalytic activity measurements, and investigation of the NEMCA effect. J Catal 251(2):474–484. https://doi.org/10.1016/j.jcat.2007.06.031
93. de Lucas-Consuegra A, González-Cobos J, García-Rodríguez Y, Mosquera A, Endrino JL, Valverde JL (2012) Enhancing the catalytic activity and selectivity of the partial oxidation of methanol by electrochemical promotion. J Catal 293:149–157. https://doi.org/10.1016/j.jcat.2012.06.016

94. González-Cobos J, Rico VJ, González-Elipe AR, Valverde JL, de Lucas-Consuegra A (2015) Electrochemical activation of an oblique angle deposited Cu catalyst film for H_2 production. Cat Sci Technol 5(4):2203–2214. https://doi.org/10.1039/C4CY01524J
95. Makri M, Vayenas CG, Bebelis S, Besocke KH, Cavalca C (1996) Atomic resolution STM imaging of electrochemically controlled reversible promoter dosing of catalysts. Surf Sci 369(1–3):351–359. https://doi.org/10.1016/S0039-6028(96)00911-9
96. Vayenas CG, Archonta D, Tsiplakides D (2003) Scanning tunneling microscopy observation of the origin of electrochemical promotion and metal–support interactions. J Electroanal Chem 554-555:301–306. https://doi.org/10.1016/S0022-0728(03)00240-7
97. Thursfield A, Brosda S, Pliangos C, Schober T, Vayenas CG (2003) Electrochemical promotion of an oxidation reaction using a proton conductor. Electrochim Acta 48(25–26): 3779–3788. https://doi.org/10.1016/S0013-4686(03)00511-5
98. Vayenas CG, Brosda S, Pliangos C (2001) Rules and mathematical modeling of electrochemical and chemical promotion: 1. Reaction classification and promotional rules. J Catal 203(2): 329–350. https://doi.org/10.1006/jcat.2001.3348
99. Brosda S, Vayenas CG, Wei J (2006) Rules of chemical promotion. Appl Catal B 68(3–4): 109–124. https://doi.org/10.1016/j.apcatb.2006.07.021
100. Vayenas CG, Brosda S (2014) Electron donation–backdonation and the rules of catalytic promotion. Top Catal 57(14–16):1287–1301. https://doi.org/10.1007/s11244-014-0294-4
101. Brosda S, Vayenas CG (2002) Rules and mathematical modeling of electrochemical and classical promotion 2. Modeling. J Catal 208(1):38–53. https://doi.org/10.1006/jcat.2002.3549
102. Vayenas CG, Pliangos C, Brosda S, Tsiplakides D (2003) Promotion, electrochemical promotion, and metal–support interactions: the unifying role of spillover. In: Wieckowski A, Savinova ER, Vayenas CG (eds) Catalysis and electrocatalysis at nanoparticle surfaces, Ch.19. Marcel Dekker, Inc, New York, pp 667–744
103. Nicole J, Tsiplakides D, Pliangos C, Verykios XE, Comninellis C, Vayenas CG (2001) Electrochemical promotion and metal–support interactions. J Catal 204(1):23–34. https://doi.org/10.1006/jcat.2001.3360
104. Sanabria-Chinchilla J, Asazawa K, Sakamoto T, Yamada K, Tanaka H, Strasser P (2011) Noble metal-free hydrazine fuel cell catalysts: EPOC effect in competing chemical and electrochemical reaction pathways. J Am Chem Soc 133(14):5425–5431. https://doi.org/10.1021/ja111160r
105. Cai F, Gao D, Zhou H, Wang G, He T, Gong H, Miao S, Yang F, Wang J, Bao X (2017) Electrochemical promotion of catalysis over Pd nanoparticles for CO_2 reduction. Chem Sci 8(4):2569–2573. https://doi.org/10.1039/C6SC04966D
106. Petrushina IM, Bandur VA, Cappeln F, Bjerrum NJ (2000) Electrochemical promotion of sulfur dioxide catalytic oxidation. J Electrochem Soc 147(8):3010–3013. https://doi.org/10.1149/1.1393640
107. Ruiz-López E, Caravaca A, Vernoux P, Dorado F, de Lucas-Consuegra A (2020) Over-faradaic hydrogen production in methanol electrolysis cells. Chem. Eng. J 396: Art. No. 125217. https://doi.org/10.1016/j.cej.2020.125217
108. Jahromi AF, Ruiz-López E, Dorado F, Baranova EA, de Lucas-Consuegra A (2022) Electrochemical promotion of ethanol partial oxidation and reforming reactions for hydrogen production. Renew Energy 183:515–523. https://doi.org/10.1016/j.renene.2021.11.041
109. Zagoraios D, Tsatsos S, Kennou S, Vayenas CG, Kyriakou G, Katsaounis A (2020) Tuning the RWGS reaction via EPOC and in situ electro-oxidation of cobalt nanoparticles. ACS Catal 10(24):14916–14927. https://doi.org/10.1021/acscatal.0c04133
110. Zagoraios D, Panaritis C, Krassakopoulou A, Baranova EA, Katsaounis A, Vayenas CG (2020) Electrochemical promotion of Ru nanoparticles deposited on a proton conductor electrolyte during CO_2 hydrogenation. Appl Catal B 276:119148. https://doi.org/10.1016/j.apcatb.2020.119148

111. Kotsiras A, Kalaitzidou I, Grigoriou D, Symillidis A, Makri M, Katsaounis A, Vayenas CG (2018) Electrochemical promotion of nanodispersed Ru-Co catalysts for the hydrogenation of CO_2. Appl Catal B 232:60–68. https://doi.org/10.1016/j.apcatb.2018.03.031
112. Souentie S, Hammad A, Brosda S, Foti G, Vayenas CG (2008) Electrochemical promotion of NO reduction by C_2H_4 in 10% O_2 using a monolithic electropromoted reactor with Rh/YSZ/Pt elements. J Appl Electrochem 38(8):1159–1170. https://doi.org/10.1007/s10800-008-9548-9
113. Makri M, Katsaounis A, Vayenas CG (2015) Electrochemical promotion of CO_2 hydrogenation on Ru catalyst–electrodes supported on a K–β''–Al_2O_3 solid electrolyte. Electrochim Acta 179:556–564. https://doi.org/10.1016/j.electacta.2015.03.144
114. Kalaitzidou I, Makri M, Theleritis D, Katsaounis A, Vayenas CG (2016) Comparative study of the electrochemical promotion of CO_2 hydrogenation on Ru using Na^+, K^+, H^+ and O^{2-} conducting solid electrolytes. Surf Sci 646:194–203. https://doi.org/10.1016/j.susc.2015.09.011
115. Kalaitzidou I, Katsaounis A, Norby T, Vayenas CG (2015) Electrochemical promotion of the hydrogenation of CO_2 on Ru deposited on a BZY proton conductor. J Catal 331:98–109. https://doi.org/10.1016/j.jcat.2015.08.023
116. Theleritis D, Souentie S, Siokou A, Katsaounis A, Vayenas CG (2012) Hydrogenation of CO_2 over Ru/YSZ electropromoted catalysts. ACS Catal 2(5):770–780. https://doi.org/10.1021/cs300072a
117. Ruiz E, Cillero D, Martínez PJ, Morales Á, Vicente GS, de Diego G, Sánchez JM (2013) Bench scale study of electrochemically promoted catalytic CO_2 hydrogenation to renewable fuels. Catal Today 210:55–66. https://doi.org/10.1016/j.cattod.2012.10.025
118. Papaioannou EI, Souentie S, Hammad A, Vayenas CG (2009) Electrochemical promotion of the CO_2 hydrogenation reaction using thin Rh, Pt and Cu films in a monolithic reactor at atmospheric pressure. Catal Today 146(3–4):336–344. https://doi.org/10.1016/j.cattod.2009.06.008
119. de Lucas-Consuegra A, Caravaca A, González-Cobos J, Valverde JL, Dorado F (2011) Electrochemical activation of a non noble metal catalyst for the water–gas shift reaction. Catal Commun 15(1):6–9. https://doi.org/10.1016/j.catcom.2011.08.007
120. González-Cobos J, Ruiz-López E, Valverde JL, de Lucas-Consuegra A (2016) Electrochemical promotion of a dispersed Ni catalyst for H_2 production via partial oxidation of methanol. Int J Hydrog Energy 41(42):19418–19429. https://doi.org/10.1016/j.ijhydene.2016.06.027
121. Ruiz E, Cillero D, Martínez PJ, Morales Á, Vicente GS, de Diego G, Sánchez JM (2014) Electrochemical synthesis of fuels by CO_2 hydrogenation on Cu in a potassium ion conducting membrane reactor at bench scale. Catal Today 236(Part A):108–120. https://doi.org/10.1016/j.cattod.2014.01.016
122. Panaritis C, Zgheib J, Ebrahim SAH, Couillard M, Baranova EA (2020) Electrochemical in-situ activation of Fe-oxide nanowires for the reverse water gas shift reaction. Appl Catal B 269:Article 118826 (11 pages). https://doi.org/10.1016/j.apcatb.2020.118826
123. Khechfe AA, Sullivan MM, Zagoraios D, Katsaounis A, Vayenas CG, Román-Leshkov Y (2022) Non-faradaic electrochemical promotion of Brønsted acid-catalyzed dehydration reactions over molybdenum oxide. ACS Catal 12(2):906–912. https://doi.org/10.1021/acscatal.1c04885
124. Pacchioni G, Illas F, Neophytides S, Vayenas CG (1996) Quantum-chemical study of electrochemical promotion in catalysis. J Phys Chem 100(41):16653–16661. https://doi.org/10.1021/jp9612386
125. Leiva EPM, Vázquez C, Rojas MI, Mariscal MM (2008) Computer simulation of the effective double layer occurring on a catalyst surface under electro-chemical promotion conditions. J Appl Electrochem 38(8):1065–1073. https://doi.org/10.1007/s10800-008-9539-x
126. Panaritis C, Hajar YM, Treps L, Michel C, Baranova EA, Steinmann SN (2020) Demystifying the atomistic origin of the electric field effect on methane oxidation. J Phys Chem Lett 11(17):6976–6981. https://doi.org/10.1021/acs.jpclett.0c01485

127. Anastasijevic NA (2009) NEMCA—from discovery to technology. Catal Today 146(3–4): 308–311. https://doi.org/10.1016/j.cattod.2009.02.020
128. Dole HAE, Baranova EA (2016) Implementation of nanostructured catalysts in the electrochemical promotion of catalysis. In: Aliofkhazraei M, Makhlouf ASH (eds) Handbook of nanoelectrochemistry. Springer International Publishing AG Switzerland, Cham, pp 1095–1124
129. Marwood M, Vayenas CG (1997) Electrochemical promotion of electronically isolated Pt catalysts on stabilized zirconia. J Catal 168(2):538–542. https://doi.org/10.1006/jcat.1997.1677
130. Balomenou S, Pitselis G, Polydoros D, Giannikos A, Vradis A, Frenzel A, Pliangos C, Pütter H, Vayenas CG (2000) Electrochemical promotion of Pd, Fe and distributed Pt catalyst-electrodes. Solid State Ionics 136-137:857–862. https://doi.org/10.1016/S0167-2738(00)00524-5
131. Wodiunig S, Bokeloh F, Nicole J, Comninellis C (1999) Electrochemical promotion of RuO_2 catalyst dispersed on an yttria-stabilized zirconia monolith. Electrochem Solid-State Lett 2(6): 281–283. https://doi.org/10.1149/1.1390811
132. Wodiunig S, Bokeloh F, Comninellis C (2000) Electrochemical promotion of bipolar electrodes: an estimation of the current bypass. Electrochim Acta 46(2–3):357–363. https://doi.org/10.1016/S0013-4686(00)00592-2
133. Xia C, Hugentobler M, Li Y, Foti G, Comninellis C, Harbich W (2010) Electrochemical promotion of CO combustion over non-percolated Pt particles supported on YSZ using a novel bipolar configuration. Electrochem Commun 13(1):99–101. https://doi.org/10.1016/j.elecom.2010.11.026
134. Xia C, Hugentobler M, Li Y, Comninellis C, Harbich W (2010) Quantifying electrochemical promotion of induced bipolar Pt particles supported on YSZ. Electrochem Commun 12(11): 1551–1554. https://doi.org/10.1016/j.elecom.2010.08.031
135. Roche V, Revel R, Vernoux P (2010) Electrochemical promotion of YSZ monolith honeycomb for deep oxidation of methane. Catal Commun 11(13):1076–1080. https://doi.org/10.1016/j.catcom.2010.05.005
136. Balomenou S, Tsiplakides D, Katsaounis A, Thiemann-Handler S, Cramer B, Foti G, Vayenas CG (2004) Novel monolithic electrochemically promoted catalytic reactor for environmentally important reactions. Appl Catal B 52(3):181–196. https://doi.org/10.1016/j.apcatb.2004.04.007
137. Chatzilias C, Martino E, Katsaounis A, Vayenas CG (2021) Electrochemical promotion of CO_2 hydrogenation in a monolithic electrochemically promoted reactor (MEPR). Appl Catal B 284:119695. https://doi.org/10.1016/j.apcatb.2020.119695
138. Hammad A, Souentie S, Balomenou S, Tsiplakides D, Figueroa JC, Cavalca C, Pereira CJ, Vayenas CG (2008) Tailor-structured skeletal Pt catalysts employed in a monolithic electropromoted reactor. J Appl Electrochem 38(8):1171–1176. https://doi.org/10.1007/s10800-008-9533-3
139. Balomenou SP, Tsiplakides D, Vayenas CG, Poulston S, Houel V, Collier P, Konstandopoulos AG, Agrafiotis C (2007) Electrochemical promotion in a monolith electrochemical plate reactor applied to simulated and real automotive pollution control. Top Catal 44(3): 481–486. https://doi.org/10.1007/s11244-006-0140-4
140. Hammad A, Souentie S, Papaioannou EI, Balomenou S, Tsiplakides D, Figueroa JC, Cavalca C, Pereira CJ (2011) Electrochemical promotion of the SO_2 oxidation over thin Pt films interfaced with YSZ in a monolithic electropromoted reactor. Appl Catal B 103(3–4): 336–342. https://doi.org/10.1016/j.apcatb.2011.01.040
141. Chatzilias C, Martino E, Tsatsos S, Kyriakou G, Katsaounis A, Vayenas CG (2022) Kinetic study of CO_2 hydrogenation on Ru/YSZ catalyst using a monolithic electropromoted reactor (MEPR). Chem Eng J 430 (Part 3):132967 (11 pages). https://doi.org/10.1016/j.cej.2021.132967

142. Marwood M, Vayenas CG (1998) Electrochemical promotion of a dispersed platinum catalyst. J Catal 178(2):429–440. https://doi.org/10.1006/jcat.1998.2156
143. Jiménez V, Jiménez-Borja C, Sánchez P, Romero A, Papaioannou EI, Theleritis D, Souentie S, Brosda S, Valverde JL (2011) Electrochemical promotion of the CO_2 hydrogenation reaction on composite Ni or Ru impregnated carbon nanofiber catalyst-electrodes deposited on YSZ. Appl Catal B 107(1–2):210–220. https://doi.org/10.1016/j.apcatb.2011.07.016
144. de Lucas-Consuegra A, González-Cobos J, Carcelén V, Magén C, Endrino JL, Valverde JL (2013) Electrochemical promotion of Pt nanoparticles dispersed on a diamond-like carbon matrix: a novel electrocatalytic system for H_2 production. J Catal 307:18–26. https://doi.org/10.1016/j.jcat.2013.06.012
145. Matei F, Jiménez-Borja C, Canales-Vázquez J, Brosda S, Dorado F, Valverde JL, Ciuparu D (2013) Enhanced electropromotion of methane combustion on palladium catalysts deposited on highly porous supports. Appl Catal B 132-133:80–89. https://doi.org/10.1016/j.apcatb.2012.11.011
146. Jiménez-Borja C, Brosda S, Matei F, Makri M, Delgado B, Sapountzi F, Ciuparu D, Dorado F, Valverde JL, Vayenas CG (2012) Electrochemical promotion of methane oxidation on Pd catalyst-electrodes deposited on Y_2O_3-stabilized-ZrO_2. Appl Catal B 128:48–54. https://doi.org/10.1016/j.apcatb.2012.02.011
147. Makri M, Symillidis A, Grigoriou D, Katsaounis A, Vayenas CG (2018) Electrochemical promotion of CO_2 reduction on a dispersed Ru/YSZ catalyst supported on YSZ solid electrolyte. Mater Today: Proc 5(14):27617–27625. https://doi.org/10.1016/j.matpr.2018.09.082
148. de Lucas-Consuegra A, Caravaca A, Martínez PJ, Endrino JL, Dorado F, Valverde JL (2010) Development of a new electrochemical catalyst with an electrochemically assisted regeneration ability for H_2 production at low temperatures. J Catal 274(2):251–258. https://doi.org/10.1016/j.jcat.2010.07.007
149. Kambolis A, Lizarraga L, Tsampas MN, Burel L, Rieu M, Viricelle JP, Vernoux P (2012) Electrochemical promotion of catalysis with highly dispersed Pt nanoparticles. Electrochem Commun 19:5–8. https://doi.org/10.1016/j.elecom.2012.02.041
150. Dole HAE, Safady LF, Ntais S, Couillard M, Baranova EA (2014) Electrochemically enhanced metal-support interaction of highly dispersed Ru nanoparticles with a CeO_2 support. J Catal 318:85–94. https://doi.org/10.1016/j.jcat.2014.07.003
151. González-Cobos J, Horwat D, Ghanbaja J, Valverde JL, de Lucas-Consuegra A (2014) Electrochemical activation of Au nanoparticles for the selective partial oxidation of methanol. J Catal 317:293–302. https://doi.org/10.1016/j.jcat.2014.06.022
152. Zagoraios D, Athanasiadi A, Kalaitzidou I, Ntais S, Katsaounis A, Caravaca A, Vernoux P, Vayenas CG (2020) Electrochemical promotion of methane oxidation over nanodispersed Pd/Co_3O_4 catalysts. Catal Today 355:910–920. https://doi.org/10.1016/j.cattod.2019.02.030
153. Cavalca CA, Larsen G, Vayenas CG, Haller GL (1993) Electrochemical modification of CH_3OH oxidation selectivity and activity on a Pt single-pellet catalytic reactor. J Phys Chem 97(23):6115–6119. https://doi.org/10.1021/j100125a005
154. Poulidi D, Thursfield A, Metcalfe IS (2007) Electrochemical promotion of catalysis controlled by chemical potential difference across a mixed ionic-electronic conducting ceramic membrane – an example of wireless NEMCA. Top Catal 44(3):435–449. https://doi.org/10.1007/s11244-006-0136-0
155. Poulidi D, Mather GC, Metcalfe IS (2007) Wireless electrochemical modification of catalytic activity on a mixed protonic–electronic conductor. Solid State Ionics 178(7–10):675–680. https://doi.org/10.1016/j.ssi.2007.02.022
156. Poulidi D, Anderson C, Metcalfe IS (2008) Remote control of the activity of a Pt catalyst supported on a mixed ionic electronic conducting membrane. Solid State Ionics 179(27–32):1347–1350. https://doi.org/10.1016/j.ssi.2008.01.056
157. Stavrakakis E, West M, Johnston S, McIllwaine R, Poulidi D (2019) Hydration, CO_2 stability and wireless electrochemical promotion studies on yttria-doped Ba (Ce, Zr) O_3 perovskites. Ionics 25:1243–1257. https://doi.org/10.1007/s11581-019-02836-6

158. Poulidi D, Rivas ME, Zydorczak B, Wu Z, Li K, Metcalfe IS (2012) Electrochemical promotion of a Pt catalyst supported on $La_{0.6}Sr_{0.4}Co_{0.2}Fe_{0.8}O_{3-\delta}$ hollow fibre membranes. Solid State Ionics 225:382–385. https://doi.org/10.1016/j.ssi.2012.03.010
159. Vernoux P, Guth M, Li X (2009) Ionically conducting ceramics as alternative catalyst supports. Electrochem Solid-State Lett 12(7):E9–E11. https://doi.org/10.1149/1.3122746
160. Fortunato MA, Princivalle A, Capdeillayre C, Petigny N, Tardivat C, Guizard C, Tsampas MN, Sapountzi FM, Vernoux P (2014) Role of lattice oxygen in the propane combustion over Pt/yttria-stabilized zirconia: isotopic studies. Top Catal 57(14–16):1277–1286. https://doi.org/10.1007/s11244-014-0293-5
161. Dole HAE, Isaifan RJ, Sapountzi FM, Lizarraga L, Aubert D, Princivalle A, Vernoux P, Baranova EA (2013) Low temperature toluene oxidation over Pt nanoparticles supported on yttria stabilized-zirconia. Catal Lett 143(10):996–1002. https://doi.org/10.1007/s10562-013-1071-x
162. Isaifan R, Dole H, Obeid E, Lizarraga L, Baranova EA, Vernoux P (2019) Catalytic CO oxidation over Pt nanoparticles prepared from the polyol reduction method supported on yttria-stabilized zirconia. ECS Trans 35(28):43–57. https://doi.org/10.1149/1.3641818
163. Isaifan RJ, Dole HAE, Obeid E, Lizarraga L, Vernoux P, Baranova EA (2012) Metal-support interaction of Pt nanoparticles with ionically and non-ionically conductive supports for CO oxidation. Electrochem Solid-State Lett 15(3):E14-E17. https://doi.org/10.1149/2.024203esl
164. Isaifan RJ, Baranova EA (2015) Effect of ionically conductive supports on the catalytic activity of platinum and ruthenium nanoparticles for ethylene complete oxidation. Catal Today 241(Part A):107–113. https://doi.org/10.1016/j.cattod.2014.03.061
165. Dole HAE, Costa ACGSA, Couillard M, Baranova EA (2016) Quantifying metal support interaction in ceria-supported Pt, PtSn and Ru nanoparticles using electrochemical technique. J Catal 333:40–50. https://doi.org/10.1016/j.jcat.2015.10.015
166. Dole HAE, Baranova EA (2016) Ethylene oxidation in an oxygen-deficient environment: why ceria is an active support? ChemCatChem 8(11):1977–1986. https://doi.org/10.1002/cctc.201600142
167. Isaifan RJ, Ntais S, Couillard M, Baranova EA (2015) Size-dependent activity of Pt/yttria-stabilized zirconia catalyst for ethylene and carbon monoxide oxidation in oxygen-free gas environment. J Catal 324:32–40. https://doi.org/10.1016/j.jcat.2015.01.010
168. Yentekakis IV, Goula G, Kampouri S, Betsi-Argyropoulou I, Panagiotopoulou P, Taylor MJ, Kyriakou G, Lambert RM (2017) Ir-catalysed nitrous oxide (N_2O) decomposition: effect of Ir particle size and metal–support interactions. Catal Lett 148(1):341–347. https://doi.org/10.1007/s10562-017-2233-z
169. Goula G, Botzolaki G, Osatiashtiani A, Parlett CMA, Kyriakou G, Lambert RM, Yentekakis IV (2019) Oxidative thermal sintering and redispersion of Rh nanoparticles on supports with high oxygen ion lability. Catalysts 9(6):541 (16 pages). https://doi.org/10.3390/catal9060541
170. Wang Z, Huang H, Liu H, Zhou X (2012) Self-sustained electrochemical promotion catalysts for partial oxidation reforming of heavy hydrocarbons. Int J Hydrog Energy 37(23):17928–17935. https://doi.org/10.1016/j.ijhydene.2012.09.072
171. Zhou X, Huang H, Liu H (2013) Study of partial oxidation reforming of methane to syngas over self-sustained electrochemical promotion catalyst. Int J Hydrog Energy 38(15):6391–6396. https://doi.org/10.1016/j.ijhydene.2013.03.047
172. Hernandez WY, Hadjar A, Giroir-Fendler A, Andy P, Princivalle A, Klotz M, Marouf A, Guizard C, Tardivat C, Viazzi C, Vernoux P (2015) Electrochemically-assisted NO_x storage–reduction catalysts. Catal Today 241(Part A):143–150. https://doi.org/10.1016/j.cattod.2014.03.076

Part II
EPOC in Nano-Dispersed Catalysts

Chapter 3
The Quest of Electropromoted Nano-dispersed Catalysts

Arash Fellah Jahromi, Christopher Panaritis, and Elena A. Baranova

Abstract Electrochemical promotion of catalysis (EPOC) also known as non-Faradaic electrochemical modification of catalytic activity (NEMCA) phenomenon of nano-dispersed catalytic systems has been of paramount interest since the pioneering studies of Vayenas and co-workers in the 1980s. A typical heterogeneous catalyst consists of a nano-sized active phase dispersed on high-surface-area support. This allows decreasing the noble metal catalyst loading while considerably increasing the number of surface-active sites available for the reaction. In EPOC studies the catalyst-working electrode is often fabricated as a continuous, porous film with low dispersion; however, more and more works on the fabrication and study of EPOC with nanostructured, dispersed catalysts have emerged recently. This chapter presents a review of EPOC studies with nano-sized, electropromoted catalytic systems reported in the last decade. The first section discusses the origin of EPOC, the main parameters, and the rules. The second part provides the observation of the EPOC effect for both noble and non-noble nanoparticle catalysts. The third part examines recent advances in density functional theory (DFT) for the understanding of electrified interfaces in catalysis, followed by recent advances in self-sustained EPOC. Finally, the last section highlights the research gaps in understanding and applying electrochemically promoted nanostructured catalysts to technologically important processes.

Keywords Electrochemical promotion · NEMCA · Metal-support interaction · Nanoparticle · Heterogeneous catalysis · Nanostructured catalyst · Density functional theory

A. Fellah Jahromi · C. Panaritis · E. A. Baranova (✉)
Department of Chemical and Biological Engineering, Centre for Catalysis Research and Innovation (CCRI), University of Ottawa, Ottawa, ON, Canada
e-mail: afell085@uottawa.ca; cpana054@uottawa.ca; Elena.Baranova@uottawa.ca

P. Vernoux, C. G. Vayenas (eds.), *Recent Advances in Electrochemical Promotion of Catalysis*, Modern Aspects of Electrochemistry 61,
https://doi.org/10.1007/978-3-031-13893-5_3

Abbreviations

ALD	Atomic layer deposition
BZY	$BaZr_{0.85}Y_{0.15}O_{3-\alpha}$
DFT	Density functional theory
DLC	Diamond-like carbon
EDX	Energy-dispersive X-ray
EMF	Electromotive force
EPOC	Electrochemical promotion of catalysis
GO	Graphene oxide
LSCF/GDC	$La_{0.6}Sr_{0.4}Co_{0.2}Fe_{0.8}O_{3-\delta}/Ce_{0.9}Gd_{0.1}O_{1.95}$
LSM/GDC	$(La_{0.8}Sr_{0.2})_{0.95}\ MnO_{3-\delta}/Ce_{0.9}Gd_{0.1}O_{1.95}$
MIEC	Mixed ionic-electronic conductive
MSI	Metal-support interaction
NAS-XPS	Near-ambient pressure X-ray photoelectron spectroscopy
NEMCA	Non-Faradaic electrochemical modification of catalytic activity
NPs	Nanoparticles
P-EPOC	Permanent or persistent electrochemical promotion of catalysis
PM-IRRAS	Polarization modulation infrared reflection absorption spectroscopy
PVD	Physical vapor deposition
PVP	Polyvinylpyrrolidone
RHE	Reversible hydrogen electrode
RWGS	Reverse water-gas shift
SHE	Standard hydrogen electrode
SMSI	Strong metal-support interaction
SRM	Steam reforming of methanol
SSEP	Self-sustained electrochemical promotion
SS-EPOC	Self-sustained electrochemical promotion of catalysis
TGA	Thermogravimetric analysis
TMAOH	Tetramethylammonium hydroxide
TOF	Turnover frequency
tpb	Three-phase boundary
TPD	Temperature program desorption
VOCs	Volatile organic compounds
WGS	Water-gas shift
XAS	X-ray absorption spectroscopy
YSZ	Yttria-stabilized zirconia

3.1 Introduction to Electrochemical Promotion of Catalysis

EPOC or NEMCA phenomenon allows for in situ control of the activity and selectivity of a catalyst towards a favorable reaction rate and products in a reversible manner through the application of electric stimuli (constant current or potential)

[1]. Since the first discovery of the EPOC phenomenon by Vayenas and collaborators [1–3], well over 100 catalytic processes have been studied and demonstrated exceptional enhancement activity and selectivity [4, 5]. As selectivity and activity show a long-life trade-off in heterogeneous catalytic reactions, EPOC can be a noticeable step to resolving and aligning both parameters for reactions and catalysts [6]. To date, the application of EPOC includes, among others, environmental reactions (methane oxidation, abatement of volatile organic compounds (VOCs), and NO_x reduction) [7–11] and production of various chemicals (hydrogen, ammonia, methane, carbon monoxide, etc.) in gas and liquid phases [12–18].

The origin of EPOC is based on the action of ionic promoters' spillover and/or backspillover from the support-solid electrolyte to/away from the deposited catalyst. An electric current or potential is manipulated to control the flux of promoters onto/from the catalyst surface through the three-phase (solid electrolyte-gas) boundary. In a typical EPOC cell, the catalyst-working electrode is polarized using an inert counter electrode that results in the supply/removal of ionic promoters to/from the catalyst surface. This permits to in situ modify the work function of the metal or metal oxide catalyst and as a result its catalytic activity and, in several instances, selectivity in a sustainable and reversible manner. Several promoters have been investigated including positive promoters, e.g., alkali, H^+, and Ag^+, or negative ones, e.g., O^{2-} and F^- [14]. Yttria-stabilized zirconia (YSZ) is the popular choice of solid electrolytes among researchers due to its remarkable stability and bulk ionic conductivity of O^{2-} at temperatures as low as 300 °C [19, 20].

The main parameters to quantify the EPOC phenomenon are the apparent Faradic efficiency (Λ) (Eq. 3.1) and the rate enhancement ratio (ρ) (Eq. 3.2) [4]:

$$\Lambda = \frac{r - r_0}{I/nF} \tag{3.1}$$

$$\rho = \frac{r}{r_0} \tag{3.2}$$

where r_0 is the open-circuit (zero voltage) rate (mol s^{-1}), r is the rate of reaction (mol s^{-1}), I is the current measured across the cell (A), F is Faraday's constant (96,485 C mol^{-1}), and n is the number of electrons. Electrochemical promotion occurs when $\rho \neq 1$ and it is non-Faradic when $|\Lambda| > 1$. The apparent Faradaic efficiency could be below 1 and still indicate the EPOC effect, when the conducting ion from the solid electrolyte does not participate in the electrochemical reaction but alters the catalytic properties (i.e., catalyst work function, oxidation state, surface coverage, etc.) that lead towards the final product [4].

To investigate the behavior of a catalyst under EPOC conditions, it is important to provide information on the electronic properties of the reactants (electron donor or acceptor) [21] and the apparent orders of reaction rate. Therefore, four principal rules were defined to aid in predicting the behavior of the catalytic systems [22]. The four rules were first proposed in [4, 23, 24] and well established in [25]:

R1. Electrophobic (nucleophilic): with an increase in work function (applied potential), the reaction rate shows ascending trend.
R2. Electrophilic: reaction rate exhibits descending behavior with an increase in applied potential.
R3. Volcano-type: the variation of applied potential results in a maximum value and then decreases.
R4. Inverted-volcano type: reaction rate demonstrates a minimum value that ascends once the applied potential varies.

Studies of EPOC reversibility by Comninellis and co-workers led to the discovery of permanent or persistent electrochemical promotion of catalysis (P-EPOC) [26]. In P-EPOC, the catalytic rate after the current/potential interruption is maintained at a higher value than the original open-circuit rate (r_0). The magnitude of the current or potential and the duration of polarization strongly impact the reversibility properties of EPOC [26]. The permanent rate enhancement parameter (γ) (Eq. 3.3), analogous to the rate enhancement ratio of EPOC, is given by

$$\gamma = \frac{r_p}{r_0} \tag{3.3}$$

where r_p is the new steady-state catalytic rate (mol s^{-1}) after potential/current interruption and r_0 is the open-circuit (zero voltage) rate (mol s^{-1}) similar to Eq. (3.2) [26].

Since the year 2000, there are a number of excellent books, book chapters, and comprehensive reviews on the EPOC phenomenon that present and discuss its origin, mechanism, rules, and concept of EPOC, as well as its application to numerous catalytic reactions [14, 27–29]. In this chapter, we focus on reviewing the application of EPOC to nano-sized, highly dispersed catalytic systems published since 2010. In particular, the preparation of mono- and bimetallic nano-catalysts and their implementation into solid-state electrochemical cells for efficient polarization and promotion are discussed. A particular emphasis is made on the functional similarity between metal-support interaction (MSI), also called self-sustained EPOC (SS-EPOC or SSEP), observed between nanoparticles and ionically conductive or mixed ionic-electronic conductive (MIEC) ceramic supports and conventional EPOC phenomenon.

3.2 Electrochemical Promotion of Nanoparticle Catalysts

3.2.1 Pt-Based Nanostructured Catalyst

Nanostructured platinum has been widely investigated in EPOC studies in the last decade thanks to its excellent activity and stability in various reactions, as well as ease of Pt synthesis using various physical (sputtering, physical vapor deposition

(PVD), atomic layer deposition (ALD), etc.) and chemical (chemical vapor deposition, impregnation, polyol method, etc.) techniques. EPOC of Pt nanoparticles was studied for oxidation [30, 31], light alkane production [32, 33], oxidation of aromatic hydrocarbons, e.g., toluene [34], water-gas shift (WGS)/reverse water-gas shift reaction (RWGS) [35, 36], and alcohol synthesis [13] as well as various methane-oriented reactions [37–39].

A pioneering study that employed non-percolated Pt nanoparticles of well-defined size and dispersion was reported by the group of Comninellis and coworkers [4, 31, 39]. In these studies, CO oxidation over electropromoted Pt nanoparticles (NPs), prepared via sputtering deposition, has been studied focusing on fundamental concepts, metal characteristics, supports, and the mode of polarization (bipolar and monopolar) [31, 39]. Pt nanoparticles of the controlled size and size distribution were investigated in the bipolar cell configuration on YSZ (1.7×10^9 Pt particles per cm^2) for CO oxidation at 300 °C [39]. A quantifying method was proposed to distinguish classical electrochemical promotion (EP) from bipolar electrochemical promotion with the aid of isotopically labeled oxygen [39]. Two stages of polarization in the absence and presence of reactive gas were presented. In the absence of reactive gas, only large particles were polarized, whereas increasing the current led to the polarization of smaller particles. With the presence of reactive gas, an equivalent number of completely galvanized cells (n_{cell}) increased and resulted in a boost of the enhancement ratio, as well as CO_2 formation (as indicated by $C^{16}O_2$ and $C^{16}O^{18}O$). However, a considerable difference was observed between the Faradaic efficiency, Eq. (3.2) ($\Lambda = 1.8$) [4], and the modified bipolar efficiency ($\Lambda = 0.086$), where no electrochemical promotion occurs [39]. This behavior was due to nonuniform current distribution and the presence of high local current densities.

Furthermore, Pt nanoparticles of 40 nm average size (1.7×10^9 particles per cm^2 of YSZ) were investigated for CO oxidation [31] where comblike gold electrodes served as a strong electrical field (27,000 Vm^{-1}) at 1μA to polarize Pt nanoparticles. Pt NPs were prepared using sputter deposition following calcination at 700 °C for 4 h. Although only 5% of the active surface area was covered by Pt, the bipolar electrochemical promotion resulted in an enhancement ratio of 500, and operando tuning of catalytic activity was observed at a low current of 0.1μA. As the relaxation step upon current interruption was slow (shown as a slow decrease in the $C^{16}O_2$ and $C^{16}O^{18}O$ formation rate), the electrochemical promotion was determined as a persistent P-EPOC effect [40] where ^{16}O species were stored on the surface as Pt-oxide (PtO_x). Once polarization was relaxed, the stored oxygen species were made available as sacrificial promoters for the reaction [41].

Another significant EPOC breakthrough using highly dispersed Pt NPs catalyst was reported by the group of Vernoux [42]. Pt NPs prepared via wet impregnation on porous $La_{0.6}Sr_{0.4}Co_{0.2}Fe_{0.8}O_{3-\delta}$-$Ce_{0.9}Gd_{0.1}O_{1.95}$ (Pt/LSCF/GDC) were investigated for deep oxidation of propane at low temperatures (267–338 °C) with maximum promotion parameters of $\rho = 1.38$ and $\Lambda = 85$ [42]. The particle size of Pt NPs was in the range of 3 to 20 nm with 15% dispersion. Pt/LSCF/GDC resulted in a remarkable decrease in activation temperature of propane oxidation from 350 °C

to 250 °C in comparison to bare LSCF/GDC. An increase in partial pressure of C_3H_8 from 2200 ppm to 3880 ppm (keeping $P_{O2} = 2.2\%$) resulted in an open-circuit rate enhancement from 2.7×10^{-8} to 19×10^{-8} mol O s^{-1} (or 56%) but only a slight variation in the open-circuit potential (ΔV_{WR}) from −85 to −73 mV in disagreement with solid electrolyte potentiometry (SEP) [43]. The authors concluded that measured potentials and currents for the Pt/LSCF/GDC film corresponded to the electrochemical properties of the LSCF/GDC MIEC layer and not to the Pt NP activity. Under polarization ($I = +200\mu A$), the rate enhancement ratio showed two peaks at 267 °C (Fig. 3.1 (bottom)), while at higher temperatures, one peak was observed. Such results are explained by the low conductivity of LSCF/GDC at relatively low temperatures, which requires time to delocalize the current onto the overall layer of the working electrode. Equally important, the gradual delocalization acts as a proof for homogeneous dispersion of Pt NPs into the LSF/GDF phase.

One of the pioneer studies of active support and EPOC was conducted by the same research group [44]. The authors carried out an investigation of the reaction mechanism of propane combustion over Pt nanoparticles, synthesized with wet impregnation, on YSZ, SiO_2, and ZrO_2. The contribution of the lattice oxygen was investigated using $^{18}O_2$ temperature-programmed desorption (TPD) for all described catalytic systems. Pt deposited on YSZ demonstrated the oxidation of propane by lattice oxygen from YSZ. The strong interaction of nanoparticles and support promoted the state of the catalyst in agreement with the EPOC mechanism.

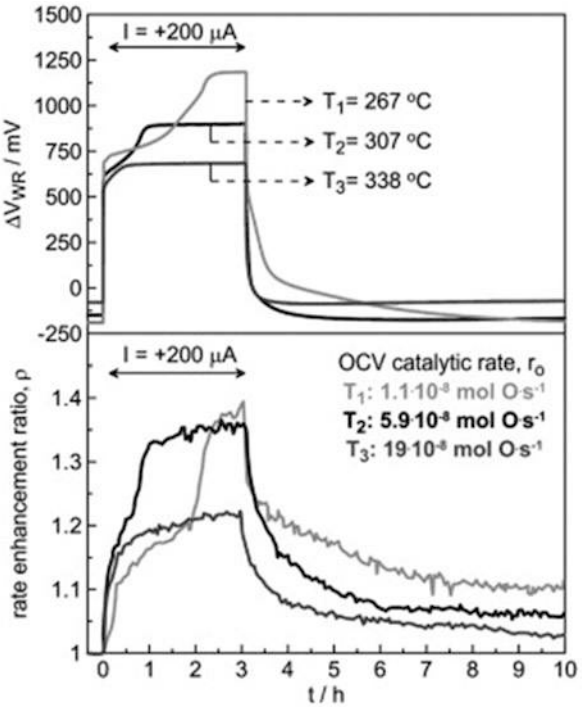

Fig. 3.1 Variation of potential (top) and enhancement ratio (bottom) upon the application of + 200μA at three distinct temperature: $T_1 = 267$ °C, $T_2 = 307$ °C, and $T_3 = 338$ °C. Reactant partial pressure: C_3H_8/O_2: 3880 ppm/2.2%. (Reprinted with permission from Ref. [42], Copyright 2012, Elsevier)

Methanol conversion to hydrogen through steam reforming and partial oxidation was studied using electropromoted nano-dispersed Pt catalysts, deposited by the filter cathodic arc deposition technique [13]. The dispersed Pt NPs (3 nm average size) over diamond-like carbon (Pt-DLC) were deposited on K-β''-Al_2O_3 solid electrolyte. The resulting Pt-DLC underwent high-temperature pre-treatment to attain desirable electrical conductivity. The conductivity increase was confirmed by the scanning transmission microscopy (STEM) and electron energy-loss spectroscopy (EELS) techniques, where the transition from sp^3 carbon into sp^2-hybridized graphitic carbon was observed. The maximum enhancement ratio of 2.5 and 3.5 times was attained under partial oxidation of methanol and steam reforming of methanol (SRM) reactions as a function of H_2 production rate, respectively. The observed steam reforming results were due to the formation of bicarbonate and potassium carbonate promoting species that were also observed using dense Pt films [45]. A comparative study between Pt-DLC catalyst films and pure dense Pt demonstrated that a higher activity was obtained for Pt-DLC due to a lower Pt particle size (3 nm). The maximum enhancement ratio of H_2 for the steam reforming reaction was $\rho = 3.4$ at 360 °C and for partial oxidation was $\rho = 2.5$ at 280 °C. In other studies by de Lucas-Consuegra *et al.*, H_2 production was enhanced 5-fold over dense Pt film [46] for SRM and 6-fold for partial oxidation [45] of methanol using the same NEMCA cell as in [13].

The application of novel techniques for nanoparticle synthesis is important from a fundamental and practical point of view. ALD technique fabricates well-defined nanoparticles and nano-layers. Pt NPs (6.5 nm) were deposited by the ALD on a porous composite backbone fabricated by $(La_{0.8}Sr_{0.2})_{0.95}MnO_{3-\delta}/Ce_{0.9}Gd_{0.1}O_{1.95}$ (LSM/GDC) inspired from solid oxide electrolyte cells (SOEC) [47]. The Pt NPs on LSM/GDC led to a 27% to 33% increase in the catalytic rate (i.e., $\rho = 1.27–1.33$) with respect to the open-circuit and resulted in an apparent Faradaic efficiency between 1000% and 3860% at 300 °C for C_3H_8 oxidation. Long-term stability of 13 h of continuous polarization (100μA) led to a marginal decrease of 5×10^{-10} mol s^{-1} in CO_2 production, signifying a stable conversion. The authors concluded that the catalyst agglomerated at higher temperatures (425 °C) and was in a stable active state [47].

The functional similarity between EPOC and MSI was investigated using Pt and RuO_2 NPs (~2 nm average diameter) for complete ethylene oxidation [48]. The authors synthesized Pt and RuO_x NPs using the polyol reduction method [49] and deposited them directly on the YSZ solid electrolyte disk resulting in free-standing NPs. In addition, the same NPs were dispersed (1 wt.%) on CeO_2, TiO_2, and YSZ powder supports [48] resulting in supported NPs. The closed-circuit reaction rate increased with anodic current (Fig. 3.2a). In addition, the relaxation time (τ), i.e., the time required to reach 63% of steady-state reaction rate under closed-circuit, decreased as a function of current, e.g., 100μA ($\tau = 1.5$ min) and 15μA ($\tau = 5$ min). The enhancement ratio of 1.7 and apparent Faradaic efficiency of 90 were reported for free-standing Pt NPs in this study (Fig. 3.2b).

Only free-standing Pt and RuO_x NPs were electrochemically promoted (Fig. 3.3), while the supported catalysts were already in the promoted MSI state. Figure 3.3

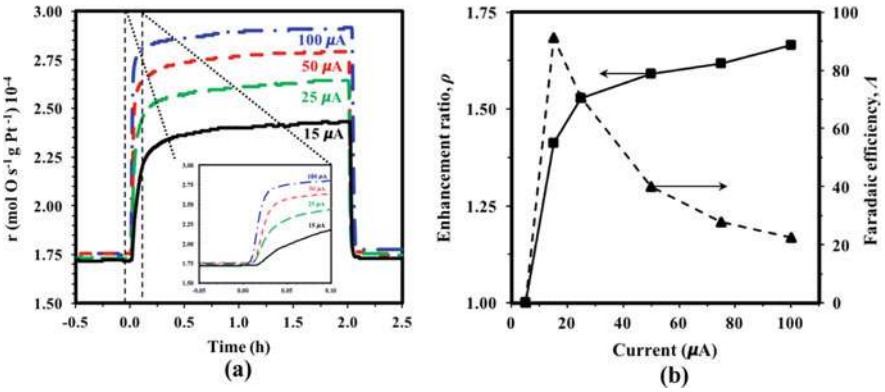

Fig. 3.2 (**a**) Transient rate response of Pt NPs under constant current; (**b**) variation of enhancement ratio ρ and apparent Faradaic efficiency Λ upon applying similar constant current denoted in (**a**). $T = 350$ °C, 3 kPa of O_2 and 0.012 kPa of C_2H_4, flow rate of 100 mL min^{-1}. (Reprinted with permission from Ref. [48], Copyright 2017, Elsevier)

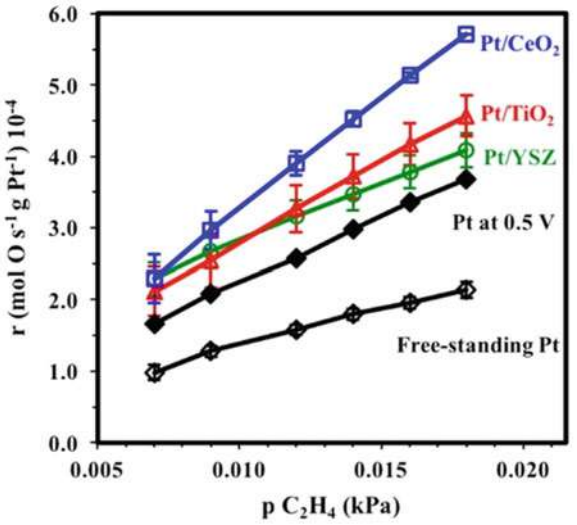

Fig. 3.3 Catalytic rate vs. partial pressure of C_2H_4 for: Pt-based NPs (free-standing and supported). Experimental conditions: $T = 350$ °C, 3 kPa of O_2 and various partial pressures of C_2H_4 as indicated in the figure, and flow rate of 100 mL min^{-1}. (Reprinted with permission from Ref. [48], Copyright 2019, Elsevier)

shows that the specific reaction rate increased with increasing C_2H_4 partial pressure for all Pt catalysts, where the reaction rate of unpromoted free-standing Pt NPs was the lowest and increased significantly under polarization or by interfacing Pt with active ionic ceramic supports. A comparable degree of promotion was achieved under open-circuit conditions for dispersed Pt NPs on CeO_2, TiO_2, and YSZ supports and EPOC of free-standing Pt NPs. These findings further confirmed the functional equivalence of EPOC and MSI with highly dispersed Pt NPs.

Therefore, the synthesis and application of size-controlled mono- and bimetallic NPs for electrochemical promotion studies in the last decade led to the advancement and better understanding of the MSI phenomenon, in particular, the MSI mechanism with ionically and mixed ionic-electronic conducting supports that will be discussed later in Sect. 4 [5]. The summary of EPOC studies with Pt NPs is shown in Table 3.1.

3.2.1.1 Pd-Based Nanostructured Catalyst

Palladium (Pd) has been widely studied for catalytic reaction development, particularly for energy and environmental application. Pd is the most active metal for the complete oxidation of methane in conventional heterogeneous catalysis and in EPOC studies [4, 52–56]. Recently, EPOC of nanostructured Pd films [37] deposited inside a monolith honeycomb (600 channels) YSZ (8 mol% Y_2O_3) solid electrolyte was reported for deep methane oxidation. Pd NPs were deposited into the YSZ monolith via the electroless plating technique reported earlier [50]. A maximum electrochemical promotion of Pd/YSZ under oxidizing conditions of CH_4/O_2: 2%/10% and under −2 V resulted in $\Lambda = 47$ at 400 °C. In this study, electrochemical promotion was observed at both negative and positive potentials [52].

In the work of Matei et al. [51], Pd NPs (8 nm average size) were prepared by the impregnation method on YSZ solid electrolyte of different porosity for complete methane oxidation. The authors demonstrated that a more porous YSZ increased the activity of Pd towards methane combustion due to a 4.5-time increase in the catalyst dispersion when compared with dense YSZ [51]. The porosity of the support impacted the transformation between metallic Pd and more active PdO_x. Another study [9] reported EPOC of Pd NPs synthesized via polyol method (average particle size of 5–35 nm) and deposited on YSZ for methane oxidation. Both positive and negative polarization at relatively low temperatures (340 °C) resulted in the reaction rate increase. Enhancement under negative polarization was explained by competitive adsorption of CH_4 and O_2 under stoichiometric, reducing, and oxidizing conditions. This competitive adsorption was mechanistically explained by the formation of PdO_x which can be limited at low O_2 partial pressure (<5 kPa). Higher oxygen partial pressure resulted in the full coverage of the catalyst surface and blockage of CH_4 adsorption sites leading to a decrease in the reaction rate.

Zagoraios et al. [52] evaluated EPOC of Pd/Co_3O_4 nanoparticles (4 nm average size) prepared by the polyol method for complete methane oxidation. To this end, Pd colloidal NPs were dispersed on commercial porous Co_3O_4 semiconductor powder and deposited on YSZ solid electrolyte disk. Pd/Co_3O_4 was compared to a Pd thin film (1.5 mg cm^{-2}) prepared using Pd commercial paste (Engelhard A1121). The open-circuit catalytic activity for Pd/Co_3O_4 was 12 times higher than the Pd film. Under anodic polarization, the catalytic rate of the Pd film increased 12-fold, while for Pd/Co_3O_4, the catalytic rate increased 2-fold. Pd/Co_3O_4 required half the time to reach a promoted state over the Pd film, due to the shorter diffusion path over the nanoparticles. Even though the Pd film experienced a higher electrochemical promotion effect, the overall catalytic activity for Pd/Co_3O_4 outperformed Pd film. Pd

Table 3.1 Examples of nano-dispersed electropromoted Pt catalysts

Catalyst	Synthesis or deposition method	Reaction	Electrolyte	Reactants	ρ	Λ	Total flow and/or reactant mixture	T (°C)	Ref. and year
Pt	Sputtering	CO oxidation	YSZ	CO, O_2	≤ 2	1.8	High vacuum	300	[39], 2010
Pt	Sputtering	CO oxidation	YSZ	CO, O_2	500	1.5	High vacuum	300	[31], 2011
Pt	Wet impregnation	C_3H_8 oxidation	LSCF/GDC	C_3H_8, O_2	1.38	85	C_3H_8/O_2: 2200 ppm and 3880 ppm/2.2%	267–338	[42], 2012
Pt	Filter cathodic arc deposition technique	CH_3OH steam reforming (SR) and partial oxidation (POX)	K–$\beta''Al_2O_3$	CH_3OH, O_2; CH_3OH, H_2O	SR: 3.4 @ 360 °C; POX: 2.5 @ 280 °C	–	6 L. h^{-1} CH_3OH/H_2O: 4%/4.8%; CH_3OH/O_2: 11%/0.9%	250–360	[13], 2013
Pt	Wet impregnation	C_3H_8 combustion	YSZ; SiO_2; ZrO_2	C_3H_8, O_2	–	–	1.8 L. h^{-1}	25–600	[44], 2014
Pt	Atomic layer deposition	C_3H_8 oxidation	LSM/GDC	C_3H_8, O_2	1.27–1.33	10–38.6	6 L. h^{-1} P_{C3H8}/P_{O2}: 0.22 kPa/2.2 kPa	300	[47], 2017
Pt	Polyol reduction	C_2H_4 oxidation	YSZ	C_2H_4, O_2	1.8	23	6 L. h^{-1} P_{C2H4}/PO_2: 0.012 kPa/3 kPa	350	[48], 2017

nanoparticles deposited on Co_3O_4 powder resulted in an MSI which enhanced the catalytic properties of Pd/Co_3O_4 by cycling oxygen during open-circuit conditions and directing oxygen and electrons under polarization.

Persistent EPOC (P-EPOC) was observed during methane oxidation over Pd NPs (5 nm average size), synthesized using the polyol method [53]. EPOC of Pd NPs on YSZ solid electrolyte showed an electrophobic behavior with an apparent Faradaic efficiency of 3000 (at $I = 1\mu A$) and a maximum rate enhancement ratio of $\rho = 2.7$ under a 2 kPa and 4 kPa gas composition of CH_4 and O_2, respectively (Fig. 3.4). The degree of p-EPOC increased with polarization time due to the continuous increase in the amount of O^{2-} stored in the PdO_x active phase [53]. The relationship between the duration of polarization and the time required to obtain the initial value of the open-circuit rate is shown in Fig. 3.4a (insert) with a slope of 0.5, along with the corresponding current (Fig. 3.4b). Thus, p-EPOC occurred due to the stored oxygen ions in PdO_x that acted as sacrificial promoters when polarization was interrupted.

Bimetallic nano-sized catalysts have attracted considerable attention, to achieve bi-functionality to increase and/or stabilize the catalytic activity and reduce the amount of noble metals [54, 55]. EPOC of the bimetallic Ni9Pd (90:10 at% of Ni to Pd) nanoparticles was studied for the complete oxidation of methane [54]. The Ni9Pd NPs were synthesized using a modified polyol method and deposited on the YSZ disk. The resulting structure of NPs was a core double-shell with Pd located at the core, Ni as the inner shell, and a second 3- to 4-nm-thick Pd outer shell (Fig. 3.5) [54]. Such a structure significantly enhanced the catalytic activity and stability under open-circuit when compared with monometallic Ni and Pd. The EPOC was observed under positive polarization in a reversible and controllable manner that increased the reaction rate by 240% ($\rho = 2.4$) at 425 °C (Fig. 3.6a). The highest promotion was attained under fuel-rich conditions if compared to fuel-lean and stochiometric gas composition. This catalytic system met economic and performance criteria, where

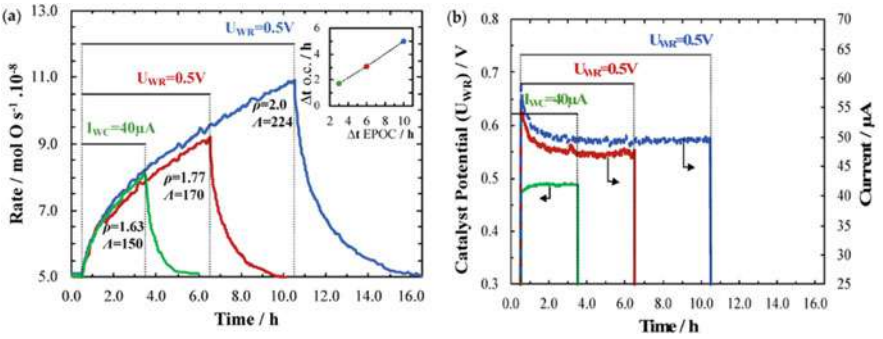

Fig. 3.4 (**a**) Transient rate response of Pd/YSZ polarized for 3.5 h, 6.5 h, and 10.5 h. Insert in (**a**) time after polarization to reach the initial open-circuit as a function of polarization time; (**b**) corresponding potential/current recorded at potentiostatic or galvanostatic application. Conditions: $T = 425$ °C, 2 kPa of CH_4 and 4 kPa of O_2, and flow rate of 100 mL min^{-1}. (Reprinted under an open access Creative Common CC BY license from Ref. [53], Copyright 2019, Molecular Diversity Preservation International)

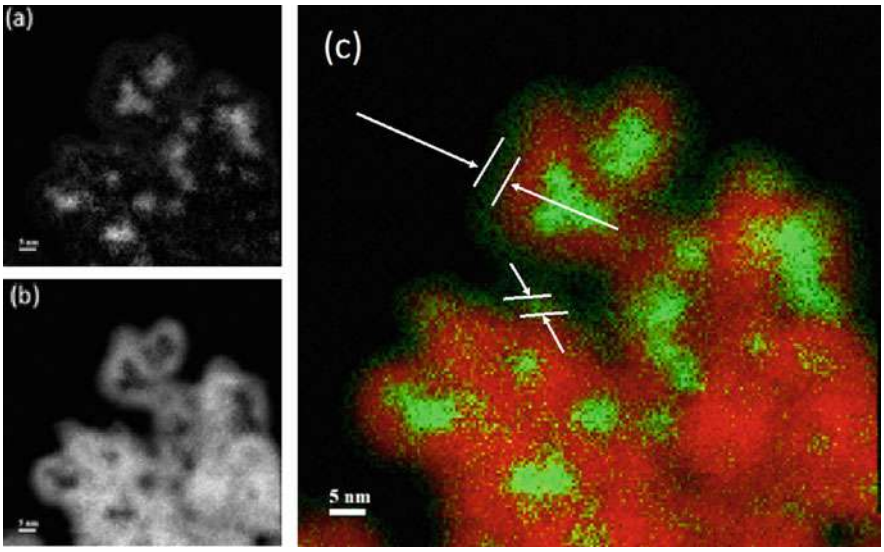

Fig. 3.5 HAADF STEM-EELS and element mapping under different signal range showing (**a**) Pd at signal range: 364.3–468.0 eV, (**b**) Ni at signal range: 848.0–885.8 eV and (**c**) illustration of double-shell structure (colored coded map) with Pd (green) as the core, Ni (red) inner shell, and Pd outer shell with average particle size of 3–4 nm. (Reprinted with permission from Ref. [54], Copyright 2019, Elsevier)

the costly Pd phase was minimized while maintaining the high active surface area and synergistic interaction between Ni and Pd. A maximum rate enhancement ratio and Faradaic efficiency of 1.3 and 39, respectively, occurred at $U_{WR} = 0.25$ V and P_{O2}/P_{CH4} ratio of 0.1 (Fig. 3.6b).

Electrochemical promotion of Pd was also investigated for CO_2 hydrogenation [56] and electrochemical CO_2 reduction reactions [57] with the goal of waste carbon dioxide utilization and transformation to useful chemicals, such as CO [56], formate [57], or methane [58]. CO_2 hydrogenation reaction pathways vary over different catalysts under atmospheric pressure, such as RWGS, methanation, or conversion to formate in aqueous media [57]. CO_2 hydrogenation was studied by Bebelis *et al.* over a thin-film coating of Pd (A1122 Engelhard Pd paste) on solid electrolytes YSZ and Na-$\beta''Al_2O_3$ [56]. Only the RWGS reaction was observed at 533 °C and 605 °C for a CO_2/H_2 ratio of 1:2.3. For Pd/YSZ, the RWGS was enhanced under anodic and cathodic polarization indicating an "inverted-volcano" behavior. For Pd/β''-Al_2O_3, the RWGS rate increased under negative polarization where Na^+ is supplied to the gas-exposed catalyst surface resulting in a 6-time rate increase. This behavior is explained by the coverage increase of the Na positive promoter and simultaneous drop of the catalyst work function. Consequently, the CO_2 adsorption was enhanced leading to an increase in the CO formation rate.

Electrochemical promotion of Pd NPs for CO_2 electroreduction in an aqueous 1 M $KHCO_3$ solution saturated with H_2/CO_2 was reported recently [57]. The Pd NPs

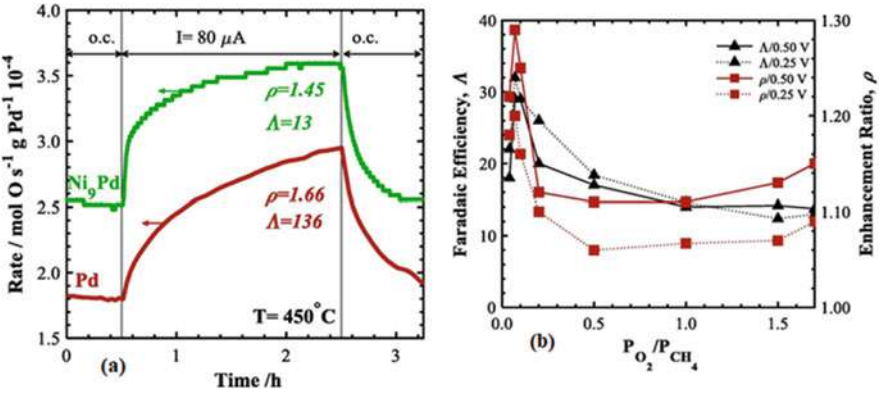

Fig. 3.6 (**a**) Catalytic rate response of Pd and Ni9Pd upon the application of $I = 80\mu A$. Experimental condition: $T = 450\ ^{\circ}C$, $P_{CH4} = 2$ kPa, $P_{O2} = 4$ kPa, and He balanced. (**b**) Enhancement ratio and apparent Faradaic efficiency obtained for Ni9Pd as a function of step change of U_{WR} to 0.25 V and 0.5 V, respectively. Experimental conditions: $T = 450\ ^{\circ}C$, $P_{CH4} = 10$ kPa, and a variable P_{O2}/P_{CH4} ratio. (Reprinted with permission from Ref. [54], Copyright 2019, Elsevier)

with an average particle size of 3.7 nm were synthesized using the sodium borohydride reduction method. The catalyst layer was composed of a catalyst ink of Pd/C and Nafion ionomer deposited on carbon paper (Toray TGP-H-060). The experiments were carried out in an H-type electrochemical cell (Fig. 3.7a) under ambient temperature. Working and counter electrode cell compartments were separated by a Nafion 115 membrane. Both electrochemical and catalytic reduction of CO_2 took place over Pd/C. Electrochemical promotion of Pd/C catalyst under negative polarization (in the range of −0.1 and −0.4 vs. RHE) showed that the formate production rate increased between 10 and 143 times depending on the Pd particle size and applied potential (Fig. 3.7b). Electrochemical polarization activated H_2 from the electrolyte solution and stabilized the active phase of PdH_x to promote catalytic CO_2 reduction. Authors suggested that electrocatalytic and catalytic reduction of CO_2 shared the same $HCOO^*$ intermediate that resulted in formate rate increase [57]. The reaction mechanism was explained by the weakening of the hydrogen adsorption bond on PdH_x under negative polarization, at an optimal value of −0.2 V with respect to the maximum enhancement ratio. The relationship between NP size and enhancement ratio is illustrated in Fig. 3.7b [57]. Decreasing the particle size increased the enhancement ratio for all applied potentials.

In a recent work [59], catalytic non-Faradaic CO_2 hydrogenation to formate in aqueous media was significantly enhanced via polarization. The reaction rate of formate production increased by three orders of magnitude due to local pH changes under polarization. Small polarization affected a nonequilibrium local environment in the vicinity of the electrode, leading to a coexistence of high alkalinity and high CO_2 concentration. The local pH changes were different from the electrolyte bulk, where alkalinity and CO_2 concentration were inversely correlated. These early works on CO_2 hydrogenation in aqueous media [57, 59] show a significant potential of the

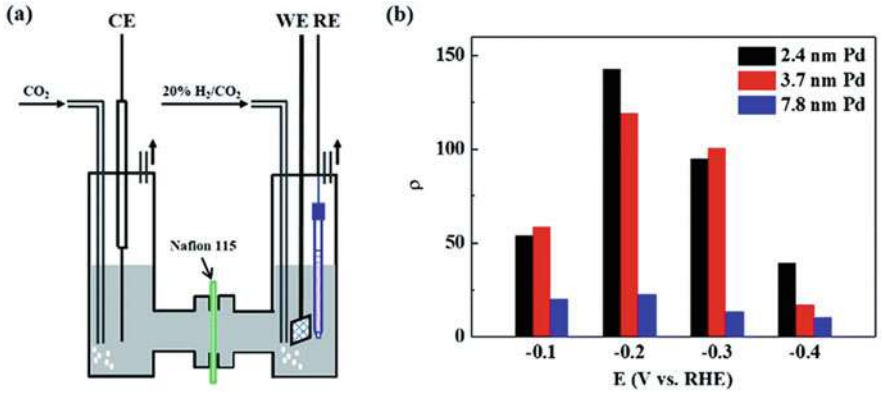

Fig. 3.7 (**a**) Schematic of the H-cell for CO_2 reduction. (**b**) Rate enhancement ratios for formate production at different negative potentials for Pd NPs with an average size of 2.4 nm, 3.7 nm, and 7.8 nm in 20% H_2/CO_2-saturated 1 M $KHCO_3$ solution under ambient temperature. (Reprinted from Ref. [57] licensed under a Creative Commons Attribution 3.0 Unported License (materials can be used without requesting further permissions); Copyright 2017, The Royal Society of Chemistry)

EPOC phenomenon for the field of CO_2 conversion and utilization not only in the gas phase but also in liquid-phase catalytic reactions in combination with electrocatalysis. Table 3.2 shows the summary of some examples of electropromoted Pd NPs catalysts that were discussed in Sect. 3.2.2.

3.2.2 Ru-Based Nanostructured Catalyst

Free-standing RuO_2 nanoparticles (0.8 nm average size) deposited on YSZ solid-electrolyte were studied for the complete ethylene oxidation [61]. The catalyst was evaluated experimentally and theoretically, using DFT calculations to provide an atomistic understanding of the role of O^{2-} in promoting RuO_2. Free-standing RuO_2 nanoparticles [62] were synthesized through the polyol method using tetramethylammonium hydroxide (TMAOH) to adjust the pH. Under reaction conditions ($P_{C2H4} = 0.012$ kP and $P_{O2} = 3$ kPa), the CO_2 rate increased under both positive and negative polarization or otherwise followed an inverted-volcano EPOC behavior (Fig. 3.8a, b). Theoretically, RuO_x structures were examined as a function of potential and oxygen coverage, correlated to the experimental data. The DFT part of this work is discussed in detail in Sect. 3.3.

Ruthenium is active for CO_2 hydrogenation reactions because it can activate CO_2 and H_2, to produce CH_4 and CO through the methanation and RWGS, respectively. Kotsiras *et al.* [63] studied nano-dispersed Ru-Co nanoparticles (6–8 nm) deposited on an interlayer Ru film (2.1 mg cm^{-2}) on the proton conductor (H^+) barium zirconia yttria-doped (BZY, $BaZr_{0.85}Y_{0.15}O_{3-\alpha}$ + 1 wt% NiO) solid electrolyte for CO_2 hydrogenation [63]. The Ru-Co nanoparticles were synthesized on BZY powder

Table 3.2 Examples of nano-dispersed electropromoted Pd catalysts

Catalyst	Synthesis or deposition method	Reaction	Electrolyte	Reactants	ρ	Λ	Total flow and/or reactant mixture	T (°C)	Ref. and year
Pd	Impregnation	CH_4 oxidation	Porous YSZ	CH_4, O_2	1.2 @ 400 °C	6 @ 400 °C	6 L. h^{-1} P_{CH4}/PO_2: 1.3 kPa/4.5 kPa	350–430	[51], 2013
Pd	Wet impregnation	CH_4 oxidation	YSZ	CH_4, O_2	5	~32	3 L. h^{-1} P_{CH4}/PO_2: 1 kPa/5 kPa	340	[9], 2018
Pd	Polyol reduction	Complete methane oxidation	YSZ	CH_4, O_2	2.7	3000	6 L. h^{-1} PCH_4/PO_2: 2 kPa/4 kPa	425	[53], 2019
Ni9Pd	Modified polyol	Complete methane oxidation	YSZ	CH_4, O_2	2.4	25	P_{CH4}/PO_2: 10 kPa/1 kPa	425	[54], 2019
Pd	Thin coating	RWGS	YSZ; Na–β″Al_2O_3	CO_2, H_2	YSZ: 6.1 @ Na–β Al_2O_3: 6.7 @ 605 °C	–	P_{CO2}/P_{H2}: 2.1–3.5	533–605	[56], 2008
Pd	Sodium borohydride reduction	CO_2 reduction (aq. rxn.) to formate	1 M $KHCO_3$	CO_2, H_2	10–143	–	20% H_2/CO_2 saturated	Ambient	[57], 2017
Pd	Pre-fabricated Pd/C (fuel cell store [60])	CO_2 hydrogenation to formate	50 mM $KHCO_3$/0.5 M $NaClO_4$	CO_2, H_2	3	–	H_2/CO_2: 20%/80%	Ambient (24 ± 1)	[59], 2020

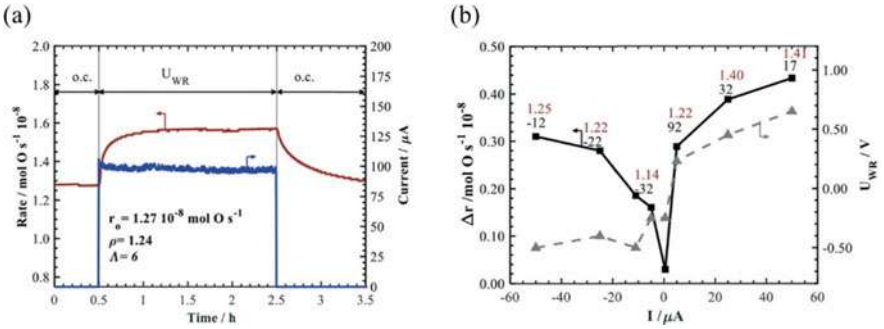

Fig. 3.8 Transient reaction rate response of free-standing RuO_2 nanoparticles (**a**) under $U_{WR} = 1$ V and (**b**) summary of the rate enhancement ratio as a function of potential. Experimental conditions: $T = 350$ °C, $P_{C2H4} = 0.012$ kPa, $P_{O2} = 3$ kPa, and total flow rate = 100 mL min^{-1}. (Reprinted with permission from Ref. [61], Copyright 2020, Elsevier)

via the wet impregnation method. The interlayer Ru film was used to disperse the Ru-Co nanoparticles, ensuring electrical contact and closing the circuit. The selectivity to CO was 84% due to the spontaneous migration of protons backspilling over on Ru-Co at 450 °C and CO_2/H_2 ratio of 1:7. Under 1.5 V the Ru-Co/BZY/Ru deposited on BZY solid- electrolyte promoted the methanation rate ($\rho = 2.7$) and suppressed the CO rate ($\rho = 0.8$) while under −1.5 V promoted the methanation ($\rho = 1.1$) and CO rate ($\rho = 1.05$).

In another study [16, 62], RuO_2 nanoparticles (0.8 nm average size) were deposited on YSZ and BZY solid electrolytes and evaluated for the CO_2 hydrogenation reaction in the temperature range of 250 °C to 400 °C. Under open-circuit conditions and a CO_2/H_2 ratio of 1:7, Ru nanoparticles were selective to CO (>75%) over CH_4, which was assigned to the small size of the nanoparticles and high dispersion on the solid electrolyte. Positive polarization increased the CH_4 production rate ($\rho = 1.8$ and 1.5 for YSZ and BZY, respectively) and suppressed CO formation. Negative polarization decreased the CH_4 rate and minimally affected the CO rate. The same electrochemical behavior was observed regardless of the type of solid electrolyte and followed the same results when a Ru film of 3μm was deposited on YSZ, BZY, Na-Al_2O_3, and K-Al_2O_3 solid electrolytes [63–66].

3.2.2.1 Rh-Based Nanostructured Catalyst

The first EPOC studies of the rhodium (Rh) nanostructured catalyst electrode for ethylene complete oxidation were reported in the early 2000s [67–69]. Recently, an elegant work by Katsaounis et al. [70] reported a fundamental study on the dependency of the Rh oxidation state and its stability under polarization using near-ambient pressure X-ray photoelectron spectroscopy (NAP-XPS). To this end, a Rh nano-film (thickness of <40 nm) catalyst was sputtered on a YSZ solid electrolyte (Rh/YSZ) using DC magnetron sputtering. NAS-XPS results revealed that the

supply of oxygen ions onto the pre-oxidized Rh surface promotes the shift to a metallic state by facilitating the reduction of the Rh surface under C_2H_4. Thus, a Rh oxide layer (RhO_x, $x < 2$) is present and stabilized under certain experimental conditions.

Closed-circuit results were examined at a potential difference of 1.5 V between the Rh catalyst-working electrode and counter electrode and continuous current flow. The mixture ratio (oxidizing, stoichiometric, and reducing) versus the current reveals that the stoichiometric ratio ($C_2H_4/O_2 = 0.33$) secured the maximum value of current (+100μA) as the optimal partial oxide layer was formed. Under reducing conditions ($C_2H_4/O_2 > 0.33$), the current decreased. Thus, RhO_x surface films can be stabilized under mild reducing and stoichiometric mixtures. This study provided spectrometric evidence to support the contribution of anodic polarization on the pre-oxidized Rh surface and the alteration of surface oxidation and subsequent reduction step from RhO_x to Rh metallic. This observation is in line with the sacrificial promoting ion model for EPOC and MSI [4, 71, 72].

3.2.2.2 Au-, Ag-, and Cu-Based Nanostructured Catalyst

Gold (Au)-based catalysts were disregarded for many years since they were viewed as inert and inactive in heterogeneous catalysis and in EPOC application. Haruta et al. [73–75] demonstrated that Au is active in the nanoparticle range (≤10 nm). In recent years, several studies on the electrochemical promotion of Au NPs have been reported [79–82]. González-Cobos et al. [76] promoted Au nanoparticles towards the partial oxidation of methanol. The catalytic system consisted of a 7% atomic weight of Au (3.3 nm, synthesized via magnetron sputtering) supported on a thin film (170 nm) of YSZ. Then, the Au-YSZ catalyst was deposited on the K-β″Al_2O_3 solid electrolyte. Catalytic measurements were conducted under $CH_3OH/O_2 = 5.9\%/0.43\%$ at 280 °C. Au nanoparticles resulted in a promising selectivity towards methyl formate ($HCOOCH_3$) and H_2 with a five- and nine-fold increase in production rate with respect to open-circuit conditions, respectively [77–79]. Analysis of the results revealed that the observed EPOC effect was only sensitive to the rate of K^+ supply and coverage. The optimal promoter coverage was 0.5 at 280 °C and $V_{WR} \leq -0.5$ V and resulted in an enhancement ratio of 9, 2, and 5 for H_2, CO_2, and $HCOOCH_3$ production, respectively.

Silver (Ag)-based catalysts have been widely used to study the EPOC effect since its discovery and in recent studies [80]. Ag nanoparticles deposited via evaporative PVD on a YSZ solid electrolyte were characterized through cyclic voltammetry to study the growth of silver oxides in the vicinity of the three-phase boundary. The results demonstrated that both anodic and cathodic polarization affected the oxidation state of Ag, where anodic polarization contributed to the formation of Ag_2O over metallic Ag [81]. Kalaitzidou et al. developed an Ag-coating film (10–25μm thickness) electrochemical cell using the screen-printing deposition on YSZ to study the EPOC effect of propylene combustion [82]. The authors showed that high catalytic activity towards propylene conversion is attainable under the high coverage

of propylene and oxygen over the surface of the catalyst-working electrode (Ag). The highest enhancement ratio ($\rho = 1.34$) was obtained by applying +25μA under lean-burn conditions, whereas stoichiometric conditions gave the highest enhancement ratio equal to 1.03 under +2μA polarization. The promotion was amplified under lean-burn (oxidizing atmosphere) conditions. This technology can aid in the abatement of propylene from the air.

Table 3.3 summarizes EPOC studies with Ru-, Rh-, Au-, and Ag-based nanoparticles for various catalytic processes.

Copper is an economic option in comparison with noble metals such as Pt, Rh, Pd, and Ru and can be an attractive catalytic system in EPOC studies. González-Cobos et al. [83] studied the electrochemical promotion of Cu deposited on K-β″Al_2O_3 for the partial oxidation of methanol to produce H_2 at a relatively low temperature of 320 °C. Nanostructured Cu was prepared via oblique angle physical vapor deposition with a thickness of ~0.8μm, a porosity of ~50 nm, and a nanocolumn cross-sectional diameter of 120 nm. The applied polarization ($I < 0$ and $V_{WR} = 0$ with $V_{ocp} \leq +0.5$ V) resulted in a remarkable enhancement in catalytic activity and a subsequent three-fold increase in production rates of methyl formate ($C_2H_2O_2$) and H_2 ($\rho_{max} = 2.7$ for $C_2H_2O_2$, $\rho_{max} = 2.63$ for H_2). The work function of Cu decreased due to the migration of positive promoters (K^+) and enhanced the reaction. These species altered the chemisorption of the O_2 molecules (electron acceptor) in a favorable manner upon the consumption of CH_3OH. The post-mortem energy-dispersive X-ray (EDX) and XPS characterization determined that the electropromoted state caused the formation of potassium-derived by-products (K_xO_y and/or carbonates).

In another study, Ruiz et al. [84] conducted a bench-scale study on CO_2 hydrogenation over Cu nanoparticles deposited on K-β″Al_2O_3 solid electrolyte. Cu nanoparticles with an average diameter of 23 nm were deposited on K-β″Al_2O_3 using electroless deposition. The reactant ratio of H_2/CO_2 was modified to 2, 3, and 4 based on post-combustion CO_2 capture exit streams to investigate the practical application and scalability of the process. The results revealed that the determining parameter to control selectivity was affiliated to Cu^+ ions and large Cu particles that were selective towards CH_3OH and an unconventional selectivity to CH_4 and CO. Selectivity values of C_2H_6O, CH_3OH, and C_2H_5OH were boosted by a maximum of 34%, 340%, and 220% via polarization (in a range between −2 and 4 V). The optimal reaction temperature was 325 °C, and the maximum selectivity was attained by a feed ratio of H_2/CO_2 of 2:1. Selectivity of dimethyl ether decreased with an increase in the reactant ratio. Thus, this study is one of the forward steps for EPOC commercialization because the flow rate was high (522 L h^{-1} = 8700 mL min^{-1}), and industrial feed ratios were selected.

In a recent study, EPOC of Cu NPs deposited on the YSZ was investigated for RWGS. Cu NPs of 20 nm average size were synthesized via the polyol method and deposited on the YSZ disk [85]. Only positive polarization increased RWGS, and the highest rate increase occurred under +2 V at a CO_2/H_2 ratio of 1:1 at 400 °C. The resulting rate enhancement ratio (ρ) was 1.2, and the Faradaic efficiency (Λ) was

Table 3.3 Examples of nano-dispersed electropromoted catalyst from Sects. 3.2.3, 3.24 and 3.2.5

Catalyst	Synthesis or deposition method	Reaction	Electrolyte	Reactants	ρ	Λ	Total flow and/or reactant mixture	T (°C)	Ref. and year
RuO_2	Polyol reduction	Complete C_2H_4 oxidation	YSZ	C_2H_4, O_2	1.24	6	3 L. h^{-1} P_{C2H4}/PO_2: 0.012 kPa/3 kPa	350	[61], 2019
Ru-Co	Wet impregnation	CO_2 hydrogenation	BZY	CO_2, H_2	CO: 0.8, CH4: 2.7 @ 1.5 V; CO: 1.1, CH4: 1.05 @ −1.5 V	–	12 L. h^{-1} P_{CO2}/P_{H2}: 1 kPa/7 kPa	450	[63], 2018
RuO_2	Wet impregnation	CO_2 hydrogenation	BZY	CO_2, H_2	CH_4: 1.5 @ 350 °C	CH_4: 8.6 @ 350 °C	6 L. h^{-1} P_{CO2}/P_{H2}: 1 kPa/7 kPa	250–400	[16], 2020
RuO_2	Polyol reduction	CO_2 hydrogenation	YSZ	CO_2, H_2	CH_4: 1.8	CH_4: 34	6 L. h^{-1} P_{CO2}/P_{H2}: 1 kPa/7 kPa	250	[62], 2020
Rh	DC magnetron sputtering	C_2H_4 oxidation	YSZ	C_2H_4, O_2	–	–	P_{C2H4}/PO_2: 0–9 (reducing: 0.3, oxidative: 3.6	400	[70], 2018
Au-YSZ	Magnetron sputtering	CH_3OH partial oxidation (POX)	K–$\beta''Al_2O_3$	CH_3OH, O_2	H_2: 9; CO_2: 2; $HCOOCH_3$: 5	–	6 L. h^{-1} CH_3OH/O_2: 5.9%/0.43%	280	[76], 2014
Ag	Screen-printing	C_3H_6 oxidation	YSZ	C_3H_6, O_2	Lean-burn: 1.34; stoichio.: 1.03	Lean-burn: 137; stoichio.: 571	Stoichio.: 6 L h^{-1} and C_3H_6/O_2: 0.1%/0.45%; Lean-burn: 3 L. h^{-1} and C_3H_6/O_2: 0.1%/3.6%	300	[82], 2018

6.52. TEM, XPS, and cyclic voltammetry confirmed the active state of Cu as Cu_2O and CuO indicating that the reaction over Cu/YSZ followed the redox mechanism.

3.2.2.3 Ni-, Fe-, and Co-Based Nanostructured Catalyst

Nickel is an alternative to noble metals and economically preferable over noble metal catalysts [54, 86, 87]. Various Ni catalyst electrodes have been studied for a number of reactions deposited on solid electrolytes supplying positive [88–91] or negative promoters [54].

Nickel electrode deposited using oblique angle PVD on K-β″Al_2O_3 was applied in methanol steam reforming. The research group of de Lucas-Consuegra [89] studied the contribution of formed graphene oxide on H_2 storage and production during methanol steam reforming over Ni at 280 °C. The proposed mechanism was based on the chemisorption of H_2 on the active sites of Ni and the role graphene oxide (GO) had on the spillover of H_2 under the K^+ promotion effect. Such a porous catalytic system increased the possibility of GO aggregate formation, whereas H_2 storage and production were controlled by varying current/potential under fixed experimental conditions.

In another study, Espinos et al. [90] elucidated the EPOC mechanism over alkaline ionic conducting materials via the in situ near-ambient pressure photoemission (NAP) spectroscopy technique. They revisited the migration of K^+ ions with regard to diffusion of positive promoter ions or their reduction, by applying various polarization modes. It was proposed that ions adsorbed at the three-phase boundary had two different modes of transport: (i) onto the surface of the catalyst exposed to reactants and (ii) into the inner interfaces or grain boundaries of the catalyst. Both modes are at equilibrium where backward and forward migration continuously take place; however, the first mode of transport is favorable with respect to energy.

As one of the early works on Ni deposited on alkali (K^+) solid electrolytes, de Lucas-Consuegra et al. [91] investigated the water-gas shift reaction ($T = 350$ °C and CO/H_2O ratio of 1:3) over Ni NPs (100 nm and film dispersion of 0.84%). The authors observed that with negative polarization, K^+ ions migrated onto the catalyst surface to promote the selectivity towards CO and H_2 with an increase in the H_2 catalytic rate ($\rho_{H2} = 2.7$). The reversibility of the EPOC effect can be explained by the activation of the chemisorption process for H_2O molecules and subsequent generation of OH species.

In the most recent research conducted over Ni-based catalysts [88] for CO_2 hydrogenation, three catalyst-working electrodes were investigated with respect to CO_2 and CH_4 production: (i) Ni/K-β″Al_2O_3, (ii) Ni-αAl_2O_3/K-β″Al_2O_3 (40 mg Ni, 20 mg α-Al_2O_3, and ethylene glycol), and (iii) Au-Ni (30%)-αAl_2O_3/K-β″Al_2O_3 (mixture of 40 mg Au ink and 20 mg α-Al_2O_3 previously impregnated with Ni (30%)). The mean particle diameter (after reduction through TPR) of the first sample (denoted as sample N) was 39.9 nm, whereas the particle size of the second sample (labeled as NA) and the third sample (labeled as GNA) was 37.5 and 35.2 nm, respectively. The authors showed that with the addition of α-Al_2O_3 to NA, the

dispersion of Ni was improved, and all samples were porous (based on SEM analysis) which remarkably enhanced the diffusion of reactants and products. NA catalyst showed the highest activity explained by an increase in the porosity of the catalyst film (composed of Ni). In addition, the CO formation rate was dependent on two parameters: (i) a direct relationship with the CO_2 feed and (ii) an inverse variation with changes in applied potential (where a decrease in potential resulted in an increase in the CO production rate). Although CO formation gave promising results under negative polarization, CH_4 production was favored by introducing positive potential (spillover of K^+ onto solid electrolyte and removal from the catalyst surface). In addition, increasing H_2 concentration (electron donor) demonstrated a positive impact on CH_4 production due to its electrophilic nature. Finally, the rate of consumption of CO_2 profoundly increased, and the EPOC effect exhibited a reproducible and reversible trend.

Progress towards the use of transition metals has been pioneered in the use of nanostructured FeO_x catalysts for the RWGS reaction. Monometallic FeO_x nanowires ($Ø = 5$ nm) deposited as a nano-film on YSZ solid electrolyte responded to the application of polarization with a CO rate increase of 200% ($\rho = 2$). FeO_x nanowires were synthesized through the polyol synthesis method with TMAOH. This was the first EPOC study where non-noble metal nanostructured catalysts were studied to electrochemically activate FeO_x for the RWGS reaction. Under open-circuit conditions, the CO_2 conversion varied as a function of temperature, relating to the oxidation state of FeO_x. XPS and cyclic voltammetry (CV) characterization provided insight on the state changes of FeO_x cycling between $Fe_2O_3 \rightarrow Fe_3O_4 \rightarrow FeO \rightarrow Fe \rightarrow Fe_xC$ from −1.6 eV to 1.6 eV (U_{WR}) under a CO_2/H_2 ratio of 1:1 (Fig. 3.9a) [17]. Figure 3.9b [17] summarizes an interesting electrochemical response to the application of $U_{WR} = 2$ V at 350 °C. A potential difference of 2 V initially electrochemically oxidized Fe-carbide that was formed during open-circuit conditions. As polarization continued, FeO_x was saturated with oxygen (Fe_3O_4/FeO), reaching an active state to favor RWGS. Once polarization was interrupted, the stored oxygen in FeO_x was made available for the RWGS reaction resulting in a P-EPOC for 5 h. FeO_x is active for the RWGS reaction as Fe_3O_4, FeO, and Fe, while Fe_2O_3 and Fe_xC phases are inactive. The efficiency of the RWGS reaction was ensured by the in situ control of the oxidation state. To evaluate the presence of the Fe_xC phase, CO_2 and H_2 were left to react on FeO_x for 12 h and then replaced by He, and polarization then supplied Fe_xC with oxygen to produce CO in the absence of CO_2. Additionally, negative polarization led to a $\rho = 2.4$ and $\Lambda = 4$ at 350°C, following inverted-volcano behavior. Overall, this study showed how the oxidation state of Fe can be manipulated electrochemically to favor the RWGS catalytic reaction. The advantage of the inverted-volcano effect is the increase in catalytic rate during positive and negative polarization that allows the counter and working electrodes to be composed of the same metal, where both sides are efficiently promoted under polarization.

In another study [92], FeO_x nanowires decorated by Ru clusters (20 at.%) have been shown to inhibit Fe_xC formation, allowing FeO_x to remain in an oxide state during open-circuit conditions (Fig. 3.10 [92]). The Ru/FeO_x catalyst was

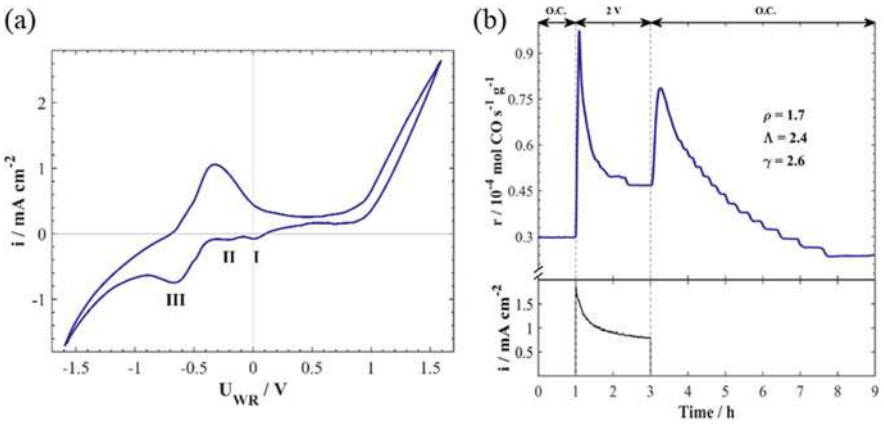

Fig. 3.9 Cyclic voltammetry of FeO_x nanowires deposited on YSZ under reaction conditions at 350 °C (**a**) stable CV and (**b**) transient response at 350 °C for 2 V under reaction conditions and current response. $CO_2/H_2 = 1{:}1$, and 100 mL min^{-1}. (Reprinted with permission from Ref. [17]; Copyright 2020, Elsevier)

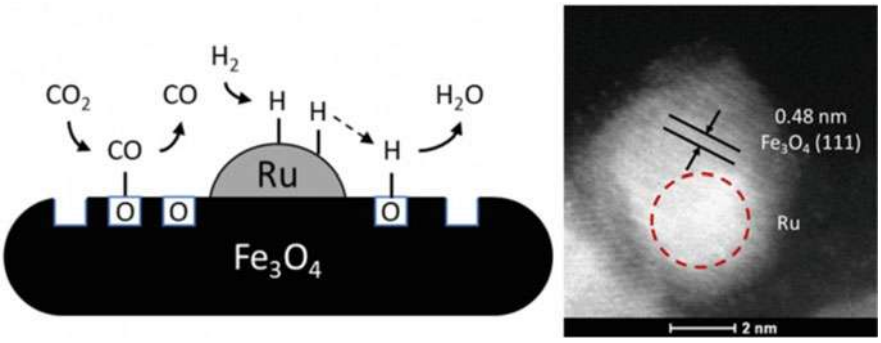

Fig. 3.10 Mechanism of the RWGS reaction on the Ru/FeO_x catalyst. (Reprinted with permission from Ref. [92]; Copyright 2020, Elsevier)

synthesized through a two-step polyol method where FeO_x nanowires were first synthesized followed by Ru clusters reduced on FeO_x. Polarization of Ru/FeO_x led to a reversible catalytic rate increase of $\rho = 2.4$. Positive polarization shared a similar response to FeO_x with the absence of the initial CO rate. Ru inhibited the formation of Fe_xC by ensuring it remained as Fe_3O_4, as shown in the STEM images. The presence of Ru was shown to favor the adsorption of H_2 and its dissociation into H, where it can spill over onto FeO_x to keep it oxidized.

Zagoraios et al. [93] studied free-standing Co nanoparticles (20 nm) synthesized through the polyol method deposited on YSZ and BZY for the RWGS reaction. XPS and imaging characterizations confirmed that polarization affected the work function and oxidation state of the Co catalyst surface. Figure 3.11 [93] displays the transients

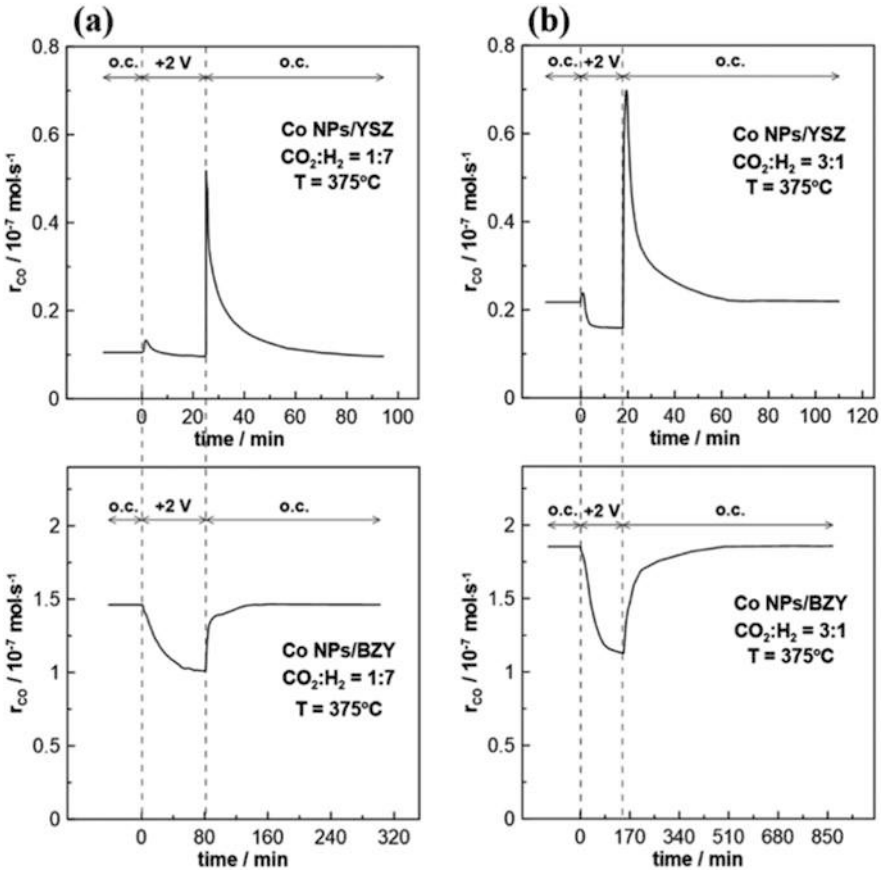

Fig. 3.11 Transient rate response of Co nanoparticles under 2 V polarization for (**a**) Co NPs/YSZ and (**b**) Co NPs/BZY, under reducing and oxidizing conditions at 375 °C. (Reprinted with permission from Ref. [93]; Copyright 2020, American Chemical Society)

of Co nanoparticles deposited on YSZ (O^{2-}) and BZY (H^+) under a potential difference of 2 V. For YSZ, the CO rate decreased as CoO_x was fully oxidized, followed by a spike in the catalytic CO rate of 650%, once potential was interrupted. Similar to FeO_x on YSZ, oxygen is stored as CoO_x and made available for the reaction. In the case of BZY, the CO rate response followed the kinetic behavior of the RWGS reaction and the absence of the post-polarization promotion. Regardless of the type of ionic species, the RWGS reaction for Co nanoparticles followed electrophilic behavior. The authors showed with XPS characterization that Co_3O_4 is dominant on the Co nanoparticles exposed to gaseous oxidation, while for 2 V polarization a mixed $Co^{2+,3+}/Co^{2+}$ state was formed. XPS confirmed that polarization affected the oxidation state of the Co nanoparticles providing a method to tailor the catalytic activity to favor the RWGS reaction. This study supports the unique

behavior exhibited by transition metals that are influenced by polarization to tailor the reaction.

Table 3.4 summarizes EPOC studies over Cu, Ni, Fe, and Co nanoparticles for various catalytic processes that were discussed in Sects. 3.2.5 and 3.2.6.

3.3 Study of EPOC Using Density Functional Theory

DFT is a unique tool to elucidate the atomic nature of the catalytic reaction. Numerous studies have been conducted using DFT calculations to supplement experimental results; however, only a handful have rationalized the EPOC effect [94–96]. Atomic slabs of Pt(111), RuO_2(110), and Ru(0001) were used to simulate small, free-standing Pt, Ru, and RuO_x nanoparticles (1–3 nm) and to establish a computational method to evaluate the EPOC effect by using the surface charging method or grand-canonical DFT [61]. Polarization was simulated through the addition and removal of electrons following the linearized Poisson-Boltzmann equation from VASPsol. Omitting many computational details, this method is used to control the number of electrons for the metal, which modifies the surface charge and work function of the slab. The model is not limited to the type of reaction since it affects the properties of the metal and the molecules.

The first study to apply the electrochemical model was on the RuO_2 (110) surface, where it was used to describe the electrochemical behavior of RuO_x nanoparticles for the complete oxidation of C_2H_4 [61]. The surface energies were measured as a function of potential and oxygen surface coverage. DFT calculations confirmed that under positive polarization simulated conditions (removal of electrons) facilitate the cleavage of the C–C bond to activate C_2H_4 on the RuO_2 (110) surface. Under negative polarization, DFT confirmed O_2 dissociation as the rate-limiting step justifying the inverted-volcano behavior. Thus, DFT calculations identified how polarization affected the binding energy of each molecule.

To provide insight into the origin of the "two oxygen species" that were demonstrated upon positive polarization through XPS, TPD, and cyclic voltammetry characterizations over Pt catalyst-working electrode [97–99], DFT calculations were carried out using Pt(111) slab for the complete oxidation of CH_4 [100]. The hypothesis was that one species originated from YSZ, while the other one was from the gas phase, relating to one oxygen atom on Pt(111) and α-PtO_2, respectively. DFT calculations were compared alongside the experimental methane oxidation reaction, where the reaction followed inverted-volcano behavior (i.e., catalytic rate increased under positive and negative application). Pt(111), 0.25 monolayer (ML) of O on Pt (111), and α-PtO_2 on Pt(111) were evaluated under the influence of polarization and are summarized in Fig. 3.12 [100], in the potential difference range of −1 to 1 U/V vs SHE. Evaluating the activation energy (E_a) of methane on the surface, above $U_{WR} > 1$ U/V vs SHE, the most stable surface was α-PtO_2 on top of Pt(111). In the range of 0 to 1 U/V vs SHE, one oxygen atom (0.25 ML) on Pt(111) was the most stable, which displayed the highest E_a. While for negative polarization, the Pt(111)

Table 3.4 Examples of nano-dispersed electropromoted catalysts (Sects. 3.2.5 and 3.2.6)

Catalyst	Synthesis method	Reaction	Electrolyte	Reactants	ρ	Λ	Total flow and/or reactant mixture	T (°C)	Ref. and year
Cu	Electroless deposition	CO_2 hydrogenation	K–β″ Al_2O_3	CO_2, H_2	C_2H_6O: 3.4; CH_3OH: 34; C_2H_5OH:22	–	522 L. h^{-1} H_2/CO_2: 2, 3, 4	325	[84], 2014
Cu	Oblique angle physical vapor deposition	CH_3OH partial oxidation (POX)	K–β″ Al_2O_3	CH_3OH, O_2	$C_2H_2O_2$: 2.7; H_2: 2.63	–	6 L. h^{-1} CH_3OH/O_2: 4.4%/0.3%	320	[83], 2015
Cu	Polyol	RWGS	YSZ	CO_2, H_2	1.2	6.52	6 L. h^{-1} H_2/CO_2: 1:1	400	[85], 2022
Ni	Thermal decomposition	WGS	K–β″ Al_2O_3	CO, H_2O	H_2: 2.7	–	6 L. h^{-1} CO/H_2O: 1:3	350	[91], 2011
Ni	Deposition	CO_2 hydrogenation	K–β″ Al_2O_3	CO_2, H_2	CO_2: 1–2, CO: 1–3.2, CH_4: 0.5–1	–	6 L. h^{-1} H_2/CO_2: 30%: 1.5%	240	[88], 2015
FeO_x	Polyol	RWGS	YSZ	CO_2, H_2	1.7 @ +2 V	2.4 @ +2 V	6 L. h^{-1} H_2/CO_2: 1:1	350	[17], 2020
FeO_x −20 at.% Ru	2-step polyol	RWGS	YSZ	CO_2, H_2	2.4	0.5	6 L. h^{-1} H_2/CO_2: 1:1	350	[92], 2020
Co	Polyol	RWGS	YSZ; BZY	CO_2, H_2	YSZ: 6.5	–	6 L. h^{-1} H_2/CO_2: 7:1	350	[93], 2020

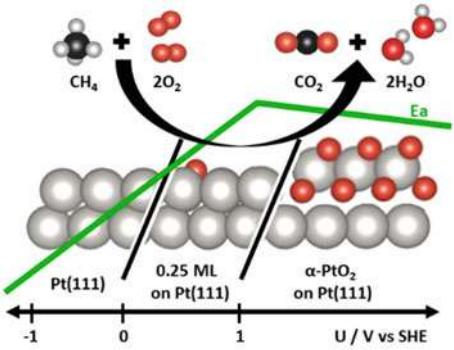

Fig. 3.12 Summary of the Pt(111) surface for the CH_4 oxidation reaction as a function of potential and oxygen coverage with corresponding activation energy (E_a). The Pt(111) is strongly influenced by polarization resulting in the change in activation energy of the reaction. (Reprinted with permission from Ref. [100]; Copyright 2020, American Chemical Society)

surface is favored. The initial hypothesis was that Pt(111) favors the dissociation of O_2, but the E_a energy was lower than CH_4 in the whole potential range. Thus, the authors concluded that the inverted-volcano effect was affiliated with the surface state change influenced by the potential conditions. When compared with the experimental E_a energies [101], the theoretical trend lines up with the negative application, while the positive is not as steep and is affiliated to other oxide surfaces that have not been evaluated. Thus, decades after the discovery of the NEMCA/EPOC effect, DFT calculations provide a way to back up the experimental observations.

Furthermore, the CO_2 hydrogenation reaction was evaluated on the Ru(0001) slab to elucidate the EPOC effect of Ru where positive polarization led to CH_4 formation and negative polarization led to CO formation regardless of the type of ionic species in the solid electrolyte. DFT calculations were performed without taking into account the type of ionic species (i.e., O^{2-}, H^+, Na^+, K^+); instead only polarization is analyzed by adding and removing electrons on Ru(0001). The intermediates were evaluated as a function of potential where the binding energy of the CHO and CO molecules was discovered to influence the selectivity of the reaction (Fig. 3.13) [62]. For positive polarization, CO is strongly adsorbed increasing its hydrogenation towards CH_4, by enhancing the adsorption strength of the CHO* intermediate. For negative polarization, the CO bond is weakened allowing it to likely desorb. The energies under the influence are close in value, which further explains the selectivity between CH_4 and CO for a Ru catalyst. Thus, a universal mechanism for Ru (nanoparticles, sputtered, thick porous layer, etc.) influenced by polarization can be used to model and simulate electrochemical polarization and its behavior.

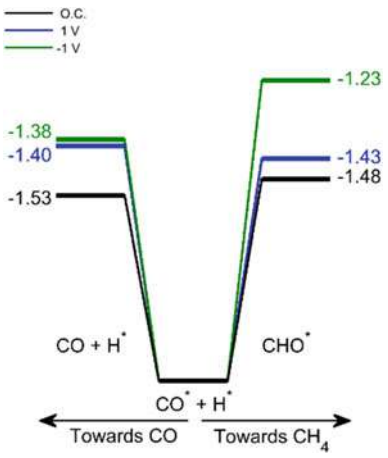

Fig. 3.13 Branching of the CO* + O* intermediate towards CO and CHO* as a function of potential at 250 °C on Ru(0001) for CO_2 hydrogenation. Energies provided in eV. (Reprinted with permission from Ref. [62]; Copyright 2020, Elsevier)

3.3.1 Recent Advancement of Self-Sustained Electrochemical Promotion

Metal-support interaction (MSI) and EPOC have long been considered two different phenomena in heterogeneous catalysis; however, in the last two decades, it has been shown that, functionally, MIEC and ionic conducting materials, both phenomena are linked by the transfer of ionic species at the metal-ceramic interfaces. Understanding the metal-support interaction and its link with EPOC was first observed in 2001 in collaborative work between the research groups of Vayenas, Verykios, and Comninellis [102]. In this work, the reaction of ethylene complete oxidation was investigated over a highly dispersed Rh catalyst deposited on TiO_2, γ-Al_2O_3, WO_3-doped TiO_2, SiO_2, and YSZ supports. In addition, a Rh thin-film catalyst-working electrode was deposited on YSZ for EPOC experiments. The application of potential to the Rh catalyst-working electrode resulted in similar behavior to Rh dispersed on supports, proving how EPOC can be functionally like the MSI effect, where EPOC is in situ controlled via electrochemical stimuli (see Fig. 1.12). In the MSI effect, the conducting supports (e.g., CeO_2, TiO_2) not only enhance catalyst dispersion but also change the catalyst properties by changing the d-bond centers of the surface (metallic state) that interact with the oxide support. The strong metal-support interaction (SMSI) initially coined by Tauster [103–106] implies the coverage of nanoparticles by suboxides that originate from the support under reducing conditions [103–105, 107]. These suboxides are recognized as atomic layers with a presumably amorphous character. A trade-off between the blockage of active sites by suboxides and alteration of local electronic structures was investigated, and the latter case outweighs the former as the role of suboxides as Lewis acids caused the activation of reactants and subsequent tuning of the catalytic performance [108].

Furthermore, extensive research on the functional similarity of EPOC and MSI with ionic and MIEC catalyst supports has been carried out in the last decade. The first confirmation of the existence and the role of ionic species (O^{2-}) from the support was reported by Vernoux et al. in the instance of Pt deposited on a YSZ powder support for deep propane oxidation [109]. The authors used TPD to study the oxidation state of nano-dispersed Pt synthesized via the impregnation method on YSZ support. Three states were determined via TPD (Fig. 3.15): state (I) TPD spectrum under 1 h exposure of oxygen to the surface of the fresh Pt/YSZ at 300 °C, state (II) spectrum recorded after cooling down to 300 °C and again exposure to oxygen for 1 h (following the completion of the first state and increasing the temperature to 700 °C), and state (III) spectrum taken after cooling down to 500 °C and exposing to oxygen for 1 h, cooling down to 300 °C and subsequent exposure to 1% O_2 for 1 h, and lastly cooling down to room temperature under oxygen purging. Catalytic measurements were carried out under the conditions of states II and III with 2000 ppm C_3H_8 and 1% O_2. The TPD analysis showed the presence of $O^{\delta-}$ at 595 °C that was assigned to $O^{\delta-}$ from YSZ support (state I) in agreement with the previous studies by Katsaounis et al. [110] and Li et al. [111]. Catalytic results under states II and III showed that O^{2-} species were thermally induced and originated from YSZ, which resulted in a strong promotion of propane deep oxidation (Fig. 3.14). Thermal migration of O^{2-} was proven by TPD analysis for propane combustion over Pt/YSZ and can be considered as a key step for advancing the understanding of the MSI with ionically conducting ceramics as active supports. The effect was coined self-sustained electrochemical promotion (SS-EPOC or SSEP) to indicate that this is MSI with ionically conductive supports, where the charge transfer occurs via ionic species that migrate to the gas-exposed catalyst surface to modify its properties. SS-EPOC or MSI for a Pt/YSZ catalytic

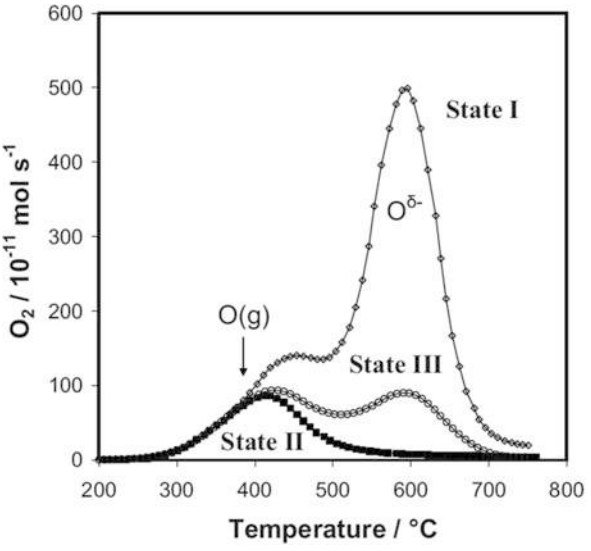

Fig. 3.14 Spectra of O_2– TPD taken after O_2 adsorption over Pt/YSZ (powdered). (Reprinted with permission from Ref. [109]; Copyright 2009, IOP Science)

system was demonstrated for CO, C_2H_4, and toluene oxidation reactions [30, 34, 112, 113].

The charge transfer and modification of the catalyst electronic state were confirmed by ex situ XPS investigations of Pt NPs deposited on YSZ powder support [114]. Pt nanoparticles with four different average sizes ranging from 1.9 to 6.7 nm were dispersed on YSZ powder. For all catalysts, the Pt4f peak was found at lower binding energies compared to the position of the peak of a Pt bulk foil. The Pt4f XPS peak shifted by as much as 0.9 eV for the smallest Pt NPs compared to the peak position of the Pt foil. In addition, changes were found on the Y3d, Zr3d, and O1s spectra after Pt nanoparticle deposition. All these confirmed a charge transfer from the oxide support to the Pt NPs and that this effect was particle size dependent, where the highest electronic modification was observed for the smallest catalyst (Fig. 3.15).

The particle size effect on the extent of MSI [115] was investigated over Pt/YSZ powder catalyst for the oxidation of CO and C_2H_4 in oxygen-free and oxygen-rich environments. In this work, Pt nanoparticles of various average sizes were synthesized via the polyol method and deposited as 1 wt% on YSZ powder. This work demonstrated that oxygen ions from the support take part in the reaction even at temperatures below 100 °C. The proposed mechanism for CO and C_2H_4 oxidation in the absence of oxygen in the gas feed was explained through the formation of local nano-galvanic cells in the vicinity of the three-phase boundary (tpb). In the spontaneous nano-galvanic cell, the oxidation of CO and C_2H_4 was accompanied by the electroreduction of zirconia. The smallest Pt NPs with a mean diameter of 1.9 nm displayed the highest activity and turnover frequency (TOF), whereas no activity was observed for larger particle size (6.7 nm) in an oxygen-deficient environment (Fig. 3.16). As for the oxygen-rich environment, the reaction took place at a lower temperature. Two contributing oxidizing mechanisms under oxygen-rich conditions were proposed: (i) thermally induced backspillover of O^{2-} from YSZ to the surface of the catalyst (metal/gas interface) and (ii) electroreduction at the three-phase boundary.

Furthermore, the effect of the ionically conducting support, i.e., pure ionic (YSZ or SDC) vs. MIEC (CeO_2) and non-conducting γ-Al_2O_3 and carbon black, was studied for ethylene and carbon monoxide oxidation over Pt NPs (2.5 nm average size) [8]. To this end, 1 wt% of Pt NPs was deposited on YSZ, CeO_2, SDC ($Sm_{0.2}Ce_{0.8}O_{1.9}$), γ-Al_2O_3, and carbon black [8]. Catalytic activity measurements showed that Pt/C and Pt/γ-Al_2O_3 were both inactive under a zero-oxygen environment, whereas the rest of the samples exhibited high catalytic activity in the oxygen-deficient environment with complete oxidation of CO and C_2H_4 below 220 °C. The highest catalytic activity for C_2H_4 oxidation was observed for Pt/SDC, explained by the higher bulk ionic conductivity of SDC [8] and the facile oxygen release from CeO_2 if compared to YSZ. The surface O^{2-} resulted in electrochemical oxidation of CO and C_2H_4 by O^{2-} in the vicinity of the tpb at temperatures as low as 70 °C. In the presence of O_2 (P_{O2} = 3.5 kPa), both chemical and electrochemical oxidation of C_2H_4 and CO took place simultaneously, leading to even lower light-off temperatures for both reactions. This effect was also demonstrated for different metal catalysts and supports [116–118].

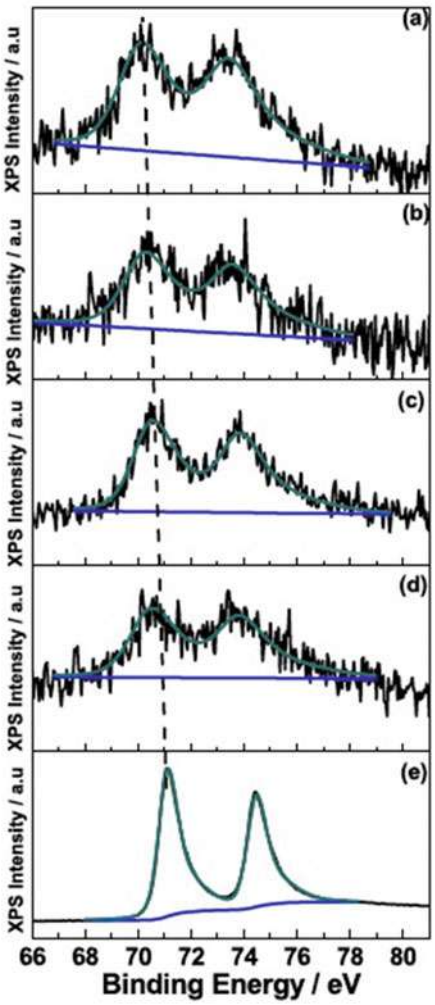

Fig. 3.15 Pt4f XPS peaks of the Pt/YSZ catalysts of various average sizes: (**a**) 1.9 ± 0.4 nm, (**b**) 3.0 ± 0.8 nm, (**c**) 4.4 ± 0.3 nm, (**d**) 6.7 ± 1 nm, (**e**) sputtered Pt foil. (Reprinted with permission from Ref. [114]; Copyright 2014, Elsevier)

An MSI study by Dole et al. [119] investigated the effect of particle size and synthesis parameters on catalytic oxidation of CO. A modified alcohol method was developed that included polyvinylpyrrolidone (PVP) at an optimal PVP/Au ratio of 10:1. Au nanoparticles of 13.1 nm and 17.1 nm supported on YSZ were compared. It was found that calcination is inevitable to remove PVP and achieve activity even though it may increase the particle size. The optimal calcination temperature was based on thermogravimetric analysis (TGA), associated with mass loss of PVP and all species at temperature values of 300 °C and 600 °C, respectively. Higher activity was achieved with lower particle size (13.1 nm), and different calcination temperature did not result in a noticeable change in CO conversion.

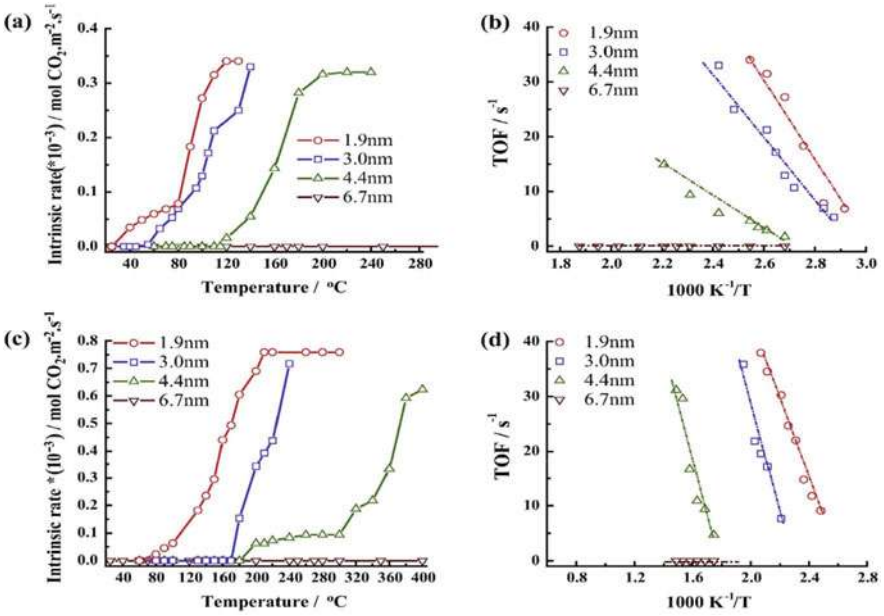

Fig. 3.16 Impact of Pt particle size on YSZ support on the electrooxidation of CO: (**a**) intrinsic rate (normalized with respect to catalyst active surface area), (**b**) turnover frequency, and C_2H_4 electrooxidation (**c**) intrinsic rate (normalized with respect to catalyst active surface area), and (**d**) turnover frequency, both under oxygen-deficient conditions. Flow rate = 77 mL min^{-1}, and concentration reactant = 909 ppm. He balanced. (Reprinted with permission from Ref. [115], Copyright 2015, Elsevier)

The application of electrochemical methods, e.g., cyclic voltammetry, steady-state polarization, chronoamperometry, and chronopotentiometry, has been used in EPOC studies, to in situ characterize, promote, and shed light on the state of the catalyst-working electrode under EPOC conditions. Recently, the use of electrochemical techniques was extended to studying the MSI effect in highly dispersed catalytic systems [117, 120]. The steady-state polarization measurements were carried out to find an exchange current (I_0) of CeO_2-supported Pt- and Ru-based catalysts and link this quantity to the open-circuit catalytic rates. To correlate catalytic and electrochemical measurements, I_0 of each catalyst was obtained from Tafel plots (Fig. 3.18). According to EPOC theory, a good electrocatalyst (high electrochemical reaction rates at the tpb and high I_0) will show an insignificant catalytic rate promotion under polarization because of competing electrochemical reaction and backspillover migration [5, 117]. The following empirical equation was proposed to define an apparent Faradaic efficiency in addition to the fundamental Eq. (3.1) [4]:

$$|\Lambda| \approx \frac{nFr_0}{I_o} \tag{3.4}$$

where r_0 is the open-circuit catalytic rate, I_0 exchange current, n is the number of electrons, and F is Faradic efficiency.

It was found that Eq. (3.4) is also applicable to describe and predict the self-sustained EPOC for the supported and unsupported catalysts in the instance of ethylene oxidation [117]:

$$|\Lambda_{\mathrm{MSI}}| \approx \frac{2Fr_0}{I_0} \left(\text{for } O^{2-} \text{ conducting system}\right) \tag{3.5}$$

where $|\Lambda_{\mathrm{MSI}}|$ is the self-sustained apparent Faradaic efficiency and other parameters are the same as in Eq. (3.4).

The presence of ceria enhanced the catalytic reaction rate when compared to the free-standing Pt and Ru nanoparticles [117, 120]. The proposed metal-support interaction rate enhancement ratios, ρ_{MSI}, defined as the ratio between the reaction rate of supported NPs over the rate of unsupported (free-standing) NPs was found to be equal to 14. Polarization measurements established that higher exchange current, I_0, values corresponded to the lower open-circuit catalytic rates. The lowest self-induced Faradaic efficiency value ($|\Lambda_{\mathrm{MSI}}| = 20$) was for the free-standing Pt nanoparticles, while the highest value ($|\Lambda_{\mathrm{MSI}}| = 1053$) corresponded to 1 wt% Pt/CeO_2.

The role of ceria in enhancing the reaction rate created an analogy to the heterojunction phenomenon called the dissimilarity in metal-support work function ($\varphi_{\mathrm{Ru}} = 4.71$ eV, $\varphi_{\mathrm{Pt}} = 5.93$ eV, $\varphi_{\mathrm{CeO_2}} = 4.69$ eV). The difference in work function caused a driving force to transfer O^{2-} from the support (CeO_2) to the metallic catalyst (e.g., Pt, Ru), which is tangible to classical EPOC, where the migration of promoters backspillover under anodic polarization for negative conducting ceramics. The mechanism of self-sustained EPOC and conventional EPOC [5] is illustrated in Fig. 3.17 [118].

The self-induced apparent Faradaic efficiency concept (Eq. 3.5) was further extended to Ni NPs for the complete ethylene oxidation [120]. Ni nanoparticles supported on YSZ and CeO_2 were synthesized using the hydrazine reduction method [121]. The three catalytic systems were free-standing Ni nanoparticles, Ni/CeO_2 (1 wt.% CeO_2), and Ni/YSZ (1 wt.% YSZ). Free-standing Ni NPs, Ni/CeO_2, and Ni/YSZ converted 35%, 43%, and 5% of ethylene at 350 °C, respectively. The apparent Faradic efficiency of MSI (Λ_{MSI}) was calculated based on exchange current density extracted from Tafel plot analysis and revealed that the Λ_{MSI} for Ni/CeO_2 is 2-fold higher than Ni/YSZ. Figure 3.18 shows the summary of catalytic and electrochemical results for several mono- and bimetallic nanoparticles for ethylene oxidation reaction [117, 120]. In all cases, the highest electrochemical rate (high i_0) corresponded to the lowest catalytic rate in agreement with the EPOC backspillover mechanism.

SSEP has been investigated for CO_2 hydrogenation reaction, where commercial Co_3O_4 powder support was used to disperse Ru nanoparticles of ~1 nm average size [62]. Ru NPs were dispersed on Co_3O_4 and deposited on BZY for CO_2 hydrogenation (Fig. 3.19 [16]). Selectivity to CH_4 and CO was 40% and 60%, respectively.

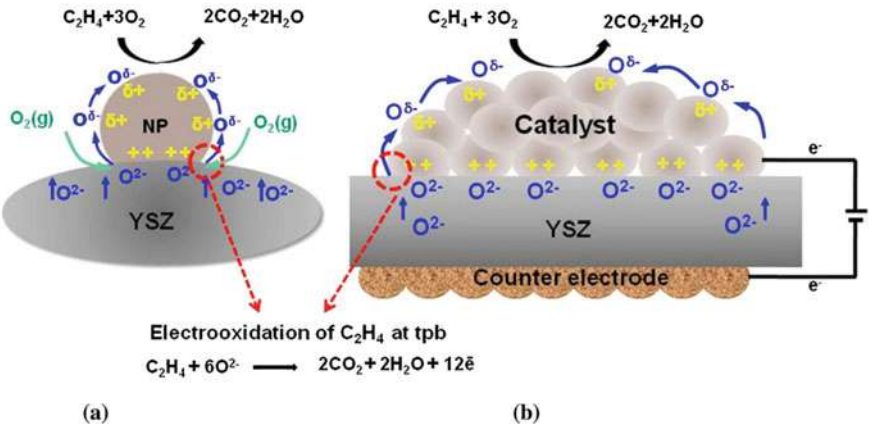

Fig. 3.17 Mechanistic view on processes carrying out over nanoparticles smaller than 5 nm for ethylene oxidation: (**a**) self-sustained EPOC and (**b**) conventional EPOC over electropromoted cell. (Reprinted with permission from Ref. [118]; Copyright 2015, Elsevier)

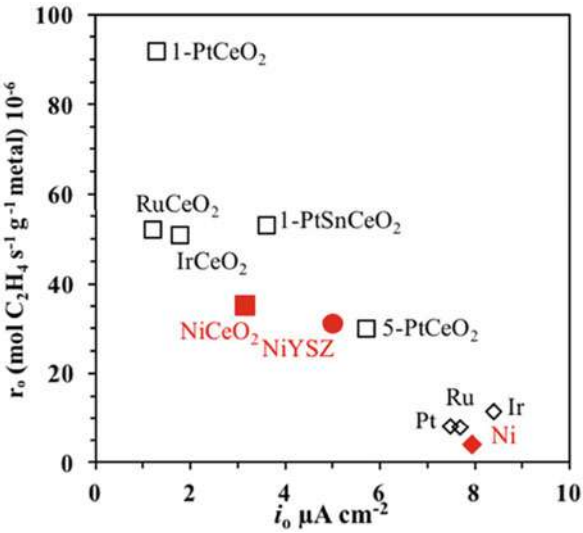

Fig. 3.18 Normalized catalytic rate (r_0) at 350 °C (0.012 kPa C_2H_4, 3 kPa O_2, He balanced) obtained at 350 °C under open-circuit condition and its variation versus exchange current density (i_0). Free-standing Ni, Ni/CeO_2, and 1 wt% Ni/YSZ are shown with red squares. Black symbols correspond to literature results [122, 123]. (Reprinted with permission from Ref. [120]; Copyright 2017, IOP Science)

Under reducing conditions ($CO_2/H_2 = 1:7$), CH_4 selectivity surpassed CO. Only the RWGS reaction was affected under the application of potential following electrophilic behavior where the CO rate decreased under positive polarization and increased during negative polarization. The spontaneous migration of H^+ from BZY aided in reducing Co_3O_4 to cycle oxygen by creating vacancies. Above 350 °C, Co_3O_4 conducted protons from BZY and electrons onto the Ru nanoparticles. The change in catalytic rate was minimally affected by ~10%, where it was suggested that Ru/Co_3O_4 was already in a promoted state or SSEP.

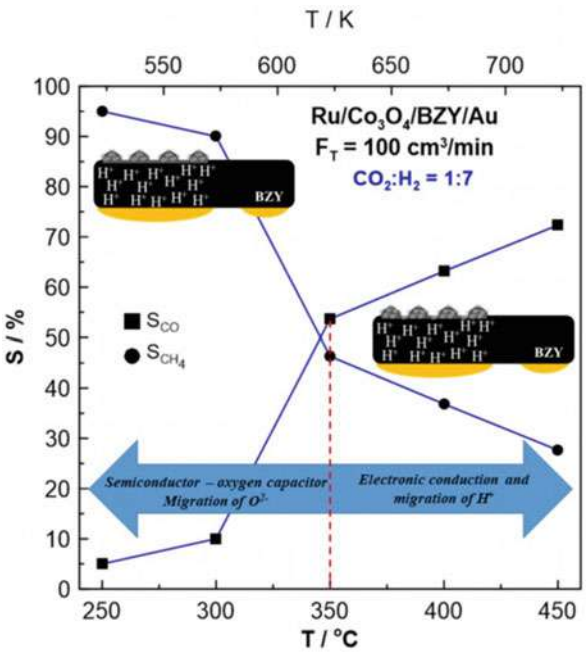

Fig. 3.19 Electrochemical activity of Ru/Co_3O_4 as a function of temperature. Under 350 °C Co_3O_4 cycles oxygen with Ru and the reactants, above 350 °C H^+ ions from BZY migrate on the Ru/Co_3O_4. (Reprinted with permission from Ref. [16]; Copyright 2020, Elsevier)

The ability of Co_3O_4 to act as a conduit of protons and electrons replaces the need to employ a conductive film to polarize the catalyst as shown in the Ru-Co nanoparticles deposited on the Ru intermediate film [63].

Panaritis *et al.* [124] carried out an electrochemical study of FeO_x nanowires dispersed on Co_3O_4 commercial powder support for RWGS. The authors found that Co_3O_4 influenced the morphology of FeO_x nanowires. When FeO_x was dispersed on Co_3O_4, the morphology of the nanowires (length ~100–500 nm, diameter ~5 nm) changed to spherical particles of 5 nm. Under open-circuit conditions, FeO_x/Co_3O_4 outperformed FeO_x/Al_2O_3 by 20 times. Under anodic and cathodic polarization, the CO rate decreased by 10% (or $\rho = 0.9$) or referred to as volcano behavior. Polarization led to the suppression in the catalytic rate of FeO_x/Co_3O_4 by altering the oxidation state of Co_3O_4 and as a result its MSI effect with FeO_x. Electrochemical polarization was used as a tool to study the MSI or SSEP effect between FeO_x and Co_3O_4. Thus, under polarization, the active state of FeO_x/Co_3O_4 is hindered suggesting that the catalyst is in an SSEP state under reaction conditions.

Another interesting aspect of promotion termed electric field promotion has been reported in recent years [125–133]. In [127, 128], the authors proposed a mechanism of ultra-lean methane oxidation over different Pd-Ce-Zr catalysts in a fixed-bed reactor under 0.2% CH_4 mixed with 10% O_2 and N_2 balance. The catalytic reactor consisted of two stainless steel electrodes positioned with no gap (Fig. 3.20). The product analysis was carried out by FTIR spectroscopy, and the increase in turnover frequency (under direct electric field) was normalized based on consumed power per

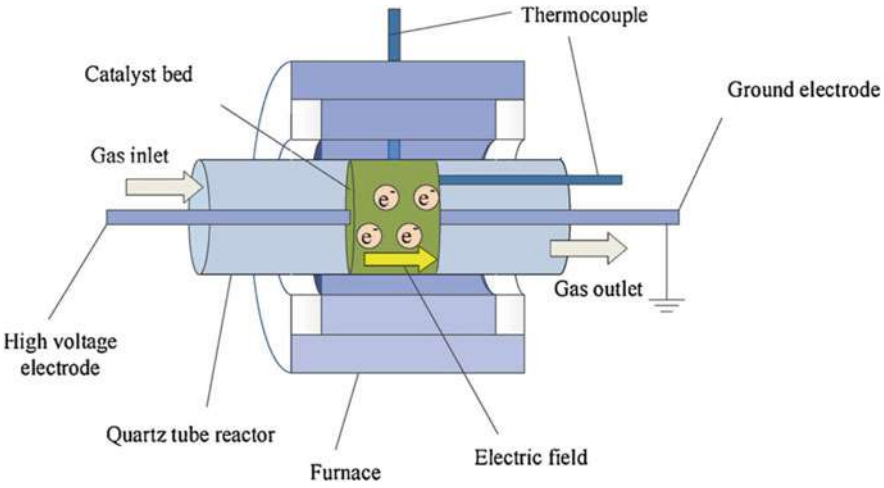

Fig. 3.20 Schematic representation of experimental setup design combining the catalytic process with an electric field. (Reprinted with permission from Ref. [125]; Copyright 2018, Elsevier)

run referred to as ΔTOF^{*} [$s^{-1}w^{-1}$]. The decrease in the light-off temperature and increase in ΔTOF^{*} was due to an electric field that resulted in the release of lattice oxygen ions present in the support. Thus, more surface localized oxygen was produced to oxidize Pd^{0}. This in turn promoted the dissociative chemisorption of CH_4 and its subsequent dehydrogenation while eliminating formate intermediates. Therefore, carbonates were directly formed through CH species. In addition, the reducibility of PdO_x was favorably altered via an electric field, which led to CH_4 oxidation at a lower temperature. Other examples of electric field promotion include oxidation of benzene [129, 130], toluene [131], naphthalene[132], and lean methane combustion over Mn_xCo_y [133].

3.4 Conclusion and Prospective Research Gaps

This chapter provides an overview of recent advances in EPOC of nanostructured catalysis covering both classical and self-sustained EPOC. The last two decades witnessed a large growth in the use of highly dispersed, nano-sized catalytic systems in electrochemical promotion studies. Furthermore, these studies confirmed the functional similarity between EPOC and MSI when ionically conductive ceramics are used as active supports, and the mechanism involved in both phenomena has been further elucidated. As we demonstrate in this review, the nanoparticle catalytic systems could be efficiently electropromoted for reforming, oxidation, and hydrogenation reactions. The application of various synthesis procedures (sputtering, PVD, ALD, impregnation, polyol, and hydrazine reduction methods) led to the

fabrication of mono- and bimetallic catalysts of well-defined size, composition, as well as bulk and surface structure. Furthermore, theoretical calculations based on DFT were discussed for Pt(111), RuO_2(110), and Ru(0001) surfaces that closely model the real nanoparticle systems. Despite tremendous progress in EPOC with noble (Pt, Pd, Rh, Au, etc.) and especially with non-noble (Fe, Co, Cu, Ni) metal and metal oxide nanoparticles, there are still several research gaps that need to be addressed for the future advancement of EPOC with a goal of developing and fabricating active and stable catalytic systems:

1. Further Development and Application of In Situ and Operando Techniques for EPOC and MSI Investigation

Additional experimental in situ observations of EPOC are still needed. Diffuse reflectance infrared Fourier transform spectroscopy (DRIFTS) is an informative technique to in situ analyze reaction mechanisms for the highly dispersed powder catalysts commonly used in MSI studies. This technique requires highly dispersed powder samples and shows limitations for studying thin films due to their low surface area and dispersion. Instead, the polarization modulation infrared reflection absorption spectroscopy (PM-IRRAS) technique could be employed to study the electrode surfaces of thin films for EPOC applications [134, 135]. Urakawa et al. demonstrated how the surface species change on the surface of a Pt thin film (40 nm) during CO oxidation using PM-IRRAS. With a modification in the reactor design and configuration, the same film can be studied under polarization with solid electrolyte support. In situ XPS measurements are useful to identify the change in the oxidation state of the catalyst-working electrode as a function of applied potential and differentiate between electrochemically induced $O^{\delta-}$ on the surface over chemisorbed atomic oxygen [70]. Both in situ approaches require specific reactor configurations that ensure electrochemical conductivity between the electrodes and high temperature to ensure ionic conductivity from the solid electrolyte to promote the catalyst-working electrode. Other important techniques like in situ X-ray absorption spectroscopy (XAS) and various electron microscopies could further shed light on the EPOC phenomenon.

2. Cell Design for Efficient NP Polarization

As discussed throughout this chapter, the use of nanoparticles as a catalyst-working electrode has clear advantages over the micrometer-thick, continuous film electrodes. However, when moving from a uniform porous, thick metal or metal oxide film, where one point of contact with the electrode is enough to ensure conductivity, to NPs, novel cell designs and current collectors are required. For nanostructured electrodes, composed of non-percolated single NPs or NPs islands, there are many challenges in assuring the conductivity and the uniform current distribution. New current collector design and electrode configurations are needed. The inert current collector in the form of a mesh, rings, or any other pattern could be deposited over the catalyst. Other approaches could include an inert, conductive interlayer between the solid electrolyte and catalytic NPs. The application of bipolar and wireless EPOC configurations is very promising in this regard. For instance,

researchers designed different current collectors: (i) direct polarization, e.g., using a gold mesh [17, 48, 112], and (ii) sputtering catalyst on the conductive support [8, 115, 118, 136]. As one of the recent advances in sputtering techniques, Vernoux's group [136] designed a current collector inspired from fuel cell technology for SS-EPOC of NO_x storage-reduction reactions (see Fig. 2.21 in Chap. 2). This current collector was prepared by dispersing Pt and Rh NPs on YSZ (acting as nanometric electrodes). Then, Pt/Rh/YSZ catalytic systems (in the form of a powder) were deposited in the location of the porous structure of the SiC diesel particulate filter (DPFs). DPFs can play the role of the external circuit to transport electrons between nanoparticles and, in the case of being doped with N, enhance their electronic conductivity. Two scenarios of using Pt/Rh/YSZ over N-doped SiC and un-doped SiC were studied under cycling conditions (lean/rich). The following observations were reported: (i) overproduction of CO_2 under rich cycle (absence of oxygen) explained by CO electrochemical reaction [8, 115, 118], (ii) N-doped SiC displayed the highest catalytic activity, and (iii) O^{2-} backspillover (from YSZ onto the surface of Pt) with NPs smaller than 5 nm while >10 nm required the existence of electromotive force (EMF). Such EMF can be induced via two distinct metals and a conductor with sufficient electronic conductivity.

Furthermore, the wireless electrochemical promotion has a great potential for practical application of the EPOC phenomenon. Stavrakakis et al. [137] studied wireless EPOC on modified catalytic membrane reactors employing $BaCe_{1-x}Y_xO_{3-\delta}$ (BCY) and $BaCe_{0.8-y}\ Zr_yY_{0.2}\ O_{3-\delta}$ (BCZY) conductive membrane supports. In this study, wireless EPOC configuration [138–143] utilized the chemical potential difference between the dense membrane support with a Pt film (synthesized via sol-gel method) painted on both sides of BCZY disk (Fig. 3.21). Catalytic CO oxidation was carried out with a total flow rate of 200 mL min^{-1} and partial pressure of 1 kPa and 10 kPa for CO and O_2, respectively, where the high partial pressure for oxygen was selected to prevent carbon deposition and subsequent poisoning. In addition, H_2/H_2O flowing through the sweep side of a dual-chamber reactor supplied promoters to the catalyst and reaction side. The best performance was obtained by BCZ20Y20 where a 10% promotion reaction rate was reported at 650 °C with a reversible EPOC behavior and tenable membrane stability. The barrier is to explain the suppressed promotion in subsequent H_2/H_2O and Ar sweep cycles in which the former sweep generated an H_2 chemical potential gradient from sweep to reaction side and emerged the ambipolar diffusion of H^+ (proton) and $O^{\delta-}$ ions. In the second and third cycles, the promotion is completely suppressed as two conducting (or competing) mechanisms: (i) hydrogen chemical potential gradient and (ii) ambipolar diffusion of proton and oxygen ions might reach an equilibrium.

Using Pt NPs instead of a Pt film might shift the competing mechanism in a favorable way to obtain the desirable flux of $O^{\delta-}$ and H^+ ions to carry out promotion through subsequent cycles (the second and third one). This possible anticipation of NPs may preserve sustainable and stable CO oxidation. In addition, using BCZY as a solid electrolyte in other types of EPOC reactions may exhibit positive enhancement with respect to activation and reaction temperature, stability, and promotion.

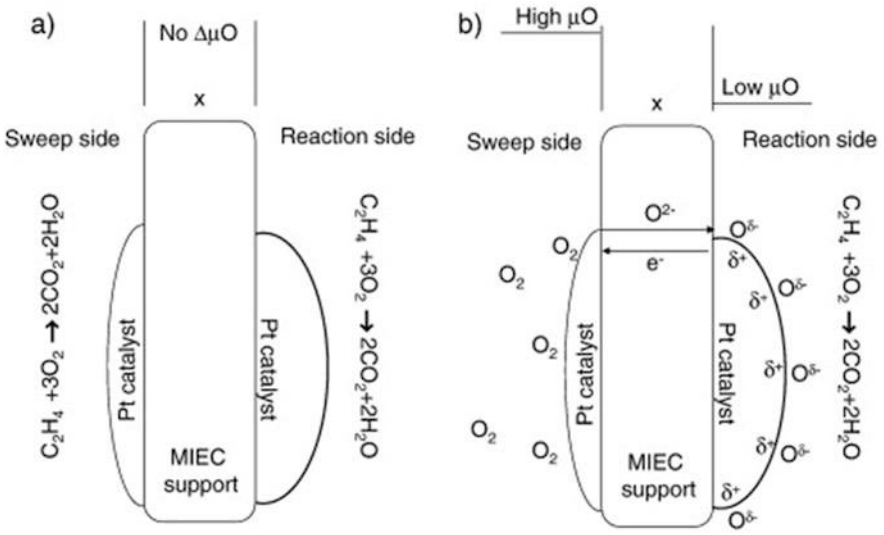

Fig. 3.21 Operation and promotional mechanism of wireless EPOC configuration: (**a**) symmetrical operation and (**b**) O_2 sweep. (Reprinted with permission from Ref. [142]; Copyright 2008, Elsevier)

3. Development of Catalytic Systems Without Noble Metal Content or with Reduced Noble Metal Content

Various nanostructured catalytic systems (non-noble or with reduced metal content) have been studied for EPOC reactions over the last 10 years for complete methane oxidation over Ni9Pd [54]; RWGS reactions over Co [93], FeO_x [17], $RuFeO_x$ [92], and Cu; WGR over Ni[91]; CO_2 hydrogenation over Ni [88] and Cu [84]; and partial oxidation of methanol over Cu[83]. Further development and implementation of nanostructured bimetallic and ternary catalysts for EPOC of other environmentally and technologically important reactions are needed.

4. Development and Application of Novel Conducting Ceramics and Polymers as Solid Electrolytes

Yttria-stabilized zirconia is the most used solid electrolyte in EPOC studies to date. YSZ requires high temperatures of at least of 280 °C to have an observable bulk ionic conductivity [5]. In addition to low ionic conductivity, YSZ is quite expensive: 0.56 USD g^{-1} [144, 145]. In laboratory experiments, a relatively thick (several mm) YSZ disk is used as a solid electrolyte, which has limitations for a scale-up application. A recent study attempted to synthesize thin-film NEMCA cells on conventional alumina supports with and without $BiCuVO_x$ [146]. Another direction is the development of novel solid-state electrolytes that display high ionic conductivity at lower temperatures with high chemical and mechanical stability. This could reduce the temperature required for ionic conductivity and extend EPOC to a wide range of low-temperature reactions and systems.

References

1. Stoukides M, Vayenas CG (1981) The effect of electrochemical oxygen pumping on the rate and selectivity of ethylene oxidation on polycrystalline silver. J Catal 70:137–146. https://doi.org/10.1016/0021-9517(81)90323-7
2. Bebelis S, Vayanes CG (1989) Non-faradaic electrochemical modification of catalytic activity 1. The case of ethylene oxidation on Pt. J Catal 118:125–146. https://doi.org/10.1016/0021-9517(89)90306-0
3. Vayanes CG, Bebelis S (1999) Electrochemical promotion of heterogeneous catalysis. Catal Today 51:581–594. https://doi.org/10.1016/S0920-5861(99)00042-5
4. Vayenas CG, Bebelis S, Pliangos C, Brosda S (2001) Electrochemical activation of catalysis promotion, electrochemical promotion, and metal-support interactions. Kluwer Academic Publishers
5. Vernoux P, Lizarraga L, Tsampas MN, Sapountzi FM, De Lucas-Consuegra A, Valverde JL, Souentie S, Vayenas CG, Tsiplakides D, Balomenou S, Baranova EA (2013) Ionically conducting ceramics as active catalyst supports. Chem Rev 113:8192–8260. https://doi.org/10.1021/cr4000336
6. Urquhart AJ, Williams FJ, Lambert RM (2005) Electrochemical promotion by potassium of Rh-catalysed fischer-tropsch synthesis at high pressure. Catal Lett 103:137–141. https://doi.org/10.1007/s10562-005-6519-1
7. Panaritis C, Edake M, Couillard M, Einakchi R, Baranova EA (2018) Insight towards the role of ceria-based supports for reverse water gas shift reaction over RuFe nanoparticles. J CO2 Util 26:350–358. https://doi.org/10.1016/j.jcou.2018.05.024
8. Isaifan RJ, Baranova EA (2013) Catalytic electrooxidation of volatile organic compounds by oxygen-ion conducting ceramics in oxygen-free gas environment. Electrochem Commun 27:164–167. https://doi.org/10.1016/j.elecom.2012.11.021
9. Kalaitzidou I, Zagoraios D, Brosda S, Katsaounis A, Vernoux P, Vayenas CG (2018) Electrochemical promotion of methane oxidation on Pd nanoparticles deposited on YSZ. Mater Today Proc 5:27345–27352. https://doi.org/10.1016/J.MATPR.2018.09.050
10. Jiménez-Borja C, Dorado F, de Lucas-Consuegra A, Vargas JMG, Valverde JL (2011) Electrochemical promotion of CH4 combustion over a Pd/CeO2–YSZ catalyst. Fuel Cells 11:131–139. https://doi.org/10.1002/fuce.201000058
11. Nakos A, Souentie S, Katsaounis A (2010) Electrochemical promotion of methane oxidation on Rh/YSZ. Appl Catal B Environ 101:31–37. https://doi.org/10.1016/J.APCATB.2010.08.030
12. López ER, Dorado F, de Lucas-Consuegra A (2019) Electrochemical promotion for hydrogen production via ethanol steam reforming reaction. Appl Catal B Environ 243:355–364. https://doi.org/10.1016/j.apcatb.2018.10.062
13. De Lucas-Consuegra A, González-Cobos J, Carcelén V, Magén C, Endrino JL, Valverde JL (2013) Electrochemical promotion of Pt nanoparticles dispersed on a diamond-like carbon matrix: a novel electrocatalytic system for H2 production. J Catal 307:18–26. https://doi.org/10.1016/j.jcat.2013.06.012
14. Vernoux P (2017) Recent advances in electrochemical promotion of catalysis. Catalysis 29:29–59. https://doi.org/10.1039/9781788010634-00029
15. Jiménez V, Jiménez-Borja C, Sánchez P, Romero A, Papaioannou EI, Theleritis D, Souentie S, Brosda S, Valverde JL (2011) Electrochemical promotion of the CO2 hydrogenation reaction on composite ni or ru impregnated carbon nanofiber catalyst-electrodes deposited on YSZ. Appl Catal B Environ 107:210–220. https://doi.org/10.1016/j.apcatb.2011.07.016
16. Zagoraios D, Panaritis C, Krassakopoulou A, Baranova EA, Katsaounis A, Vayenas CG (2020) Electrochemical promotion of Ru nanoparticles deposited on a proton conductor electrolyte during CO2 hydrogenation. Appl Catal B Environ 276:119148. https://doi.org/10.1016/j.apcatb.2020.119148

17. Panaritis C, Zgheib J, Ebrahim SAH, Couillard M, Baranova EA (2020) Electrochemical in-situ activation of Fe-oxide nanowires for the reverse water gas shift reaction. Appl Catal B Environ 269:118826. https://doi.org/10.1016/j.apcatb.2020.118826
18. Fellah Jahromi A, Ruiz-López E, Dorado F, Baranova EA, de Lucas-Consuegra A (2022) Electrochemical promotion of ethanol partial oxidation and reforming reactions for hydrogen production. Renew Energy 183:515–523. https://doi.org/10.1016/J.RENENE.2021.11.041
19. Shim JH, Park JS, Holme TP, Crabb K, Lee W, Kim YB, Tian X, Gür TM, Prinz FB (2012) Enhanced oxygen exchange and incorporation at surface grain boundaries on an oxide ion conductor. Acta Mater 60:1–7. https://doi.org/10.1016/J.ACTAMAT.2011.09.050
20. Siebert E, Djurado E, Pagnier T, Roux C, Vernoux P (2005) In-situ high temperature study of oxygen adsorbed on Pt/YSZ under conditions of electrochemical promotion of catalysis. In: Risoe international symposium on materials science. Roskilde
21. Skriver HL, Rosengaard NM (1992) Surface energy and work function of elemental metals. Phys Rev B 46:7157–7168. https://doi.org/10.1103/PhysRevB.46.7157
22. Vayenas CG, Brosda S (2014) Electron donation-Backdonation and the rules of catalytic promotion. Top Catal 57:1287–1301. https://doi.org/10.1007/s11244-014-0294-4
23. Vayenas CG, Brosda S, Pliangos C (2001) Rules and mathematical modeling of electrochemical and chemical promotion: 1. Reaction classification and promotional rules. J Catal 203: 329–350. https://doi.org/10.1006/jcat.2001.3348
24. Brosda S, Vayenas CG (2002) Rules and mathematical modeling of electrochemical and classical promotion: 2. Modeling. J Catal 208:38–53. https://doi.org/10.1006/jcat.2002.3549
25. Brosda S, Vayenas CG, Wei J (2006) Rules of chemical promotion. Appl Catal B Environ 68: 109–124. https://doi.org/10.1016/j.apcatb.2006.07.021
26. Nicole J, Tsiplakides D, Wodiunig S, Comninellis C (1997) Activation of catalyst for gas-phase combustion by electrochemical pretreatment. J Electrochem Soc 144. https://doi.org/10.1149/1.1838143
27. González-Cobos J, de Lucas-Consuegra A (2016) A review of surface analysis techniques for the investigation of the phenomenon of electrochemical promotion of catalysis with alkaline ionic conductors. Catalysts 6. https://doi.org/10.3390/catal6010015
28. Yentekakis IV, Vernoux P, Goula G, Caravaca A (2019) Electropositive promotion by alkalis or alkaline earths of Pt-group metals in emissions control catalysis: a status report. Catalysts 9: 157. https://doi.org/10.3390/catal9020157
29. Katsaounis A (2009) Recent developments and trends in the electrochemical promotion of catalysis (EPOC). J Appl Electrochem 405(40):885–902. https://doi.org/10.1007/S10800-009-9938-7
30. Isaifan RJ, Dole HAE, Obeid E, Lizarraga L, Vernoux P, Baranova EA (2012) Metal-support interaction of Pt nanoparticles with ionically and non-ionically conductive supports for CO oxidation. Electrochem Solid-State Lett 15:E14. https://doi.org/10.1149/2.024203esl
31. Xia C, Hugentobler M, Li Y, Foti G, Comninellis C, Harbich W (2011) Electrochemical promotion of CO combustion over non-percolated Pt particles supported on YSZ using a novel bipolar configuration. Electrochem Commun 13:99–101. https://doi.org/10.1016/j.elecom.2010.11.026
32. Marwood M, Vayenas CG (1998) Electrochemical promotion of a dispersed platinum catalyst. J Catal 178:429–440. https://doi.org/10.1006/jcat.1998.2156
33. Vernoux P, Gaillard F, Bultel L, Siebert E, Primet M (2002) Electrochemical promotion of propane and propene oxidation on Pt/YSZ. J Catal 208. https://doi.org/10.1006/jcat.2002.3573
34. Dole HAE, Isaifan RJ, Sapountzi FM, Lizarraga L, Aubert D, Princivalle A, Vernoux P, Baranova EA (2013) Low temperature toluene oxidation over Pt nanoparticles supported on yttria stabilized-zirconia. Catal Lett 143:996–1002. https://doi.org/10.1007/s10562-013-1071-x
35. Souentie S, Lizarraga L, Kambolis A, Alves-Fortunato M, Valverde JL, Vernoux P (2011) Electrochemical promotion of the water-gas shift reaction on Pt/YSZ. J Catal 283:124–132. https://doi.org/10.1016/j.jcat.2011.07.009

36. Palma V, Ruocco C, Cortese M, Renda S, Meloni E, Festa G, Martino M (2020) Platinum based catalysts in the water gas shift reaction: recent advances. Metals (Basel) 10:1–74. https://doi.org/10.3390/met10070866
37. Roche V, Revel R, Vernoux P (2010) Electrochemical promotion of YSZ monolith honeycomb for deep oxidation of methane. Catal Commun 11. https://doi.org/10.1016/j.catcom.2010.05.005
38. De Lucas-Consuegra A, Caravaca A, Martínez PJ, Endrino JL, Dorado F, Valverde JL (2010) Development of a new electrochemical catalyst with an electrochemically assisted regeneration ability for H2 production at low temperatures. J Catal 274:251–258. https://doi.org/10.1016/j.jcat.2010.07.007
39. Xia C, Hugentobler M, Yongdan-Li CC, Harbich W (2010) Quantifying electrochemical promotion of induced bipolar Pt particles supported on YSZ. Electrochem Commun 12:1551–1554. https://doi.org/10.1016/j.elecom.2010.08.031
40. Falgairette C, Xia C, Li Y, Harbich W, Foti G, Comninellis C (2010) Investigation of the Pt/YSZ interface at low oxygen partial pressure by solid electrochemical mass spectroscopy under high vacuum conditions. J Appl Electrochem 4010(40):1901–1907. https://doi.org/10.1007/S10800-010-0160-4
41. Jaccoud A, Falgairette C, Fóti G, Comninellis C (2007) Charge storage in the O2(g),Pt/YSZ system. Electrochim Acta 52:7927–7935. doi: https://doi.org/10.1016/j.electacta.2007.06.046
42. Kambolis A, Lizarraga L, Tsampas MN, Burel L, Rieu M, Viricelle J-P, Vernoux P (2012) Electrochemical promotion of catalysis with highly dispersed Pt nanoparticles. Electrochem Commun:19. https://doi.org/10.1016/j.elecom.2012.02.041
43. Li X, Gaillard F, Vernoux P (2005) The relationship of the catalytic activity and the open-circuit potential of Pt interfaced with YSZ. Ionics 111(11):103–111. https://doi.org/10.1007/BF02430408
44. Fortunato MA, Princivalle A, Capdeillayre C, Petigny N, Tardivat C, Guizard C, Tsampas MN, Sapountzi FM, Vernoux P (2014) Role of lattice oxygen in the propane combustion over Pt/Yttria-stabilized zirconia: isotopic studies. Top Catal 57:1277–1286. https://doi.org/10.1007/s11244-014-0293-5
45. De Lucas-Consuegra A, González-Cobos J, García-Rodríguez Y, Mosquera A, Endrino JL, Valverde JL (2012) Enhancing the catalytic activity and selectivity of the partial oxidation of methanol by electrochemical promotion. J Catal 293:149–157. https://doi.org/10.1016/j.jcat.2012.06.016
46. De Lucas-Consuegra A, González-Cobos J, Gacia-Rodriguez Y, Endrino JL, Valverde JL (2012) Electrochemical activation of the catalytic methanol reforming reaction for H 2 production. Electrochem Commun 19:55–58. https://doi.org/10.1016/j.elecom.2012.03.016
47. Hajar Y, Di Palma V, Kyriakou V, Verheijen MA, Baranova EA, Vernoux P, Kessels WMM, Creatore M, van de Sanden MCM, Tsampas M (2017) Atomic layer deposition of highly dispersed Pt nanoparticles on a high surface area electrode backbone for electrochemical promotion of catalysis. Electrochem Commun:84. https://doi.org/10.1016/j.elecom.2017.09.023
48. Hajar YM, Patel KD, Tariq U, Baranova EA (2017) Functional equivalence of electrochemical promotion and metal support interaction for Pt and RuO2 nanoparticles. J Catal 352:42–51. https://doi.org/10.1016/j.jcat.2017.05.001
49. Baranova EA, Bock C, Ilin D, Wang D, MacDougall B (2006) Infrared spectroscopy on size-controlled synthesized Pt-based nano-catalysts. Surf Sci 600:3502–3511. https://doi.org/10.1016/j.susc.2006.07.005
50. Yeung KL, Christiansen SC, Varma A (1999) Palladium composite membranes by electroless plating technique: relationships between plating kinetics, film microstructure and membrane performance. J Memb Sci 159:107–122. https://doi.org/10.1016/S0376-7388(99)00041-1
51. Matei F, Jiménez-Borja C, Canales-Vázquez J, Brosda S, Dorado F, Valverde JL, Ciuparu D (2013) Enhanced electropromotion of methane combustion on palladium catalysts deposited on highly porous supports. Appl Catal B Environ 132–133:80–89. https://doi.org/10.1016/j.apcatb.2012.11.011

52. Zagoraios D, Athanasiadi A, Kalaitzidou I, Ntais S, Katsaounis A, Caravaca A, Vernoux P, Vayenas CG (2020) Electrochemical promotion of methane oxidation over nanodispersed Pd/Co3O4 catalysts. Catal Today 355:910–920. https://doi.org/10.1016/J.CATTOD.2019.02.030
53. Hajar YM, Venkatesh B, Baranova EA (2019) Electrochemical promotion of nanostructured palladium catalyst for complete methane oxidation. Catalysts 9:48. https://doi.org/10.3390/catal9010048
54. Hajar YM, Venkatesh B, Houache MSE, Liu H, Safari R, Prabhudev S, Botton GA, Baranova EA (2019) Electrochemical promotion of Bi-metallic Ni9Pd core double-shell nanoparticles for complete methane oxidation. J Catal 374:127–135. https://doi.org/10.1016/j.jcat.2019.04.026
55. Chang Q, Xu Y, Duan Z, Xiao F, Fu F, Hong Y, Kim J, Choi S-I, Su D, Shao M (2017) Structural evolution of Sub-10 nm octahedral platinum–nickel bimetallic nanocrystals. Nano Lett 17:3926–3931. https://doi.org/10.1021/ACS.NANOLETT.7B01510
56. Bebelis S, Karasali H, Vayenas CG (2008) Electrochemical promotion of the CO2 hydrogenation on Pd/YSZ and Pd/β″-Al2O3 catalyst-electrodes. Solid State Ionics 179:1391–1395. https://doi.org/10.1016/j.ssi.2008.02.043
57. Cai F, Gao D, Zhou H, Wang G, He T, Gong H, Miao S, Yang F, Wang J, Bao X (2017) Electrochemical promotion of catalysis over Pd nanoparticles for CO2 reduction. Chem Sci 8:2569–2573. https://doi.org/10.1039/c6sc04966d
58. Solymosi F, Erdöhelyi A (1980) Hydrogenation of CO2 to CH4 over alumina-supported noble metals. J Mol Catal 8:471–474. https://doi.org/10.1016/0304-5102(80)80086-1
59. Ryu J, Surendranath Y (2020) Polarization-induced local pH swing promotes Pd-catalyzed CO2 hydrogenation. J Am Chem Soc 142:13384–13390. https://doi.org/10.1021/jacs.0c01123
60. Fuel Cell Store (2020) Fuel cell store
61. Hajar YM, Treps L, Michel C, Baranova EA, Steinmann SN (2019) Theoretical insight into the origin of the electrochemical promotion of ethylene oxidation on ruthenium oxide. Cat Sci Technol 9:5915–5926. https://doi.org/10.1039/c9cy01421g
62. Panaritis C, Michel C, Couillard M, Baranova EA, Steinmann SN (2020) Elucidating the role of electrochemical polarization on the selectivity of the CO2 hydrogenation reaction over Ru. Electrochim Acta 350:136405. https://doi.org/10.1016/j.electacta.2020.136405
63. Kotsiras A, Kalaitzidou I, Grigoriou D, Symillidis A, Makri M, Katsaounis A, Vayenas CG (2018) Electrochemical promotion of nanodispersed Ru-Co catalysts for the hydrogenation of CO2. Appl Catal B Environ 232:60–68. https://doi.org/10.1016/j.apcatb.2018.03.031
64. Theleritis D, Souentie S, Siokou A, Katsaounis A, Vayenas CG (2012) Hydrogenation of CO2 over Ru/YSZ Electropromoted catalysts. ACS Catal 2:770–780. https://doi.org/10.1021/CS300072A
65. Theleritis D, Makri M, Souentie S, Caravaca A, Katsaounis A, Vayenas CG (2014) Comparative study of the electrochemical promotion of CO2 hydrogenation over Ru-supported catalysts using electronegative and electropositive promoters. ChemElectroChem 1:254–262. https://doi.org/10.1002/CELC.201300185
66. Kalaitzidou I, Makri M, Theleritis D, Katsaounis A, Vayenas CG (2016) Comparative study of the electrochemical promotion of CO2 hydrogenation on Ru using Na+, K+, H+ and O2- conducting solid electrolytes. Surf Sci 646:194–203. https://doi.org/10.1016/j.susc.2015.09.011
67. Baranova EA, Thursfield A, Brosda S, Fóti G, Comninellis C, Vayenas CG (2005) Electrochemical promotion of ethylene oxidation over Rh catalyst thin films sputtered on YSZ and TiO[sub 2]/YSZ supports. J Electrochem Soc 152:E40. https://doi.org/10.1149/1.1839511
68. Baranova EA, Thursfield A, Brosda S, Fóti G, Comninellis C, Vayenas CG (2005) Electrochemically induced oscillations of C2H4 oxidation over thin sputtered Rh catalyst films. Catal Lett 1051(105):15–21. https://doi.org/10.1007/S10562-005-7999-8

69. Pliangos C, Yentekakis IV, Verykios XE, Vayenas CG (1995) Non-faradaic electrochemical modification of catalytic activity: VIII. Rh-catalyzed C2H4 oxidation. J Catal 154:124–136. https://doi.org/10.1006/JCAT.1995.1154
70. Katsaounis A, Teschner D, Zafeiratos S (2018) The effect of polarization and reaction mixture on the Rh/YSZ oxidation state during ethylene oxidation studied by near ambient pressure XPS. Top Catal 61:2142–2151. https://doi.org/10.1007/s11244-018-1073-4
71. Katsaounis A, Nikopoulou Z, Verykios XE, Vayenas CG (2004) Comparative isotope-aided investigation of electrochemical promotion and metal–support interactions: 2. CO oxidation by 18O2 on electropromoted Pt films deposited on YSZ and on nanodispersed Pt/YSZ catalysts. J Catal 226:197–209. https://doi.org/10.1016/J.JCAT.2004.05.009
72. Vayenas CG, Koutsodontis CG (2008) Non-faradaic electrochemical activation of catalysis. J Chem Phys 128:182506. https://doi.org/10.1063/1.2824944
73. Kishi K, Daté M, Haruta M (2001) Effect of gold on the oxidation of the Si(1 1 1)-7×7 surface. Surf Sci 486:L475–L479. https://doi.org/10.1016/S0039-6028(01)01083-4
74. Haruta M (2003) When gold is not noble: catalysis by nanoparticles. Chem Rec 3:75–87. https://doi.org/10.1002/TCR.10053
75. Haruta M (2004) Gold as a novel catalyst in the 21st century: preparation, working mechanism and applications. ChemInform 35. https://doi.org/10.1002/CHIN.200444247
76. González-Cobos J, Horwat D, Ghanbaja J, Valverde JL, De Lucas-Consuegra A (2014) Electrochemical activation of Au nanoparticles for the selective partial oxidation of methanol. J Catal 317:293–302. https://doi.org/10.1016/j.jcat.2014.06.022
77. Pestryakov AN, Lunin VV, Bogdanchikova N, Temkin ON, Smolentseva E (2013) Active states of gold in small and big metal particles in CO and methanol selective oxidation. Fuel 110:48–53. https://doi.org/10.1016/J.FUEL.2012.10.012
78. Chang FW, Lai SC, Roselin LS (2008) Hydrogen production by partial oxidation of methanol over ZnO-promoted Au/Al2O3 catalysts. J Mol Catal A Chem 282:129–135. https://doi.org/10.1016/J.MOLCATA.2007.12.002
79. Kähler K, Holz MC, Rohe M, Van Veen AC, Muhler M (2013) Methanol oxidation as probe reaction for active sites in Au/ZnO and Au/TiO2 catalysts. J Catal 299:162–170. https://doi.org/10.1016/J.JCAT.2012.12.001
80. Cavoué T, Caravaca A, Kalaitzidou I, Gaillard F, Rieu M, Viricelle JP, Vernoux P (2019) Ethylene epoxidation on Ag/YSZ electrochemical catalysts: understanding of oxygen electrode reactions. Electrochem Commun 105:106495. https://doi.org/10.1016/j.elecom.2019.106495
81. Fee M, Ntais S, Weck A, Baranova EA (2014) Electrochemical behavior of silver thin films interfaced with yttria-stabilized zirconia. J Solid State Electrochem 188(18):2267–2277. https://doi.org/10.1007/S10008-014-2477-0
82. Kalaitzidou I, Cavoué T, Boreave A, Burel L, Gaillard F, Retailleau-Mevel L, Baranova EA, Rieu M, Viricelle JP, Horwat D, Vernoux P (2018) Electrochemical promotion of propylene combustion on Ag catalytic coatings. Catal Commun 104:28–31. https://doi.org/10.1016/j.catcom.2017.10.005
83. González-Cobos J, Rico VJ, González-Elipe AR, Valverde JL, De Lucas-Consuegra A (2015) Electrochemical activation of an oblique angle deposited Cu catalyst film for H2 production. Cat Sci Technol 5:2203–2214. https://doi.org/10.1039/c4cy01524j
84. Ruiz E, Cillero D, Martínez PJ, Morales Á, Vicente GS, De Diego G, Sánchez JM (2014) Electrochemical synthesis of fuels by CO2 hydrogenation on Cu in a potassium ion conducting membrane reactor at bench scale. Catal Today 236:108–120. https://doi.org/10.1016/j.cattod.2014.01.016
85. Wang J, Couillard M, Baranova E (2022) Electrochemical promotion of copper nanoparticles for the reverse water gas shift reaction. Cat Sci Technol. https://doi.org/10.1039/D1CY02315B

86. Persson K, Ersson A, Colussi S, Trovarelli A, Järås SG (2006) Catalytic combustion of methane over bimetallic Pd–Pt catalysts: the influence of support materials. Appl Catal B Environ 66:175–185. https://doi.org/10.1016/J.APCATB.2006.03.010
87. Persson K, Ersson A, Jansson K, Iverlund N, Järås S (2005) Influence of co-metals on bimetallic palladium catalysts for methane combustion. J Catal 231:139–150. https://doi.org/10.1016/J.JCAT.2005.01.001
88. Gutiérrez-Guerra N, González-Cobos J, Serrano-Ruiz JC, Valverde JL, De Lucas-Consuegra A (2015) Electrochemical activation of Ni catalysts with potassium ionic conductors for CO2 hydrogenation. Top Catal 58:1256–1269. https://doi.org/10.1007/s11244-015-0488-4
89. González-Cobos J, Rico VJ, González-Elipe AR, Valverde JL, De Lucas-Consuegra A (2016) Electrocatalytic system for the simultaneous hydrogen production and storage from methanol. ACS Catal 6:1942–1951. https://doi.org/10.1021/acscatal.5b02844
90. Espinós JP, Rico VJ, González-Cobos J, Sánchez-Valencia JR, Pérez-Dieste V, Escudero C, de Lucas-Consuegra A, González-Elipe AR (2018) In situ monitoring of the phenomenon of electrochemical promotion of catalysis. J Catal 358:27–34. https://doi.org/10.1016/j.jcat.2017.11.027
91. De Lucas-Consuegra A, Caravaca A, González-Cobos J, Valverde JL, Dorado F (2011) Electrochemical activation of a non noble metal catalyst for the water-gas shift reaction. Catal Commun 15:6–9. https://doi.org/10.1016/j.catcom.2011.08.007
92. Panaritis C, Zgheib J, Couillard M, Baranova EA (2020) The role of Ru clusters in Fe carbide suppression for the reverse water gas shift reaction over electropromoted Ru/FeOx catalysts. Electrochem Commun 119:106824. https://doi.org/10.1016/j.elecom.2020.106824
93. Zagoraios D, Tsatsos S, Kennou S, Vayenas CG, Kyriakou G, Katsaounis A (2020) Tuning the RWGS reaction via EPOC and in situ electro-oxidation of cobalt nanoparticles. ACS Catal:14916–14927. https://doi.org/10.1021/ACSCATAL.0C04133
94. Leiva EPM, Vázquez C, Rojas MI, Mariscal MM (2008) Computer simulation of the effective double layer occurring on a catalyst surface under electro-chemical promotion conditions. J Appl Electrochem 38:1065–1073. https://doi.org/10.1007/S10800-008-9539-X/FIGURES/9
95. Pacchioni G, Lomas JR, Illas F (1997) Electric field effects in heterogeneous catalysis. J Mol Catal A Chem 119:263–273. https://doi.org/10.1016/S1381-1169(96)00490-6
96. Steinmann SN, Michel C, Schwiedernoch R, Filhol JS, Sautet P (2015) Modeling the HCOOH/CO2 electrocatalytic reaction: when details are key. ChemPhysChem 16:2307–2311. https://doi.org/10.1002/CPHC.201500187
97. Neophytides SG, Vayenas CG (1995) TPD and cyclic voltammetric investigation of the origin of electrochemical promotion in catalysis. J Phys Chem 99:17063–17067. https://doi.org/10.1021/j100047a001
98. Ladas S, Kennou S, Bebelis S, Vayenas CG (2002) Origin of non-faradaic electrochemical modification of catalytic activity. J Phys Chem 97:8845–8848. https://doi.org/10.1021/J100137A004
99. Tsampas MN, Sapountzi FM, Boréave A, Vernoux P (2013) Isotopical labeling mechanistic studies of electrochemical promotion of propane combustion on Pt/YSZ. Electrochem Commun 26. https://doi.org/10.1016/j.elecom.2012.09.043
100. Panaritis C, Hajar YM, Treps L, Michel C, Baranova EA, Steinmann SN (2020) Demystifying the atomistic origin of the electric field effect on methane oxidation. J Phys Chem Lett 11:6976–6981. https://doi.org/10.1021/acs.jpclett.0c01485
101. Tsiakaras P, Vayenas CG (1993) Non-faradaic electrochemical modification of catalytic activity: VII. The case of methane oxidation on platinum. J Catal 140:53–70. https://doi.org/10.1006/JCAT.1993.1068
102. Nicole J, Comninellis C, Tsiplakides D, Pliangos C, Verykios XE, Vayenas CG (2001) Electrochemical promotion and metal-support interactions. J Catal 204:23–34. https://doi.org/10.1006/jcat.2001.3360

103. Tauster SJ, Fung SC, Garten RL (1978) Strong metal-support interactions. Group 8 noble metals supported on titanium dioxide. J Am Chem Soc 100:170–175. https://doi.org/10.1021/ja00469a029
104. Tauster SJ, Fung SC, Baker RTK, Horsley JA (1981) Strong interactions in supported-metal catalysts. Science (80–) 211:1121–1125. https://doi.org/10.1126/science.211.4487.1121
105. Spichiger-Ulmann M, Monnier A, Koudelka M, Augustynski J (1986) Spectroscopic and electrochemical study of the state of Pt in Pt-TiO2 catalysts. ACS Symp Ser:212–227. https://doi.org/10.1021/BK-1986-0298.CH021
106. Tauster SJ (2002) Strong metal-support interactions. Acc Chem Res 20:389–394. https://doi.org/10.1021/AR00143A001
107. van Deelen TW, Hernández Mejía C, de Jong KP (2019) Control of metal-support interactions in heterogeneous catalysts to enhance activity and selectivity. Nat Catal 211(2):955–970. https://doi.org/10.1038/s41929-019-0364-x
108. Chen MS, Goodman DW (2007) Interaction of Au with titania: the role of reduced Ti. Top Catal 44:41–47. https://doi.org/10.1007/s11244-007-0276-x
109. Vernoux P, Guth M, Li X (2009) Ionically conducting ceramics as alternative catalyst supports. Electrochem Solid-State Lett 12. https://doi.org/10.1149/1.3122746
110. Katsaounis A, Nikopoulou Z, Verykios XE, Vayenas CG (2004) Comparative isotope-aided investigation of electrochemical promotion and metal-support interactions 1. 18O2 TPD of electropromoted Pt films deposited on YSZ and of dispersed Pt/YSZ catalysts. J Catal 222:192–206. https://doi.org/10.1016/j.jcat.2003.10.010
111. Li X, Gaillard F, Vernoux P (2007) Investigations under real operating conditions of the electrochemical promotion by O_2 temperature programmed desorption measurements. Top Catal 44. https://doi.org/10.1007/s11244-006-0131-5
112. Dole HAE, Safady LF, Ntais S, Couillard M, Baranova EA (2014) Improved catalytic reactor for the electrochemical promotion of highly dispersed Ru nanoparticles with CeO2 support. In: ECS transactions. Electrochemical Society, pp 65–74
113. Isaifan R, Dole H, Obeid E, Lizarraga L, Baranova EA, Vernoux P (2011) Catalytic CO oxidation over Pt nanoparticles prepared from the polyol reduction method supported on Yttria-stabilized zirconia. ECS Trans 35:43. https://doi.org/10.1149/1.3641818
114. Ntais S, Isaifan RJ, Baranova EA (2014) An X-ray photoelectron spectroscopy study of platinum nanoparticles on yttria-stabilized zirconia ionic support: insight into metal support interaction. Mater Chem Phys 148:673–679. https://doi.org/10.1016/J.MATCHEMPHYS.2014.08.033
115. Isaifan RJ, Ntais S, Couillard M, Baranova EA (2015) Size-dependent activity of Pt/yttria-stabilized zirconia catalyst for ethylene and carbon monoxide oxidation in oxygen-free gas environment. J Catal 324:32–40. https://doi.org/10.1016/j.jcat.2015.01.010
116. Dole HAE, Baranova EA (2016) Ethylene oxidation in an oxygen-deficient environment: why ceria is an active support? ChemCatChem 8:1977–1986. https://doi.org/10.1002/CCTC.201600142
117. Dole HAE, Costa ACGSA, Couillard M, Baranova EA (2016) Quantifying metal support interaction in ceria-supported Pt, PtSn and Ru nanoparticles using electrochemical technique. J Catal 333:40–50. https://doi.org/10.1016/j.jcat.2015.10.015
118. Isaifan RJ, Baranova EA (2015) Effect of ionically conductive supports on the catalytic activity of platinum and ruthenium nanoparticles for ethylene complete oxidation. Catal Today 241:107–113. https://doi.org/10.1016/j.cattod.2014.03.061
119. Dole HA, Kim JM, Lizarraga L, Vernoux P, Baranova EA (2012) Catalytic CO oxidation over au nanoparticles supported on Yttria-stabilized zirconia. ECS Trans 45:265. https://doi.org/10.1149/1.3701316
120. Hajar YM, Houache MSE, Tariq U, Vernoux P, Baranova EA (2017) Nanoscopic Ni interfaced with oxygen conductive supports: link between electrochemical and catalytic studies. ECS Trans 77:51–66. https://doi.org/10.1149/07710.0051ecst
121. Eluri R, Paul B (2012) Synthesis of nickel nanoparticles by hydrazine reduction: mechanistic study and continuous flow synthesis. J Nanopart Res 14. https://doi.org/10.1007/s11051-012-0800-1

122. González-Cobos J, López-Pedrajas D, Ruiz-López E, Valverde JL, de Lucas-Consuegra A (2015) Applications of the electrochemical promotion of catalysis in methanol conversion processes. Top Catal 58:1290–1302. https://doi.org/10.1007/s11244-015-0493-7
123. Khan MS, Lee SB, Song RH, Lee JW, Lim TH, Park SJ (2016) Fundamental mechanisms involved in the degradation of nickel–yttria stabilized zirconia (Ni–YSZ) anode during solid oxide fuel cells operation: a review. Ceram Int 42:35–48. https://doi.org/10.1016/J.CERAMINT.2015.09.006
124. Panaritis C, Yan S, Couillard M, Baranova EA (2021) Electrochemical study of the metal-support interaction between FeOx nanoparticles and cobalt oxide support for the reverse water gas shift reaction. J CO2 Util 101824. https://doi.org/10.1016/J.JCOU.2021.101824
125. Li K, Liu K, Ni H, Guan B, Zhan R, Huang Z, Lin H (2018) Electric field promoted ultra-lean methane oxidation over Pd-Ce-Zr catalysts at low temperature. Mol Catal 459:78–88. https://doi.org/10.1016/j.mcat.2018.08.021
126. He L, Fan Y, Bellettre J, Yue J, Luo L (2020) A review on catalytic methane combustion at low temperatures: catalysts, mechanisms, reaction conditions and reactor designs. Renew Sust Energ Rev 119:109589. https://doi.org/10.1016/J.RSER.2019.109589
127. Guan B, Lin H, Zhu L, Huang Z (2011) Selective catalytic reduction of NOx with NH3 over Mn, Ce substitution Ti0.9V0.1O2−δ nanocomposites catalysts prepared by self-propagating high-temperature synthesis method. J Phys Chem C 115:12850–12863. https://doi.org/10.1021/JP112283G
128. Roy S, Viswanath B, Hegde MS, Madras G (2008) Low-temperature selective catalytic reduction of NO with NH3 over Ti0.9M0.1O2-δ (M = Cr, Mn, Fe, Co, Cu). J Phys Chem C 112:6002–6012. https://doi.org/10.1021/JP7117086/SUPPL_FILE/JP7117086-FILE002.PDF
129. Zhao X, Xu D, Wang Y, Zheng Z, Li K, Zhang Y, Zhan R, Lin H (2021) Electric field assisted benzene oxidation over Pt-Ce-Zr nano-catalysts at low temperature. J Hazard Mater 407:124349. https://doi.org/10.1016/J.JHAZMAT.2020.124349
130. Shen F, Li K, Xu D, Li X, Zhao X, Chen T, Zhan R, Lin H (2019) Electric field promoted complete oxidation of benzene over PdCexCoy catalysts at low temperature. Catalysis 9:1071. https://doi.org/10.3390/CATAL9121071
131. Mo S, Zhang Q, Li J, Sun Y, Ren Q, Zou S, Zhang Q, Lu J, Fu M, Mo D, Wu J, Huang H, Ye D (2020) Highly efficient mesoporous MnO2 catalysts for the total toluene oxidation: oxygen-vacancy defect engineering and involved intermediates using in situ DRIFTS. Appl Catal B Environ 264:118464. https://doi.org/10.1016/J.APCATB.2019.118464
132. Shen F, Li K, Xu D, Yan R, Chen T, Zhan R, Lin H (2019) Electric field promoted oxidation of naphthalene over Cu/Ce0.55Zr0.45Ox catalysts at low temperature. Mol Catal 476:110536. https://doi.org/10.1016/J.MCAT.2019.110536
133. Li K, Xu D, Liu K, Ni H, Shen F, Chen T, Guan B, Zhan R, Huang Z, Lin H (2019) Catalytic combustion of lean methane assisted by an electric field over MnxCoy catalysts at low temperature. J Phys Chem C 123:10377–10388. https://doi.org/10.1021/ACS.JPCC.9B00496
134. Monyoncho EA, Zamlynny V, Woo TK, Baranova EA (2018) The utility of polarization modulation infrared reflection absorption spectroscopy (PM-IRRAS) in surface and: in situ studies: new data processing and presentation approach. Analyst 143:2563–2573. https://doi.org/10.1039/c8an00572a
135. Urakawa A, Bürgi T, Schläpfer HP, Baiker A (2006) Simultaneous in situ monitoring of surface and gas species and surface properties by modulation excitation polarization-modulation infrared reflection-absorption spectroscopy: CO oxidation over Pt film. J Chem Phys 124:054717. https://doi.org/10.1063/1.2159484
136. Hernandez WY, Hadjar A, Giroir-Fendler A, Andy P, Princivalle A, Klotz M, Marouf A, Guizard C, Tardivat C, Viazzi C, Vernoux P (2015) Electrochemically-assisted NOx storage-reduction catalysts. Catal Today 241:143–150. https://doi.org/10.1016/j.cattod.2014.03.076

137. Stavrakakis E, West M, Johnston S, McIllwaine R, Poulidi D (2019) Hydration, CO2 stability and wireless electrochemical promotion studies on yttria-doped Ba (Ce, Zr) O3 perovskites. Ionics (Kiel) 25:1243–1257. https://doi.org/10.1007/s11581-019-02836-6
138. Poulidi D, Thursfield A, Metcalfe IS (2007) Electrochemical promotion of catalysis controlled by chemical potential difference across a mixed ionic-electronic conducting ceramic membrane – an example of wireless NEMCA. Top Catal 44:435–449. https://doi.org/10.1007/s11244-006-0136-0
139. Poulidi D, Metcalfe IS (2008) Comparative studies between classic and wireless electrochemical promotion of a Pt catalyst for ethylene oxidation. J Appl Electrochem 388(38):1121–1126. https://doi.org/10.1007/S10800-008-9525-3
140. Poulidi D, Metcalfe IS (2010) In situ catalyst activity control in a novel membrane reactor-reaction driven wireless electrochemical promotion of catalysis. Chem Eng Sci 65:446–450. https://doi.org/10.1016/j.ces.2009.06.013
141. Poulidi D, Rivas ME, Zydorczak B, Wu Z, Li K, Metcalfe IS (2012) Electrochemical promotion of a Pt catalyst supported on La0.6Sr0.4Co0.2Fe0.8O3 − δ hollow fibre membranes. Solid State Ionics 225:382–385. https://doi.org/10.1016/J.SSI.2012.03.010
142. Poulidi D, Anderson C, Metcalfe IS (2008) Remote control of the activity of a Pt catalyst supported on a mixed ionic electronic conducting membrane. Solid State Ionics 179:1347–1350. https://doi.org/10.1016/J.SSI.2008.01.056
143. Poulidi D, Mather GC, Metcalfe IS (2007) Wireless electrochemical modification of catalytic activity on a mixed protonic–electronic conductor. Solid State Ionics 178:675–680. https://doi.org/10.1016/J.SSI.2007.02.022
144. Fuelcell Store (2022) Yttria-stabilized zirconia (8% Y). Standard Grade Powder
145. Inframat Advanced Materials (2022) 8 mol% yttria stabilized zirconia (YSZ) Nano Powder, 99.9+%, 30–60 nm
146. Lelalertsupakul W, Assabumrungrat S, Bumroongsakulsawat P (2020) Electrochemical promotion of propane oxidation at Pt/BiCuVOx-YSZ thin-film cells: economical use of YSZ. J Environ Chem Eng 8. https://doi.org/10.1016/j.jece.2020.104141

Chapter 4
The Effective-Double-Layer as an Efficient Tool for the Design of Sinter-Resistant Catalysts

Ioannis V. Yentekakis

Abstract Effective promotion of catalytic reactions is always a grand challenge for heterogeneous catalysis. As it has been well-established, electrochemical promotion of catalysis (EPOC) through the *effective-double-layer* (EDL) created on catalyst particle surfaces is a unique, ultra-effective method for catalyst promotion. Nevertheless, catalyst nanoparticle (NP) stabilization at the typically elevated operation temperatures of catalysis is at least of equivalent, unless of much more importance, since sintering of NPs is inevitably a leading cause of catalyst degradation used for energy, environmental, and large-scale synthesis of commodity chemical applications with obvious economic drawbacks. We have recently discovered that the *effective-double-layer*, spontaneously created on catalyst nanoparticle surfaces via *metal-support* interactions with supports that have high lattice oxygen lability and mobility, can play a critical, additional to activity promotion, role, that is, the unprecedented stabilization of catalyst nanoparticles dispersed on them (i.e., anti-sinter catalysts). In addition to the experimental findings, we proposed a plausible model – based on the *effective-double-layer* approach introduced by Vayenas and co-workers for metal-support interactions – which streamlines and convincingly interprets the observed resistance to sintering, even redispersion of NPs. In this chapter all relevant experimental results obtained so far and their interpretation by means of the proposed mechanistic model are discussed.

Keywords Electrochemical promotion of catalysis · Effective-double-layer · Lattice oxygen lability · Resistance to sintering

I. V. Yentekakis (✉)
Laboratory of Physical Chemistry & Chemical Processes, School of Chemical & Environmental Engineering, Technical University of Crete (TUC), Chania, Greece
e-mail: yyentek@chenveng.tuc.gr

P. Vernoux, C. G. Vayenas (eds.), *Recent Advances in Electrochemical Promotion of Catalysis*, Modern Aspects of Electrochemistry 61,
https://doi.org/10.1007/978-3-031-13893-5_4

4.1 Introduction

Industrial heterogeneous catalysts typically consist of metal particles well(nano)-dispersed on high-surface-area supports such as metal oxides and mixed oxides, zeolites, etc. Restricting the active phases to the nanoscale, the so-called nanoparticles (NPs) maximize both the number of active catalytic sites and the undercoordinated (direct interactive) area between the active phase and the support [1, 2]. Such nanostructured catalysts are endowed with significant advantages, e.g., (i) efficient use of rare and expensive platinum group metals (PGMs) which are common catalysts in a variety of practical applications and (ii) increased number of undercoordinated (i.e., support-tuned) active metal sites, usually leading to beneficial effects on catalytic performance caused by wider metal-support interactions and the potential additional contribution of bifunctional reaction mechanisms [3–10].

Thanks to the development of new catalyst synthesis methods or the optimization of existing ones, through which we can achieve very narrow particle size distributions of deposited NPs up to the level of atomic dispersions [1, 2, 11–15], significant advances in nanocatalysis are currently being made regarding catalysts' activity.

However, promoting catalytic activity is a major issue, but catalyst stability is just as or even more important. Deterioration of catalytic performance via thermal agglomeration (particles sintering) under the typical elevated temperatures of catalyst operation, or during specific processes applied for catalyst regeneration, remains a key problem that has received much attention both for reasons of fundamental significance and practical importance [16–20]. In fact, thermal sintering is a leading cause of the degradation of industrial catalysts used for large-scale synthesis of commodity chemical, energy, and environmental applications.

In this chapter, we summarize recent results of our group showing that the lack of resistance, the resistance, or even redispersion of catalyst nanoparticles deposited on oxide supports strongly depends on the lattice oxygen ion lability/oxygen storage capacity (OSC) of the support [21–27]. It was found that the higher the oxygen ion lability/capacity of the support, the lower the propensity of the nanoparticles to agglomerate and, most importantly, the higher the propensity towards redispersion at high temperatures [24]. A model is also presented and analyzed that deciphers the role of the *effective-double-layer (EDL)* [$O^{\delta-}$, δ^{+}] – spontaneously created on the catalyst nanoparticle surfaces via thermally driven lattice oxygen spillover from supports with substantial OSC onto the nanoparticle surfaces – in the sintering behavior of the nanoparticles [21–27]. The model explains the observed anti-sintering behavior in terms of the two well-known particle agglomeration mechanisms, i.e., Ostwald ripening (OR) of atomic species and large particle migration and coalescence (PMC), governing sintering phenomena. It also provides a consistent explanation of the redispersion phenomena observed in our studies.

4.2 Catalyst Nanoparticle Sintering: A Leading Cause of the Degradation of Industrial Catalysts

Two basic mechanisms for catalytic particle agglomeration are generally accepted today, which have been demonstrated by advanced *operando* spectroscopic and microscopic methods (e.g., in situ XRD and in situ HRTEM) [17–20]. These mechanisms are schematically shown in Fig. 4.1 [24]. Specifically, one involves migration of large nanoparticles and subsequent coalescence (PMC; Fig. 4.1 case (i)) and the other net transport of single atomic species from smaller to larger nanoparticles that is so-called atomic ripening (AR; Fig. 4.1 case (ii)), which includes the particular case of Ostwald ripening (OR) (path b in Fig. 4.1 case (ii)). AR refers to any path of atom migration, either over the surface of the support or via the vapor phase [18]. Modes of sintering (PMC or OR) are strongly dependent on the metal-support couple under consideration and temperature and reaction conditions applied.

To distinguish between PMC and OR mechanisms operated on samples experienced to a variety of sintering protocols by means of traditional ex situ techniques, e.g., transmission electron microscopy (TEM), is nontrivial and rather impossible. Modern state-of-the-art in situ high-resolution transmission electron microscopy (in situ HRTEM) and other *operando* techniques have significantly increased our knowledge on the issue. Through them clear evidence that OR is the dominant mechanism in some specific catalytic systems has been provided [28, 29], although other authors point to the importance of PMC in controlling sintering of dispersed nanoparticles [14, 15], claiming that OR of supported noble metal NPs is a slow process that typically dominates the late stages of growth of large (ca. >5 nm) immobile NPs at high temperatures (400 – 1000 ° C) and over long time scales (hours to years).

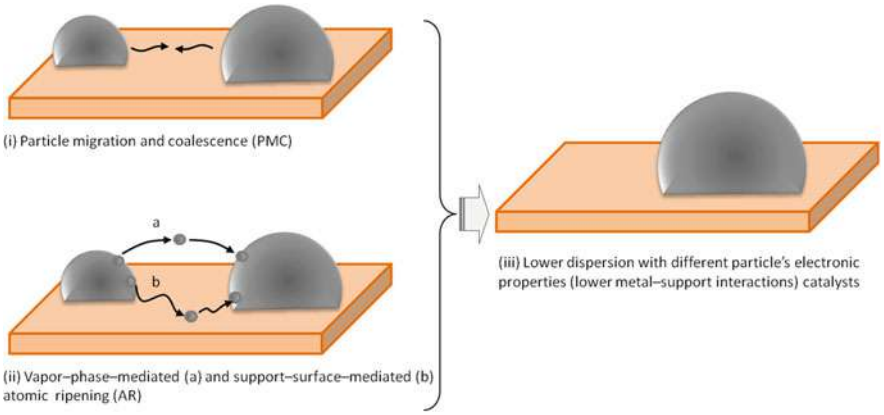

Fig. 4.1 Schematic of potential sintering mechanisms of catalytic nanoparticles leading to sintering, fewer undercoordinated sites, and reduced metal-support interaction. (Reused from Ref. [24] Open Access under a CC BY 4.0 license, https://creativecommons.org/licenses/by/4.0/)

The true is that all heterogeneous catalysts are inevitably subjected to sintering during operation at elevated temperatures or regeneration processes [16, 20]. Therefore, regardless of sintering mechanism, the effect poses a grand challenge for the development of sinter-resistant catalysts [17, 18].

A synopsis of our knowledge about particle agglomeration is as follows: Sintering is unambiguously a strong function of temperature regardless the prevailing sintering mechanism (PMC and OR), both of which require breaking of the bonds between metal atoms as well as between metal atoms and the surface of the support.

The respective Hütting ($T_H = 0.3T_{melting}$) and Tamman ($T_T = 0.5T_{melting}$) temperatures can provide a first indication of the temperatures at which surface and bulk atoms are mobilized (i.e., detached from large particles and diffused on the support surface) [16, 20]. Indeed, the susceptibility to sintering of some common heterogeneous catalysts (e.g., PGMs, Ni, Cu, Ag) in their metallic state (under reducing atmosphere) is in accordance with their T_H and T_T temperatures. That is, their stability generally decreases with decreasing T_H and T_T temperatures in the sequence: Ru > Ir > Rh > Pt > Pd > Ni > Cu > Ag [20]. Of course, the actual order is dependent on metal-support adhesion energy and possible strong interactions that can influence the ultimate sintering behavior.

Particles existing in their oxidation state the Hütting and Tamman temperatures are of less use for the prediction of nanoparticle stability. Particle volatility, thermal stability (some metal oxides decompose before T_H or T_T are reached), and the strength of the metal oxide-support interaction are the main factors responsible for the observed discrepancies [16, 20]. For example, Fiedorow et al. [30] investigating the stability of PGM particles supported on a relatively "inert" support (γ - Al_2O_3) obtained the following stability sequence in oxidizing atmospheres: Rh > Pt > Ir > Ru. This does not coincide with the predicted sequence based on the T_T of the respective PGM oxides: RuO_2(735K) > Rh_2O_3(687K) > IrO_2(685K) > PtO_2(362K). However, under reducing conditions in which the nanoparticles were in their metallic state, the stability sequence of the particles obtained, i.e., Ir $\sim$ Ru > Rh > pt, was consistent with their T_T.

It has also been widely observed that in the presence of significant metal-support interactions, simplified predictions based only on T_H or T_T are substantially altered. Therefore, such interactions have been adopted as key factors and tools in strategies aimed at designing sinter-resistant catalysts [17]. Supports with sufficient population of lattice oxygen defects such as ceria- or zirconia-based materials and perovskites are first in the list of these efforts. These materials provide high population of surface oxygen vacancies that can act as trapping centers for the dispersed active phases. The phenomenon is described as "atom trapping," a term reflecting the immobilization of isolated single atoms at support sites (oxygen vacancies) during their diffusion on the surface of the support [11–13], and has been used to design anti-sintering catalysts [21–27, 31, 32].

4.3 The Effective-Double-Layer (EDL) Approach for Conventional Catalyst Promotion

First at the Massachusetts Institute of Technology (MIT, USA) in 1981, and continuing at the University of Patras (UP, GR), Professor Vayenas and co-workers began publishing about a new physicochemical phenomenon they discovered, originally called "non-Faradaic electrochemical modification of catalytic activity" (NEMCA), later referred to as "electrochemical promotion of catalysis" (EPOC) [e.g., 33, 34, 35 and 36]. This new phenomenon allows for dramatic, in situ controlled, and reversible enhancement of catalyst activity and is achieved by the use of solid-state electrochemical galvanic cells of the type (Fig. 4.2a) [37]:

Working – catalyst electrode//ion conducting solid electrolyte//inert counter electrode

In brief, using such an electrochemical device (Fig. 4.2a), the chemisorptive properties and catalytic performance of metal catalysts interfaced with solid electrolytes (ionic conductors) are subjected to in situ controlled electrochemical promotion via external current or voltage applications, imposed between the catalyst metal film and the separate counter electrode. Catalytic promotion is therefore caused by the ions (promoter species) supplied from the solid electrolyte to the catalyst-electrode surface by means of the imposed external bias; ion flux follows Faraday's law, i.e., $r_z = I/zF$ (I is the applied current, z is the ion's charge, and F is Faraday's constant). According to the EPOC theory, the as-spillover ions onto the gas-exposed catalyst surface, together with their compensating charge in the metal (i.e., surface dipoles), establish an *effective-double-layer* (EDL) on the catalytically active surface altering its electron availability (the so-called work function) as schematically shown in Fig. 4.2b [e.g., 34, 37, 38, and 39]. As a result, the binding strength of chemisorbed reactants and intermediates is strongly affected, resulting in a significant modification on catalytic reaction rate. Typically, the resulted rate modification, r_{EPOC}-r_o, is significantly larger than the rate of ion flux causing it, i.e., $\Lambda = (r_{EPOC}\text{-}r_o)/(I/zF) >> 1$, which indicates a non-Faradaic behavior. In such EPOC phenomena, the net gain on the catalytic activity is described by the "rate enhancement ratio," $\rho = r_{EPOC}/r_o$, which is the ratio of the promoted (via EPOC) rate, r_{EPOC}, and the unpromoted (without application of external bias) one, r_o; up to *two orders of magnitude* rate enhancements have been achieved by this advanced way of promotion [34].

In addition to these great advantages, the EPOC method allows the use of promoter species that cannot be applied by conventional promotion methods due to their *sacrificial* nature (they participate in the reaction schemes or are desorbed, so they are quickly removed from the catalyst surface) [38, 39]. A typical example is the O^{2-} ion, which has been used as a promoter in most EPOC studies [34].

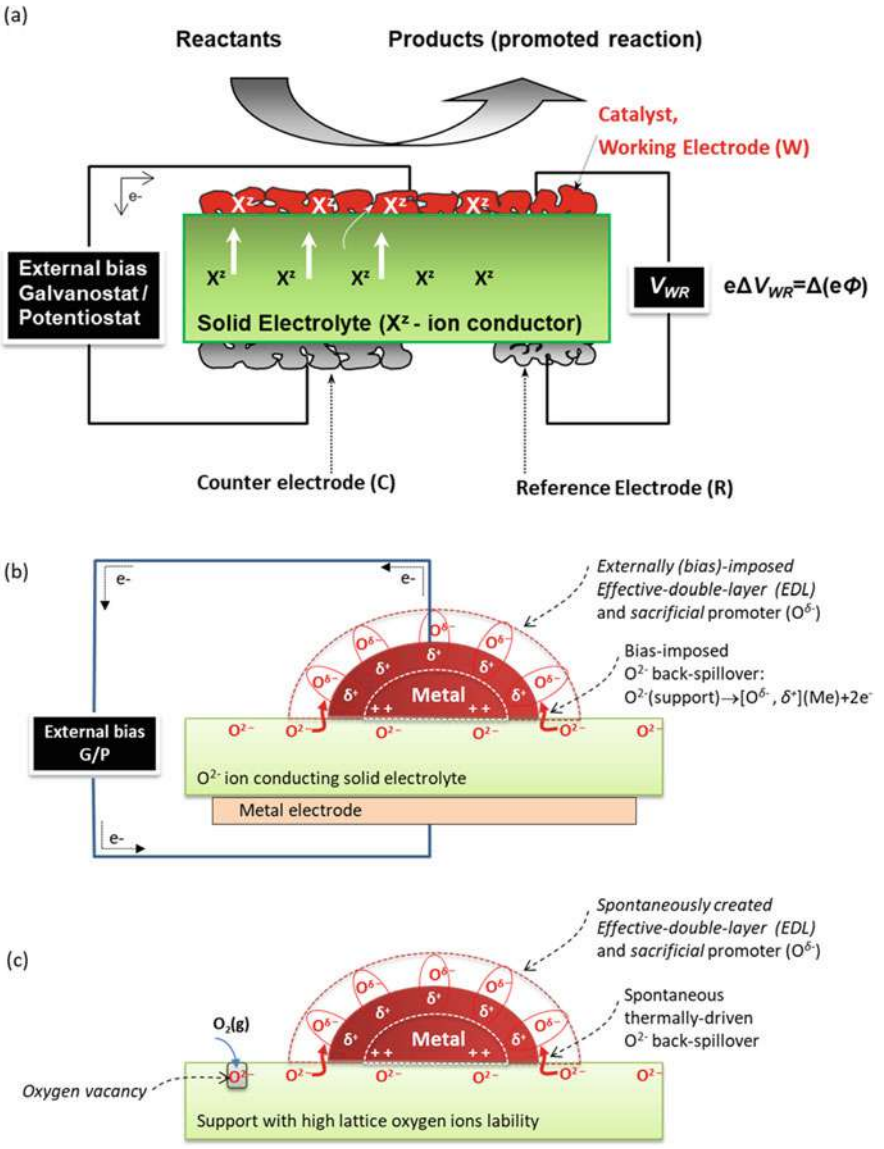

Fig. 4.2 (**a**) A typical solid-state electrochemical galvanic cell through which the electrochemical promotion of catalysis (EPOC) can be applied. (Adapted from Ref. [37] Open Access under a CC BY 4.0 license, https://creativecommons.org/licenses/by/4.0/. (**b**) Creation of the *effective-double-layer* [$O^{\delta-}$, δ^+] via externally imposed bias using O^{2-} ion conducting solid electrolyte. (**c**) Spontaneously created *effective-double-layer* via thermally driven O^{2-} ion back-spillover (wireless EDL creation) on catalyst nanoparticles dispersed on supports with high lattice oxygen ion lability and storage capacity)

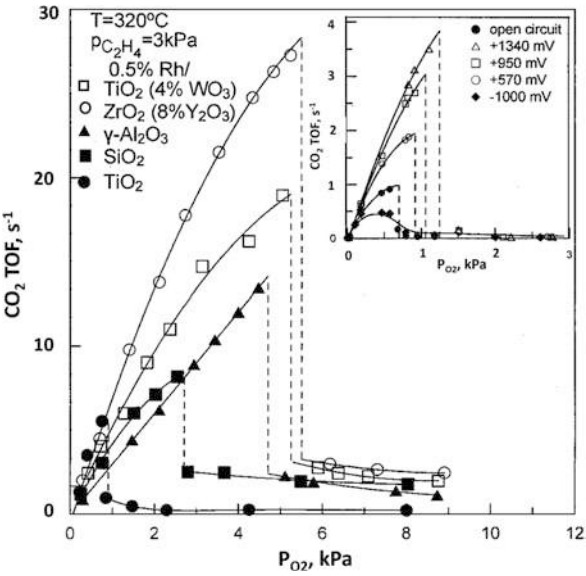

Fig. 4.3 C_2H_6 oxidation over Rh/YSZ electrocatalyst (for EPOC studies) and over traditionally supported Rh/TiO_2, Rh/SiO_2, Rh/YSZ, and $Rh/TiO_2(WO_3)$ catalysts (for metal-support interaction studies): promotion of the intrinsic activity of Rh induced via EPOC concept was similar with the support-mediated promotion by supports with high oxygen storage capacity and mobility. (Reproduced with permission form Ref. [5]. Copyright 1995. Elsevier)

However, there is a technical difficulty in implementing EPOC on large-scale systems/processes. It is the necessity of cables for the application of external bias (Fig. 4.2b). This necessity becomes even more critical when using *sacrificial promoters* that require a constant supply of these species in order to keep their surface concentration constant at the desired level.

This technical difficulty seems to be manageable after the works of Yentekakis et al. [4] and Pliangos et al. [5], who demonstrated for the first time that promotional effects of O^{2-} ions imposed by external bias (i.e., via the EPOC concept, Fig. 4.2a) are similar to those obtained spontaneously (i.e., wirelessly, without external bias) on highly dispersed traditional catalyst formulations, that provided the catalyst supports with high lattice oxygen ion lability/mobility (Fig. 4.3) [4, 5]. These important experimental findings led to an innovative and reasonable interpretation by Vayenas and co-workers of *metal-support interactions* (MSI) in catalysis, which also points to their common origin with EPOC [9]. It was suggested that an *effective-double-layer* [$O^{\delta-}$, δ^+], spontaneously created (via thermally driven O^{2-} ion back-spillover) in the case of MSI (Fig. 4.2c) or externally imposed (via external bias) in EPOC (Fig. 4.2b), is the common origin of the promotional effects in both methods of promotion.

Today, the spontaneous back-spillover O^{2-} ions from supports characterized with high lattice oxygen ion lability and mobility (e.g., CeO_2-containing supports) and the as created EDL, [$O^{\delta-}$, δ^+], on the surface of metal particles, are issues widely accepted and used to interpret metal-support interactions in full analogy with the electrochemically generated EDL previously invoked to explain EPOC phenomena [3, 10].

4.4 The Additional Effect of the *Effective-Double-Layer* (EDL) in Heterogeneous Catalysis: Catalyst Nanoparticle Stabilization and Redispersion

4.4.1 Correlation of EDL with Catalyst Nanostructure Stabilization: Experimental Findings

In a series of publications, we have recently reported [21–27] that the resistance, or lack of resistance to sintering, or even the redispersion of supported catalyst particles experienced to high-temperature oxidative conditions is a strong function of the support lattice oxygen ion lability or equivalently its total oxygen storage capacity (t-OSC). These systematic experimental studies enabled us to decipher the phenomenon and finally to provide a plausible model that implicates the *effective-double-layer*, [$O^{\delta-}$, δ^{+}], spontaneously created on the catalyst nanoparticle surfaces via thermally driven lattice oxygen spillover from supports with substantial oxygen ion lability onto the nanoparticle surfaces [3, 9, 10, 38, 39], which adequately explains all the experimental findings of the nanoparticle sintering or even redispersion characteristics in terms of both OR and PMC mechanisms involved. That is, we argue that the *effective-double-layer* (EDL) approach of Vayenas and co-workers for metal-support interactions has a dual functional role of great significance in heterogeneous catalysis: *EDL simultaneously controls both the intrinsic activity and the nanostructure stability of supported catalysts*. Therefore, it is offered as an effective tool for the design of highly active (promoted) and at the same time very stable catalysts, which is a long-term goal of industrial catalysis.

So far, our studies have been carried out using nanoparticles of two different metals, namely, Ir [21–23, 26, 27] and Rh [24, 25, 27]. According to the literature, under conditions of oxidative thermal sintering, Ir has a higher propensity for agglomeration than Rh [20, 30]. Such nanoparticles were dispersed in a series of selected oxide and mixed oxide supports, bearing in mind that it encompasses a wide range of oxygen lattice ion lability/storage capacity, namely, γ-Al_2O_3, yttria-stabilized-zirconia (YSZ: 8 mol% Y_2O_3-ZrO_2), alumina-ceria-zirconia (ACZ: 80 wt % Al_2O_3–20 wt % $Ce_{0.5}Zr_{0.5}O_{2-\delta}$), ceria-zirconia (CZ: $Ce_{0.5}Zr_{0.5}O_{2-\delta}$), and gadolinia-doped-ceria (GDC: 10 mol% Gd_2O_3-CeO_2). Table 4.1 summarizes the above

Table 4.1 Total surface area (S_{BET}) and total oxygen storage capacity (t-OSC) of the materials used as supports for the dispersion of catalyst nanoparticles in our sintering behavior studies [21–27]

Supports	S_{BET} (m^2/g)	OSC (μmolO_2/g)
γ-Al_2O_3 (100% Al_2O_3)	178	0
YSZ (8 mol% Y_2O_3-ZrO_2)	5	6
ACZ (80wt%Al_2O_3–20wt%$Ce_{0.5}Zr_{0.5}O_{2-\delta}$)	149	110
GDC (10 mol% Gd_2O_3-CeO_2)	10	186
CZ ($Ce_{0.5}Zr_{0.5}O_{2-\delta}$)	22	557

Table 4.2 Characteristics of fresh and sintered catalysts

Catalysts	S_{BET} (m^2/g)	D_{metal} (%)	Mean metal particle size (nm)[a] H_2-chem/TEM	Ref.
Ir-based catalysts[b]				
0.7 wt% Ir/γ - Al_2O_3-*fresh*	159	88	0.8/1.2 ± 0.4	[21–23]
0.7 wt% Ir/γ - Al_2O_3-*sinter@750*	140	3	28.8/14.5 ± 6.5	
0.7 wt% Ir/YSZ-*fresh*	4	33	2.2/1.2 ± 0.4	
0.7 wt% Ir/YSZ-*sinter@750*	4	3	22.6/10.5 ± 5.5	
0.4 wt% Ir/GDC-*fresh*	10	48	1.5/1.7 ± 0.5	
0.4 wt% Ir/GDC-*sinter@750*	10	41	1.8/2.0 ± 1.0	
0.4 wt% Ir/ACZ-*fresh*	73	41	1.8/1.6 ± 0.5	
0.4 wt% Ir/ACZ-*sinter@750*	64	45	1.6/1.9 ± 0.4	
1.0 wt% Ir/γ - Al_2O_3-*fresh*	167	70	1.0/1.2 ± 0.3	[26]
1.0 wt% Ir/γ - Al_2O_3-*sinter@750*	140	5	13.6/n.m.	
0.4 wt% Ir/ACZ-*fresh*	73	41	1.7/1.8 ± 0.5	
0.04 wt% Ir/ACZ-*sinter@750*	64	34	2.1/n.m.	
0.6 wt% Ir/CZ-*fresh*	17	61	1.2/1.3 ± 0.4	
0.6 wt% Ir/CZ-*sinter@750*	16	44	1.6/n.m.	
Rh-based catalysts[b]				
1.0 wt% Rh/γ - Al_2O_3-*fresh*	160	88	1.2/1.3 ± 0.4	[24, 25]
1.0 wt% Rh/γ - Al_2O_3-*sinter@750*	159	69	1.6/1.6 ± 0.3	
1.0 wt% Rh/γ - Al_2O_3-*sinter@850*	140	41	2.6/1.6 ± 0.3	
0.8 wt% Rh/ACZ-*fresh*	136	77	1.8/1.5 ± 0.5	
0.8 wt% Rh/ACZ-*sinter@750*	n.m	91	1.4/2.0 ± 0.8	
0.8 wt% Rh/ACZ-*sinter@850*	n.m	81	1.7/1.5 ± 0.4	
0.8 wt% Rh/CZ-*fresh*	17	27	5.0/5.1 ± 1.7	
0.8 wt% Rh/CZ-*sinter@750*	12	65	2.1/2.5 ± 0.7	
0.8 wt% Rh/CZ-*sinter@850*	n.m	62	2.2/2.0 ± 0.7	

[a] The mean metal particle size compares values estimated via H_2 chemisorption and HRTEM
[b] Ir and Rh contents were measured via ICP-OES

supports, their total surface area (S_{BET}), and oxygen storage capacity (OSC), while Table 4.2 the corresponding Ir- or Rh-based catalysts synthesized with their main characteristics before ("*fresh*" samples) and after undergoing thermal aging under oxidative conditions ("*sinter*" samples).

The estimated OSC values of the supports by using hydrogen temperature-programed reduction (H_2-TPR) measurements are summarized in Table 4.1; γ-Al_2O_3 and YSZ have zero to low OSC values, whereas ACZ, GDC, and CZ have moderate to high OSC values. As an example, Fig. 4.4a shows the reducibility performance (H_2-TPR profiles) of γ-Al_2O_3, ACZ, and CZ supports; the total amount of H_2 consumed, determined from the integrated area of the respective TPR profiles in the time interval of the experiment, is used for the estimation of the total oxygen storage capacity (t-OSC) of the supports [21–27]; the high OSC values of ACZ and CZ reflect the $Ce^{4+} \rightarrow Ce^{3+}$ reduction of these CeO_2-containing supports. When the metal nanoparticles are dispersed on the supports the main reduction peaks are shifted towards lower temperatures (i.e., the reducibility is promoted); their t-OSC

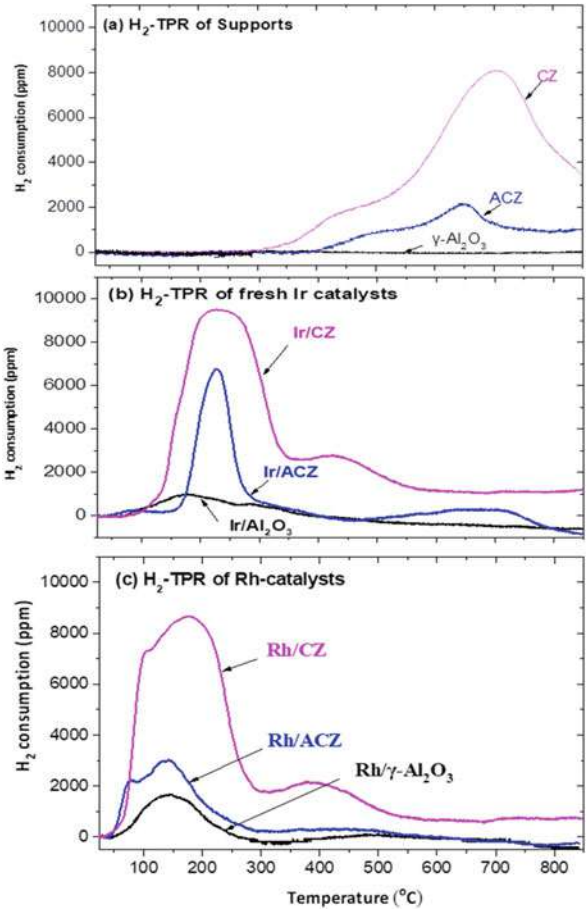

Fig. 4.4 H_2-TPR profiles of the γ-Al_2O_3, ACZ, and CZ supports (**a**) and the counterpart Ir (**b**) [26] and Rh (c) [24]–based catalysts. (Adapted from Refs [24, 26]. Open Access under a CC BY 4.0 license, https://creativecommons.org/licenses/by/4.0/)

values however are only slightly increased reflecting the contribution of the reduction of IrO_2- or Rh_2O_3-oxidized particles (Fig. 4.4b,c).

Sintering performance of supported Ir and Rh nanoparticles on supports with different OSC values was investigated on samples that underwent thermal aging at oxidative environment (air). Nanoparticle sizes were estimated by the use of isothermal H_2 chemisorption and corroborated by HRTEM measurements on both fresh and sintered samples (Table 4.2).

Representative HRTEM images and corresponding particle distribution profiles depicting the sintering behavior of Ir and Rh nanoparticles on the different supports are shown in Figs. 4.5, 4.6, and 4.7. As can be seen in Fig. 4.5, all the fresh Ir/γ-Al_2O_3, Ir/YSZ, Ir/GDC, and Ir/ACZ showed small iridium particles (ca. 1–2 nm), regardless of the nature and surface area of the support used. However, the sintered samples exhibited a very strong dependence of Ir particle size on the nature of the support: Ir particles supported on γ-Al_2O_3 underwent extensive growth (Figs. 4.5 and 4.6 items a and b; Table 4.2).

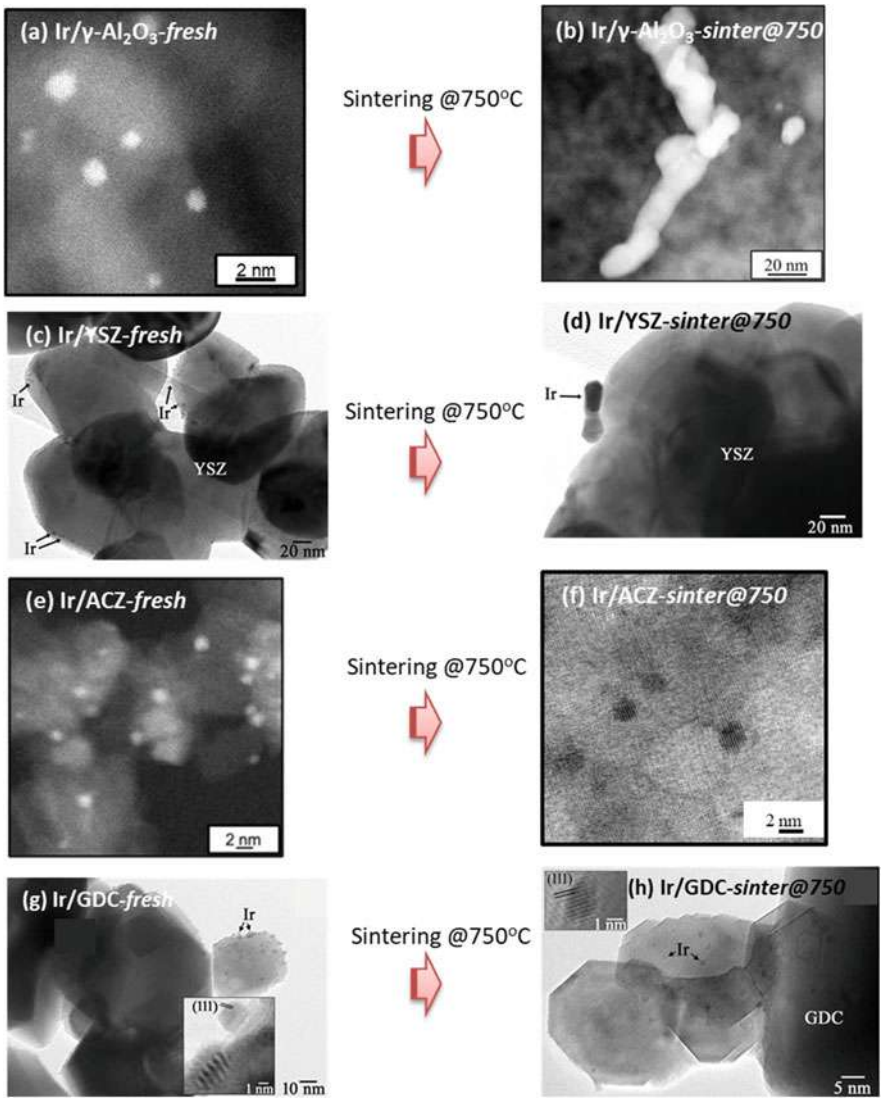

Fig. 4.5 HRTEM images of the fresh (**a**, **c**, **e**, **g**) and sinter@750 (**b**, **d**, **f**, **h**) Ir/γ-Al_2O_3, Ir/YSZ, Ir/ACZ, and Ir/GDC catalysts, respectively [27]

In a similar manner, Ir particles supported on YSZ had undergone significant increase in size (Figs. 4.5 and 4.6 items c and d; Table 4.2) and some changes in shape after sintering, but significantly less than that observed on Ir/γ-Al_2O_3 sample. In contrast, Ir nanoparticles supported on ACZ (Figs. 4.5 and 4.6 items e and f; Table 4.2) and GDC (Figs. 4.5 and 4.6, items g and h; Table 4.2) retained their original small sizes and uniform spatial distribution after sintering.

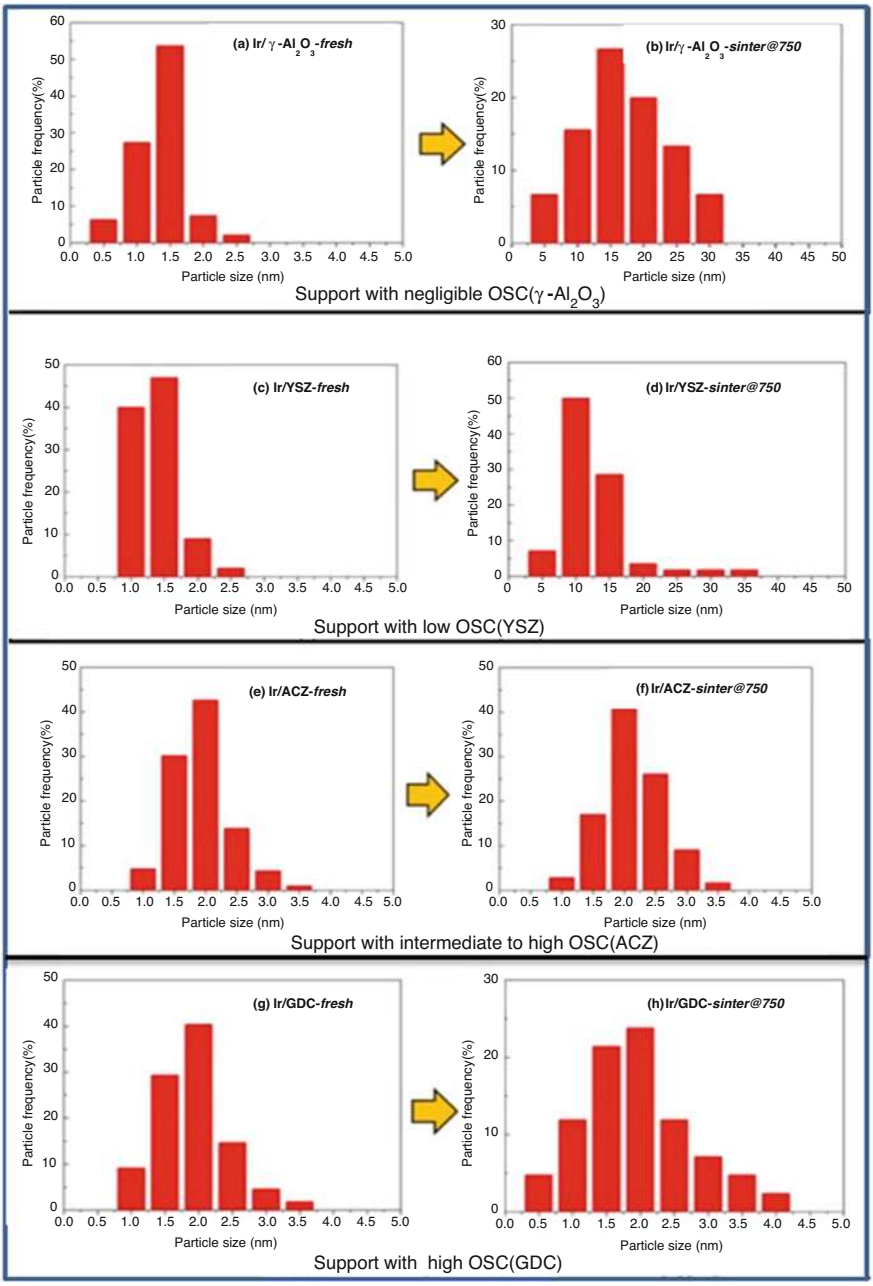

Fig. 4.6 TEM size distribution profiles for fresh (**a**, **c**, **e**, **g**) and sinter@750 (**b**, **d**, **f**, **h**) Ir/γ-Al_2O_3, Ir/YSZ, Ir/ACZ, and Ir/GDC catalysts, respectively. (Reproduced with permission form ref. [22]. Copyright 2016, Elsevier)

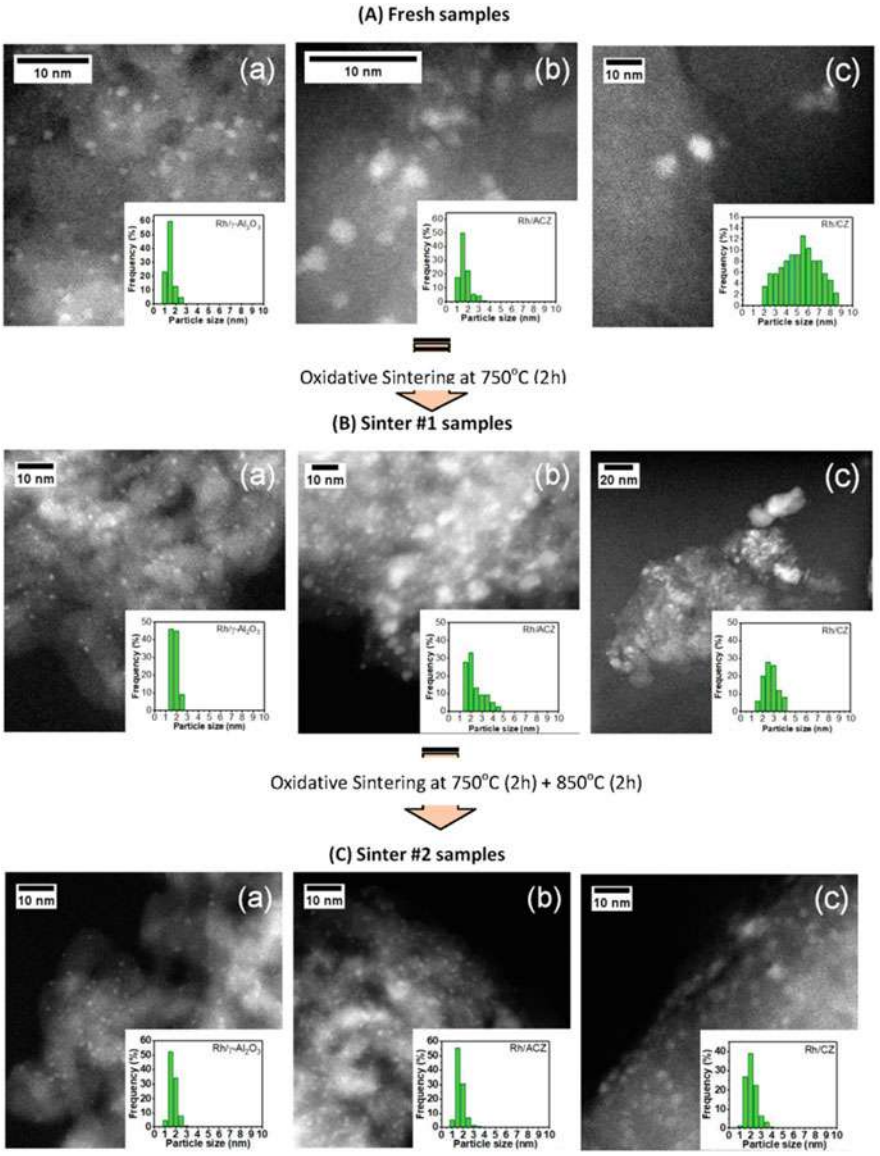

Fig. 4.7 HRTEM images and particle size distributions for (**a**) fresh, (**b**) sinter #1 (oxidative sintering at 750 °C for 2 h), and (**c**) sinter #2 (oxidative sintering at 750 °C for 2 h + at 850 °C for 2 h) of (**a**) Rh/γ-Al_2O_3, (**b**) Rh/ACZ, and (**c**) Rh/CZ catalysts. (Reused from Ref. [24] Open Access under a CC BY 4.0 license, https://creativecommons.org/licenses/by/4.0/)

Similar anti-sintering effects through supports with high OSCs were obtained during thermal sintering at oxidative atmosphere of supported Rh nanoparticles (Fig. 4.7 and Table 4.2) [24]. Once again Rh nanoparticles supported on γ-Al_2O_3

systematically increase in size upon increasing sintering temperature (from 1.2 nm on Rh/γ-Al_2O_3-*fresh* to 1.6 nm and 2.6 nm on Rh/γ-Al_2O_3-*sinter@750* and Rh/γ-Al_2O_3-*sinter@850* catalysts, respectively, as shown in Table 4.2 and Fig. 4.7, images A(a), B(a), and C(a)). In contrast, Rh nanoparticles supported on ACZ and CZ not only retain small sizes after sintering procedure but also undergo *redispersion*, which is much more pronounced in the case of the latter, Rh/CZ. Specifically, an initial mean particle size of 1.8 nm on fresh Rh/ACZ (Fig. 4.7, image A(b)) goes to 1.4 nm after 2 h of sintering at 750 °C (Fig. 4.7, image B(b)) and then results in some slight particle growth after 2 additional hours sintering at 850 °C (Fig. 4.7, image C(b)), thus finally retaining a marginal redispersion of ~6% after the end of the sintering procedure (Table 4.2). For Rh NPs supported on CZ, an initial mean particle size of 5 nm on the fresh sample (Fig. 4.7, image A(c)) becomes 2.1 nm on Rh/CZ-*sinter@750* (Fig. 4.7, image B(c)) and then undergoes to 2.2 nm on Rh/CZ-*sinter@850* sample (Fig. 4.7, image C(c)), i.e., accomplishing a redispersion of ~58% (Table 4.2) [24, 27].

The key observation arising from the aforementioned results is that the strong resistance to sintering, or even redispersion, in an oxidizing environment of catalyst NPs on supports with high oxygen ion lability/storage capacity is dramatically different from their vulnerable behavior on supports with negligible or low oxygen ion lability. Supports without or negligible OSC, such as γ-Al_2O_3 (OSC~0 μmol O_2/g) and YSZ (OSC~6 μmol O_2/g), do not actually prevent particle growth. In striking contrast, high OSC supports such as ACZ (OSC~110 μmol O_2/g), GDC (OSC~186 μmol O_2/g), and CZ (OSC~557 μmol O_2/g) significantly prevent particle sintering as shown for both Ir and Rh metals investigated, and more importantly they can promote particle redispersion as demonstrated for Rh.

The aforementioned strong dependence of the sintering behavior of Ir and Rh nanoparticles on the support OSC is clearly shown in Figs. 4.8, 4.9, and 4.10, respectively. The figures illustrate the NP growth and/or redispersion (defined by Eq. 4.1) versus support's OSC [23, 24, 27]:

$$\%particle\ growth = 100 \cdot (PS - PS^{\circ})/PS^{\circ} \tag{4.1}$$

where *PS* denotes mean metal particle size and the superscript "°" refers to fresh (un-sintered) samples; negative values of the "*% particle growth*" parameter indicate *redispersion*.

Obviously (Fig. 4.8), Ir nanoparticles are dramatically susceptible to sintering on supports with about zero (γ-Al_2O_3) and low (YSZ) OSCs, exhibiting as high as 3500% and 930% particle growth, respectively [23]. In striking contrast their propensity to sintering becomes negligible, namely, −13% (redispersion), 16%, and 10%, when supported on supports with intermediate to high OSCs, i.e., on ACZ, GDC, and CZ with 110, 186, and 557 μmol O_2/g OSC, respectively.

Similarly (Figs. 4.9 and 4.10), Rh nanoparticles supported on γ-Al_2O_3 (OSC~0 μmol O_2/g) underwent an about 33% growth after sintering at 750 °C and significantly higher (~117%) after an additional sintering at 850 °C. However, when Rh particles are dispersed on ACZ (OSC~110 μmol O_2/g), and especially on CZ

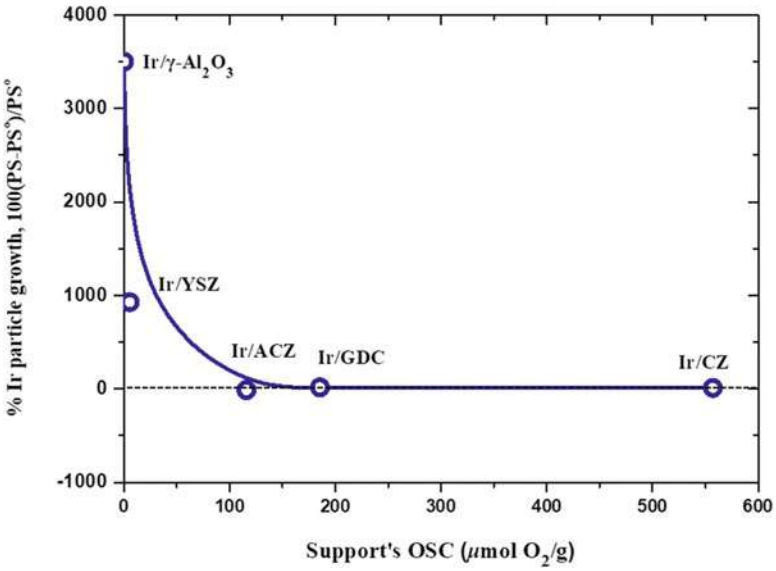

Fig. 4.8 Correlation of the sintering behavior (% particle growth) of supported iridium nanoparticles with the oxygen storage capacity (OSC) of the support. (Reproduced with permission from ref. [23]. Copyright 2017, Springer)

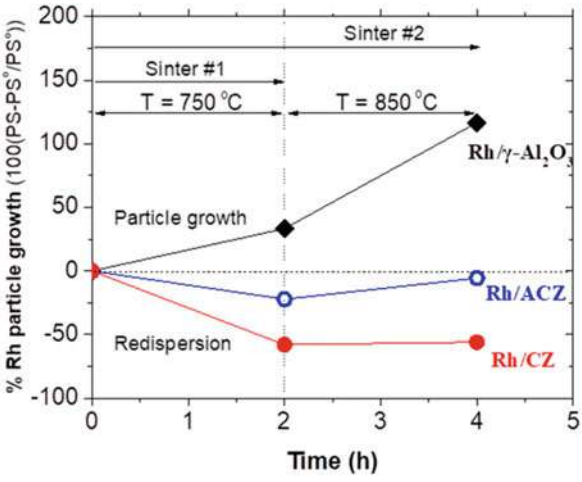

Fig. 4.9 *% particle growth* (positive values) or *redispersion* (negative values) of Rh nanoparticles dispersed on γ-Al_2O_3, ACZ, and CZ supports versus sintering time and temperature under oxidizing environment (20% O_2/He). (Reused from Ref. [24] Open Access under a CC BY 4.0 license, https://creativecommons.org/licenses/by/4.0/)

(OSC~557 μmol O_2/g), not only their agglomeration is prevented, but they end up redispersed [24]: For Rh/ACZ, an initial about 22% redispersion obtained after 2 h oxidative aging at 750 °C is followed by particle growth after 2 additional hours heating at 850 °C, finally leading to only a slight redispersion of 6% (−6% Rh particle growth); for Rh/CZ, the initial redispersion of 58% (−58% Rh particle growth) occurred during 2 h of heating at 750 °C and remained unaffected after 2 additional hours heating at 850 °C.

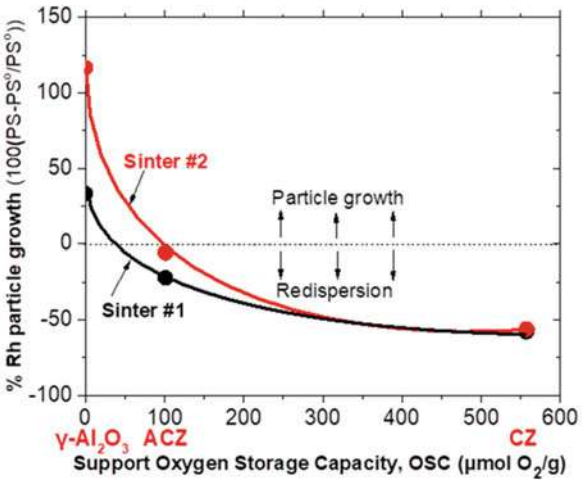

Fig. 4.10 *% Rh particle growth* (+) or *redispersion* (−) versus OSC of the support for sinter #1 (thermal sintering for 2 h at 750 °C with 20%O_2/He) and sinter #2 (thermal sintering for 2 h at 750 °C plus 2 h at 850 °C with 20%O_2/He) conditions. (Reused from Ref. [24] Open Access under a CC BY 4.0 license, https://creativecommons.org/licenses/by/4.0/)

4.4.2 *Correlation of EDL with Catalyst Nanostructure Stabilization: The EDL-Based Model for Sinter-Resistant and Redispersion Behavior*

A mechanistic model was developed by our group, which adequately and consistently explains the experimental findings concerning both resistance to oxidative thermal sintering and redispersion of metal nanoparticles dispersed on oxide supports with high lattice oxygen lability/storage capacity [21–27].

The model deciphers the dominant role of the *effective-double-layer* [$O^{\delta-}$, δ^+] on particle sintering behavior and demonstrates for the very first time that spontaneous, thermally driven, O^{2-} back-spillover from high OSC supports onto catalyst nanoparticle surfaces can affect and control not only their intrinsic activity (a well-known effect [e.g., 3–6, 9, 10, 38, 39]) but also their sintering behavior [21–27]. That is, the *effective-double-layer* [$O^{\delta-}$, δ^+] plays a highly important *dual function* role in heterogeneous catalysis, as schematically shown in Fig. 4.11.

What we argue is that the spontaneously created EDL, [$O^{\delta-}$, δ^+], endows catalyst particles with a negative charge at their gas-exposed surfaces, leading to interparticle repulsion at short range, thus preventing particle-particle encounters followed by coalescence (i.e., PMC [18–20]): *The higher the lability and capacity of O^{2-} ions in the support, the lower the vulnerability of the nanoparticles to sintering in an oxidative environment* [21–27].

Our model also involves *atomic trapping* as an additional contributing factor in the sinter-resistant mechanism: Labile support lattice oxygen creates surface oxygen vacancies ($V_O^{\cdot\cdot}$) [3] that act as traps for very small (atomic) metal particles, thus inhibiting their diffusion and agglomeration [22–24, 27]. At the same time, the presence of EDL and the concomitant $O^{\delta-}$-modified surface barrier of the large catalyst particles increases the activation energies for detachment and reattachment

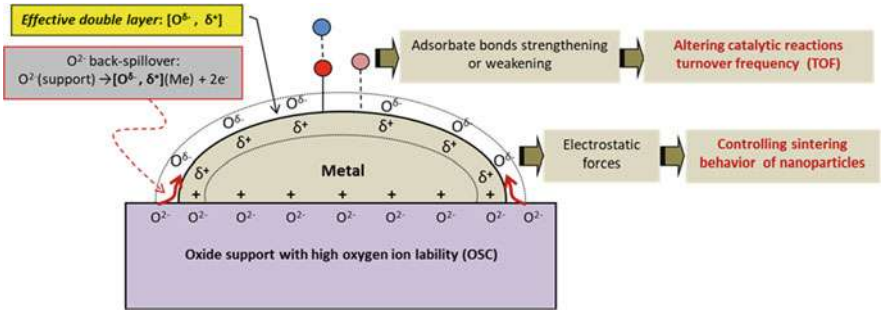

Fig. 4.11 The dual functional role of the *effective-double-layer* [$O^{\delta-}$, δ^+] in heterogeneous catalysis: promotion of the intrinsic catalytic activity and stabilization of catalyst nanostructure. (Reused from Ref. [24] Open Access under a CC BY 4.0 license, https://creativecommons.org/licenses/by/4.0/)

of metal entities whose transport would otherwise lead to continuous growth of large particles at the expense of smaller particles according to the Ostwald ripening (OR) mechanism of particle growth [22–24, 27]. Such effects on surface particle diffusion will be negligible or low for supports with low lattice oxygen lability (e.g., Al_2O_3, YSZ), which therefore cannot prevent particle agglomeration through either PMC or OR pathways. Therefore, the best supports for providing sintering resistance will be those with the highest O^{2-} ion mobility, such as CeO_2, doped with gadolinium, zirconium, and other additives that increase the defects of ceria lattice, increasing oxygen ion vacancies and consequently O^{2-} capacity and mobility [40, 41]. All the contributing factors on the control of the sintering and/or redispersion behavior according to our EDL-based model are schematically depicted in Fig. 4.12 [24]. There are three main pathways (I, II, and III) associated with particle size growth, and our model includes the key factors that are expected to control their contribution and intensity.

Path I (Fig. 4.12): It concerns large particle migration and coalescence (PMC), which according to our model is considered to be strongly inhibited by electrostatic interparticle repulsion due to the presence of the EDL and the consequent coating of particles with a net negative charge ($O^{\delta-}$).

Path II (a) and (b) (Fig. 4.12): It concerns the Ostwald ripening (OR) sequence, i.e., atom detachment (IIa) and reattachment (IIb), both of which are supposed to be inhibited by the increased activation energies resulting from the $O^{\delta-}$-encaptured particle surfaces.

Path III (Fig. 4.12): It concerns the diffusion of detached atomic species from smaller particles towards larger ones, which is strongly inhibited by atom trapping at surface oxygen vacancy ($V_O^{\cdot\cdot}$) centers.

According to these factors proposed in our EDL-based model to be critical to the sintering behavior of the catalyst nanoparticles, the experimental findings in Sect. 4.4.1 (Figs. 4.5, 4.6, 4.7, 4.8, 4.9 and 4.10 and Table 4.2) can be consistently rationalized as follows.

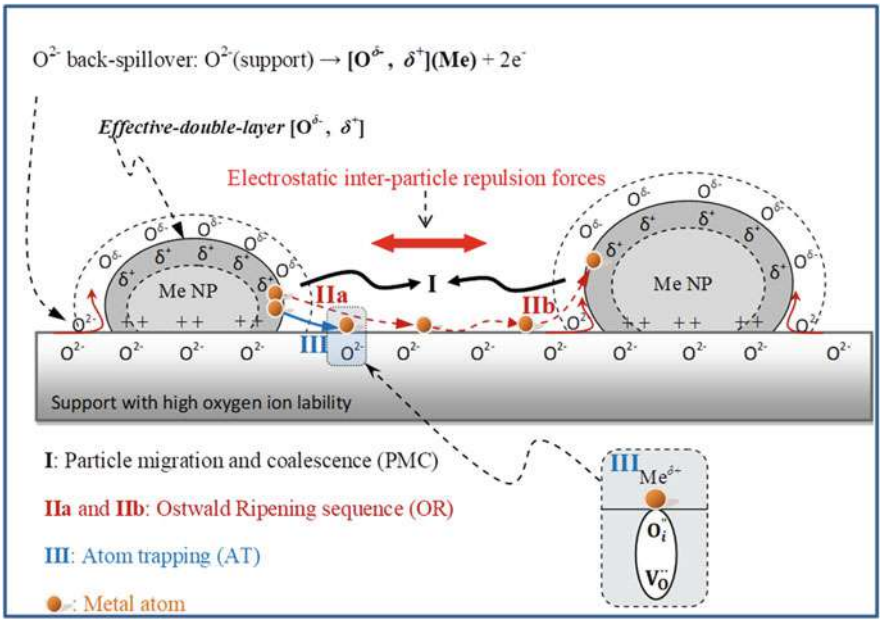

Fig. 4.12 Model deciphering the sintering resistance of dispersed catalyst nanoparticles against PMC and OR agglomeration mechanisms as well as redispersion phenomena, resulting from the simultaneous action of (i) the EDL and its subsequent interparticle repulsion forces and the suppression of detachment/reattachment of atom species and (ii) the atom trapping at support surface oxygen ion vacancies. $O_i^{''}$ is the Krönger-Vink notation for interstitial (labile) O^{2-} ions; their concentration is determined by the equilibrium $O_O \leftrightarrow V_O + O_i^{''}$ between lattice oxygen O_O and oxygen ion vacancies [27]. (Adapted from Ref. [24] Open Access under a CC BY 4.0 license, https://creativecommons.org/licenses/by/4.0/)

- In the absence of the *effective-double-layer* (e.g., when γ-Al_2O_3 support is used), none of the above potential anti-sintering factors (I, II, and III) are at work to protect particle agglomeration; the obtained severe Ir and Rh nanoparticle agglomeration on Ir/γ-Al_2O_3 (Fig. 4.8) and Rh/γ-Al_2O_3 (Figs. 4.9 and 4.10) catalysts is then easily understandable. The extent of agglomeration mainly depends on the nature of the metal particle (Ir is more sensitive to agglomerate than Rh).
- The presence of the *effective-double-layer*, with its accompanying effects on paths I and II, can lead to either moderate or substantial sinter protection, or even redispersion, depending on the intensity of the EDL and the transport properties of the metal particles (metal nature).

Thus, for Ir nanoparticles dispersed on YSZ support, which is characterized by low OSC, therefore capable of creating only low-intensity EDL, some (albeit limited) attenuation of particle size growth tendency is achievable compared to that observed for Ir/γ-Al_2O_3 (Fig. 4.8) [23].

For Ir or Rh nanoparticles dispersed on ACZ, which is characterized by moderate OSC, not only sintering protection but even redisperison of NPs is achievable after thermal aging at oxidizing conditions (Figs. 4.9 and 4.10; Table 4.2). Especially, for Rh/ACZ an initial slight redispersion after 2 h at oxidative sintering conditions was almost quenched after 4 h at the same conditions (Fig. 4.9) [24]. Obviously, even moderate-intensity EDL appears to be capable of suppressing the PMC mechanism of particle aggregation (path I) through the interparticle repulsion forces developed. However, path IIa, i.e., atomic species detachment via Ostwald ripening mechanism, still seems to work. These detached species are then diffused onto the two separate entities (alumina or CZ) of the ACZ surface, initially having a fairly good chance of encountering trapping centers (oxygen vacancies) on the CZ component of the ACZ, where they are immobilized; otherwise, they are recaptured by large particles. The possibility of diffusion of some detached atoms onto the surface of the alumina component of the ACZ support is not negligible. In that case their trapping as atomic entities is also limited. Therefore, the whole scenario suggests moderate redispersion as indeed observed (Fig. 4.9). By increasing the sintering time, the population of the trapping centers is gradually decreasing, which is able to reverse the final net redispersion effect, as actually observed (Fig. 4.9) [24].

For Rh nanoparticles dispersed in CZ support characterized by high OSC, the expected dense EDL on the surface of NPs strongly suppresses PMC (path I). Paths IIa and IIb are also inhibited because of the high intensity of the EDL. At the same time, the coexisting high population of support trapping centers (surface oxygen vacancies) is capable of extensive and effective trapping of potentially detached individual species, significantly reducing their surface mobility, thus minimizing the probability of path IIb. The pronounced Rh redispersion obtained even after prolonged sintering (Figs. 4.9 and 4.10) is in accordance with the above considerations.

Finally, although effective anti-sintering behavior was obtained for Ir nanoparticles dispersed on supports with OSC (i.e., on Ir/GDC and Ir/CZ catalysts; Fig. 4.8) [23], no redispersion was observed as that discussed above for Rh NPs dispersed on similar supports [24]. This implies that the nature of the NP and its own thermal transport properties combined with the intensity of the EDL, the population of the support trapping centers (surface oxygen vacancies), and the sintering temperature imposed are all critical factors that compete with or act in parallel, determining the net agglomeration/redispersion result.

4.5 EDL-Induced Anti-sintering Behavior Evaluated by Selected Catalytic Reactions

Three catalytic reaction systems of high environmental and energy importance [41–43] were selected to exemplify and evaluate thermal aging stability of the catalysts according to the aforementioned EDL-governed anti-sintering and redispersion phenomena. These reaction systems were:

The dry (CO_2) reforming of methane (DRM)

$$CH_4 + CO_2 \rightarrow 2H_2 + 2CO \quad (R.1)$$

The CO_2 methanation

$$CO_2 + 4H_2 \rightarrow CH_4 + 2H_2O \quad (R.2)$$

The direct nitrous oxide decomposition (deN_2O):

$$N_2O \rightarrow N_2 + ½O_2 \quad (R.3)$$

The scope of these studies was to verify that under conditions of steady-state catalytic reaction the behavior of the catalysts was indeed consistent with their independently measured sintering characteristics (Sect. 4.4).

4.5.1 Dry Reforming of Methane Reaction

Catalysis of DRM (reaction R.1) is of tremendous interest, ranking among the top issues of applied catalysis in the light of environmental protection, renewable energy production, and circular economy, because it involves the simultaneous reduction of two key greenhouse gases (CO_2 and CH_4) producing synthesis gas (CO + H_2) and provides an efficient way for CO_2 utilization (recycling) as well as the direct implementation of biogas [3, 42–47]. Synthesis gas (syngas) is an important building block for large-scale industrial processes to produce hydrogen, ammonia, and Fischer–Tropsch-derived liquid energy carriers and chemicals [3, 44].

Typically operating at high temperatures (ca. 700–850 °C), where catalyst particle agglomeration is the main cause of catalyst deactivation, DRM catalysts are prone to such deactivation. At the same time, large crystallites are susceptible and accelerate carbon deposition and accumulation, which is an additional factor for DRM catalyst deactivation. To eliminate the latter cause of DRM deactivation, catalyst regeneration procedures are followed, typically involving high-temperature oxidation-reduction cycles for carbon combustion. However, during such regeneration procedures, particle agglomeration and therefore the permanent catalyst deactivation is again a critical problem. Consequently, discovering means and ways to stabilize DRM catalysts with particles at the nanoscale level is a grand challenge [42, 43].

DRM time-on-stream stability studies performed on Ir/γ-Al_2O_3, Ir/YSZ, and Ir/GDC catalysts, which were subjected to two successive high-temperature oxidation-reduction cycles (750 °C), showed that while Ir/γ-Al_2O_3 and Ir/YSZ underwent significant and progressive permanent deactivation, Ir/GDC DRM performance remained very stable after the two sintering steps imposed (Figs. 4.13 and 4.14) [21, 27]. Specifically, for Ir particles dispersed on γ-Al_2O_3 and YSZ supports with

low OSC values, the sintering process resulted in a significant deactivation: the high (~90%) initial CH_4 conversion efficiency of the fresh catalysts was decreased to ~60% after 1 h sintering and then to ~20% after 1 additional hour of sintering at the same temperature (Fig. 4.14). In striking contrast, Ir nanoparticles dispersed on GDC, a support with significant OSC, offered extremely stable behavior during the same sintering process, maintaining methane conversion to the initial level of fresh sample (> 80%), regardless of whether it has been subjected to sintering conditions. It is apparent that the present DRM performance evaluation results are in remarkable agreement with the sintering behavior of these catalysts presented in Sect. 4.4 (Table 4.2 and Fig. 4.8).

Similar to the above studies, additional studies were recently performed with a series of Ir/γ - Al_2O_3, Ir/ACZ, and Ir/CZ catalysts [26]. The imposed sintering procedure was slightly different, involving a longer total period of time of imposition of thermal sintering conditions, i.e., 4 instead of 2 h; the results were very similar (Fig. 4.15), and our main conclusions were confirmed once again. Table 4.3 summarizes results concerning the sintering behavior of Ir-based catalysts exemplified via DRM reaction [21, 26].

Taking into account recent results demonstrating that supports with high oxygen storage capacity and lability characteristics can induce bifunctional mechanism for DRM promotion through the oxygen vacancies in the support and the EDL created on catalyst particle surfaces [3], and the results analyzed herein showing that the creation of EDL is a factor protecting catalyst particle against agglomeration, we can conclude that new horizons are opened for the design of effective and stable DRM catalyst formulations.

4.5.2 *CO_2 Methanation Reaction*

Despite their finite amounts in nature and the fact that their use inevitably leads to the emission of tremendous quantities of CO_2 in the atmosphere, fossil fuels (coal, oil, and natural gas) unfortunately remain the dominant source of energy in the industrial, commercial, residential, and transportation sectors. However, with CO_2 to be the dominant greenhouse gas and to have the major contribution to the greenhouse effect and the concomitant global warming and climate change, its emission control has become a critical and urgent environmental issue [43, 48–51]. A possible mitigation of this problem can be provided by energy models accompanied with a reduced environmental footprint which commonly combines *circular economy* strategies [44, 52–54]. CO_2 capture and utilization (recycling) through its conversion to added-value products and fuels are nowadays among the approaches that receive intense research and technological interest [43, 44, 48–54]. The catalytic hydrogenation of CO_2 towards CH_4, also known as the *Sabatier reaction* (R.2), is among the top approaches in respect to the aforementioned strategies [48, 51, 52]. Notably, the hydrogen demands for CO_2 methanation (R.1) can be provided via a solar- or wind-powered water-splitting system. This further expands the eco-friendly and

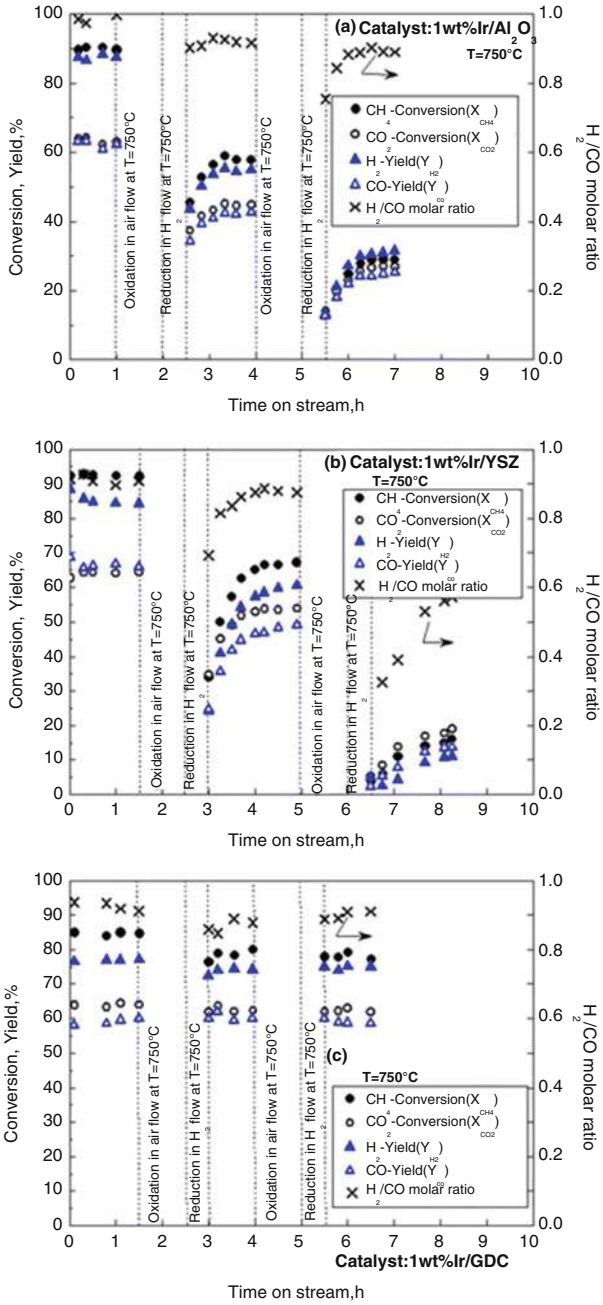

Fig. 4.13 Time-on-stream DRM stability experiments on Ir/γ - Al_2O_3 (**a**), Ir/YSZ (**b**), and Ir/GDC (**c**) catalysts upon repeated (subsequent) oxidation-reduction cycles. *Conditions*: T = 750 °C; *feed composition*: $[CH_4] = 35.5$ % , $[CO_2] = 64.5$ % ($CO_2/CH_4 = 1.8/1$); $F_{t,\,in} = 50$ cm^3/min .. Catalyst mass w_{cat} = 100 mg. (Reproduced with permission from Ref. [21]. Copyright 2015, Springer Nature)

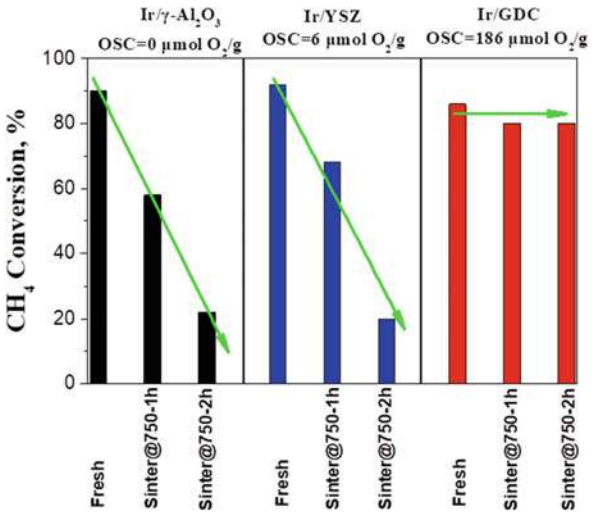

Fig. 4.14 CH_4 conversion efficiency of fresh and sintered Ir/γ-Al_2O_3, Ir/YSZ, and Ir/GDC catalysts under DRM reaction at 750 °C and $CH_4/CO_2 = 35.5\ \% / 64.5\ \%$. Sinter@750-1 h and Sinter@750-2 h represent catalysts sintered in air flow at 750 °C for 1 and 2 h in total, respectively [27]

sustainability character of the CO_2 methanation concept, also known as *power-to-gas* process [52, 54], which attracts even intense interest as a promising method for the "storage" of hydrogen, thereby overcoming the safety challenges of direct storage and transport of the latter. Methane can then have a variety of important applications, including domestic, industrial, power plants, and other natural gas-related sectors, distributed through the ever-growing natural gas grid.

Using the Rh-series of catalysts listed in Table 4.2, we were enabled to evaluate the catalyst turnover frequency (TOF) performance in respect to the EDL-induced effects via both active sites' promotion (electronic metal-support interactions) and particle size. A volcano-type variation of methanation turnover frequency was found in respect to support OSC, i.e., to the intensity of the created EDL. Between the γ-Al_2O_3, ACZ, and CZ supports that were used for Rh nanoparticle dispersion, the support with intermediate OSC value (i.e., ACZ with OSC~100 μmol O_2/g) offered the optimal TOF promotion via the intermediate intensity EDL created (Fig. 4.16); to minimize the contribution of particle size effects that could lead to misleading conclusions, the catalysts compared in Fig. 4.16 have chosen to have quite similar mean Rh particle size values. It was concluded that the *effective-double-layer* created on the surface of Rh particles via O^{2-} back-spillover from supports with intermediate and high oxygen lability (ACZ and CZ respectively) and its concomitant effect on strengthening the Rh—CO bond (CO is a critical intermediate of CO_2 methanation pathway) fits well with the experimental results of Fig. 4.16; a high-intensity EDL (i.e., in the case of CZ) causes over-strengthening of Rh—CO bond, thus CO-poisoning [25]. This effect also accounts for the final competition result between the methanation and reverse water-gas shift reactions during CO_2 hydrogenation [25].

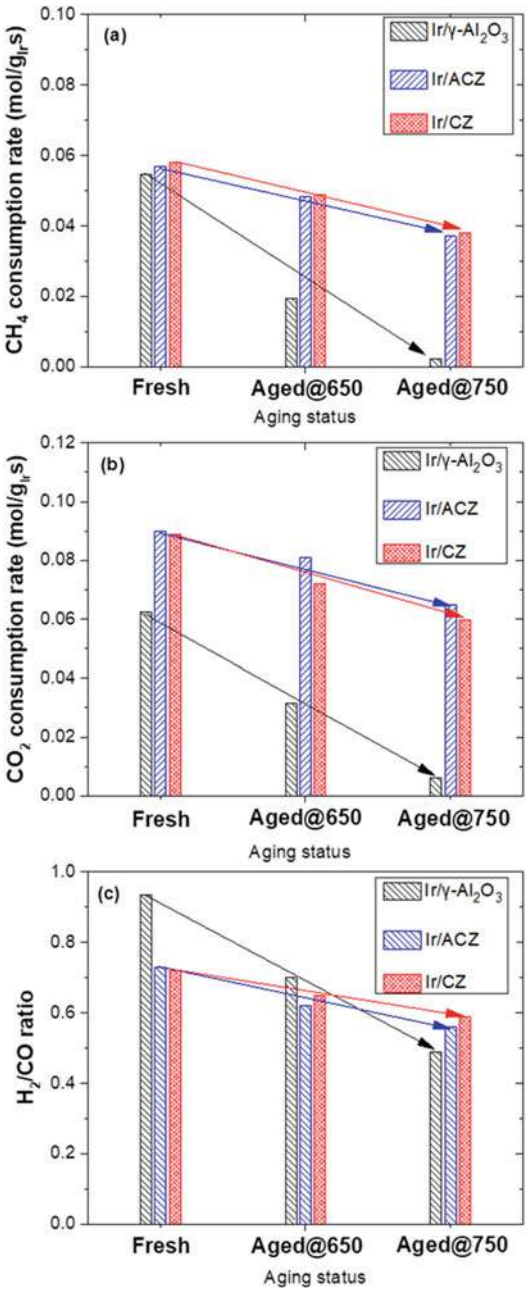

Fig. 4.15 The effects of consecutive oxidative thermal aging on the DRM performance, i.e., methane consumption rate (**a**), carbon dioxide consumption rate (**b**), and H_2/CO molar ratio (**c**) of Ir/γ-Al_2O_3, Ir/ACZ, and Ir/CZ catalysts. Aging protocols: (i) Aged@650 (2 h in situ oxidation with 50 mL/min flow of 20% O_2/He at 650 °C); (ii) Aged@750 (consecutive 2 h additional in situ oxidation with 50 mL/min flow of 20% O_2/He at 750 °C). DRM performance was evaluated at 750 °C, equimolar feed composition $[CH_4] = [CO_2] = 50\%$ at a total pressure of $m_{cat} = 50$mg, WGHSV = 120, 000 mL/g_{cat} · h. (Reused from Ref. [6] Open Access under a CC BY 4.0 license, https://creativecommons.org/licenses/by/4.0/)

Table 4.3 Normalized percentage deactivation of catalysts DRM performance, $\Delta r_{CH_4}^{norm.}(\%)$ and $\Delta r_{CO_2}^{norm.}(\%)\left(\Delta r_i^{norm.}(\%) = 100 \cdot \left|r_i^a - r_i^f\right| / r_i^f \text{ where } i \text{ denotes } CH_4 \text{ or } CO_2\ [26]\right)$, after exposure of the catalysts to oxidative thermal sintering protocols

Catalyst	Support *t-OSC* (μmol O_2/g)	$\Delta r_{CH_4}^{norm.}(\%)$		$\Delta r_{CO_2}^{norm.}(\%)$		Ref.
		First sintering	Second sintering	First sintering	Second sintering	
Ir/γ-Al_2O_3	0	64.5[a]	95.7[b]	49.5[a]	90.2[b]	[26]
Ir/ACZ	110	15.1[a]	35.1[b]	10.0[a]	27.8[b]	[26]
Ir/CZ	557	15.5[a]	34.5[b]	19.1[a]	33.0[b]	[26]
Ir/γ-Al_2O_3	0	35.6[c]	68.8[d]	29.0[c]	58.1[d]	[21]
Ir/YSZ	6	28.3[c]	81.5[d]	14.7[c]	69.0[d]	[21]
Ir/GDC	186	5.9[c]	5.2[d]	0.0[c]	0.0[d]	[21]

[a]Sintering protocol: 2 h at 650 °C; DRM testing conditions: $[CH_4] = [CO_2] = 50\ \%$ ($CO_2/CH_4 = 1/1$), WGHSV = 120, 000 mL/$g_{cat} \cdot h$

[b]Sintering protocol: 2 h at 650 °C plus 2 h at 750 °C; DRM testing conditions: $[CH_4] = [CO_2] = 50\ \%$ ($CO_2/CH_4 = 1/1$), WGHSV = 120, 000 mL/$g_{cat} \cdot h$

[c]Sintering protocol: 1 h at 750 °C; DRM testing conditions: $[CH_4] = 35.5\ \%$, $[CO_2] = 64.5\ \%$ ($CO_2/CH_4 = 1.8/1$), WGHSV = 30, 000mL/$g_{cat} \cdot h$

[d]Sintering protocol: 2 h at 750 °C; DRM testing conditions: $[CH_4] = 35.5\ \%$, $[CO_2] = 64.5\ \%$ ($CO_2/CH_4 = 1.8/1$), WGHSV = 30, 000mL/$g_{cat} \cdot h$

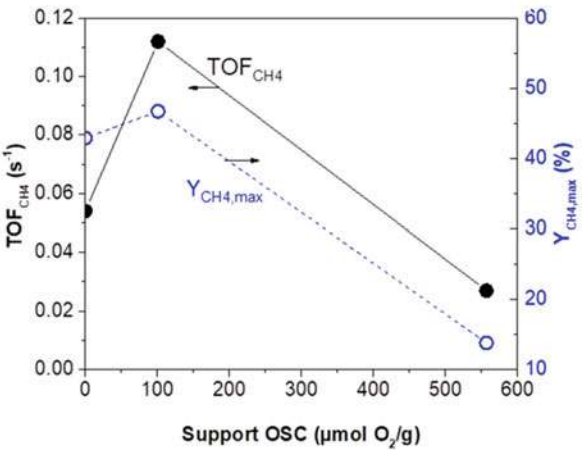

Fig. 4.16 Dependence of methane turnover frequency (TOF_{CH4}) at T = 280 ° C and maximum methane yield ($Y_{CH4,\ max}$) on support oxygen storage capacity. Experimental conditions: feed composition of 5% CO_2/20 % H_2/75% Ar at 1 bar; mass of catalyst m_{cat} = 50 mg; fixed mean contact time of CO_2 at $\tau(CO_2) \sim 1.3$ s. (Reused from Ref. [25] Open Access under a CC BY 4.0 license, https://creativecommons.org/licenses/by/4.0/)

Moreover, CO_2 methanation has been reported as a structure-sensitive reaction [e.g., 55, 56] where particle size affects methanation efficiency in a way that still remains unclear, often found to be favored on larger particles [56]. Evidently, any further insight elucidating what are the main material properties and how they interact, affecting the structural sensitivity of the reaction, will provide advantages and benefits for the design and optimization of CO_2 methanation catalysts. Our methodology, i.e., the EDL-based method on controlling the particle size (stability

and/or redistribution) of supported catalysts, has allowed us to shed light on and decipher this phenomenon as well. Specifically, we found that, for Rh/γ-Al_2O_3 (lack of OSC and thus EDL) CO_2 methanation reaction (R.2) was strongly favored on small particles, and the opposite for Rh/CZ (high OSC ∼ 560 μmol O_2/g and thus high intensity EDL) due to the simultaneous aforementioned reverse (over-promotion) effects of EDL on Rh—CO adsorption bond, which are further favored on lower in size particles, that correspond to a larger amount of undercoordinated sites leading to enhanced metal-support interactions [25].

That is, EDL provides an effective method for fine-tuning of these two critical parameters, i.e., particle size and surface electronic properties, resulting in the design novel CO_2 methanation catalyst formulations that are optimized in activity and stability (Fig. 4.17).

4.5.3 N_2O Decomposition Reaction

Having a global warming potential as high as ~300, nitrous oxide (N_2O) is a powerful greenhouse gas significantly contributing to global warming. It is also the dominant stratospheric ozone-depleting gas. Therefore, the abatement of N_2O from anthropogenic sources, such as mobile or stationary fossil fuel combustion processes and certain industries (e.g., adipic acid and nitric acid industries where N_2O is emitted as a by-product), is an urgent need [57–59]. The catalytic decomposition of N_2O to N_2 and O_2 is the most promising approach [59].

Catalytic N_2O decomposition on Ir nanoparticles is a reaction with well-known particle size dependence (i.e., structure-sensitive reaction), practically favored on larger Ir particles [60]. Although due to this fact the N_2O decomposition reaction is an inverse example, we used it to verify that under conditions of steady-state catalytic reaction the behavior of the four Ir/γ-Al_2O_3, Ir/YSZ, Ir/GDC, and Ir/ACZ (Table 4.2) was indeed consistent with their independently measured sintering characteristics [22, 23]. The following key points emerged from these studies: (i) the particle size dependence of Ir-catalyzed N_2O decomposition was clearly verified – larger Ir particles strongly favor N_2O decomposition (Fig. 4.18); (ii) partially oxidized Ir particle surface favors the reaction; and (iii) in the case of supports characterized by high OSC, which strongly favored the persistence of small catalyst particles, simultaneous stronger catalyst-support interactions further depressed N_2O decomposition turnover frequencies (Fig. 4.18).

That is, for this particular reaction, the net effect of Ir particle size and metal-support interactions (both EDL-derived effects) was a strong N_2O-TOF degradation for Ir nanoparticles dispersed on high OSC supports, which favor the maintenance of small particles.

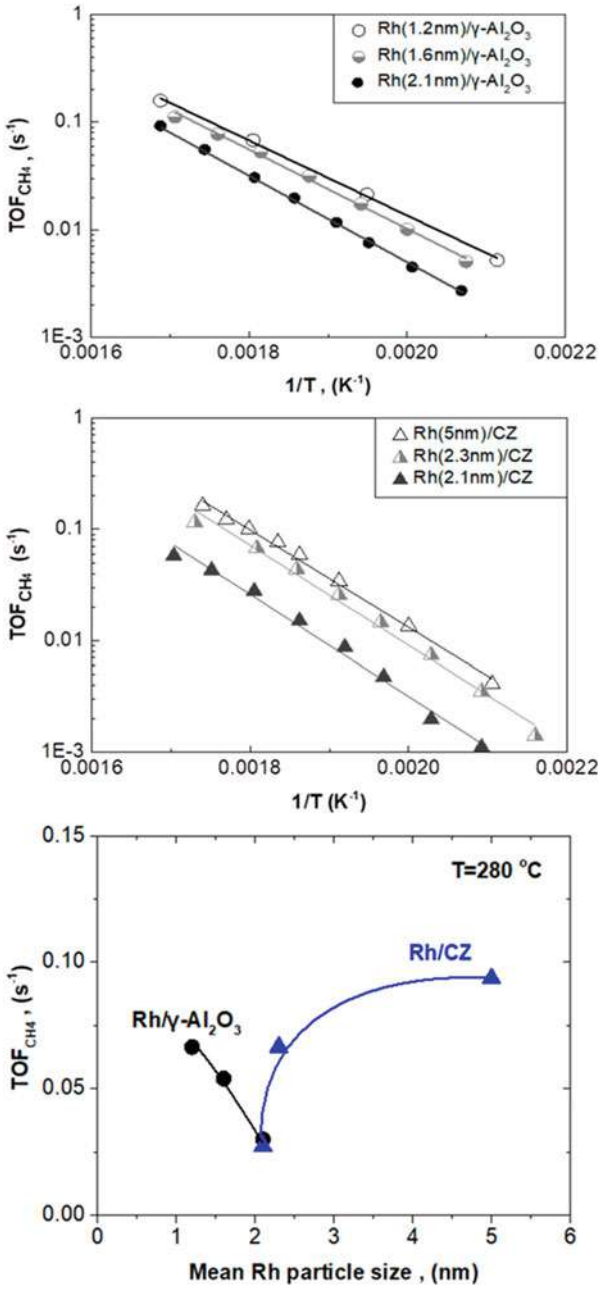

Fig. 4.17 Effect of Rh particle size on the turnover frequency of CO_2 formation (TOF_{CH4}) obtained over Rh/γ - Al_2O_3 and Rh/CZ catalysts at T = 280 ° C. Experimental conditions: feed composition of 5% CO_2/20 % H_2/75% Ar at 1 bar; mass of catalyst $m_{cat} = 50$ mg; fixed mean contact time of CO_2 at $\tau(CO_2) \sim 1.3$ s, and the reaction to be operated at the differential mode. (Reused from Ref. [25] Open Access under a CC BY 4.0 license, https://creativecommons.org/licenses/by/4.0/)

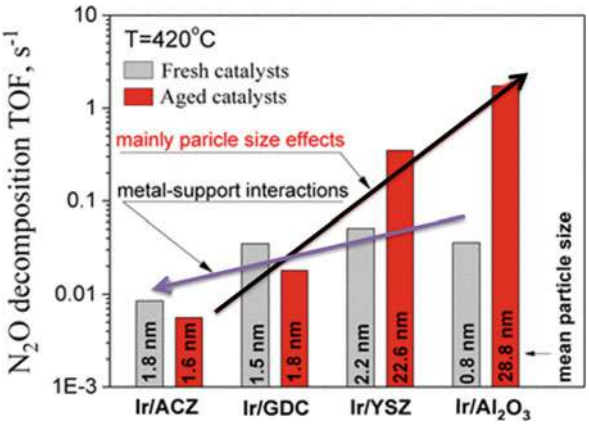

Fig. 4.18 Direct N_2O decomposition on fresh and sintered at oxidizing conditions Ir/γ-Al_2O_3, Ir/YSZ, Ir/ACZ, and Ir/GDC catalysts. Combined effects of metal-support interactions and particle size on N_2O decomposition turnover frequency. Conditions: 1000 ppm N_2O/He, $F_t = 150 cm^3/min$, $w_{cat} = 50$ mg. (Reproduced with permission from Ref. [23]. Copyright 2018, Springer Nature)

4.6 Conclusions and Prospects

This chapter reviews our team's results on a new phenomenon in heterogeneous catalysis, that is, catalysts' nanostructure stabilization by means of the *effective-double-layer (EDL)*. As we recently discovered, the EDL approach, introduced by Vayenas and co-workers some years ago to interpret metal-support interactions and concomitant catalyst promotion effects, an additional and equally important effect of EDL on the overall behavior of heterogeneous catalysts is the protection of the catalytic nanoparticles against agglomeration (thermal sintering), and under certain conditions even the in situ redispersion of the nanoparticles. This *dual function* role of EDL on catalysts behavior can be used as an effective tool to design highly active and at the same time highly stable catalyst formulations, which is a long-term goal in industrial catalysis.

The following key issues and conclusions can be drawn from these experimental findings:

- The sintering behavior of catalyst nanoparticles dispersed on oxide supports strongly correlates with the oxygen storage capacity (OSC) of the support. Specifically, catalyst NPs dispersed on a variety of oxide supports with different lattice oxygen lability and storage capacity (OSC) exhibit markedly different thermal sintering characteristics under oxidative environments.
- Supports with negligible or low OSC, e.g., γ-Al_2O_3 and YSZ, provide no or little resistance to sintering, respectively.
- In striking contrast, high resistance to sintering and even redispersion of catalyst nanoparticles occur on supports characterized by moderate and high OSC values, e.g., ACZ, GDC, and CZ. The higher the OSC of the support, the greater the

stability and/or the extent of particle redispersion; the latter also depends on the nature of metal, and when it exists, it is increased with increasing sintering temperature.

An EDL-based mechanistic model is developed, adequately explains all the experimental findings, and deciphers the role of EDL on the observed sintering behavior of metal NPs (Ir and Rh nanoparticles have been investigated so far under these issues). In accord to this model, the resistance to sintering and/or the redispersion of catalyst NPs is due to the synergistic action of three main factors:

- The presence of the spontaneously formed EDL ($[O^{\delta-}, \delta^{+}]$) on the catalyst particles, resulting from the thermally driven oxygen back-spillover from high OSC supports; this endows the NPs with a surface layer of net negative charge ($O^{\delta-}$), which quenches large particle migration and coalescence (PMC) via the resulting interparticle electrostatic repulsion forces.
- Atom species detachment and reattachment from catalyst crystallites, following the Oswald ripening (OR) mechanism of NP size growth, are both inhibited due to the increased activation energies of these steps resulting from the $O^{\delta-}$-encaptured particle surfaces.
- The trapping of the catalyst atomic particles detached from large crystallites by surface oxygen vacancies on the support, suppressing diffusion of these species and their subsequent attachment to larger particles; the higher the population of surface oxygen vacancies on the support, the greater the redispersion of the NPs.

In light of these findings, a new methodology for in situ on-stream controlled redispersion of metal catalysts may be devised, with potentially major implications for industrial heterogeneous catalysis. Supports capable to create the *effective-double-layer*, which strongly favor the persistence of small catalyst particles and simultaneously alter reaction turnover frequencies, can consist the basis of strategies for the production of active and stable catalyst formulations.

It should be noted that in the studies analyzed in this chapter, we have introduced the qualitative term "oxygen lability" because oxygen ion mobilities were not available for all the mixed oxide supports investigated. However, combining available oxygen ion mobility values with our experimentally determined oxygen storage capacity (OSC) data, a close correlation was found between these properties, which enabled us to rank these oxides as indicated in this chapter, in terms of their propensity to provide spillover oxygen. Future work could focus on which is the most appropriate and direct parameter or combination of parameters that will best reflect the propensity of a material to provide spillover oxygen, creating the EDL.

In addition, further experimental work on the sintering behavior of other combinations of NPs (e.g., Pt, Ni, Ag, and Ru) and supports (e.g., CeO_2-, ZrO_2-, TiO_2-based mixed oxides and perovskites), which will be also confirmed via functional density theory (DFT) calculations, will be useful for a deeper understanding of the sintering/redispersion behavior of nanoparticles, by means of our model. Such a more complete overview of the parameters and factors involved can lead to the transformation of the present model into a parametric mathematical one, capable of

quantitatively predicting sintering/redistribution phenomena in supported catalysts. Moreover, the use of the EPOC type reactor cells (i.e., *dispersed catalyst working electrode//O^{2-}-conducting solid electrolyte//counter electrode*) through which the EDL intensity will be in situ controlled by external bias (instead of changing support materials for nanoparticle dispersion) will be even more essential and advantageous for a deeper understanding of the EDL-sintering correlation, along with the practical value of the process which could provide an in situ, external bias controlled, methodology for catalyst nanoparticle size adjustment. Work is underway to achieve these goals.

References

1. Flytzani-Stephanopoulos M, Gates BC (2012) Atomically dispersed supported metal catalysts. Ann Rev Chem Biomol Eng 3:545–574. https://www.annualreviews.org/doi/pdf/10.1146/annurev-chembioeng-062011-080939
2. Yang XF, Wang A, Qiao B, Li J, Liu J, Zhang T (2013) Single-atom catalysts: a new frontier in heterogeneous catalysis. Acc Chem Res 46:1740–1748. https://doi.org/10.1021/ar300361m
3. Yentekakis IV, Goula G, Hatzisymeon M, Betsi-Argyropoulou I, Botzolaki G, Kousi K, Kontarides DI, Taylor MJ, Parlett CMA, Osatiashtiani A et al (2019) Effect of support oxygen storage capacity on the catalytic performance of Rh nanoparticles for CO_2 reforming of methane. Appl Catal B 243:490–501. https://doi.org/10.1016/j.apcatb.2018.10.048
4. Yentekakis IV, Pliangos CA, Papadakis VG, Verykios XE, Vayenas CG (1995) Support and NEMCA induced promotional effects on the activity of automotive exhaust catalysts. Stud Surf Sci Catal 96:375–385. https://doi.org/10.1016/S0167-2991(06)81444-8
5. Pliangos A, Yentekakis IV, Papadakis VG, Vayenas CG, Verykios XE (1997) Support-induced promotional effects on the activity of automotive exhaust catalysts: 1. The case of oxidation of light hydrocarbons (C_2H_4). Appl Catal B Environ 14:161–173. https://doi.org/10.1016/S0926-3373(97)00020-9
6. Papadakis VG, Pliangos CA, Yentekakis IV, Verykios XE, Vayenas CG (1996) Development of high performance, Pd-based, three-way catalysts. Catal Today 29:71–75. https://doi.org/10.1016/0920-5861(95)00268-5
7. Konsolakis M, Drosou C, Yentekakis IV (2012) Support mediated promotional effects of rare earth oxides (CeO_2 and La_2O_3) on N_2O decomposition and N_2O reduction by CO and C_3H_6 over Pt/Al_2O_3 structured catalysts. Appl Catal B 123–124:405–413. https://doi.org/10.1016/j.apcatb.2012.04.048
8. Papavasiliou A, Tsetsekou A, Matsuka V, Konsolakis M, Yentekakis IV (2010) An investigation of the role of Zr and La dopants into $Ce_{1-x-y}Zr_xLa_yO_\delta$ enriched γ-Al_2O_3 TWC washcoats. Appl Catal A 382:73–84. https://doi.org/10.1016/j.apcata.2010.04.025
9. Nicole J, Tsiplakides D, Pliangos C, Verykios XE, Comninellis C, Vayenas CG (2001) Electrochemical promotion and metal-support interactions. J Catal 204:23–34. https://doi.org/10.1006/jcat.2001.3360
10. Vernoux P, Lizarraga L, Tsampas MN, Sapountzi FM, De Lucas-Consuegra A, Valverde JL, Souentie S, Vayenas CG, Tsiplakides D, Balomenou S, Baranova A (2013) Ionically conducting ceramics as active catalyst supports. Chem Rev 113:8192–8260. https://doi.org/10.1021/cr4000336
11. Datye A, Wang Y (2018) Atom trapping: a novel approach to generate thermally stable and regenerable single-atom catalysts. Natl Sci Rev 5:630–632. https://doi.org/10.1093/nsr/nwy093

12. Qiao B, Wang A, Yang X, Allard LF, Jiang Z, Cui Y, Liu J, Li J, Zhang T (2011) Single-atom catalysis of CO oxidation using $Pt_1/FeOx$. Nat Chem 3:634–641. https://doi.org/10.1038/nchem.1095
13. Jones J, Xiong H, DeLaRiva AT, Peterson EJ, Pham H, Challa SR, Qi G, Oh S, Wiebenga MH, Hernandez XIP, Wang Y, Datye AK (2016) Thermally stable single-atom platinum-on-ceria catalysts via atom trapping. Science 353:150–154. https://doi.org/10.1126/science.aaf8800
14. Grillo F, van Bui H, Moulijn JA, Kreutzer MT, van Ommen R (2017) Understanding and controlling the aggregative growth of platinum nanoparticles in atomic layer deposition: an avenue to size selection. J. Phys. Chem. Lett 8:975–983. https://doi.org/10.1021/acs.jpclett.6b02978
15. Grillo F, van Bui H, La Zara D, Aarnink AI, Kovalgin AY, Kooyman P, Kreutzer MT, van Ommen R (2018) From single atoms to nanoparticles: autocatalysis and metal aggregation in atomic layer deposition of Pt on TiO_2 nanopowder. Small 14:1800765. https://doi.org/10.1002/smll.201800765
16. Moulijn JA, van Diepen AE, Kapteijn F (2001) Catalyst deactivation: is it predictable? What to do? Appl. Catal. A 212:3–16. https://doi.org/10.1016/S0926-860X(00)00842-5
17. Dai Y, Lu P, Cao Z, Campbell CT, Xia Y (2018) The physical chemistry and materials science behind sinter-resistant catalysts. Chem Soc Rev 47:4314–4331. https://doi.org/10.1039/c7cs00650k
18. Goodman ED, Schwalbe JA, Cargnello M (2017) Mechanistic understanding and rational design of sinter-resistant heterogeneous catalysts. ACS Catal 7:7156–7173. https://doi.org/10.1021/acscatal.7b01975
19. Hansen TW, DeLaRiva AT, Challa SR, Datye AK (2013) Sintering of catalytic nanoparticles: particle migration or Ostwald ripening? Acc Chem Res 46:1720–1730. https://doi.org/10.1021/ar3002427
20. Argyle MD, Bartholomew CH (2015) Heterogeneous catalyst deactivation and regeneration: a review. Catalysts 5:145–269. https://doi.org/10.3390/catal5010145
21. Yentekakis IV, Goula G, Panagiotopoulou P, Katsoni A, Diamadopoulos E, Mantzavinos D, Delimitis A (2015) Dry reforming of methane: catalytic performance and stability of Ir catalysts supported on γ - Al_2O_3, $Zr_{0.92}Y_{0.08}O_{2-\delta}$ (YSZ) or $Ce_{0.9}Gd_{0.1}O_{2-\delta}$ (GDC) supports. Top Catal 58:1228–1241. https://doi.org/10.1007/s11244-015-0490-x
22. Yentekakis IV, Goula G, Panagiotopoulou P, Kampouri S, Taylor MJ, Kyriakou G, Lambert RM (2016) Stabilization of catalyst particles against sintering on oxide supports with high oxygen ion lability exemplified by Ir-catalysed decomposition of N_2O. Appl Catal B Environ 192:357–364. https://doi.org/10.1016/j.apcatb.2016.04.011
23. Yentekakis IV, Goula G, Kampouri S, Betsi-Argyropoulou I, Panagiotopoulou P, Taylor MJ, Kyriakou G, Lambert RM (2018) Ir-catalyzed nitrous oxide (N_2O) decomposition: effect of the Ir particle size and metal-support interactions. Catal Lett 148:341–347. https://doi.org/10.1007/s10562-017-2233-z
24. Goula G, Botzolaki G, Osatiashtiani A, Parlett CMA, Kyriakou G, Lambert RM, Yentekakis IV (2019) Oxidative thermal sintering and redispersion of Rh nanoparticles on supports with high oxygen ion lability. Catalysts 9:541. https://doi.org/10.3390/catal9060541
25. Botzolaki G, Goula G, Rontogianni A, Nikolaraki E, Chalmpes N, Zygouri P, Karakassides M, Gournis D, Charisiou N, Goula M, Papadopoulos S, Yentekakis IV (2020) CO_2 methanation on supported Rh nanoparticles: the combined effect of support oxygen storage capacity and Rh particle size. Catalysts 10:944. https://doi.org/10.3390/catal10080944
26. Nikolaraki E, Goula G, Panagiotopoulou P, Taylor MJ, Kousi K, Kyriakou G, Kondarides D, Lambert RM, Yentekakis IV (2021) Support induced effects on the Ir nanoparticles activity, selectivity and stability performance under CO_2 reforming of methane. Nano 11:2880. https://doi.org/10.3390/nano11112880
27. Yentekakis IV (2019) An additional innovative effect of the effective-double-layer in heterogeneous catalysis: Stabilization of catalysts' nanoparticles against thermal sintering. In Vayenas Intl. Symp/physical chemistry and its applications for sustainable development F. Kongoli,

E. Aifantis, C. Cavalca, A. de Lucas Consuegra, A. Efstathiou, M. Fardis, D. Grigoriou, A. Lemonidou, S.G. Neophytides, Y. Roman, M. Stoukides, M. Sullivan, P. Vernoux, X. Verykios, I. Yentekakis Sustainable Industrial Processing Summit SIPS2019 Volume 10: Vayenas Intl. Symp/physical chemistry and its applications for sustainable development, pp 222–245). Montreal: FLOGEN Star Outreach. https://www.flogen.org/sips2019/paper-10-127.html

28. Simonsen SB, Chorkendorff I, Dahl S, Skoglundh M, Sehested J, Helveg S (2010) Direct observations of oxygen-induced platinum nanoparticle ripening studied by in situ TEM. J Am Chem Soc 132:7968–7975. https://doi.org/10.1021/ja910094r
29. DeLaRiva AT, Hansen TW, Challa SR, Datye AK (2013) In situ transmission electron microscopy of catalyst sintering. J Catal 308:291–305. https://doi.org/10.1016/j.jcat.2013.08.018
30. Fiedorow RMJ, Chahar BS, Wanke SE (1978) The sintering of supported metal catalysts. II. Comparison of sintering rates of supported Pt, Ir, and Rh catalysts in hydrogen and oxygen. J Catal 51:193–202. https://doi.org/10.1016/0021-9517(78)90293-2
31. Nagai Y, Hirabayashi T, Dohmae K, Takagi N, Minami T, Shinjoh H, Matsumoto S (2006) Sintering inhibition mechanism of platinum supported on ceria-based oxide and Pt-oxide-support interaction. J Catal 242:103–109. https://doi.org/10.1016/j.jcat.2006.06.002
32. Hatanaka M, Takahashi N, Tanabe T, Nagai Y, Dohmae K, Aoki Y, Yoshida T, Shinjoh H (2010) Ideal Pt loading for a Pt/CeO_2-based catalyst stabilized by Pt-O-Ce bond. Appl Catal B 99:336–342. https://doi.org/10.1016/j.apcatb1010.07.003
33. Stoukides M, Vayenas CG (1981) The effect of electrochemical oxygen pumping on the rate and selectivity of ethylene oxidation on polycrystalline silver. J Catal 70:137–146. https://doi.org/10.1016/0021-9517(81)90323-7
34. Vayenas CG, Bebelis S, Yentekakis IV, Lintz HG (1992) Non-faradaic electrochemical modification of catalytic activity: a status report. Catal Today 11:303–442. https://doi.org/10.1016/0920-5861(92)80002-5
35. Yentekakis IV, Vayenas CG (1988) The effect of electrochemical oxygen pumping on the steady-state and oscillatory behaviour of CO oxidation on polycrystalline Pt. J Catal 111:170–188. https://doi.org/10.1016/0021-9517(88)90075-9
36. Vayenas CG, Bebelis S, Neophytides S (1988) Non-faradaic electrochemical modification of catalytic activity. J Phys Chem 92:5083–5085. https://doi.org/10.1021/j100329a007
37. Yentekakis IV, Vernoux P, Goula G, Caravaca A (2019) Electropositive promotion by alkalis or alkaline earths of Pt-group metals in emissions control catalysis: a status report. Catalysts 9:157. https://doi.org/10.3390/catal9020157
38. Vayenas CG, Brosda S, Pliangos C (2003) The double-layer approach to promotion, electrocatalysis, electrochemical promotion, and metal–support interactions. J Catal 216:487–504. https://doi.org/10.1016/S0021-9517(02)00127-6
39. Vayenas CG (2013) Promotion, electrochemical promotion and metal–support interactions: their common features. Catal Lett 143:1085–1097. https://doi.org/10.1007/s10562-013-1128-x
40. Montini T, Melchionna M, Monai M, Fornasiero P (2016) Fundamentals and catalytic applications of CeO_2-based materials. Chem Rev 116:5987–6041. https://doi.org/10.1021/acs.chemrev.5b00603
41. Ivanova AS (2009) Physicochemical and catalytic properties of systems based on CeO_2. Kinet Catal 50:797–815. https://doi.org/10.1134/S0023158409060020
42. Yentekakis IV, Panagiotopoulou P, Artemakis G (2021) A review of recent efforts to promote dry reforming of methane (DRM) to syngas production via bimetallic catalyst formulations. Appl Catal B Environ 296:120210. https://doi.org/10.1016/j.apcatb.2021.120210
43. Yentekakis IV, Dong F (2020) Grand challenges for catalytic remediation in environmental and energy applications towards a cleaner and sustainable future. Front Environ Chem 1:5. https://doi.org/10.3389/fenvc.2020.00005

44. Yentekakis IV, Goula G (2017) Biogas management: advanced utilization for production of renewable energy and added-value chemicals. Front Environ Sci 5:7. https://doi.org/10.3389/fenvs.2017.00007
45. Pakhare D, Spivey J (2014) A review of dry (CO_2) reforming of methane over noble metal catalysts. Chem Soc Rev 43:7813–7837. https://doi.org/10.1039/c3cs60395d
46. Lavoie JM (2014) Review on dry reforming of methane, a potentially more environmentally-friendly approach to the increasing natural gas exploitation. Front Chem 2:81. https://doi.org/10.3389/fchem.2014.00081
47. Akri M, Zhao S, Li X, Zang K, Lee AF, Isaacs MA, Xi W, Gangarajula Y, Luo J, Ren Y, Cui YT, Li L, Su Y, Pan X, Wen W, Pan Y, Wilson K, Li L, Qiao B (2019) Atomically dispersed nickel as coke-resistant active sites for methane dry reforming. Nat Commun 10:5181. https://doi.org/10.1038/s41467-019-12843-w
48. Wang W, Wang SP, Ma XB, Gong JL (2011) Recent advances in catalytic hydrogenation of carbon dioxide. Chem Soc Rev 40:3703–3727. https://doi.org/10.1039/C1CS15008A
49. Ye RP, Ding J, Gong W, Argyle MD, Zhong Q, Wang Y, Russell CK, Xu Z, Russell AG, Li Q, Fan M, Yao YG (2019) CO_2 hydrogenation to high-value products via heterogeneous catalysis. Nat Commun 10:5698. https://doi.org/10.1038/s41467-019-13638-9
50. Gao W, Liang S, Wang R, Jiang Q, Zhang Y, Zheng Q, Xie B, Toe CY, Zhu X, Wang J, Huang L, Gao Y, Wang Z, Jo C, Wang Q, Wang L, Liu Y, Louis B, Scott J, Roger AC, Aman R, He H, Park SE (2020) Industrial carbon dioxide capture and utilization: state of the art and future challenges. Chem Soc Rev 49:8584–8686. https://doi.org/10.1039/D0CS00025F
51. Tsiotsias AI, Charisiou ND, Yentekakis IV, Goula MA (2020) The role of alkali and alkaline earth metals in the CO_2 methanation reaction and the combined capture and methanation of CO_2. Catalysts 10:812. https://doi.org/10.3390/catal10070812
52. Vogt C, Monai M, Kramer GJ, Weckhuysen BM (2019) The renaissance of the Sabatier reaction and its applications on Earth and in space. Nat Catal 2:188–197. https://doi.org/10.1038/s41929-019-0244-4
53. Pan SY, Chiang PC, Pan W, Kim H (2018) Advances in state-of-art valorization technologies for captured CO_2 toward sustainable carbon cycle. Crit Rev Env Sci Technol 48:471–534. https://doi.org/10.1080/10643389.2018.1469943
54. Ghaiba K, Ben-Faresb FZ (2018) Power-to-methane: a state-of-the-art review. Renew Sust Energ Rev 81:433–446. https://doi.org/10.1016/j.rser.2017.08.004
55. Italiano C, Llorca J, Pino L, Farraro M, Antonucci V, Vita A (2020) CO and CO_2 methanation over Ni catalysts supported on CeO_2, Al_2O_3 and Y_2O_3 oxides. Appl Catal B 264:118494. https://doi.org/10.1016/j.apcatb.2019.118494
56. Karelovic A, Ruiz P (2012) CO_2 hydrogenation at low temperature over Rh/-Al_2O_3 catalysts: effect of the metal particle size on catalytic performances and reaction mechanism. Appl Catal B Environ 113–114:237–249. https://doi.org/10.1016/j.apcatb.2011.11.043
57. Wuebbles DJ (2009) Nitrous oxide: no laughing matter. Science 326:56–57. https://doi.org/10.1126/science.1179571
58. Ravishankara AR, Daniel JS, Portmann RW (2009) Nitrous oxide (N_2O): the dominant ozone-depleting substance emitted in the 21st century. Science 326:123–125. https://doi.org/10.1126/science.1176985
59. Centi G, Perathoner S, Vazzana F, Marella M, Tomaselli M, Mantegazza M (2000) Novel catalysts and catalytic technologies for N_2O removal from industrial emissions containing O_2, H_2 and SO_2. Adv Environ Res 4:325–338. https://doi.org/10.1016/S1093-0191(00)00032-0
60. Ohnishi C, Iwamoto S, Inoue M (2008) Direct decomposition of nitrous oxide in the presence of oxygen over iridium catalyst supported on alumina. Chem Eng Sci 63:5076–5082. https://doi.org/10.1016/j.ces.2007.08.011

Part III
EPOC to Face Environmental Challenges

Chapter 5
EPOC with Alkaline Conductors: Implementations in Emission Control Catalysis

Ioannis V. Yentekakis, Philippe Vernoux, and Angel Caravaca

Abstract Rapid global industrialization, increasing human population and energy demand, and at the same time fossil fuels remaining the dominant source of energy in transport, industry, trade, and housing have led to massive increases in a variety of pollutants (mainly VOCs, NO_x, N_2O, CO_x, and SO_x) in the atmosphere with their known destructive effects on the environment and the consequent climate change. Emission control catalysis (ECC) is one of the most efficient and cost-effective end-of-pipe technologies for reducing emissions. The application of electrochemical promotion of catalysis (EPOC), especially that achieved through alkaline conductors (alkaline-EPOC), has been found to be extremely effective in ECC-related reaction systems. Its use made it possible to decipher the role and mode of action of alkaline promoters on these reactions, thus enabling the successful transfer of the obtained knowledge to the design of highly effective and simple, alkaline-promoted conventional catalyst formulations (alkaline-CPC), readily applicable in exhaust gas systems. Catalytic performance improvements by up to two orders of magnitude have been achieved on representative ECC-related reactions (e.g., deNO_x) via alkaline-EPOC and/or alkaline-CPC application. This chapter summarizes and critically discusses the literature findings on the topic.

I. V. Yentekakis (✉)
Laboratory of Physical Chemistry & Chemical Processes, School of Chemical & Environmental Engineering, Technical University of Crete (TUC), Chania, Greece
e-mail: yyentek@chenveng.tuc.gr

P. Vernoux
Université de Lyon, Institut de Recherches sur la Catalyse et l'Environnement de Lyon, UMR 5256, CNRS, Université Claude Bernard Lyon 1, Villeurbanne, France
e-mail: philippe.vernoux@ircelyon.univ-lyon1.fr

A. Caravaca
Departamento de Ingeniería Mecánica, Universidad Politécnica de Madrid, Madrid, Spain
e-mail: angel.caravaca@upm.es

P. Vernoux, C. G. Vayenas (eds.), *Recent Advances in Electrochemical Promotion of Catalysis*, Modern Aspects of Electrochemistry 61,
https://doi.org/10.1007/978-3-031-13893-5_5

Keywords Alkaline promotion · Conventional catalyst promotion · Electrochemical promotion · Emission control catalysis · Nitrogen oxides · Volatile organic compounds

5.1 Introduction

Emission control catalysis has often been demonstrated as one of the most efficient and cost-effective end-of-pipe technologies for the mitigation of several atmospheric pollutants massively produced from both stationary fossil fuel combustion processes and mobile (transportation) sources [1]. In the case of mobile sources, three-way catalytic converters (TWCs) have more than 40 years of successful implementation for the remediation of cars' emissions via the simultaneous occurrence of several CO and HC oxidation and NO_x reduction reactions summarized in Scheme 5.1.

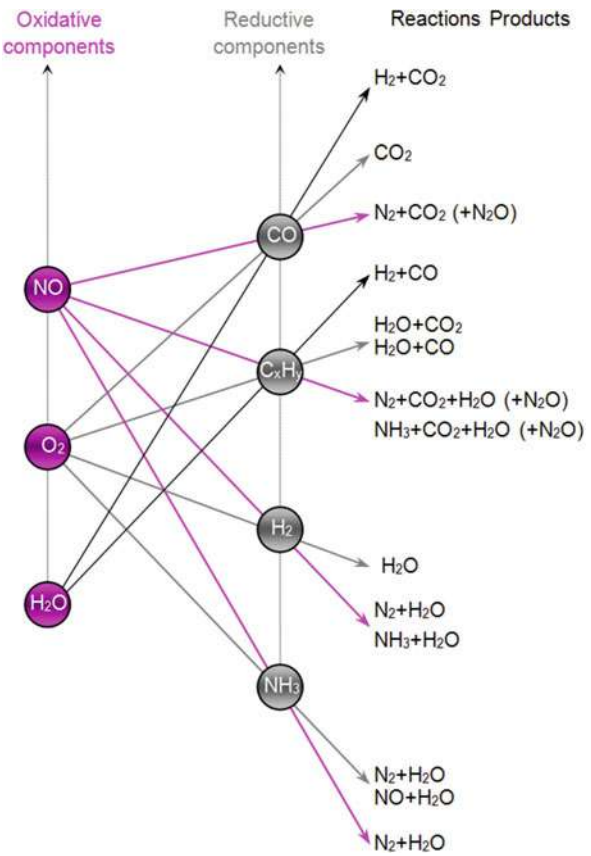

Scheme 5.1 Possible parallel reactions taking place in TWCs

However, besides the fact that we are currently in the "fourth generation" of commercial TWCs, some major aspects concerning the economy, the material formulations, their operational lifetime behavior, and noble metals' recycling still remain to be resolved [2, 3], specifically:

(i) The typical bi- or tri-metallic (Pt/Rh, Pd/Rh, Pt/Pd/Rh) formulations of commercial TWCs, with the role of rare and expensive Rh to be essential for the NO_x reduction reactions, increase their cost.
(ii) Noble metals' recovery from such complex formulations is almost marginally profitable due to the costly final separation of the recovered NMs.
(iii) The formation (into TWC) and thus the effluent of small but significant amount of the undesirable N_2O as byproduct of the NO_x reduction reactions (see Scheme 5.1) – N_2O has an outstanding global warming potential (310 times greater than that of CO_2) and a harmful impact on stratospheric ozone depletion.
(iv) The quite narrow operating air/fuel window (lambda window) for effective elimination of the three main pollutants that reduces TWC tolerance to the lean-rich swings in engine exhaust gas composition during operation and more importantly makes them inefficient in controlling NO_x emissions from the advanced diesel and lean-burn engines as well as stationary fossil fuels and solid waste combustion processes that operate at net oxidizing conditions.

Therefore, research in the topic remains challenging. Goals are focused on developing lower NM loading but more efficient catalysts, if possible monometallic (e.g., Pt-only, Pd-only) in order to eliminate the use of Rh, easily recyclable, particularly selective toward N_2 instead of N_2O in deNO_x reactions, and more tolerant in oxygen-rich conditions [1–3].

Catalysts' promotion, which can be imposed either via the use of surface promoters (surface or direct promotion) or via "active" supports (support-mediated promotion, metal-support interactions (MSI)) and/or support doping (dopant-induced metal-support interactions (DIMSI)), employed for years is still the main strategy for improving catalysts' performance.

More recently, the electrochemical promotion of catalysis (EPOC), discovered by Vayenas and co-workers in the 1980s, originally described as "non-Faradaic electrochemical modification of catalytic activity (NEMCA)," is an advanced, highly effective, in situ controlled and reversible, electrochemically guided method of promoting and optimizing catalysts' performance [4–7]. Besides the above, other important advantages of EPOC are (i) it can be used for employing promoters that cannot be applied by traditional methods due to their reactivity and thus consumption during operation (sacrificial promoters [8]) and (ii) it provides an effective tool for an in-depth investigation of the way of action of promoters and a probe of in situ scanning in order to readily find out the optimal promoter loading for any specific catalytic system at the chosen operating conditions (i.e., promotion optimization).

The insight gained from the EPOC studies provided an in-depth understanding of the role and mode of action of promoters in catalysis, allowing Vayenas and

co-workers to interpret catalyst promotion by providing rules governing it and clarifying the relationship between EPOC and classic promotion [8–10].

In this respect, using EPOC by means of a galvanic cell (such as shown in Fig. 5.1a), an electrochemically (Faradaic law) controlled migration of promoting ion species from the solid electrolyte support onto the catalyst surface can be imposed via external bias application, and thus an effective (overall neutral) double layer is developed on the catalyst surface (Fig. 5.1b, c). Figure 5.1b shows the case of imposition of an electronegative promoter (O^{2-}), while Fig. 5.1c shows the imposition of an electropositive promoter (alkali ion, Na^{+}); both configurations are reliable, as long as the appropriate solid electrolyte support is available. The electrocatalytic reactions taking place in each case at the three-phase-boundary

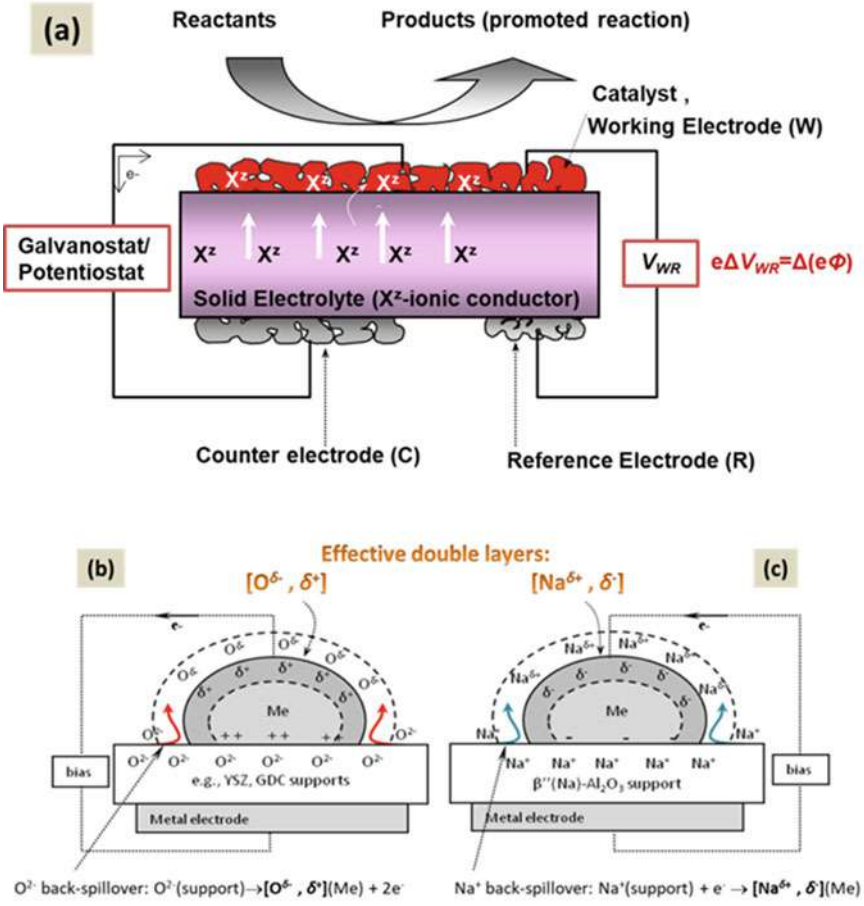

Fig. 5.1 Schematic of the galvanic cell through which the implementation of EPOC is conducted (**a**) and the *effective double layers* are formed by application of an electronegative (**b**) or electropositive (**c**) promoter

metal-solid electrolyte-gas that leads to the formation of the effective double layer $[O^{\delta-}, \delta^+]$ (Fig. 5.1b) or $[Na^{\delta+}, \delta^-]$ (Fig. 5.1c) are, respectively [7, 11]:

$$O^{2-}(\text{from support}) \rightarrow \left[O^{\delta-}, \delta^+\right] \text{ (on metal)} + 2e^- \tag{5.1}$$

$$Na^+(\text{from support}) + e^-(\text{from metal}) \rightarrow \left[Na^{\delta+}, \delta^-\right] \text{ (on metal)} \tag{5.2}$$

Since these electrochemically driven adatoms are imposed on the catalyst surface, they are evenly spread over the entire metal surface due to strong repulsive dipole–dipole interactions, which establish a homogeneous, neutral, effective double layer, corresponding to an electrically modified metal surface, practically an electron-deficient (i.e., higher work function) or electron-enriched (i.e., lower work function) metal surface due to the δ^+ or δ^- charge respectively located at the metal side interface half-layer. This electrically modified surface interacts with the co-adsorbed reactants and reaction intermediates and products, changing their binding energies (in respect to those on a promoter-free metal surface), producing pronounced alterations in catalytic performance [7], that is, electrochemistry has nothing to do with changes in catalytic phenomena other than to provide the ability for in situ changing the promoter loading, i.e., electrochemistry just plays the role of the promoter species bearer (forward or backward).

The promoting species O^{2-} and alkali ions shown in Fig. 5.1b, c, respectively, and the corresponding effective double layers formed, are the two of most commonly used in EPOC studies. Besides their opposite effect on the catalyst work function, and thus on the concomitant promotion, there is an additional key difference of crucial practical importance. While O^{2-} species are typically scavenged from catalyst surface due to their participation in reactions as *sacrificial* promoter [8], thus in order to maintain a certain $[O^{\delta-}, \delta^+]$ effective double layer, an external bias has to be constantly applied, alkali ions are stable promoters, not participating in scavenging reactions; therefore, once applied to the catalyst surface, the created double layer (e.g., $[Na^{\delta+}, \delta^-]$) remains stable so that no further external bias is required.

Alkaline conductors available for the construction of galvanic cells suitable for EPOC implementation are Na^+- or K^+-substituted β- and β''-aluminas $(Na \text{ or } K)_{1+x}Al_{11}O_{17+x/2}$ and $(Na \text{ or } K)_{1+x}M_xAl_{11-x}O_{17}$, respectively, as well as NaSiCon ($Na_3Zr_2Si_2PO_{12}$) [2, 7]. The constructed galvanic cells typically have the following configuration (Fig. 5.1a):

$$\text{Catalyst electrode/alkali conductor/inert counter electrode (e.g., Au)} \tag{5.3}$$

As commonly followed in EPOC studies, such cells can be operated under two distinct modes:

(i) *Potentiostatic operation*, which corresponds to imposition of a constant catalyst polarization (V_{WR}) via the potentiostat (Fig. 5.1a). This is a *steady-state* operation achieved very rapidly after a fast transfer of the appropriate amount of alkali ions onto the catalyst surface (as a Dirac function) until the system obtains the

specified V_{WR} value. Then the alkali ion flux (current) vanishes to zero, and V_{WR} remains at the set value, that is, the catalyst surface is experienced at a constant amount of alkali promoter species – a constant effective double layer and catalyst work function have been achieved. This mode of operation is typically conducted to study the reflex of the performance of a reaction on an EPOC-modified value of the work function ($e\Phi$) of the catalyst surface [7, 11], since Eq. (5.4) has been evidenced [12].

$$e\Delta V_{WR} = \Delta(e\Phi) \tag{5.4}$$

(ii) *Galvanostatic operation*, which corresponds to continuous supply of a constant current (I) via the galvanostat. This is a transient mode of operation during which alkali ions are transferred with a constant flux (Faraday's law, I/F) and accumulated onto the catalysts' surface increasing their coverage, θ_{Alk}, according to Eq. 5.5 [7, 11]:

$$\theta_{Alk} = (-It/FN_0) \tag{5.5}$$

where t is the time of current (I) application, F is Faraday's constant, and N_0 is the number of catalysts' active sites.

This mode of operation provides an efficient and rapid method for assessing the response of the reaction to promoter coverage, allowing fast determination of the optimal promoter loading at any set of reaction conditions employed (i.e., promotion optimization). In addition, recording the catalyst polarization transient (i.e., the time variation of catalyst potential, V_{WR}) during galvanostatic operation, this permits establishment of the relationship $\theta_{Alk}(V_{WR})$ between alkali coverage (θ_{Alk}) and catalyst potential (V_{WR}) and then of the catalyst coverage and catalyst work function by considering the direct proportional relation of V_{WR} and $e\Phi$ given in Eq. 5.4. An experimental example is shown in Fig. 5.2.

Combination of the two modes of operation in EPOC studies allows an in-depth insight in the overall context of the promotion under study and the particular effect of all main parameters on the catalytic system under promotion.

In this chapter and in a first step, the most important results reported in the literature regarding the application of alkali-EPOC to reactions that play a major role in emission control catalysis will be analyzed. To this end, reactions involving CO and light hydrocarbon oxidation or NO_x reduction will be in our central attention. Then, studies involving transfer of the findings and knowledge obtained by the application of alkali-EPOC for the design of effective conventionally promoted catalyst (CPC) formulations for direct practical application in emission control catalysis reactions will also be discussed. A complete list of the above cases is illustrated in Table 5.1.

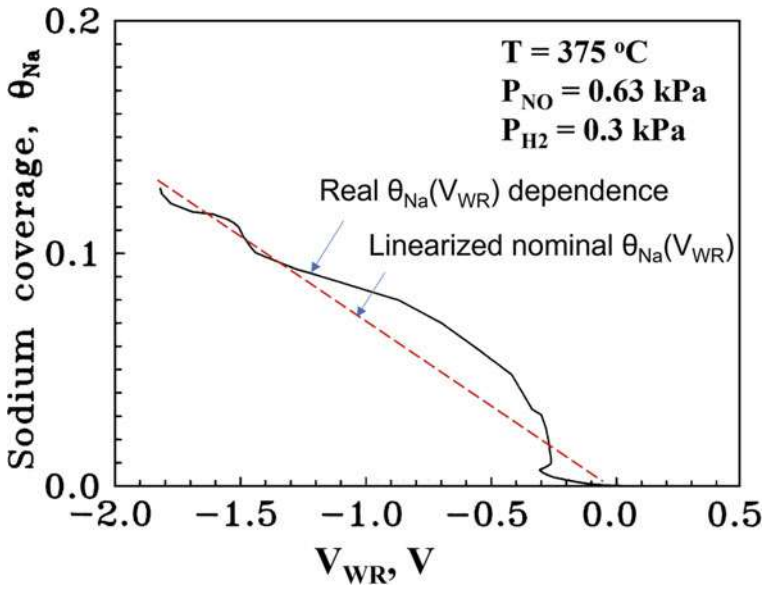

Fig. 5.2 NO + H_2 reaction under alkaline (Na)-EPOC: dependence of sodium coverage θ_{Na} on catalyst potential V_{WR} under specific reaction conditions. (Reproduced with permission from Ref. [13]. Copyright 1997, Elsevier)

In order to have a solid basis for comparison within each case but also between them, the following well-known parameters [7] will be used to account the promotion findings:

(i) The *rate enhancement ratio* (ρ) will be used in both EPOC and CPC cases:

$$\rho = r_p/r_o \quad (p = \text{EPOC-or CPC-promoted catalysts}) \tag{5.6}$$

where r_o is the unpromoted rate and r_p is the alkali-promoted rate; either this promotion was obtained electrochemically (p = EPOC) or by using conventional promotion methods (p = CPC). ρ values actually indicate the net gain of the promotion on the catalytic reaction system applied.

(ii) The *Faradaic efficiency* (Λ) which actually describes the magnitude of promotion. This is applicable only to EPOC systems, no meaning in CPC systems.

$$\Lambda = \Delta r/(I/zF) = (r_{\text{EPOC}} - r_o)/(I/zF) \tag{5.7}$$

where F is the Faradaic constant and I is the applied current. Z is the charge of the promoting ion which is equal to +1 in the present case of alkali promotion. It is worth noting that at steady-state potentiostatic operation, by definition, Λ values tend to infinity. Indeed, in most alkali-EPOC studies, Λ values as high as ~10^3–10^5 have

Table 5.1 Model reactions and simulated practical emissions investigated in the context of alkaline promotion via EPOC or CPC methods

Reaction category	Specific reaction	Active phase studied	Promotion method employed	Refs.
Oxidations	CO oxidation: $CO + ½O_2 \rightarrow CO_2$	Pt, Pd	EPOC/CPC	[11, 16]/[45–47]
	Preferential CO oxidation (PROX): $CO + ½O_2$ ($+H_2$ excess) $\rightarrow CO_2 + H_2O$	Pt	EPOC/CPC	[17]/[48–55]
	Alkene oxidation: $C_\nu H_{2\nu} + {}^{3\nu}/_2O_2 \rightarrow \nu CO_2 + \nu H_2O$	Pt	EPOC/CPC	[14, 18–23]/[57]
	Alkane oxidation: $C_\nu H_{2\nu+2} + {}^{(3\nu+1)}/_2O_2 \rightarrow \nu CO_2 + (\nu+1)H_2O$	Pt	EPOC	[24, 25]
NO_x and N_2O reductions	NO reduction by CO: $NO + CO \rightarrow CO_2 + ½\ N_2$ ($+N_2O$)	Pt, Rh, Pd	EPOC/CPC	[26–29]/[58–60]
	NO reduction by alkenes: $3\nu NO + C_\nu H_{2\nu} \rightarrow \nu CO_2 + {}^{3\nu}/_2N_2 + \nu H_2O$ ($+N_2O$)	Pt, Rh, Ir	EPOC/CPC	[30–33, 43, 44]/[43, 44, 59, 62–67]
	NO reduction by alkanes: $(3\nu+1)NO + C_\nu H_{2\nu+2} \rightarrow \nu CO_2 + {}^{(3\nu+1)}/_2N_2 + (\nu+1)H_2O$	Pd	CPC	[68, 69]
	NO reduction by H_2: $NO + H_2 \rightarrow ½\ N_2 + H_2O$ ($+N_2O$)	Pt, Pd	EPOC/CPC	[13]/[72, 73, 78]
	Direct N_2O decomposition: N_2O (presence of O_2) $\rightarrow N_2 + ½O_2$	Pt, Rh, Ir	CPC	[79–82, 85]
	N_2O reduction (by CO or HCs): N_2O + (CO or HC) $\rightarrow N_2 + CO_2 + H_2O$	Pt, Pd	EPOC/CPC	[41, 42, 84]/[81, 83, 84]
Simulated real conditions	*TWC*: $NO + CO + C_3H_6 + O_2$ (stoich.) ($+CO_2 + H_2O$) $\rightarrow N_2 + CO_2 + H_2O$ ($+N_2O$)	Pt, Pd, Rh	CPC	[86–91, 93–96]
	Lean-burn and diesel: $NO + C_3H_6 + O_2$ (excess) $\rightarrow N_2 + CO_2 + H_2O$ ($+N_2O$)	Pt	EPOC/CPC	[34–40]/[57, 97]
	Two-stroke engine exhaust: $CO + C_3H_6 + H_2 + O_2 + CO_2 + H_2O \rightarrow CO_2 + H_2O$	Pt	CPC	[92]

been obtained [11, 14]. However, in the case of lower Λ values in alkali-EPOC, a mechanism decreasing the amount of alkali on catalyst surface could possibly be at work; therefore, a small current maintains to keep V_{WR} at the set value. Lower Λ values have been observed in case of reactions operated at net reducing conditions [15]; this probably indicates that at such conditions, alkalis can exist partially at the reduced state characterized by low melting point and high volatility, easily escaping in the gas phase.

(iii) The promotion index (PI_i), useful to quantify the alkali promotion [7, 11]:

$$PI_i = (\Delta r/r_o)/\Delta\theta_i \tag{5.8}$$

where $\Delta\theta_i$ is the change of the coverage of the promoting species i such as $Na^{\delta+}$ and $K^{\delta+}$. PI_i is positive for a promoting action of the imposed adatom species and negative for a possible poisoning role (in case of pure site blocking $PI_i = -1$); as we shall see, alkali promotion often shows a volcano-type behavior in respect to alkali coverage, i.e., it can exhibit either promotional or poisonous behavior depending on the promoter loading.

5.2 Alkaline-EPOC for Emission Control Reactions

5.2.1 *Alkaline-EPOC Studies on CO and Light Hydrocarbon Oxidation Reactions*

Table 5.2 summarizes studies concerning CO and light hydrocarbon oxidation reactions, catalyzed by Pt-group metals and promoted by alkalis via the EPOC method [11, 14, 16–25]. It can be seen that all these studies were performed on Pt catalyst, while the alkali conductors used as source of the alkali ion promoter species were (Na)$\beta''Al_2O_3$ or NaSiCon ($Na_3Zr_2Si_2PO_{12}$) for applying Na^+ species and (K)$\beta''Al_2O_3$ for applying K^+ species. Most probably, Pt was preferred in these studies (Table 5.2) as the most promising (in activity and stability) candidate, already used in three-way catalytic chemistry, to replace the rarer and more expensive Rh.

The first study concerning electrochemical promotion of CO oxidation by sodium was performed by Yentekakis et al. [11] in a wide range of operational conditions (CO/O_2 gas-phase composition, temperature, galvanostatic and potentiostatic operation modes) on a Pt film electrocatalyst interfaced with a Na^+-conducting $\beta''Al_2O_3$ solid electrolyte (Table 5.2). It was found that promotion phenomena were strongly dependent on the CO/O_2 gas-phase composition and on the amount of alkali species (θ_{Na} coverage) supplied – a large number of experimental data acquired lead to the construction of a complete illustration of the kinetic behavior under Na promotion (Fig. 5.3a). As can be seen in Fig. 5.3, the reaction rate is markedly enhanced ($\rho \sim 6$) at Na coverage values of ca. 0.02–0.04 under CO-rich conditions (Fig. 5.3b, case

Table 5.2 Alkaline-EPOC studies on CO and light hydrocarbon (alkenes and alkanes) oxidation reactions

Reaction	Catalyst/alkali conductor	Reaction conditions	Maximum ρ values and other highlights	Refs.
$CO + O_2$	Pt/(Na)$\beta''Al_2O_3$	T = 300–450 °C; [CO] = 0–6%, [O_2] = 0–6%	ρ = 6 with θ_{Na} = 0.04 at T = 350 °C and CO-rich conditions	[11]
$CO + O_2$	Pt/(K)$\beta''Al_2O_3$	T = 200–350 °C; [CO] = [O_2] = 0.5%	ρ = 11 at T = 278 °C	[16]
$CO + O_2 + H_2$ (PROX)	Pt/(K)βAl_2O_3	T = 195 °C; [CO] = 0.4%, [O_2] = 0.2%, [H_2] = 16%; θ_K = 0–0.04	ρ = 1.3 and ~10% increase in CO oxidation selectivity, with θ_K = 0.02–0.04	[17]
$C_2H_4 + O_2$	Pt/(Na)$\beta''Al_2O_3$	T = 291 °C; [C_2H_4] = 0.021%, [O_2] = 5%; θ_{Na} = 0–0.03	Poisoning: a θ_{Na} >0.015 suffices to cause a 70% rate inhibition	[14]
$C_2H_4 + O_2$	Pt/(Na)$\beta''Al_2O_3$	T = 300–470 °C; [C_2H_4] = 4.2%, [O_2] = 8% and 16.2%; θ_{Na} = 0–0.35	ρ = 2 with θ_{Na} = 0.08 at T = 280 °C	[18]
$C_3H_6 + O_2$	Pt/(Na)$\beta''Al_2O_3$	T = 340 °C; [C_3H_6] = 0.62%, [O_2] = 0–7%	ρ = 2.3 at T = 340 °C, [O_2]/[C_2H_4] =2	[19]
			Formation of 3D Na2CO3 species	
$C_3H_6 + O_2$	Pt/ $Na_3Zr_2Si_2PO_{12}$ (NaSiCon)	T = 300 °C; C_3H_6/O_2 = 0.04%/0.2% (stoic.) and C_3H_6/O_2 = 0.04%/8.3% (O_2-rich); θ_{Na} = 0–6%	ρ = 3.5 with θ_{Na} = 3.6% at T = 300 °C, [C_3H_6]/[O_2] = 0.04/0.2	[20] [21]
			Formation of Na_2CO_3 and $NaHCO_3$ phases	
$C_3H_6 + O_2$	Pt/(K)βAl_2O_3	T = 190–310 °C; [C_3H_6] = 0.2%, [O_2] = 1–7%	ρ = 7 at T = 200 °C and [C_3H_6]/[O_2] = 0.2%/7%	[22] [23]
$C_3H_8 + O_2$	Pt/(Na)$\beta''Al_2O_3$	T = 320–440 °C; [C_3H_8] = 0.2%, [O_2] = 1%; θ_{Na} = 0–3%	Poisoning: ρ~0.002 with θ_{Na} >0.025 at 440 °C	[24] [25]
			Na forms carbonate, bicarbonate, and oxide phases	

(i)), where CO oxidation kinetics obey negative order in CO and positive order in O_2. In this promoting region, enhancement factor (or "*Faradaic efficiency*") Λ values measured were typically 10^3–10^5, while PI_i values up to 250 were achieved showing that Na is a very pronounced promoter species for the Pt-catalyzed CO oxidation. Higher Na coverages cause strong attenuation of catalyst activity; a volcano-type behavior of CO oxidation rate versus θ_{Na} is thus clear. On the contrary, at O_2-rich

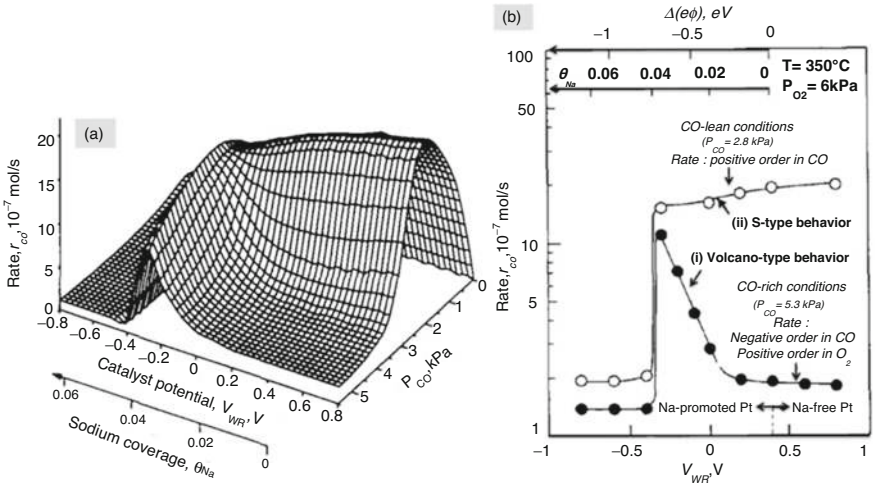

Fig. 5.3 (**a**) Three-dimensional presentation of the effect of partial pressure of CO (P_{CO}), catalyst potential (V_{WR}), and the corresponding Na promoter coverage (θ_{Na}) on the rate of CO oxidation on a Pt electrocatalyst deposited on a (Na)$\beta''Al_2O_3$ sodium ion conductor under EPOC conditions. (**b**) Dependence of CO oxidation rate on Pt electrocatalyst potential (V_{WR}) and the corresponding work function ($e\Phi$) and sodium coverage (θ_{Na}) at certain CO-rich (i) and CO-lean (ii) reaction conditions. Other conditions: $T = 350\,^{\circ}C$, $P_{O2} = 6$ kPa. (Reproduced with permission from Ref. [11]. Copyright 1994, Elsevier)

conditions (Fig. 5.3b, case (ii)), where the rate is of positive order in CO, only poisoning phenomena can be observed upon increasing θ_{Na} (S-type behavior).

Taking into account the modifications on the chemisorptive properties of CO and O_2 reactants on Pt sites caused by the created [$Na^{\delta+}$, δ^-] effective double layer (Fig. 5.1c), which leads to an electron-enriched (δ^-) lower work function Pt surface, it was concluded that at CO-rich conditions and for Na coverages up to ~0.04, the promotional effect is resulted by an enhancement in oxygen chemisorption (more pronounced compared to CO) due to strengthening of the Pt–O bond (O is an electrophilic adsorbate). The poisoning behavior at $\theta_{Na} > 0.04$ was attributed to active site blocking phenomena due to the formation of a CO–Na–Pt surface complex.

De Lucas-Consuegra and co-workers using a Pt/(K)$\beta''Al_2O_3$/Au galvanic cell with a K^+-conducting solid electrolyte performed EPOC studies for both CO oxidation [16] and preferential CO oxidation (PROX) [17] reactions. In the former study, conducted at low temperatures (ca. 200–350 °C) and equimolar reactant composition ([CO] = [O_2] = 5000 ppm), rate enhancement ratios ρ of about 11 and *light-off* temperature that decreases by ~40 °C were achieved [16] (Table 5.2). Provided that both CO and O_2 are electron acceptor (electrophilic) adsorbates, the resulted electron-enriched Pt surface, due to the formed [$K^{\delta+}$, δ^-] effective double layer, favors the adsorption of both reactants. However, a more pronounced enhancement of the adsorption of oxygen at the expense of CO on a Pt surface predominately

covered by CO under unpromoted conditions was considered to be responsible for the obtained promotion. In the case of PROX reaction [17], a rate enhancement up to $\rho = 1.3$ at a potassium coverage θ_K~0.02–0.04 was achieved at 195 °C and feed composition of $CO/O_2/H_2 = 0.4\%/0.2\%/16\%$. A concomitant increase in CO_2 selectivity of ~10% was recorded as well (Table 5.2). The effect of the alkali on the chemisorptive bonds of CO, H, and O on Pt surface was considered to be the origin of the observed promotional phenomena.

Taking into account the above literature findings of alkali-EPOC studies on CO oxidation reaction, the following general remarks and common features can be highlighted: only Pt was investigated so far for CO oxidation under alkali-EPOC conditions, probably due to its being a promising candidate to replace Rh in TWCs accounting its original performance (activity and stability) on the titled reaction. The general view is that alkalines can induce both promotional and poisonous effects on the reaction, depending on reaction conditions and promoter loading. Specifically, alkalines efficiently promote Pt-catalyzed CO oxidation only at CO-rich conditions at which CO coverage predominates on the catalyst surface; this is valid not necessarily at $CO/O_2 > 1$ in the gas phase, due to the higher propensity of CO to adsorb on Pt sites. However, the promotion follows a volcano-type behavior upon increasing alkali coverage at generally low values (up to ca. 0.04), thus reversing to poisoning for high promoter coverages. In contrast, no or moderate promotion and more often poisonous effects are caused by alkalis under O_2-rich conditions. Best overall rate enhancements up to $\rho \sim 11$ were achieved by K promotion. Alkali-EPOC was also found to be effective in the Pt-catalyzed preferential CO oxidation in hydrogen-rich conditions (PROX reaction) allowing activation of Pt at lower temperatures and attenuation of the inhibiting effect of H_2. The alkaline-induced pronounced enhancement on oxygen adsorption compared to that of CO was a key argument upon explaining all the above findings, whereas the formation of large surface alkali complexes was considered responsible in cases of poisoning at high alkali coverages.

Alkaline-EPOC was also found very effective in light alkene (C_2H_4, C_3H_6) oxidation reactions (Table 5.2). Using Pt/(Na)$\beta''Al_2O_3$/Au galvanic cells, Bebelis et al. [14] and Harkness et al. [18] investigating the C_2H_4 oxidation reaction demonstrated both promoting and poisoning effects induced by Na, depending on the alkali coverage: $\theta_{Na} < \sim 0.08$ caused promotion (up to $\rho \sim 2$) with Λ values of the order of 10^4, whereas $\theta_{Na} > 0.08$ induced rate inhibition even below the original unpromoted rate (Fig. 5.4). As shown in Fig. 5.4, galvanostatic and potentiostatic operations of EPOC coincide. The interpretation of the experimental findings was based on the alkali-induced enhancement chemisorption of the electrophilic oxygen adsorbate at the expense of C_2H_4 (electrophobic adsorbate) in case of promotion, while poisoning at high alkali coverages was attributed to Pt site blocking by surface Na compound accumulation together with an overstretching of the Pt–O bond reducing oxygen reactivity.

A model Pt(111)–Na-dosed catalyst used in the second study [18] was found to mirror the behavior of the electrochemically promoted Pt/(Na)$\beta''Al_2O_3$ electrocatalyst. This was a strong indication that Na supplied via electrochemical

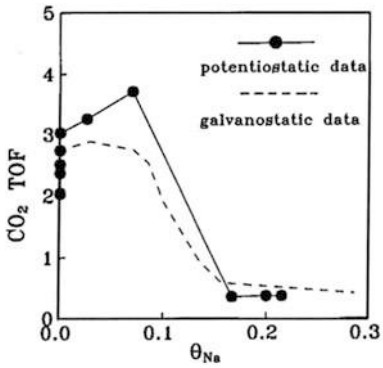

Fig. 5.4 $C_2H_4 + O_2$ reaction under alkaline (Na)-EPOC conditions: rate as a function of Na coverage for both potentiostatic and galvanostatic experiments for $[O_2] = 8.0\%$ and $[C_2H_4] = 4.2\%$ (balance He) mixture at 352 °C. (Reprinted with permission from Ref. [18]. Copyright 1996, Elsevier)

polarization is indeed the key species inducing the promoting or poisoning phenomena in alkaline-EPOC systems and demonstrated for the very first time (nowadays well-documented) that electrochemical promotion of catalysis (EPOC) and conventional catalyst promotion (CCP) by surface-imposed alkali adatoms obey the same physiochemical rules.

The Pt-catalyzed propylene oxidation has been also extensively studied. Filkin et al. [19] investigated the Pt-catalyzed propene (C_3H_6) oxidation under alkaline-EPOC using a Pt/(Na)$\beta''Al_2O_3$/Au galvanic cell. Fully reversible promotion and poisoning effects were observed as a function of electrochemically applied or removed Na^+ ions. Maximum rate enhancement ratio of the order of $\rho = 2.3$ was obtained at $[O_2]/[C_3H_6] = 2$ and a moderate Na coverage (not specified), while higher Na coverages caused poisoning of the reaction. The intensity of Na promotion was found to be strongly influenced by the value of $[O_2]/[C_3H_6]$ ratio, increasing as $[O_2]/[C_3H_6]$ ratio decreases. The authors explained promotion and poisoning findings in terms of a Na-modified chemisorption of the reactants: Na enhances oxygen chemisorption and inhibits propylene chemisorption on a Langmuir–Hinshelwood-type reaction in which the rate is strongly affected by the relative coverages of the competitive adsorbed reactants. Using X-ray photoelectron spectroscopy (XPS), Auger electron spectroscopy (AES), and postreaction Na K-edge XANES (X-ray absorption near-edge structure), the authors demonstrated that under reaction conditions, the promoter phase consists of small amounts of 3D sodium carbonate crystallites; thick layers of this sodium surface compound were responsible for rate inhibition in the poisoning regime. They also showed that although these promoter and poisoning phases were stable at reaction temperatures investigated, these were readily destroyed via electrochemical Na pumping away from the catalyst by the application of opposite-sign polarizations [19].

Vernoux and co-workers [20, 21] investigated the same reaction system (i.e., Pt-catalyzed propylene oxidation under Na-EPOC conditions) using an alternative Na^+ conductor, namely, NaSiCon ($Na_3Zr_2Si_2PO_{12}$). The EPOC experiments were performed at 300 °C and two different propene/oxygen gas-phase compositions, near-stoichiometric ($[O_2]/[C_3H_6] = 0.2\%/0.04\%$) and excess oxygen ($[O_2]/[C_3H_6] = 8.3\%/0.04\%$) conditions (Table 5.2). They found that under oxygen excess

conditions, $\theta_{Na} > 0.03$ causes a slight poisoning to the reaction rate ($\rho \sim 0.8$). However, under near-stoichiometric conditions, sodium strongly promotes the reaction offering rate enhancement ratios up to $\rho = 3.5$ at an optimal sodium coverage of $\theta_{Na} \sim 0.036$ since the rate was then slightly decreased for higher θ_{Na} values. In agreement with the findings of Filkin et al. [19], the authors indicated (using cyclic voltammetry) that during reaction, Na exists in the form of surface complex species, namely, Na_2CO_3 and $NaHCO_3$ phases; this fact, however, did not prevent Na-induced promotion.

Alkaline-EPOC studies on propene oxidation reaction were continued by de Lucas-Consuegra et al. [22, 23] but now using a K^+-conducting $\beta''Al_2O_3$ solid electrolyte (Table 5.2). The authors found that at low temperatures (ca. 200–300 °C), the reaction can be strongly promoted under both near-stoichiometric and oxygen-rich conditions. Rate enhancement ratios of the order of $\rho = 7$ were achieved for a catalyst polarization of about −2 V. Using cyclic voltammetry, FTIR, and SEM-EDX, the authors identified the formation of stable potassium oxide and superoxide species responsible for the promotional phenomena upon electrical polarization. These species were considerably stable, thus causing permanent promotional effects when no external bias was disconnected.

In contrast to alkenes, in the case of alkane oxidation, alkalis were found to be only poisonous surface adatoms. In a sodium-EPOC study of propane oxidation over Pt electrocatalyst using a Pt/(Na)$\beta''Al_2O_3$/Au galvanic cell, Kotsionopoulos and Bebelis [24, 25] found severe rate inhibition by electrochemically supplied Na even at low sodium coverages, over a wide range of $[C_3H_8]/[O_2]$ ratios (Table 5.2). For example, at 320 °C and stoichiometric reaction conditions ($[O_2]/[C_3H_8] = 1\%/0.2\%$), a Na coverage as small as $\theta_{Na} \sim 0.025\%$ was enough to decrease the reaction rate for 625 times; this poisonous effect of Na was more pronounced at higher temperatures. The poisoning performance of alkali for alkane oxidation can be attributed to the originally (before alkali supply) weak adsorption of alkanes on Pt surface compared to that of oxygen. Therefore, a further weakening of the alkane adsorption (electrophobic adsorbate) on the electron-enriched surface via the $[Na^{\delta+}, \delta^-]$ effective double layer causes an even more unequal distribution of the reactants and consequently less reaction probability. In agreement with the previous reports, the authors observed that under alkaline-EPOC conditions, the supplied alkali ions on the catalyst surface form surface complexes, mainly carbonate, bicarbonate, and oxide species [25].

Overviewing these findings obtained upon alkaline-EPOC studies of light alkene and alkane oxidation reactions (Table 5.2), the following general features and conclusions can emerge. Alkali promotion of platinum-group metals is detrimental for alkane oxidation due to the low adsorption propensity of alkanes on the catalyst surface which becomes worse due to the alkali-induced weakening of their adsorption bond and the simultaneous strengthening of oxygen adsorption bond that leads to self-poisoning of the reaction (O-poisoning of the surface). On the contrary, alkene oxidation is substantially promoted by alkalines due to the opposite trend of their adsorption characteristics compared to alkanes, which is strong initial adsorption propensity on the alkali-free metal surface. Therefore, an alkali-induced

enhancement on oxygen adsorption counterbalances its coverage on a catalyst surface predominantly covered by alkene molecules on the unpromoted surface, resulting in an enhancement on reaction probability. As in the case of CO oxidation, alkene oxidation also follows volcano-type promotion upon increasing alkali coverage, resulting from the competitive adsorption of the reactants (LH-type reactions) and the formation of 3D alkali carbonates during reaction that leads to excessive site blocking when alkali coverage becomes high.

5.2.2 *Alkaline-EPOC Studies on deNO$_x$ and deN$_2$O Reactions*

The reduction of NO_x by reducing agents such as CO, light hydrocarbons, or H_2, which co-exist in the exhaust gases of mobile and stationary combustion processes, and their behavior under alkaline-EPOC conditions were systems that found particular attention by several research groups [13, 26–42] (Table 5.3).

The first relevant study was conducted in 1996 through a collaboration of Vayenas and Lambert groups who studied the Pt/NO+CO catalytic system under alkaline (Na)-EPOC that was applied by means of a Pt/(Na)β″Al_2O_3/Au galvanic cell [26, 27]. CO/NO gas composition, sodium coverage, and temperature were found to be the main factors determining the promotion. For high CO/NO ratios, the Na-promoting intensity was marginal, attributed to the formation of extensive CO islands that limit NO chemisorption. At low CO/NO ratios, the effect of Na was also relatively small, because the CO + O step of the deNO$_x$ reaction pathway is limited by the low CO coverage. However, at the intermediate CO/NO ratios, where the above constrains are not valid, Na strongly promotes the reaction ($\rho_{N2} = 13$; see Table 5.3) with concomitant increase (up to ~30%) of system selectivity toward N_2 instead of N_2O as well (Fig. 5.5). The Na-induced promotion in rate and selectivity was rationally interpreted in terms of an enhancement on NO vs. CO chemisorption and the concomitant extended dissociation of the chemisorbed NO molecules.

The same reaction (CO + NO) but now on Rh catalyst was studied under sodium-EPOC by the research group of Lambert using a Rh/(Na)β″Al_2O_3/Au galvanic cell [28, 29]. The authors showed that NO + CO can also be promoted over Rh catalyst, but not as effective as that obtained on Pt [26, 27]. Maximum rate enhancement ratios of the order of $\rho_{N2} \sim 3$ were observed at stoichiometric CO/NO gas composition for a $\theta_{Na} = 0.02$ (Table 5.3) followed by a large increase in N_2 selectivity as well ($\Delta S_{N2} = 56\%$, thus achieving a value of 80% on the Na-promoted Rh catalyst). Using XPS and work function ($\Delta e\Phi$) measurements, the authors also demonstrated that the Na coverage on the catalyst surface is indeed controlled through the externally imposed catalyst potential, while a linear relationship of catalyst work function and θ_{Na} with catalyst potential was experimentally evidenced (Fig. 5.6) [29].

Table 5.3 Alkaline-EPOC studies on $deNO_x$ and deN_2O reactions

Reaction	Catalyst/ alkali conductor	Reaction conditions	Maximum ρ values and other highlights	Refs.
NO + CO	Pt/(Na)β'' Al_2O_3	T = 300–400 °C; [CO] = 0–1.5%, [NO] = 0–1.5%, θ_{Na} = 0–0.2	ρ_{N2} = 13, ρ_{CO2} = 4.8, ΔS_{N2} = +45% at 348 °C, θ_{Na} > 0.03	[26, 27]
NO + CO	Rh/ (Na)β'' Al_2O_3	T = 307 °C; [CO] = 0–1.1%, [NO] = 0–2%, θ_{Na} ~ 0–1	ρ_{N2}~3.1, ρ_{CO2}~1.4, ρ_{N2O} = 0.3, ΔS_{N2} = +50% at 307 °C and θ_{Na}~0.011–0.02	[28, 29]
			V_{WR}, θ_{Na}, and $\Delta e\Phi$ were directly correlated	
NO + C_2H_4	Pt/(Na)β'' Al_2O_3	T = 275–450 °C; [NO] = 0.5–1%, [C_2H_4] = 1–3%; θ_{Na} = 0–0.4	ρ_{CO2} = 15 with θ_{Na} = ~0.3 at 402 °C and [C_2H_4] = 1.5%, [NO] = 0.65%	[30]
NO + C_3H_6	Pt/(Na)β'' Al_2O_3	T = 330–400 °C; [NO] = 0–6%, [C_3H_6] = 0–0.4%, θ_{Na} = 0–1	ρ_{N2}~ρ_{CO2} = 7, ρ_{N2O} = 3, ΔS_{N2} = +20% at 375 °C, [C_3H_6] = 0.6%, [NO] = 1.3%, θ_{Na} = 0.3	[31]
			The promoter phase consists of $NaNO_2$/$NaNO_3$	
NO + C_3H_6 + O_2	Rh/ (Na)β'' Al_2O_3	T = 350 °C; [NO] = 1–9%, [C_3H_6] = 0–4%, [O_2] = 0–2%	ρ_{N2} = 2.4, ρ_{CO2} = 1.7, ρ_{N2O} = 0.4, ΔS_{N2} = +37% at 350 °C, [C_3H_6] = [NO] = 1%, θ_{Na} = 0.2 Alkali consists of carbonate and/or nitrate phases	[32, 33]
			XPS showed reversible Na transport via external bias	
NO + H_2	Pt/(Na)β'' Al_2O_3	T = 300–450 °C; [NO] = 0–1.6%, [H_2] = 0–1%, θ_{Na} = 0–0.12	ρ_{N2} = 30, ρ_{N2O} = 6, ΔS_{N2} = +40% at 375 °C, [NO] = 0.6%, [H_2] = 0.3%, θ_{Na} ~ 6%	[13]
NO + C_3H_6 + O_2 excess	Pt/ NaSiCon	T = 200–400 °C; [NO] = 0.2%, [C_3H_6] = 0.2%, [O_2] = 5%	ρ_{N2} ~ ρ_{CO2} ~ 1.7, ρ_{N2O} ~ 1.1, ΔS_{N2} = +20% at T = 295 °C	[34]
NO + C_3H_6 + O_2 excess	Pt/(Na)β'' Al_2O_3	T = 220–300 °C; [NO] = 0.2%, [C_3H_6] = 0.2%, [O_2] = 0.5–5%, θ_{Na} = 0–0.08	ρ_{N2} ~ ρ_{CO2} ~ 1.4, ΔS_{N2} = +20% at 220 °C, [O_2] = 5%, θ_{Na} = ~0.08	[35, 36]

(continued)

Table 5.3 (continued)

Reaction	Catalyst/ alkali conductor	Reaction conditions	Maximum ρ values and other highlights	Refs.
NO + C_3H_6 + O_2 excess + H_2O	Pt/(K)β Al_2O_3	T = 180–400 °C; [NO] = 0.2%, [C_3H_6] = 0.2%, [O_2] = 5%, [H_2O] = 5%	K depresses the inhibitory effect of H_2O in lean deNO$_x$	[37]
			K forms stable nitrates on Pt, i.e., can operate as NSR system	
NO + C_3H_6 + O_2 excess	Pt/(K)β Al_2O_3	T = 250–370 °C; [NO] = 0.1%, [C_3H_6] = 0.1%, [O_2] = 5%	The electrochemically assisted NSR process of the Pt/(K)βAl_2O_3/Pt cell is demonstrated	[38, 39]
			Max. deNO$_x$ to N_2 yield obtained at T = 300 °C	
NO + C_3H_6 + O_2 excess	Ir/(K)β'' Al_2O_3	T = 250–400 °C; [NO] = 0.2%, [C_3H_6] = 0.2%, [O_2] = 0–5%, θ_K = 0–1.0	Marginal promotion of K in the absence of O_2	[40]
			Strong poisoning at oxidizing conditions	
N_2O + C_3H_6 + O_2	Pt/(K)β'' Al_2O_3	T = 180–580 °C; [N_2O] = 0.1%, [C_2H_6] = 0.2%, [O_2] = 0.2–1.0%, θ_K = 0–0.9	ρ_{N2O} = 38.5, ρ_{C3H6} = 1.2 at 450 °C, [N_2O] = 0.1%, [C_2H_6] = 0.2%, [O_2] = 0.2%, $\theta_K \sim 0.4$	[41, 42]

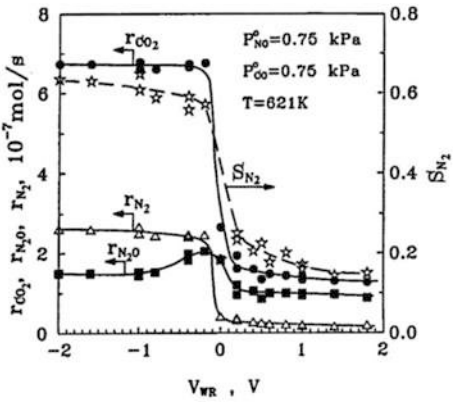

Fig. 5.5 NO + CO reaction under alkaline (Na)-EPOC conditions: effect of catalyst potential on the CO_2, N_2, and N_2O formation rates and the selectivity toward N_2 over Pt catalyst. Conditions: [NO] = [CO] = 0.75%, T = 348 °C. Data was acquired in a Pt/(Na)$\beta''Al_2O_3$/Au galvanic cell. (Reprinted with permission from Ref. [26]. Copyright 2005, Elsevier)

Alkaline-EPOC on NO reduction by hydrocarbons has received even more research interest (Table 5.3). Starting with the NO reduction by alkenes, the first works were demonstrated by Harkness and Lambert [30] and Yentekakis et al. [31] (Fig. 5.7).

In the first publication [30], the NO reduction by ethylene (NO + C_2H_4) in a Pt/(Na)$\beta''Al_2O_3$/Au galvanic cell was conducted, where it was shown that the rate of

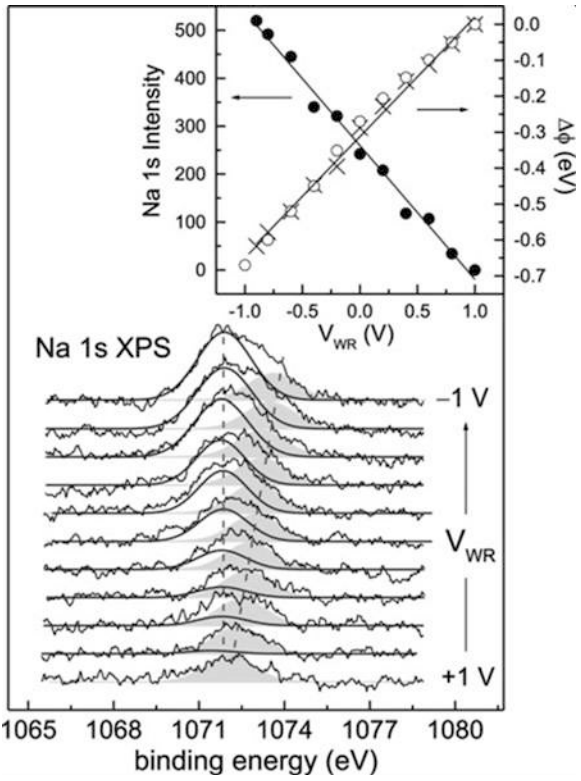

Fig. 5.6 Na 1s XPS spectra versus catalyst potential (V_{WR}) for Rh film interfaced with (Na)$\beta''Al_2O_3$ Na^+ ion conductor, at 307 °C and UHV conditions. The inset shows the integrated Na 1s XPS intensity due to sodium on the Rh surface (θ_{Na}) and associated work function change ($\Delta\Phi$) of the Rh film as a function of V_{WR}. Data was acquired using a Rh/(Na)$\beta''Al_2O_3$/Au galvanic cell. (Reprinted with permission from Ref. [29]. Copyright 2001, Elsevier)

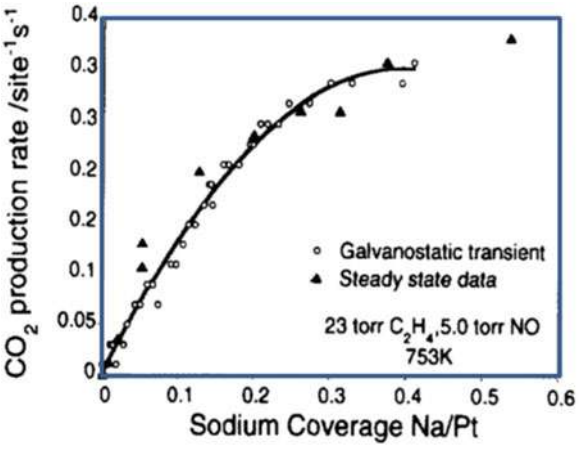

Fig. 5.7 Transient galvanostatic and steady-state potentiostatic data obtained during an alkaline (Na)-EPOC study of NO + C_2H_4 reaction over Pt electrocatalyst. Electrochemically promoted CO_2 production rate as a function of Na coverage. (Reproduced with permission from Ref. [30]. Copyright 1995, Elsevier)

the reaction linearly increased with θ_{Na} at low and intermediate θ_{Na} values (typically <0.3), achieving a plateau for higher values. Rate enhancement ratio values as high as $\rho = 15$ were obtained. In the second publication [31], propylene was used as

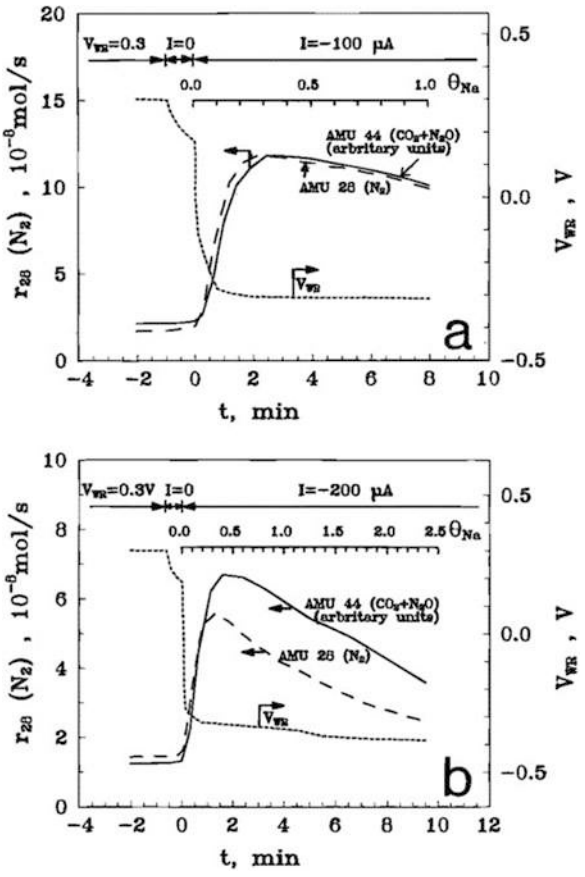

Fig. 5.8 Galvanostatic transients showing response of mass 44 rate ($N_2O + CO_2$) (solid line), N_2 rate (broken line), and catalyst potential (dotted line), in response to a step change in constant applied current. Conditions: (a) $P^0_{NO} = 1.3$ kPa, $P^0_{C3H6} = 0.6$ kPa, $T = 375$ °C; (b) $P^0_{NO} = 0.8$ kPa, $P^0_{C3H6} = 0.4$ kPa, $T = 375$ °C. (Reproduced with permission from Ref. [31]. Copyright 1997, ACS)

reactant ($NO + C_3H_6$) in a similar to the above galvanic cell, where very pronounced NO reduction rate enhancements were also achieved via EPOC in the whole range of reaction conditions applied (Fig. 5.8). The promotional effects were maximized at $\theta_{Na} \sim 0.4$, for which value the maximum rate enhancements were about $\rho = 7$ for both CO_2 and N_2 rates that followed by N_2 selectivity increases as well, from 60% on the unpromoted Pt to 80% on the optimal Na-promoted Pt. Higher Na coverages caused a gradual decrease of the promoting phenomena. As shown in Fig. 5.8, rate promotion although attenuated for high θ_{Na} values remains valid even for $\theta_{Na} > 1$. This suggests that a substantial amount of Na is present as 3D crystallites with a mixture of $NaNO_2$ and $NaNO_3$ phases, as demonstrated by XPS; at high Na loadings, these surface promoter compounds gradually inhibit reaction due to active site blocking. A Na-induced strengthening of the NO chemisorbed bond relative to propene was indicated by the kinetic data. The accompanied weakening of the N–O bond in the adsorbed NO molecules and the concomitant extended NO dissociation were considered for the interpretation of the observed promotional effects.

In two subsequent reports by the group of Lambert in Cambridge University, alkaline-EPOC was also used for the study of NO reduction by propylene over Rh,

using a Rh/(Na)$\beta''Al_2O_3$/Au galvanic cell, in the absence [32] or in the presence of O_2 [33]. They found that in the absence of O_2, a low sodium coverage ($\theta_{Na} \sim 0.02$) can cause a very large increase in the N_2 selectivity from 45% on the unpromoted Rh to 82% on the Na-promoted Rh together with rate enhancement ratio values of $\rho = 2.4$, 1.7, and 0.4 for the N_2, CO_2, and N_2O productions, respectively (Table 5.3). In the presence of O_2 [33], it was shown that upon increasing O_2 concentration in the reactant mixture, the promotional effects of Na were progressively attenuated and finally reversed to poisoning for $[O_2] = 2\%$. Using XPS and Auger spectroscopies, the authors also demonstrated that (i) a reversible transport of Na occurs between the solid electrolyte and the metal film catalyst whose potential (external bias) determines the sodium coverage and (ii), under promoted conditions, the alkali surface phase consists of nitrate, carbonate, or both depending on gas-phase composition but still acts as a promoter, i.e., the chemical identity of the counterion appeared not to play a significant role.

The only alkaline-EPOC work on NO reduction by hydrogen was reported by Marina et al. [13], who studied the effect of Na on the Pt-catalyzed NO reduction by H_2 using a Pt/(Na)$\beta''Al_2O_3$/Au galvanic cell reactor. Rate enhancement ratio values as high as $\rho_{N2} = 30$ were achieved for the formation of N_2, accompanied by significant increases in N_2 selectivity ($\Delta S_{N2} = \sim 40\%$ between unpromoted and optimally Na-promoted catalyst) with an optimal Na coverage of $\theta_{Na} = 0.06$ at 375 °C (Table 5.3). The promotional effects of Na were applicable in a wide range of H_2/NO gas-phase compositions (ca. 0.1–3.0) and temperatures (ca. 300–450 °C).

Following these first very encouraging results of alkaline-EPOC on the reduction of NO by either CO or hydrocarbons and H_2, the Vernoux and Valverde research groups in France and Spain, respectively, focused on similar systems, contributing substantially to further knowledge about the action of alkaline promoters and related phenomena, as well as to explore the usefulness and extend the applications of the titled promotion method (Table 5.3) [34–39]. Although there are no alkaline-EPOC studies on simulated exhaust conditions of stoichiometric gasoline engines, some studies of the above research groups have focused on simulated lean-burn or diesel engine emissions, i.e., on reactions involving the reduction of NO_x by hydrocarbons in conditions of excess oxygen.

Specifically, Vernoux et al. [34] performed a sodium-EPOC study of NO_x reduction by propene at excess oxygen (typical of diesel exhaust conditions) via a galvanic cell of the type of Pt/NaSiCon/Au that was based on a new type of Na^+ ion conductor, namely, NaSiCon ($Na_3Zr_2Si_2PO_{12}$), rather than (Na)$\beta''Al_2O_3$ typically used before. At a temperature of 300 °C and by using very low overpotentials (−100 mV), the authors found a strong enhancement on both the catalytic activity and the selectivity to N_2.

In the same line, the Spanish group performed several EPOC studies by using Na and K promoters by means of (Na)β″Al_2O_3 and (K)β″Al_2O_3 alkali ion conductors, respectively. Under lean-burn conditions, at low reaction temperatures (220 °C), rate enhancement ratios up to $\rho = 1.4$ were obtained for the NO reduction rate over a Pt electrocatalyst (Table 5.3) [35, 36]. As the temperature of the reaction increased, the Na-induced promotion decreased or even turned into poisoning. This was due to an

increase in oxygen coverage at the Pt surface with temperature, accompanied by inhibition of C_3H_6 adsorption. However, in the whole temperature region studied, Na ions caused a large increase in N_2 selectivity (up to 90%), minimizing the formation of undesirable N_2O. Regarding the effect of O_2 on the EPOC system, Na promotion was progressively attenuated upon increasing oxygen concentration (from 0 to 5%), as a result of the increased competitive adsorption of O_2 to the expense of C_3H_6. In all cases, the presence of sodium ions induced an increase in the nitrogen selectivity by promoting the NO adsorption and subsequent dissociation.

The research team extended their studies of alkaline-EPOC in lean-burn conditions investigating for the very first time the effect of the presence of H_2O in the feed stream, using now K^+ as the promoting ion (i.e., via a Pt/(K)βAl_2O_3/Au galvanic cell) [37] in order to approach even better real working conditions of lean-burn engines. The authors demonstrated that K promoter can decrease the well-known inhibitory effect of water for the reduction of NO by propylene. They once again verified that the K species form stable nitrate compounds on the Pt surface. This observation prompted them to conduct new series of alkaline-EPOC studies, bearing in mind the application of EPOC to *NO_x storage/reduction* (NSR) technology developed by Toyota in the early 1990s as a potential method of treating lean-burn engine emissions. The ability of alkaline elements to readily store NO_x (in the form of nitrites/nitrates) under oxygen excess conditions and then release NO_2 when switching to reducing conditions are key issues of NSR technology; during the latter step, NO_2 is easily reduced by the HCs, CO, or H_2 components accompanying NO_x in automotive exhaust emissions, that is, under NSR operation, the alkaline elements function in two ways: as promoters to enhance the NO oxidation to NO_2 and as trappers storing NO_2 in the form of nitrites/nitrates in order to release it under reducing environments. De Lucas-Consuegra et al. demonstrated, for the very first time, the possibility to perform the NSR process via EPOC, using Pt catalysts supported on (K)$\beta''Al_2O_3$ solid electrolytes (to supply the K promoter species) [38, 39]. Performing experiments under lean-burn conditions and even under the presence of steam, the authors found that K^+ ions electrochemically transferred to the Pt catalyst play a double role in the NSR process, as a promoter for the NO oxidation toward NO_2 and as storage sites through the formation of KNO_3. A maximum yield of the Pt/(K)βAl_2O_3 NSR catalyst to effectively reduce NO_x to N_2 was obtained at a very suitable temperature of ~300 °C for both lean-burn gasoline and diesel engines (Fig. 5.9).

Finally, Goula et al. [40] studied the NO + C_3H_6 + O_2 reaction at a reactants' mixture of 2000 ppm NO and 2000 ppm C_3H_6 and a variety of oxygen concentrations (ca. 0–5%) under alkaline (K)-EPOC conditions using Ir as electrocatalyst (Table 5.3). For all oxygen concentrations used, electrochemical supply of potassium to the catalyst surface caused detrimental effects on Ir catalytic performance in respect to the titled reaction. Only in the absence of oxygen a slight promoting effect on selectivity toward N_2 but not on the rates was observed. Obviously, this behavior of Ir under alkali promotion significantly differs from that of Pt at similar conditions and is understood in the light of an easier achievable on Ir surface (compared to Pt) extensive adsorption of O_2 in the expense of the hydrocarbon adsorption, leading to O-poisoning.

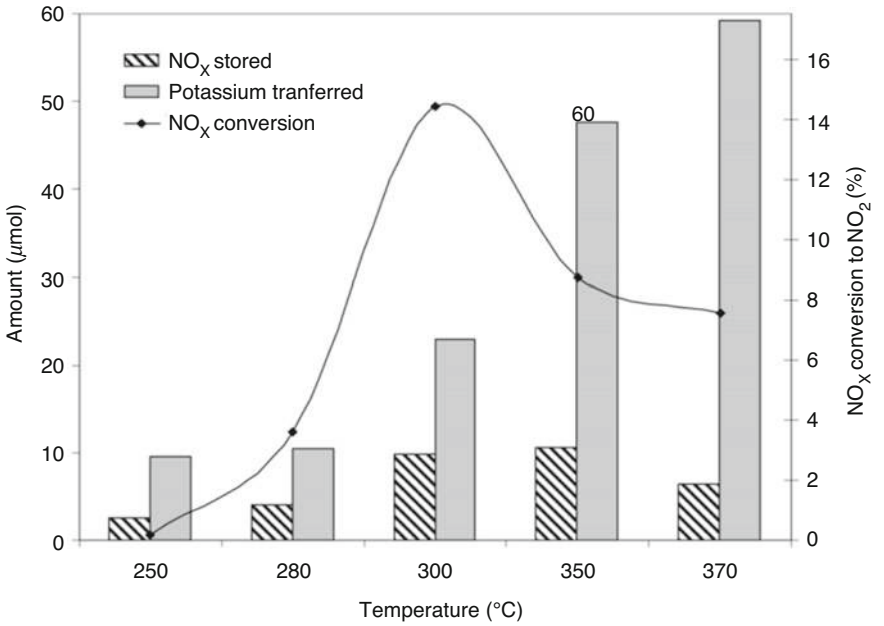

Fig. 5.9 Influence of the reaction temperature on the amount of NO_x stored, on potassium transferred, and on the NO_x conversion to N_2 during NO_x storage/reduction experiments. Lean phase ($NO/C_3H_6/O_2$: 1000 ppm/1000 ppm/5% O_2), 6 min of duration, $V_{cell} = -1.5$ V. Rich phase ($NO/C_3H_6/O_2$: 1000 ppm/1000 ppm/0.5% O_2), 5 min of duration, $V_{cell} = 3$ V. Data was acquired in a Pt/(K)βAl_2O_3/Au galvanic cell. (Reprinted with permission from Ref. [38]. Copyright 2011, Elsevier)

The catalytic abatement of N_2O from effluent gases is currently a topic of intense research interest since the recognition of its dominant role in stratospheric ozone depletion besides the fact that it is a very powerful greenhouse gas with a global warming potential of about 310. Although it is not a primary molecule emitted from combustion engines and processes, it is a byproduct of the NO_x reduction reactions taking place in catalytic converters. N_2O is also emitted in high quantities by the adipic and nitric acid industries and by stationary fuel combustion processes and agricultural activities (fertilizer use).

De Lucas-Consuegra et al. [41, 42] were the first who studied the N_2O reduction by propene via alkaline (K^+)-EPOC over Pt, using a Pt/(K)$\beta''Al_2O_3$/Au cell reactor. Maximum rate enhancement ratios obtained were as high as $\rho \sim 10$ at $T = 400$–450 °C and a reactant composition $N_2O/C_3H_6/O_2 = 1000$ ppm/2000 ppm/2000 ppm (Table 5.3). High K coverages (ca. $\theta_K = 0.7$) were necessary in order to achieve such large rate enhancements. K promotion was found to be practically constant at such high ρ values in a range of ~2000–7000 ppm concentration of oxygen in the reaction mixture. However, at larger O_2 concentrations (>9000 ppm), the promoting phenomena were practically vanished. It was also

demonstrated that potassium addition strongly decreased the inhibiting effect of water vapor in the feed.

5.3 Successful Transfer of the Alkaline-EPOC Obtained Insight to the Design of Conventional Catalyst Formulations

Early in the discovery of the EPOC phenomenon, and before Vayenas clarified and formulated the rules governing promotion in catalysis and highlighted the similarities between electrochemical promotion (EPOC) and conventional promotion in catalysis (CPC) [8–10], there was a belief and some indications that the two modes of promotion were governed by the same physicochemical properties and rules [7]. The favorable characteristic of alkaline promoters not to be sacrificed during reactions (permanent promoters) allowed the conduct of EPOC and CPC studies in a close comparative approach and therefore the experimental demonstration of the very close relationship of the two phenomena. Such studies have also highlighted the value of using EPOC as an effective research tool (probe) for exploring the effect of a range of promoters and in a wide range of conditions on a catalytic system of interest, determining their optimal loadings, before effectively applying them to the design of optimally promoted conventional catalyst formulations.

This research concept was for the very first time successfully implemented by Yentekakis and Lambert research groups in collaboration [43, 44]. In this work, the authors studied in close comparison the Pt-catalyzed NO + C_3H_6 reaction under promotion by Na, which was imposed by both electrochemical promotion (EPOC, using a Pt/(Na)$\beta''Al_2O_3$/Au electrochemical cell) and conventional promotion (CPC, using Pt(Na)/γ-Al_2O_3 catalysts where Na was added by impregnation). As shown in Fig. 5.10, very close similarities were found between the performance of the electrochemically promoted and conventionally promoted systems; catalyst performance was in both cases optimized at a Na coverage of $\theta_{Na} \sim 0.04$ [44]. Using Na 1s XPS, the authors also confirmed that electro-pumped Na is indistinguishable from Na put down by other ways (e.g., vacuum deposition).

It is worth noting that in order to obtain an efficient comparison between the two methods of promotion, the knowledge of the alkali coverage in both cases is a key issue. As we have seen, in EPOC studies, the alkali coverage (θ_{Akl}) is easily estimated by performing a galvanostatic transient experiment and using Eq. 5.5. In the case of CPC studies, Eq. 5.9 can be used to estimate alkali coverage (θ_{Alk}) from its wt% value on the catalyst prepared via conventional routes (e.g., impregnation) [2, 44]:

$$\theta_{Alk} = (\text{wt\% of alkali on the catalyst}/100) \cdot (N_{AV}/M_{Alk} \cdot A \cdot d) \qquad (5.9)$$

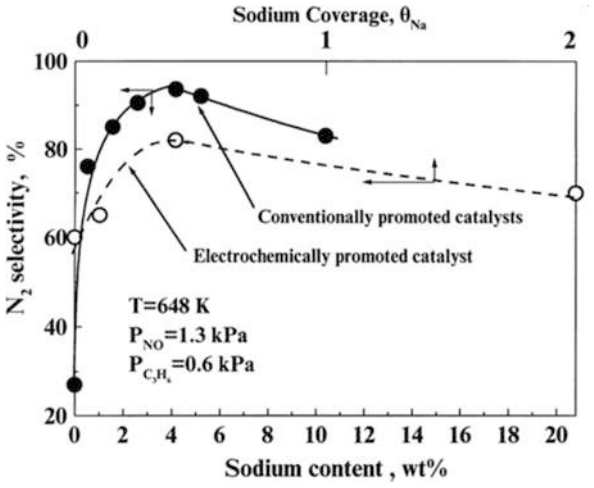

Fig. 5.10 NO + C_3H_6 reaction under alkaline (Na) promotion: comparison of electrochemically promoted (EPOC, Pt/(Na)$\beta''Al_2O_3$/Au galvanic cell) and conventionally promoted (CPC, Na-dosed Pt/γ-Al_2O_3) Pt catalysts with respect to N_2 selectivity under the NO + C_3H_6 reaction. Reaction conditions: $T = 375$ °C, [NO] = 1.3%, and [C_3H_6] = 0.6%. Similar well-correlated dependences of the variation of N_2 selectivity on nominal sodium coverage (θ_{Na}, upper abscissa) were obtained by the two methods of promotion (EPOC and CPC) applied. (Reprinted with permission from Ref. [44]. Copyright 2000, Elsevier)

where N_{AV} is the Avogadro number, M_{Alk} is the molecular weight of alkali used, A is the total (BET) surface area of the catalyst (m^2/g), and d is the surface density (atoms/m^2) of the active metal (d is equal to $1.53 \cdot 10^{19}$, $1.27 \cdot 10^{19}$, and $1.33 \cdot 10^{19}$ atoms/m^2 for {111} crystallites of Pt, Pd, and Rh, respectively) [2]. A probably better estimation of the nominal θ_{Alk} can be obtained if in Eq. 5.9 the surface density of the alkali adatom is used instead of that of the active metal (i.e., $8.84 \cdot 10^{19}$, $3.314 \cdot 10^{19}$, $1.8 \cdot 10^{19}$, $1.115 \cdot 10^{19}$, or $1.45 \cdot 10^{19}$ atoms/m^2 for Li, Na, K, Cs, or Rb, respectively; values were calculated on the basis of the alkali ionic radius) [2]. Bearing in mind that some issues related to alkali distribution, such as preference between active metal or support surface and formation of 2D and/or 3D aggregates, are not clear yet, it is apparent that Eq. 5.9 provides a quite rough estimation of alkali coverage, which, however, in the absence of more rigorous estimations or experimental measurements, can be applicable as a first approximation upon comparing the EPOC and CPC methods of promotion.

After all the above, particularly encouraging results obtained from the alkaline-EPOC studies of catalytic reactions related to emission control, the research groups that had contributed to in-depth understanding and exploring the usefulness of the electrochemical promotion phenomenon turned their efforts to design real catalytic systems in which the acquired EPOC insights were effectively integrated. Many other groups worldwide have also contributed to the alkaline promotion of emission control catalytic systems. Besides the studies on "model" reactions related to emission control catalysis, these efforts have been extended to a variety of catalytic

materials (supports and alkaline promoters), as well as different conditions to cover all the main sources of emissions, using simulated emissions of stoichiometric gasoline, lean-burn, and diesel engines as well as stationary and solid waste combustion processes. The obtained results of applying alkali promotion on these more realistic systems were spectacular. Many of these are gathered in three separated tables, namely, Table 5.4 (for CO oxidation and hydrocarbon oxidation), Table 5.5 (for deNO_x and deN_2O reactions), and Table 5.6 (for simulated realistic exhaust conditions), while some representative ones from each case are analyzed below in a more detail.

5.3.1 *Alkaline-CPC Studies on CO and Hydrocarbon Oxidation Reactions*

Regarding CO oxidation, the case of its preferential oxidation under H_2-rich conditions (PROX reaction) has received more intense interest in alkaline promotion studies [45–56] (Table 5.4). This is due to the critical importance of PROX to produce pure H_2 through the selective removal of CO from hydrocarbons reforming gas (CO + H_2) [1]. To this end, Minemura et al. [48, 49] showed that the addition of alkalis (Li, Na, K, Rb, and Cs) in a Pt/γ-Al_2O_3 catalyst results in very significant promotional effects on the selective oxidation of CO under H_2-rich conditions. Similar to EPOC results, this promotion followed a volcano-type behavior upon increasing alkali loading, thus providing a specific optimal loading for each alkali: 10–15, 3, and 5 (Na or K)/Pt, Cs/Pt, and Rb/Pt content ratios, respectively. Turnover rate enhancement ratio values up to $\rho = 10$ for the optimal K promotion at $T = 100$ °C [48] and even better (up to $\rho = 20$) at 80 °C [49] were achieved. Further studies by the research group, focused on the optimal promoter (K) when applying different supports (Al_2O_3, SiO_2, ZrO_2, Nb_2O_5, and TiO_2), have shown that the most remarkable promoting effects are obtained on γ-Al_2O_3-supported Pt [50]. Corroborative characterization studies by means of a variety of techniques enabled the authors to consistently interpret the promotion features [51, 52].

A K-induced weakening in the strength of CO adsorption on Pt and drastic changes on the adsorption site of CO (bridge and threefold hollow CO species) on the Pt(10wt%K)/γ-Al_2O_3 catalyst, found by using FTIR spectroscopy, were considered responsible for the observed promotional effects attributed to the change in the electronic state of K-modified platinum [51, 52]. OH co-adsorbed species (originating from H_2 and O_2 interaction under PROX conditions) that promote the CO oxidation were found by in situ FTIR on the highly active K-modified Pt/γ-Al_2O_3 catalyst [52]. The inhibiting effects on PROX reaction under over-promotion conditions (beyond the optimal promoter loading) were attributed to aggregation of Pt metal particles caused by the larger amount of alkali metal used [52].

More than *one order of magnitude* turnover rate enhancements of PROX reaction accompanied by CO oxidation selectivity higher than 90% were obtained by Pedrero

Table 5.4 Alkaline-CPC studies on CO and hydrocarbon oxidation reactions

Reaction	Catalyst	Promoter	Reaction conditions	Maximum achievements	Refs.
$CO + O_2$	PdO/SnO_2	Na	$T = 150$ °C; [CO]/[O] = 1.25 and 0.5 Na loading: 0.1 wt%	$\rho = 2.6$, $\Delta T_{50} = -25$ °C (at [CO]/[O] = 1.25) $\rho = 1.3$, $\Delta T_{50} = -8$ °C (at [CO]/[O] = 0.5)	[45, 46]
$CO + O_2$	$Pd/\gamma\text{-}Al_2O_3$	Ba	$T = 50$–250 °C; [CO] = 2.2%, $[O_2] = 1.1\%$ Ba loading: 0–15 wt%	$\Delta T_{50} = -45$ °C, with 10 wt% Ba on Pd/Al_2O_3	[47]
$CO + O_2 + H_2$ (PROX)	$Pt/(\gamma\text{-}Al_2O_3, SiO_2, ZrO_2, Nb_2O_5, TiO_2)$	Li, Na, K, Rb, Cs	$T = 100$–160 °C; [CO] = $[O_2] = 0.2\%$ Alkali/Pt molar ratio = 0–20	$\rho = 10$ by K promotion, at K/Pt = 10	[48–52]
$CO + O_2 + H_2$ (PROX)	Pt/SiO_2	Na, Rb, Cs	$T = 110$ °C; [CO] = $[O_2] = 1\%$, $[H_2] = 70\%$ Cs = 0–6 atoms/nm^2	$\rho = 10$, $\Delta S_{CO} = +30\%$ (60%→90%) by Cs, with a surface density = 1.6 Cs atom/nm^2	[53]
$CO + O_2 + H_2$ (PROX)	$Pt/\gamma\text{-}Al_2O_3$, $PtCo/Al_2O_3$	Na	$T = 25$–300 °C; [CO] = $[O_2] = 0.1\%$, $[H_2] = 1\%$ Na loading: 0.5–3 wt%	$\Delta X_{CO} = +75\%$ (25%→100%) on 2 wt% Na-promoted $PtCo/Al_2O_3$	[54]
$CO + O_2 + H_2$ (PROX)	$Pt/\gamma\text{-}Al_2O_3$	Mg	$T = 100$–250 °C; [CO] = 1%, $[O_2] = 0.75\%$, $[H_2] = 65\%$, $[CO_2] = 20\%$, $[H_2O] = 2\%$ Mg loading = 3 wt%	$\Delta T_{50} = -20$ °C for $CO + O_2$ reaction + 2% H_2O $\Delta X_{CO} > 35\%$, $\Delta S_{CO} > 15\%$ for PROX reaction (max $X_{CO} = 93\%$, max $S_{CO} = 62\%$) at 170 °C	[55]
$C_3H_6 + O_2$	$Pt/\gamma\text{-}Al_2O_3$	Na	$T = 100$–500 °C; $[C_3H_6] = 1000$ ppm, $[O_2] = 5\%$ Na loading: 0–4.2 wt%	$\rho \sim 10$, $\Delta T_{50} = -60$ °C with 2.6 wt% Na ($\theta_{Na} \sim 0.23$)	[57]

Table 5.5 Alkaline-CPC studies on deNO_x and deN_2O reactions

Reaction	Catalyst	Promoter	Reaction conditions	Maximum ρ achievements and other highlights	Refs.
NO + CO	Pt/γ-Al_2O_3	K, Rb, Cs	T = 150–500 °C; [CO], [NO] = 0–3% Alkali loading: 0–24 wt%	Optimal promotion by Rb: $\rho_{N2} = 110$, $\rho_{CO2} = 45$, $\rho_{N2O} = 7$, ΔS_{N2} = +58% (24% → 82%) with 15.5 wt% Rb at T = 350 °C and [CO] = 0.5%, [NO] = 1% $\Delta T_{50} = -150$ °C with >9.7 wt% Rb at [NO] = [CO] = 1000 ppm	[58]
NO + CO	Pd/YSZ	Na	T = 352 °C; [CO], [NO] = 0–4% Na loading: 0–0.102 wt% (θ_{Na} = 0–0.3)	$\rho_{N2} = 2$, $\rho_{CO2} = 1.5$, $\rho_{N2O} = 1$, ΔS_{N2} = +20% (50% → 70%) with 0.034 wt% Na at T = 352 °C, [CO] = [NO] = 1%	[59]
NO + CO + O_2	Pd/γ-Al_2O_3; Pd/CZ	Ba	T = 50–300 °C; [CO] = 2.2%, [NO] = 0.2%, [O_2] = 1% Ba loading: 0–15 wt%	$\Delta T_{50(CO)} = -40$ °C and $\Delta T_{50(NO)} = -33$ °C with 15 wt% Ba on Pd/γ-Al_2O_3 (promotion) $\Delta T_{50(CO)}$ = +97 °C and $\Delta T_{50(NO)}$ = +99 °C with 10 wt% Ba on Pd/CZ (strong poisoning)	[60]
NO + C_3H_6	Pt/γ-Al_2O_3 and Pt/(Na)$\beta''Al_2O_3$ (CPC vs. EPOC)	Na, Li, K, Rb, Cs	T = 200–500 °C; [NO] = 0–7%, [C_3H_6] = 0.3 and 0.6% Alkali loading: 0–24 wt%	Extraordinarily effective promotion, *by up to two orders of magnitude* (Rb being the best overall, 420-fold rate increases): $\rho_{N2} = 420$, $\rho_{CO2} = 280$, $\rho_{N2O} = 25$, ΔS_{N2} = +75% (20 → 95%), with 9.7 wt% Rb at T = 375 °C, [NO] = 1.3%, [C_3H_6] = 0.3% Optimal alkali loadings: Li = 1.25 wt %, Na = 4.16 wt%, K = 7.1 wt%, Rb = 9.7 wt%, Cs = 15 wt%	[43, 44, 62, 63]

(continued)

Table 5.5 (continued)

Reaction	Catalyst	Promoter	Reaction conditions	Maximum ρ achievements and other highlights	Refs.
NO + C_3H_6	Pt/γ-Al_2O_3	Ba	T = 200–500 °C; [NO] = 0–5%, [C_3H_6] = 0–2% Ba loading: 0–22.3 wt%	Extraordinarily effective promotion, *by up to two orders of magnitude*: ρ_{N2} = 165, ρ_{CO2} = 110, ρ_{N2O} = 9, ΔS_{N2} = +49% (45 → 94%), $\Delta T_{50\ (NO)}$ = −124 °C, with 9.7 wt% Ba at 450 °C, [NO] = 1.3%, [C_3H_6] = 0.3%	[64, 65]
NO + C_3H_6	Pd/YSZ	Li, Na, K, Cs	T = 250–450 °C; [NO], [C_3H_6] = 0–8% Na loading: 0–0.102 wt% (θ_{Na} = 0–0.3)	Best promotion obtained by Na: $\rho_{N2} \sim \rho_{CO2}$ = 7, ρ_{N2O} = 1.5, ΔS_{N2} = +20% (75% → 95%) with a θ_{Na} = ~0.2 (0.068 wt% Na) at 380 °C, [NO] = 1%, [C_3H_6] = 0.8%; ΔT_{50} = −110 °C, at [C_3H_6] = [NO] = 0.8%	[59, 66]
NO + C_3H_6	Rh/γ-Al_2O_3	Na	T = 200–550 °C; [NO] = 0–1%, [C_3H_6] = 0.1% Na loading: 0–11.3 wt%	ρ_{N2} = 3.3, ρ_{CO2} = 2.7, ρ_{N2O} = 2, ΔS_{N2} = +29% (43 → 72%) with 7.3 wt % Na at T = 375 °C and [NO] = [C_3H_6] = 0.3%	[67]
NO + CH_4	Pd/YSZ	Na	T = 350–450 °C; [NO] = 0–1.5 %, [CH_4] = 0–20% Na loading: 0–0.102 wt% (θ_{Na} = 0–0.3)	Only Na-induced poisoning was obtained	[68, 69]
NO + H_2 + O_2	Pt/γ-Al_2O_3, Pt/SiO_2	Na	T = 50–200 °C; [NO] = 0.1%, [H_2] = 0.4%, [O_2] = 6% Na_2O loading: 0–10 wt%	ΔX_{NO} = +20% (75%→90%) with 0.27 wt% Na_2O loading at T = 125 °C	[72]
NO + H_2 + O_2	Pt/ZSM-5	Na, K, Cs, Mg, Ca, Ba	T = 40–110 °C; [NO] = 0.08%, [H_2] = 0.08–0.56%, [O_2] = 10% O_2 Na loading: 0–20 wt%	Optimum promotion was achieved by Na at an optimal promoter loading of ca.10–15 wt% Na: NO_x conversion >90% with a selectivity toward N_2 ~ 50%	[73]

$NO + H_2 + CO + O_2$	$Pd/\gamma\text{-}Al_2O_3$, $Pd/\gamma\text{-}Al_2O_3\text{-}TiO_2$	K	$T = 50$–$400\ ^\circ C$; $[NO] = 0.1\%$, $[CO] = 0.25\%$, $[H_2] = 0.75\%$, $[O_2] = 6\%$ K loading: 0–3 wt%	Synergy between support-mediated (TiO_2 into Al_2O_3) and surface-induced (K addition) promotions, providing 90% NO_x conversion with $S_{N2} > 85\%$ in 180–300 °C and $\Delta T_{50} = -40\ ^\circ C$ on the optimal 0.5 wt% Pd (*0.25 wt% K*)/γ-Al_2O_3-*10 wt% TiO_2* catalyst	[78]
N_2O dec.	$Rh/\gamma\text{-}Al_2O_3$	Li, Na, K, Cs	$T = 250$–$450\ ^\circ C$; $[N_2O] = 1\%$ Alkali loading: 0.033–0.099 wt% (as oxide)	$\Delta T_{50} = -60\ ^\circ C$ for Li and Na promotion; $\Delta T_{50} = -70\ ^\circ C$ for K promotion; $\Delta T_{50} = -90\ ^\circ C$ for Cs promotion with an optimal promoter loading ~0.078 wt % alkali oxide	[79]
N_2O dec. Presence or absence of O_2	Rh/Al_2O_3	Mg, Sr	$T = 250$–$450\ ^\circ C$; $[N_2O] = 0.1\%$; $[N_2O] = 0.1\% + [O_2] = 5\%$ Mg and Sr loading: 5 wt%	$\Delta T_{50} = -45$ and $-50\ ^\circ C$ in the absence and presence of O_2, respectively, with a Sr loading = 5 wt% $\Delta T_{50} = +10$ and $-15\ ^\circ C$ in the absence and presence of O_2, respectively, with a Mg loading = 5 wt%	[80]
N_2O dec. Presence or absence of O_2, CO, and H_2O	Pt/Al_2O_3-(CeO_2-La_2O_3)	K	$T = 200$–$600\ ^\circ C$; $[N_2O] = 0.1\%$; $[N_2O] = 0.1\% + [O_2] = 2\%$; $[N_2O] = 0.1\% + [CO] = 1\%$; $[N_2O] = 0.1\% + [CO] = 1\% + [O_2] = 2\%$ K loading: 0–2.0 wt%	Promotion in all feed compositions examined: $\Delta T_{100} = -60\ ^\circ C$ under N_2O feed $\Delta T_{100} = -50\ ^\circ C$ under $N_2O + O_2$ feed $\Delta T_{100} = -45^\circ C$ under $N_2O + CO + O_2$ feed	[81]
N_2O dec. Presence or absence of O_2	$Ir/\gamma\text{-}Al_2O_3$	K	$T = 300$–$600\ ^\circ C$; $[N_2O] = 0.1\%$; $[N_2O] = 0.1\% + [O_2] = 2\%$ K loading: 0–1.0 wt%	K induces poisoning in the Ir-catalyzed N_2O decomposition at O_2-deficient conditions K is a promoter under O_2 excess conditions: $\Delta T_{50} = -80\ ^\circ C$ under $[N_2O] = 0.1\% + [O_2] = 2\%$ and an optimal K loading = 0.5wt%	[82]

(continued)

Table 5.5 (continued)

Reaction	Catalyst	Promoter	Reaction conditions	Maximum ρ achievements and other highlights	Refs.
$N_2O + CH_4$ $N_2O + C_3H_8$ $N_2O + C_3H_6$ Presence or absence of O_2	Pd/γ-Al_2O_3 and Pd/(K)$\beta''Al_2O_3$ CPC vs. EPOC	K	T = 100–500 °C; $[N_2O] = 0.15\%$ with $[CH_4] = 0.6\%$; $[C_3H_8] = 0.2\%$; $[C_2H_6] = 0.2\%$; and or not $[O_2] = 3\%$ K loading: 0–9.0 wt%	K strongly promotes N_2O reduction by C_3H_8 or C_3H_6 K slightly inhibits N_2O reduction by CH_4 CPC vs. EPOC K-induced promotions were similar $\Delta T_{50} = -100$ °C with 9 wt% K ($[N_2O] = 0.15\% + [C_3H_8] = 0.2\%$) $\Delta T_{50} = -135$ °C with 9 wt% K ($[N_2O] = 0.15\% + [C_2H_6] = 0.2\%$) $\Delta T_{50} = +25$ °C with 9 wt% K ($[N_2O] = 0.15\% + [CH_4] = 0.6\%$)	[83, 84]
N_2O, NO simultaneous dec.	Pt/(ROX 0.8)	K	$T = 50$–500 °C; $[NO] = 0.1\%$; $[N_2O] = 0.05\%$; $[N_2O] = 0.05 + [NO] = 0.1\%$ K loading: 3 and 5 wt%	K simultaneously promotes both NO and N_2O conversions: 100% conversion of both N_2O and NO over 0.1 wt% Pt(5 wt% K)/Al_2O_3 at $T = 350$ °C and $[N_2O] = 0.05\% + [NO] = 1\%$	[85]

Table 5.6 Alkaline-CPC studies on simulated realistic exhaust conditions

Reactants	Catalyst	Promoter	Conditions	Promotion highlights and achievements	Refs.
NO, C_3H_6, CO, O_2 (simulated TWC conditions at SP)	Pt/γ-Al_2O_3	Na	T = 200–500 °C; [NO] = 1000 ppm, [CO] = 7000 ppm, $[C_3H_6]$ = 1067 ppm, $[O_2]$ = 7800 ppm (S = SP = 1); w/F = 6×10^{-3} g s/cm^3 Na loading: 0–10.4 wt%	CO, C_3H_6, and NO conversions reached 100%, 100%, and >91% at T = 400 °C for Na loadings >4.18 wt% $\Delta T_{50(CO)} = -79$ °C, $\Delta T_{50(C3H6)} = -77$ °C, $\Delta T_{50(NO)} = -93$ °C, $\Delta S_{N2} = +81\%$	[86]
NO, C_3H_6, CO, O_2 (simulated TWC conditions around SP)	Pd/γ-Al_2O_3 Rh/γ-Al_2O_3	Na	T = 100–340 °C [NO] = 1000 ppm, [CO] = 7000 ppm, $[C_3H_6]$ = 1067 ppm, $6970 \leq [O_2] \leq 8630$ ppm ($0.9 \leq S \leq 1.1$); w/F = 15×10^{-3} g·s/cm^3; Na loading: 0–12 wt%	For Pd catalyst: Na > 3.5 wt% was beneficial under both oxidizing and reducing conditions ($\Delta T_{50(CO)} = -48$ °C, $\Delta T_{50(C3H6)} = -35$ °C, $\Delta T_{50(NO)} = -38$ °C (S = 1), and $\Delta S_{N2} = +35\%$ (S > 1.04)) For Rh catalyst: Na addition was detrimental	[87, 88]
NO, C_3H_6, CO, O_2, H_2, CO_2, H_2O (simulated TWC conditions at varying S)	Pt/MoO_3-SiO_2	Na_2O	T = 100–600 °C; (0.40–1.21%) O_2 + 0.12% NO + (490–620 ppm) C_3H_6 + (0.45–1.50%) CO + (0.15–0.50%) H_2 + 10.0% CO_2 + 3.0% H_2O; w/F = 9.91×10^{-3} g·s/cm^3; Na_2O loading: 0.05–1.0 wt%	Under stoichiometric conditions: a wider window of NO_x conversion was obtained by PtMoNa/SiO_2	[89]
NO, C_3H_6, CO, O_2, H_2, CO_2, H_2O (simulated TWC conditions)	Pt/γ-Al_2O_3 Rh/γ-Al_2O_3	Ba	T = 100–400 °C [NO] = 1000 ppm, $[C_3H_6]$ = 334 ppm, [CO] = 1%, $[H_2]$ = 0.3%, $[CO_2]$ = 12%, $[H_2O]$ = 3%, $[O_2]$ = 0.75% GHSV = 200,000 h^{-1}; 5.8–46 wt% Ba	Ba promotes Pt/γ-Al_2O_3 activity but not Rh/γ-Al_2O_3: $\Delta T_{50(NO)} = -30$ °C over Pt(46wt% Ba)/γ-Al_2O_3 $\Delta T_{50(NO)} = +15$ °C over Rh(46wt% Ba)/γ-Al_2O_3	[90]

(continued)

Table 5.6 (continued)

Reactants	Catalyst	Promoter	Conditions	Promotion highlights and achievements	Refs.
Real exhaust gas from a car engine	5 wt% Pd-commercial TWC	Ba, Sr, La	T = 300–600 °C GHSV = 68,000 h^{-1} Ba, Sr, or La loading: 5 wt%	The TWC performance of the Pd-based commercial catalyst was significantly improved by the addition of Ba, Sr, or La following the order Ba > Sr > La	[91]
C_3H_6, CO, H_2, O_2, CO_2, H_2O (simulated two-stroke motorcycle emissions)	Pt/γ-Al_2O_3	Na, K	T = 150–450 °C [CO] = 1–4.14%, [C_3H_6] = 0.08–0.7%, [O_2] = 0.9–0.96%, [H_2] = 0.2%, [CO_2] = 10%, [H_2O] = 0 or 10% S = 1, 0.17, and 0.31; 4.5 wt% Na; 7.6 wt% K	Promotion by both alkalis (superior to that of K): $\Delta T_{50(CO)} = -90$ °C, $\Delta T_{50\ (C3H6)} = -110$ °C at $S = 1$, no H_2O $\Delta X_{CO} = +51$ and +48 at $S = 0.31$, without and with H_2O, respectively $\Delta X_{CO} = +22$ and +48 at $S = 0.17$, without and with H_2O, respectively	[92]
NO, C_3H_6, CO, O_2, CO_2, H_2O (simulated TWC conditions)	0.5wt%Pt/(γ-Al_2O_3-CeO_2-La_2O_3) vs. commercial Pt/Rh-TWC	Na	T = 150–500 °C [NO] = 0.1%, [CO] = 0.7%, [C_3H_6] = 0.1067%, [O_2] = 0.78%, [H_2O] = 10%, [CO_2] = 10% GHSV = 50,500 h^{-1} Na loading: 5 and 10 wt% (in washcoat)	The Na-promoted monometallic (Pt-only) TWC, with 4.5-fold less PGMs, exhibits similar performance with the commercial TWC and better N_2 selectivity (~100% in the range 150–500 °C) Marginal impact of H_2O and CO_2 on Na/Pt-TWC A synergy between surface promoter (Na) and structural promoters (CeO_2, La_2O_3) was resulted Significant resistant to deactivation, even at 800 °C Na promotion remains valid even after aging due to the formation of β'-β''(Na)Al_2O_3 that act as permanent spontaneous Na sources	[93–96]

NO, C_3H_6, O_2 excess (simulated lean-burn conditions)	Pt/γ-Al_2O_3	Na	T = 200–450 °C [NO] = [C_3H_6] = 0.1%, [O_2] = 5% Na loading: 0–4.2 wt%	Strong promotion with an optimal Na loading = 2.6 wt% Na (higher loadings cause inhibition) $\Delta T_{50(C3H6)} \sim \Delta T_{50(NOx)} = -65$ °C; $\Delta S_{N2} = +40\%$ at T > 320 °C	[57]
NO, C_3H_6 or C_3H_8, O_2 excess (simulated lean-burn conditions)	Pt/γ-Al_2O_3	Na	T = 200–650 °C [NO] = [HC] = 0.2%, [O_2] = 5% GHSV = 20,000 h^{-1} Na loadings: 0–5 wt%	Under C_3H_6/NO/O_2 reaction: strong promotion ($\Delta T_{50(C3H6)} = -39$ °C; $\Delta S_{N2} = +20\%$ for $T > 280$ °C, optimized at 5 wt% Na) Under C_3H_8/NO/O_2 reaction: severe poisoning ($\Delta T_{50(C3H8)} = +191$ °C at 5 wt% Na loading)	[97]

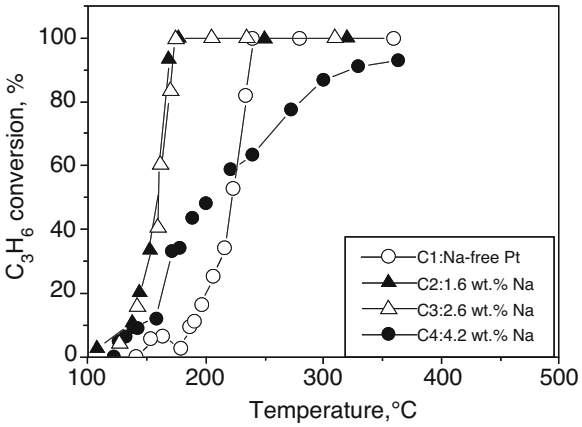

Fig. 5.11 The effect of temperature on C_3H_6 conversion over Na-dosed Pt(Na)/γ-Al_2O_3 catalysts under $C_3H_6 + O_2$ excess reaction: 1000 ppm C_3H_6 + 5% O_2; $w_{cat} = 70$ mg; total flow rate varying as $F_t = 210$, 126, 62.5, and 52 cm^3/min for C1, C2, C3, and C4 catalysts, respectively, in order to keep the *effective contact time* of C_3H_6 constant at $\tau = 4$ s (τ is defined as surface Pt atoms/reactant molecules/s). (Reprinted with permission from Ref. [57]. Copyright 2005, Elsevier)

et al. [53] by an optimal surface concentration of Cs of 1.6 atoms/nm^2 during an alkali (Na, Rb, or Cs) promotion study over Pt/SiO_2 catalysts (Table 5.4). The promotional effects of alkalis were interpreted in terms of both the electronic alkali–metal interactions and the inhibition of spillover-mediated H_2 oxidation pathways induced by alkalis.

Using an alkaline earth promoter (Mg), Cho et al. [55] obtained a notable increase on both CO oxidation rate and selectivity under PROX conditions over Pt/Al_2O_3 (Table 5.4): at 170 °C, maximum values obtained for CO conversion and CO_2 selectivity on Mg-promoted Pt/Al_2O_3 catalysts were 93.1 and 62%, respectively, compared to 70.2 and 46.8% (at 200 °C) over the unpromoted Pt/Al_2O_3 catalysts. The authors also investigated the response of their Mg-promoted catalytic system under the presence of CO_2 and H_2O in the feed, as well as in the absence of excess H_2. The superior performance of Mg-modified catalysts was attributed to an increase in Pt electron density, as well as to an increase of hydroxyl groups on catalyst surface.

Literature up to 2010 concerning CO PROX reaction over platinum-group metal catalysts (PGMs) under alkali promotion imposed by conventional routes (CPC) has been reviewed by Liu et al. [56].

Regarding hydrocarbon oxidation reactions under alkaline promotion, a CPC study has been reported by Yentekakis and co-workers [57]. They studied the oxidation of propene over Na-promoted Pt/γ-Al_2O_3 catalysts in oxygen excess conditions, typical of lean-burn combustion engines (1000 ppm propene + 5% O_2). Significant activity enhancements were obtained for Na loadings of ca. 1.6–2.6 wt% or equivalently for nominal Na coverages of ca. $\theta_{Na} \sim 0.11$–0.23 (Eq. 5.9), whereas higher Na coverages were found to be poisonous (Fig. 5.11). Rate

enhancement ratios as high as $\rho \sim 10$ can be calculated from their results (Table 5.4). A Na-induced enhancement of the adsorption of oxygen on a Pt surface predominately covered by propene (even at excess oxygen gas-phase conditions) was considered to be the origin of the promotional phenomena observed on the Na-promoted Pt/γ-Al_2O_3.

5.3.2 *Alkaline-CPC Studies on deNO$_x$ and deN$_2$O Reactions*

A number of studies on this topic can be found in the literature as summarized in Table 5.5. Among them, Yentekakis and co-workers reported on the NO reduction by CO over K-, Rb-, and Cs-promoted conventional Pt/γ-Al_2O_3 catalysts [58].

The study was performed in a wide range of temperature (ca. 150–500 °C), partial pressures of reactants, and promoter loadings. All alkalis were found to be very active promoters of the reaction, Pb promotion being the best overall offering rate enhancement ratios (ρ) as high as 110, 45, and 7 for the formation of N_2, CO_2, and N_2O, respectively (Fig. 5.12a), accompanied by substantial increases in N_2 selectivity by up to ~60 additional percentage units, thus achieving very high values, typically > ~ 85%, on the optimally promoted 0.5wt%Pt(9.7wt%Rb)/γ-Al_2O_3 at $T >$ ~ 350 °C [58]. Light-off experiments under stoichiometric reaction conditions

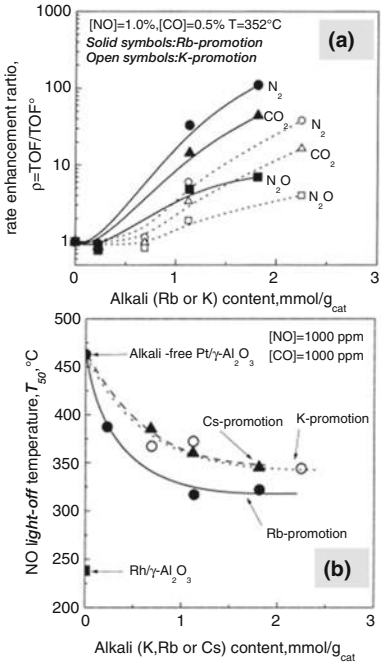

Fig. 5.12 NO + CO reaction under alkaline (K, Rb, Cs)-CPC conditions. (**a**) N_2, CO_2, and N_2O turnover rate (TOF) enhancement ratios achieved by Rb and K promotion of Pt/γ-Al_2O_3 catalyst. Reaction conditions: $T = 352$ °C, [NO] = 1%, [CO] = 0.5%. Solid lines and symbols refer to Rb promotion, and dashed lines and open symbols refer to K promotion. (**b**) Temperature for 50% NO conversion (T_{50}) as a function of alkali (K, Rb, or Cs) content of Pt/γ-Al_2O_3 catalyst. Conditions: [NO] = [CO] = 1000 ppm, $F_t = 80$ cm^3/min, catalyst weight 8(±0.2) mg. (Reprinted with permission from Ref. [58]. Copyright 2001, Elsevier)

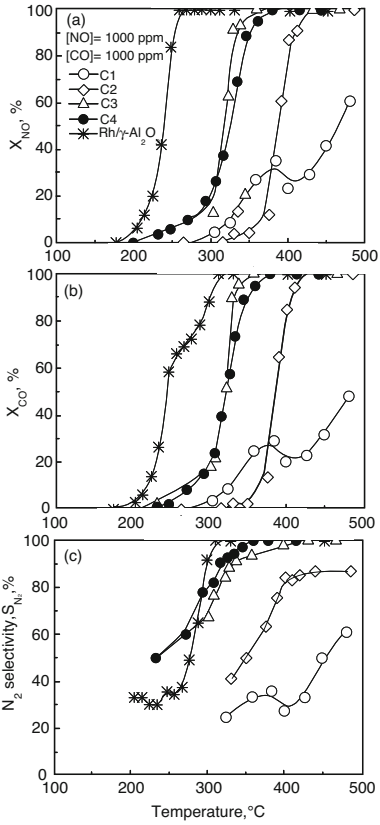

Fig. 5.13 Conversion of NO (**a**) and CO (**b**) and the corresponding N_2 selectivity (**c**), for Rb-promoted Pt/γ-Al_2O_3 catalysts as a function of temperature at constant reactor inlet conditions: [NO] = 1000 ppm, [CO] = 1000 ppm, total gas flow rate 80 cm^3/min, catalyst weight 8(±0.2) mg (w/f = 6×10^{-3} g s/cm^3). Comparison with the behavior of 0.5 wt% Rh/γ-Al_2O_3 catalyst. (Reprinted with permission from Ref. [58]. Copyright 2001, Elsevier)

showed that the NO conversion performance of the alkali-free 0.5wt%Pt/γ-Al_2O_3 catalyst is very poor in the temperature interval 100–500 °C (never exceeding 60%), whereas the optimally promoted 0.5wt%Pt(9.7wt%Rb)/γ-Al_2O_3 one exhibited 100% conversion of both NO and CO with 100% selectivity toward N_2 at ~350 °C (Fig. 5.13). Moreover, an about 115 °C decrease on the NO T_{50} temperature was obtained for K and Cs promotion and an even larger (150 °C) for Rb promotion (Fig. 5.12b).

The alkali-induced changes in the chemisorption bond strengths of CO, NO, and the dissociation products of the latter were taken into account to rationalize the promotional effects observed. The superior promotion of Rb compared to that of K was attributed to its larger size and thus to the greater electric field experienced by co-adsorbed species located at adjacent sites [58].

The NO + CO reaction under Na promotion was also studied by Yentekakis research group on Pd active phase supported on 10 mol% Y_2O_3-stabilized ZrO_2 (YSZ) using different loadings of alkali promoter [59]. On this active phase, both promoting and poisoning effects, regarding the Na loading, were induced by Na; the optimal promoter loading should be dependent from the CO/NO reactant

composition. A promoter coverage of $\theta_{Na} = 0.03$, obtained with an ~0.02–0.03 wt% Na addition on the catalysts (Eq. 5.9), was found to be optimal at 352 °C and equimolar CO/NO composition ([CO] = [NO] = 1%) leading to rate enhancement ratios for N_2 and CO_2 formation by up to $\rho = 2$ and an improvement in N_2 selectivity of about 20% in comparison to the unpromoted Pd/YSZ catalyst (Table 5.5) [59]. From a first comparative overview of the alkali promotion of CO+NO on Pt- and Pd-based catalysts [58, 59], it is apparent that Pt is more susceptible to this kind of promotion.

The effect of an alkaline earth (Ba) promotion on CO+NO reaction in the presence of oxygen was studied by Tanikawa and Egawa [60] on Pd supported on alumina and ceria–zirconia catalysts (Pd/γ-Al_2O_3 and Pd/CZ). While they found promotional effects of Ba on Pd/γ-Al_2O_3, which were gradually increasing as a function of Ba loading up to 15 wt%, only poisoning effects on Pd/CZ were recorded (Table 5.5).

From the same point of view and reaction (NO+CO), Lepage et al. [61] studied the effect of both alkali and alkaline earth promoters (Na^+, Rb^+, Cs^+, Mg^{2+}, Ca^{2+}, Sr^{2+}, and Ba^{2+}) on Rh nanoparticles supported on a series of Y zeolites by means of infrared spectroscopy of NO adsorption to monitor the electronic modifications of Rh nanoparticles. The observed decrease in NO reduction ignition temperature (T_{10}) with increasing ionic radius-to-charge ratio was related to the degree of electron transfer from Rh particles to the adsorbed NO molecules. This was confirmed by the red shift of the IR band of linearly adsorbed NO with increasing the radius/charge ratio of promoter elements.

Alkaline-CPC studies for the reduction of NO by hydrocarbons (alkenes or alkanes) have received more intense interest. Yentekakis' group in a series of publications on Pt- and Pd-based catalysts showed that the NO+propene reaction can undergo extraordinarily effective promotion by alkaline promoters [62–66], with that on Pt, however, to be more pronounced compared to Pd. Specifically, it was demonstrated that Pt nanoparticles dispersed on γ-Al_2O_3 (Pt/γ-Al_2O_3) are subjected to extraordinarily effective promotion by all Li, Na, K, Rb, and Cs alkalis [62, 63] and alkaline earths (Ba) [64, 65] in both activity and N_2 selectivity during the NO +propene reaction in the whole temperature interval of three-way catalytic converters interest (ca. 200–550 °C). In the case of alkali promotion [62, 63], rate increases by *two orders of magnitude* were achieved, while the selectivity toward N_2 was improved from about 20% over the alkali-free unpromoted Pt/γ-Al_2O_3 catalyst to more than 95% over the optimally alkali-promoted ones. Best promotion was offered by Rb, for which rate enhancement ratios as high as ρ = 420, 280, and 25 were obtained for N_2, CO_2, and N_2O formation rates, respectively (Table 5.5). Similar to corresponding EPOC studies [31], volcano-type behavior was found to be followed upon increases of promoter loadings for all Li, Na, K, Rb, and Cs alkalis (see, e.g., Na in Fig. 5.14) [62, 63]; the resulted optimal alkali loadings were, respectively, 1.25 wt% Li, 4.18 wt% Na, 7.1 wt% K, 9.7 wt% Rb, and 15 wt% Cs.

In Fig. 5.15, a representative light-off diagram of the aforementioned very spectacular alkali promotion of Pt/γ-Al_2O_3 is presented, bearing in mind the reactant concentration and temperature conditions existed in TWCs. As can be seen, the

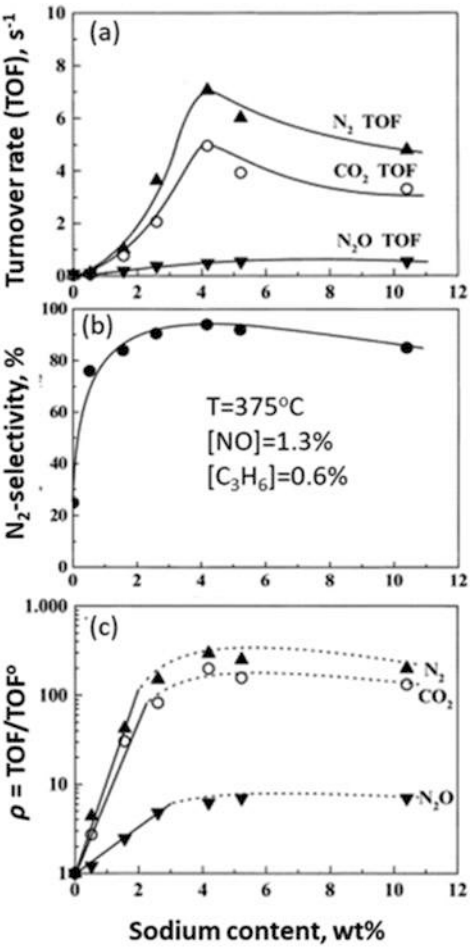

Fig. 5.14 NO + C_3H_6 reaction. The effect of Na content in 0.5wt%Pt(Na)/-Al_2O_3 catalyst on the turnover (TOF) formation rates of N_2, CO_2, and N_2O (**a**) and on N_2 selectivity (**b**) and rate enhancement ratios achieved (**c**). Reactor outlet conditions: $T = 375$ °C, [NO] = 1.3%, [C_3H_6] = 0.6%. (Adapted with permission from Ref. [62]. Copyright 1999, Elsevier)

marginal (~10%) NO conversion efficiency of unpromoted Pt/γ-Al_2O_3 can be readily improved by alkalis (e.g., Na) to values up to 100% in the temperature window of TWCs interest, offering at the same time selectivities toward N_2 as high as 95% [62].

Similar in trend (volcano-type) and intensity ($\rho = 165$, 110, and 9, for N_2, CO_2, and N_2O formation rates; ΔS_{N2} ~+50%), promotion was found on Ba-promoted Pt (Ba)/γ-Al_2O_3 catalysts for the same reaction (NO + C_3H_6) at 450 °C and an optimal Ba loading of 15.2 wt% Ba (Table 5.5) [64, 65].

Remarkable, but not so intense as above, promotion was achieved over Pd catalysts promoted by Li, Na, K, and Cs, namely, Pd(alkali)/YSZ [59, 66]: rate enhancement ratios (ρ) by up to *one order of magnitude* and N_2 selectivities up to 95% were achieved with an optimal promoter loading of 0.06 wt% Na (Table 5.5) [66]. A strengthening of the chemisorption bond of NO relative to propene that

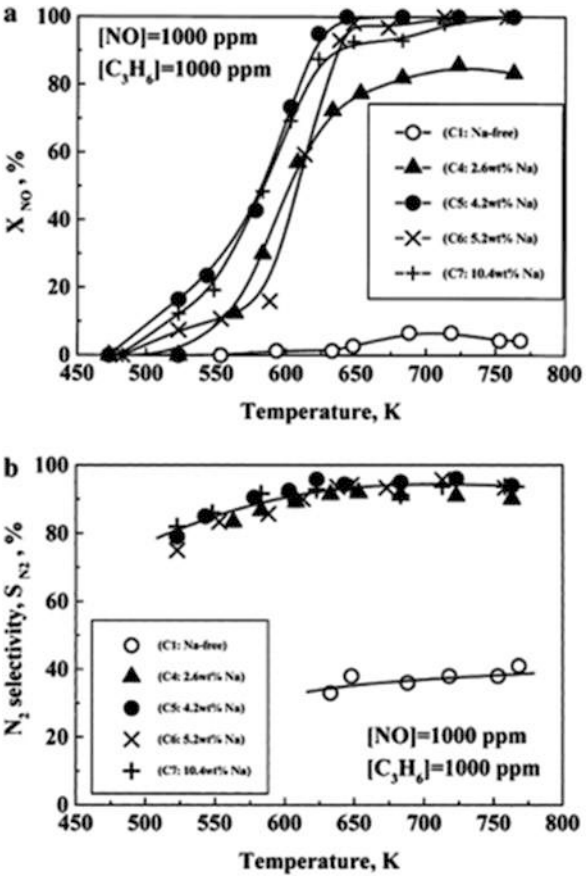

Fig. 5.15 NO + C_3H_6 reaction. The conversion of NO (**a**) and the corresponding selectivity toward N_2 (**b**) for Na-promoted 0.5wt% Pt/γ-Al_2O_3 catalysts, as a function of temperature at constant reactor inlet conditions: [NO] = [C_3H_6] = 1000 ppm, total flow rate F_t = 80 cm^3 STP/min, catalyst weight 8(±0.2) mg. (Reprinted with permission from Ref. [62]. Copyright 1999, Elsevier)

causes weakening of the N–O bond of the adsorbed NO molecules facilitating their dissociative chemisorption was considered as the origin of the promotional effects. The effect of residual chloride derived from chlorine-containing precursors used for catalyst preparation on Ba promotion performance was also examined in Ref. [59]. It was demonstrated that although all the original chloride is retained in the catalyst, Ba promotion remains effective and identical to that of chloride-free Ba-promoted catalysts. The formation of stable 2D $BaCl_2$ phase on the surface of the catalyst was detected. This implies that the promoting effect of Ba through these species overwhelms the poisoning effect of chloride resulting in a large net promotion, a finding of significant practical importance.

Further knowledge on this catalytic system, i.e., NO + C_3H_6 reaction under alkaline-CPC, was acquired by the studies of Lambert's team working on a different

active phase, namely, Rh [67]; Rh is a critical noble metal in the current commercial TWC formulations, as the main constituent associated with the effective reduction of NO_x. They found notable alkali (Na)-induced rate enhancement ratios up to $\rho \sim 3$ accompanied with significant enhancements on the selectivity toward N_2, from 53% on the unpromoted Rh/γ-Al_2O_3 catalyst up to 90% on the optimally Na-promoted catalyst with 7.3 wt% Na (optimal promoter loading). Higher Na loadings were poisonous for the catalytic system leading its performance below to its initial Na-free one. The authors also demonstrated that Na suppresses the formation of CO and HCN. Comparing these findings with that obtained on Pt or Pd active phases, it is apparent that the degree of promotional effect of alkalis on the NO reduction chemistry of Rh is substantially lower than that on Pt and Pd; the latter were the most spectacular achievements so far on alkaline-promoted emission control catalytic systems.

In the case of NO reduction by alkanes, the findings of alkaline promotion were completely different. In a study of NO reduction by methane on Na-dosed Pd/YSZ catalysts, Yentekakis and co-workers [68, 69] found only a poisonous effect of Na addition on both activity and selectivity for any Na loading (0–0.102 wt% Na) and reaction conditions applied ([NO] = 0–1.5%, [CH_4] = 0–25%, T = 350–500 °C). Representative results are shown in Fig. 5.16. The low tendency of CH_4 to adsorb, which becomes even worse on the Na-modified Pd surface (electrophobic adsorbate), and the much more pronounced adsorption of the competitive NO adsorbate (further enhanced by Na addition, electrophilic adsorbate) were the arguments for explaining the obtained behavior [68, 69].

It is worth noting the similarities on the effect of electropositive (alkaline) promotion of Pt-group metals (PGMs) between the alkanes' or alkenes' oxidation by dioxygen and by NO independently of the way (EPOC or CPC) this promotion is applied. When the oxidation process involves alkenes, electropositive promoters induce strong promotion, while when it involves alkanes, electropositive promoters induce poisoning. This is consistent to different trend of alkenes' and alkanes' adsorption on the PGM surfaces (strong and weak, respectively [70]) and the influence of the promotion on it regarding the EPOC theory [7–10], as well as the fact that in both cases the oxidant species are mainly based on adsorbed atomic oxygen derived by the dissociative chemisorption either of molecular oxygen or NO [57].

Besides hydrocarbons, H_2 is also used in alkaline-CPC studies since it is one of the gases present in combustion exhaust stream. Hydrogen could also be externally supplied, by the use of a hydrocarbon reformer or another source of safe in situ hydrogen generator, for the reduction of NO_x from stationary power sources and chemical plants. On the other hand, the NH_3-selective catalytic reduction process (NH_3-SCR), which is currently one of the most performing technologies for deNO_x processes in stationary power applications and chemical plants, experiences several drawbacks related to the storage and slip of ammonia. The growing interest for the H_2-SCR of NO_x is therefore understandable [71]. Most of these studies have used Pt-group metals as catalysts.

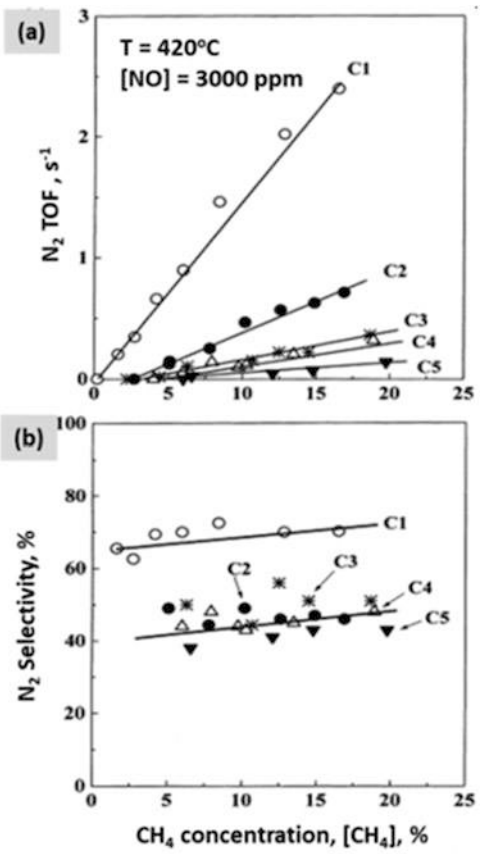

Fig. 5.16 NO + CH_4 reaction: the effect of Na content of the 0.5wt%Pd (Na)/γ-Al_2O_3 catalyst on the turnover frequency of N_2 production (**a**) and the corresponding N_2 selectivity (**b**). Reaction conditions: [NO] = 3000 ppm, varying [CH_4] = 0–25%, T = 420 °C. Catalyst codes regarding their Na content: C1 (Na-free), C2 (0.017 wt % Na), C3 (0.034 wt% Na), C4 (0.068 wt% Na), and C5 (0.102 wt% Na). (Reproduced with permission from Ref. [68]. Copyright 1998, Elsevier)

Burch and Coleman [72] studied the lean (O_2 excess) deNOx by H_2 over Na_2O-modified Pt/Al_2O_3 and Pt/SiO_2 catalysts, at low temperatures (<200 °C) representative of automotive "cold-start" conditions, and found that small Na loadings significantly increase the NO conversion rate, while larger loadings led to severe poisoning. Regarding the selectivity of the system toward N_2, it remained unaffected at temperatures less than 140 °C, while an adverse effect was recorded at higher temperatures (Table 5.5). In the same line, Machida et al. [73] investigated the effect of alkalis (Na, K, Cs) and alkaline earths (Mg, Ca, Ba) on Pt/ZSM5 catalysts for the H_2-SCR of NO_x under O_2 excess (10% O_2). The optimum promotional effects were obtained with Na promoter at loadings of 10–15 wt%, which exhibited NO_x conversion higher than 90% and N_2 selectivity of ~50%. Based on in situ DRIFTS studies, the promotional effect of Na was attributed to an enhancement of the adsorption of NO as NO_2-type species, which then serve as intermediates toward N_2 formation. However, when CO co-exists in exhaust streams (e.g., in automotive emissions), Pt-based catalysts are not the best choice for H_2-SCR of NO_x, due to the strong adsorption of CO on Pt surface which inhibits NO_x reduction [74]. As

demonstrated by Lambert's research team, Pd is a preferred active phase for such applications, which overcomes this poisoning effect of CO leading to good NO_x conversions at stream containing H_2 + CO [74–77]. Guided by these findings, Yentekakis and co-workers [78] studied the lean NO_x reduction by H_2 + CO over K-modified Pd/Al_2O_3 and Pd/Al_2O_3-TiO_2 catalysts. They found that potassium is a very active promoter of these catalysts for H_2-SCR process, while acting synergistically with the support-mediated promotion (addition of TiO_2 in Al_2O_3) leads to significant enhancements of both NO_x conversion activity and N_2 selectivity of Pd on the doubly promoted $Pd(K)/Al_2O_3$-TiO_2; a potassium loading of ~0.25 wt% optimized the catalyst performance offering up to ~90% NO_x conversion accompanied by a N_2 selectivity >85% in the temperature range of 180–300 °C (Table 5.5).

The environmentally important N_2O reduction/decomposition reaction has also attended remarkable interest by several research groups in the light of alkaline-CPC methodology (Table 5.5) [79–85]. Specifically, Haber et al. [79] studied the N_2O decomposition reaction over Rh supported on alkali (Li, Na, K, and Cs)-modified Al_2O_3 supports. They found that the pre-deposition of alkali metals on Al_2O_3 support results in a notable increase of Rh dispersion, which then improves catalyst efficiency on N_2O decomposition. Optimum promotion was obtained at ~0.078 mol % alkali loading.

Combined support-mediated (using CeO_2 and La_2O_3 modifiers of the Al_2O_3 support) and surface-induced (using alkalis) promotion was applied by Yentekakis research team [81] to improve the deN_2O performance of Pt/γ-Al_2O_3. The obtained doubly promoted $Pt(K)/Al_2O_3$-(20wt%CeO_2-La_2O_3) catalyst composite with 2 wt% K loading offered 100% N_2O conversion at a temperature of only 440 °C; the bare Pt/γ-Al_2O_3 did not exceed ~35% N_2O conversion even at 600 °C (Fig. 5.17). In respect to the impact of CO, O_2, and H_2O co-feed, the authors found the following deN_2O efficiency sequence in all promoted or non-promoted catalysts: $N_2O + CO >> N_2O > N_2O + O_2 > N_2O + O_2 + CO$ (Fig. 5.17b). Water co-feed was detrimental to deN_2O performance but in a partially reversible manner after its removal from the feed stream; the catalytic efficiency was totally restored by adding H_2 into $N_2O + H_2O$ feed. The research team extended their studies on a different noble metal, performing K promotion of Ir/γ-Al_2O_3 catalyst on N_2O decomposition under both deficient and O_2 excess conditions [82]. In the absence of O_2 and varying K loading in the range of 0–1 wt%, the authors found poisoning effect of the alkali on deN_2O catalytic efficiency. On the contrary, a pronounced K-induced promotion on deN_2O efficiency was found in the case of oxygen excess conditions, indicating that K prohibits the O-poisoning of the catalysts, which is the typical problem in deN_2O catalytic chemistry. The effect of alkali on the adsorption properties of Ir involving strengthening of the Ir–O bond of adsorbed O species with concomitant changes on the oxidation state of the metal was considered for the interpretation of the promotional and/or poisoning effects observed.

The N_2O reduction by hydrocarbons, alkanes (CH_4, C_3H_8) and alkenes (C_3H_6), was extensively studied by Pekridis et al. under alkali (K)-CPC conditions on Pd/γ-Al_2O_3 catalysts [83, 84]. It was found that K strongly enhanced the N_2O reduction by propane or propene, resulting in notably lower N_2O light-off

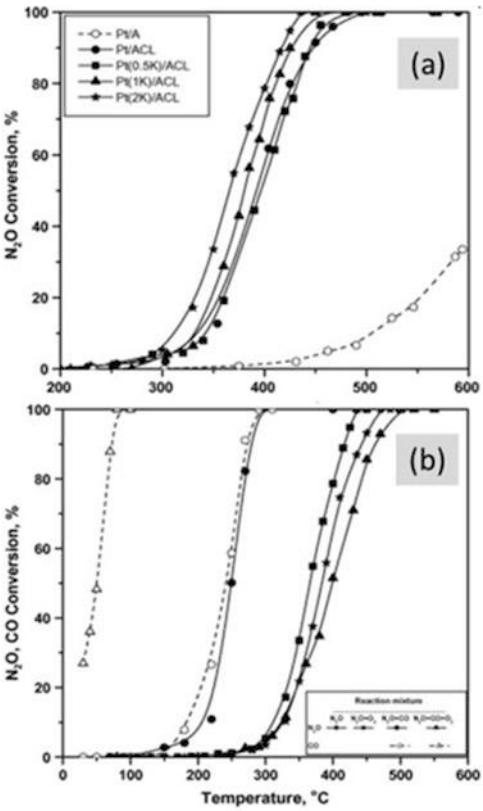

Fig. 5.17 (**a**) N_2O conversion profiles as a function of temperature (light-off curves) for bare Pt/γ-Al_2O_3, structurally promoted Pt/ACL, and doubly promoted Pt(K)/ACL catalysts under direct decomposition of N_2O; feed: 0.1% N_2O, GHSV = 10,000 h^{-1}. (**b**) N_2O (and CO) conversion profiles obtained over the optimally doubly promoted Pt(2wt%K)/ACL catalyst under direct N_2O decomposition or N_2O + CO reaction in the absence or presence of O_2; feeds: 0.1% N_2O; 0.1% N_2O + 2% O_2; 0.1% N_2O + 0.1% CO; 0.1% N_2O + 0.1% CO + 2% O_2. GHSV = 10,000 h^{-1}. (Reprinted with permission from Ref. [81]. Copyright 2013, Elsevier)

temperatures (~100 °C) compared to the unpromoted catalyst [83]. However, a slight inhibition upon K promotion was obtained when CH_4 was used as a reducing agent. K-induced modifications on the electronic, acidic, and structural properties of Pd/Al_2O_3 catalyst, which in turn affects the reactants' chemisorption bonds and consequently reactivity, were evidenced by XPS, in situ DRIFT spectroscopy of CO adsorption, and FTIR-pyridine adsorption and undertaken to explain the way of action of alkali promoters on deN_2O performance. Specifically, addition of K on Pd/Al_2O_3 decreases the adsorption strength of electron donor adsorbates, such as C_3H_8 and C_3H_6, enhancing the N_2O adsorption through an electron transfer from metal sites to N_2O antibonding orbitals. Both factors act synergistically toward increasing active sites for N_2O adsorption/decomposition. However, in the case of CH_4, K enhances the adsorption strength of N_2O and its dissociation products (O_{ads}), at the expense of weakly bonded CH_4, leading to poisoning by strongly bonded oxygen atoms. In Ref. [84], the authors conducted parallel studies of the same catalytic system under potassium-EPOC conditions using a Pd/(K)$\beta''Al_2O_3$/Au galvanic cell. The obtained results matched the promotion characteristics of the corresponding potassium-CPC study on Pd(K)/γ-Al_2O_3 catalyst very well,

experimentally evidencing once again the similarities of the two methods of promotion and demonstrating that electrochemical promotion is an effective and rapid tool for investigation of the role of a promoter on a catalytic system, allowing the transfer of the obtained insight to the design of optimal conventional catalyst formulations.

Goncalves and Figueiredo [85] studied the effect of potassium on the simultaneous reduction of NO + N_2O mixtures over Pt catalyst supported on activated carbon (ROX 0.8). A synergistic effect between K and Pt was found to offer high activity at relatively low temperatures. Specifically, at 350 °C, a very stable of about 100% conversion for both NO and N_2O was achieved over a 5 wt% K/0.1 wt% Pt catalyst, in opposite to the monometallic 0.5 wt% K or 0.1 wt% Pt counterparts; the latter showed only 25% conversion for NO and 90% and 0% for N_2O, respectively.

5.3.3 *Alkaline-CPC Studies on Simulated Realistic Exhaust Conditions*

The studies analyzed so far concerned "model" reactions associated with emission control catalysis. As we have seen, alkalis and alkaline earths were found to strongly promote reactions related with the emission control catalytic systems; therefore, testing the effectiveness of these new catalyst formulations at conditions that simulate real emissions was a reasonable consequence (Table 5.6).

The first work for this purpose was performed by Yentekakis and Lambert research teams in collaboration who studied the Na-promoted Pt/γ-Al_2O_3 catalyst formulations under simulated exhaust conditions of the stoichiometric gasoline engines operated at the stoichiometric point, using a feed mixture consisting (v/v) 1000 ppm NO + 1067 ppm C_3H_6 + 7000 ppm CO + 7800 ppm O_2 [86]. The stoichiometric point (SP) corresponds to the value equal to 1 of the stoichiometric number (S), calculated by Eq. 5.10:

$$S = (2[O_2] + [NO])/([CO] + 9[C_3H_6]) \tag{5.10}$$

A series of Pt(Na:0–10wt%)/γ-Al_2O_3 catalysts were tested under these conditions in the temperature range of 200–500 °C typical of TWCs, and representative results showing the effect of the promoter loading on the overall NO, CO, and C_3H_6 simultaneous conversions and N_2 selectivity at the mean temperature of TWC operation (400°C) are shown in Fig. 5.18 [86]. The results were very spectacular: the conversions of all three pollutants (NO, CO, and C_3H_6) reach 100% at sodium contents larger than ca. 4.2 wt% (θ_{Na}~0.4), accompanied with N_2 selectivity values >95% at this region of promoter loading (Fig. 5.18). A significant decrease in the light-off temperatures of pollutants' conversion of ~100 °C was also reported.

Lambert's team continued this motif, studying the performance of Na-promoted Pd/γ-Al_2O_3 and Rh/γ-Al_2O_3 catalysts operating under simulated TWC conditions over a range of stoichiometries from fuel-rich to fuel-lean conditions, $0.90 < S < 1.1$

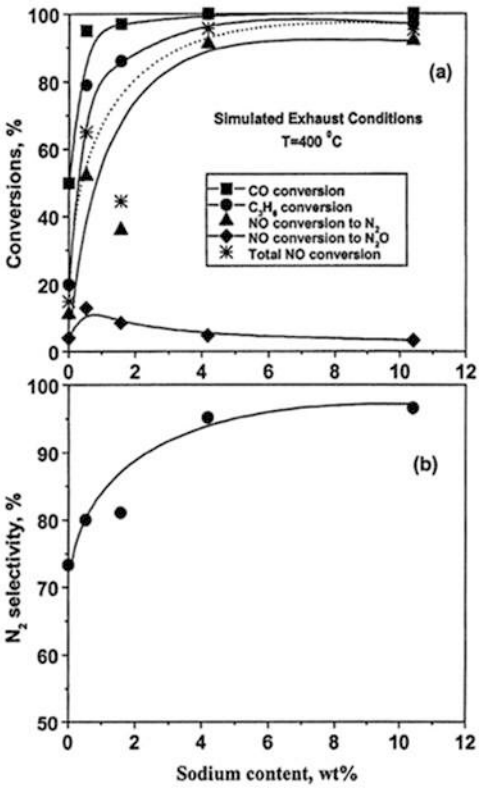

Fig. 5.18 Performance output of Na-promoted Pt/γ-Al_2O_3 catalysts operated at simulated exhaust conditions of conventional stoichiometric gasoline engines ($T = 400$ °C, 1000 ppm NO, 1067 ppm CO, and 7800 ppm O_2; $F_t = 80$ cm^3 STP/min; $m_{cat} = 8$ mg). Effect of Na loading on reactants' conversions (**a**) and selectivity toward N_2 (**b**). (Reprinted with permission from Ref. [86]. Copyright 2000, Elsevier)

(Table 5.6) [87, 88]. In the case of Pd/γ-Al_2O_3 catalysts, they found once again very spectacular promotional effects of Na [87], but not as high as those described above for Na-promoted Pt/γ-Al_2O_3 catalysts [86]. The beneficial effects of sodium were at work under both sides of the stoichiometric point (fuel-rich and fuel-lean conditions). However, the response of the Na-promoted Rh(Na)/γ-Al_2O_3 catalysts under similar TWC conditions was very different compared with that of Pd(Na)/γ-Al_2O_3: detrimental effect causing severe activity poisoning and N_2 selectivity reduction over the greater part of the temperature interval of 200–400 °C were recorded [83]. This was attributed to the enhanced oxygen adsorption on the Rh active sites at the expense of the hydrocarbon, while in the case of Pd, the beneficial effects were considered as a consequence of Na-promoted NO dissociation, together with inhibition of self-poisoning due to excessive propene adsorption [88]. It is worth noting that NO dissociative chemisorption takes place spontaneously on Rh but not on Pd.

Three-way performance around the stoichiometric point using Na_2O-promoted mono- and bimetallic catalysts, Pt/SiO_2 and PtMo/SiO_2, was studied by Tanaka et al. [89]. They also reported beneficial effects of the addition of a small amount of Na_2O on their catalysts that resulted in a widening of the active window around the SP (Table 5.6). Shinjoh et al. [90] have investigated the effect of an alkaline earth

(Ba) modifier on the catalytic activity of Pt/γ-Al_2O_3 and Rh/γ-Al_2O_3 catalysts under simulated automotive exhaust conditions at the stoichiometric point. The composition of the simulated exhaust gas used in their study was even more realistic: 1% CO, 0.3% H_2, 0.1% C_3H_6, 0.1% NO, 0.75% O_2, 3% H_2O, and 12% CO_2. They found that the TWC performance of Pt/γ-Al_2O_3 catalysts was improved by Ba, offering ~30 °C lower light-off temperatures compared to those for the unpromoted catalysts (Table 5.6). On the other hand, in a similar manner with the findings of Lambert and co-workers for Na-dosed Rh/γ-Al_2O_3 catalysts [88], the overall performance of their Ba-dosed Rh/γ-Al_2O_3 catalysts deteriorated with Ba addition. The authors concluded that Ba addition on Rh results in strong adsorption of oxygen species, suppressing hydrocarbon chemisorption and thus the reaction between them [90].

Kobayashi et al. [91] studied the effect of Ba, Sr, and La on a commercial 5 wt% Pd-only TWC catalyst (N.E. ChemCat Corp.) and achieved improvements on its three-way performance by the addition of all three elements.

Lee and Chen [92] investigated the impact of alkali (Na and K) addition on a Pt/γ-Al_2O_3 catalyst in the temperature interval of 150–450 °C using a gas mixture simulating two-stroke motorcycle emissions (with varying stoichiometric number, $S = 1$, 0.31, and 0.17). Operating at $S = 1$, significant improvements on CO and C_3H_6 conversions were achieved by both alkalis, with K-induced promotion being superior. Under O_2-deficient conditions, alkali addition enhanced CO conversion but not that of propene, which was reduced. The presence of water in the gas mixture was found to have a positive impact on promoted catalyst performance, in particular in the case of K promotion (Table 5.6).

Yentekakis and co-workers [93, 94] developed a monolithic-type catalytic converter with a washcoat containing only one noble metal (Pt-only TWC) that was optimally promoted by Na. Operating this novel TWC under simulated exhaust conditions in a wide temperature range (150–500 °C), they found similar performance to that of a commercial bimetallic (Pt/Rh)-TWC catalyst (Fig. 5.19a, Table 5.6), even with the 4.5-fold lower noble metal loading in this novel TWC. It is worth emphasizing that such a novel formulation and design of TWC are subjected to much lower production cost (use of only one noble metal at much lower loading, without the necessity of scarce Rh) and cost-effective recycling. Most recent tests of the novel TWCs after aging at extremely high temperature conditions (>800 °C) have shown a significant resistance to deactivation (Fig. 5.19b) [95, 96], indicating that the promoter phase (Na) does not actually escape from the catalyst composite even at such very high temperatures, due to its stabilization via the formation of new β' and β'' sodium-alumina phases as verified by TEM and XRD studies [95, 96]. These stable Na-containing phases, in direct interaction with the active phase (Pt), then act as a spontaneous (thermal diffusion-driven) Na promoter source during TWC operation causing permanent promotion [95, 96].

Alkaline-CPC studies performed under simulated exhaust conditions of lean-burn and diesel engines have also been reported by Vernoux et al. [97] and Yentekakis et al. [57]. Both research groups independently investigated the promotional effects

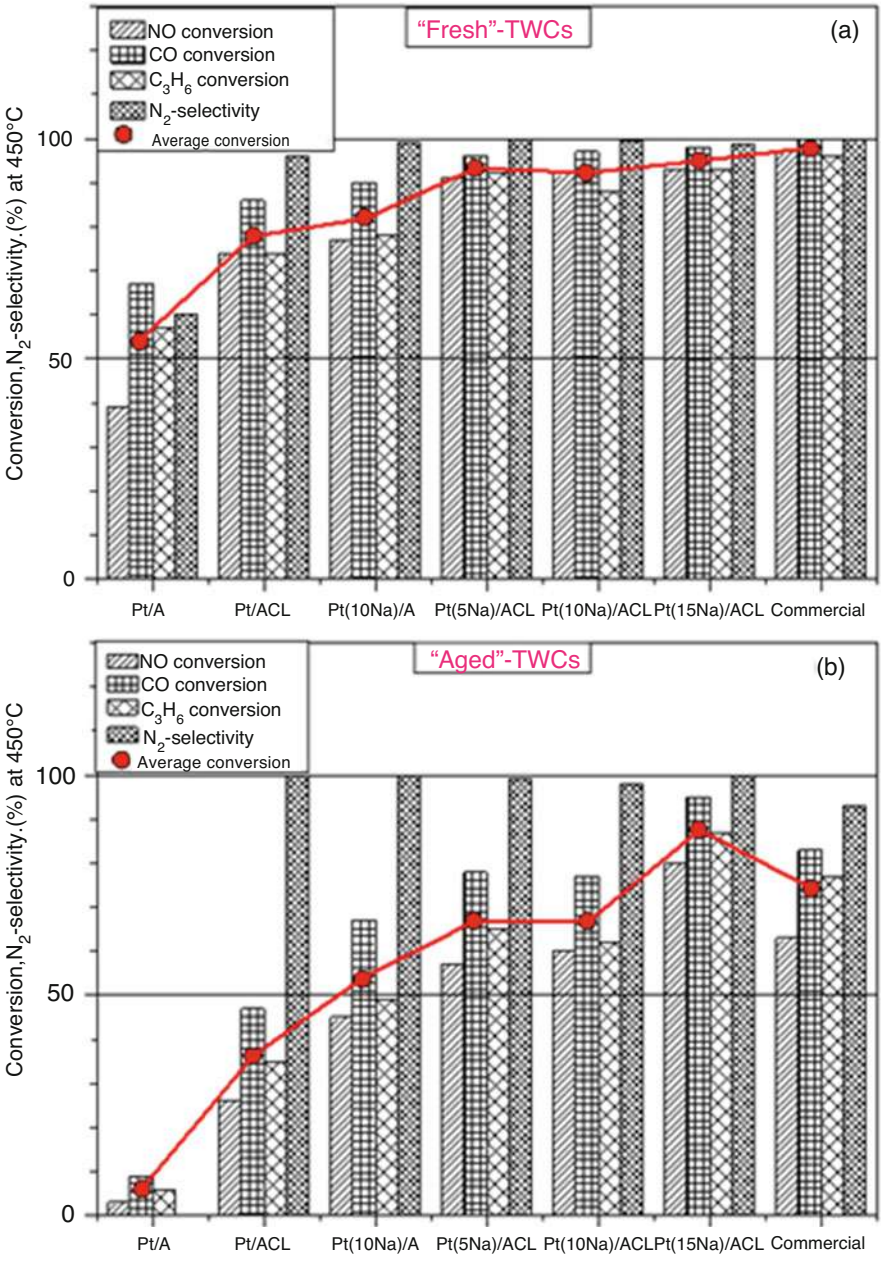

Fig. 5.19 Three-way catalytic performance at 450 °C of "fresh" (**a**) and "aged" (**b**) TWC samples at simulated stoichiometric gasoline engine exhaust conditions (0.1% NO + 0.7% CO + 0.1067% C_3H_6 + 0.78% O_2, balanced with He at 1 bar; $F_t = 3200$ cm^3/min). (Reproduced with permission from Ref. [96]. Copyright 2011, Elsevier)

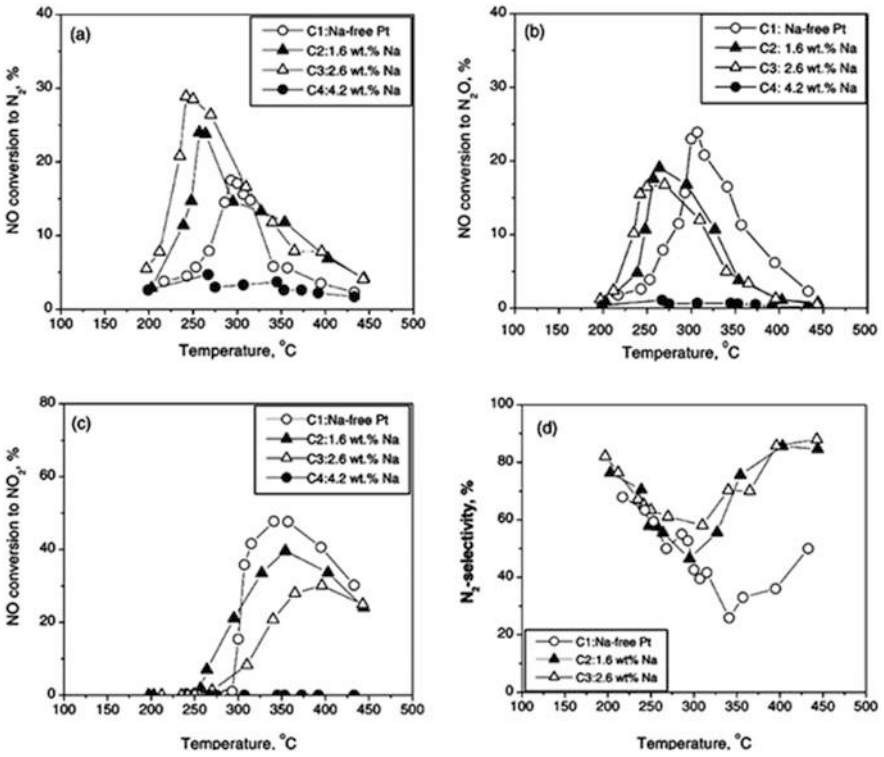

Fig. 5.20 C_3H_6 + NO + O_2 reaction on Na-promoted Pt/γ-Al_2O_3 catalysts. The effect of temperature on the conversion of NO to various N-containing products and the corresponding N_2 selectivity: (**a**) NO conversion to N_2, (**b**) NO conversion to N_2O, (**c**) NO conversion to NO_2, (**d**) N_2 selectivity. Conditions: 1000 ppm NO, 1000 ppm C_3H_6, 5% O_2, reactant contact time 4 s (Reprinted with permission from Ref. [57]. Copyright 2005, Elsevier)

of Na on Pt/γ-Al_2O_3 catalysts for the NO + propene + excess O_2 reaction and found significant beneficial effects on both deNO_x activity and N_2 selectivity at low and intermediate Na loadings [57, 97]; at high Na loadings, the alkali caused performance inhibition [57] (Table 5.6). The effects, promoting or poisoning (depending on promoter loading), were interpreted in terms of the alkali-induced changes on the relative adsorption strengths of reactants and intermediates on a highly populated surface with electrophilic and electrophobic adsorbates. The beneficial role of Na was possessed in a relatively narrow window of Na loading (ca. 0–2.6 wt% Na), while over-promotion to the optimal value of ~2.6 wt% Na causes significant inhibition of the catalyst performance (Fig. 5.20) [57].

5.4 The Role and Way of Action of Alkaline Promoters in Systems Associated with Emission Control Catalysis

The results presented in the previous sections demonstrated that alkalis and alkaline earths supplied either electrochemically (alkaline-EPOC) or conventionally (alkaline-CPC) on platinum-group metal surfaces can markedly improve their catalytic properties (activity and selectivity) for reactions of high significance in emission control systems, such as CO and hydrocarbon oxidation and NO_x and N_2O reduction, as well as for more complex reaction systems that mirror practical applications (e.g., stoichiometric gasoline, lean-burn and diesel engine exhaust gases) (Tables 5.2, 5.3, 5.4, 5.5 and 5.6). Independently of the method used, i.e., electrochemical promotion of catalysis (EPOC) or conventional promotion of catalysis (CPC), the resulted promotional effects were at least qualitatively similar, thus demonstrating the common origin of the two promotion methods. This has been experimentally demonstrated by conducting parallel comparative EPOC vs. CPC studies (e.g., [43, 44, 84]) and latterly was thoroughly interpreted on a theoretical basis by Vayenas and co-workers [8–10].

Nevertheless, the intensity of the promotion obtained via the alkaline-CPC method is typically more spectacular, likely due to the better alkali-to-metal interactions allowed in the well-dispersed catalyst nanoparticles associated with CPC method, compared to the film-type catalysts of EPOC method. These issues boost the practical importance of the subject and its promising features for direct implementations on several challenging environmental protection systems.

Bearing in mind the similarities of EPOC and CPC concepts of promotion, these will be hereafter considered as identical phenomena; the mechanistic model described below interpreting the mode of action of alkaline promoters may be considered valid for both promotion methods. In fact, in the vast majority of publications reviewed here, the authors relied on it to consistently interpret specific promotion phenomena appearing at the different reaction systems they explored. The main body of the model is described below, and several direct spectroscopic evidences supporting its consistency are presented.

As mentioned at the beginning of this chapter, using EPOC (via a galvanic cell as it was described by the formula 5.3 and Fig. 5.1), one can electrochemically control (via Faraday's law) the migration of promoting species (e.g., Na^+, Fig. 5.1c) from the solid electrolyte onto the catalyst/gas interface, where an effective and overall neutral double layer [$Na^{\delta+}$, δ^-] is formed through this ion's back-spillover imposed electrochemically (reaction 5.2) [7–11]. Note that δ^- is the image charge in the metal of the positively charged $Na^{\delta+}$ species on the metal surface; the charge δ is about 0.8–0.5, decreasing with increasing Na coverage [7]. In a number of studies involving X-ray photoelectron spectroscopy (XPS), the groups of Lambert and Yentekakis have doubtlessly shown that in EPOC studies that concern PGM films interfaced with an alkali-conducting solid electrolyte, the promoting species are indeed alkaline ions reversibly supplied by the external bias onto the catalyst surface [19, 28, 29, 31–33, 43, 44]. The authors have also shown that under reaction conditions, the

electrochemically supplied alkali ions form stable surface compounds (e.g., alkali nitrites, nitrates, and carbonates) that can act as promoters even existing in such formulations, which, in excess, induce geometric, active site blocking, phenomena, and thus poisoning effects on PGM activity (the so-called over-promotion). Direct evidences and similar conclusions about the origin of alkaline-EPOC have also been provided by the Vayenas group through scanning tunneling microscopy (STM) studies [98, 99].

In fact, an identical configuration of alkali species on the catalyst surface (therefore, similar accompanied promotional/poisoning effects [43, 44]) is expected when these species are introduced by conventional (CPC) methods (e.g., impregnation, vapor deposition, etc.) on conventional catalyst formulations (i.e., highly dispersed catalysts).

Eventually, an electrically modified metal surface, actually an electron-enriched, lower work function metal surface due to the δ^- charge located at the metal side interface half-layer, is resulted independently of the promotion method employed. This electrically modified surface interacts with the co-adsorbed reactants and reaction intermediates and products, changing their binding energies (in respect to those on an unpromoted metal surface), creating pronounced alterations in catalytic performance. Therefore, the main feature of the alkaline-promoted (either via EPOC or CPC) catalyst particles is their resulted electron-enriched, lower work function surface.

The concomitant alterations on the adsorption characteristics of the co-adsorbed reactants over an alkaline-modified metal surface are of course subjected to the electronic properties of the reactants, i.e., electrophilic (electron acceptor) or electrophobic (electron donor) [100]. Theoretical predictions [101] have shown that alkali-promoted Pt-group metal (PGM) surfaces appear strengthening in the bonds of the metal–electron acceptor (electrophilic) adsorbates, such as PGM–NO, PGM–O_2, PGM–N, PGM–O, and PGM–CO, and weakening in the bonds of the metal–electron donor (electrophobic) adsorbates, such as PGM–hydrocarbons (and their fragments) and occasionally PGM–CO since CO can behave either as an electrophilic or as an electrophobic adsorbate [100].

Alkali-induced changes on the chemisorption characteristics of several reactants have also been directly evidenced by experiments. To this end, Vernoux et al. [97] using temperature-programmed desorption (TPD) after adsorption of oxygen on Na-dosed Pt/Al_2O_3 catalysts demonstrated that the adsorption strength of the atomic oxygen (electron acceptor adsorbate) on the Pt component of the catalyst is enhanced by Na addition; the oxygen desorption peak corresponding to Pt–O interaction was shifted to higher temperatures with increasing Na loading of the catalyst, directly evidencing a strengthening of the Pt–O bond. Koukiou et al. [102] using in situ diffuse reflectance infrared Fourier transform spectroscopy (DRIFTS) have shown that increasing Na loading in a Pt(Na)/γ-Al_2O_3 catalyst causes a pronounced and progressive red shift of the N–O stretching frequency (Fig. 5.21) associated with molecular NO adsorbed on the Pt component of the supported catalyst. As shown in the figure, at the highest sodium loading (10 wt% Na, nominal sodium coverage $\theta_{Na} = 0.5$), a 1681 cm^{-1} species is observed that corresponds to an activated $NO^{\delta-}$

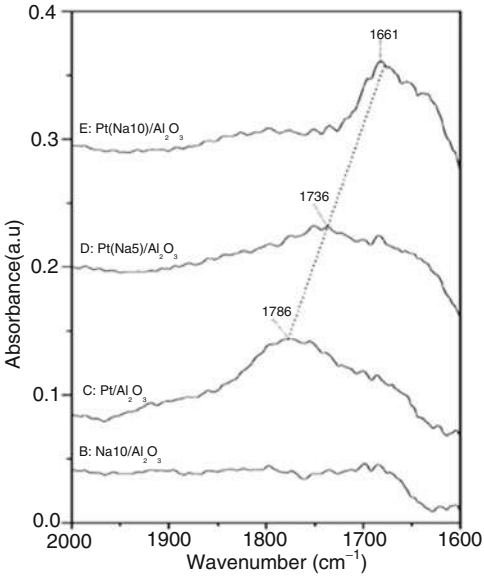

Fig. 5.21 DRIFT spectra (expanded scale for the region 2000–1600 cm^{-1} and subtracting spectrum of pure Al_2O_3) obtained with 10wt %Na/γ-Al_2O_3 (**b**), Pt/γ-Al_2O_3 (**c**), Pt (Na5)/γ-Al_2O_3 (**d**), and Pt (Na10)/γ-Al_2O_3 (**e**) samples after NO adsorption for 1 min at 27 °C. (Reprinted with permission from Ref. [102]. Copyright 2007, Elsevier)

species with bond order 2, that is, a negatively charged adsorbate with increased electron density in the π* antibonding orbital. Therefore, according to the authors, the red shifts shown in Fig. 5.21 are due to the resulting metal → adsorbate charge transfer that acts to weaken the N–O bond, red-shifting its vibration frequency and promoting its dissociation, rather than to alkali-induced changes in the relative populations of various forms of adsorbed NO.

TPD experiments conducted by Harkness and Lambert [103] to investigate the chemisorption characteristics of NO on Na-dosed Pt{111} surface demonstrated that the presence of Na on the Pt{111} single crystal causes an increase in the adsorption energy of NO (i.e., strengthening of the metal–NO bond) accompanied by a monotonically increased NO dissociation (i.e., N_2 desorption) as a function of Na coverage. In the same line, TPD studies by Garfungel et al. [104], involving the interaction of NO with K-dosed Pt{111}, yielded the same evidences: a K-induced increase in the Pt–NO bond strength accompanied by K-promoted NO dissociation.

A number of early and recent studies concern the chemisorption of CO on alkali-modified PGM surfaces. Bertolini et al. [105] studied the chemisorption of CO on K-modified Pt(100) model surfaces by means of TPD and Auger electron spectroscopy (AES). The observed progressive strengthening of the Pt–CO bond (i.e., shift of the CO desorption peak to higher temperatures) as a function of K coverage at low θ_K values (ca. 0–0.4) was attributed to long range uniform electronic modifications (i.e., work function changes), due to charge transfer; uniformly distributed, due to electrostatic repulsing forces, $K^{\delta+}$ ($\delta \sim 1$) adspecies appear on the K-dosed surface. Such an electron-enriched (lower work function) Pt surface strengthens the adsorption of CO via substantial charge donation from the K-modified Pt surface into the 2π* orbitals of CO [105]. At high K coverages (ca. 0.45–1), short range interactions

between the CO and K adspecies, that is, an even more direct bonding of CO with K (formation of CO–K–Pt surface complexes), were considered. On the other hand, Pitchon et al. studied the effect of Li, Na, K, and Cs on CO adsorption characteristics over dispersed Pd/SiO_2 [106]. They demonstrated drastic changes in the infrared spectrum of CO adsorbed on Pd sites; a significant weakening on the strength of the C–O bond of adsorbed CO molecules caused the appearance of a new νCO band at low infrared frequency – the extent of the interaction was dependent on the nature of the alkali. These influences were assigned to a localized interaction "Pd–CO–alkali" rather than to long range electronic modifications. Liotta et al. [107] studied the effect of Na on the adsorption of CO on Pd-based supported catalysts, using SiO_2 and pumice supports, by means of FTIR spectroscopy. Depending on the support used, the appearance of both electronic and geometric effects was evidenced, attributed to the different localization of sodium ions in the catalysts. An electronic density transfer to Pd due to the presence of alkali was invoked that produces a red shift (toward lower frequencies) of the CO bands of the IR spectra of chemisorbed CO, owing to an enhanced transfer of electron density from the metal to the π^* molecular orbitals of CO (electrophilic behavior of adsorbed CO).

Using in situ DRIFTS, Yentekakis and co-workers recently demonstrated that electron-enriched Pt surfaces resulted by combined application of alkali-induced surface promotion and support-mediated promotion by ceria-based mixed oxides [93–95]. Operating these doubly promoted $Pt(Na)/Al_2O_3$-(CeO_2-La_2O_3) catalysts under TWC conditions, a substantial population of adsorbed species at 2060 cm^{-1} was detected attributed to CO on reduced Pt^0 sites when CeO_2-La_2O_3 was incorporated into the Al_2O_3 support. This feature was substantially exacerbated when Na promoter was also incorporated in the catalyst formulation, while at the same time, the formation of active Pt–NCO intermediates at about 2180 cm^{-1} (resulted from an enhanced NO decomposition) was facilitated by alkali promotion on the doubly promoted $Pt(Na)/Al_2O_3$-(CeO_2-La_2O_3) catalyst (Fig. 5.22). On the unpromoted Pt/Al_2O_3 catalyst, CO species adsorbed on positively charged Pt sites ($Pt^{\delta+}$–CO) were assigned (Fig. 5.22).

All the aforementioned studies in this chapter unambiguously lead to the main conclusion that alkali adatoms on PGM surfaces provide electron-enriched metal sites (lower work function surfaces), which favor the adsorption of electron donor (electrophilic) co-adsorbates and inhibit the adsorption of electron acceptor (electrophobic) co-adsorbates. Besides these electronic effects, geometric type influences can also emerge due to the formation of alkali–reactant–metal surface complexes. However, the promotional effect of alkalis is practically not eliminated due to the existence of such surface complexes, except at high alkali loadings where extensive coverage of the surface by such large species creates active site blocking (geometric constrains). This is one of the main causes, but not the only one, of the common volcano-type behavior of the intensity of promotion versus alkali loading. Such modifications on the reactants' chemisorptive bonds are accompanied by alterations in the activation energies of the catalytic reactions (showed in many alkaline-EPOC and alkaline-CPC studies (e.g., [11, 26, 27, 64, 66])) and in some cases on their mechanism (e.g., on the rate determination step [26, 27, 31, 62, 63, 94,

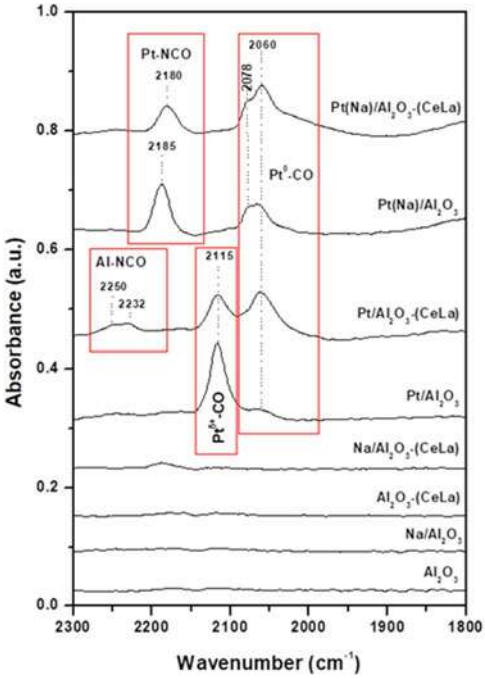

Fig. 5.22 In situ DRIFT spectra during simulated TWC reaction conditions (1000 ppm NO + 1067 ppm C_3H_6 + 7000 ppm CO + 7800 ppm O_2; $F_t = 80$ cm^3/min; $T = 200$ °C). (Reproduced with permission from Ref. [94]. Copyright 2008, Elsevier)

102]), which resulted in dramatic changes on the catalytic system intrinsic activity and/or selectivity. The individual characteristics of the promotion are subjected to both the catalytic system under consideration (active metal, promoter nature and loading, reactants) and the reaction conditions imposed. These issues were considered in the vast majority of alkaline-promoted emission control catalysis reaction studies to explain the promotion phenomena observed.

Below, the Pt-catalyzed NO + C_3H_6 reaction has been selected as a representative one to decipher the mode of action of alkalis in promoting catalytic systems associated with emission control reactions. It is recalled that rate enhancement ratios as high as $\rho \sim 400$ (40,000% rate increases, Fig. 5.15) were achieved by alkaline promotion on this system accompanied by large increases on its selectivity toward N_2, as well [62–65].

First, it is well established that NO + C_3H_6 reaction over Pt obeys Langmuir–Hinshelwood-type kinetics with characteristic rate maxima reflecting competitive adsorption of the two NO and C_3H_6 reactants on Pt active sites (Fig. 5.23) [31]. On the unpromoted Pt, these rate maxima occurred at very low C_3H_6/NO ratios (<0.08), that is, very high NO concentrations relative to C_3H_6 are necessary in order to achieve a comparable coverage of both reactants on the Pt surface, thus maximizing the rate [31, 64], reflecting a weaker adsorption of NO on Pt sites relative to C_3H_6 [31, 64, 69, 70] mainly due to the presence of π-electrons in the alkene structure. As a consequence, in a wide range of reactants' partial pressure and temperature conditions, the unpromoted (alkali-free) Pt surface is predominantly covered by propene

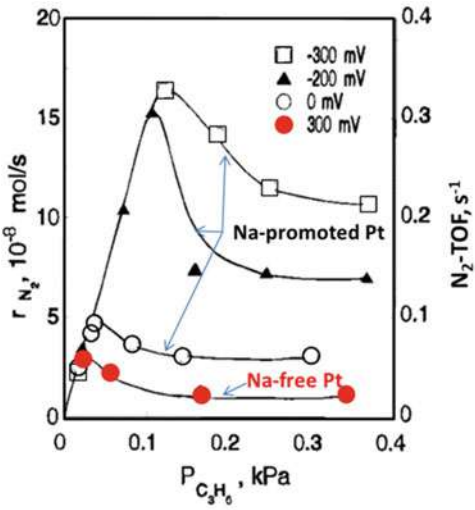

Fig. 5.23 NO + C_3H_6 reaction over Pt. Dependence of N_2 formation rate on propene partial pressure (P_{C3H6}) at constant P_{NO} = 1.4 kPa and T = 375 °C and at different catalyst potentials V_{WR} (i.e., alkaline (Na)-EPOC conditions via a Pt/(Na)β'' Al_2O_3/Au galvanic cell). V_{WR} = 300 mV corresponds to Na-free unpromoted Pt. Results depict a typical LH-type kinetics of the reaction. (Reproduced with permission from Ref. [31]. Copyright 1997, ACS)

and propene-derived fragments, as schematically shown in Fig. 5.24a, resulting in a quite low unpromoted reaction rate, r_o (Figs. 5.23 and 5.24a).

Addition of Na, which is accompanied by the formation of the [$Na^{\delta+}$, δ^-] effective double layer, with the metal side δ^- charge to provide an electron-enriched (lower work function) Pt surface that in effect favors the adsorption of electrophilic co-adsorbates (NO and its fragments) and inhibits that of electrophobic co-adsorbates (C_3H_6 and its fragments), as shown in the following reaction scheme:

$$NO(g) \rightarrow NO_{ads} \quad \text{(enhanced by Na addition)} \tag{5.11}$$

$$NO_{ads} \rightarrow N_{ads} + O_{ads} \quad \text{(enhanced by Na addition)} \tag{5.12}$$

$$C_3H_6(g) \rightarrow C_3H_{6,ads} \quad \text{(inhibited by Na addition)} \tag{5.13}$$

$$N_{ads} + N_{ads} \rightarrow N_2(g) \quad \text{(enhanced by Na addition)} \tag{5.14}$$

$$N_{ads} + NO_{ads} \rightarrow N_2O(g) \quad \text{(inhibited by Na addition)} \tag{5.15}$$

$$O_{ads} + H/C \text{ species} \rightarrow CO_2(g) + H_2O(g) \quad \text{(enhanced by Na addition)} \tag{5.16}$$

The resulted effects are schematically depicted in Fig. 5.24b and are:

(i) Strengthening of the Pt–NO bond with a concomitant enhancement population of NO molecules on the Na-modified Pt surface (5.11) – the relative surface populations of NO and propene are optimized.

(ii) Strong enhancement of the dissociative adsorption of NO (5.12) as a result of the Pt–NO bond strengthening and the concomitant weakening of the N–O bond in the adsorbed NO molecules – the surface is enriched with very active atomic oxygen species (Fig. 5.24b).

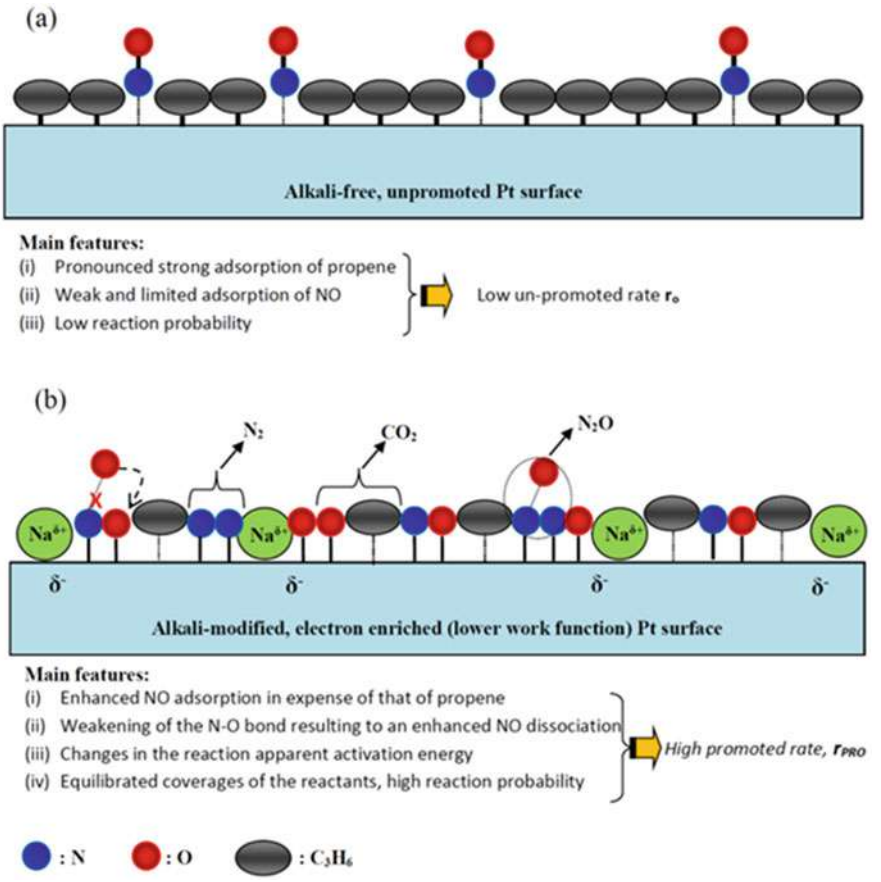

Fig. 5.24 Schematic of the mechanism of action of Na as promoter on the Pt-catalyzed NO + C_3H_6 reaction. Expected distribution of reactants and/or intermediates over the unpromoted surface (**a**) and the Na-promoted surface (**b**). (Reused from Ref. [2] open access under a CC BY 4.0 license (https://creativecommons.org/licenses/by/4.0/))

(iii) Weakening of the strength of the Pt–C_3H_6 bond – an equilibrated population of more active (due to their weaker adsorption) hydrocarbonaceous species is resulted (5.13, Fig. 5.24b).

All these factors operate together in increasing the reaction probability of NO and propene, leading to extraordinarily high rate enhancement ratios $\rho = r_p/r_o$ (ca. 420 for N_2 production) as achieved experimentally through both the EPOC method and the CPC method [31, 62–65]. Notably, these gains in catalytic activity did not reflect the maximum of the LH rate curve of the unpromoted Pt (Fig. 5.23), that is, were not restricted by the optimal balance of the competitive reactants' coverages, but extraordinarily larger due to the synergy of the aforementioned factors.

The resulted increase in N_2 selectivity can also be rationalized in similar terms. According to the reaction network 5.10, 5.11, 5.12, 5.13, 5.14, 5.15 and 5.16, the production rates of N_2 and N_2O depend on the extent of NO dissociation (5.12), which is followed by the elementary reactions 5.14 and 5.15. The observed increase in the N_2 selectivity upon Na addition is a consequence of increased NO dissociation, that is, less molecular NO and more atomic N on the surface. According to Lang et al. [101], the electrostatic field produced by Na^+ can shift the $\pi*$ orbital energy of NO adsorbed in the vicinity of an alkali ion below the Pt Fermi level. Then, valence electrons from the metal can populate the NO $\pi*$ orbital energy, resulting in weakening of the N–O bond and a strengthening of the Pt–N bond. Both factors favor reaction R.17 over reaction R.18, leading to higher N_2 selectivity.

Finally, a brief overview of alkaline promotion in the main reaction/catalyst systems implicated in emission control catalysis is as follows:

(i) *CO oxidation* (*by* O_2) (e.g., [11, 16]): Strong promotion observed only under CO-rich conditions. It is understandable in terms of a pronounced strengthening of O adsorption, compared to that of CO (both reactants are electrophilic adsorbates) at conditions (CO-rich) where CO coverage predominates, and formation of CO islands suppresses reaction probability. The alkali causes destruction of CO islands by increasing the population of O species on the surface.

(ii) *Alkene oxidation* (*by* O_2) and *NO reduction (by alkenes)* (e.g., [18–23, 57, 62–66, 97]): Alkenes are characterized by their strong propensity to adsorb on platinum-group metals. As electrophobic adsorbates, their adsorption is restricted on electron-enriched (lower work function) surfaces resulting from alkaline promotion, while at the same time, the adsorption of the electrophilic adsorbates limiting on the surface reactant O or NO is enhanced leading to a more ideal distribution and bond strength of the reactants on the catalyst surface; both factors enhance reaction probability. Note that, in the case of NO, its alkali-promoted dissociation plays an additional important role.

(iii) *Alkane oxidation* (*by* O_2) (e.g., [24, 25]): In opposite to alkenes, alkanes (in particular CH_4) have very low propensity for adsorption (activation) on platinum-group metal surfaces [70]. Their adsorption becomes even worse on alkali-modified electron-enriched surfaces, a factor that causes inhibition (O-poisoning) of the reaction [24, 25].

(iv) *NO reduction (by alkenes)* (e.g., [57, 59, 62–67, 97]): Similar to case (ii), and further considering that the alkaline-promoted dissociation of adsorbed NO molecules plays an additional important role in the ultimately unprecedented enhancement in rate and N_2 selectivity found in this reaction system. After that, the adsorbed O species derived from the

(continued)

NO dissociation behaves identically to those derived from the adsorption of O_2.

(v) *NO reduction* (*by alkanes*) [68, 69, 97]: Similar considerations to case (iii). The enhanced adsorption/dissociation of NO molecules at the expense of the already weak adsorption of alkanes causes O-poisoning of the system (O species come from NO dissociation).

(vi) *NO reduction* (*by CO*) (e.g., [26–29, 58–61]): Significant alkaline promotion was achieved in this reaction system, as in case (iv). The comparatively stronger enhancement of NO adsorption (→dissociation) than that of the competitive reactant CO was considered to be the main factor that causes promotion.

(vii) *N_2O decomposition and reduction* (e.g., [41, 42, 79–85]): Promotional effects found were attributed to an alkaline-induced enhancement in N_2O adsorption and concomitant dissociation. However, the effects (promoting or poisoning and their intensity) were found to be very sensitive to other molecules, e.g., O_2, H_2O, CO, or H/Cs, co-existing in the reaction mixture.

In addition, the active metal and promoter nature and the loading of the latter are key factors on the degree of promotion achieved; the following issues are highlighted:

(i) *The nature of the metal on the promotional characteristics*: Focusing on the reactions that were found to be more susceptible in alkali promotion, i.e., NO reduction by alkenes, the following increasing order of the intensity of promotion can be observed regarding the active metal used, Ir ~ Rh < Pd < Pt, that is, marginal alkali-induced promotion over Rh or Ir [32, 33, 40, 67], large on Pd [59, 66], and unprecedented on Pt (e.g., [31, 62–65, 97]). This is related to the different adsorption propensity of NO on these metals: NO has high adsorption propensity on Ir and Rh, which is extendedly dissociative; on Pd, it is less and partially dissociative, while on Pt, it is even less and non-dissociative. Therefore, enhancing NO adsorption by alkali promotion on Ir and Rh surfaces has no further practical value (NO adsorption/dissociation is close to ideal on the unpromoted Ir and Rh catalysts), while on Pt, the non-dissociative and quite limited NO adsorption can become much stronger and fully dissociative, enabling Pt to behave like Rh or Ir (e.g., [57, 62, 63, 86]).

(ii) *Optimal alkali promoter loading in relation to the active metal used*: Comparing the amount of alkali required to optimize the promotion for a certain reaction on the various Pt-group metals, the following general trend merges: only a small alkali loading is required in the case of Rh and Ir (ca. θ_{Alkali}~1–3%), higher for Pd (θ_{Alkali}~5–10%), and much higher for Pt (θ_{Alkali}~15–40%) (e.g., [18, 26, 27, 30, 31, 62, 63]). This is readily understood using similar considerations as above: Rh and Ir electron

(continued)

availability (work function) is by its own close to the optimal value for the reactions under consideration, and only a small amount of alkali is necessary to reach the optimal work function value. The opposite is true for Pd and in particular for Pt; these two metals show a higher work function (5.55 and 5.67 eV, respectively) than Rh and Ir (4.98 and 5.27, respectively).

(iii) *Optimal alkali promoter loading in relation to alkali nature*: For a certain catalytic systems and operating conditions, the amount of alkali that is needed to optimize promotion depends on the chemical identity of the alkali: heavier alkalis appear to be more effective than the lighter ones (e.g., [63]). This is fully consistent to the EPOC theory, i.e., the effective double layer approach considered, and to the theoretical predictions of Lang et al. [101], who have shown that the larger the alkali cation, the greater the effect its electric field has on an electron acceptor adsorbate (e.g., NO).

(iv) *Alkaline promotion of complex reaction systems*: In such cases, e.g., simulated automotive exhaust gas mixtures, the decipherment of promotional phenomena is usually more complex and should consider all possible influences, synergistic or competitive, caused by the modified work function of the metal on all electrophilic and/or electrophobic reactant species and intermediates on such a densely populated surface with all these competing adsorbed species (e.g., [57, 78, 86, 97]).

(v) *The stability of alkali promotion*: It is of particular practical significance the fact that alkalis and alkaline earths are typically permanent promoters due to the fact that they do not participate in the reaction networks. Therefore, since the optimal alkali load is incorporated on the catalyst, regardless of the method employed (EPOC or CPC), its amount remains practically constant for a very long time offering promotion. This explains the high values of Faradaic efficiency (ca. $\Lambda \sim 10^3$–10^5) typically achieved in alkaline-EPOC studies (e.g., [11, 14, 18, 26, 27]).

(vi) *The volcano-type feature of alkaline promotion*: As we have seen, a common feature of the resulted alkaline promotion in the vast majority of the catalytic systems studied is the volcano-type behavior of its intensity versus promoter loading, that is, outgoing of the optimal amount of the promoter (the so-called over-promotion), the reaction is gradually inhibited following negative *PI* values (e.g., [11, 26, 27, 31, 57, 62, 63]). This phenomenon was attributed to two main factors: (i) overstrengthening of the adsorption bond of the electrophilic adsorbate (electronic effect) and (ii) formation of extended 2D and 3D surface complexes of the alkali promoter with the reactant species and/or reaction intermediates (e.g., alkali nitrites/nitrates, carbonates, oxides, and superoxides, depending on the reaction atmosphere) that can block

(continued)

active sites (geometric effect). These two factors can operate together, suppressing reaction rates in the case of over-promoted catalysts. Noteworthy, formation of such 2D or 3D surface alkali complex species can be valid even at low promoter loadings (promoting region), without actually cancelling the promoting role of the alkali (e.g., [20–24, 28–33]). On the opposite, and for the benefit of maintaining the promotion at elevated temperatures of catalytic interest, such surface alkali complexes are thermally stable species, thus overcoming the inherent disadvantage of alkali metals, which is their high volatility when alone.

5.5 Conclusions and Perspectives

In this chapter, the applicability and effectiveness of the use of the advanced alkaline-EPOC in dealing with performance problems (in activity, selectivity, stability, and recycling) of catalytic systems focusing on emission control of automotive and stationary combustion processes have been reviewed, classified, and analyzed.

As an in situ, reversible, and well-controlled method of promotion, EPOC offered various ways for an in-depth understanding of the phenomena and key factors governing alkaline promotion of emission control reactions. Moreover, due to the advantageous characteristic of the alkalis to serve as permanent promoters (not participating on side *sacrificial* reactions), the alkaline-EPOC was successfully used as an effective research tool (probe) for exploring the effect of an alkali in a wide range of conditions on the catalytic system under consideration, thus allowing the transfer of the obtained insight to the design of optimally promoted conventional catalyst formulation (i.e., realistic alkaline-CPC systems). Although the resulting promotion by the two systems (alkaline-EPOC and alkaline-CPC) was qualitatively similar, in reality, the results achieved by alkaline-CPC systems were always more spectacular than that of corresponding alkaline-EPOC, apparently due to the more favorable and efficient alkali-to-metal interactions in case of nano-dispersed metal particles that appear in supported-type conventional catalysts.

Most contributions to the topic, in both the above directions (alkaline-EPOC and alkaline-CPC), came from the research teams of Vayenas in Patras, Greece; Yentekakis in Chania, Greece; Lambert in Cambridge, United Kingdom; Vernoux in Lyon, France; and Valverde and de Lucas-Consuegra in Castilla-La Mancha, Spain, who worked independently or in collaboration, as well as from some other groups around the world.

Specifically, they have demonstrated that the vast majority of the catalytic reaction systems associated with the abatement of the main pollutants of combustion processes, i.e., CO and hydrocarbon oxidation and NO_x and N_2O reduction, are

subjected to remarkable activity and selectivity improvements by alkaline-EPOC and corresponding alkaline-CPC. The only exception is the oxidation of light alkanes by dioxygen or NO, for which alkalis serve as reaction inhibitors.

It is not unrealistic to say that the above efforts have already resulted in the design of novel, optimally promoted (with alkalis) three-way catalytic converters for the control of stoichiometric gasoline engine emissions that overcome all the basic problems of the commercial bi- and tri-metallic TWCs emerged during their long-term use. These new alkali-promoted TWCs are cost-effective and easily recyclable due to their low noble metal loading and simple monometallic (e.g., Pt-only, no Rh use) composition, highly stable even in extremely high temperature conditions, extremely effective for simultaneous removal of the three main automotive exhaust pollutants, and highly selective (~100%) toward N_2 instead of N_2O.

In lean (oxygen excess) deNO_x catalytic systems, aimed at controlling emissions from lean-burn and diesel engines and stationary combustion processes, alkaline promotion is also effective in improving both activity and selectivity, but we are rather far from the point to claim that a fully suitable to use alkali-promoted catalytic system has been designed. In this case, a synergy of engineering and alkaline promotion strategies could provide acceptable solutions. To this end, for example, the coupling of alkaline-EPOC and *NO_x storage/reduction (NSR)* technology, as proposed by the Spanish team, seems to be a promising approach as it will be discussed in Chap. 9.

We can also conclude that (i) a high level of knowledge has already been gained on the mechanism of action of alkaline promoters in emission control catalysis systems, (ii) optimally designed systems in this light can be implemented immediately, (iii) the subject has still many rough open fields for research, and (iv) similar considerations and transfer of the knowledge gained in the field could be directly useful for the design of materials and systems related to energy processes (e.g., CO_2 hydrogenation toward renewable fuels, dry reforming of natural gas and biogas toward syngas production, etc.).

References

1. Yentekakis IV, Dong F (2020) Grand challenges for catalytic remediation in environmental and energy applications toward a cleaner and sustainable future. Front Environ Chem 1:5. https://doi.org/10.3389/fenvc.2020.00005
2. Yentekakis IV, Vernoux P, Goula G, Caravaca A (2019) Electropositive promotion by alkalis or alkaline earths of Pt-group metals in emissions control catalysis: a status report. Catalysts 9: 157. https://doi.org/10.3390/catal9020157
3. Yentekakis IV, Konsolakis M (2016) Three-way catalysis. In: Perovskites and related mixed oxides: concepts and applications. Wiley-VCH, Vergal GmbH & Co. KGaA, Weinheim, pp 559–586. https://onlinelibrary.wiley.com/doi/pdf/10.1002/9783527686605.ch25
4. Stoukides M, Vayenas CG (1981) The effect of electrochemical oxygen pumping on the rate and selectivity of ethylene oxidation on polycrystalline silver. J Catal 70:137–146. https://doi.org/10.1016/0021-9517(81)90323-7

5. Yentekakis IV, Vayenas CG (1988) The effect of electrochemical oxygen pumping on the steady-state and oscillatory behaviour of CO oxidation on polycrystalline Pt. J Catal 111:170–188. https://doi.org/10.1016/0021-9517(88)90075-9
6. Vayenas CG, Bebelis S, Neophytides S (1988) Non-faradaic electrochemical modification of catalytic activity. J Phys Chem 92:5083–5085. https://doi.org/10.1021/j100329a007
7. Vayenas CG, Bebelis S, Yentekakis IV, Lintz H-G (1992) Non-faradaic electrochemical modification of catalytic activity: a status report. Catal Today 11:303–442. https://doi.org/10.1016/0920-5861(92)80002-5
8. Vayenas CG (2013) Promotion, electrochemical promotion and metal–support interactions: their common features. Catal Lett 143:1085–1097. https://doi.org/10.1007/s10562-013-1128-x
9. Vayenas CG, Brosda S, Pliangos C (2001) Rules and mathematical modeling of electrochemical and chemical promotion: 1. Reaction classification and promotional rules. J Catal 203:329–350. https://doi.org/10.1006/jcat.2001.3348
10. Vayenas CG, Brosda S, Pliangos C (2003) The double-layer approach to promotion, electrocatalysis, electrochemical promotion, and metal–support interactions. J Catal 216:487–504. https://doi.org/10.1016/S0021-9517(02)00127-6
11. Yentekakis IV, Moggridge G, Vayenas CG, Lambert RM (1994) In situ controlled promotion of catalyst surfaces via NEMCA: the effect of Na on the Pt-catalysed CO oxidation. J Catal 146:292–305. https://doi.org/10.1016/0021-9517(94)90033-7
12. Vayenas CG, Bebelis S, Ladas S (1990) Dependence of catalytic rates on catalyst work function. Nature 343:625–627. https://doi.org/10.1038/343625a0
13. Marina OA, Yentekakis IV, Vayenas CG, Palermo A, Lambert RM (1997) In situ controlled promotion of catalyst surfaces via NEMCA: the effect of Na on the Pt-catalysed NO reduction by H_2. J Catal 166:218–228. https://doi.org/10.1006/jcat.1997.1551
14. Vayenas CG, Bebelis S, Despotopoulou M (1991) Non-faradaic electrochemical modification of catalytic activity: 4. The use of β''-Al_2O_3 as the solid electrolyte. J Catal 128:415–435. https://doi.org/10.1016/0021-9517(91)90300-S
15. Díez-Ramírez J, Kyriakou V, Garagounis I, Vourros A, Vasileiou E, Sánchez P, Dorado F, Stoukides M (2017) Enhancement of ammonia synthesis on a Co_3Mo_3N-Ag electrocatalyst in a K-βAl_2O_3 solid electrolyte cell. ACS Sustain Chem Eng 5:8844–8851. https://doi.org/10.1021/acssuschemeng.7b01618
16. de Lucas-Consuegra A, Dorado F, Valverde JL, Karoum R, Vernoux P (2008) Electrochemical activation of Pt catalyst by potassium for low temperature CO deep oxidation. Catal Commun 9:17–20. https://doi.org/10.1016/j.catcom.2007.04.038
17. de Lucas-Consuegra A, Princivalle A, Caravaca A, Dorado F, Guizard C, Valverde JL, Vernoux P (2010) Preferential CO oxidation in hydrogen-rich stream over an electrochemically promoted Pt catalyst. Appl Catal B 94:281–287. https://doi.org/10.1016/j.apcatb.2009.11.019
18. Harkness IR, Hardacre C, Lambert RM, Yentekakis IV, Vayenas CG (1996) Ethylene oxidation over platinum: *in situ* electrochemically controlled promotion using Na–β'' alumina and studies with a Pt(111)/Na model catalyst. J Catal 160:19–26. https://doi.org/10.1006/jcat.1996.0119
19. Filkin NC, Tikhov MS, Palermo A, Lambert RM (1999) A kinetic and spectroscopic study of the in situ electrochemical promotion by sodium of the platinum-catalysed combustion of propene. J Phys Chem A 103:2680–2687. https://doi.org/10.1021/jp984186o
20. Vernoux P, Gaillard F, Lopez C, Siebert E (2004) In-situ electrochemical control of the catalytic activity of platinum for the propene oxidation. Solid State Ionics 175:609–613. https://doi.org/10.1016/j.ssi.2004.01.075
21. Billard A, Vernoux P (2007) Electrochemical catalysts for hydrocarbon combustion. Top Catal 44:369–377. https://doi.org/10.1007/s11244-006-0129-z
22. de Lucas-Consuegra A, Dorado F, Valverde JL, Karoum R, Vernoux P (2007) Low-temperature propene combustion over Pt/K-βAl_2O_3 electrochemical catalyst:

characterization, catalytic activity measurements and investigation of the NEMCA effect. J Catal 251:474–484. https://doi.org/10.1016/j.jcat.2007.06.031
23. de Lucas-Consuegra A, Dorado F, Jimenez-Borja C, Caravaca A, Vernoux P, Valverde JL (2009) Use of potassium conductors in the electrochemical promotion of environmental catalysis. Catal Today 146:293–298. https://doi.org/10.1016/j.cattod.2009.04.009
24. Kotsionopoulos N, Bebelis S (2007) *In situ* electrochemical modification of catalytic activity for propane combustion of Pt/β''-Al_2O_3 catalyst-electrodes. Top Catal 44:379–389. https://doi.org/10.1007/s11244-006-0130-6
25. Kotsionopoulos N, Bebelis S (2010) Electrochemical characterization of the Pt/β''-Al_2O_3 system under conditions of in situ electrochemical modification of catalytic activity for propane combustion. J Appl Electrochem 40:1883–1891. https://doi.org/10.1007/s10800-010-0158-y
26. Palermo A, Lambert RM, Harkness IR, Yentekakis IV, Marina OA, Vayenas CG (1996) Electrochemical promotion by Na of the platinum-catalysed reaction between CO and NO. J Catal 161:471–479. https://doi.org/10.1006/jcat.1996.0206
27. Palermo A, Tikhov MS, Filkin NC, Lambert RM, Yentekakis IV, Vayenas CG (1996) Electrochemical promotion of NO reduction by CO and by propene. Stud Surf Sci Catal 101:513–522. https://doi.org/10.1016/S0167-2991(96)80262-X
28. Williams FJ, Palermo A, Tikhov MS, Lambert RM (2000) Electrochemical promotion by sodium of the rhodium-catalysed NO + CO reaction. J Phys Chem B 104:11883–11890. https://doi.org/10.1021/jp001689x
29. Williams FJ, Palermo A, Tikhov MS, Lambert RM (2001) Mechanism of alkali promotion in heterogeneous catalysis under realistic conditions: application of electron spectroscopy and electrochemical promotion to the reduction of NO by CO and by propene over rhodium. Surf Sci 482–485:177–182. https://doi.org/10.1016/S0039-6028(00)01040-2
30. Harkness IR, Lambert RM (1995) Electrochemical promotion of the NO + ethylene reaction over platinum. J Catal 152:211–214. https://doi.org/10.1006/jcat.1995.1075
31. Yentekakis IV, Palermo A, Filkin N, Tikhov MS, Lambert RM (1997) *In situ* electrochemical promotion by sodium of the platinum-catalysed reduction of NO by propene. J Phys Chem B 101:3759–3768. https://doi.org/10.1021/jp963052c
32. Williams FJ, Palermo A, Tikhov MS, Lambert RM (2001) Electrochemical promotion by sodium of the rhodium-catalysed reduction of NO by propene: kinetics and spectroscopy. J Phys Chem B 105:1381–1388. https://doi.org/10.1021/jp003269d
33. Williams FJ, Tikhov MS, Palermo A, Macleod N, Lambert RM (2001) Electrochemical promotion of rhodium-catalysed NO reduction by CO and by propene in the presence of oxygen. J Phys Chem B 105:2800–2808. https://doi.org/10.1021/jp004131y
34. Vernoux P, Gaillard F, Lopez C, Siebert E (2003) Coupling catalysis to electrochemistry: a solution to selective reduction of nitrogen oxides in lean-burn engine exhausts? J Catal 217: 203–208. https://doi.org/10.1016/S0021-9517(03)00052-6
35. Dorado F, de Lucas-Consuegra A, Jimenez C, Valverde JL (2007) Influence of the reaction temperature on the electrochemical promoted catalytic behaviour of platinum impregnated catalysts for the reduction of nitrogen oxides under lean burn conditions. Appl Catal A 321: 86–92. https://doi.org/10.1016/j.apcata.2007.01.035
36. Dorado F, de Lucas-Consuegra A, Vernoux P, Valverde JL (2007) Electrochemical promotion of platinum impregnated catalyst for the selective catalytic reduction of NO by propene in presence of oxygen. Appl Catal B 73:42–50. https://doi.org/10.1016/j.apcatb.2006.12.001
37. de Lucas-Consuegra A, Caravaca A, Dorado F, Valverde JL (2009) Pt/K–βAl_2O_3 solid electrolyte cell as a "smart electrochemical catalyst" for the effective removal of NO_x under wet reaction conditions. Catal Today 146:330–335. https://doi.org/10.1016/j.cattod.2009.02.043
38. de Lucas-Consuegra A, Caravaca A, Sanchez P, Dorado F, Valverde JL (2008) A new improvement of catalysis by solid-state electrochemistry: an electrochemically assisted NO_x storage/reduction catalyst. J Catal 259:54–65. https://doi.org/10.1016/j.jcat.2008.07.008

39. de Lucas-Consuegra A, Caravaca A, Martin de Vidales MJ, Dorado F, Balomenou S, Tsiplakides D, Vernoux P, Valverde JL (2009) An electrochemically assisted NO_x storage/reduction catalyst operating under fixed lean burn conditions. Catal Commun 11:247–251. https://doi.org/10.1016/j.catcom.2009.10.004
40. Goula G, Katzourakis P, Vakakis N, Papadam T, Konsolakis M, Tikhov M, Yentekakis IV (2007) The effect of potassium on the Ir/C_3H_6+NO+O_2 catalytic system. Catal Today 127: 199–206. https://doi.org/10.1016/j.cattod.2007.03.008
41. de Lucas-Consuegra A, Dorado F, Jimenez-Borja C, Valverde JL (2008) Influence of the reaction conditions on the electrochemical promotion by potassium for the selective catalytic reduction of N_2O by C_3H_6 on platinum. Appl Catal B 78:222–231. https://doi.org/10.1016/j.apcatb.2007.09.027
42. de Lucas-Consuegra A, Dorado F, Jimenez-Borja C, Valverde JL (2008) Electrochemical promotion of Pt impregnated catalyst for the treatment of automotive exhaust emissions. J Appl Electrochem 38:1151–1157. https://doi.org/10.1007/s10800-008-9559-6
43. Konsolakis M, Palermo A, Tikhov MS, Lambert RM, Yentekakis IV (1998) Electrochemical vs. conventional promotion: a new tool to design effective, highly dispersed conventional catalysts. Ionics 4:148–156. https://doi.org/10.1007/BF02375793
44. Yentekakis IV, Konsolakis M, Lambert RM, Palermo A, Tikhov M (2000) Successful application of electrochemical promotion to the design of effective conventional catalyst formulations. Solid State Ionics 136(137):783–790. https://doi.org/10.1016/S0167-2738(00)00547-6
45. Mirkelamoglu B, Karakas G (2005) CO oxidation over palladium- and sodium-promoted tin dioxide: catalyst characterization and temperature-programmed studies. Appl Catal A 281: 275–284. https://doi.org/10.1016/j.apcata.2004.11.036
46. Mirkelamoglu B, Karakas G (2006) The role of alkali-metal promotion on CO oxidation over PdO/SnO_2 catalysts. Appl Catal A 299:84–94. https://doi.org/10.1016/j.apcata.2005.10.003
47. Tanikawa K, Egawa C (2011) Effect of barium addition on CO oxidation activity of palladium catalysts. Appl Catal A 403:12–17. https://doi.org/10.1016/j.apcata.2011.06.007
48. Minemura Y, Kuriyama M, Ito S, Tomishige K, Kunimori K (2006) Additive effect of alkali metal ions on preferential CO oxidation over Pt/Al_2O_3. Catal Commun 7:623–626. https://doi.org/10.1016/j.catcom.2006.01.028
49. Minemura Y, Ito S, Miyao T, Naito S, Tomishige K, Kunimori K (2005) Preferential CO oxidation promoted by the presence of H_2 over K–Pt/Al_2O_3. Chem Commun 11:1429–1431. https://doi.org/10.1039/B416565A
50. Tanaka H, Kuriyama M, Ishida Y, Ito S, Tomishige K, Kunimori K (2008) Preferential CO oxidation in hydrogen-rich stream over Pt catalysts modified with alkali metals: Part I. Catalytic performance. Appl Catal A 343:117–124. https://doi.org/10.1016/j.apcata.2008.03.030
51. Kuriyama M, Tanaka H, Ito S, Kubota T, Miyao T, Naito S, Timoshige K, Kunimori K (2007) Promoting mechanism of potassium in preferential CO oxidation on Pt/Al_2O_3. J Catal 252:39–48. https://doi.org/10.1016/j.jcat.2007.09.001
52. Tanaka H, Kuriyama M, Ishida Y, Ito S, Kubota T, Miyao T, Naito S, Tomishige K, Kunimori K (2008) Preferential CO oxidation in hydrogen-rich stream over Pt catalysts modified with alkali metals: Part II. Catalyst characterization and role of alkali metals. Appl Catal A 343: 125–133. https://doi.org/10.1016/j.apcata.2008.03.029
53. Pedrero C, Waku T, Iglesia E (2005) Oxidation of CO in H_2–CO mixtures catalysed by platinum: alkali effects on rates and selectivity. J Catal 233:242–255. https://doi.org/10.1016/j.jcat.2005.04.005
54. Kwak C, Park TJ, Suh DJ (2005) Effects of sodium addition on the performance of PtCo/Al_2O_3 catalysts for preferential oxidation of carbon monoxide from hydrogen-rich fuels. Appl Catal A 278:181–186. https://doi.org/10.1016/j.apcata.2004.05.025

55. Cho SH, Park JS, Choi SH, Kim SH (2006) Effect of magnesium on preferential oxidation of carbon monoxide on platinum catalyst in hydrogen-rich stream. J Power Sources 156:260–266. https://doi.org/10.1016/j.jpowsour.2005.06.019
56. Liu K, Wang A, Zhang T (2012) Recent advances in preferential oxidation of CO reaction over platinum group metal catalysts. ACS Catal 2:1165–1178. https://doi.org/10.1021/cs200418w
57. Yentekakis IV, Tellou V, Botzolaki G, Rapakousios IA (2005) A comparative study of the C_3H_6 + NO + O_2, C_3H_6 + O_2 and NO + O_2 reactions in excess oxygen over Na-modified Pt/γ-Al_2O_3 catalysts. Appl Catal B 56:29–239. https://doi.org/10.1016/j.apcatb.2004.08.017
58. Konsolakis M, Yentekakis IV, Palermo A, Lambert RM (2001) Optimal promotion by rubidium of the CO + NO reaction over Pt/γ-Al_2O_3 catalysts. Appl Catal B 33:293–302. https://doi.org/10.1016/S0926-3373(01)00183-7
59. Konsolakis M, Yentekakis IV (2007) NO reduction by propene or CO over alkali-promoted Pd/YSZ catalysts. J Hazard Mater 149:619–624. https://doi.org/10.1016/j.jhazmat.2007.06.085
60. Tanikawa K, Egawa C (2011) Effect of barium addition over palladium catalyst for CO–NO–O_2 reaction. J Mol Catal A 349:94–99. https://doi.org/10.1016/j.molcata.2011.08.025
61. Lepage M, Visser T, Soulimani F, Inglesias-Juez A, Weckhuysen BM (2010) Promotion effects in the reduction of NO by CO over zeolite-supported Rh catalysts. J Phys Chem C 114:2282–2292. https://doi.org/10.1021/jp910371j
62. Yentekakis IV, Konsolakis M, Lambert RM, Macleod N, Nalbantian L (1999) Extraordinarily effective promotion by sodium in emission control catalysis: NO reduction by propene over Na-promoted Pt/γ-Al_2O_3. Appl Catal B 22:123–133. https://doi.org/10.1016/S0926-3373(99)00042-9
63. Konsolakis M, Yentekakis IV (2001) Strong promotional effects of Li, K, Rb and Cs on the Pt-catalysed reduction of NO by propene. Appl Catal B 29:103–113. https://doi.org/10.1016/S0926-3373(00)00195-8
64. Konsolakis M, Yentekakis IV (2001) The reduction of NO by propene over Ba-promoted Pt/γ-Al_2O_3 catalysts. J Catal 198:142–150. https://doi.org/10.1006/jcat.2000.3123
65. Yentekakis IV, Lambert RM, Konsolakis M, Kallithrakas-Kontos N (2002) On the effects of residual chloride and of barium promotion on Pt/-Al_2O_3 catalysts in the reduction of NO by propene. Catal Lett 81:181–185. https://doi.org/10.1023/A:1016520921545
66. Yentekakis IV, Lambert RM, Tikhov M, Konsolakis M, Kiousis V (1998) Promotion by sodium in emission control catalysis: a kinetic and spectroscopic study of the Pd-catalysed reduction of NO by propene. J Catal 176:82–92. https://doi.org/10.1006/jcat.1998.2041
67. Macleod N, Isaac J, Lambert RM (2000) Sodium promotion of the NO+C_3H_6 reaction over Rh/-Al_2O_3 catalysts. J Catal 193:115–122. https://doi.org/10.1006/jcat.2000.2882
68. Yentekakis IV, Lambert RM, Konsolakis M, Kiousis V (1998) The effect of sodium on the Pd-catalysed reduction of NO by methane. Appl Catal B 18:293–305. https://doi.org/10.1016/S0926-3373(98)00049-6
69. Yentekakis IV, Konsolakis M, Kiousis V, Lambert RM, Tikhov M (1999) Promotion by sodium in emission control catalysis: the difference between alkanes and alkenes in the Pd-catalysed reduction of NO by hydrocarbons. G-NEST Int J 1:121–130
70. Burch R, Watling TC (1997) The difference between alkanes and alkenes in the reduction of NO by hydrocarbons over Pt catalysts under lean-burn conditions. Catal Lett 43:19–23. https://doi.org/10.1023/A:1018974102756
71. Machida M, Ikeda S, Kurogi D, Kijima T (2001) Low temperature catalytic NO_x-H_2 reactions over Pt/TiO_2-ZrO_2 in an excess oxygen. Appl Catal B 35:107–116. https://doi.org/10.1016/S0926-3373(01)00243-0
72. Burch R, Coleman MD (2002) An investigation of promoter effects in the reduction of NO by H_2 under lean-burn conditions. J Catal 208:435–447. https://doi.org/10.1006/jcat.2002.3596
73. Machida M, Watanabe T (2004) Effect of Na-addition on catalytic activity of Pt-ZSM-5 for low-temperature NO–H_2–O_2 reactions. Appl Catal B 52:281–286. https://doi.org/10.1016/j.apcatb.2004.05.001

74. Macleod N, Lambert RM (2002) Lean NO_x reduction with CO + H_2 mixtures over Pt/Al_2O_3 and Pd/Al_2O_3 catalysts. Appl Catal B 35:269–279. https://doi.org/10.1016/S0926-3373(01)00264-8
75. Macleod N, Lambert RM (2002) Low-temperature NO_x reduction with H_2+CO under oxygen-rich conditions over a $Pd/TiO_2/Al_2O_3$ catalyst. Catal Commun 3:61–65. https://doi.org/10.1016/S1566-7367(02)00050-X
76. Macleod N, Lambert RM (2003) In situ ammonia generation as a strategy for catalytic NO_x reduction under oxygen rich conditions. Chem Commun 11:1300–1301. https://doi.org/10.1039/B302959J
77. Macleod N, Lambert RM (2003) An in situ DRIFTS study of efficient lean NOx reduction with H_2 + CO over Pd/Al_2O_3: the key role of transient NCO formation in the subsequent generation of ammonia. Appl Catal B 46:483–495. https://doi.org/10.1016/S0926-3373(03)00289-3
78. Konsolakis M, Vrontaki M, Avgouropoulos G, Ioannides T, Yentekakis IV (2006) Novel doubly-promoted catalysts for the lean NO_x reduction by H_2 + CO: $Pd(K)/Al_2O_3$–(TiO_2). Appl Catal B 68:59–67. https://doi.org/10.1016/j.apcatb.2006.07.011
79. Haber J, Nattich M, Machej T (2008) Alkali-metal promoted rhodium-on-alumina catalysts for nitrous oxide decomposition. Appl Catal B 77:278–283. https://doi.org/10.1016/j.apcatb.2007.07.028
80. Parres-Esclaped S, Lopez-Suerez FE, Bueno-Lopez A, Illan-Gomez MJ, Ura B, Trawcczynski J (2009) $Rh–Sr/Al_2O_3$ catalyst for N_2O decomposition in the presence of O_2. Top Catal 52:1832–1836. https://doi.org/10.1007/s11244-009-9353-7
81. Konsolakis M, Aligizou F, Goula G, Yentekakis IV (2013) N_2O decomposition over doubly-promoted $Pt(K)/Al_2O_3$-(CeO_2-La_2O_3) structured catalysts: on the combined effects of promotion and feed composition. Chem Eng J 230:286–295. https://doi.org/10.1016/j.cej.2013.06.083
82. Papista E, Pachatouridou E, Goula MA, Marnellos GE, Iliopoulou E, Konsolakis M, Yentekakis IV (2016) Effect of alkali promoters (K) on nitrous oxide abatement over Ir/Al2O3 catalysts. Top Catal 59:1020–1027. https://doi.org/10.1007/s11244-016-0584-0
83. Pekridis G, Kaklidis N, Konsolakis M, Iliopoulou EF, Yentekakis IV, Marnellos G (2011) Correlation of surface characteristics with catalytic performance of potassium promoted Pd/Al_2O_3 catalysts: the case of N_2O reduction by alkanes or alkenes. Top Catal 54:1135–1142. https://doi.org/10.1007/s11244-011-9735-5
84. Pekridis G, Kaklidis N, Konsolakis M, Athanasiou C, Yentekakis IV, Marnellos GE (2011) A comparison between electrochemical and conventional catalyst promotion: the case of N_2O reduction by alkanes or alkenes over K-modified Pd catalysts. Solid State Ionics 192:653–658. https://doi.org/10.1016/j.ssi.2010.03.024
85. Goncalves F, Figueiredo JL (2006) Synergistic effect between Pt and K in the catalytic reduction of NO and N_2O. Appl Catal B 62:181–192. https://doi.org/10.1016/j.apcatb.2005.07.005
86. Konsolakis M, Macleod N, Isaac J, Yentekakis IV, Lambert RM (2000) Strong promotion by Na of Pt/γ-Al_2O_3 catalysts operated under simulated exhaust conditions. J Catal 193:330–337. https://doi.org/10.1006/jcat.2000.2888
87. Macleod N, Isaac J, Lambert RM (2001) Sodium promotion of Pd/γ-Al_2O_3 catalysts operated under simulated "three-way" conditions. J Catal 198:128–135. https://doi.org/10.1006/jcat.2000.3113
88. Macleod N, Isaac J, Lambert RM (2001) A comparison of sodium-modified Rh/γ-Al_2O_3 and Pd/γ-Al_2O_3 catalysts operated under simulated TWC conditions. Appl Catal B 33:335–343. https://doi.org/10.1016/S0926-3373(01)00191-6
89. Tanaka T, Yokota K, Isomura N, Doi H, Sugiura M (1998) Effect of the addition of Mo and Na to Pt catalysts on the selective reduction of NO. Appl Catal B 16:199–208. https://doi.org/10.1016/S0926-3373(97)00074-X

90. Shinjoh H, Tanabe T, Sobukawa H, Sugiura M (2001) Effect of Ba addition on catalytic activity of Pt and Rh catalysts loaded on γ-alumina. Top Catal 16(17):95–99. https://doi.org/10.1023/A:1016686932085
91. Kobayashi T, Yamada T, Kayano K (2001) Effect of basic metal additives on NOx reduction property of Pd-based three-way catalyst. Appl Catal B 30:287–292. https://doi.org/10.1016/S0926-3373(00)00240-X
92. Lee CH, Chen YW (1997) Effect of basic additives on Pt/Al_2O_3 for CO and propylene oxidation under oxygen-deficient conditions. Ind Eng Chem Res 36:1498–1506. https://doi.org/10.1021/ie960414u
93. Yentekakis IV, Konsolakis M, Rapakousios IA, Matsouka V (2007) Novel electropositively promoted monometallic (Pt-only) catalytic converters for automotive pollution control. Top Catal 42–43:393–397. https://doi.org/10.1007/s11244-007-0212-0
94. Matsouka V, Konsolakis M, Lambert RM, Yentekakis IV (2008) In situ DRIFTS study of the effect of structure (CeO_2-La_2O_3) and surface (Na) modifiers on the catalytic and surface behaviour of Pt/γ-Al_2O_3 catalyst under simulated exhaust conditions. Appl Catal B 84:715–722. https://doi.org/10.1016/j.apcatb.2008.06.004
95. Matsouka V, Konsolakis M, Yentekakis IV, Papavasiliou A, Tsetsekou A, Boukos N (2011) Thermal aging behavior of Pt-only TWC converters under simulated exhaust conditions: effect of rare earths (CeO_2, La_2O_3) and alkali (Na) modifiers. Top Catal 54:1124–1134. https://doi.org/10.1007/s11244-011-9734-6
96. Papavasiliou A, Tsetsekou A, Matsouka V, Konsolakis M, Yentekakis IV, Boukos N (2011) Synergistic structural and surface promotion of monometallic (Pt) TWCs: effectiveness and thermal aging tolerance. Appl Catal B 106:228–241. https://doi.org/10.1016/j.apcatb.2011.05.030
97. Vernoux P, Leinekugel-Le-Cocq AY, Gaillard F (2003) Effect of the addition of Na on Pt/Al_2O_3 catalysts for the reduction of NO by C_3H_8 and C_3H_6 under lean-burn conditions. J Catal 219:247–257. https://doi.org/10.1016/S0021-9517(03)00200-8
98. Makri M, Vayenas CG, Bebelis S, Besocke KH, Gavalca C (1996) Atomic resolution STM imaging of electrochemically controlled reversible promoter dosing of catalysts. Surf Sci 369:351–359. https://doi.org/10.1016/S0039-6028(96)00911-9
99. Archonta D, Frantzis A, Tsiplakides D, Vayenas CG (2006) STM observation of the origin of electrochemical promotion on metal catalyst-electrodes interfaced with YSZ and β''-Al_2O_3. Solid State Ionics 26–32:2221–2225. https://doi.org/10.1016/j.ssi.2006.02.026
100. Vayenas CG, Brosda S (2014) Electron donation–backdonation and the rules of catalytic promotion. Top Catal 57:1287–1301. https://doi.org/10.1007/s11244-014-0294-4
101. Lang ND, Holloway S, Norskov JK (1985) Electrostatic adsorbate-adsorbate interactions: the poisoning and promotion of the molecular adsorption reaction. Surf Sci 150:24–38. https://doi.org/10.1016/0039-6028(85)90208-0
102. Koukiou S, Konsolakis M, Lambert RM, Yentekakis IV (2007) Spectroscopic evidence for the mode of action of alkali promoters in Pt-catalyzed de-NO_x chemistry. Appl Catal B 76:101–106. https://doi.org/10.1016/j.apcatb.2007.05.014
103. Harkness IR, Lambert RM (1997) Chemisorption and reactivity of nitric oxide on Na-dosed platinum{111}. J Chem Soc Faraday Trans 93:1425–1429. https://doi.org/10.1039/A606375F
104. Garfunkel EL, Maj JJ, Frost JC, Farias MH, Somorjai GA (1983) Interaction of potassium with π-electron orbital containing molecules on platinum(111). J Phys Chem 87:3629–3635. https://doi.org/10.1021/j100242a012
105. Bertolini JC, Derichele P, Massardier J (1985) The influence of potassium and the role of coadsorbed oxygen on the chemisorptive properties of Pt(100). Surf Sci 160:531–541. https://doi.org/10.1016/0039-6028(85)90792-7
106. Pitchon V, Primet M, Praliaud H (1990) Alkali addition to silica-supported palladium: infrared investigation of the carbon monoxide chemisorptions. Appl Catal 62:317–334. https://doi.org/10.1016/S0166-9834(00)82255-1
107. Liotta FL, Martin GA, Deganello G (1996) The influence of alkali metal ions in the chemisorption of CO andCO_2 on supported palladium catalysts: a fourier transform infrared spectroscopic study. J Catal 164:322–333. https://doi.org/10.1006/jcat.1996.0388

Chapter 6
Electrochemical Promotion of Catalysis for CO_2 Valorization

Christos Chatzilias, Eftychia Martino, Dimitrios Zagoraios, Georgios Kyriakou, and Alexandros Katsaounis

Abstract Carbon dioxide management is of foremost importance in terms of climate change mitigation, environmental sustainability, and the production of renewable energy. CO_2 is an important source of carbon which can be converted into useful chemicals and fuels by catalytic processes. In this respect, the catalytic hydrogenation of CO_2, leading to products such as methane, carbon monoxide, or even hydrocarbons and alcohols with more than one carbon atom, is gaining continuous research importance. Such processes are possible with a variety of metal-based catalysts operated under different conditions and catalytic chemical reactor systems. The phenomenon of electrochemical promotion of catalysis (EPOC) is an important tool in the field of catalysis and electrochemistry, through which one can modify and control the catalytic properties of a conductive catalytic film interfaced on an ionic solid electrolyte. This chapter provides an overview of recent EPOC studies of the CO_2 hydrogenation reaction on simple conductive metal films, metal nanoparticles, and supported catalysts (powders) deposited on different solid electrolytes. Furthermore, the use of monolithic scaled-up electropromoted reactors for the CO_2 hydrogenation reaction is presented, as a step towards the development and commercialization of the electrochemical promotion of catalysis.

Keywords CO_2 hydrogenation · RWGS · EPOC · NEMCA · Methanation

C. Chatzilias · E. Martino · D. Zagoraios · G. Kyriakou · A. Katsaounis (✉)
Department of Chemical Engineering, University of Patras, Patras, Greece
e-mail: chatzilias@chemeng.upatras.gr; martino@chemeng.upatras.gr; zagoraios@chemeng.upatras.gr; kyriakg@chemeng.upatras.gr; alex.katsaounis@chemeng.upatras.gr

P. Vernoux, C. G. Vayenas (eds.), *Recent Advances in Electrochemical Promotion of Catalysis*, Modern Aspects of Electrochemistry 61,
https://doi.org/10.1007/978-3-031-13893-5_6

6.1 Introduction

6.1.1 CO_2 Management

The greenhouse effect has become one of the greatest burning issues with environmental, economic, and social impact for the current century. Carbon dioxide (CO_2) levels in the earth's atmosphere have increased dramatically, with the global average being 30% higher than it used to be in the period of the industrial revolution. Specifically, the preindustrial CO_2 concentration levels were approximately 280 ppm, whereas today that the society has become urban, modern, and industrial the concentration reaches almost 410 ppm [1]. This rise inevitably led to unprecedented planet atmospheric temperature increase, intensifying the greenhouse effect more than ever [2].

Many international policies and legislations, such as the Kyoto Protocol, EU Emissions Trading Scheme, Climate Change Act 2008, and the Carbon Plan [3–6], have been adopted in the interest of carbon footprint reduction. During the latest United Nations Climate Change Conference (COP26), the importance of the Paris Agreement was highlighted with very urgent updates. Countries are confronted with ambitious 2030 emission reduction targets that align with reaching a net zero by the middle of the century. To deliver on these stretching targets, countries will need to accelerate the phase-out of coal, curtail deforestation, speed up the switch to electric vehicles, and encourage investment in renewables [7].

Under this framework, the CO_2 Capture and Storage (CCS) is one of the most promising technologies for controlling and reducing CO_2 emissions. Applications that separate CO_2 from large fossil fuel units, including natural gas production and ammonia synthesis industries, are already in operation [8, 9]. The high cost involved in capturing, transporting, and storing CO_2 remains an important barrier that has to be overcome so that CCS becomes the dominant method of CO_2 handling [10–12]. Moreover, the uncertainty of long-term storage capacity of CO_2 together with the dangers associated with leaks during transportation and at the site of underground storage has initiated a major interest in developing alternative CO_2 management methods [13, 14].

In addition to CCS, other alternative processes, like the CO_2 hydrogenation reaction leading to useful fuels and chemicals, are also vital in managing CO_2 [15–20]. CO_2 hydrogenation offers two main advantages: it can stop the galloping CO_2 increase in the atmosphere and at the same time produce fuels such as methane, methanol, ethanol, or even carbon monoxide which can be further hydrogenated to offer higher hydrocarbons.

In the current chapter, the thermodynamic properties, the reaction mechanisms, and the most common catalytic systems used for the CO_2 hydrogenation reaction towards two common products, CO and CH_4, are described in detail. Furthermore, the phenomenon of electrochemical promotion of catalysis (EPOC) is introduced, together with its theoretical background, governing rules, and types of EPOC reactors.

6.1.2 CO_2 Hydrogenation

Carbon dioxide has the potential of becoming an important, economic, safe, and renewable source of carbon for the synthesis of a variety chemicals and fuels [21, 22]. Utilization of CO_2 as raw material not only contributes to the global climate change regulation but also offers a significant challenge in exploring new ideas and opportunities for catalytic and industrial development [23–25]. However, at present, CO_2 is not widely used as a carbon source in industrial applications. Its use is limited to processes concerning urea production and its derivatives such as salicylic acid and carbonates [26]. This is mainly attributed to high CO_2 thermodynamic stability, which practically means high amounts of energy for the electroreduction processes used for CO_2 conversion to useful chemicals [1, 27].

Hydrogen is a high energy content fuel, which can be used to overcome this barrier, as a reactant for the CO_2 conversion. From a mechanistic point of view, there are two competitive routes that occur in the CO_2 hydrogenation reaction, the direct route, which is the modified Fischer-Tropsch mechanism, as well as the indirect route via the methanol-mediated mechanism [28, 29].

6.1.2.1 Thermodynamic Considerations

The heterogeneous Fischer-Tropsch CO_2 hydrogenation (Eq. 6.1) reaction integrates the reduction of CO_2 to CO through the reverse water-gas shift reaction (Eq. 6.2) and to hydrocarbons by the hydrogenation of CO via the Fischer-Tropsch Synthesis (Eq. 6.3). The structure and the composition of the catalyst, the source of hydrogen, as well as the reaction conditions are some of the parameters that play a crucial role in the physical and chemical deactivation [30, 31] of the catalytic system used and consequently to the CO_2 conversion and product distribution. The product variety includes methane, syngas, methanol, ethanol, formic acid, light olefins, liquid fuels, and higher alcohols [31–33] (Fig. 6.1).

$$nCO_2 + (3n+1)H_2 \leftrightarrow C_nH_{2n+2} + 2nH_2O \tag{6.1}$$

$$CO_2 + H_2 \leftrightarrow CO + H_2O \qquad \Delta H^{o}_{r,298K} = 41.5\ \text{kJ/mol} \tag{6.2}$$

$$nCO + (2n+1)H_2 \leftrightarrow C_nH_{2n+2} + nH_2O \tag{6.3}$$

The high global energy demands have turned the interest to renewable energy sources, resulting in many cases of an excess of energy, either due to the high distance between the production site and the distribution grid or to the reduced energy demands at the time of the production. This excess of energy can be wisely used in hydrogen production through the electrolysis process, which can be considered as a renewable storage route and can also be used for the elevated temperatures necessary for the CO_2 hydrogenation process. The utilization of renewable energy either for H_2 production [34] or for the energy demands of the CO_2 hydrogenation, as well as the possible product distribution of this reaction, is shown in Fig. 6.1 [35].

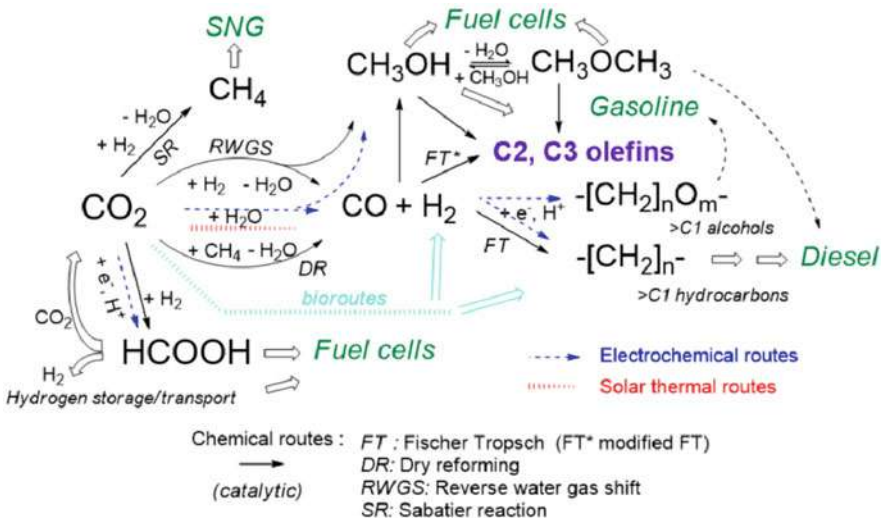

Fig. 6.1 Schematic representation of the CO_2 conversion possible routes integrating renewable energy sources. (Reprinted with permission from [35])

In the first step, prior to any hydrocarbon formation, the RWGS reaction converts CO_2 to CO, by dissociation, leading to adsorbed *CO precursor molecules on the catalyst surface. The RWGS, which is a mildly endothermic reaction, requires high temperatures (higher than 500 °C) to achieve high CO_2 conversions. The RWGS can be considered as a process itself or as an intermediate reaction in other CO_2 conversion processes. A strong example is the CO_2 methanation, which can occur through a consecutive pathway, with the RWGS reaction as the first step. Therefore, substituting $n = 1$ in Eqs. 6.1 and 6.3, the CO_2 and CO methanation reactions appear (Eqs. 6.4 and 6.5, respectively), which were first discovered by Paul Sabatier and Jean-Baptiste Senderens [36]. These two reactions have been studied under various conditions using plenty of catalysts over 100 years [1]. The methanation reaction is favored at low temperatures, due to its exothermic character.

CO_2 methanation reaction

$$CO_2 + 4H_2 \rightarrow CH_4 + 2H_2O \quad \Delta H^{o}_{r,298K} = -165\ \text{kJ/mol} \tag{6.4}$$

CO methanation reaction

$$CO + 3H_2 \rightarrow CH_4 + H_2O \quad \Delta H^{o}_{r,298K} = -206\ \text{kJ/mol} \tag{6.5}$$

The methanation reaction is mainly affecting the process selectivity under atmospheric pressure, even though other oxygenated compounds are likely to be produced like dimethyl ether, alcohols, and larger alkanes [37].

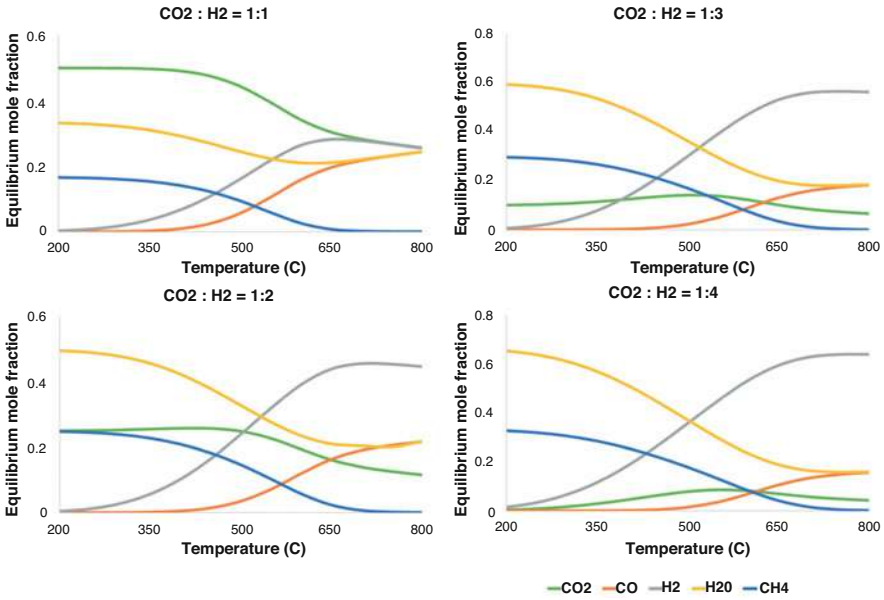

Fig. 6.2 Effect of temperature on the thermodynamic equilibrium of the RWGS reaction at 1 bar for different CO_2/H_2 compositions. Modelled in Aspen Plus using an RGibbs reactor and the Peng–Robinson property method. (Reprinted with permission from [37])

The thermodynamic equilibrium compositions from the CO_2 hydrogenation to methane and CO through the RWGS reaction and the methanation reaction under different H_2/CO_2 compositions are shown in Fig. 6.2. Temperature variation leads to different product distribution under a given feed stream. The main product in the temperature range of 100–700 °C appears to be the methane either by the Sabatier reaction or via the CO hydrogenation reaction, whereas at a higher temperatures (higher than 600 °C), CO is the dominant product. This suggests that the proper catalysts should be used to achieve the desired composition under as low temperature as possible to avoid undesired phenomena such as sintering. Therefore, based on the thermodynamics of the system under atmospheric pressure conditions, the conversion of CO_2 through the RWGS reaction route is enhanced with temperature increase, where the equilibrium conversion to CO increases. In contrast, the equilibrium constant and consequently the equilibrium conversion for the methanation reaction decreases with increasing temperature. However, the reduction of the fully oxidized CO_2 to methane is a process involving eight electrons, which means slow kinetics leading to low CO_2 conversion. Therefore, the utilization of proper catalysts leading to high CO_2 conversion rates to methane as well as to increased methane selectivity is necessary.

It is worth mentioning the significance of the H_2/CO_2 ratio on the equilibrium conversion of CO_2. High H_2/CO_2 ratios result in higher CO_2 conversions, pointing out that H_2 is acting as a limiting reactant during CO_2 hydrogenation. Furthermore,

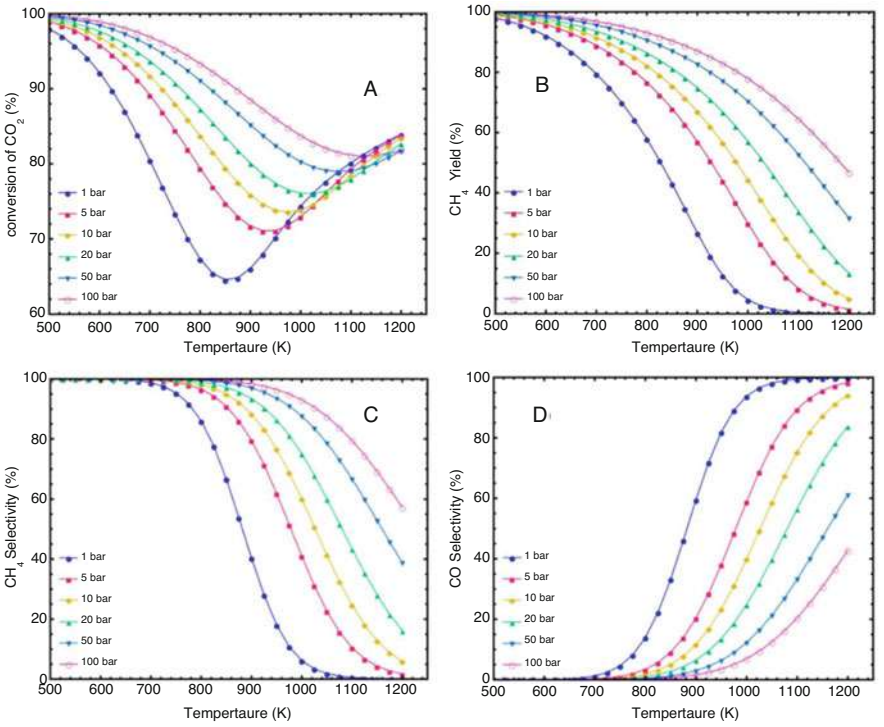

Fig. 6.3 Effect of pressure on (**a**) CO_2 conversion, (**b**) CH_4 yield, (**c**) CH_4 selectivity, and (**d**) CO selectivity. (Reprinted with permission from [1])

the CO selectivity during CO_2 methanation is an important factor. The higher the H_2/CO_2 ratio, the lower the CO formation (Fig. 6.2). It must be pointed out that carbon formation is not expected at high H_2/CO_2 ($\geq$4). Operating at high H_2/CO_2 ratios is preferable because the carbon formation is suppressed with the drawback of remaining hydrogen unused. The carbon formation can be prevented by shifting the reaction to the left by using steam (H_2O is a byproduct of the reaction) [35].

As expected, for the CO_2 methanation reaction, thermodynamics predict that the optimum temperature operation range is at low levels (<300 °C) for atmospheric pressure. The expected conversion reaches 90% with a high selectivity to methane. Nevertheless, this window widens while the pressure rises as shown in Fig. 6.3 [2]. Pressure is a significant factor for increasing the methane yield and selectivity. Great enhancement of CO_2 conversion is achieved under very high pressures (100 bar) compared to that observed under atmospheric pressures. It is worth mentioning that at low temperatures the rise in pressure has a little effect on the methane production, as well as in the RWGS reaction and consequently to the CO_2 conversion. However, in a higher temperature range, this increase is enormous. The opposite behavior is observed for the RWGS reaction selectivity by increasing the

temperature where the selectivity is dramatically dropping with high reactor pressures.

The optimal reactor system operation conditions should include considerations concerning the equipment safety which is preserved under low pressures as well as the constant temperature maintenance, which can be easily disturbed due to the exothermic nature of the methanation reaction.

6.1.2.2 CO_2 Hydrogenation Reaction Mechanisms

Although the Sabatier reaction is thermodynamically favored at low temperatures, the reaction kinetics are very slow resulting in very low CO_2 conversions. Therefore, in order to maximize the efficiency of the system and to increase the overall reactant conversion, the intense study of the kinetics of the hydrogenation of CO_2 under the utilization of a catalyst is required. CO_2 hydrogenation has been studied in a variety of catalytic systems. Figure 6.4 shows the predominant mechanisms of the reaction with CO, CH_3OH, and CH_4 as products.

The preferred pathway for the CO_2 hydrogenation is primarily controlled by the binding capability of the catalyst with the key reaction intermediates [39].

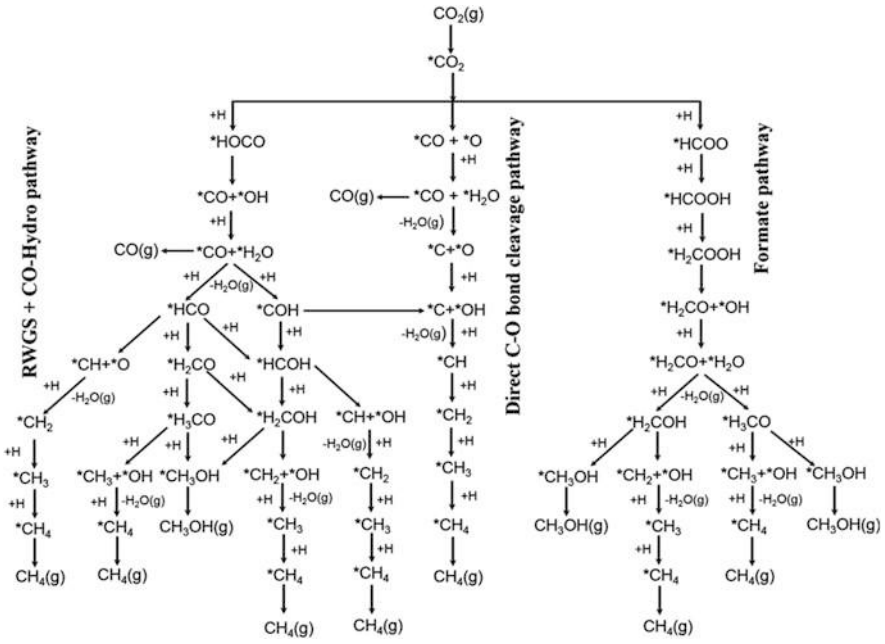

Fig. 6.4 Possible reaction pathways of CO_2 hydrogenation to CO, CH_3OH, and CH_4. * indicates adsorbed species. (Reprinted with permission from [38])

The Case of the Reverse Water-Gas Shift (RWGS) Reaction

Two different mechanisms (Fig. 6.5) have been proposed for the RWGS reaction: (i) the direct reduction of CO_2 into CO and O (redox mechanism) and (ii) the formation of formic species (HCOO) and/or carboxylic (COOH) intermediates (associative mechanism) [40].

The redox mechanism includes the CO_2 dissociation on the catalytic surface into CO and O, with the reduction of the superficial O by H_2 to produce H_2O, and eventually leading to the desorption of CO and H_2O. It is clear that this reaction path does not require the interaction of CO_2 with H_2 (hydrogen only "cleans" the catalytic surface from the adsorbed oxygen).

On the other hand, in the associative mechanism, H_2 is first transferred to CO_2, resulting in the formation of intermediate species, which are then decomposed into CO. Alternatively, CO_2-activated species on the surface react with H-dissociated species leading to intermediates that decompose to the reaction products [37, 41]. The main associative reaction pathways proposed are formyl, formate, carboxyl, and formic acid as potential intermediates.

It is very likely that under specific catalyst conditions, other alternative mechanisms exist. However, the dominant mechanism will depend intrinsically on the catalytic system used, its physicochemical properties, and structural characteristics both in the micro and macro scales [42].

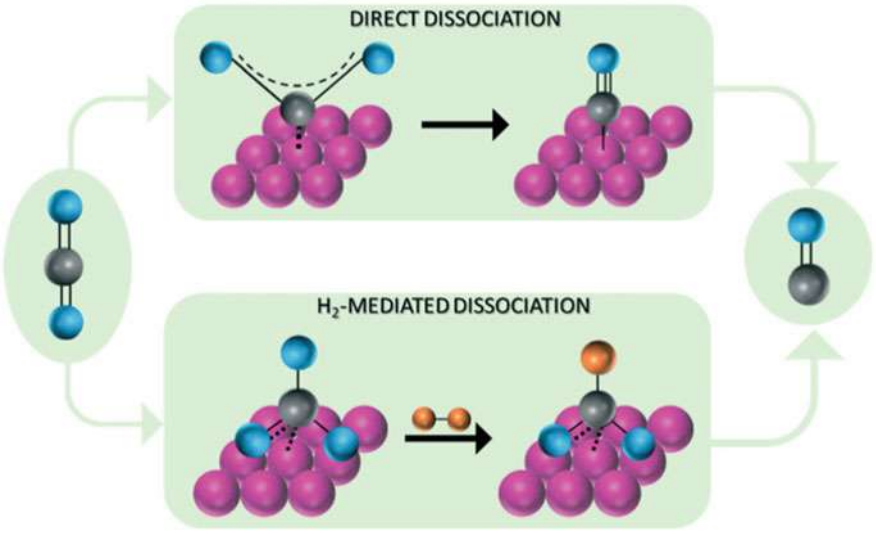

Fig. 6.5 Simplified RWGS mechanism for redox and H-assisted CO_2 dissociations processes. (Reprinted with permission from [37])

The Case of the Methanation Reaction (Sabatier)

Although the CO_2 methanation seems to be a simple reaction, it is quite challenging to precisely determine its mechanism. Two well-established mechanisms have been proposed from 1970 until today: the associative and the dissociative categories [42].

Under the associative scheme, CO_2 adsorbs associatively and reacts with adsorbed hydrogen atoms to form oxygenates, which are further hydrogenated to formate $HCOO_{ad}$ and formyl CHO_{ad} species. The most common intermediate observed in various studies is the formate species, which is considered to form methane in successive surface hydrogenation steps. In this mechanism CO intermediate is not formed [1, 42, 43]. The dissociative mechanism involves the adsorption of CO_2 onto the catalytic surface which splits into a carbonyl and an oxygen atom. Consequently, the carbonyl, CO_{ad}, carbon, and C_{ad} are playing the role of the intermediates. The reaction follows the CO methanation mechanism, which is closely related to the Fischer-Tropsch mechanism [2].

It is worth noting that the production of water affects negatively the methanation reaction, and its removal from the catalytic sites increases the yield of CH_4 and minimizes the CO release as a side product [44].

The species involved in these mechanisms were detected by a variety of spectroscopic techniques, including diffuse reflectance infrared Fourier transformed spectroscopy (DRIFTS), Raman spectroscopy [45], infrared spectroscopy [46, 47], and Fourier [48–50].

The Case of the CO_2 Hydrogenation to Methanol

The mechanism pathways describe the CO_2 hydrogenation to methanol production is supported by plenty of experimental studies as well as theoretical calculations [51–54]. Two are the main pathways: the RWGS + CO-Hydro pathway and the formate pathway. There are many intermediates involved in both pathways through different routes (Fig. 6.4).

The RWGS + CO-Hydro pathway involves adsorbed CO as an intermediate formed via the carboxylate (*HOCO) species or through the breaking of C-O bond and further hydrogenation to the production of CH_3OH. The second mechanism includes the pathway which is associated with the formate (*HCOO) intermediate formed as the initial step during the adsorbed CO_2 hydrogenation, which eventually produces CH_3OH via the $C-O$ bond cleavage of the $*H_2COOH$ intermediate.

6.1.2.3 CO_2 Hydrogenation Reaction Catalysts

The CO_2 hydrogenation reaction takes place over a variety of metallic particles, such as Ni, Cu, Ru, Rh, Pt, Pd Ir, Fe, and Co supported on metal oxides, including TiO_2, SiO_2, Al_2O_3, CeO_2, ZrO_2, γ-Al_2O_3, ZnO, MgO, etc. [18, 51, 55–60]. Generally, the electrocatalytic activity of the catalysts produced by these metals is heavily affected

by the type of support utilized. It is reported in the literature that the metal-support interactions are modifying the properties of the active metallic phase (i.e., morphology and dispersion), thereby affecting the catalytic activity, the yield, and selectivity of the reaction.

Ru has found to be one of the most active catalysts for the CO_2 methanation reaction, even with low metal loading supported catalysts. The CH_4 yield over Ru-supported catalysts is strongly affected by the metal loading, the metal particle size, structure and distribution, and the metal-support interactions [61]. Ru-based catalysts on various oxide materials, including both reducible supports with lattice oxygen vacancies such as CeO_2, ZrO_2, and TiO_2 and without oxygen vacancies like Al_2O_3 and SiO_2, show high activity and selectivity to methane [62]. The most effective and active catalyst for the CO_2 methanation reaction has been found the Ru/TiO_2 [63]. The TiO_2 crystalline plan was found to strongly affect the electronic properties of Ru, which also has an impact on the catalyst structure and therefore influences the performance of the catalyst for the CO_2 methanation reaction [64].

Rh-based catalysts have also been found to be highly active and selective for the methanation reaction catalysts, especially at low temperatures. According to the literature, the intrinsic activity of $Rh/\gamma\text{-}Al_2O_3$ strongly depends on the Rh particle size. More specifically, at low temperatures, large particles result in the promotion of the CH_4 rate turnover frequency, since the high proportion of lateral faces favor the C-O bond cleavage, which is the rate-determining step of the reaction, with a lower activation energy [65]. As regards the supports, various metal oxides have been found to promote the methanation reaction, including TiO_2, SiO_2, Al_2O_3, and CeO_2 [66, 67]. Although, all the aforementioned supports lead to relatively high yields, the performance of TiO_2 is outstanding, which is the most effective support for Rh towards the methanation reaction [65].

Nickel catalysts are also widely used for the CO_2 methanation reaction. Their low price together with their good performance makes them an attractive alternative to the more expensive Ru and Rh catalysts. However, it should be noted that their performance is better at elevated temperatures, with the danger of particle sintering and agglomeration. Other studies have shown that Co is the most active catalyst among the Group VIII metals for CO_2 methanation, with a higher resistivity to deactivation compared to Ni [68].

In general, with respect to the methanation reaction, the activity among the most used metals is ranked as Ru > Rh > Ni > Fe > Co > Os > Pt > Ir > Mo > Pd, whereas the selectivity order follows the trend Pd > Pt > Ir > Ni > Rh > Co > Fe > Ru > Mo [31].

Regarding the RWGS reaction, a variety of catalytic system based on noble metals and on transition metals have been extensively studied. Typically, the metal catalyst's performances are improved when combined with reducible oxides such as CeO_2, Mn_2O_3, CrO_3, FeO_x, or TiO_2 [69].

Precious metals including Pt, Pd, Rh, and Au and non-precious metals such as Cu, Fe, and Ni over metal oxides favor the RWGS reaction [68]. Pt is a highly active and selective metal for the RWGS reaction. However, the type of the metal oxide support plays a significant role to the performance of the catalyst. It was found that between

Pt/γ-Al_2O_3 and Pt/CeO_2, the first was less active and more selective to CO at similar metal loadings and reactant conversion [70].

While the Pt-based catalysts performance shows high conversions, the Cu-supported catalysts belong to the most active metals with high selectivity to CO. An extensive study of its properties and the way that its surface morphology and particle size distribution is affecting the CO_2 hydrogenation reaction has been done showing that highly dispersed Cu nanoparticles over ZnO performed high activity for CO_2 hydrogenation reaction to produce CO [71].

Furthermore, one more metal on the list of the most selective for the RWGS reaction is Rh. Catalytic experiments on Rh/TiO_2 catalysts (with low Rh loadings) have shown that the selectivity to CO is higher than that to methane at 200 °C, under both reducing and oxidizing operating conditions [72].

The bimetallic Pt-Ni, Pt-Co, and Pd-Ni catalyst performance for the CO_2 hydrogenation to the RWGS reaction was profound, and interestingly these catalysts showed higher activity and RWGS selectivity compared to the monometallic ones on the same support [70, 73].

The production of methanol from CO_2 is of great interest, due to the challenging thermodynamic barriers that must be overcome. Low temperatures and high pressures (mainly over 5 bar) are necessary for methanol production, with a great risk for the formation of several by-products, such as CO, formic acid, and ethanol. Therefore, the optimum catalyst development is deemed inevitable.

Cu-supported catalysts have been meticulously studied, since they exhibit the highest activation among other elements, in combination with a series of promoters including B, Si, Zn, Ag, Cr, Ti, Ce, Ze, Al, V, and Ga [74]. Cu-ZnO-Al_2O_3 has been the most widely used catalyst for CO_2 hydrogenation to methanol [75, 76]. New catalysts are being developed to overcome the deactivation, sintering, and phase segregation problems that the Cu-based catalysts are displaying. For this reason, In-based materials are being investigated [77], and many bimetallic catalysts such as Ni-Ga, Co-Cu, Pd-Cu, and Au-Cu seem to be very promising materials for methanol production through CO_2 hydrogenation [74].

It is worth mentioning that the utilization of bimetallic catalysts can strongly affect the selectivity of the CO_2 hydrogenation, because the introduction of a second material changes the structure and the morphology of the active catalytic surface, leading to changes of metal-intermediate bond strength.

6.2 Electrochemical Promotion of Catalysis

6.2.1 EPOC: Concept, Theory, and Definitions

Electrochemical promotion of catalysis (EPOC), also known as non-Faradaic electrochemical modification of catalytic activity (NEMCA), is a phenomenon which targets the catalytic reaction rate increase using electrochemistry [78–96]. EPOC was discovered by M. Stoukides and C. Vayenas in the early 1980s and has been

widely studied by various research groups [97–106] using a plethora of catalytic reactions in more than 100 catalytic systems. It shows similar features with classical chemical promotion as well as with the metal-support interactions (MSI) [103, 107–110].

In EPOC studies, the catalytic reaction takes place on the surface of a conductive film (working electrode), which is deposited on a solid electrolyte. The latter allows the orientated migration of ionic species to the catalyst (working electrode), by applying small currents or potentials between the working catalyst-electrode and an inert Au counter electrode [98], deposited on the other side of the electrolyte. This ionic migration to the three-phase boundaries (tpb, solid electrolyte-catalyst-gas/liquid phase) results in the formation of an effective double layer leading to a significant change of the catalytic properties turning them into electronic promoters. Also, these ionic promoters can participate in the promoting reactions as sacrificial species. In addition, the benefit of the EPOC effect is connected to the in situ generation, control, and optimization of these promoters by a small current or potential application and as well as with the reversibility of this process.

The explanation of the EPOC effect can be given via the formation of an effective overall neutral double layer created via the application of an electrical current (or potential) on the catalytic surface (Fig. 6.6) [98, 111, 112]. The ionic direction is dictated by the applied potential between the working and counter electrode. The creation of the effective double layer affects the catalyst work function and furthermore the chemisorption energy of the reactants and the intermediate compounds leading to a change of the catalytic activity and selectivity in a very pronounced and predictable manner.

Therefore, the coverages of the reactants on the catalytic surface also change, and as a result, the catalytic rate increases or decreases according to the kinetics of the reaction. This modification of catalytic rate is non-Faradaic since the total reaction rate upon polarization is significantly higher (or lower) than the sum of the catalytic rate under open-circuit conditions (no polarization) and the rate of electrochemical reactions (following Faraday's law).

The EPOC phenomenon can be applied on metal catalysts deposited on solid electrolytes, such as YSZ (O^{2-} conductor), β''-Al_2O_3 (Na^+ or K^+ conductor), and $BaZrO_{0.85}Y_{0.15}O_{3-\alpha}$, BZY, (proton conductor), or mixed electronic-ionic conductors, like titania (TiO_2) or ceria (CeO_2) [84, 98, 109, 113].

Three parameters have been introduced for the quantification of the EPOC phenomenon i.e., the rate enhancement ratio, ρ, defined by Eq. 6.6; the apparent Faradaic efficiency, Λ, defined by Eq. 6.7; and the conversion enhancement index (CEI) defined by Eq. 6.8:

$$\rho = \frac{r}{r_o} \tag{6.6}$$

$$\Lambda = \frac{\Delta r}{(\mathrm{I}/nF)} \tag{6.7}$$

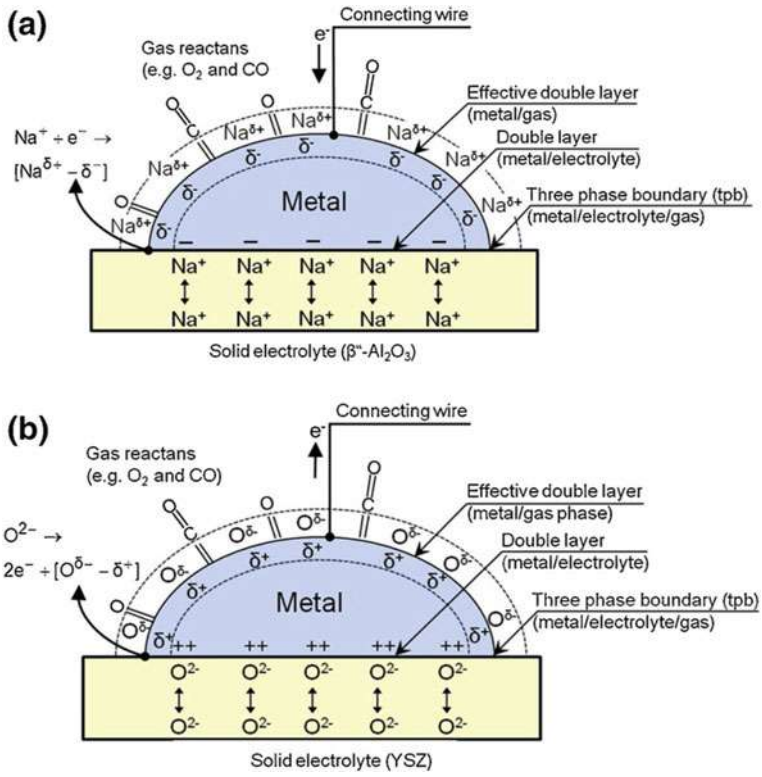

Fig. 6.6 Schematic representation of a metal electrode deposited on (**a**) Na-β″-Al_2O_3, a Na^+ conductor, and (**b**) YSZ, an O^{2-} conductor, showing the location of the tpb, of the classical double layer at the metal-support interface and of the effective double layer at the metal-gas interface. (Reprinted with permission from [111])

$$\mathrm{CEI} = \frac{X_i - X_i^o}{X_i^o}\% \tag{6.8}$$

In these equations, the electropromoted catalytic rate is denoted by r, whereas the open-circuit catalytic rate (unpromoted state) is r_o. Δr stands for the observed difference of the catalytic rate (in g-eq/s) during polarization (i.e., under the application of potential/current between the working and counter electrodes), F is the Faraday constant (96,485 C/mol), I is the applied current, and n is the ion charge. Additionally, the conversion of the reactant I, with and without polarization, is denoted by X_i and X_i^o, respectively [96, 106].

The overall rate increase upon polarization is expressed by the rate enhancement ratio, ρ. The apparent Faradaic efficiency, Λ, is used to express the number of additional reactant molecules which are forced to react due to the introduction of one molecule of the promotional species (e.g., in the case of YSZ, O^{2-} is the

promotional species) on the catalytically active electrode surface. In other words, Λ is used to correlate the change of the catalytic rate when a potential is applied with the rate of ion migration from the solid electrolyte (Faraday's law). The main distinguishing featuring of EPOC is connected to the observed Λ values. When $|\Lambda| \geq 1$, a non-Faradaic change of the catalytic rate is observed, because product formation outweighs the O^{2-} supplied to the reaction. Electrolysis is limited to $|\Lambda| \leq 1$ [98].

The response of an electrocatalytic system under the EPOC phenomenon can be easily predicted via the rules that have been developed over the years. These rules are valid for both classical promotions and for the electrochemical promotion of catalysis [98, 111, 114–116].

The prediction of the manner that the applied potential or current is affecting the electrocatalytic system is facilitated by the kinetic study of the examined reaction. The kinetic study is performed by investigating the effect of partial pressure of the electron acceptor (A) and the electron donor (D) reactants on the catalytic rate. All the catalytic systems studied have shown the existence of four distinct types of reaction behavior: electrophobic (or nucleophilic, $\partial r/\partial U > 0$), electrophilic (or nucleophobic, $\partial r/\partial U < 0$), volcano-type (maximum in a rate vs. potential plot), and inverted volcano-type (minimum in a rate vs. potential plot) behavior. All the four types of behavior and the corresponding rules (discussed in detail in Chaps. 1 and 2) describe the EPOC phenomenon [98, 111, 114–116] (see Fig. 1.11 in Chap. 1 and Fig. 2.15 in Chap. 2 where a characteristic example is given for each reaction type [80, 81, 86, 117]).

6.2.2 *Experimental Set-Up for EPOC Studies*

The catalytic sample most commonly consists of a solid electrolyte/ion conductor (disc or tube) and three metal electrodes. On one side of the electrolyte, the counter (CE) and reference (RE) electrodes are deposited by brush painting of a gold (i.e., inert) organometallic paste or metal precursor solution, followed by a calcination process. The catalyst, which also serves as the working electrode (WE), is deposited on the other side of the electrolyte (opposite to the CE) via calcination of an organometallic paste, wet impregnation of a metal precursor/solvent solution, or dropwise from a colloidal solution/suspension by a micropipette. The catalytic sample (WE/solid electrolyte/CE, RE), also called electrochemical catalyst, is then placed in a single pellet or a fuel cell type reactor (Fig. 6.7). The main difference between these two types of reactors is that in the single pellet (or single chamber) reactor all electrodes (WE, CE, and RE) are exposed to the reaction mixture, compared to the fuel cell reactor where only the WE is exposed to the reaction mixture, whereas CE and RE electrodes are in a separate compartment and are exposed to a reference gas (e.g., air). The main advantage of the "single chamber" type reactor is its simplicity and the ability to use cheaper solid electrolyte elements

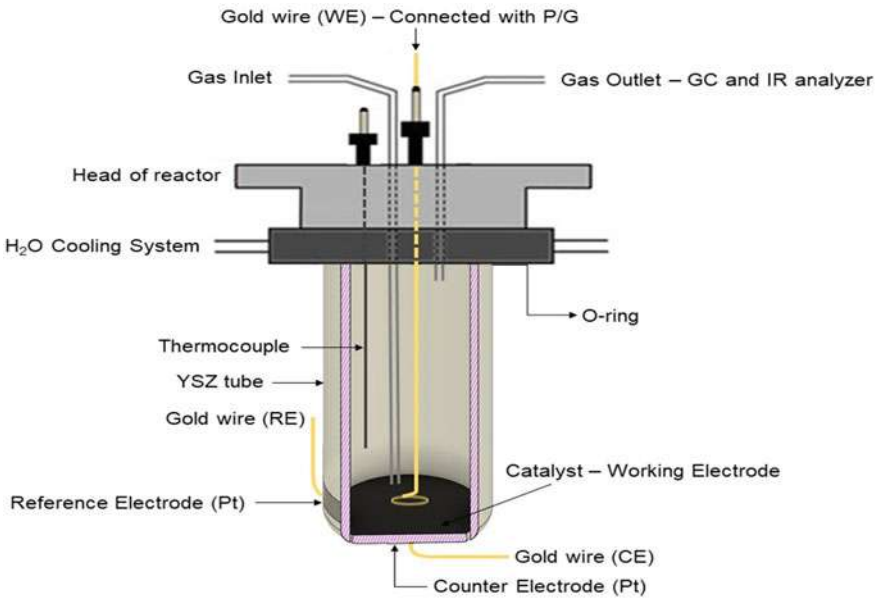

Fig. 6.7 Schematic presentation of the fuel cell type reactor

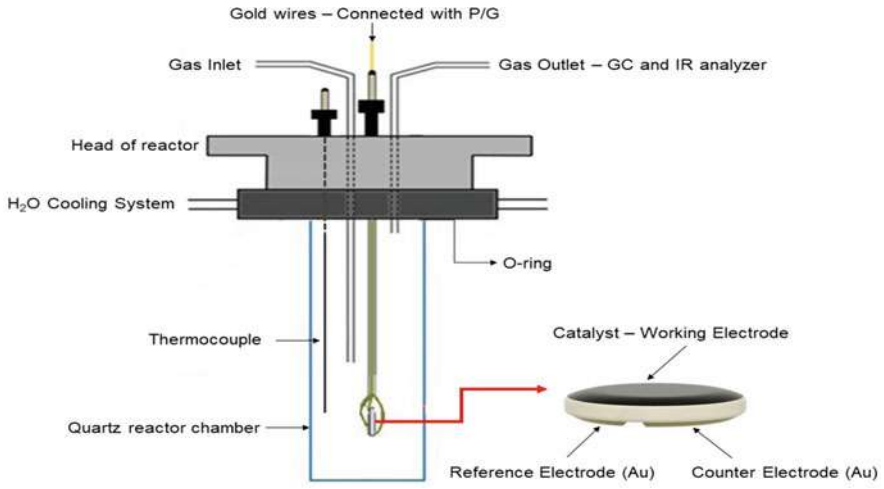

Fig. 6.8 Schematic presentation of the single chamber type reactor

(discs instead of tubes). The "single chamber" reactor is made of a quartz tube closed at one end (Fig. 6.8). The open end of the tube is mounted on a stainless steel cap, which has provisions for the introduction of reactants and removal of products as well as for the insertion of a thermocouple and connecting wires to the electrodes of the cell. The catalytic sample is appropriately clamped inside the reactor. Au wires

are normally used to connect the catalyst-working electrode as well as the two Au auxiliary electrodes with the external circuit. These wires are mechanically pressed onto the corresponding electrodes, using an appropriate ceramic holder. A thermocouple, inserted in a closed-end quartz tube, is used to measure the temperature of the solid electrolyte pellet. The reactor inlet gas line is designed to be very close to the WE surface, creating enough turbulence so that the reactor resembles a continuous stirred tank reactor operation (CSTR reactor). In order to operate at high and constant temperatures, the reactor is in turn placed in an oven.

The experimental set-up used in EPOC studies can be separated into four parts: the gas controller system (electronic mass flow meters), the reactor, the gas analysis system (on-line gas chromatograph, infrared analyzer (IR), mass spectrometer, etc.), and the electrochemical control equipment (potentiostat/galvanostat (P/G)). Crucially, prior to any EPOC experiment, it is important to examine if the catalytic reaction is subjected or not to any internal or external mass transfer limitations within the reaction operating temperature range. This is necessary as mass transfer limitations can potentially obscure and in some cases even completely hide the electrochemical promotion effect. Examining for the presence or absence of external mass transfer limitations is a straightforward procedure, compared to the case of internal mass transfer limitations. One has to simply vary the total volumetric flow rate while holding the partial pressure of the reactant's constant. When external mass transfer limitations are absent, then the consumption rate of the reactants does not vary with the flow rate. Beyond mass transfer limitations, when performing EPOC experiments, it is crucial to calculate the maximum mass-balance allowable rate enhancement. This is closely connected to the conversion of the limiting reactant under open-circuit conditions since its conversion cannot be greater than 100%. In this regard maintaining a low conversion under open-circuit conditions (typically this is achieved by utilizing small amounts of catalyst) leads to a pronounced rate enhancement ratio.

In a typical EPOC experiment, kinetic measurements under both open- and closed-circuit (i.e., electropromotion) conditions are carried out. In addition, the effect of catalyst potential (or work function) on the catalytic rate and the selectivity under transient and steady-state conditions is also studied. When carrying out kinetic measurements, the partial pressure of each reactant is varied while keeping the partial pressures of the other reactants constant. Differential operation of the reactor (typically by keeping the conversion below 5%) allows for a relatively easy analysis of the kinetic data, even if the reactor does not exhibit identical behavior to that of a continuous stirred tank reactor.

6.3 Electrochemical Promotion of the CO_2 Hydrogenation Reaction

The electrochemical promotion of the carbon dioxide (CO_2) hydrogenation reaction targets not only to increase the overall CO_2 conversion to added-value chemicals and fuels but also to the in situ tuning of the product selectivity. The latter is typically

achieved by the addition of electronegative or electropositive promoters on the catalytic surface, resulting in a predictable switch of the reaction selectivity. The main products of the CO_2 hydrogenation reaction under atmospheric pressure and medium temperatures (200 °C < T < 500 °C) are methane (CH_4) and carbon monoxide (CO) via the methanation (i.e., Sabatier) reaction and the reverse water-gas shift (RWGS) reaction, respectively. The presence of electropositive or electronegative promoters on the catalytic surface can strongly affect the bond strength of the adsorbed species with the catalyst surface. More specifically, electropositive promoters enhance the chemisorption of electron acceptor and weaken the bond of electron donor species, whereas electronegative promoters have the opposite effect. If we consider the case of CO_2 hydrogenation, under anodic polarization, electropositive species (e.g., H^+ in the case of BZY, Na^+ or K^+ in the case of Al_2O_3) are removed, while electronegative species (e.g., O^{2-} in the case of YSZ) are supplied to the catalyst surface. Therefore, an increase of the catalyst work function is expected together with an enhancement in the chemisorption of hydrogen (i.e., electron donor) supplied from the gas phase. On the other hand, cathodic polarization results in a decrease of the catalyst work function, accompanied with an increase in the electron acceptor (i.e., CO_2) surface coverage.

6.3.1 Kinetic Studies of CO_2 Hydrogenation Reaction

Over the past years, the kinetics of CO_2 hydrogenation to CH_4 and CO have been studied on Rh, Pd, and Ru porous catalyst films using both electronegative and electropositive promoters [101, 118, 119].

More specifically, regarding the Ru catalysts, the effect of the nature of the electrolyte used on the selectivity of the reaction was investigated at temperatures between 200 and 340 °C and pressures up to 5 bar. Interestingly, it was found that the electrochemical behavior of the promoted catalytic reactions is independent of the nature of the electrolyte. For example, Ru catalysts deposited on both YSZ electrolyte (O^{2-} conductor) and β''-Al_2O_3 (Na^+ conductor) resulted in an enhancement of the methanization rate (i.e., CH_4 formation) upon positive polarization, i.e., through O^{2-} supply or Na^+ removal from the catalyst surface. The opposite effect is observed when using a negative applied potential, which suppresses CH_4 production and enhances the production of CO through the RWGS reaction. Under highly reducing conditions, sodium can also promote the methanation reaction up to a coverage of 20%, which can be attributed to enhanced CO_2 chemisorption. Moreover, high pressure favors CH_4 production, whereas CO production is enhanced at high temperatures, low H_2/CO_2 ratios, and atmospheric pressure. In all cases, the observed electrocatalytic behavior is well aligned with the predictions made based upon the rules of electrochemical promotion. In a more recent study, the kinetics and the electrochemical promotion of CO_2 hydrogenation reaction to CH_4 and CO were compared for Ru porous catalytic films deposited on Na^+, K^+, H^+, and O^{2-} conducting solid electrolyte supports [102]. It was found that in all four cases

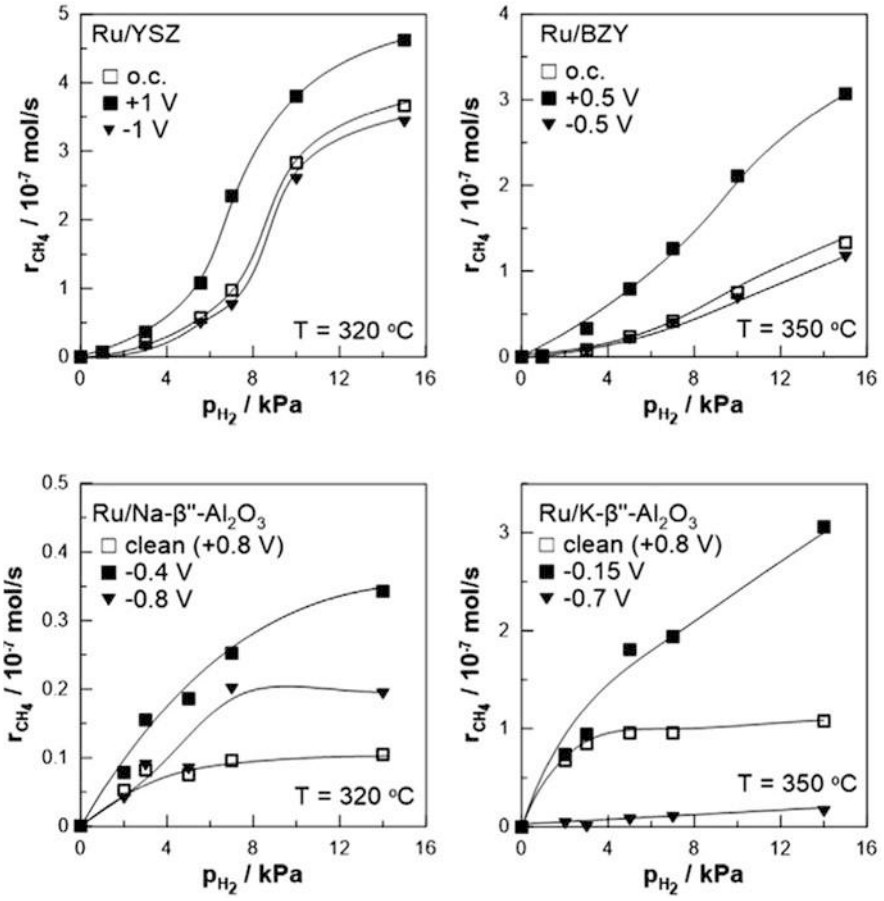

Fig. 6.9 Effect of P_{H2} and of catalyst potential on the rate of CO_2 methanation on the Ru/YSZ, Ru/BZY, Ru/Na-β″-Al_2O_3, and Ru/K- β″-Al_2O_3 catalysts. $P_{CO2} = 1$ kPa. (Reprinted with permission from [102])

increasing catalyst potential (or work function) enhances the methanation rate and selectivity (i.e., electrophobic behavior). As shown in Figs. 6.9 and 6.10, in all catalytic systems the methanation reaction rate is positive order in H_2 and exhibits a maximum with respect to CO_2, which implies strong adsorption of CO_2. For $P_{CO2} > 1$ kPa, the methanation reaction is zero to negative order in CO_2. According to these results and the rules mentioned in paragraph 6.3.1, methanation reaction is expected to have an electrophobic behavior. At the same time the reverse water-gas shift (RWGS) reaction (Figs. 6.11 and 6.12), which occurs in parallel with the methanation reaction, exhibits a maximum with increasing partial pressure of H_2 and is positive order with respect to CO_2 (i.e., prediction for electrophilic behavior). Note that for the case of YSZ and BZY supports, the unpromoted state corresponds to zero applied current or potential, denoted as o.c. (open-circuit).

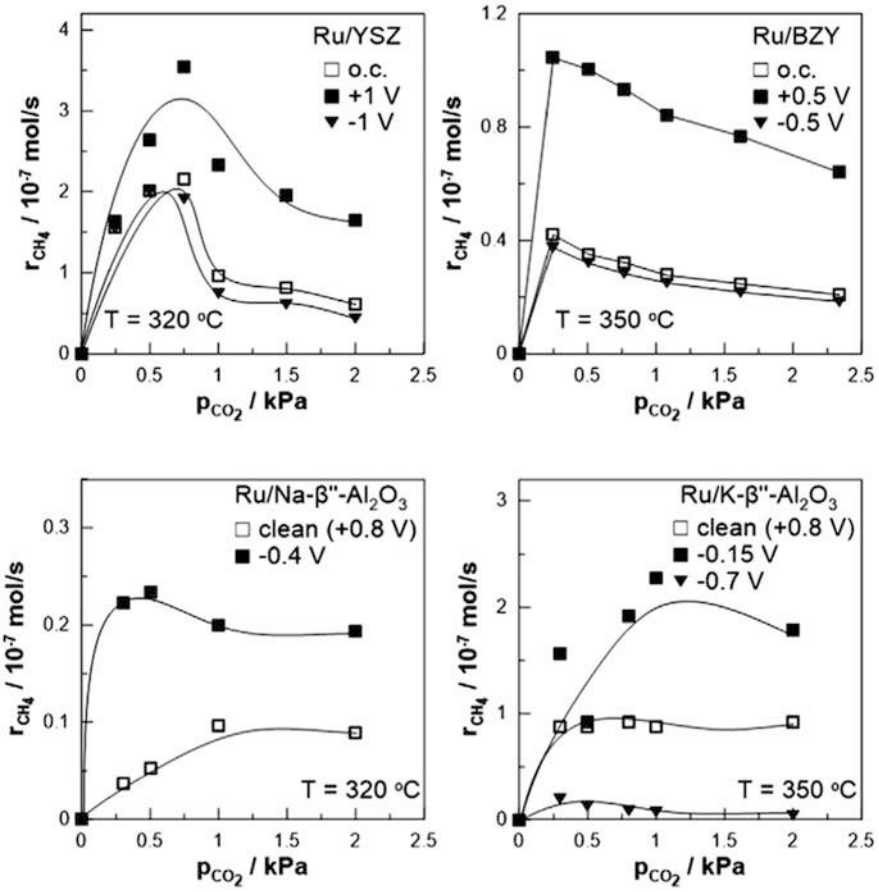

Fig. 6.10 Effect of P_{CO2} and of catalyst potential on the rate of CO_2 methanation on the Ru/YSZ, Ru/BZY, Ru/Na-β″-Al_2O_3, and Ru/K- β″-Al_2O_3 catalysts. $P_{H2} = 7$ kPa. (Reprinted with permission from [102])

Nevertheless, in the case of the Na-β″-Al_2O_3 and K-β″-Al_2O_3 supports, the unpromoted state corresponds to a cleaned surface, which is obtained after positive potential application ($U_{WR} = +0.8$ V) for 30 min. In all cases, the observed behavior is in excellent agreement with the promotional rules which can be rationalized both via "through the vacuum" interactions by considering the attractive or repulsive dipole-dipole interactions in the effective double layer present at the metal-gas interface [98, 112, 120] and via "through the metal" interactions by considering the electron donation and backdonation [111, 120] between the metal and the adsorbed species.

Bebelis et al. [119] studied the kinetics of the methanation and the RWGS reaction on porous Rh catalyst-electrodes deposited on YSZ, under atmospheric pressure at temperatures between 328 and 391 °C (Fig. 6.13). The catalytic rate of

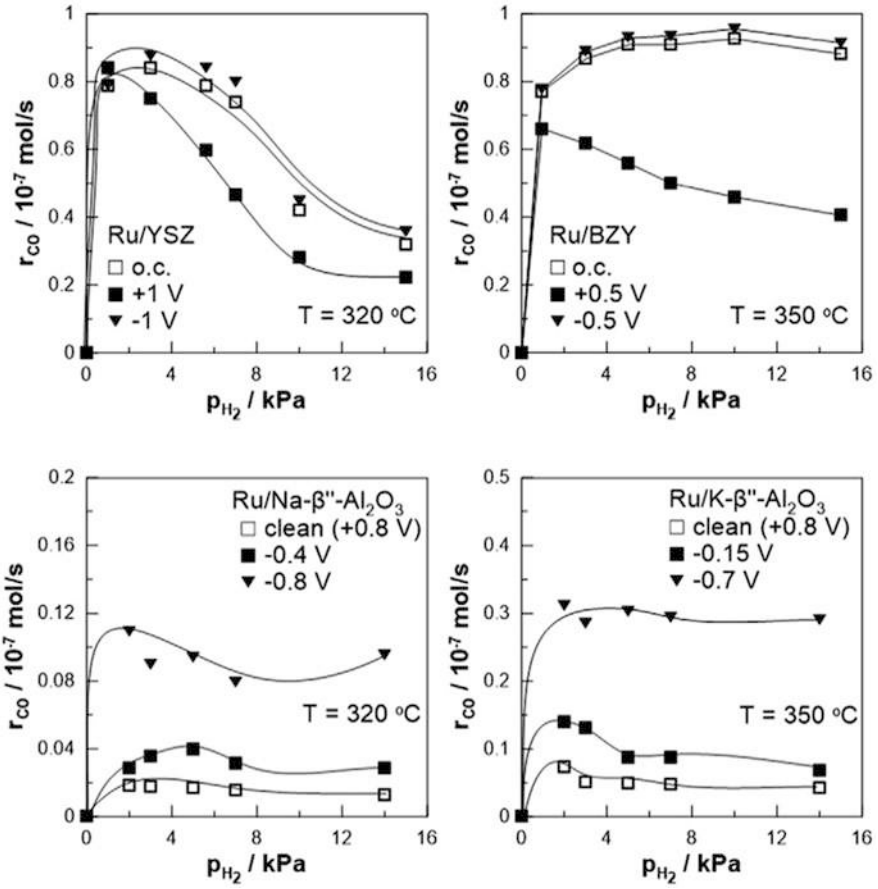

Fig. 6.11 Effect of P_{H2} and of catalyst potential on the rate of RWGS reaction on the Ru/YSZ, Ru/BZY, Ru/Na-β″-Al_2O_3, and Ru/K-β″-Al_2O_3 catalysts. $P_{CO2} = 1$ kPa. (Reprinted with permission from [102])

CH_4 formation increases with increasing H_2 and is zero-order in respect to the CO_2 partial pressure (reaching a plateau beyond a partial pressure value, which depends on the reactor temperature). On the other hand, the catalytic formation of CO increases linearly both with H_2 and CO_2 partial pressures (Fig. 6.13). The observed electrophobic and electrophilic behavior for the methanation and the RWGS reaction, respectively, is in agreement with the chemical and electrochemical promotion rules [119].

In another study [121], Bebelis et al. studied the kinetics of the methanation and the RWGS reaction over Pd catalyst-electrodes on YSZ, under atmospheric pressure and temperatures between 533 and 605 °C (Fig. 6.14). In that system, the only observed products were CO and H_2O (i.e., RWGS reaction). It was found that the CO production rate was positive order in respect to hydrogen (electron donor) and

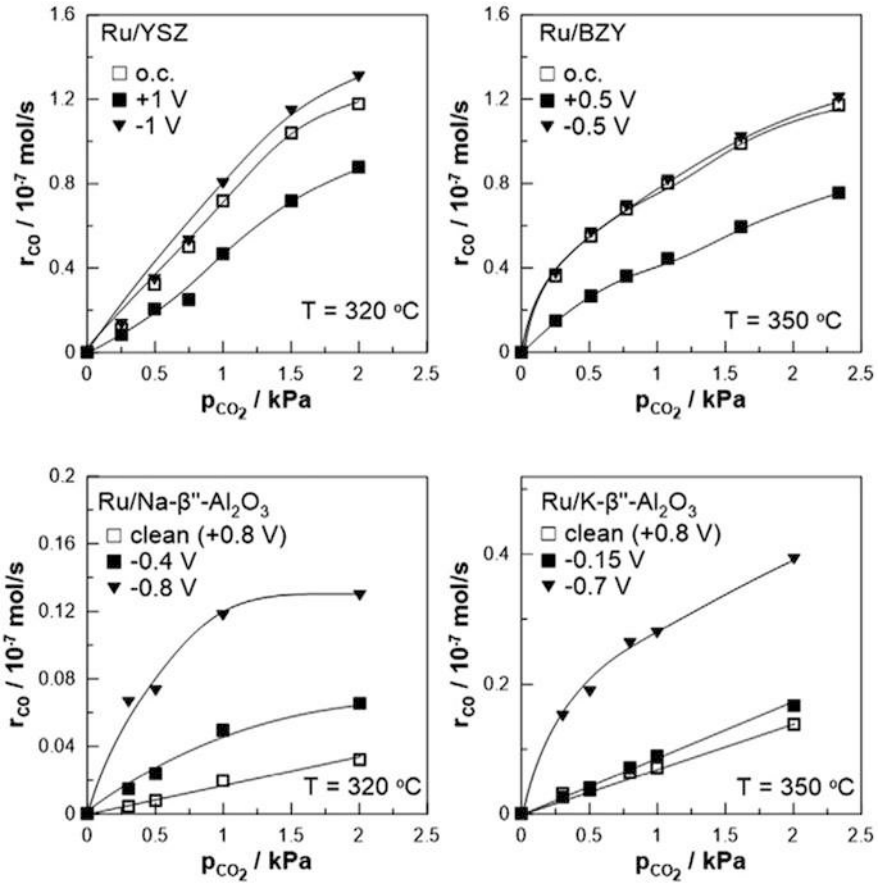

Fig. 6.12 Effect of P_{CO2} and of catalyst potential on the rate of RWGS reaction on the Ru/YSZ, Ru/BZY, Ru/Na-β″-Al_2O_3, and Ru/K-β″-Al_2O_3 catalysts. $P_{H2} = 7$ kPa. (Reprinted with permission from [102])

CO_2 (electron acceptor) as well (Fig. 6.14) confirming the observed inverted volcano behavior.

6.3.2 Electrochemical Promotion of Metal Films

The first study of the CO_2 hydrogenation reaction was carried out in 2008 by Prof. Vayenas group [119]. The electrochemical promotion experiments were performed in a fuel cell type reactor, under atmospheric total pressure conditions and a temperature range of 346–477 °C. The working electrode (i.e., Rh film catalyst) was deposited on the inner bottom side of an YSZ tube by application of thin coating

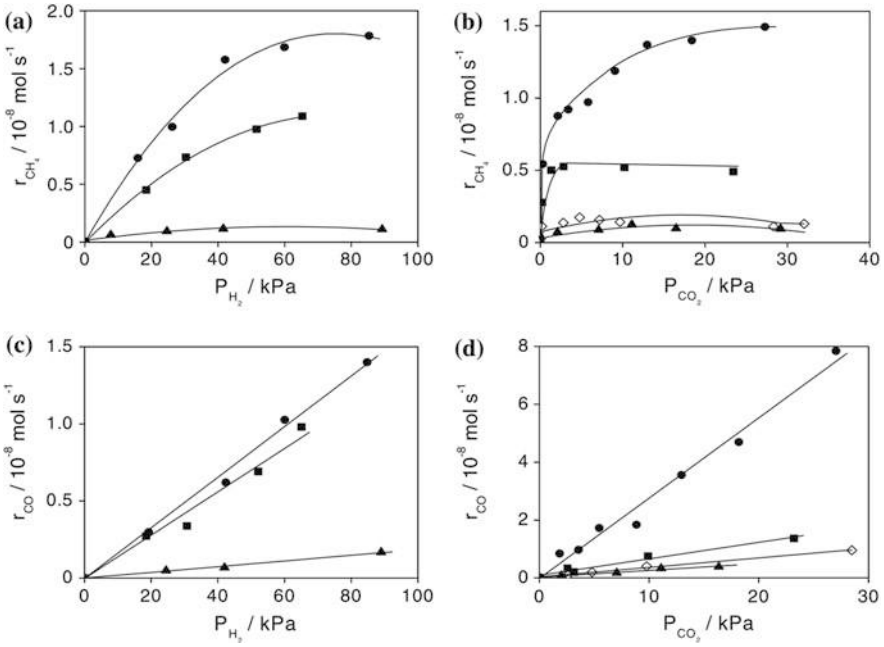

Fig. 6.13 Dependence of the CH_4 (**a**, **b**) and CO (**c**, **d**) formation rates on P_{H2} at $P_{CO2} = 5.5$ kPa and on P_{CO2} at $P_{H2} = 63$ kPa. ($N = 4.2 \times 10^{-6}$ mol Rh). Flow rate 15–50 cm^3 min^{-1}. (▲) 328 °C, (◊) 355 °C, (■) 372 °C, (●) 391 °C. (Reprinted with permission from [119])

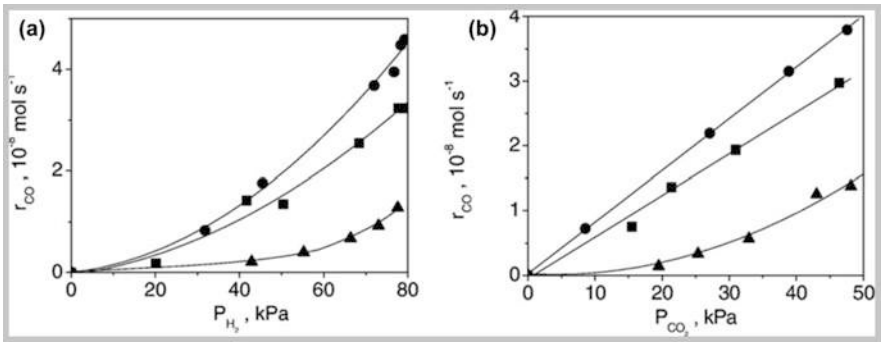

Fig. 6.14 Dependence of the CO production rate on H_2 partial pressure at $P_{CO2} = 21$ kPa (**a**) and on CO_2 partial pressure at $P_{H2} = 49$ kPa (**b**). Pd/YSZ. ($N = 4.1 \times 10^{-7}$ mol Pd). (▲) 490 °C, (■) 533 °C, (●) 560 °C. Fv = 103–300 cm3 min^{-1} (Reprinted with permission from [121])

of Rh organometallic paste followed by calcination in air, first at 400 °C (5 °C min^{-1}) for 2 h and then at 950 °C (5 °C min^{-1}). A thin coating of Pt organometallic paste was deposited on the outer bottom side of an YSZ tube, displaying the counter electrode. Prior to the experiments, the electrodes were reduced at 240 °C for 16 h

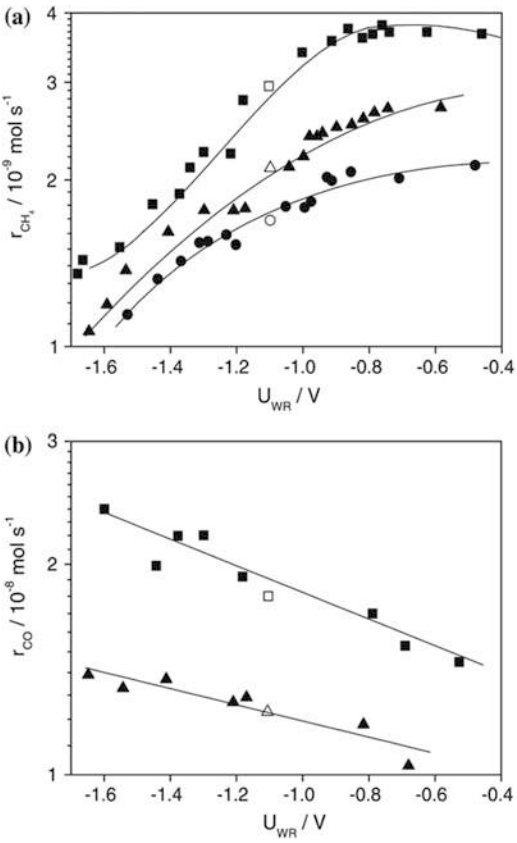

Fig. 6.15 Effect of catalyst potential U_{WR} on the CH_4 production rate (**a**) and on the CO production rate (**b**) for catalyst-electrode R1 (N = 3.9 9 10^{-7} mol Rh). Open symbols correspond to open-circuit conditions. P_{CO2} = 1 kPa, P_{H2} = 1.5 kPa. (●) 400 °C (flow rate 27 cm^3 min^{-1}), (▲) 451 °C (flow rate 38 cm^3 min^{-1}), (■) 468 °C (flow rate 38.5 cm^3 min^{-1}). (Reprinted with permission from [119])

under a 2% H_2 in He flow. The only detected products (under operating conditions: $CO_2/H_2 \sim 2$) were CH_4 and CO. Figure 6.15a, b shows the effect of the ohmic-drop-free catalyst potential (U_{WR}) on the rate of CH_4 and CO production in the temperature range 400–468 °C. The CH_4 formation rate increased up to 2.7 times upon positive potential application (i.e., electrophobic behavior), while rate enhancement ratios of CO up to 1.7 were observed upon negative polarization (i.e., electrophilic behavior). The resulted catalytic rate changes were non-Faradaic, with Λ values approximately equal to 210 and 125 for CH_4 and CO, respectively.

The observed electrochemical promotion behavior (under anodic polarization conditions) can be ascribed to the preferential formation of electron donor hydrogenated carbonylic species on the Rh surface. This leads to the formation of CH_4 and to the decreasing coverage of more electron acceptor carbonylic species resulting in CO formation. However, high operating temperatures led to methane selectivity values up to 40%, even under polarization (i.e., closed-circuit) conditions, suggesting that CO is the dominant product, following the thermodynamics of the system. The same year, a similar EPOC study was published over Pd film catalysts [118]. The Pd electrodes were deposited on the inner bottom side of YSZ and (Na^+)-

β''-Al_2O_3 tubes in the form of a thin film of Pd organometallic paste, followed by a calcination and pretreatment process, as described in detail in a previous study [119]. The reaction was also studied in a fuel cell type reactor, under atmospheric pressure and at a temperature range from 490 to 590 °C in the case of the Pd/YSZ system and 545–605 °C in the case of Pd/β''-Al_2O_3 system. EPOC experiments were performed for P_{CO2}/P_{H2} ratios ranging from 2.1 to 3.5. The only products detected were CO and H_2O through the RWGS reaction. In the case of Pd/YSZ sample, CO formation was enhanced up to approximately 6 times by applying either negative or positive overpotentials (i.e., "inverted volcano" behavior). The rate was observed to change up to almost 150 times higher than the corresponding pumping rate of oxygen ions (i.e., $\Lambda \leq 150$). On the other hand, in the case of Pd/β''-Al_2O_3 sample, the CO formation rate increased by supplying sodium ions (i.e., Na^+) onto the Pd surface. The rate was found to increase up to 6.7 times by decreasing the catalyst potential by 0.34 V.

The first report of the electrochemical promotion of the CO_2 hydrogenation reaction in a single pellet reactor was in 2011 by Jiménez et al. [122]. In this study, composite Ni- and Ru-impregnated carbon nanofibers (CNFs) deposited on an YSZ solid electrolyte disc were used as the working electrodes. Experiments took place at a temperature range of 200–440 °C and atmospheric pressure. The only products observed were CH_4 and CO under both open-circuit and electrochemical promotion conditions. Ni-based catalyst-electrodes show methane selectivity up to 55% at 300 °C, while the Ru-based catalyst exhibits selectivity up to 75% at 390 °C. The application of negative potential or current changes slightly the catalytic activity of composite CNF electrodes. The observed behavior is electrophilic, leading to CH_4 rate enhancement ratio values below 3. The authors suggested that the observed weak electropromotion can be rationalized on the basis of the limited transport of promoting or poisoning O^{2-} species along the CNF structure. Although the selectivity to CH_4 for the Ni-based catalysts is low (20–55%), Ru-based catalysts exhibit remarkable improvement of methane selectivity (up to 76%) under negative applied potential.

A year later, in 2012, this reaction was studied over a Ru film catalyst on a single pellet (i.e., single chamber) reactor [123]. The catalyst was prepared by the wet impregnation method of a Ru precursor/isopropanol solution. The Ru catalytic film (i.e., WE) was deposited on one side of an YSZ pellet, whereas gold (Au) counter and reference electrodes were deposited on the other side of the electrolyte by brush painting of an Au organometallic paste. Prior to any hydrogenation activity measurement, a calcination process in air and a reduction pretreatment was performed. The final mass of the catalyst film was ~3 mg. Indeed, methane was found to be the dominant reaction product at temperatures up to 240 °C, while the selectivity to CO increased by increasing the operating temperature. It was found that the supply of O^{2-} on the ruthenium surface results to a significant increase in the selectivity and the rate of formation of CH_4, which is also accompanied by a considerable decrease in the formation rate of CO. Figure 6.16 shows the effect of applied potential on the formation rate and selectivity to CH_4 and CO at 220 °C under steady-state conditions. The CH_4 selectivity was ~56% at open-circuit. Application of a positive

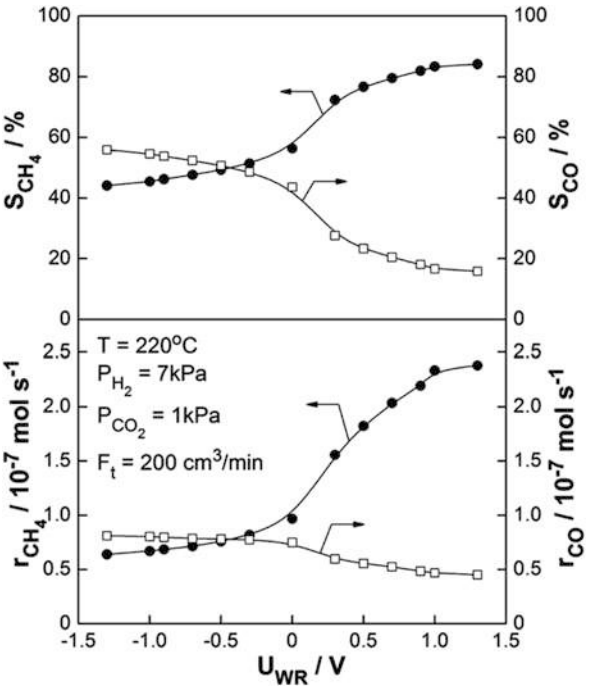

Fig. 6.16 Steady-state effect of catalyst potential on the selectivity to CH_4 and CO. $P_{H2} = 7$ kPa, $P_{CO2} = 1$ kPa, $F_T = 200$ cm^3/min. $T = 220$ °C. (Reprinted with permission from [123])

potential produced a monotonic increase in the selectivity, reaching ~84% at +1.3 V. Application of a negative potential caused a decrease of up to 44% at −1.3 V. Conversely, the formation rate and selectivity to CO exhibited the opposite behavior. Figure 6.16 shows a monotonic decrease of the CO selectivity from ~58% at −1.3 V to ~18% at +1.3 V.

According to the authors, this is a very rare case where the electrochemical promotion is found to promote a catalytic reaction (i.e., Sabatier reaction) and at the same time to poison a reaction (i.e., RWGS reaction) proceeding in parallel with the promoted one. The apparent Faradic efficiency values were found to be of the order of 10–10^3, which were among the highest reported in the EPOC literature for hydrogenation reactions. After a series of ex situ XPS measurements, both in the fresh and in the used sample, it was suggested that under open-circuit conditions, the catalyst surface consists of ~20% RuO_2 that suppresses the methanation rate. Upon positive polarization, RuO_2 is partially decomposed into RuO_x (where $x < 2$), contributing to the strengthening of the hydrogen (i.e., electron donor) bond with the active catalytic sites (whereas the opposite occurs with CO_2) and therefore enhancing the production of CH_4. Both kinetic and electropromotion results can be interpreted, using the rules of electrochemical promotion, in terms of the changes in the surface RuO_x/Ru ratio induced via potential application, as confirmed via XPS analysis.

Furthermore, two new EPOC studies [124, 125] proved once again that this phenomenon is reproducible and reversible, with the benefit of pronounced reaction

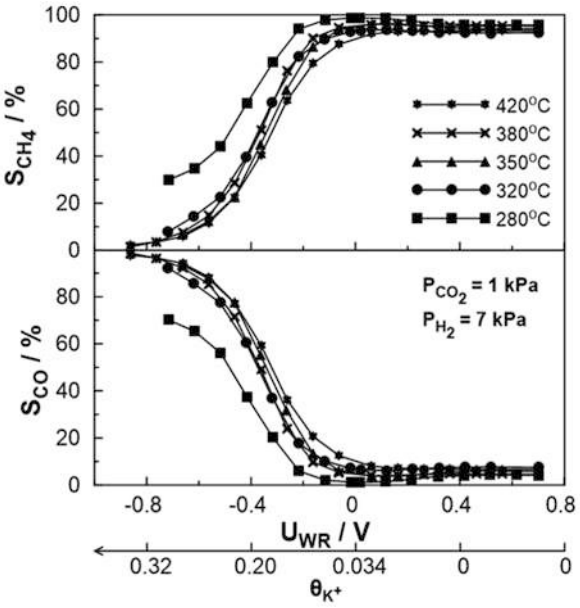

Fig. 6.17 Steady-state effect of catalyst potential and corresponding K^+ coverage on the selectivities to CH_4 and to CO at various temperatures. $P_{H2} = 7$ kPa, $P_{CO2} = 1$ kPa, $F_T = 100$ cm^3/min. (Reprinted with permission from [124])

selectivity tuning under closed-circuit conditions. In both studies, the Ru catalyst films were deposited following the wet impregnation method. In the case of the $Ru/Al_2O_3(K^+)$ sample [124], the selectivity to CH_4 was varied reversibly between 0.01% and 98% by varying the catalyst potential between −0.8 and + 0.4 V, which corresponds to an alteration in the K^+ coverage on the catalyst surface between 0.32 and 0 (Fig. 6.17).

The authors suggested that this intense alteration in the reaction selectivity to methane is attributed to the higher dipole moment of K^+ compared to that of O^{2-} and Na^+. Increasing the K^+ surface coverage (decreasing potential) leads to a monotonic increase of the CO rate of formation (i.e., electrophilic behavior) and to a decrease in the formation rate of CH_4 (i.e., electrophobic behavior). At lower temperatures (i.e., $T < 380$ °C), the rate of the methanation reaction exhibits a volcano-type behavior displaying a local maximum at intermediate potential values and K^+ coverage. Moreover, in this work, apart from the classical cyclic voltammograms (I vs U plots) for CH_4 and CO formation, rate cyclic voltammograms were obtained by plotting the rates of the electropromoted catalytic reactions as a function of the catalyst potential. A general rule which emerges from the rate cyclic voltammograms is the following: (a) an electrophobic catalytic reaction leads to a counterclockwise hysteresis of its rate cyclic voltammogram, (b) an electrophilic catalytic reaction leads to a clockwise hysteresis of its rate cyclic voltammogram, and (c) when a reaction shows a volcano-like behavior, then the rate cyclic voltammogram displays a crossing. It worth noting that case (c) also applies for inverted volcano-type catalytic reactions. In parallel, the same year, the reaction was studied for the very first time using a proton conductor/solid electrolyte (i.e., BZY) [125]. The

experiments were performed in a temperature range of 300–450 °C, in order to ensure pure proton conductivity of the electrolyte, which at low temperatures also shows oxygen ion conductivity. CO and CH_4 were the only products observed, and by altering the catalyst potential by less than 1.2 V, the selectivity to CH_4 could be reversibly tuned in the range of 15–65%. Both the CH_4 selectivity and rate could be significantly increased via the electrochemically controlled atomic H spillover from the surface of the catalyst to the proton-conducting support (i.e., electrophobic behavior). The is a strongly non-Faradaic effect with the methanation apparent Faradaic efficiency reaching values up to 500, which depends strongly on the thickness of the porous Ru catalyst film. Additionally, in this study, the dependence of the catalytic activity and selectivity of CO_2 hydrogenation to the catalyst loading was also investigated. The catalytic rate, and therefore the metal surface area, increases when the Ru loading also increases. However, this also leads to a decrease of the exchange current and thus to the length of the tpb. According to the authors, the application of a positive potential results to the deprotonation of adsorbed formic acid and the formation of anionic formate species at the metal/support/gas (i.e., Ru/BZY/gas) three phase boundaries (tpb). The formate species can then backspillover (migrate) over the entire metal-gas interface, leading to an increase in work function of the catalyst. Therefore, on the basis of the experimental data, it is not possible to conclude which of the two is the prevailing reaction mechanisms, and it is likely that they both act in parallel. In summary, the authors point out that this is a special case where the same electrochemically produced species act simultaneously as a powerful promoter for a catalytic reaction (methanation) but also as a poison for a competitive parallel reaction (RWGS).

According to the above results over Ru porous catalyst films deposited on Na^+, K^+, H^+, and O^{2-} conducting solid electrolyte supports [102], the catalytic rate of CO formation decreases monotonically with increasing potential (i.e., electrophilic behavior) as presented in Fig. 6.18, bottom. On the other hand, the rate of CH_4 production (Fig. 6.18, top) increases monotonically with potential (i.e., electrophobic behavior) only for the YSZ and BZY supports. In the case of the Na-β''-Al_2O_3 and K-β''-Al_2O_3 supports, the catalytic rate of methanation exhibits a maximum with increasing potential, (i.e., it exhibits volcano-type behavior). The results are in excellent agreement with the promotional rules and the observed kinetics.

In addition to Ru active catalysts, a PdZn alloy has been also used as an electrocatalytic film for the CO_2 hydrogenation reaction resulted in methanol (CH_3OH) formation [126]. The PdZn catalyst films were deposited by impregnation on (K^+ and Na^+)-$\beta''Al_2O_3$ pellets. During the electrochemical promotion, a low quantity of ions increases the formation rate of CH_3OH, and a high quantity leads to the poisoning of the PdZn active sites. The dynamic and stable responses of the reaction rates for CO_2, CO, and CH_3OH for the catalyst PdZn/K under several reaction conditions are shown in Fig. 6.19.

The reaction rates of CO_2 and CO are fairly similar, since the contribution of the CH_3OH formation rate to the total rate is low. The reaction rates of CO_2 and CO increased with temperature due to the endothermic nature of the RWGS reaction.

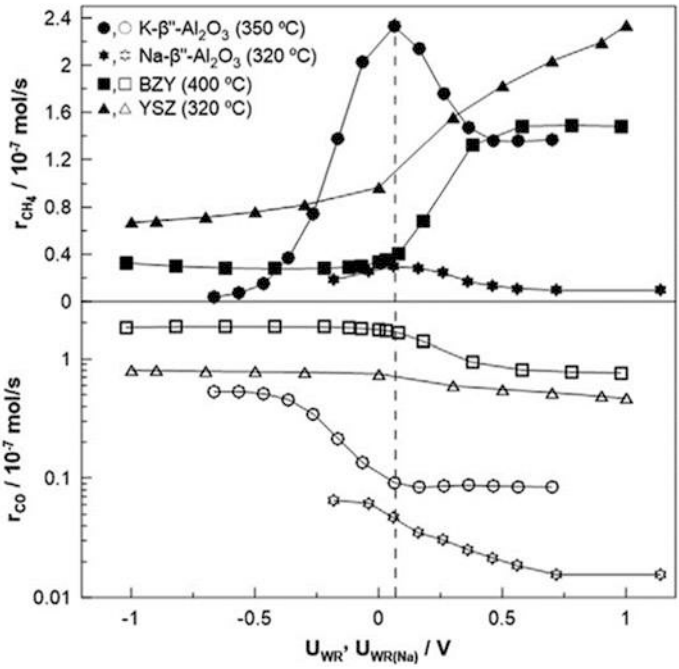

Fig. 6.18 Effect of catalyst potential on the rates of CH_4 and CO formation on the Ru/YSZ, Ru/BZY, Ru/Na-β″-Al_2O_3, and Ru/K- β″-Al_2O_3 catalysts. $P_{H2} = 7$ kPa, $P_{CO2} = 1$ kPa. (Reprinted with permission from [102])

When the H_2/CO_2 ratio in the feed atmosphere was decreased, higher reaction rates were obtained for CO and CO_2, but with larger transients being observed. The highest methanol selectivity was found for the highest H_2/CO_2 ratio (2.5% CO_2/ 97.5% H_2) at 300 °C and + 2 V. The catalysts that have palladium and the palladium-zinc alloy in their structure show an electrophilic behavior in the CO formation, and when only the alloy is formed in the catalyst, the CO has the same behavior found for the methanol. Apparent Faradaic efficiency values above 1000 were obtained under different studied conditions.

6.3.3 Electrochemical Promotion of Metal Nanoparticles (NPs)

In an attempt to minimize the total cost of the process, increase the active surface area, and utilize the exceptional properties of nanosized metal particles, a new era in EPOC literature has begun. Thin films of both noble and non-noble transition metals are studied during the last 2 years [105, 127–130]. In the noble metal category, free-standing (i.e., unsupported) Ru NPs (1–2 nm) deposited on YSZ pellets were studied

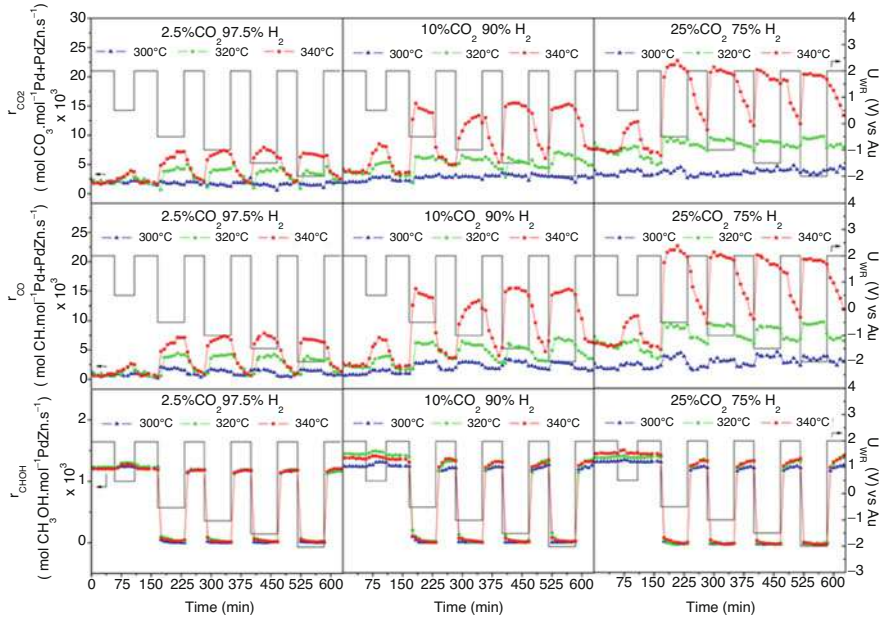

Fig. 6.19 Influence of the applied potential vs. time on the reaction rate values of CO_2 consumption, CO production, and CH_3OH formation for the catalyst PdZn/K under three different feed ratios: 25% CO_2 and H_2, 10% CO_2 and 90% H_2, and 2.5% CO_2 and 97.5% H_2 at the temperature of 300 (blue), 320 (green), and 340 °C (red). (Reprinted with permission from [126])

under atmospheric pressure conditions in conjunction with density functional theory (DFT) computations [127]. Under positive polarization, the methanation reaction was promoted, and the competitive RWGS reaction was impeded. On the other hand, negative polarization resulted in suppressing permanently the methanation reaction and minimally affecting the RWGS reaction. Based on DFT calculations, it was confirmed that on Ru-based catalysts, the selectivity of the reaction is not driven by the nature of the migrating species but by the induced polarization. The combination of periodic DFT and experiments showed that the relative adsorption energy of CO and CHO as a function of the electrochemical potential at the catalyst surface is key for determining the selectivity between CO and CH_4 production. In addition, free-standing Ru NPs on BZY were also investigated for the CO_2 hydrogenation reaction under atmospheric pressure conditions [128]. In that work, both methanation and RWGS reactions take place simultaneously over the Ru NPs with a superior selectivity to CO. The latter is attributed both to the spontaneous thermal migration of protons from BZY to the catalyst surface and the presence of nanosized and well-dispersed metal particles, where CO desorption (instead of its further hydrogenation) is favored. In parallel, a new chapter in EPOC phenomenon has opened by utilizing non-noble transition metal catalysts (such as Fe and Co) deposited onto solid electrolytes with oxygen ion conductivity [105, 129, 130]. In this case, upon positive

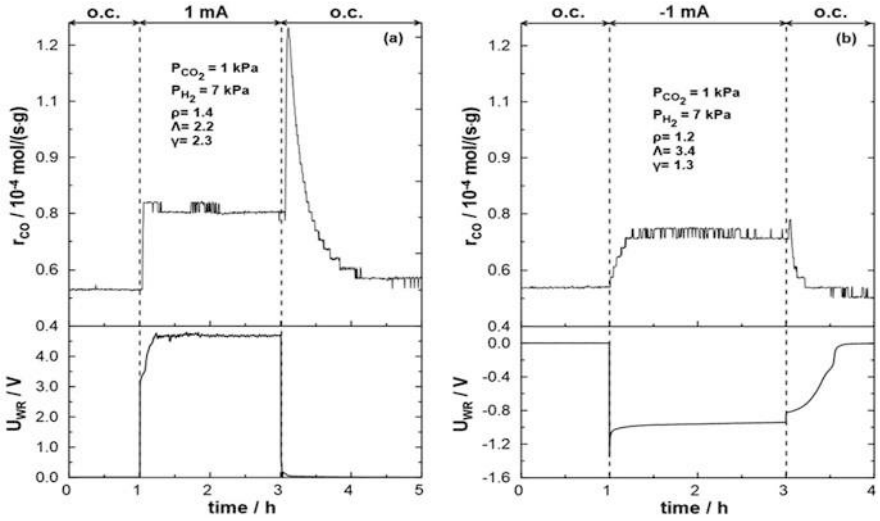

Fig. 6.20 Transient rate responses of Ru/FeOx under galvanostatic conditions at 400 °C: left hand (**a**) + 1 mA and right-hand side (**b**) −1 mA. The gas composition is indicated in each panel. $P_{H2} = 7$ kPa, $P_{CO2} = 1$ kPa, $T = 400$ °C, $F_T = 100$ cm^3/min. (Reprinted with permission from [105])

polarization, in addition to the work function and chemisorption bond strength change, oxygen ions can electro-oxidize the metal particles, thus forming in situ active metal oxides. The presence of these oxides has a beneficial impact on the RWGS activity and selectivity, whereas upon potential interruption, they can be reversibly reduced to the initial metal oxidation state. Cyclic voltammetry and ex situ XPS analysis confirmed the formation and the presence of both Fe and Co oxides during polarization, displaying two unexpected rate peaks in the rate transients. This behavior deviates from the classical electrochemical promotion behavior, where the catalytic rate after a constant potential or current application changes gradually and monotonically to a new steady-state value, while after interruption it returns to its initial value, also in a monotonous way. More specifically, in the FeO_x nanowire/YSZ system [100], the first- and the second-rate peaks are attributed to the electro-oxidation of an inactive iron carbide (i.e., FeC_x) and the subsequent change of the Fe valence state, respectively. Figure 6.20 displays the effect of reducing conditions ($CO_2/H_2 = 1{:}7$) with applied currents of 1 and − 1 mA, respectively. Figure 6.20a shows that positive current application leads to a constant increase in the CO rate with $\rho = 1.4$ and $\Lambda = 2.2$ in the new steady state. Once current is interrupted at 3 h, oxygen (from YSZ) stored in the form of FeO_x (active phase) is made available for the RWGS reaction, resulting in an increased reaction rate (i.e., rate peak) and a permanent EPOC effect (i.e., $\gamma = 2.3$) before it returns to the o.c. value. Figure 6.20b displays the transient response under negative current −1 mA, with a steady-state rate increase of 1.2 at a Λ value of 3.4, exhibiting also a slight permanent EPOC effect ($\gamma = 1.3$).

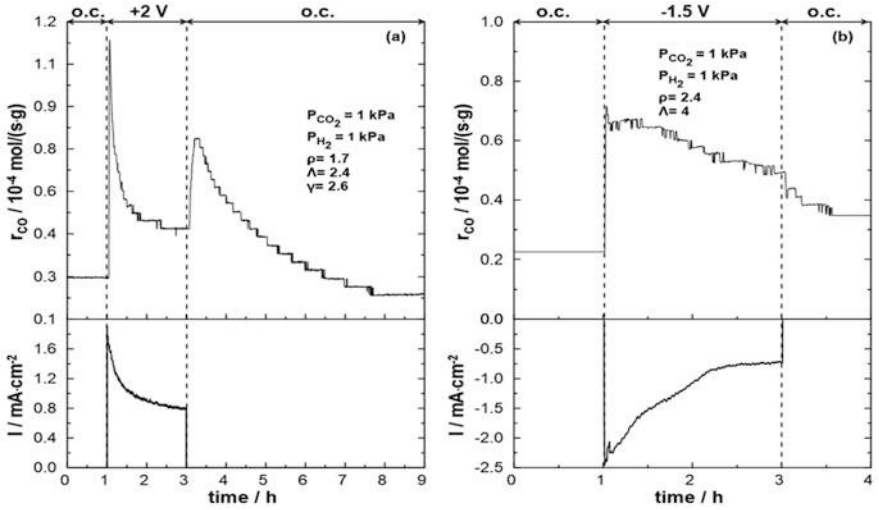

Fig. 6.21 Transient response for (**a**) + 2 V and (**b**) -1.5 V application. The lower figures show the corresponding current or potential response. P_{H2} = 1 kPa, P_{CO2} = 1 kPa, T = 335 °C, F_T = 100 cm^3/min. (Reprinted with permission from [129])

Meanwhile, the effect of adding Ru clusters to FeO_x nanowires was investigated [105]. Based on the experimental results, the presence of Ru increases the catalytic activity compared to that of the pure FeO_x nanowires, since it inhibits the formation of iron carbides, which act as a reducing component and stabilize the FeO_x active state for the RWGS reaction.

Figure 6.21a, b shows a rate increase under application of +2 V and − 1.5 V at 350 °C, respectively. Application of a positive polarization (Fig. 6.21a) leads to a rate increase (ρ_{max} = 2.6) followed by subsequent decrease and rate stabilization after 1 h. The current response mirrors the CO rate increase spike, suggesting a change in conductivity which initially increases followed by a gradual decrease as FeO_x further oxidizes. Once the potential application is interrupted, the reaction rate showed a "new promoted transient" before returning to its initial open-circuit value, similar to the FeO_x nanowire/YSZ system [129].

Negative application in Fig. 6.21b leads to the reduction of the FeO_x catalyst by forcing $O^{\delta-}$ to migrate towards the YSZ through the tpb. Thus, the catalyst is in a more reduced state, which in turn increases the cycling exchange of O originating from the dissociation of CO_2 into CO and O, overall increasing the coverage of CO_2 on the surface.

Besides, in the Co NPs/YSZ system [130], the migrating O^{2-} (from YSZ) can cause an electrochemical oxidation of Co at the tpb, affecting the ratio of the formed metal oxides (as confirmed by XPS) and thus the activity and selectivity of the RWGS reaction. Therefore, the increased activity towards the RWGS reaction can be also rationalized by the modification of the surface work function associated both with the application of a positive potential and with the presence of different oxides

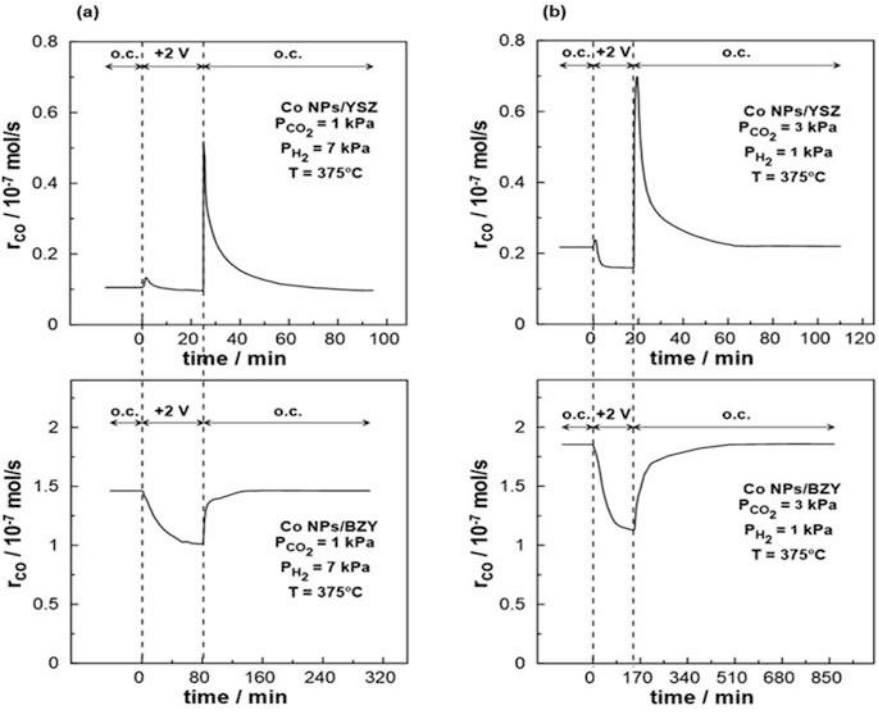

Fig. 6.22 Comparison of the transient effect of the constant applied positive (+2 V) potential on the catalytic rate of CO formation for Co NPs deposited on YSZ and BZY under (**a**) reducing and (**b**) oxidizing reaction conditions, $T = 375$ °C. (Reprinted with permission from [130])

(depending on the polarization time, current value, and reaction conditions) on the catalyst surface. To shed further light on the above interpretation and, in particular, on the electrochemical formation of cobalt oxide upon oxygen ion supply to the surface, the catalytic behavior of Co NPs on YSZ (O^{2-} conductor) was compared with that of Co NPs deposited on a proton conductor (BZY). The comparison was carried out at 375 °C both under oxidizing ($CO_2/H_2 = 3{:}1$) and reducing ($CO_2/H_2 = 1{:}7$) conditions (Fig. 6.22).

Irrespective of the reaction conditions, in the case of YSZ sample, two rate peaks are observed attributed to the oxidation state change from Co^0 to Co^{2+}, which is further oxidized to Co_3O_4, along with the modification of the catalyst work function. However, in the case of BZY conductor (i.e., when an oxygen ion conductor is not used), the observed catalytic activity was the one expected according to the kinetics of the RWGS reaction, following the well-established rules of standard chemical promotion. Thus, the observed behavior of the rate is related to the supply of oxygen ions and their interaction with the surface of the Co catalyst. Nevertheless, irrespectively of the promoting species (electropositive or electronegative), an electrophilic behavior is observed for the reaction. A similar behavior has been seen for Ni NPs on YSZ. In particular, cyclic voltammetry reveals that O^{2-} can electro-

oxidize the Ni nanoparticles leading to an enhancement of the rate of RWGS reaction up to 40% due to the in situ formation of NiO_x species. This interesting response is related to the structure of the formed catalyst nanofilm leading to an increased tpb length [131]. In short, migrating O^{2-} apart from forming the well-known "effective" double layer can also react electrochemically with the reactants, desorb as gaseous O_2, and electro-oxidize the non-noble transition metal-based electrodes. *Hence, the EPOC effect appears to be an effective tool for the in situ (re)generation of non-noble transition metal oxides, modifying both the physicochemical and the catalytic properties of metal nanoparticles*.

An interesting and novel study on electrochemical promotion of CO_2 reduction in aqueous media was published recently by Cai et al. [132]. In this study carbon dioxide was reduced to produce formate over Pd nanoparticles (NPs) in an aqueous $KHCO_3$ solution (1 M). Applying a negative potential over differently sized Pd NPs improved significantly the rate of formate production (as compared to the rate value at open-circuit), with an enhancement ratio of the rate ranging from 10 to 143. The electrocatalytic and thermocatalytic CO_2 reduction competes with one another and is promoted by introducing H_2 in the feed or applying a negative potential, respectively.

6.3.4 Electrochemical Promotion of Dispersed Catalysts

In recent years, the EPOC effect has been explored over metal-supported catalysts [103, 133]. In the first study [133], the dispersed catalyst 2% Ru/YSZ powder catalyst (prepared employing the wet impregnation method) was deposited on an YSZ solid electrolyte using a catalyst powder terpineol solution. A Ru interlayer film (between the solid electrolyte and the dispersed catalyst), with total mass of 2.5 mg, was also used to enhance the catalyst-solid electrolyte adhesion and increase the electronic conductivity of the electrode.

Four different metal loadings of Ru/YSZ catalyst, varying from 2.3 to 5.1 mg/cm^2, were studied. The experiments were carried out at a temperatures range of 280–380 °C and atmospheric pressure. Figure 6.23 depicts the effect of applied potential on the selectivity of the reaction towards CH_4 and CO at 340 °C for all samples. Positive potential favors the selectivity to methane with simultaneous decrease of the selectivity to CO. Although the selectivity to CO in the case of Ru film is very high (~65%) and that to CH_4 is low (~35%), addition of the Ru/YSZ powder leads to a decrease of the CO selectivity and to an increase of the CH_4 selectivity. In all cases, positive potential enhances methane production, whereas a negative one enhances the production of CO. Apparent Faradaic efficiencies and rate enhancement ratios of methane up to 800 and 3 were observed, respectively.

Interestingly, the authors note that the increased selectivity to methane when using the dispersed catalyst can be explained from the fact that the catalyst is already in a promoted state, due to thermal migration of the O^{2-} from the support to the Ru metallic particles. The results are in full agreement with the idea that on anionic

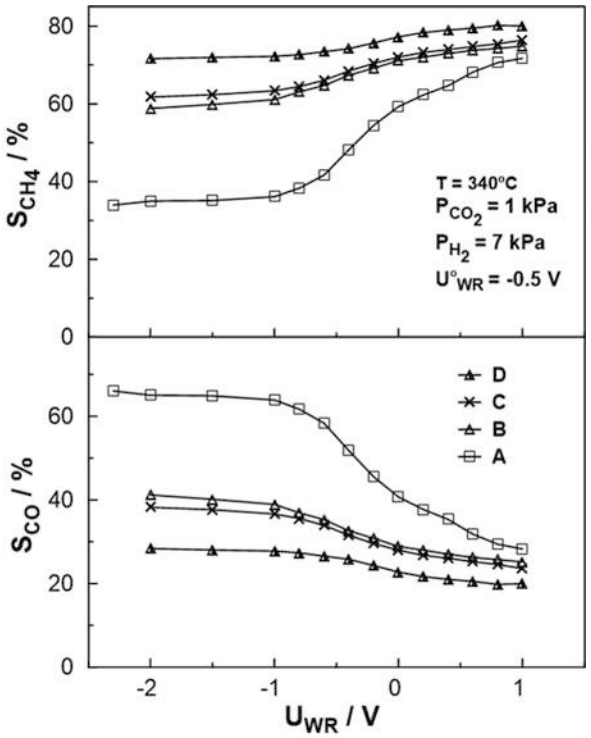

Fig. 6.23 Effect of potential on the selectivity of the products at 340 °C. A, Ru/YSZ; B, A+ 2.3 mg powder Ru/YSZ; C, A + 3 mg powder Ru/YSZ; D, A + 5.1 mg powder Ru/YSZ. $P_{H2} = 7$ kPa, $P_{CO2} = 1$ kPa, $T = 340$ °C, $F_T = 300$ cm^3/min. (Reprinted with permission from [133])

supports (such as YSZ) the metal particles are thermally "decorated" by oxygen ions (O^{2-}) which modify the chemisorptive properties of the catalysts (i.e., increasing the metal work function and thus leading to an enhancement of the CH_4 formation rate). This effect of the support on catalytic activity and/or selectivity was termed in the literature as metal-support interactions (MSI). The exact opposite behavior was observed in the case where a nanodispersed catalyst (2%Ru-15%Co supported on BZY powder) deposited on a porous Ru catalyst (interlayer) film supported on a BZY (i.e., proton conductor) disc [103]. Following exactly the same deposition technique as in Ref. [133] but using BZY both as catalytic support and solid electrolyte, experiments were performed up to 460 °C. Figure 6.24 shows the effect of dispersed Ru-Co/BZY catalyst loading and catalyst potential on the methane and CO production rate enhancement ratios under reducing reaction conditions. Interestingly, the methane rate enhancement ratio increases with dispersed catalyst loading, whereas the opposite is observed for the CO formation. In general, the higher the applied potential, the higher is the observed rate enhancement.

Figure 6.25 relates the selectivity of CO and CH_4 with the catalyst potential for various catalyst loadings. Evidently, the electrochemical promotion of the catalytic reaction has a significant impact on the selectivity of the dispersed catalyst. More specifically, varying the potential of the catalyst between 0 and + 1.5 V, the selectivity to CH_4 rises from 16% to 41%. Interestingly, a high selectivity to CO is

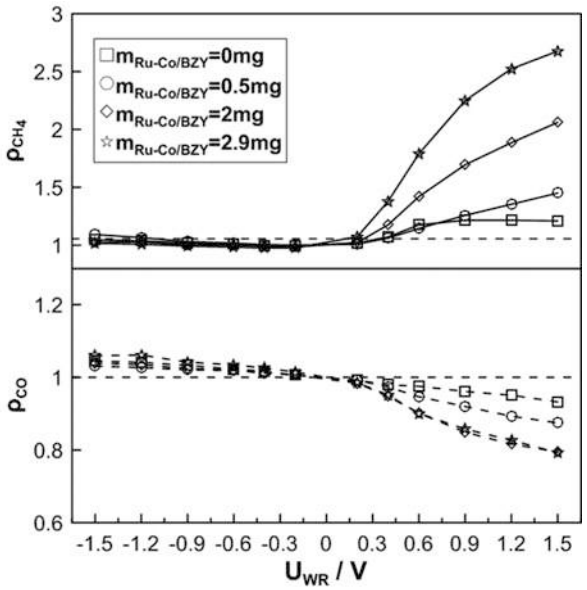

Fig. 6.24 Effect of dispersed Ru-Co/BZY catalyst loading and catalyst potential on the methane and CO production rate enhancement ratios. $P_{H2} = 7$ kPa, $P_{CO2} = 1$ kPa, $T = 450$ °C, $F_T = 200$ cm^3/min. (Reprinted with permission from [103])

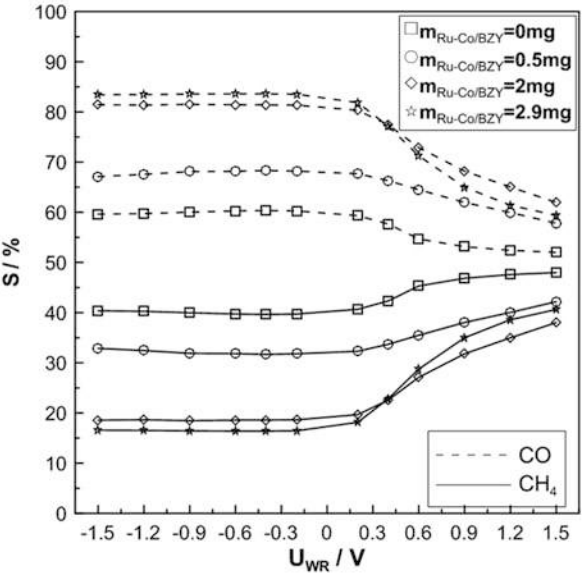

Fig. 6.25 Effect of catalyst potential and dispersed Ru-Co/BZY catalyst loading on the selectivity to CH_4 and CO. $P_{H2} = 7$ kPa, $P_{CO2} = 1$ kPa, $T = 450$ °C, $F_T = 200$ cm^3/min. (Reprinted with permission from [103])

observed when Ru is dispersed on the BZY powder. This is most likely related to the easier thermal spillover (transport) of protons on the nanoparticle surface as compared to the much higher surface area of the film. Therefore, as the catalyst loading on top of the Ru film increases, CO formation (through the RWGS) also increases leading to a higher CO selectivity. The current effect is non-Faradaic, with the

Faradaic efficiency reaching values as high as 60. Independently of the solid electrolyte utilized (BZY or YSZ), CO production is favored under negative polarization, while methane is favored under positive potentials. Subsequently, the use of a proton conductor (i.e., BZY) corresponds to negative applied potential (hence lower work function) of the catalyst, while the use of an oxygen ion conductor (i.e., YSZ) corresponds to positive applied potential (hence higher work function). Thus, it can be concluded once more that both MSI and EPOC are functionally identical and only operationally different [134, 135], since they are both related to ion spillover. Therefore, EPOC appears to be a rather valuable tool to investigate MSI effects and to guide the choice of a catalyst support.

A step forward for the practical utilization of the EPOC effect in the modern catalytic chemical industry has been achieved by using a semiconducting material (i.e., Co_3O_4) as the metal support [128]. The nanodispersed catalyst Ru/Co_3O_4 (2 wt. %) was drop-deposited directly (without the use of any conductive interlayer film as in Refs. [103, 133]) on BZY via a micropipette containing the catalyst powder-isopropanol solution resulting in 2.6 mg deposited powder mass. The observed electropromotion of the nanodispersed catalyst is non-Faradaic with apparent Faradaic efficiency values of CO reaching the value of -19 (i.e., electrophilic RWGS reaction), whereas the rate enhancement ratio remains low (i.e., $\rho_{CO} \leq 1.1$) due to enhanced thermally metal-support interactions (at $T = 400$ and 425 °C). Based on the experimental results, at low temperatures (below 350 °C), Co_3O_4 behaves like a p-type semiconductor, inhibiting electron conductivity and thus the electrochemical promotion. In contrast, at high temperatures, Co_3O_4 acts as a mixed ionic-electronic conductor for the conduction of both protons and electrons. The presence of electronic conduction activates proton migration from the BZY to the supported Ru nanoparticles (Ru NPs); thus electropromotion is allowed. The combined synergistic effect of proton and electron conductivity related to BZY and Co_3O_4, respectively, gives rise to a superior catalytic activity resulting in a "wireless" EPOC effect. It is also notable that although the $2\%Ru/Co_3O_4$ is already in a promoted state (via MSI), it can be further promoted via the EPOC effect (application of an electrical potential). In other words, *the nanodispersed catalyst, which is already promoted through the spontaneous thermal diffusion (MSI effect), can be further promoted by electrochemical means (EPOC effect) which leads to an increase of the* H^+ *surface coverage*.

6.3.5 Electrochemical Promotion in Scaled-Up Electropromoted Reactors

Although several studies in the literature report the electropromotion of the CO_2 hydrogenation reaction, nearly all of them were carried out with laboratory-scale reactors. In an attempt to scale up the EPOC effect, a monolithic electropromoted reactor (MEPR) (similar to that proposed by Balomenou et al. [136]) was used to

study the CO_2 hydrogenation reaction. The MEPR can be considered as a hybrid of a classical monolithic honeycomb reactor and a flat- or ribbed-plate solid oxide fuel cell. In contrast to the fuel cell case, where fuel and air gas streams are kept separated, in MEPR there is only one gas stream containing all reactants and products, as in a classical catalytic reactor (Fig. 6.26).

In 2009, Papaioannou et al. [137] used a monolithic electropromoted reactor (MEPR) with 22 thin Rh/YSZ/Pt or Cu/TiO_2/YSZ/Au plates in order to investigate the hydrogenation of CO_2 at atmospheric pressure, temperatures between 220 and 380 °C, and total gas flow rate equal to 1000 $cm^3 \cdot min^{-1}$. The working electrodes were deposited by magnetron sputtering of pure Rh and Cu metal targets. The utilization of Rh/YSZ/Pt cells led to CO, CH_4, and C_2H_4 formation, while both positive and negative applied potentials significantly enhance the total hydrogenation rate ($\rho_{CH4,max} \sim 6.5$, $\rho_{CO,max} \sim 7.5$, and $\rho_{C2H4,max} \sim 20$), displaying an inverted volcano behavior. Although the rate enhancement ratios were remarkable, the Faradaic efficiencies were small ($\Lambda < 1$), as well as the selectivity to CH_4 which was the main product.

In the same study, Cu/TiO_2/YSZ/Au cells were also used to explore the electrochemical promotion of the CO_2 hydrogenation reaction. TiO_2 was incorporated as an

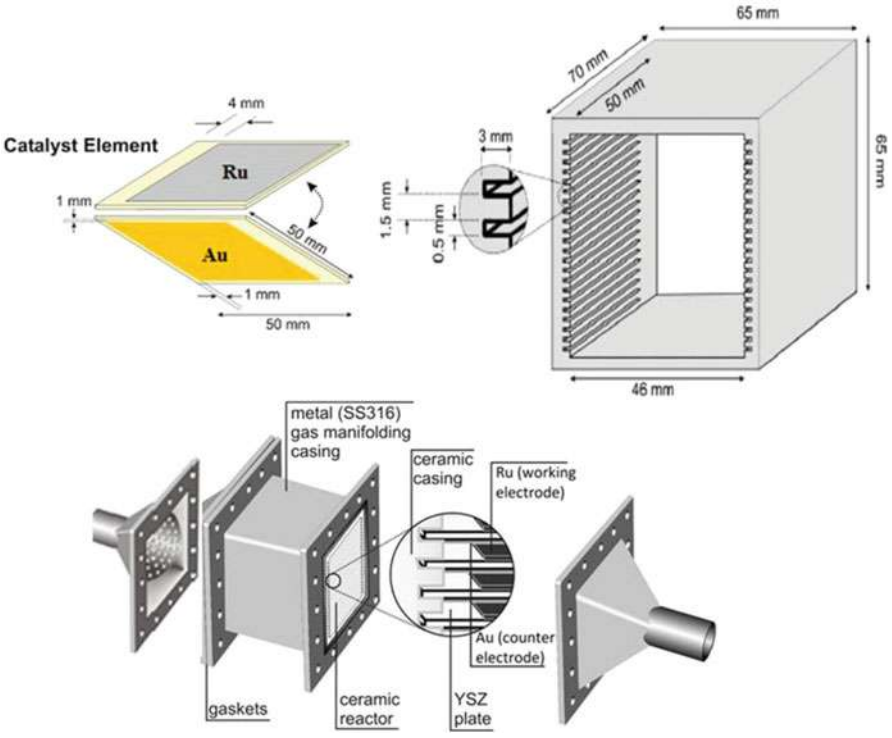

Fig. 6.26 Schematic and dimensions of the monolithic electropromoted reactor (MEPR). (Reprinted with permission from [106])

intermediate layer since Cu showed low activity and conductivity. The composite system, in addition to CO and CH_4, was also found to produce C_2H_4 with a selectivity value up to 2%. CH_4 was the dominant product with selectivity values up to 80%. Both positive and negative applied potentials significantly enhanced the hydrogenation rate, as well as the selectivity to C_2H_4. Moreover, it was also found that the addition of small (0.5 kPa) amounts of CH_3OH in the gas feed had a pronounced promotional effect on the reaction rate and on the selectivity of the $Cu/TiO_2/YSZ/Au$ cells. The presence of CH_3OH in the reaction mixture reduced the required temperature (up to 100 °C) for the selective conversion of CO_2 to CH_4 leading in almost 100% CH_4 selectivity under open-circuit and polarization conditions at temperatures between 220 and 380 °C. According to the authors, CH_3OH adsorption effectively blocks the active surface sites catalyzing the RWGS reaction and at the same time forms adsorbed intermediates favoring the Sabatier reaction.

Recently, a monolithic electropromoted reactor (MEPR) loaded with nine parallelly connected Ru/YSZ/Au electrochemical cells was used to study both the electrochemical promotion and the kinetics of the CO_2 hydrogenation reaction [96, 106]. This was the first time that a complete kinetic study of CO_2 hydrogenation reaction was carried out in a scaled-up electropromoted reactor [96]. This work showed that with increasing hydrogen partial pressure (electron donor), an increase in the production rate of methane is also observed accompanied with a simultaneous decrease in the formation of CO. The methanation reaction appears to have a positive order in hydrogen and the RWGS reaction a negative one. On the other hand, increasing the CO_2 partial pressure (electron acceptor) leads to the reverse behavior. The kinetic results together with the rules of electrochemical and chemical promotion suggest that with increasing catalyst potential an increase of the rate methanation reaction (electrophobic behavior) and a decrease of the rate of the RWGS reaction (electrophilic behavior) should be observed. The potentiostatic transient for anodic polarization (i.e., supplying O^{2-} to the surface of the catalyst) and cathodic polarization (i.e., removing O^{2-} from the surface of the catalyst) is displayed in Fig. 6.27, left [96]. The results were obtained at 370 °C with a total gas flow rate of 1000 cm^3/min and under highly reducing gas feed composition (P_{CO2}/P_{H2} = 1:10). For open-circuit conditions, the conversion of CO_2 at the beginning is approximately 34%, while after the constant application of +2.5 V, it shows an increase of up to 42%. Furthermore, a 30% enhancement of the methanation reaction is observed with the Faradaic efficiency Λ_{CH4} being equal to 4.2, which implies a non-Faradaic behavior. In contrast, the RWGS reaction is suppressed (electrophobic behavior) showing a 40% drop from the initial value of its catalytic rate. Negative polarization leads to an almost 4% decrease in the conversion of CO_2, accompanied with a 10% decrease in the methanation rate and a 70% enhancement in the rate of the RWGS reaction. Figure 6.27, right, shows the potentiostatic transient obtained at the same gas flow rate and temperature but with P_{CO2}/P_{H2} = 3:2 (oxidizing conditions) [96]. As expected, under these conditions the dominant reaction is the RWGS. Application of +2.5 V lowers the conversion of CO_2 by 0.5%. Although the rate of the methanation reaction is very low, the positive polarization enhances it by 60%, with the CO production rate being lowered by 20%.

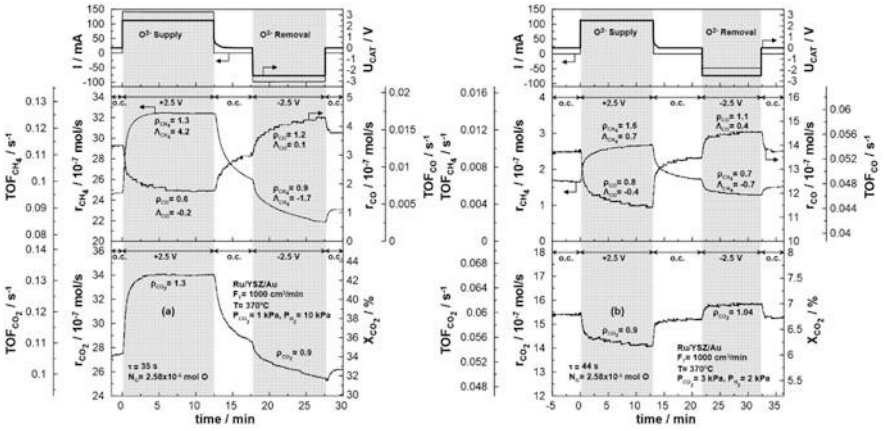

Fig. 6.27 Transient effect of constant positive (+2.5 V) and negative (−2.5 V) applied potential on the current (top), the catalytic rates and TOFs of CH_4 (middle left), CO (middle right), and CO_2 reduction (bottom left), as well as on the CO_2 conversion (bottom right). $P_{H2} = 7$ kPa, $P_{CO2} = 1$ kPa, $F_T = 1000$ cm^3/min, $T = 370$ °C. (Reprinted with permission from [96])

On the contrary, the application of a negative potential increases the rate of CO production by approximately 10% and decreases the CH_4 production by 30%. Figure 6.27 also shows the turnover frequencies (TOFs) of CH_4, CO, and CO_2. These TOFs were calculated based on catalytic rates and the calculated reactive oxygen uptake (N_G) which corresponds to the active surface area of the catalyst.

The CO and CH_4 selectivity for both open-circuit and ± 2.5 V polarization conditions as a function of temperature is displayed in Fig. 6.28. Clearly, temperatures up to 300 °C favor the methanation reaction. Despite the fact that the methane selectivity gradually reduces with temperature (down to 84% at 370 °C), it can increase up to 92% with the application of a positive polarization. In contrast, polarizing negatively leads to a reduction from 84 down to approximately 73%. As expected, the CO selectivity displays the opposite effect.

Besides, Fig. 6.29 presents the calculated yields for both methane and CO production. The maximum yield to methane (i.e., Y_{CH4}) and carbon monoxide (i.e., Y_{CO}), observed under open-circuit conditions, is 24% and 5%, respectively, at 370 °C. These values can be enhanced to 32% (Y_{CH4}, via anodic polarization) and 7% (Y_{CO}, via cathodic polarization) or decreased to 18% (Y_{CH4}, via cathodic polarization) and 3% (Y_{CO}, via anodic polarization). The qualitative features of electropromotion agreed with previous EPOC studies of CO_2 hydrogenation in laboratory-scale reactors showing a successful scale up of EPOC.

The present chapter highlights the effectiveness of electrochemical promotion of catalysis for carbon dioxide hydrogenation, a reaction of high industrial and environmental importance. Future perspectives include the utilization and electrochemical promotion of nanoparticles and/or metal oxide catalyst films in an effort to minimize the use of noble metals and to reduce the catalyst cost. Special attention should be devoted in the electrochemical promotion of catalysts that favor the

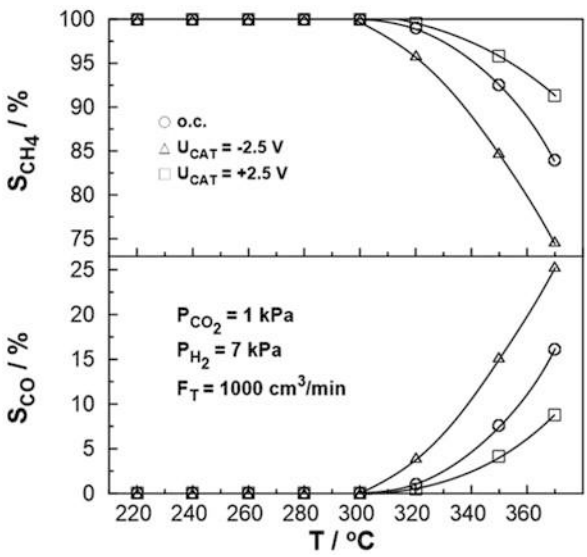

Fig. 6.28 Steady-state effect of temperature on the selectivity to CH_4 (top) and CO (bottom) under open-circuit (o.c.), positive (+2.5 V), and negative (−2.5 V) polarization. $P_{H2} = 7$ kPa, $P_{CO2} = 1$ kPa, $F_T = 1000$ cm^3/min. (Reprinted with permission from [106])

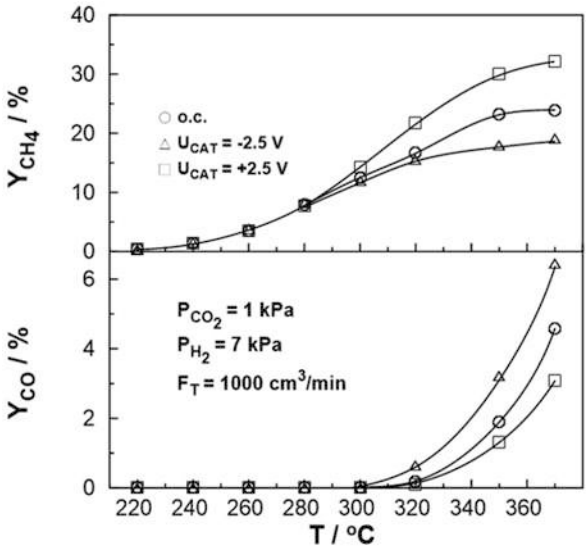

Fig. 6.29 Steady-state effect of temperature on the yields of CH_4 (top) and CO (bottom) under open-circuit (o.c.), positive (+2.5 V), and negative (−2.5 V) polarization. $P_{H2} = 7$ kPa, $P_{CO2} = 1$ kPa, $F_T = 1000$ cm^3/min. (Reprinted with permission from [106])

production of higher hydrocarbons, specific alcohols, and/or aldehydes. Application of EPOC in low-temperature liquid-phase systems is also an area of strategic importance for the future. Coupling the above catalytic technologies and hydrogen produced from renewable energy sources (e.g., via water electrolysis) presents a realistic target for CO_2 management.

6.4 Conclusions

The capture and catalytic treatment of carbon dioxide constitutes a feasible and effective solution in reducing its concentrations in the atmosphere and for climate change mitigation. The catalytic hydrogenation of carbon dioxide for the production of useful chemicals and hydrocarbons is important in terms of cyclic economy and sustainable development and offers a prospect in tackling the greenhouse effect. Electrochemical promotion of catalysis (EPOC) can contribute significantly to improving the performance of catalysts supported on solid electrolytes and more specifically to the modification and control of the catalytic activity and selectivity. A summary of the relevant literature has shown that metal catalysts based on Rh, Ru, Pd, Cu, and Co can be promoted and controlled in a reversible manner by electrochemical means to give products such as methane and carbon monoxide with significant conversions and remarkable selectivities up to 100%. Successful EPOC studies on CO_2 hydrogenation have been reported not only on conventional catalytic metal conductive films but also on metal nanoparticles or even dispersed catalysts (powders). The successful use of semi-pilot-scale monolithic electropromoted reactors seems to pave the way for the commercialization of electrochemical promotion of catalysis for the CO_2 hydrogenation reaction.

References

1. Hussain I, Jalil AA, Hassan NS, Hamid MYS (2021) Recent advances in catalytic systems for CO2 conversion to substitute natural gas (SNG): perspective and challenges. J Energy Chem 62:377–407
2. Mebrahtu C, Krebs F, Abate S, Perathoner S, Centi G, Palkovits R (2019) CO2 methanation: principles and challenges. Stud Surf Sci Catal 178:85–103. https://doi.org/10.1016/B978-0-444-64127-4.00005-7
3. Maamoun N (2019) The Kyoto protocol: empirical evidence of a hidden success. J Environ Econ Manage 95. https://doi.org/10.1016/j.jeem.2019.04.001
4. Efthymiou M, Papatheodorou A (2019) EU emissions trading scheme in aviation: policy analysis and suggestions. J Clean Prod 237. https://doi.org/10.1016/j.jclepro.2019.117734
5. HM Government (2019) The Climate Change Act 2008 (2050 Target Amendment) Order 2019
6. Department of Energy and Climate Change (2011) The Carbon Plan: delivering our low carbon future. Executive summary
7. Johnson B (2021) COP26 explained. UN climate change conference UK 2021
8. Grande CA, Roussanaly S, Anantharaman R, Lindqvist K, Singh P, Kemper J (2017) CO_2 capture in natural gas production by adsorption processes. Energy Procedia 114:2259–2264
9. Haugen HA, Eldrup NH, Fatnes AM, Leren E (2017) Commercial capture and transport of CO_2 from production of ammonia. Energy Procedia 114:6133–6140
10. Ajayi T, Gomes JS, Bera A (2019) A review of CO_2 storage in geological formations emphasizing modeling, monitoring and capacity estimation approaches. Pet Sci 16:1028–1063
11. Davies DP, Adcock PL, Turpin M, Rowen SJ (2000) Stainless steel as a bipolar plate material for solid polymer fuel cells. J Power Sources 86:237–242. https://doi.org/10.1016/S0378-7753(99)00524-8

12. Godin J, Liu W, Ren S, Xu CC (2021) Advances in recovery and utilization of carbon dioxide: a brief review. J Environ Chem Eng 9:105644. https://doi.org/10.1016/J.JECE.2021.105644
13. Kelemen P, Benson SM, Pilorgé H, Psarras P, Wilcox J (2019) An overview of the status and challenges of CO_2 storage in minerals and geological formations. Front Clim 1. https://doi.org/10.3389/fclim.2019.00009
14. Leiss W, Krewski D (2019) Environmental scan and issue awareness: risk management challenges for CCS. Int J Risk Assess Manag 22. https://doi.org/10.1504/IJRAM.2019.103340
15. Saeidi S, Najari S, Fazlollahi F, Nikoo MK, Sefidkon F, Klemeš JJ, Baxter LL (2017) Mechanisms and kinetics of CO_2 hydrogenation to value-added products: a detailed review on current status and future trends. Renew Sust Energ Rev 80:1292–1311. https://doi.org/10.1016/J.RSER.2017.05.204
16. Gao YN, Liu S, Zhao Z, Tao HC, Sun ZY (2018) Heterogeneous catalysis of CO_2 hydrogenation to C2+ products. Wuli Huaxue Xuebao/Acta Phys – Chim Sin 34:858–872
17. Zhang S, Wu Z, Liu X, Hua K, Shao Z, Wei B, Huang C, Wang H, Sun Y (2021) A short review of recent advances in direct CO2 hydrogenation to alcohols. Top Catal 64:371–394
18. Gao P, Zhang L, Li S, Zhou Z, Sun Y (2020) Novel heterogeneous catalysts for CO_2 hydrogenation to liquid fuels. ACS Cent Sci 6. https://doi.org/10.1021/acscentsci.0c00976
19. He Z, Cui M, Qian Q, Zhang J, Liu H, Han B (2019) Synthesis of liquid fuel via direct hydrogenation of CO_2. Proc Natl Acad Sci U S A 116. https://doi.org/10.1073/pnas.1821231116
20. Xu D, Wang Y, Ding M, Hong X, Liu G, Tsang SCE (2021) Advances in higher alcohol synthesis from CO_2 hydrogenation. Chem 7:849–881
21. Goeppert A, Czaun M, Surya Prakash GK, Olah GA (2012) Air as the renewable carbon source of the future: an overview of CO_2 capture from the atmosphere. Energy Environ Sci 5:7833
22. Barbarossa V, Vanga G, Viscardi R, Gattia DM (2014) CO_2 as carbon source for fuel synthesis. Energy Procedia 45:1325–1329. https://doi.org/10.1016/J.EGYPRO.2014.01.138
23. Aresta M, Dibenedetto A (2007) Utilisation of CO_2 as a chemical feedstock: opportunities and challenges. Dalton Trans. 28:2975–2992. https://doi.org/10.1039/B700658F
24. Al-Mamoori A, Krishnamurthy A, Rownaghi AA, Rezaei F (2017) Carbon capture and utilization update. Energ Technol 5:834–849
25. Jiang Z, Xiao T, Kuznetsov VL, Edwards PP (2010) Turning carbon dioxide into fuel. Philos Trans R Soc A Math Phys Eng Sci 368:3343–3364
26. Pérez-Fortes M, Bocin-Dumitriu A, Tzimas E (2014) CO_2 utilization pathways: techno-economic assessment and market opportunities. Energy Procedia 63:7968–7975
27. Younas M, Loong Kong L, Bashir MJK, Nadeem H, Shehzad A, Sethupathi S (2016) Recent advancements, fundamental challenges, and opportunities in catalytic methanation of CO_2. Energy Fuels 30:8815–8831
28. Wei J, Ge Q, Yao R, Wen Z, Fang C, Guo L, Xu H, Sun J (2017) Directly converting CO_2 into a gasoline fuel. Nat Commun 8. https://doi.org/10.1038/ncomms15174
29. Gao P, Li S, Bu X, Dang S, Liu Z, Wang H, Zhong L, Qiu M, Yang C, Cai J, Wei W, Sun Y (2017) Direct conversion of CO_2 into liquid fuels with high selectivity over a bifunctional catalyst. Nat Chem 9. https://doi.org/10.1038/nchem.2794
30. Konsolakis M, Lykaki M, Stefa S, Carabineiro SAC, Varvoutis G, Papista E, Marnellos GE (2019) CO_2 hydrogenation over nanoceria-supported transition metal catalysts: role of ceria morphology (nanorods versus nanocubes) and active phase nature (co versus cu). Nano 9. https://doi.org/10.3390/nano9121739
31. Fan WK, Tahir M (2021) Recent trends in developments of active metals and heterogenous materials for catalytic CO_2 hydrogenation to renewable methane: a review. J Environ Chem Eng 9. https://doi.org/10.1016/j.jece.2021.105460
32. Ye R, Ding J, Gong W, Argyle MD, Zhong Q, Wang Y, Russell CK, Xu Z, Russell AG, Li Q, Fan M, Yao Y (2019) CO_2 hydrogenation to high-value products via heterogeneous catalysis. Nat Commun 10:5698. https://doi.org/10.1038/s41467-019-13638-9

33. Bahmanpour AM, Signorile M, Kröcher O (2021) Recent progress in syngas production via catalytic CO_2 hydrogenation reaction. Appl Catal B Environ 295:120319. https://doi.org/10.1016/j.apcatb.2021.120319
34. Hosseini SE, Wahid MA (2016) Hydrogen production from renewable and sustainable energy resources: promising green energy carrier for clean development. Renew Sust Energ Rev 57:850–866
35. Centi G, Quadrelli EA, Perathoner S (2013) Catalysis for CO_2 conversion: a key technology for rapid introduction of renewable energy in the value chain of chemical industries. Energy Environ Sci 6:1711–1731
36. Sabatier P, Senderens JB (1902) New synthesis of methane. Comptes Rendus l'Académie des Sci Paris 134:514–516
37. González-Castaño M, Dorneanu B, Arellano-García H (2021) The reverse water gas shift reaction: a process systems engineering perspective. React Chem Eng 6:954–976
38. Kattel S, Liu P, Chen JG (2017) Tuning selectivity of CO_2 hydrogenation reactions at the metal/oxide interface. J Am Chem Soc 139:9739–9754
39. Kattel S, Yan B, Yang Y, Chen JG, Liu P (2016) Optimizing binding energies of key intermediates for CO2 hydrogenation to methanol over oxide-supported copper. J Am Chem Soc 138. https://doi.org/10.1021/jacs.6b05791
40. Tada S, Thiel I, Lo HK, Copéret C (2015) CO_2 hydrogenation: supported nanoparticles vs. immobilized catalysts. Chimia (Aarau) 69:759–764
41. Yoo JS, Abild-Pedersen F, Nørskov JK, Studt F (2014) Theoretical analysis of transition-metal catalysts for formic acid decomposition. ACS Catal 4. https://doi.org/10.1021/cs400664z
42. Baraj E, Vagaský S, Hlinčik T, Ciahotný K, Tekáč V (2016) Reaction mechanisms of carbon dioxide methanation. Chem Pap 70:395–403
43. Galadima A, Muraza O (2019) Catalytic thermal conversion of CO_2 into fuels: perspective and challenges. Renew Sust Energ Rev 115. https://doi.org/10.1016/j.rser.2019.109333
44. Borgschulte A, Gallandat N, Probst B, Suter R, Callini E, Ferri D, Arroyo Y, Erni R, Geerlings H, Züttel A (2013) Sorption enhanced CO_2 methanation. Phys Chem Chem Phys 15. https://doi.org/10.1039/c3cp51408k
45. Westermann A, Azambre B, Bacariza MC, Graça I, Ribeiro MF, Lopes JM, Henriques C (2015) Insight into CO_2 methanation mechanism over NiUSY zeolites: an operando IR study. Appl Catal B Environ 174–175:120–125. https://doi.org/10.1016/j.apcatb.2015.02.026
46. Prairie MR, Renken A, Highfield JG, Ravindranathan Thampi K, Grätzel M (1991) A fourier transform infrared spectroscopic study of CO_2 methanation on supported ruthenium. J Catal 129:130–144. https://doi.org/10.1016/0021-9517(91)90017-X
47. Marwood M, Doepper R, Renken A (1997) In-situ surface and gas phase analysis for kinetic studies under transient conditions: the catalytic hydrogenation of CO_2. Appl Catal A Gen 151:223–246. https://doi.org/10.1016/S0926-860X(96)00267-0
48. Schild C, Wokaun A, Koeppel RA, Baiker A (1991) CO_2 hydrogenation over nickel/zirconia catalysts from amorphous precursors: on the mechanism of methane formation. J Phys Chem 95:6341–6346. https://doi.org/10.1021/j100169a049
49. Panagiotopoulou P, Kondarides DI, Verykios XE (2011) Mechanistic study of the selective methanation of CO over Ru/TiO_2 catalyst: identification of active surface species and reaction pathways. J Phys Chem C 115:1220–1230. https://doi.org/10.1021/jp106538z
50. Beuls A, Swalus C, Jacquemin M, Heyen G, Karelovic A, Ruiz P (2012) Methanation of CO_2: further insight into the mechanism over $Rh/\gamma\text{-}Al_2O_3$ catalyst. Appl Catal B Environ 113–114:2–10. https://doi.org/10.1016/j.apcatb.2011.02.033
51. Kattel S, Yu W, Yang X, Yan B, Huang Y, Wan W, Liu P, Chen JG (2016) CO_2 hydrogenation over oxide-supported PtCo catalysts: the role of the oxide support in determining the product selectivity. Angew Chem Int Ed 55. https://doi.org/10.1002/anie.201601661
52. Ye J, Liu CJ, Mei D, Ge Q (2014) Methanol synthesis from CO_2 hydrogenation over a Pd4/In2O3 model catalyst: a combined DFT and kinetic study. J Catal 317:44–53. https://doi.org/10.1016/J.JCAT.2014.06.002

53. Studt F, Sharafutdinov I, Abild-Pedersen F, Elkjær CF, Hummelshøj JS, Dahl S, Chorkendorff I, Nørskov JK (2014) Discovery of a Ni-Ga catalyst for carbon dioxide reduction to methanol. Nat Chem 6. https://doi.org/10.1038/nchem.1873
54. Zhao YF, Yang Y, Mims C, Peden CHF, Li J, Mei D (2011) Insight into methanol synthesis from CO_2 hydrogenation on Cu(1 1 1): complex reaction network and the effects of H2O. J Catal 281. https://doi.org/10.1016/j.jcat.2011.04.012
55. Kattel S, Yan B, Chen JG, Liu P (2016) CO_2 hydrogenation on Pt, Pt/SiO_2 and Pt/TiO_2: importance of synergy between Pt and oxide support. J Catal 343:115–126. https://doi.org/10.1016/j.jcat.2015.12.019
56. Koeppel RA, Baiker A, Wokaun A (1992) Copper/zirconia catalysts for the synthesis of methanol from carbon dioxide. Influence of preparation variables on structural and catalytic properties of catalysts. Appl Catal A Gen 84. https://doi.org/10.1016/0926-860X(92)80340-I
57. Lei H, Nie R, Wu G, Hou Z (2015) Hydrogenation of CO_2 to CH_3OH over Cu/ZnO catalysts with different ZnO morphology. Fuel 154. https://doi.org/10.1016/j.fuel.2015.03.052
58. Zhou B, Ou P, Pant N, Cheng S, Vanka S, Chu S, Rashid RT, Botton G, Song J, Mi Z (2020) Highly efficient binary copper iron catalyst for photoelectrochemical carbon dioxide reduction toward methane. Proc Natl Acad Sci U S A 117. https://doi.org/10.1073/pnas.1911159117
59. Shen L, Xu J, Zhu M, Han YF (2020) Essential role of the support for nickel-based CO_2 methanation catalysts. ACS Catal 10. https://doi.org/10.1021/acscatal.0c03471
60. Bacariza MC, Spataru D, Karam L, Lopes JM, Henriques C (2020) Promising catalytic systems for CO_2 hydrogenation into CH_4: a review of recent studies. PRO 8:1646
61. Chai S, Men Y, Wang J, Liu S, Song Q, An W, Kolb G (2019) Boosting CO_2 methanation activity on Ru/TiO_2 catalysts by exposing (001) facets of anatase TiO2. J CO2 Util 33. https://doi.org/10.1016/j.jcou.2019.05.031
62. Panagiotopoulou P (2017) Hydrogenation of CO2 over supported noble metal catalysts. Appl Catal A Gen 542:63–70. https://doi.org/10.1016/j.apcata.2017.05.026
63. Wang W, Wang S, Ma X, Gong J (2011) Recent advances in catalytic hydrogenation of carbon dioxide. Chem Soc Rev 40:3703–3727
64. Lin Q, Liu XY, Jiang Y, Wang Y, Huang Y, Zhang T (2014) Crystal phase effects on the structure and performance of ruthenium nanoparticles for CO_2 hydrogenation. Cat Sci Technol 4. https://doi.org/10.1039/c4cy00030g
65. Karelovic A, Ruiz P (2013) Mechanistic study of low temperature CO_2 methanation over Rh/TiO2 catalysts. J Catal 301. https://doi.org/10.1016/j.jcat.2013.02.009
66. Solymosi F, Erdöhelyi A, Bánsági T (1981) Methanation of CO_2 on supported rhodium catalyst. J Catal 68:371–382. https://doi.org/10.1016/0021-9517(81)90106-8
67. Martin NM, Velin P, Skoglundh M, Bauer M, Carlsson PA (2017) Catalytic hydrogenation of CO_2 to methane over supported Pd, Rh and Ni catalysts. Cat Sci Technol 7. https://doi.org/10.1039/c6cy02536f
68. Sreedhar I, Varun Y, Singh SA, Venugopal A, Reddy BM (2019) Developmental trends in CO_2 methanation using various catalysts. Cat Sci Technol 9. https://doi.org/10.1039/c9cy01234f
69. Puigdollers AR, Schlexer P, Tosoni S, Pacchioni G (2017) Increasing oxide reducibility: the role of metal/oxide interfaces in the formation of oxygen vacancies. ACS Catal 7:6493–6513
70. Porosoff MD, Chen JG (2013) Trends in the catalytic reduction of CO_2 by hydrogen over supported monometallic and bimetallic catalysts. J Catal 301. https://doi.org/10.1016/j.jcat.2013.01.022
71. Fujita SI, Usui M, Takezawa N (1992) Mechanism of the reverse water gas shift reaction over Cu/ZnO catalyst. J Catal 134. https://doi.org/10.1016/0021-9517(92)90223-5
72. Matsubu JC, Yang VN, Christopher P (2015) Isolated metal active site concentration and stability control catalytic CO_2 reduction selectivity. J Am Chem Soc 137. https://doi.org/10.1021/ja5128133

73. Porosoff MD, Yang X, Boscoboinik JA, Chen JG (2014) Molybdenum carbide as alternative catalysts to precious metals for highly selective reduction of CO_2 to CO. Angew Chem Int Ed 53. https://doi.org/10.1002/anie.201404109
74. Saeidi S, Najari S, Hessel V, Wilson K, Keil FJ, Concepción P, Suib SL, Rodrigues AE (2021) Recent advances in CO_2 hydrogenation to value-added products — current challenges and future directions. Prog Energy Combust Sci 85:100905–100969. https://doi.org/10.1016/j.pecs.2021.100905
75. Bansode A, Urakawa A (2014) Towards full one-pass conversion of carbon dioxide to methanol and methanol-derived products. J Catal 309. https://doi.org/10.1016/j.jcat.2013.09.005
76. Ruland H, Song H, Laudenschleger D, Stürmer S, Schmidt S, He J, Kähler K, Muhler M, Schlögl R (2020) CO_2 hydrogenation with $Cu/ZnO/Al_2O_3$: a benchmark study. ChemCatChem 12. https://doi.org/10.1002/cctc.202000195
77. Sun K, Fan Z, Ye J, Yan J, Ge Q, Li Y, He W, Yang W, Liu CJ (2015) Hydrogenation of CO2 to methanol over In2O3 catalyst. J CO2 Util 12. https://doi.org/10.1016/j.jcou.2015.09.002
78. Stoukides M, Vayenas CG (1981) The effect of electrochemical oxygen pumping on the rate and selectivity of ethylene oxidation on polycrystalline silver. J Catal 70:137–146. https://doi.org/10.1016/0021-9517(81)90323-7
79. Vayenas CG, Bebelis S, Ladas S (1990) Dependence of catalytic rates on catalyst work function. Nature 343:625–627. https://doi.org/10.1038/343625a0
80. Vayenas CG, Bebelis S, Yentekakis IV, Tsiakaras P, Karasali H (1990) Non-faradaic electrochemical modification of catalytic activity reversible promotion of platinum metals catalysts. Platin Met Rev 34:122–130
81. Vayenas CG, Neophytides S (1991) Non-faradaic electrochemical modification of catalytic activity III. The case of methanol oxidation on Pt. J Catal 127:645–664. https://doi.org/10.1016/0021-9517(91)90189-B
82. Anastasijevic NA, Baltruschat H, Heitbaum J (1993) On the hydrogen evolution during the electrochemical oxidation of aldehydes at Ib metals. Electrochim Acta 38:1067–1072. https://doi.org/10.1016/0013-4686(93)80214-K
83. Belyaev VD, Politova TI, Sobyanin VA (2000) Effect of non-faradaic electrochemical modification of catalytic activity. Solid State Ionics 136–137:721–725. https://doi.org/10.1016/S0167-2738(00)00501-4
84. Vayenas CG, Bebelis S, Despotopoulou M (1991) Non-faradaic electrochemical modification of catalytic activity 4. The use of β″-Al2O3 as the solid electrolyte. J Catal 128. https://doi.org/10.1016/0021-9517(91)90300-S
85. Baltruschat H, Anastasijevic NA, Beltowska-Brzezinska M, Hambitzer G, Heitbaum J (1990) Electrochemical detection of organic gases. The development of a formaldehyde sensor. Berichte der Bunsengesellschaft/Phys Chem Chem Phys 94. https://doi.org/10.1002/bbpc.19900940923
86. Tsiakaras P, Vayenas CG (1993) Non-faradaic electrochemical modification of catalytic activity: VII. The case of methane oxidation on platinum. J Catal 140:53–70. https://doi.org/10.1006/JCAT.1993.1068
87. Neophytides SG, Tsiplakides D, Stonehart P, Jaksic MM, Vayenas CG (1994) Electrochemical enhancement of a catalytic reaction in aqueous solution. Nature 370:45–47. https://doi.org/10.1038/370045a0
88. Makri M, Vayenas GG, Bebelis S, Besocke KH, Cavalca C (1996) Atomic resolution STM imaging of electrochemically controlled reversible promoter dosing of catalysts. Surf Sci 369:351–359. https://doi.org/10.1016/S0039-6028(96)00911-9
89. Ladas S, Bebelis S, Vayenas CG (1991) Work function measurements on catalyst films subject to in situ electrochemical promotion. Surf Sci Lett 251–252. https://doi.org/10.1016/0167-2584(91)91023-p

90. Yiokari CG, Pitselis GE, Polydoros DG, Katsaounis AD, Vayenas CG (2000) High-pressure electrochemical promotion of ammonia synthesis over an industrial iron catalyst. J Phys Chem A 104:10600–10602. https://doi.org/10.1021/jp002236v
91. Constantinou I, Bolzonella I, Pliangos C, Comninellis C, Vayenas CG (2005) Electrochemical promotion of RuO2 catalysts for the combustion of toluene and ethylene. Catal Lett 100. https://doi.org/10.1007/s10562-004-3440-y
92. Koutsodontis C, Katsaounis A, Figueroa JC, Cavalca C, Pereira C, Vayenas CG (2006) The effect of catalyst film thickness on the electrochemical promotion of ethylene oxidation on Pt. Top Catal 39. https://doi.org/10.1007/s11244-006-0042-5
93. de Lucas-Consuegra A, Dorado F, Valverde JL, Karoum R, Vernoux P (2008) Electrochemical activation of Pt catalyst by potassium for low temperature CO deep oxidation. Catal Commun 9:17–20. https://doi.org/10.1016/j.catcom.2007.04.038
94. de Lucas-Consuegra A, Princivalle A, Caravaca A, Dorado F, Guizard C, Valverde JL, Vernoux P (2010) Preferential CO oxidation in hydrogen-rich stream over an electrochemically promoted Pt catalyst. Appl Catal B Environ 94:281–287. https://doi.org/10.1016/j.apcatb.2009.11.019
95. Vayenas CG, Lambert RM, Ladas S, Bebelis S, Neophytides S, Tikhov MS, Filkin NC, Makri M, Tsiplakides D, Cavalca C, Besocke K (1997) Direct STM, XPS and TPD observation of spillover phenomena over mm distances on metal catalyst films interfaced with solid electrolytes. In: Studies in surface science and catalysis, Elsevier, pp 39–47. https://doi.org/10.1016/S0167-2991(97)80822-1
96. Chatzilias C, Martino E, Tsatsos S, Kyriakou G, Katsaounis A, Vayenas CG (2022) Kinetic study of CO2 hydrogenation on Ru/ YSZ catalyst using a monolithic electropromoted reactor (MEPR). Chem Eng J 430. https://doi.org/10.1016/j.cej.2021.132967
97. Neophytides SG, Tsiplakides D, Vayenas CG (1998) Temperature-programmed desorption of oxygen from Pt films interfaced with Y2O3-doped ZrO2. J Catal 178:414–428. https://doi.org/10.1006/jcat.1998.2155
98. Vayenas CG, Bebelis S, Pliangos C, Brosda S, Tsiplakides D (2001) Electrochemical activation of catalysis: promotion, electrochemical promotion and metal-support interactions. Kluwer Academic/Plenum Publishers, New York
99. Ouzounidou M, Skodra A, Kokkofitis C, Stoukides M (2007) Catalytic and electrocatalytic synthesis of NH3 in a H+ conducting cell by using an industrial Fe catalyst. Solid State Ionics 178:153–159. https://doi.org/10.1016/j.ssi.2006.11.019
100. Theleritis D, Souentie S, Siokou A, Katsaounis A, Vayenas CG (2012) Hydrogenation of CO 2 over Ru/YSZ electropromoted catalysts. ACS Catal 2:770–780. https://doi.org/10.1021/cs300072a
101. Theleritis D, Makri M, Souentie S, Caravaca A, Katsaounis A, Vayenas CG (2014) Comparative study of the electrochemical promotion of CO2 hydrogenation over Ru-supported catalysts using electronegative and electropositive promoters. ChemElectroChem 1:254–262. https://doi.org/10.1002/celc.201300185
102. Kalaitzidou I, Makri M, Theleritis D, Katsaounis A, Vayenas CG (2016) Comparative study of the electrochemical promotion of CO2 hydrogenation on Ru using Na+, K+, H+ and O2- conducting solid electrolytes. Surf Sci 646:194–203. https://doi.org/10.1016/j.susc.2015.09.011
103. Kotsiras A, Kalaitzidou I, Grigoriou D, Symillidis A, Makri M, Katsaounis A, Vayenas CG (2018) Electrochemical promotion of nanodispersed Ru-Co catalysts for the hydrogenation of CO2. Appl Catal B Environ 232:60–68. https://doi.org/10.1016/j.apcatb.2018.03.031
104. Hajar YM, Venkatesh B, Houache MSE, Liu H, Safari R, Prabhudev S, Botton GA, Baranova EA (2019) Electrochemical promotion of Bi-metallic Ni9Pd core double-shell nanoparticles for complete methane oxidation. J Catal 374:127–135. https://doi.org/10.1016/j.jcat.2019.04.026

105. Panaritis C, Zgheib J, Couillard M, Baranova EA (2020) The role of Ru clusters in Fe carbide suppression for the reverse water gas shift reaction over electropromoted Ru/FeOx catalysts. Electrochem Commun 119:106824. https://doi.org/10.1016/j.elecom.2020.106824
106. Chatzilias C, Martino E, Katsaounis A, Vayenas CG (2021) Electrochemical promotion of CO2 hydrogenation in a monolithic electrochemically promoted reactor (MEPR). Appl Catal B Environ 284:119695. https://doi.org/10.1016/j.apcatb.2020.119695
107. Nicole J, Comninellis C, Tsiplakides D, Pliangos C, Verykios XE, Vayenas CG (2001) Electrochemical promotion and metal-support interactions. J Catal 204:23–34. https://doi.org/10.1006/jcat.2001.3360
108. Hajar YM, Patel KD, Tariq U, Baranova EA (2017) Functional equivalence of electrochemical promotion and metal support interaction for Pt and RuO2 nanoparticles. J Catal 352:42–51. https://doi.org/10.1016/j.jcat.2017.05.001
109. Panaritis C, Edake M, Couillard M, Einakchi R, Baranova EA (2018) Insight towards the role of ceria-based supports for reverse water gas shift reaction over RuFe nanoparticles. J CO2 Util 26:350–358. https://doi.org/10.1016/j.jcou.2018.05.024
110. Vayenas CG (2013) Promotion, electrochemical promotion and metal-support interactions: their common features. Catal Lett 143:1085–1097. https://doi.org/10.1007/s10562-013-1128-x
111. Vayenas CG, Brosda S (2014) Electron donation-backdonation and the rules of catalytic promotion. Top Catal 57:1287–1301. https://doi.org/10.1007/s11244-014-0294-4
112. Vernoux P, Lizarraga L, Tsampas MN, Sapountzi FM, De Lucas-Consuegra A, Valverde JL, Souentie S, Vayenas CG, Tsiplakides D, Balomenou S, Baranova EA (2013) Ionically conducting ceramics as active catalyst supports. Chem Rev 113:8192–8260. https://doi.org/10.1021/cr4000336
113. Katsaounis A (2010) Recent developments and trends in the electrochemical promotion of catalysis (EPOC). J Appl Electrochem 40:885–902
114. Vayenas CG, Brosda S, Pliangos C (2001) Rules and mathematical modeling of electrochemical and chemical promotion: 1. Reaction classification and promotional rules. J Catal 203:329–350. https://doi.org/10.1006/jcat.2001.3348
115. Brosda S, Vayenas CG (2002) Rules and mathematical modeling of electrochemical and classical promotion: 2. Modeling J Catal 208:38–53. https://doi.org/10.1006/jcat.2002.3549
116. Brosda S, Vayenas CG, Wei J (2006) Rules of chemical promotion. Appl Catal B Environ 68:109–124. https://doi.org/10.1016/j.apcatb.2006.07.021
117. Marwood M, Kaloyannis A, Vayen CG (1996) Electrochemical promotion of the NO reduction by C2H4 on Pt/YSZ and by CO on Pd/YSZ. Ionics 2:302–311
118. Bebelis S, Karasali H, Vayenas CG (2008) Electrochemical promotion of the CO2hydrogenation on Pd/YSZ and Pd/β″-Al2O3catalyst-electrodes. Solid State Ionics 179:1391–1395. https://doi.org/10.1016/j.ssi.2008.02.043
119. Bebelis S, Karasali H, Vayenas CG (2008) Electrochemical promotion of CO2 hydrogenation on Rh/YSZ electrodes. J Appl Electrochem 38:1127–1133. https://doi.org/10.1007/s10800-008-9574-7
120. Pacchioni G, Illas F, Neophytides S, Vayenas CG (1996) Quantum-chemical study of electrochemical promotion in catalysis. J Phys Chem 100:16653–16661. https://doi.org/10.1021/jp9612386
121. Bebelis S, Karasali H, Vayenas CG (2008) Electrochemical promotion of the CO2 hydrogenation on Pd/YSZ and Pd/β″-Al2O3 catalyst-electrodes. Solid State Ionics 179:1391–1395. https://doi.org/10.1016/j.ssi.2008.02.043
122. Jiménez V, Jiménez-Borja C, Sánchez P, Romero A, Papaioannou EI, Theleritis D, Souentie S, Brosda S, Valverde JL (2011) Electrochemical promotion of the co2 hydrogenation reaction on composite ni or ru impregnated carbon nanofiber catalyst-electrodes deposited on YSZ. Appl Catal B Environ 107:210–220. https://doi.org/10.1016/j.apcatb.2011.07.016

123. Theleritis D, Souentie S, Siokou A, Katsaounis A, Vayenas CG (2012) Hydrogenation of CO2 over Ru/YSZ electropromoted catalysts. ACS Catal 2:770–780. https://doi.org/10.1021/cs300072a
124. Makri M, Katsaounis A, Vayenas CG (2015) Electrochemical promotion of CO2 hydrogenation on Ru catalyst-electrodes supported on a K-β″-Al2O3 solid electrolyte. Electrochim Acta 179:556–564. https://doi.org/10.1016/j.electacta.2015.03.144
125. Kalaitzidou I, Katsaounis A, Norby T, Vayenas CG (2015) Electrochemical promotion of the hydrogenation of CO2 on Ru deposited on a BZY proton conductor. J Catal 331:98–109. https://doi.org/10.1016/j.jcat.2015.08.023
126. Díez-Ramírez J, Sánchez P, Valverde JL, Dorado F (2016) Electrochemical promotion and characterization of PdZn alloy catalysts with K and Na ionic conductors for pure gaseous CO2 hydrogenation. J CO2 Util 16. https://doi.org/10.1016/j.jcou.2016.09.007
127. Panaritis C, Michel C, Couillard M, Baranova EA, Steinmann SN (2020) Elucidating the role of electrochemical polarization on the selectivity of the CO2 hydrogenation reaction over Ru. Electrochim Acta 350:136405. https://doi.org/10.1016/j.electacta.2020.136405
128. Zagoraios D, Panaritis C, Krassakopoulou A, Baranova EA, Katsaounis A, Vayenas CG (2020) Electrochemical promotion of Ru nanoparticles deposited on a proton conductor electrolyte during CO2 hydrogenation. Appl Catal B Environ 276:119148. https://doi.org/10.1016/j.apcatb.2020.119148
129. Panaritis C, Zgheib J, Ebrahim SAH, Couillard M, Baranova EA (2020) Electrochemical in-situ activation of Fe-oxide nanowires for the reverse water gas shift reaction. Appl Catal B Environ 269:118826. https://doi.org/10.1016/j.apcatb.2020.118826
130. Zagoraios D, Tsatsos S, Kennou S, Vayenas CG, Kyriakou G, Katsaounis A (2020) Tuning the RWGS reaction via EPOC and in situ electro-oxidation of cobalt nanoparticles. ACS Catal. 10:14916–14927. https://doi.org/10.1021/acscatal.0c04133
131. Zagoraios D, Kyriakou G, Katsaounis A (2021) Electrochemical control of the RWGS reaction over Ni nanoparticles deposited on yttria stabilized zirconia. Submitted Publication
132. Cai F, Gao D, Zhou H, Wang G, He T, Gong H, Miao S, Yang F, Wang J, Bao X (2017) Electrochemical promotion of catalysis over Pd nanoparticles for CO2 reduction. Chem Sci 8:2569–2573. https://doi.org/10.1039/c6sc04966d
133. Makri M, Symillidis A, Grigoriou D, Katsaounis A, Vayenas CG (2018) Electrochemical promotion of CO2 reduction on a dispersed Ru/YSZ catalyst supported on YSZ solid electrolyte. Mater Today Proc 5:27617–27625. https://doi.org/10.1016/J.MATPR.2018.09.082
134. Vayenas CG, Brosda S, Pliangos C (2003) The double-layer approach to promotion, electrocatalysis, electrochemical promotion, and metal–support interactions. J Catal 216:487–504. https://doi.org/10.1016/S0021-9517(02)00127-6
135. Grigoriou D, Zagoraios D, Katsaounis A, Vayenas CG (2021) The role of the promoting ionic species in electrochemical promotion and in metal-support interactions. Catal Today 363:122–127. https://doi.org/10.1016/J.CATTOD.2019.08.024
136. Balomenou S, Tsiplakides D, Katsaounis A, Thiemann-Handler S, Cramer B, Foti G, Comninellis C, Vayenas CG (2004) Novel monolithic electrochemically promoted catalytic reactor for environmentally important reactions. Appl Catal B Environ 52:181–196. https://doi.org/10.1016/j.apcatb.2004.04.007
137. Papaioannou EI, Souentie S, Hammad A, Vayenas CG (2009) Electrochemical promotion of the CO2 hydrogenation reaction using thin Rh, Pt and Cu films in a monolithic reactor at atmospheric pressure. Catal Today 146:336–344. https://doi.org/10.1016/j.cattod.2009.06.008

Part IV
EPOC to Accelerate the Energy Transition

Chapter 7
Recent Studies of Electrochemical Promotion for H_2 Production from Ethanol

Estela Ruiz-López, Fernando Dorado, and Antonio de Lucas-Consuegra

Abstract The incessant growth in global energy demand joint to the finite character of traditional energy sources and their associated greenhouse emissions has led to an energy crisis that could only be solved by changing the actual energy system. Green hydrogen could be a platform molecule to electrify and decarbonize the system, linking different energy sectors while increasing their operational flexibility. This chapter reviews the latest advances on hydrogen generation from ethanol via application of the phenomenon of electrochemical promotion of catalysis (EPOC). Due to the well-known promotional effects of alkali metals in heterogeneous catalysts for reforming and partial oxidation reactions, our investigations focused on the use of K-βAl_2O_3 solid electrolyte as the electro-active support of a Pt catalyst. The supply of K^+ under negative polarization steps strongly increased hydrogen production rates showing a reversible and controllable promotional effect in all cases. Comparing the three atmospheres (reforming, partial oxidation, and autothermal reforming) under EPOC conditions, it seems that autothermal reforming is the most suitable one. It combines both reaction routes achieving a compromise between hydrogen production and catalyst stability. All these results demonstrated the interest of the phenomenon application in ethanol conversion reactions, improving hydrogen production as well as catalyst stability.

Keywords Electrochemical promotion of catalysis · Hydrogen production · Ethanol

7.1 Introduction

The excessive consumption and depletion of fossil fuels have led to an atmospheric CO_2 level higher than 400 ppm [1], exceeding the safety limit estimated at 350 ppm [2]. Consequently, all attention is currently focused on the search for solutions to

E. Ruiz-López · F. Dorado · A. de Lucas-Consuegra (✉)
Department of Chemical Engineering, School of Chemical Sciences and Technologies, University of Castilla-La Mancha, Ciudad Real, Spain
e-mail: Fernando.Dorado@uclm.es; Antonio.LConsuegra@uclm.es

P. Vernoux, C. G. Vayenas (eds.), *Recent Advances in Electrochemical Promotion of Catalysis*, Modern Aspects of Electrochemistry 61,
https://doi.org/10.1007/978-3-031-13893-5_7

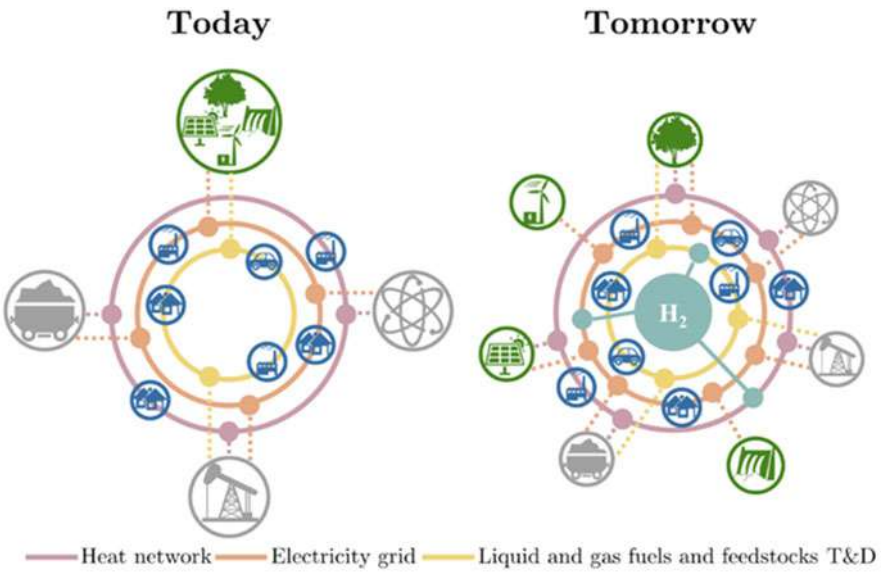

Fig. 7.1 Energy system today and in the future. (Adapted with permission from Ref. [11]. Copyright © 2020 Hydrogen TCP)

control and mitigate CO_2 emissions – solutions that imply a new energy system with an increase in electricity as an end-use energy and an encouragement in the use, implantation, and development of renewable sources to generate the mentioned electricity.

In the latest years, hydrogen generated from green sources has awaken interest as an efficient strategy to achieve the electrification and the decarbonization of the energy system. Hydrogen could link different energy sectors and networks and thus increase the operational flexibility of the future systems (as shown in Fig. 7.1).

Hydrogen, the most abundant but not directly available element, possesses higher energy content by weight than the rest of conventional fuels [3]. It is a versatile carrier that can be generated from a wide variety of sources and with a large flexibility in terms of conversion and storage methods [4].

In general terms, hydrogen can be produced from fossil fuels, biomass, or water. Biomass is able to produce it through several processes such as reforming, pyrolysis, gasification, or fermentation. Hydrogen from biomass is one of the most considerable sustainable resources since energy crops, agricultural residue and waste, forestry residue and waste, and industrial and community waste can be used as raw materials [5]. Biological hydrogen produced from biomass is especially appealing since these processes can be conducted at ambient temperature and pressure requiring less energy [6].

Water splitting processes such as electrolysis, thermolysis, or photo-electrolysis are also remarkable options to generate hydrogen since water is an abundant and inexhaustible compound [7]. Renewable energy sources could be coupled with these

processes, generating a totally free of CO_2 emission hydrogen. Among them, electrolysis is an established and well-known method, it is the most efficient process for water splitting, and it has been widely explored. Nonetheless, due to its high endothermicity, it is a high energy-demanding process that leads to high production costs [5]. Depending on the type and the number of hours of utilization of the electrolyzer, the cost of hydrogen production can oscillate in a range of 10 €/kg (utilization <1000 h) to 2–6 €/kg (utilization of 3000–4000 h), although none of them are competitive or commercially acceptable costs nowadays [8].

Currently, and despite all possibilities, around a 96% of hydrogen is produced from fossil fuels [5], being the most common routes coal gasification, hydrocarbon pyrolysis, and hydrocarbon reforming. These production methods are the most developed, used in industry, and least costly. The production costs without considering transport and distribution of these mature technologies are below 100 USD/MWh, much lower than those for electrolysis which are close to 200 USD/MWh [9]. However, the idea of a decarbonized system using hydrogen produced from fossil fuel seems contradictory. For that reason, the use of oxygenated liquid compounds obtained from renewable sources such as bioalcohols in these systems is encouraged.

Biomass-derived organic molecules such as bioalcohols are stable hydrogen-rich molecules that can be considered as a resource for hydrogen production from multiple methods including biological, thermal, or electrochemical systems [10].

Alcohols such as methanol, ethanol, or glycerol are able to replace methane in reforming and partial oxidation processes, turning them into more environmentally attractive ones.

Among the different alcohols, ethanol is one of the most attractive alternatives for hydrogen production. It can be easily generated from biomass feedstock (such as sugarcane, wheat, corn, woodchips, bagasse, waste from agro-industries, and organic fraction from municipal wastes or forestry residues). In fact, many commercial plants produce ethanol from corn in the USA and sugarcane in Brazil [12]. Brazil is indeed known for its policy on the bioethanol production and uses it in hydrous form or blended it with gasoline in transport vehicles (40% of transport fuel consumption has been replaced by sugarcane-derived bioethanol) [13], which is non-toxic (unlike methanol) and easy to store, handle, and transport, and it is globally available. Although its hydrogen content (13 wt.%) is slightly higher than the one of methanol (12.5 wt.%), its complete conversion requires breaking of the C-C bond that is more difficult than the cleavage of C-H bonds. In any case, its use is favored since CO produced during methanol electrolysis could lead to catalyst deactivation in homogeneously catalyzed processes [10].

The phenomenon of electrochemical promotion of catalysis (EPOC) [14], initially described as non-Faradaic electrochemical modification of catalytic activity (NEMCA) [15], is able to reversibly change the activity and selectivity of a metal catalyst supported on a solid electrolyte by means of external voltage application and could be a plausible alternative to induce a catalytic rate increase in reforming processes for hydrogen. The EPOC effect has already played a key role in hydrogen

production, being applied in some of the most important hydrogen production reactions (Table 7.1).

Although classical or conventional promotion and electrochemical promotion methods are functionally identical, they operate in a different way [14]. While in classical promotion the electronic promoters are chemically added onto the catalyst support together with the active phase, the electrochemical promotion allows the in situ modification and control of the amount of promoter in the reaction process. Moreover, in the case of the former one, catalysts could be deteriorated in case of promoters' evaporation or deactivation during operating conditions [16].

In general, the addition of alkali and alkaline earth metals as classical promoters enhanced catalysts' stability, as in the case of potassium promotion in methane and ethane steam reforming [17–20] or methane dry reforming [19]. Alkali promoters are prone to block the most active sites inhibiting carbon deposition although also decreasing methane conversion, being the former effect more pronounced than the latter one [16]. Moreover, the hygroscopic nature and basicity of certain alkali salts can lead to promotional effect via enhancing the catalyst activity [21].

Equivalent electrochemical promotional effect can be observed in the following presented studies, although, in this case, the in situ control of the alkali amount allows the catalyst activation and regeneration in the course of catalytic reaction, as it will be explained below.

Hydrogen production from ammonia decomposition has been boosted by alkali classical promotion [22, 23]. In 1997, this reaction was electrochemically promoted using a K^+ conductor ($Fe/K_2YZr(PO_4)_3$ as electrocatalyst) for the very first time [24]. The electrochemical supply of low amounts of potassium ions enhanced ammonia decomposition rate, the effect attributed to the strengthening of nitrogen (electron acceptor) and the consequent weakening of ammonia and hydrogen (electron donors) adsorption.

Alkali promoters also presented a beneficial effect on water-gas shift reaction. Potassium adatoms can favor the thermochemistry for water dissociation with the cleavage of O-H bonds at room temperature [25], and the electronically weakening of C-H bonds, enhancing formate composition, which is the rate-limiting step in most cases [26]. Application of EPOC effect on water-gas shift systems led to similar effects. The use of K^+ [27] and O^{2-} [28] as conductors in Ni and Pt catalysts, respectively, resulted in an electrophilic EPOC behavior in both cases. The K^+ backspillover and the O^{2-} spillover (cathodic polarizations) enhanced CO conversion. The overall catalytic activity increased due to the strengthening of the chemisorption bond of hydroxyl groups (electron acceptors) and the weakening of electron donors such as CO.

The EPOC phenomenon was applied to the methane steam reforming reaction for the first time in 1995 [29], using a Ni-based catalyst film supported on YSZ as solid electrolyte (O^{2-} conductor). The electrochemical supply of O^{2-} through a positive polarization decreased carbon deposition and enhanced methane conversion and CO production rate. Besides, catalyst was regenerated by anodic polarization, by oxidizing carbon deposits due to the presence of oxygen ions.

Table 7.1 State of the art of hydrogen production reactions promoted by EPOC phenomenon

Reaction	Catalyst	Solid electrolyte	Preparation method	Morphology	ρ	Λ	Effect	Year	Refs.
Ammonia decomposition	Fe	$K_2YZr(PO_4)_3$	Application of thin coatings of paste		3.6	120	Electrophobic	1997	[24]
		$CaZr_{0.9}In_{0.1}O_{3-\alpha}$	Application of thin coatings of paste				Electrophobic		
Water-gas shift	Pt	YSZ	Application of thin coatings of paste	Homogeneous with significant porosity	2.3	−30	Electrophilic	2011	[28]
	Ni	K-βAl_2O_3	Thermal decomposition	Foam structure typical of bulk Ni catalyst	2.7		Electrophilic		[27]
Steam reforming of methane	Ni	YSZ	Application of thin coatings of paste		57	15	Electrophobic	1995	[29]
	Pt	Na-βAl_2O_3	Application of thin coatings of paste	Pt agglomerates ranging from 0.5 to 1 lm			Electrophobic	2010	[30]
	Pt-Pt/YSZ		Application of a catalyst ink (Pt paste and Pt/YSZ catalyst powder with ethylene glycol)	Pt particles disposed in a homogeneous surface			Electrophobic		
	Pt-Pt/YSZ	YSZ		Homogeneous electrode, well adhered to the solid electrolyte, with an improved roughness			Electrophilic	2011	[31]
Partial oxidation of methane	Pt-Pt/YSZ	Na-βAl_2O_3	Application of a catalyst ink (Pt paste and Pt/YSZ catalyst powder with ethylene glycol)	Pt particles disposed in a homogeneous surface			Electrophobic	2010	[30]
	Pt-Pt/YSZ	YSZ		Homogeneous electrode, well adhered to the solid electrolyte, with an improved roughness			Electrophilic	2011	[31]
	Pt-Pt/YSZ	Na-βAl_2O_3	Application of a catalyst ink (Pt paste and Pt/YSZ	Pt particles disposed in a homogeneous surface			Electrophobic	2010	[30]

(continued)

Table 7.1 (continued)

Reaction	Catalyst	Solid electrolyte	Preparation method	Morphology	ρ	Λ	Effect	Year	Refs.
Autothermal reforming of methane	Pt-Pt/YSZ	YSZ	catalyst powder with ethylene glycol)	Homogeneous electrode, well adhered to the solid electrolyte, with an improved roughness	4		Electrophilic	2011	[31]
Methanol decomposition	Ag	YSZ	Application of thin coatings of Ag solution in butyl acetate	Porous film		6	Electrophobic	1989	[32]
	Ni	K-βAl_2O_3	Filter cathodic arc deposition		5		Volcano-type electrophilic	2015	[33]
Steam reforming of methanol	Pt	K-βAl_2O_3	Pulsed cathodic arc deposition		5		Electrophilic	2012	[34]
	Ni		Cathodic arc deposition		1.8		Electrophilic	2015	[33]
Partial oxidation of methanol	Pt		Pulse cathodic arc deposition	Dense structure	6		Electrophilic	2012	[35]
	Au/YSZ		Magnetron sputtering	Particles consisting of face-centered cubic (FCC) metallic assembly of gold atoms	8.9	−8150	Electrophilic	2014	[36]
	Ni		Cathodic arc deposition		0.5		Electrophobic	2015	[33]
	Cu		Deposited by oblique evaporation under vacuum conditions	Microstructure consisting of tilted and separated nanocolumns with $\beta = 60°$	2.63		Electrophilic		[37]
	Ni-DLC		Filter cathodic arc deposition	Face-centered cubic (FCC) crystalline structure	2.4		Electrophilic	2016	[38]

Steam reforming of ethanol	Pt	K-βAl_2O_3	Thermal deposition – Impregnation		6.78	−6145	Electrophilic	2019	[39]
Partial oxidation of ethanol	Pt	K-βAl_2O_3						2021	This chapter
Autothermal reforming of ethanol	Pt	K-βAl_2O_3						2021	This chapter

The same solid electrolyte was also used in a Pt catalyst film [31], where the hydrogen production was studied by applying the EPOC effect to partial oxidation, steam reforming, and autothermal reforming of methane. Cationic conducting solid electrolyte (Na-β"Al_2O_3) has also been used as support for a Pt catalyst in methane reforming reactions [30], for in situ catalyst activation and regeneration under different polarization conditions.

Due to the advantages of using alcohols as fuels for hydrogen production, the EPOC effect has been also applied to alcohol conversion processes. The electrochemical promotion to the methanol dehydrogenation reactions was firstly studied in 1989 [32], using an Ag catalyst supported on YSZ. The same solid electrolyte was also used to support Au nanoparticles in partial oxidation of methanol [36], leading in both cases to an increase in hydrogen production. The removal of O^{2-} ions from the catalyst surface while decreasing the applied potential led to a decrease of catalyst work function favoring the chemisorption of electron-acceptor molecules (such as methoxy group) [32]. Alkali promoter (K^+) was also applied in the methanol conversion processes such as partial oxidation, steam reforming, or methanol decomposition, supporting Pt [34, 35], Ni [33, 38], and Cu [37] catalyst films. In these alcohol conversion processes, the use of alkali promoters instead of negative promoters could provide a higher conductivity at lower temperatures, which could be pretty beneficial in the case of methanol reforming processes. This kind of promoters could also provide a higher stability, especially in hydrogen production reactions since the use of O^{2-} promoters in an oxygen-free gas-phase reaction could limit the solid electrolyte stability.

In most of the mentioned alkali-promoted cases, an electrophilic EPOC behavior was found, i.e., an increase in the hydrogen production rate under a decrease in the catalyst potential by the electrochemical supply of alkali ions to the catalyst. As in the case of classical promotion, the alkali promotional effect enhances catalyst stability and activity, as well as the selectivity toward the methanol partial oxidation instead of total oxidation and, hence, toward hydrogen [35].

In the case of ethanol as feedstock, and prior to the studies of our group, the EPOC phenomenon has only been applied to ethanol oxidation reaction. In these studies, ethanol dehydrogenation into acetaldehyde was enhanced due to the EPOC effect while using YSZ as solid electrolyte and Pt [40, 41] or perovskite [42] as catalysts. The reversible enhancement on the acetaldehyde reaction rate in the polarization of the Pt/YSZ was found to be on the order of 10^4 at low temperatures and high oxygen pressures (conditions where the maximum acetaldehyde yield was obtained). The promotional effect is more pronounced at higher oxygen partial pressures since the activation of the chemisorb oxygen atoms is higher. The origin of this effect was attributed to the observed decrease in the catalytic activation energy of ethanol dehydrogenation reaction (up to 85% lower than the one required in open-circuit conditions) [40, 41]. In the case of using a perovskite as catalyst, the kinetic behavior was affected not only by the NEMCA effect but by high temperatures, homogeneous reactions, and direct electrocatalysis [42].

In view of the importance of hydrogen production in the foresight energy future and its production from renewable sources, as well as the successfully promotional

effects of alkali metals for methane or methanol conversion processes, our group has focused on the study of hydrogen production from ethanol by the application of the alkali-EPOC phenomenon [39]. In this chapter, we reviewed some of the most promising results obtained for the ethanol steam reforming, partial oxidation, and autothermal reforming processes in a Pt/K-βAl_2O_3 electrochemical catalyst.

7.2 Ethanol Steam Reforming Reaction

Due to its favorable stoichiometric equation (Eq. 7.1), ethanol steam reforming (ESR) has been pointed out as an attractive alternative for hydrogen production compared to the most used methane steam reforming.

$$C_2H_5OH + 3H_2O \rightarrow 2CO_2 + 6H_2 \tag{7.1}$$

Consequently, ethanol steam reforming has been widely studied in different catalytic systems. Noble metals such as Au, Pd, Pt, Rh, and Ru [43–48] have been used and tested as catalysts, although attention has been also focused on the use of transient metals like Cu, Ni, Co, or Fe [49–56], as well as on bimetallic systems [57–61]. The role of the support has also been subject of study, and materials such as ZnO, Al_2O_3, Nb_2O_5, ZrO_2, CeO_2, SiO_2, La_2O_3, calcium hydroxyapatite $Ca_{10}(PO_4)_6(OH)_2$ (HAp), and mesoporous silica Santa Barbara Amorphous-15 (SBA-15) [62–64] have been tested. Besides, novel structures have been explored, like carbon nanofibers and nanotubes that have supported Co as catalyst [51], metal-carbon composites with Co-Ru as bimetallic catalyst [61], or Ni catalyst encapsulated within ultrathin graphene layers [54].

Hydrogen selective catalytic membrane reactors have been also pointed out as an alternative to highly pure hydrogen production since conventional gas separation techniques are not sufficiently cost-efficient [65]. A few studies have taken a chance on these systems [47, 65, 66]. Nonetheless, the fragility of these materials, which delimits their lifetime, is a major issue yet.

One of the main problems of ethanol steam reforming process is the catalyst deactivation due to coke deposition. For that reason, chemical promotion has been studied in different systems, to reduce coke formation and to improve catalyst resistance [67–69]. Alkali and alkali earth metals have outstood as promoters due to their basicity, which can help to suppress coke formation [63, 70], to inhibit methanation reaction [71], or even to facilitate C-C bond scission at lower temperatures [71]. Besides, this kind of promoters has been also proved to enhance CO_2 adsorption in a system able to generate hydrogen and capture CO_2 simultaneously (sorption-enhanced steam reforming) [72].

Considering the promotional effect of alkali metals, the EPOC phenomenon was applied to the ethanol steam reforming process using a Pt/ K-βAl_2O_3/Au disk as electrochemical catalyst [39]. The EPOC experiments were conducted following the procedure generally used in the conventional three-electrode electrochemical cells

[73]. This cell consists of a single-chamber solid reactor, which has been shown to behave as a well-mixed (CSTR) reactor in the range of flow rates typically used, as proved by obtaining the reactor residence time distribution with a nondispersive IR CO_2 analyzer [74, 75].

7.2.1 *Electrochemical Promotion of Pt Catalyst on Ethanol Steam Reforming*

The strong promotional effect of alkali (potassium) was analyzed through different galvanostatic, potentiostatic, or combined transients. In a galvanic-potentiostatic first experiment (Fig. 7.2), an electrophilic behavior was observed with the increase of the potassium supply, in agreement with the EPOC rules [14].

While applying a negative and constant current, where a rate of $I/nF = 1.04 \cdot 10^{-10}$ $mol_{K^+} \cdot s^{-1}$ of potassium ions was electrochemically transferred to the surface of the catalyst, it can be observed how the catalyst potential decreased, as well as catalyst work function leading to a rate increase. This enhancement can be due to an increase of the chemical bond of intermediate chemisorbed species (ethoxy molecules) and its further dehydrogenation. Regarding the potential measured between the working and reference electrodes (V_{WR}), the same trend seen in previous studies with this kind of electrolytes was observed [36, 76] – it decreased as long as the negative current was applied. Therefore, the application of negative current led to a back-spillover of K^+ ions onto the catalyst film which strongly activate the catalyst. This

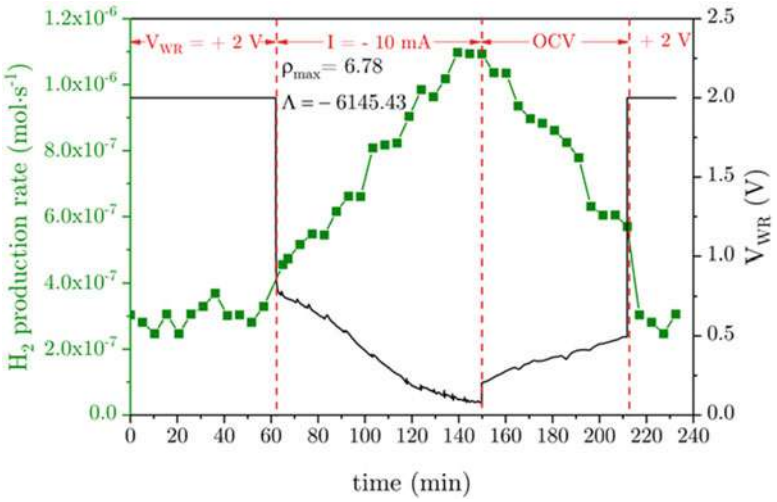

Fig. 7.2 Variations of H_2 production rates vs. time upon different potentiostatic and galvanostatic transitions. Ethanol steam reforming conditions: 3% EtOH, 9% H_2O, Ar balance. T = 450 °C. (Adapted with permission from Ref. [39]. Copyright © 2018 Elsevier B.V. All rights reserved)

activation can be quantified via different parameters such as the Faradaic efficiency (Λ) or the reaction rate enhancement ratio (ρ). These two parameters were calculated (please see Fig. 7.2), and the obtained values corroborated the strong promotional effect induced during the negative polarization step. This effect increased hydrogen production rate in more than three times vs. the absence of these promoter species. Previous studies of hydrogen production reactions electrochemically promoted with alkaline solid electrolytes have reported similar promotional parameter values [77].

The reversible character of this promotional effect was also observed in this first experiment, due to the hydrogen production rate decrease once the current application was interrupted (open-circuit conditions, at $t = 150$ min). In this step, potassium ions were gradually removed from the catalyst surface via thermal back-diffusion or sublimation until the forced fast migration of K^+ promoter back to the solid electrolyte via application of a positive overpotential (final application of +2 V at $t = 212$ min). In a previous study [78], the immediate disappearance of the K_{2p} signal from a Ni catalyst film supported on K-βAl_2O_3 was observed under the application of +2 V via in situ XPS measurements. These XPS measurements demonstrated the successive potassium reduction/diffusion steps on the solid electrolyte cell upon polarization. The electrochemical reduction led to the adsorption of atomic potassium at two different sites at the Ni catalyst: via spillover at the tpb (triple-phase boundary) gas-exposed catalyst surface and then at the inner catalyst interfaces or grain boundaries via diffusion [78]. In the present case, the fast recover of the initial catalytic activity after the positive polarization pointed out the complete reversibility of the induced EPOC effect. This behavior was also a result of the stability of the catalyst film, which was studied in more detail.

The steady-state variation of ethanol conversion and catalyst selectivity (Eqs. 7.2 and 7.3) vs. applied potential was evaluated at different reaction temperatures, as shown in Fig. 7.3.

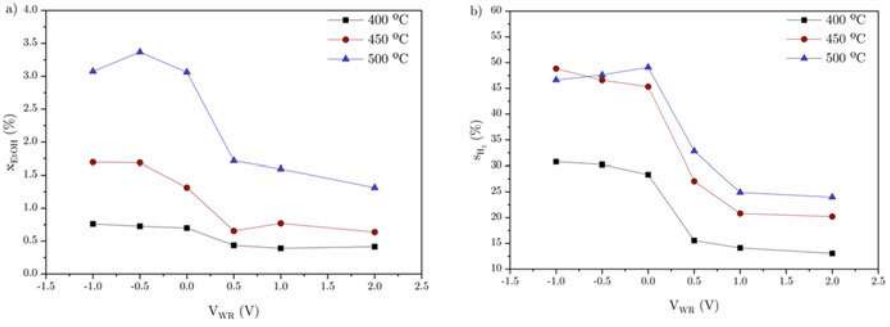

Fig. 7.3 Steady-state (**a**) EtOH conversion and (**b**) H_2 selectivity vs. applied potential (V_{WR}) at different reaction temperatures. Ethanol steam reforming conditions: 3% EtOH, 9% H_2O, Ar balance. T = 450 °C. (Adapted with permission from Ref. [39]. Copyright © 2018 Elsevier B.V. All rights reserved)

$$x_{EtOH}(\%) = \frac{(F_{EtOH,in} - F_{EtOH,out})}{F_{EtOH,in}} \cdot 100 \quad (7.2)$$

$$s_{H_2}(\%) = \frac{F_{H_2,out}}{6 \cdot (F_{EtOH,in} - F_{EtOH,out})} \cdot 100 \quad (7.3)$$

being $F_{i,in}$ and $F_{i,out}$ the inlet and outlet molar flow rate of the i species, respectively.

As expected, taking into account reaction kinetics [14], ethanol conversion increased as reaction temperature did. At all temperatures, an electrophilic EPOC effect was observed, and it was higher at higher temperatures due to the exponential nature of this effect on dehydrogenation kinetics. However, at the highest temperature (500 °C) and at low potentials (below −0.5 V), a decrease in both ethanol conversion and in hydrogen selectivity was observed.

It is well-known that an excessive promoter coverage can be produced at the most negative potentials leading to a poisoning of catalytic active sites as already studied in published works on EPOC effect for methanol reforming reactions [36]. As already commented, one of the main advantages of the electrochemical promotion vs. conventional catalytic one is its capability of controlling the amount of promoter coverage on the catalyst surface by changing reaction conditions, being able to lead to an optimal amount [79].

Compared to conventional potassium-promoted Pt/Al_2O_3 catalytic studies, where conversion values were up to 94% at 450 °C [79], low conversion values (below 4% in all cases) were obtained. These values are a consequence of the low geometric area of the catalyst film (2.01 cm^2), its low catalytic active surface area, and a high reactant bypass due to the reaction system used [80]. Nonetheless, and in view of practical applications, conversion could be increased using other reactor designs, e.g., the monolithic electro-promoted reactor (MEPR), in order to get higher catalyst surface area and higher catalytic conversion values [81].

Notwithstanding, and for comparative purposes, a previous study reported the turnover frequency (TOF) values of methanol decomposition, from the active catalyst sites. The values reported were shown to be of the same order as those reported in different conventional catalytic systems [77].

Related to the catalyst selectivity to hydrogen production, it is also interesting to note the positive effect of the electrochemical promoter, which was attributed to an increase in the kinetics of the dehydrogenation reactions. The role of the promotional effect in the reaction mechanism and hence in the hydrogen selectivity was also evaluated as detailed below.

7.2.2 The Role of the EPOC Effect on the Ethanol Steam Reforming Reaction Pathway

In order to evaluate the influence of the presence of K^+ on Pt continuous films in the reaction mechanism, H_2, CO_2, and C_2H_4O were followed up along time while

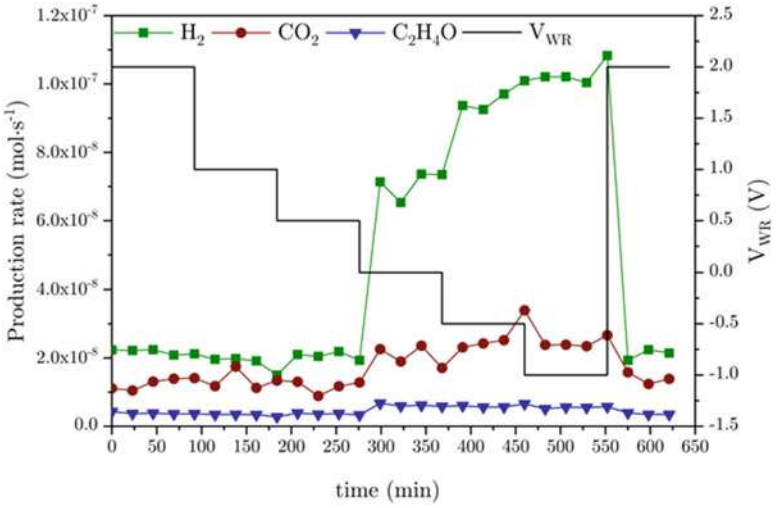

Fig. 7.4 Variations of H_2, CO_2, and C_2H_4O production rates vs. time upon different potentiostatic transitions. Ethanol steam reforming conditions: 3% EtOH, 9% H_2O, Ar balance. T = 450 °C. (Adapted with permission from Ref. [39]. Copyright © 2018 Elsevier B.V. All rights reserved)

applying different potentials at a constant temperature of 450 °C, as shown in Fig. 7.4. Once again, it could be observed the strong electrophilic EPOC effect at potentials below +0.5 V and thus an increase in the different obtained product rates. However, it was observed a higher enhancement in hydrogen production rates (five times higher while applying −1 V than +2 V) compared to the one observed in the carbonaceous product rates. Nonetheless, this was not the case for the rest of the products. The ratio between hydrogen production and the rest of the product's production rate $\left(\frac{r_{H_2}}{r_{CO_2}+r_{C_2H_4O}}\right)$ was calculated in both states, promoted state (applying −1 V) and unpromoted state (+2 V), being the second one 1.56, while the first one was up to 3.53. This fact may indicate the possible adsorption of some carbonaceous products on the catalyst surface while applying negative polarization steps. This behavior was previously reported while using a conventional Pt catalyst in catalytic ethanol steam reforming reactions [82].

As previously studied, operation parameters such as reaction temperature or catalyst characteristics (such as metal dispersion, thermal stability, metal-support interaction, or particle size) can determine the ethanol steam reforming reaction mechanism [83, 84]. As schemed in Fig. 7.5, ethanol adsorption on the catalyst surface is established as the first step in the reaction mechanism for these studied conditions [83, 85]. This adsorbed ethanol is then dehydrogenated to acetaldehyde in two reaction steps: firstly into an intermediate ethoxy molecule and, secondly, into acetaldehyde [86]. Then, hydrogen is obtained from three different reactions: H-adsorbed atom recombination, acetaldehyde steam reforming reaction, and water-gas shift reaction.

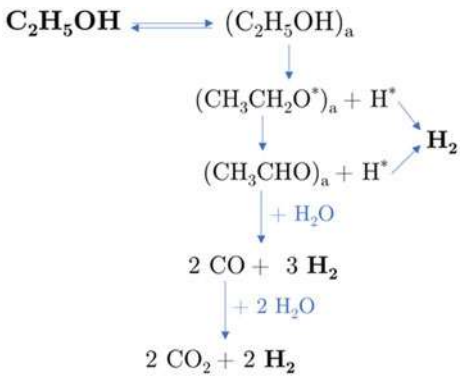

Fig. 7.5 Ethanol steam reforming reaction mechanism scheme

It was proposed that, under unpromoted conditions (+2 V), the initial ethanol dehydrogenation reactions were the rate-determining step [87]. Under these conditions, the hydrogen production was limited by the presence of a low coverage of intermediate ethoxy and acetaldehyde adsorbed molecules, leading to a low hydrogen production rate [79]. Notwithstanding, the presence of K^+ during the negative polarization steps activated the ethanol dehydrogenation reactions. The observed electrophilic behavior was explained considering the strengthening of the chemisorptive bond of electron-acceptor molecules, i.e., intermediate ethoxy molecules, while decreasing catalyst work function.

A similar electrophilic effect has been reported for the case of methanol decomposition considering the electron-acceptor character of intermediate methoxy molecules formed in these previous cases [32, 33]. Under these conditions, the hydrogen production rate may have probably increased via dehydrogenation into acetaldehyde and H atom recombination, whereas very likely, a large amount of ethoxy species and acetaldehyde molecules remained adsorbed on the Pt active sites, explaining the increase in hydrogen production but not in the carbonaceous products during the negative polarization step. This electrochemical promotion mechanism was further supported by the influence of the partial pressure of water and ethanol [39].

7.2.3 Stability Study of Ethanol Steam Reforming Reaction

The hypothesis of the adsorbed carbonaceous species was confirmed by conducting in situ temperature-programmed oxidation (TPO) experiments (Fig. 7.6b) after a long-time negative polarization step (Fig. 7.6a). The application of this negative polarization (−1.5 V) led to a continuous decrease in the catalytic activity along the time, attributed to the continuous formation and adsorption of intermediate carbonaceous species, which would block the Pt active sites.

The complete reversible character of the EPOC phenomenon was again observed after the application of an electric potential of +2 V, which also allowed regenerating

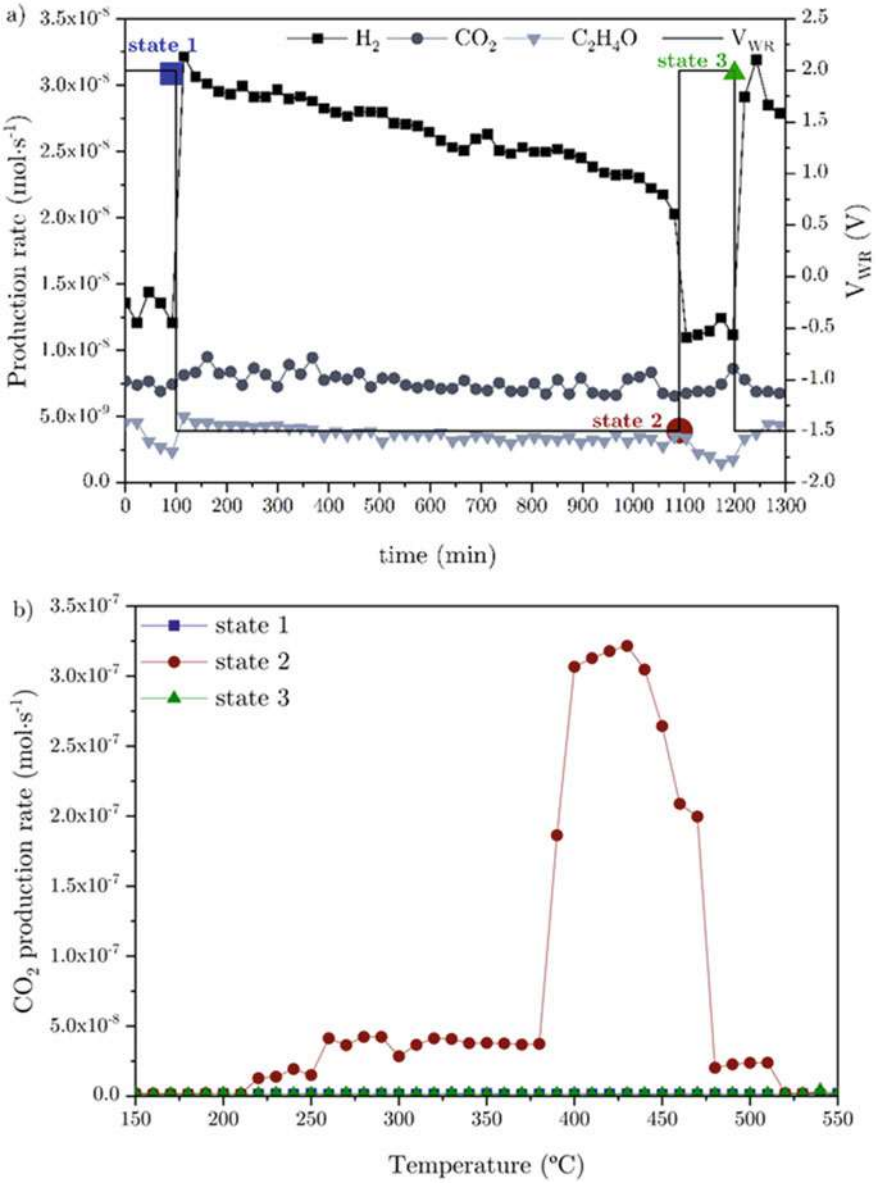

Fig. 7.6 (**a**) H_2, CO_2, and C_2H_4O production rate variation vs. time for a long EPOC experiment during a mild term. Ethanol steam reforming conditions: 3% EtOH, 9% H_2O. T = 400 °C. (**b**) CO_2 production rates vs. temperature in a temperature-programmed oxidation at three different states (pointed out in Fig. 7.6a). 2% O_2, Ar balance, heating ramp = 2 °C·min^{-1}. (Adapted with permission from Ref. [39]. Copyright © 2018 Elsevier B.V. All rights reserved)

the catalyst from such carbonaceous species deposition. After this positive overpotential application, a catalyst surface free of adsorbed carbonaceous molecule was recovered and able to be again electrochemically activated through negative polarization. The in situ TPO experiments were performed just after each polarization step denoted as the following: *state 1* after the initial polarization at +2 V at $t = 100$ min, *state 2* after the polarization at −1.5 V at $t = 1090$ min, and *state 3* after the second polarization at +2 V at $t = 1200$ min.

TPO experiments after *state 1* and *state 3* showed a C product-free and clean catalyst surface since CO_2 was not observed. Applying a positive polarization (+2 V) leads to a clean catalyst free of intermediates, while, on the contrary, applying a − 1.5 V polarization for 15 h (*state 2*) produces CO_2 originated from intermediate carbonaceous species deposited on the catalyst surface. The negative polarization induced the formation of these intermediates since the K^+ presence strengthens ethoxy intermediated molecule chemisorption, activating the dehydrogenation reactions. Raman spectroscopy and scanning electron microscopy were used as ex situ characterization techniques to further confirm the presence of these species on the catalyst surface. Two different regions can be clearly differentiated in the analyses conducted after negative polarization: a lighter zone which could correspond to an apparently clean or free of intermediate zone (region 1) and a darker one (region 2), where carbonaceous species deposition was visible at first sight (Fig. 7.7).

Unsurprisingly, the state 3 (only region 1) and state 2 spectra did not show any band, while the spectra obtained on region 2 of *state 2* showed two bands identified as the disordered graphitic lattice (D band) and ideal graphitic lattice (G band), respectively. This latter spectrum resembles a carbonaceous structure typical of

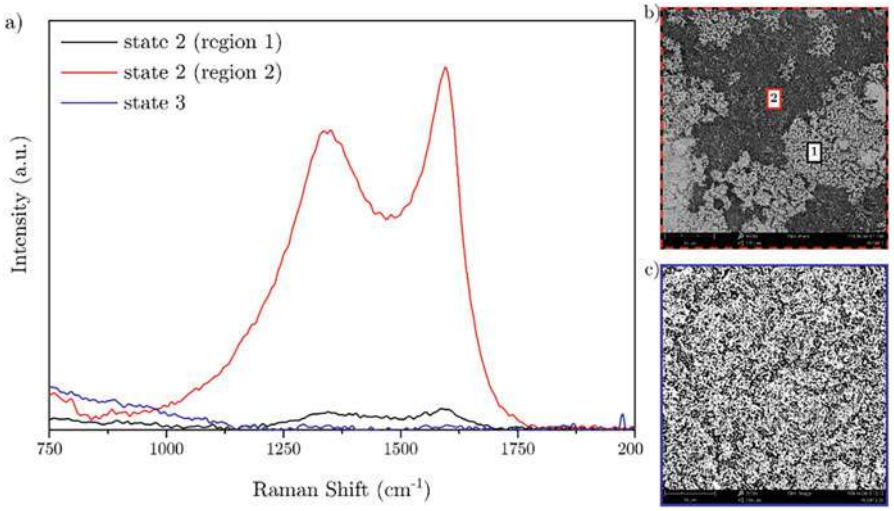

Fig. 7.7 (**a**) Raman spectra of Pt catalysts after different applied potentials at Fig. 7.6 reaction conditions. Microscopy images after different states: (**b**) *state 2* and (**c**) *state 3*. (Adapted with permission from Ref. [39]. Copyright © 2018 Elsevier B.V. All rights reserved)

pre-graphitic carbon which has been previously observed in Pt catalysts and identified as one of the main reasons of the reforming catalysts' deactivations [88].

This study confirmed the electrochemical promotion effect on the reaction of ethanol steam reforming. It also underlined the advantage of this phenomenon in terms of in situ activation of catalytic activity and hydrogen selectivity, as well as the catalyst regeneration after a carbon deposition deactivation.

7.3 Ethanol Partial Oxidation Reaction

Despite that ethanol steam reforming reaction offers higher energy efficiency since it provides the maximum theoretical yield of hydrogen [89], it is a strongly endothermic process that requires an external supply of heat, so it is limited by the heat transfer. Microchannel reactor systems or catalytic wall reactors with high-surface area catalysts are capable of increasing heat transfer, although they could compromise the compactness and the cost of the system [90]. Moreover, catalyst deactivation could hinder onboard applications [91].

Ethanol partial oxidation reaction (Eq. 7.4) can be carried out without external heat sources or heat exchangers. This reaction exhibits fast startup and quick response times and presents a simple and compact design, desirable features for automotive, mobile fuel cell applications [92]. However, the likelihood of hotspot formation could make difficult the reaction control. That fact, joint to its low hydrogen yield compared to steam reforming process, is its main drawback [57].

$$C_2H_5OH + 1/2O_2 \rightarrow 2CO + 3H_2 \tag{7.4}$$

This reaction has not been so widely studied as in the case of ethanol steam reforming reaction. Nonetheless, the role of noble metals such as Pt, Rh, Pd, or Ru as monometallic and bimetallic catalysts has been subject of study [90, 93–99]. Non-noble metals have been also used as monometallic catalysts as in the case of Ni [100] or Co [94] and as bimetallic catalyst coupled with another non-noble or noble metal [101–103]. The effect of the support and its interaction with the metallic phase has been also evaluated, testing materials such as CeO_2, Y_2O_3, Al_2O_3, ZrO_2, TiO_2, and SiO_2 [95, 97, 104].

Previous catalytic studies have already evaluated the addition of different classical promoters. For instance, the addition of a V_2O_5 phase to a Pt catalyst improved its performance probably due to the V_2O_5 redox properties [105]. Nitrogen also promoted the catalytic activity of partial oxidation processes while using a vanadium oxide catalyst supported on nitrogen-doped TiO_2 [106]. Characterization confirmed the presence of nitrogen species in the surface support and their critical role on the catalytic activity of the material due to the ethanol adsorption ability and the degree of the vanadia cluster-support interaction. The impact of Na as alkali promoter in a vanadium oxide catalyst was studied by Chimentao et al. [107], finding the influence of this promoter in dispersion, reducibility, and acidity of the catalyst and its ability

to decrease carbon deposition during reaction while using a high amount of promoter.

Our group has also evaluated the EPOC phenomenon in the ethanol partial oxidation reaction using the same Pt/K-βAl_2O_3/Au electrocatalytic system. The promotional effect at different temperatures and inlet compositions was investigated.

7.3.1 *Electrochemical Promotion of Pt Catalyst on Ethanol Partial Oxidation*

The electrophilic EPOC behavior was first demonstrated through different potentiostatic transients, as shown in Fig. 7.8. The application of potentials below −0.5 V was responsible for an increase in hydrogen production rate, i.e., for a strong activation of the ethanol partial oxidation on the Pt catalyst. This electrophilic behavior is translated into a decrease in the catalyst potential and hence catalyst work function. In a previous methanol partial oxidation study, methanol was identified as the donor molecule and O_2 as the acceptor one [35]. Similarly, ethanol was considered as the electron-donor molecule since the migration of positively charge species weakened the chemical bond between this molecule and Pt and strengthened the bond with the electron-acceptor molecule (O_2).

At the most negative potentials, a hydrogen production rate decrease was observed right after the initial strong activation. Negative potentials were responsible for a strong activation of the partial oxidation that led to the fast formation of intermediate species. These intermediate species could further react and be decomposed blocking active sites.

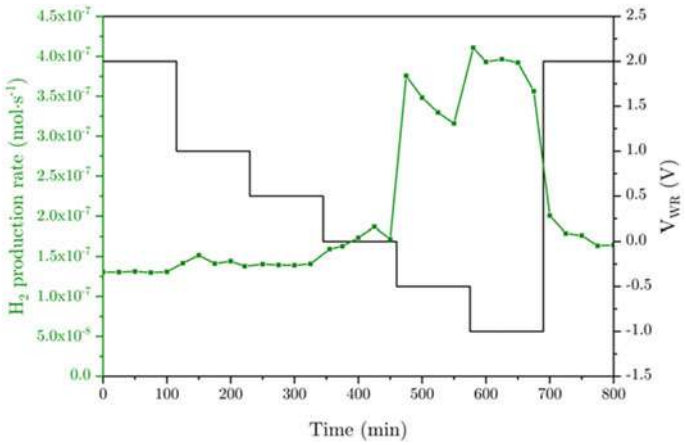

Fig. 7.8 Potentiostatic transients: hydrogen reaction rate and applied potential vs. time. Inlet composition: 3% EtOH, 1% O_2, Ar balance. T = 550 °C. (Adapted with permission from Ref. [108]. Copyright © 2022 Elsevier B.V. All rights reserved)

Catalyst deactivation has always been a major issue in steam reforming processes (as demonstrated in 7.2), and, in some extent, it has been previously observed in partial oxidation too [102]. Nonetheless, the decrease observed in Fig. 7.8 seems to be more likely due to an excess of acetate or ethoxy species adsorbed on the catalyst surface [98], which would be further reacted into acetaldehyde. This kind of behavior was observed in previous catalytic studies [94, 100] where, despite the stability of the catalyst, an initial deactivation was observed at the beginning of the reaction.

Following the trend obtained while working on ethanol steam reforming conditions, a fully reversible effect was again observed since similar hydrogen production rate values at the beginning and at the end of the experiment were obtained. This fact is also an index of the stability of the catalyst film through different polarization steps.

The positive influence of the potassium ions in the catalyst work function decrease was asserted in all O_2/EtOH molar ratios studied, and hydrogen production always showed an electrophilic behavior (Fig. 7.9).

Notwithstanding, while feeding the reactor with a 1:2 molar O_2/EtOH ratio, it can be observed a decrease in the catalytic activity at the most negative potentials, finding a maximum value at −0.5 V. Ethanol could find difficulties to be adsorbed on the catalyst surface due to the high O_2 coverage at this molar ratio. At the most negative potentials, and being ethanol the electron donor and hence, the weaken chemical Pt bond compared to the electron acceptor, ethanol molecules could not be found in the catalyst surface and oxygen would cover most of it. On the other hand, and as previously reported while working with alkali conductors [35], the number of Pt active sites could decrease due to the presence of formed and stored potassium

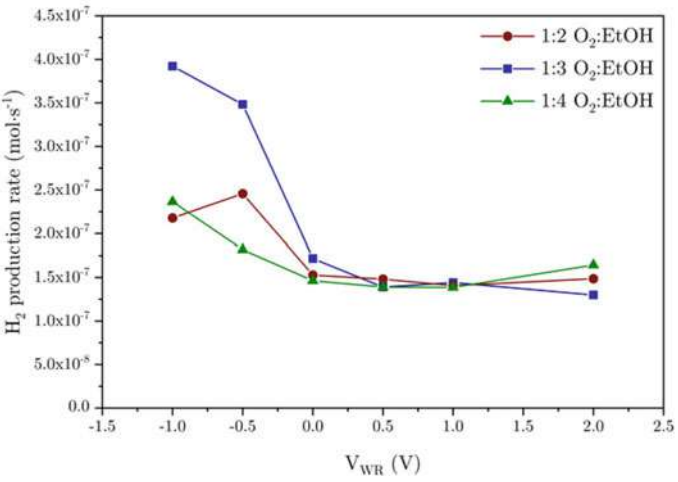

Fig. 7.9 Hydrogen production rates vs. applied potential at three different O_2/EtOH molar ratios. Inlet composition: 3% EtOH. T = 550 °C. (Adapted with permission from Ref. [108]. Copyright © 2022 Elsevier B.V. All rights reserved)

surface compounds, which would partially blocked the catalyst surface. In this latter case, the significance of the EPOC effect is not only dependent on the kinetics order of donor and acceptor molecules, and at this negative potential, an excess of promoter coverage could poison the Pt active sites [37].

Taking into account previous studies [91], the hydrogen yield is directly affected by the oxygen-to-ethanol molar ratio. High ratios would favor hydrogen oxidation, and then ethanol complete combustion could take place. The oxygen adsorption is favored by the presence of potassium ions since it is the electron-acceptor molecule instead of the ethanol adsorption (since this is the electron-donor molecule) leading to a large oxygen coverage that could possibly limit the presence of ethanol in the catalyst surface. On the contrary, very low molar ratios could not provide enough oxygen. For that reason, 1:3 O_2/EtOH molar ratio presented the highest catalytic activity and EPOC behavior.

7.3.2 The Role of the EPOC Effect on the Ethanol Partial Oxidation Reaction Pathway

The presence of oxygen and a C-C bond in the ethanol molecule make the reaction pathways for ethanol partial oxidation numerous and complex. The large number of possible by-products and its further transformations, which depend on the metal catalyst, the support, and the reaction conditions, increase the potential reaction combinations [109]. Through temperature-programmed reaction experiments (Fig. 7.10), and in order to determine the possible reaction pathway, the different product reaction rates were followed up under both promoted and unpromoted (+2 V, −0.5 V) conditions.

A possible reaction mechanism based on the products found under the explored conditions as well as on previous studies [109–111] was developed and schemed in Fig. 7.11. In this mechanism, the first step consists of two competitive reactions: the oxidative dehydrogenation and dehydration of ethanol. While dehydration reaction does not produce hydrogen as product, the oxidative dehydrogenation of ethanol generates acetaldehyde which can be reformed and then decomposed into methane and carbon monoxide. Hydrogen would finally appear as an oxidation and reforming product of these two species.

According to previous catalytic studies [97, 112], in this range of temperature, the two competitive first reaction steps can lead to noticeable amounts of water, acetaldehyde, or ethylene, while the formation of carbon monoxide (which would further produced hydrogen) needs high temperatures [91, 97]. Nonetheless, carbon monoxide could be activated at lower temperatures due to the electrochemical promotion.

Figure 7.10 confirmed this temperature activation for the oxidative dehydrogenation and dehydration reactions since the production rates of acetaldehyde and ethylene notably increased as temperature did while applying +2 V (unpromoted conditions).

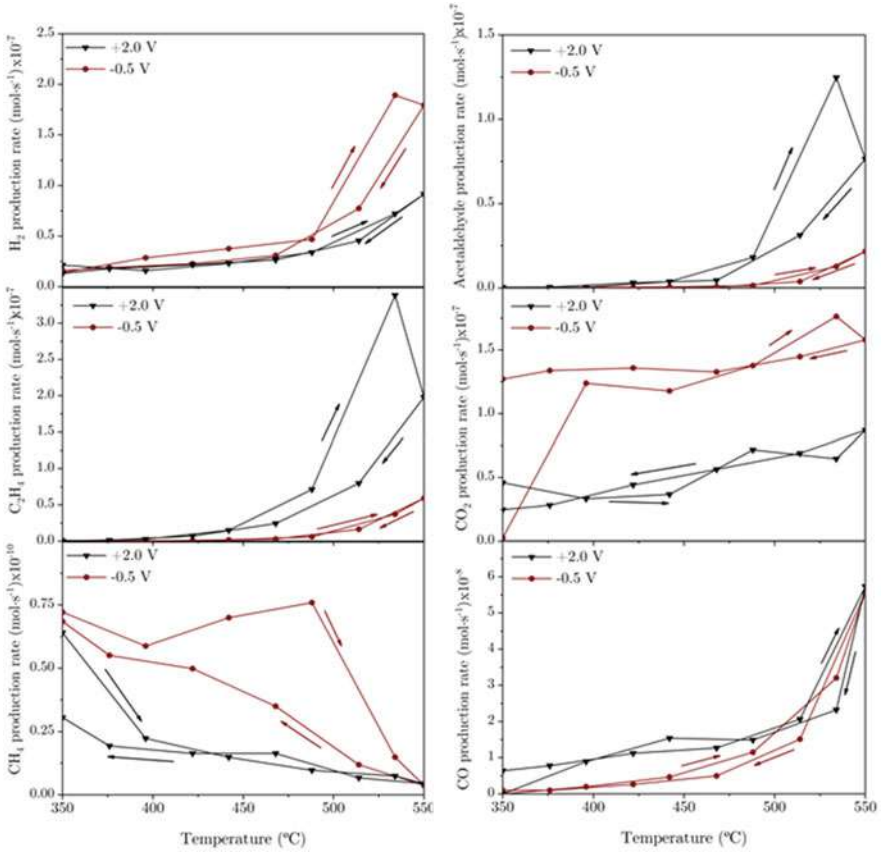

Fig. 7.10 Temperature-programmed reaction experiments (rate = 2 °C·min^{-1}): products' reaction rates vs. temperature at unpromoted (+2 V) and promoted (−0.5 V) conditions. Inlet composition: 3% EtOH, 1% O_2, Ar balance. (Adapted with permission from Ref. [108]. Copyright © 2022 Elsevier B.V. All rights reserved)

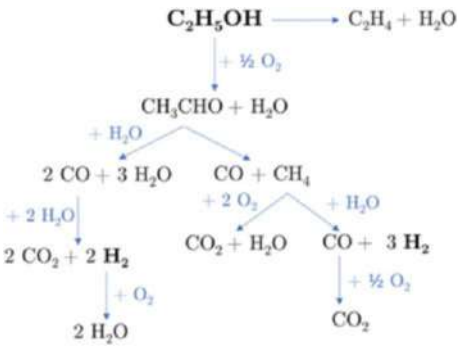

Fig. 7.11 Ethanol partial oxidation reaction mechanism scheme. (Adapted with permission from Ref. [108]. Copyright © 2022 Elsevier B.V. All rights reserved)

However, under promoted conditions, hydrogen was strongly activated at lower temperatures due to the K^+ presence on the catalyst surface. It seems that polarization favored ethanol oxidative dehydrogenation route and, hence, acetaldehyde reforming and decomposition reactions and the rest of the mechanism. Acetaldehyde oxidation was limited in the absence of promoter species, and once these species were present, an increase in hydrogen production rate was observed.

As already mentioned, the oxidative dehydrogenation and dehydration of ethanol are the two competitive steps on the reaction mechanism, and polarization activated ethanol oxidative dehydrogenation route instead of ethanol dehydration. Since ethanol dehydration reaction does not produce hydrogen, it was demonstrated the beneficial effect of EPOC application on partial ethanol oxidation, which favors ethanol oxidative dehydrogenation reaction that leads to hydrogen production.

7.4 Oxidative Steam Reforming and Comparison Between Different Reaction Atmospheres

Oxidative steam reforming or autothermal reforming process (Eq. 7.5) is the combination of both steam reforming and partial oxidation. The addition of oxygen to steam reforming conditions allows achieving an equilibrium between hydrogen selectivity and energy efficiency, besides promoting the removal of carbon species formed during reaction conditions that could deactivate the catalyst [113].

$$C_2H_5OH + 2\,H_2O + \frac{1}{2}\,O_2 \rightarrow 2\,CO_2 + 5\,H_2 \tag{7.5}$$

Our group evaluated the effect of the oxygen addition to steam reforming conditions following up the production rates under unpromoted and promoted conditions while modifying the reaction atmospheres. Hydrogen production rates vs. time through steam reforming, partial oxidation, and autothermal reforming are shown in Fig. 7.12.

In all three atmospheres, the migration of the potassium ions led to an electrophilic EPOC effect activating the different reaction mechanisms and, hence, activating hydrogen production via product reaction of all intermediate species since they were not observed under promoted conditions.

Logically, and under all conditions, hydrogen production was higher in the case of steam reforming reaction, since this reaction provides the maximum theoretical yield of hydrogen among the studied reactions [89]. Nonetheless, the hydrogen decrease slope was more pronounced in this reaction atmosphere. Considering the stability experiments shown in Sect. 7.2.3 (Stability Study of Ethanol Steam Reforming Reaction), the catalytic activity decreased along time in all cases, being more notorious under promoted conditions. As already discussed, this is attributed to the intermediate carbonaceous species deposition, which are continuously produced and absorbed blocking Pt active sites.

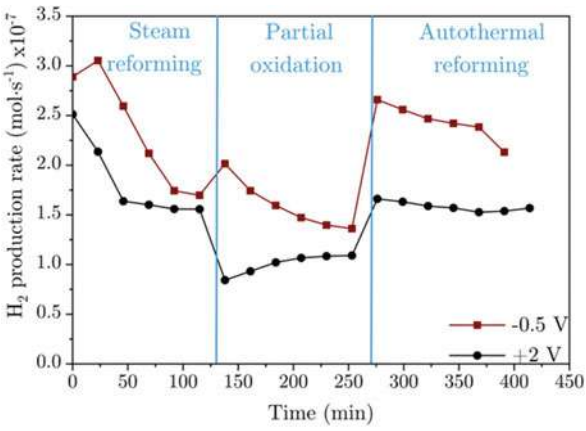

Fig. 7.12 Hydrogen production rates vs. time. Changes in the atmosphere. Steam reforming: 3% EtOH, 9% H_2O, Ar balance. Partial oxidation: 3% EtOH, 1% O_2, Ar balance. Autothermal reforming: 3% EtOH, 9% H_2O, 1% O_2, Ar balance. T = 550 °C. (Adapted with permission from Ref. [108]. Copyright © 2022 Elsevier B.V. All rights reserved)

Regarding partial oxidation atmosphere, an increase in reaction temperature activates oxidative dehydrogenation and dehydration reactions. Under unpromoted conditions, acetaldehyde reforming and decomposition reactions are the rate-limiting step of the reaction mechanism, so acetaldehyde and ethylene are produced in large amounts. The presence of potassium ions activates these reforming and decomposition reactions, favoring the ethanol oxidative dehydrogenation route and increasing hydrogen production. Comparing this atmosphere to steam reforming, it should be noticed the stable behavior of the former one, although its activity is lower. According to previous studies [114] and under unpromoted conditions, it is possible to achieve a higher acetaldehyde production if steam is replaced with oxygen, though the acetaldehyde decomposition could be hindered resulting in a decreased hydrogen selectivity. Acetaldehyde decomposition could be enhanced by polarization, but, in any case, partial oxidation reaction provides a lower theoretical yield of hydrogen (as it can be observed in Eqs. 7.1, 7.4, and 7.5).

Oxidative steam reforming or autothermal reforming combines both previously mentioned atmospheres, achieving a higher catalytic activity for hydrogen production rate than the one obtained by partial oxidation and a more stable performance than in the case of steam reforming. Although hydrogen production rates slightly decreased regarding steam reforming conditions, ethanol autothermal reforming could be the most suitable atmosphere for hydrogen production taking into account the significant deactivation that Pt catalyst suffered from exposure to steam reaction conditions.

The suitability of autothermal reforming reaction was investigated through a stability study. As shown in Fig. 7.13, two different experiments were conducted: short-time (30 min each) and long-time polarizations were applied, switching from unpromoted (+2 V) to promoted (−0.5 V) states. Both short-time and long-time polarizations showed an electrophilic, reversible, and reproducible EPOC effect. Once again, the migration of the potassium ions into the catalyst surface during the first seconds of polarization led to an increase in the hydrogen production rate. Additionally, the different obtained hydrogen production rates achieved the same

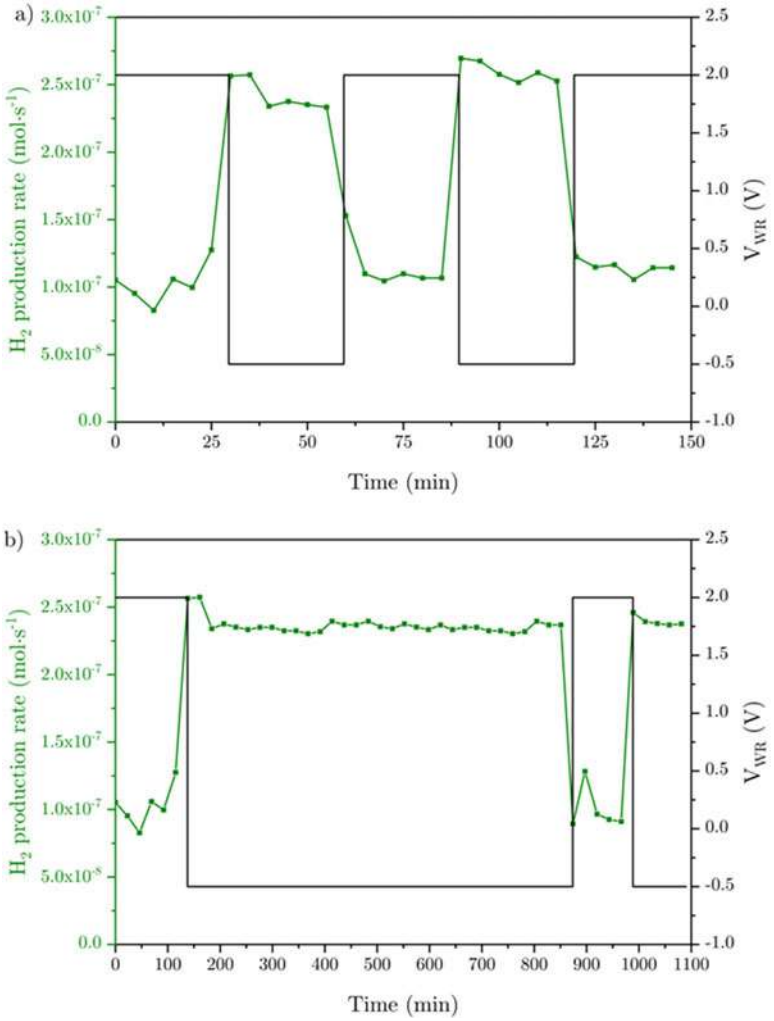

Fig. 7.13 Autothermal reforming stability tests: hydrogen production rates vs. time. (**a**) Short-time (30 min each) polarization cycles, (**b**) long-time negative polarization. Inlet composition: 3% EtOH, 9% H_2O, 1% O_2, Ar balance. T = 550 °C. (Adapted with permission from Ref. [108]. Copyright © 2022 Elsevier B.V. All rights reserved)

values for the same polarizations; here is to say the amount of electrochemically transferred potassium ions from or to the solid electrolyte during negative or positive polarizations was the same and led to a complete reversible and reproducible effect.

In the case of the long-time polarization experiment (Fig. 7.13b), and contrary to steam reforming stability study (Fig. 7.6a) where a continuous decrease in the catalytic activity along time was observed, constant values of hydrogen production rates showed that the possible catalytic deactivation is negligible under autothermal

reforming conditions. There is no loss of catalytic activity; hence, there is no loss of promotional phases or catalyst deactivation during polarization. As it has been already reported [99, 114], the continuous formation and adsorption of intermediate carbonaceous species could block catalyst active sites in steam reforming conditions leading to significant activity losses (resulting in a 50% drop of ethanol conversion in some cases [111, 115]). Nonetheless and in all cases, the addition of oxygen (autothermal reforming atmosphere) produced an appreciable improvement in the catalyst stability.

7.5 Conclusions and Prospects

This chapter has reviewed the latest efforts of our group on the electrochemical catalyst activation of hydrogen production methods from ethanol, which can be easily generated from biomass feedstock, free of CO_2 emissions. In particular, it has been focused on the application of EPOC phenomenon in traditional hydrogen production methods such as steam reforming, partial oxidation, and autothermal reforming. Drawn from these findings, key conclusions are presented below.

All the explored results led to corroborate the interest of electrochemical promotion to improve the activity of a Pt catalyst in H_2 production from ethanol steam reforming. Under the explored conditions, the promotional effect enhanced ethanol dehydrogenation reaction kinetics by strengthening the chemisorptive bond of intermediate ethoxy molecules. These species were responsible for catalyst deactivation since they remained adsorbed on its surface; however, the application of a positive potential (+2 V) allowed the complete catalyst regeneration from these species and carbon deposition (as supported by in situ and ex situ characterization techniques).

It was also observed that, under ethanol partial oxidation conditions, the migration of potassium ions weakened the Pt chemical bond with electron-donor adsorbates (ethanol) and strengthened chemical bond with electron-acceptor ones (O_2), enhancing hydrogen production. Moreover, polarization activated ethanol dehydrogenation into acetaldehyde route instead of ethanol dehydration reaction. The former one leads to further acetaldehyde reforming and decomposition reactions and hence to hydrogen production, while the latter one does not produce hydrogen. Autothermal reforming has been presented as the optimal conditions since it achieved higher hydrogen production rates than the one obtained by partial oxidation and a more stable activity than in the case of steam reforming. The addition of oxygen produced an improvement in the catalytic stability.

Due to the promising results observed from these works, it can be expected that further investigations should be focused on the EPOC phenomenon application to ethanol conversion processes using other kinds of solid electrolytes, cationic (Na-βAl_2O_3, NASICON) or anionic (YSZ), as well as solid-state protonic conductors that could be useful for providing electropositive promoters to carry out reforming reactions at the standard conditions. As already studied in methanol

conversion reactions [33, 37, 38], the use of other metals as catalysts (as Ni or Cu), instead of the noble metals, substituting the Pt group metals, would be an interesting field of research. It is also encouraged the preparation of electrochemical catalytic metallic films using advanced techniques (like cathodic arc deposition, sputtering, or oblique angle deposition) in order to improve the catalyst active surface area and decrease metal loading. In line with this, nanoparticles dispersed over mixed conductor materials used as catalysts could strengthen the EPOC effect as already observed in reverse water-gas shift or methane oxidation reactions while using Co nanoparticles supported on YSZ or nanodispersed Pd on Co_3O_4, respectively [116, 117].

Regarding the source of ethanol, further research testing real bioalcohol streams originating from biomass as feedstocks [118, 119], or even raw biomass such as lignocellulosic biomass [120], would be necessary to truly evaluate the suitability of this technology.

Finally, another interesting direction to focus on involves the development of proper design of electrochemical cells, as the MEPR already mentioned, in order to improve catalytic conversion [81], or an ethanol over-Faradaic electrolyzer. This latter concept (see Chap. 9) was first purposed by our group by using methanol as feedstock, and it consists of a new phenomenon where the electrocatalytic hydrogen production via methanol electrolysis was coupled with the electrochemical-promoted methanol dehydrogenation reaction, leading to an over-Faradaic hydrogen production [121]. Although this phenomenon was not achieved in a first test using ethanol as feedstock, further research and efforts in this direction would give rise to outstanding and very valuable results.

References

1. Gao W, Liang S, Wang R, Jiang Q, Zhang Y, Zheng Q, Xie B, Toe CY, Zhu X, Wang J, Huang L, Gao Y, Wang Z, Jo C, Wang Q, Wang L, Liu Y, Louis B, Scott J, Roger AC, Amal R, He H, Park SE (2020) Industrial carbon dioxide capture and utilization: state of the art and future challenges. Chem Soc Rev 49:8584–8686
2. Zhu DD, Liu JL, Qiao SZ (2016) Recent advances in inorganic heterogeneous electrocatalysts for reduction of carbon dioxide. Adv Mater 28:3423–3452. https://doi.org/10.1002/adma.201504766
3. Dutta S (2014) A review on production, storage of hydrogen and its utilization as an energy resource. J Ind Eng Chem 20:1148–1156
4. Khalilpour KR, Pace R, Karimi F (2020) Retrospective and prospective of the hydrogen supply chain: a longitudinal techno-historical analysis. Int J Hydrog Energy 45:34294–34315. https://doi.org/10.1016/j.ijhydene.2020.02.099
5. Abdin Z, Zafaranloo A, Rafiee A, Mérida W, Lipiński W, Khalilpour KR (2020) Hydrogen as an energy vector. Renew Sust Energ Rev 120:109620
6. Abdalla AM, Hossain S, Nisfindy OB, Azad AT, Dawood M, Azad AK (2018) Hydrogen production, storage, transportation and key challenges with applications: a review. Energy Convers Manag 165:602–627
7. Nikolaidis P, Poullikkas A (2017) A comparative overview of hydrogen production processes. Renew Sust Energ Rev 67:597–611

8. Ball M, Weeda M (2015) The hydrogen economy – vision or reality? Int J Hydrog Energy 40: 7903–7919. https://doi.org/10.1016/J.IJHYDENE.2015.04.032
9. Iea Technology Roadmap Hydrogen and Fuel Cells
10. Trincado M, Banerjee D, Grützmacher H (2014) Molecular catalysts for hydrogen production from alcohols. Energy Environ Sci 7:2464–2503
11. Hydrogen TCP – Research and Innovation in Hydrogen Technology by IEA. https://www.ieahydrogen.org/. Accessed 14 Mar 2021
12. Badwal SPS, Giddey S, Kulkarni A, Goel J, Basu S (2015) Direct ethanol fuel cells for transport and stationary applications – a comprehensive review. Appl Energy 145:80–103
13. Demirbas A (2009) Biofuels securing the planet's future energy needs. Energy Convers Manag 50:2239–2249. https://doi.org/10.1016/j.enconman.2009.05.010
14. Vayenas CG, Jaksic MM, Bebelis SI, Neophytides SG (1996) The electrochemical activation of catalytic reactions. Springer, Boston, MA, pp 57–202
15. Vayenas CG, Bebelis S, Yentekakis IV, Lintz HG (1992) Non-faradaic electrochemical modification of catalytic activity: a status report. Catal Today 11:303–438. https://doi.org/10.1016/0920-5861(92)80002-5
16. González-Cobos J, Valverde JL, de Lucas-Consuegra A (2017) Electrochemical vs. chemical promotion in the H2 production catalytic reactions. Int J Hydrog Energy 42:13712–13723. https://doi.org/10.1016/J.IJHYDENE.2017.03.085
17. Ni C, Pan L, Yuan Z, Cao L, Wang S (2014) Study of methane autothermal reforming catalyst. J Rare Earths 32:184–188. https://doi.org/10.1016/S1002-0721(14)60049-1
18. Borowiecki T, Denis A, Rawski M, Gołębiowski A, Stołecki K, Dmytrzyk J, Kotarba A (2014) Studies of potassium-promoted nickel catalysts for methane steam reforming: effect of surface potassium location. Appl Surf Sci 300:191–200. https://doi.org/10.1016/j.apsusc.2014.02.053
19. Juan-Juan J, Román-Martínez MC, Illán-Gómez MJ (2006) Effect of potassium content in the activity of K-promoted Ni/Al2O3 catalysts for the dry reforming of methane. Appl Catal A Gen 301:9–15. https://doi.org/10.1016/J.APCATA.2005.11.006
20. Graf PO, Mojet BL, Lefferts L (2009) The effect of potassium addition to Pt supported on YSZ on steam reforming of mixtures of methane and ethane. Appl Catal A Gen 362:88–94. https://doi.org/10.1016/J.APCATA.2009.04.022
21. Kusche M, Agel F, Ní Bhriain N, Kaftan A, Laurin M, Libuda J, Wasserscheid P (2014) Methanol steam reforming promoted by molten salt-modified platinum on alumina catalysts. ChemSusChem 7:2516–2526. https://doi.org/10.1002/CSSC.201402357
22. Jedynak A, Szmigiel D, Raróg W, Zieliński J, Pielaszek J, Dłużewski P, Kowalczyk Z (2002) Potassium-promoted carbon-based iron catalyst for ammonia synthesis. Effect of Fe dispersion. Catal Letters 81:213–218. https://doi.org/10.1023/A:1016533224270
23. Yan P, Guo W, Liang Z, Meng W, Yin Z, Li S, Li M, Zhang M, Yan J, Xiao D, Zou R, Ma D (2019) Highly efficient K-Fe/C catalysts derived from metal-organic frameworks towards ammonia synthesis. Nano Res 12:2341–2347. https://doi.org/10.1007/s12274-019-2349-0
24. Pitselis GE, Petrolekas PD, Vayenas CG (1997) Electrochemical promotion of ammonia decomposition over Fe catalyst films interfaced with K+- & H+- conductors. Ionics. Institute for Ionics, In, pp 110–116
25. Rodriguez JA, Remesal ER, Ramírez PJ, Orozco I, Liu Z, Graciani J, Senanayake SD, Sanz JF (2019) Water-gas shift reaction on K/Cu(111) and Cu/K/TiO2(110) surfaces: alkali promotion of water dissociation and production of H2. ACS Catal 9:10751–10760. https://doi.org/10.1021/acscatal.9b03922
26. Watson CD, Martinelli M, Cronauer DC, Kropf AJ, Marshall CL, Jacobs G (2020) Low temperature water-gas shift: optimization of K loading on Pt/m-ZrO2 for enhancing CO conversion. Appl Catal A Gen 598:117572. https://doi.org/10.1016/j.apcata.2020.117572
27. De Lucas-Consuegra A, Caravaca A, González-Cobos J, Valverde JL, Dorado F (2011) Electrochemical activation of a non-noble metal catalyst for the water-gas shift reaction. Catal Commun 15:6–9. https://doi.org/10.1016/j.catcom.2011.08.007

28. Souentie S, Lizarraga L, Kambolis A, Alves-Fortunato M, Valverde JL, Vernoux P (2011) Electrochemical promotion of the water-gas shift reaction on Pt/YSZ. J Catal 283:124–132. https://doi.org/10.1016/j.jcat.2011.07.009
29. Yentekakis IV, Jiang Y, Neophytides S, Bebelis S, Vayenas CG (1995) Catalysis, electrocatalysis and electrochemical promotion of the steam reforming of methane over Ni film and Ni-YSZ cermet anodes. Ionics (Kiel) 1:491–498. https://doi.org/10.1007/BF02375296
30. De Lucas-Consuegra A, Caravaca A, Martínez PJ, Endrino JL, Dorado F, Valverde JL (2010) Development of a new electrochemical catalyst with an electrochemically assisted regeneration ability for H2 production at low temperatures. J Catal 274:251–258. https://doi.org/10.1016/j.jcat.2010.07.007
31. Caravaca A, De Lucas-Consuegra A, Molina-Mora C, Valverde JL, Dorado F (2011) Enhanced H2 formation by electrochemical promotion in a single chamber steam electrolysis cell. Appl Catal B Environ 106:54–62. https://doi.org/10.1016/j.apcatb.2011.05.004
32. Neophytides S, Vayenas CG (1989) Non-faradaic electrochemical modification of catalytic activity. 2. The case of methanol dehydrogenation and decomposition on Ag. J Catal 118:147–163. https://doi.org/10.1016/0021-9517(89)90307-2
33. González-Cobos J, López-Pedrajas D, Ruiz-López E, Valverde JL, de Lucas-Consuegra A (2015) Applications of the electrochemical promotion of catalysis in methanol conversion processes. Top Catal 58:1290–1302. https://doi.org/10.1007/s11244-015-0493-7
34. De Lucas-Consuegra A, González-Cobos J, Gacia-Rodriguez Y, Endrino JL, Valverde JL (2012) Electrochemical activation of the catalytic methanol reforming reaction for H 2 production. Electrochem Commun 19:55–58. https://doi.org/10.1016/j.elecom.2012.03.016
35. De Lucas-Consuegra A, González-Cobos J, García-Rodríguez Y, Mosquera A, Endrino JL, Valverde JL (2012) Enhancing the catalytic activity and selectivity of the partial oxidation of methanol by electrochemical promotion. J Catal 293:149–157. https://doi.org/10.1016/j.jcat.2012.06.016
36. González-Cobos J, Horwat D, Ghanbaja J, Valverde JL, De Lucas-Consuegra A (2014) Electrochemical activation of Au nanoparticles for the selective partial oxidation of methanol. J Catal 317:293–302. https://doi.org/10.1016/j.jcat.2014.06.022
37. González-Cobos J, Rico VJ, González-Elipe AR, Valverde JL, De Lucas-Consuegra A (2015) Electrochemical activation of an oblique angle deposited Cu catalyst film for H2 production. Cat Sci Technol 5:2203–2214. https://doi.org/10.1039/c4cy01524j
38. González-Cobos J, Ruiz-López E, Valverde JL, de Lucas-Consuegra A (2016) Electrochemical promotion of a dispersed Ni catalyst for H_2 production via partial oxidation of methanol. Int J Hydrog Energy 41:19418–19429. https://doi.org/10.1016/j.ijhydene.2016.06.027
39. López ER, Dorado F, de Lucas-Consuegra A (2019) Electrochemical promotion for hydrogen production via ethanol steam reforming reaction. Appl Catal B Environ 243:355–364. https://doi.org/10.1016/j.apcatb.2018.10.062
40. Douvartzides SL, Tsiakaras PE (2002) Electrochemically promoted catalysis: the case of ethanol oxidation over Pt. J Catal 211:521–529. https://doi.org/10.1006/jcat.2002.3740
41. Tsiakaras PE, Douvartzides SL, Demin AK, Sobyanin VA (2002) The oxidation of ethanol over Pt catalyst-electrodes deposited on ZrO2 (8 mol% Y2O3). In: Solid state ionics. Elsevier, pp 721–726
42. Douvartzides S, Tsiakaras P (2000) Catalytic and electrocatalytic oxidation of ethanol over a La0.6Sr0.4Co0.8Fe0.2O3 perovskite-type catalyst. Solid State Ionics 136–137:849–855. https://doi.org/10.1016/S0167-2738(00)00521-X
43. Da Silva AGM, Fajardo HV, Balzer R, Probst LFD, Lovón ASP, Lovón-Quintana JJ, Valença GP, Schreine WH, Robles-Dutenhefner PA (2015) Versatile and efficient catalysts for energy and environmental processes: mesoporous silica containing Au, Pd and Au-Pd. J Power Sources 285:460–468. https://doi.org/10.1016/j.jpowsour.2015.03.066

44. Mudiyanselage K, Al-Shankiti I, Foulis A, Llorca J, Idriss H (2016) Reactions of ethanol over CeO2 and Ru/CeO2 catalysts. Appl Catal B Environ 197:198–205. https://doi.org/10.1016/j.apcatb.2016.03.065
45. Ghita D, Stanica Ezeanu D, Cursaru D, Rosca P (2016) Hydrogen production by steam reforming of bioethanol over Pt based catalysts. Revista de Chimie 67:145–149
46. Rodrigues TS, Silva FA, Candido EG, AGM DS, Dos RR, PHC C, Linardi M, Fonseca FC (2019) Ethanol steam reforming: understanding changes in the activity and stability of Rh/MxOy catalysts as function of the support. J Mater Sci 54:11400–11416. https://doi.org/10.1007/s10853-019-03660-z
47. Lytkina AA, Mironova EY, Orekhova NV, Ermilova MM, Yaroslavtsev AB (2019) Ru-containing catalysts for methanol and ethanol steam reforming in conventional and membrane reactors. Inorg Mater 55:547–555. https://doi.org/10.1134/S0020168519060104
48. Martinelli M, Watson CD, Jacobs G (2020) Sodium doping of Pt/m-ZrO2 promotes C–C scission and decarboxylation during ethanol steam reforming. Int J Hydrog Energy 45:18490–18501. https://doi.org/10.1016/j.ijhydene.2019.08.111
49. Deinega IV, Dolgykh LY, Staraya LA, Strizhak PE, Moroz EM, Pakharukova VP (2014) Catalytic properties of nanosized Cu/ZrO2 systems in the steam reforming of bioethanol. Theor Exp Chem 50:46–52. https://doi.org/10.1007/s11237-014-9347-9
50. Ferencz Z, Varga E, Puskás R, Kónya Z, Baán K, Oszkó A, Erdőhelyi A (2018) Reforming of ethanol on Co/Al2O3 catalysts reduced at different temperatures. J Catal 358:118–130. https://doi.org/10.1016/j.jcat.2017.12.003
51. Augusto BL, Ribeiro MC, Aires FJCS, da Silva VT, Noronha FB (2020) Hydrogen production by the steam reforming of ethanol over cobalt catalysts supported on different carbon nanostructures. Catal Today 344:66–74. https://doi.org/10.1016/j.cattod.2018.10.029
52. Palm MO, Silva Júnior ME, Cardoso LR, Duarte DA, Catapan RC (2020) On the effect of the washcoat on the partial oxidation and steam reforming of ethanol on Ni/Al2O3 monolith in short-contact-time reactors. Energy and Fuels 34:2205–2213. https://doi.org/10.1021/acs.energyfuels.9b03655
53. Nuñez Meireles M, Alonso JA, Fernández Díaz MT, Cadús LE, Aguero FN (2020) Ni particles generated in situ from spinel structures used in ethanol steam reforming reaction. Mater Today Chem 15:100213. https://doi.org/10.1016/j.mtchem.2019.100213
54. Chen D, Liu C, Mao Y, Wang W, Li T (2020) Efficient hydrogen production from ethanol steam reforming over layer-controlled graphene-encapsulated Ni catalysts. J Clean Prod 252:119907. https://doi.org/10.1016/j.jclepro.2019.119907
55. Parlett CMA, Durndell LJ, Isaacs MA, Liu X, Wu C (2020) Ethanol steam reforming for Hydrogen production over hierarchical macroporous mesoporous SBA-15 supported nickel nanoparticles. Top Catal 63:403–412. https://doi.org/10.1007/s11244-020-01265-4
56. Ishihara A, Andou A, Hashimoto T, Nasu H (2020) Steam reforming of ethanol using novel carbon-oxide composite-supported Ni, Co and Fe catalysts. Fuel Process Technol 197:106203. https://doi.org/10.1016/j.fuproc.2019.106203
57. Chen LC, Lin SD (2011) The ethanol steam reforming over Cu-Ni/SiO2 catalysts: effect of Cu/Ni ratio. Appl Catal B Environ 106:639–649. https://doi.org/10.1016/j.apcatb.2011.06.028
58. Cifuentes B, Bustamante F, Conesa JA, Córdoba LF, Cobo M (2018) Fuel-cell grade hydrogen production by coupling steam reforming of ethanol and carbon monoxide removal. Int J Hydrog Energy 43:17216–17229. https://doi.org/10.1016/j.ijhydene.2018.07.139
59. Soler L, Casanovas A, Ryan J, Angurell I, Escudero C, Pérez-Dieste V, Llorca J (2019) Dynamic reorganization of bimetallic nanoparticles under reaction depending on the support nanoshape: the case of RhPd over ceria nanocubes and nanorods under ethanol steam reforming. ACS Catal 9:3641–3647. https://doi.org/10.1021/acscatal.9b00463
60. Efimov MN, Mironova EY, Vasilev AA, Muratov DG, Averin AA, Zhilyaeva NA, Dzidziguri EL, Yaroslavtsev AB, Karpacheva GP (2019) Ethanol steam reforming over Co[sbnd]Ru nanoparticles supported on highly porous polymer-based carbon material. Catal Commun 128:105717. https://doi.org/10.1016/j.catcom.2019.105717

61. Efimov MN, Mironova EY, Pavlov AA, Vasilev AA, Muratov DG, Dzidziguri EL, Yaroslavtsev AB, Karpacheva GP (2020) Novel polyacrylonitrile-based C/Co-Ru metal-carbon nanocomposites as effective catalysts for ethanol steam reforming. Int J Nanosci:19. https://doi.org/10.1142/S0219581X19500315
62. Furtado AC, Alonso CG, Cantão MP, Fernandes-Machado NRC (2009) Bimetallic catalysts performance during ethanol steam reforming: influence of support materials. Int J Hydrog Energy 34:7189–7196. https://doi.org/10.1016/j.ijhydene.2009.06.060
63. Phung TK, Pham TLM, Nguyen ANT, Vu KB, Giang HN, Nguyen TA, Huynh TC, Pham HD (2020) Effect of supports and promoters on the performance of Ni-based catalysts in ethanol steam reforming. Chem Eng Technol 43:672–688
64. Dobosz J, Małecka M, Zawadzki M (2018) Hydrogen generation via ethanol steam reforming over Co/HAp catalysts. J Energy Inst 91:411–423. https://doi.org/10.1016/j.joei.2017.02.001
65. Jia H, Xu H, Sheng X, Yang X, Shen W, Goldbach A (2020) High-temperature ethanol steam reforming in PdCu membrane reactor. J Memb Sci 605:118083. https://doi.org/10.1016/j.memsci.2020.118083
66. Ma R, Castro-Dominguez B, Mardilovich IP, Dixon AG, Ma YH (2016) Experimental and simulation studies of the production of renewable hydrogen through ethanol steam reforming in a large-scale catalytic membrane reactor. Chem Eng J 303:302–313. https://doi.org/10.1016/j.cej.2016.06.021
67. Chagas CA, Manfro RL, Toniolo FS (2020) Production of hydrogen by steam reforming of ethanol over Pd-promoted Ni/SiO2 catalyst. Catal Letters 150:3424–3436. https://doi.org/10.1007/s10562-020-03257-1
68. Greluk M, Rotko M, Turczyniak-Surdacka S (2020) Enhanced catalytic performance of La2O3 promoted Co/CeO2 and Ni/CeO2 catalysts for effective hydrogen production by ethanol steam reforming: La2O3 promoted Co(Ni)/CeO2 catalysts in SRE. Renew Energy 155:378–395. https://doi.org/10.1016/j.renene.2020.03.117
69. Vecchietti J, Lustemberg P, Fornero EL, Calatayud M, Collins SE, Mohr S, Ganduglia-Pirovano MV, Libuda J, Bonivardi AL (2020) Controlled selectivity for ethanol steam reforming reaction over doped CeO2 surfaces: the role of gallium. Appl Catal B Environ 277:119103. https://doi.org/10.1016/j.apcatb.2020.119103
70. Kim KM, Kwak BS, Im Y, Park NK, Lee TJ, Lee ST, Kang M (2017) Effective hydrogen production from ethanol steam reforming using CoMg co-doped SiO2@Co1−xMgxO catalyst. J Ind Eng Chem 51:140–152. https://doi.org/10.1016/j.jiec.2017.02.025
71. Yoo S, Park S, Song JH, Kim DH (2020) Hydrogen production by the steam reforming of ethanol over K-promoted Co/Al2O3–CaO xerogel catalysts. Mol Catal 491:110980. https://doi.org/10.1016/j.mcat.2020.110980
72. Wang N, Feng Y, Guo X, Ni S (2020) Continuous high-purity hydrogen production by sorption enhanced steam reforming of ethanol over modified lithium silicate. Int J Hydrog Energy 46:10119–10130. https://doi.org/10.1016/j.ijhydene.2020.04.225
73. Vernoux P, Gaillard F, Lopez C, Siebert E (2003) Coupling catalysis to electrochemistry: a solution to selective reduction of nitrogen oxides in lean-burn engine exhausts? J Catal 217:203–208. https://doi.org/10.1016/S0021-9517(03)00052-6
74. Yentekakis IV, Neophytides S, Vayenas CG (1988) Solid electrolyte aided study of the mechanism of CO oxidation on polycrystalline platinum. J Catal 111:152–169. https://doi.org/10.1016/0021-9517(88)90074-7
75. Yentekakis IV, Bebelis S (1992) Study of the NEMCA effect in a single-pellet catalytic reactor. J Catal 137:278–283. https://doi.org/10.1016/0021-9517(92)90157-D
76. de Lucas-Consuegra A, Princivalle A, Caravaca A, Dorado F, Guizard C, Valverde JL, Vernoux P (2010) Preferential CO oxidation in hydrogen-rich stream over an electrochemically promoted Pt catalyst. Appl Catal B Environ 94:281–287. https://doi.org/10.1016/j.apcatb.2009.11.019
77. De Lucas-Consuegra A, González-Cobos J, Carcelén V, Magén C, Endrino JL, Valverde JL (2013) Electrochemical promotion of Pt nanoparticles dispersed on a diamond-like carbon

matrix: a novel electrocatalytic system for H2 production. J Catal 307:18–26. https://doi.org/10.1016/j.jcat.2013.06.012
78. Espinós JP, Rico VJ, González-Cobos J, Sánchez-Valencia JR, Pérez-Dieste V, Escudero C, de Lucas-Consuegra A, González-Elipe AR (2018) In situ monitoring of the phenomenon of electrochemical promotion of catalysis. J Catal 358:27–34. https://doi.org/10.1016/j.jcat.2017.11.027
79. Dömök M, Baán K, Kecskés T, Erdőhelyi A (2008) Promoting mechanism of potassium in the reforming of ethanol on Pt/Al2O3 catalyst. Catal Letters 126:49–57. https://doi.org/10.1007/s10562-008-9616-0
80. Dorado F, de Lucas-Consuegra A, Vernoux P, Valverde JL (2007) Electrochemical promotion of platinum impregnated catalyst for the selective catalytic reduction of NO by propene in presence of oxygen. Appl Catal B Environ 73:42–50. https://doi.org/10.1016/j.apcatb.2006.12.001
81. Tsiplakides D, Balomenou S (2009) Milestones and perspectives in electrochemically promoted catalysis. Catal Today 146:312–318. https://doi.org/10.1016/j.cattod.2009.05.015
82. Kourtelesis M, Panagiotopoulou P, Ladas S, Verykios XE (2015) Influence of the support on the reaction network of ethanol steam reforming at low temperatures over Pt catalysts. Top Catal 58:1202–1217. https://doi.org/10.1007/s11244-015-0485-7
83. Contreras JL, Salmones J, Colín-Luna JA, Nuño L, Quintana B, Córdova I, Zeifert B, Tapia C, Fuentes GA (2014) Catalysts for H2 production using the ethanol steam reforming (a review). Int J Hydrog Energy 39:18835–18853. https://doi.org/10.1016/j.ijhydene.2014.08.072
84. González-Gil R, Herrera C, Larrubia MA, Mariño F, Laborde M, Alemany LJ (2016) Hydrogen production by ethanol steam reforming over multimetallic RhCeNi/Al2O3 structured catalyst. Pilot-scale study. Int J Hydrog Energy 41:16786–16796. https://doi.org/10.1016/j.ijhydene.2016.06.234
85. Compagnoni M, Tripodi A, Di Michele A, Sassi P, Signoretto M, Rossetti I (2017) Low temperature ethanol steam reforming for process intensification: new Ni/MxO–ZrO2 active and stable catalysts prepared by flame spray pyrolysis. Int J Hydrog Energy 42:28193–28213. https://doi.org/10.1016/j.ijhydene.2017.09.123
86. Lang L, Zhao S, Yin X, Yang W, Wu C (2015) Catalytic activities of K-modified zeolite ZSM-5 supported rhodium catalysts in low-temperature steam reforming of bioethanol. Int J Hydrog Energy 40:9924–9934. https://doi.org/10.1016/j.ijhydene.2015.06.016
87. Dong T, Wang Z, Yuan L, Torimoto Y, Sadakata M, Li Q (2007) Hydrogen production by steam reforming of ethanol on potassium-doped 12CaO • 7Al2O3 catalyst. Catal Letters 119:29–39. https://doi.org/10.1007/s10562-007-9148-z
88. Espinat D, Dexpert H, Freund E, Martino G, Couzi M, Lespade P, Cruege F (1985) Characterization of the coke formed on reforming catalysts by laser raman spectroscopy. Appl Catal 16:343–354. https://doi.org/10.1016/S0166-9834(00)84398-5
89. da Silva VT, Mozer TS, da Costa Rubim Messeder dos Santos D, da Silva César A (2017) Hydrogen: trends, production and characterization of the main process worldwide. Int J Hydrog Energy 42:2018–2033
90. Salge JR, Deluga GA, Schmidt LD (2005) Catalytic partial oxidation of ethanol over noble metal catalysts. J Catal 235:69–78. https://doi.org/10.1016/j.jcat.2005.07.021
91. Sawatmongkhon B, Theinnoi K, Wongchang T, Haoharn C, Wongkhorsub C, Tsolakis A (2019) Hydrogen production via the catalytic partial oxidation of ethanol on a platinum-rhodium catalyst: effect of the oxygen-to-ethanol molar ratio and the addition of steam. Energy and Fuels 33:6742–6753. https://doi.org/10.1021/acs.energyfuels.9b01398
92. Mattos LV, Noronha FB (2005) Partial oxidation of ethanol on supported Pt catalysts. J Power Sources 145:10–15. https://doi.org/10.1016/j.jpowsour.2004.12.034
93. Sheng PY, Yee A, Bowmaker GA, Idriss H (2002) H2 production from ethanol over Rh-Pt/CeO2 catalysts: the role of Rh for the efficient dissociation of the carbon-carbon bond. J Catal 208:393–403. https://doi.org/10.1006/jcat.2002.3576

94. Mattos LV, Noronha FB (2005) The influence of the nature of the metal on the performance of cerium oxide supported catalysts in the partial oxidation of ethanol. J Power Sources 152:50–59. https://doi.org/10.1016/j.jpowsour.2004.12.052
95. Bi JL, Hsu SN, Yeh CT, Bin WC (2007) Low-temperature mild partial oxidation of ethanol over supported platinum catalysts. Catal Today 129:330–335. https://doi.org/10.1016/j.cattod.2006.10.011
96. Silva AM, Barandas APMG, Costa LOO, Borges LEP, Mattos LV, Noronha FB (2007) Partial oxidation of ethanol on Ru/Y2O3 and Pd/Y2O3 catalysts for hydrogen production. Catal Today 129:297–304. https://doi.org/10.1016/j.cattod.2006.09.036
97. Costa LOO, Silva AM, Borges LEP, Mattos LV, Noronha FB (2008) Partial oxidation of ethanol over Pd/CeO2 and Pd/Y2O3 catalysts. Catal Today 138:147–151. https://doi.org/10.1016/j.cattod.2008.05.003
98. Silva AM, Costa LOO, Barandas APMG, Borges LEP, Mattos LV, Noronha FB (2008) Effect of the metal nature on the reaction mechanism of the partial oxidation of ethanol over CeO2-supported Pt and Rh catalysts. Catal Today 133–135:755–761. https://doi.org/10.1016/j.cattod.2007.12.103
99. de Lima SM, da Cruz IO, Jacobs G, Davis BH, Mattos LV, Noronha FB (2008) Steam reforming, partial oxidation, and oxidative steam reforming of ethanol over Pt/CeZrO2 catalyst. J Catal 257:356–368. https://doi.org/10.1016/j.jcat.2008.05.017
100. Liguras DK, Goundani K, Verykios XE (2004) Production of hydrogen for fuel cells by catalytic partial oxidation of ethanol over structured Ni catalysts. J Power Sources 130:30–37. https://doi.org/10.1016/j.jpowsour.2003.12.008
101. Wang W, Wang Z, Ding Y, Xi J, Lu G (2002) Partial oxidation of ethanol to hydrogen over Ni-Fe catalysts. Catal Letters 81:63–68. https://doi.org/10.1023/A:1016008006076
102. Kraleva E, Rodrigues CP, Pohl MM, Ehrich H, Noronha FB (2019) Syngas production by partial oxidation of ethanol on PtNi/SiO2-CeO2 catalysts. Cat Sci Technol 9:634–645. https://doi.org/10.1039/c8cy02418a
103. Sadykov VA, Eremeev NF, Sadovskaya EM, Chesalov YA, Pavlova SN, Rogov VA, Simonov MN, Bobin AS, Glazneva TS, Smal EA, Lukashevich AI, Krasnov AV, Avdeev VI, Roger AC (2020) Detailed mechanism of ethanol transformation into syngas on catalysts based on mesoporous MgAl2O4 support loaded with Ru + Ni/(PrCeZrO or MnCr2O4) active components. Top Catal 63:166–177. https://doi.org/10.1007/s11244-020-01222-1
104. Lin YC, Chang CH, Chen CC, Jehng JM, Shyu SG (2008) Supported vanadium oxide catalysts in selective oxidation of ethanol: comparison of TiO2/SiO2 and ZrO2/SiO2 as supports. Catal Commun 9:675–679. https://doi.org/10.1016/j.catcom.2007.08.002
105. Yun D, Zhao Y, Abdullahi I, Herrera JE (2014) The effect of interstitial nitrogen in the activity of the VO x/N-TiO2 catalytic system for ethanol partial oxidation. J Mol Catal A Chem 390:169–177. https://doi.org/10.1016/j.molcata.2014.03.022
106. Silva AM, de Farias AMD, Costa LOO, Barandas APMG, Mattos LV, Fraga MA, Noronha FB (2008) Partial oxidation and water-gas shift reaction in an integrated system for hydrogen production from ethanol. Appl Catal A Gen 334:179–186. https://doi.org/10.1016/j.apcata.2007.10.004
107. Chimentão RJ, Herrera JE, Kwak JH, Medina F, Wang Y, Peden CHF (2007) Oxidation of ethanol to acetaldehyde over Na-promoted vanadium oxide catalysts. Appl Catal A Gen 332:263–272. https://doi.org/10.1016/j.apcata.2007.08.024
108. Jahromi AF, Ruiz-López E, Dorado F, Baranova EA, de Lucas-Consuegra A (2022) Electrochemical promotion of ethanol partial oxidation and reforming reactions for hydrogen production. Renew Energy 183:515–523. https://doi.org/10.1016/J.RENENE.2021.11.041
109. Schmal M, Cesar DV, Souza MMVM, Guarido CE (2011) Drifts and TPD analyses of ethanol on Pt catalysts over Al_2O_3 and ZrO_2—partial oxidation of ethanol. Can J Chem Eng 89:1166–1175. https://doi.org/10.1002/cjce.20597
110. Yao YFY (1984) Catalytic oxidation of ethanol at low concentrations. Ind Eng Chem Process Des Dev 23:60–67. https://doi.org/10.1021/i200024a011

111. Cavallaro S, Chiodo V, Freni S, Mondello N, Frusteri F (2003) Performance of Rh/Al2O3 catalyst in the steam reforming of ethanol: H2 production for MCFC. Appl Catal A Gen 249: 119–128. https://doi.org/10.1016/S0926-860X(03)00189-3
112. Livio D, Diehm C, Donazzi A, Beretta A, Deutschmann O (2013) Catalytic partial oxidation of ethanol over Rh/Al2O3: spatially resolved temperature and concentration profiles. Appl Catal A Gen 467:530–541. https://doi.org/10.1016/j.apcata.2013.07.054
113. Cai W, Wang F, Zhan E, Van Veen AC, Mirodatos C, Shen W (2008) Hydrogen production from ethanol over Ir/CeO2 catalysts: a comparative study of steam reforming, partial oxidation and oxidative steam reforming. J Catal 257:96–107. https://doi.org/10.1016/j.jcat.2008.04.009
114. De Lima SM, Da Silva AM, Da Costa LOO, Graham UM, Jacobs G, Davis BH, Mattos L V., Noronha FB (2009) Study of catalyst deactivation and reaction mechanism of steam reforming, partial oxidation, and oxidative steam reforming of ethanol over Co/CeO2 catalyst. J Catal 268:268–281. doi:https://doi.org/10.1016/j.jcat.2009.09.025
115. Cavallaro S, Chiodo V, Vita A, Freni S (2003) Hydrogen production by auto-thermal reforming of ethanol on Rh/Al2O3 catalyst. J Power Sources 123:10–16. https://doi.org/10.1016/S0378-7753(03)00437-3
116. Zagoraios D, Tsatsos S, Kennou S, Vayenas CG, Kyriakou G, Katsaounis A (2020) Tuning the RWGS reaction via EPOC and in situ electro-oxidation of cobalt nanoparticles. ACS Catal 10: 14916–14927. https://doi.org/10.1021/ACSCATAL.0C04133
117. Zagoraios D, Athanasiadi A, Kalaitzidou I, Ntais S, Katsaounis A, Caravaca A, Vernoux P, Vayenas CG (2020) Electrochemical promotion of methane oxidation over nanodispersed Pd/Co3O4 catalysts. Catal Today 355:910–920. https://doi.org/10.1016/J.CATTOD.2019.02.030
118. Le Valant A, Can F, Bion N, Duprez D, Epron F (2010) Hydrogen production from raw bioethanol steam reforming: optimization of catalyst composition with improved stability against various impurities. Int J Hydrog Energy 35:5015–5020. https://doi.org/10.1016/J.IJHYDENE.2009.09.008
119. Liu L, Hong D, Wang N, Guo X (2020) High purity H2 production from sorption enhanced bio-ethanol reforming via sol-gel-derived Ni–CaO–Al2O3 bi-functional materials. Int J Hydrog Energy 45:34449–34460. https://doi.org/10.1016/J.IJHYDENE.2020.02.158
120. Okolie JA, Mukherjee A, Nanda S, Dalai AK, Kozinski JA (2021) Next-generation biofuels and platform biochemicals from lignocellulosic biomass. Int J Energy Res 45:14145–14169. https://doi.org/10.1002/ER.6697
121. Ruiz-López E, Caravaca A, Vernoux P, Dorado F, de Lucas-Consuegra A (2020) Over-faradaic hydrogen production in methanol electrolysis cells. Chem Eng J 396:125217. https://doi.org/10.1016/J.CEJ.2020.125217

Chapter 8
Electrochemical Promotion and Related Phenomena During Ammonia Synthesis

Anastasios Vourros, Ioannis Garagounis, and Michael Stoukides

Abstract A large number of studies on the electrochemical synthesis of ammonia have been published in the past two decades, but very few of them searched for electrochemical promotion phenomena. This is because in most of the studies, pure N_2 (instead of N_2/H_2 mixture) was introduced over the cathode. In the studies on NH_3 synthesis, the Faradaic efficiency, Λ, attains very low values, and, in most cases, the phenomenon is "sub-Faradaic," i.e., $\Lambda < 1$. The Λ values are substantially larger when a mixture of N_2 and H_2, rather than N_2 alone, is introduced at the cathode. In the reaction of NH_3 decomposition, the picture is improved: in all cases, $\Lambda > 1$ and values of the order of 100 have been reported. For either reaction (synthesis or decomposition), the ρ values are comparable to those reported in previous NEMCA studies: a maximum $\rho = 220$ has been reported, while typical values are between 2 and 10. The NEMCA characteristics in NH_3 synthesis were poor primarily because its thermodynamic equilibrium limits the yield and, therefore, electrical energy must be supplied to the system in order to attain the desired conversion.

Keywords Ammonia synthesis · Electrochemical promotion · NEMCA · EPOC · Solid electrolytes

8.1 Introduction: The Synthesis of Ammonia from Its Elements

The twentieth century is full of remarkable scientific inventions and discoveries: the airplane, television, nuclear energy, antibiotics, walking on the moon, computers, DNA structure, the Internet, and many others. Nevertheless, when the scientific community was asked to name the most important achievement of the past century, none of the above won. Instead, the synthesis of ammonia from its elements

A. Vourros (✉) · I. Garagounis · M. Stoukides
Chemical Engineering Department, Aristotle University of Thessaloniki & Center for Research and Technology Hellas, Thessaloniki, Greece
e-mail: mstoukid@auth.gr

P. Vernoux, C. G. Vayenas (eds.), *Recent Advances in Electrochemical Promotion of Catalysis*, Modern Aspects of Electrochemistry 61,
https://doi.org/10.1007/978-3-031-13893-5_8

$$3\,H_2 + N_2 \rightleftarrows 2\,NH_3 \tag{8.1}$$

was on the top [1–3]. This selection is totally justified. Without ammonia, the world population could not exceed 3.5 billion. In other words, today, half of the people on earth have food to eat thanks to the discovery of the industrial synthesis of ammonia [4].

Human food must contain amino acids in order for our body to synthesize proteins. These amino acids are supplied primarily by agricultural crops. Because amino acids and proteins contain nitrogen in its atomic form, agricultural crops are limited by the availability of atomic nitrogen [4]. Nitrogen is abundant in the atmosphere but in its diatomic form, N_2. The utilization of atmospheric N_2 was achieved via its conversion into ammonia, which in turn is the basic constituent of fertilizers.

In 1913, BASF put in operation the first ammonia plant in Germany. It could produce 5 tons of ammonia per day or, equivalently, 1825 tons/year [5, 6]. Nowadays, the worldwide production of ammonia exceeds 150 million tons/year [3, 7, 8]. About 80% of it is used to make fertilizers. In the last two decades, ammonia's role in the energy economy has been upgraded considerably. One ammonia molecule can host three hydrogen atoms and does not contain carbon. Clearly, it is an attractive compound in the development of environmentally friendly processes for power generation and hydrogen storage [3, 9]. Furthermore, it can be used as a fuel in both thermal engines and fuel cells [10]. The continuous development of renewable energy technologies is expected to further upgrade the importance of ammonia in the global energy economy as this carbon-free liquid compound is both a fuel and a hydrogen carrier [11].

The dominant route to the industrial production of NH_3 is the Haber-Bosch (H-B) process, developed at the beginning of the twentieth century. Although its basic characteristics remain the same, numerous studies and research efforts have focused on the improvement and optimization of this reaction system. From the engineering point of view, it was realized early on that the conversion of reaction (8.1) is limited by thermodynamics. Because four volumes of reactants produce two volumes of product, the equilibrium conversion increases with pressure. Also, because the reaction is exothermic, the equilibrium conversion decreases with temperature. Thus, if the reaction is carried out at ambient conditions (25 °C, 1 atm), the thermodynamically predicted conversion exceeds 99%. At 25 °C, however, the reaction kinetics are too slow for industrial practice. Therefore, temperatures between 400 °C and 500 °C must be used to obtain reasonable reaction rates. At these temperatures, however, the equilibrium conversion is extremely low if the pressure is kept atmospheric. Consequently, pressures between 100 and 300 bar are used [5, 6]. Under these conditions, the reaction conversion is about 15%. The formation of the NH_3 molecule requires cleavage of the $N \equiv N$ triple bond first. This is one of the strongest bonds in nature: 945 kJ/mol [12]. The search for an effective catalyst and the elucidation of the reaction mechanism opened the road and promoted the fields of surface science and heterogeneous catalysis to a great extent.

Michel Boudart, one of the most distinguished scientists in this field, named ammonia synthesis "The Bellwether Reaction of Heterogeneous Catalysis" [13]. Today, it is generally accepted that the rate determining step in ammonia synthesis is the dissociative adsorption of molecular N_2 on the catalyst surface [14–16].

8.2 The Electrochemical Synthesis of Ammonia

As opposed to the industrial synthesis, which operates at elevated temperatures and pressures, plants can convert N_2 of the air into ammonia under ambient conditions. The nature of this reaction is essentially electrochemical: protons (H^+), electrons (e^-), and N_2 react in the presence of the metalloenzyme nitrogenase [14, 15]. According to most researchers, the enzyme-catalyzed synthesis proceeds via an associative mechanism: the N_2 molecule is partially hydrogenated before breaking the triple N ≡ N bond [14–18]. In an effort to imitate nature, several investigators studied the electrochemical synthesis of ammonia at ambient conditions using liquid (aqueous or organic) electrolytes [19–26]. Success, however, was limited. The main problem was that liquid electrolyte cells have to operate at low temperatures at which the reaction kinetics are slow.

In 1981, Iwahara and coworkers reported that certain mixed oxides of the perovskite structure exhibit significant proton (H^+) conduction at elevated temperatures, i.e., 500–900 °C [27]. Since then, a large number of proton-conducting ceramics have been synthesized. Such high-temperature proton conductors are very useful in catalytic processes because they can operate under conditions at which industrial hydro- and dehydrogenation reactions take place [28].

Using a solid-state proton conductor and the cell of Fig. 8.1, the solid-state ammonia synthesis (SSAS) was first experimentally demonstrated in 1998 [29]. Two porous film electrodes are placed on the two sides of the solid electrolyte. Hydrogen and nitrogen flow over the anodic and the cathodic electrode, respectively. By the application of an external potential across the cell, hydrogen is converted to protons at the anode:

$$3\,H_2 \rightleftarrows 6\,H^+ + 6\,e^- \tag{8.2}$$

At the cathode, N_2 reacts with H^+ to produce ammonia:

$$N_2 + 6\,H^+ + 6\,e^- \rightleftarrows 2\,NH_3 \tag{8.3}$$

The use of the solid electrolyte cell of Fig. 8.1 exhibits certain advantages when compared to the H-B process. The first is that the high-pressure requirement is counterbalanced by the supply of electrical energy. In fact, in the cell of Fig. 8.1, where hydrogen is supplied in the form of H^+, one reactant volume produces two

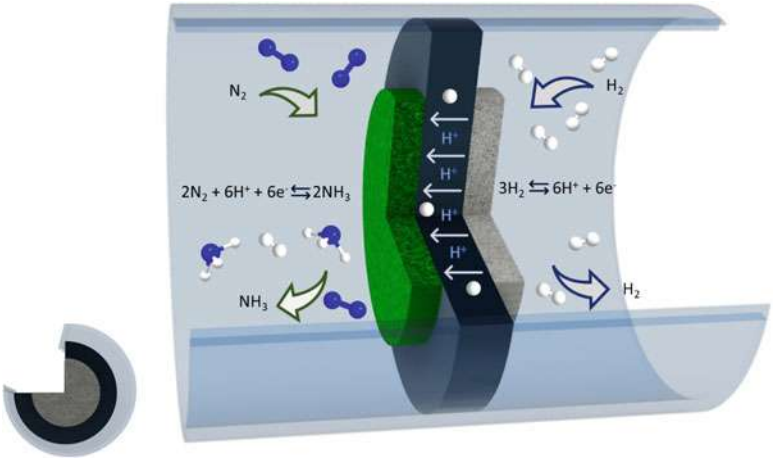

Fig. 8.1 Schematic diagram of a double-chamber solid-state H^+-conducting cell; here, NH_3 is produced from gaseous H_2 and N_2

volumes of product as shown in Eq. (8.3). Thus, the high-pressure requirement is essentially reversed. The energy input in the form of electrical work into the system allows the conversion to ammonia to attain values higher than those predicted by the thermodynamic equilibrium of reaction (8.1). This does not constitute a violation of thermodynamics. To understand how this is possible, one can consider another well-known example of an electrochemical reaction:

$$H_2O \rightleftarrows H_2 + 1/2\ O_2 \tag{8.4}$$

At 25 °C, the equilibrium constant for reaction (8.4) is of the order of 10^{-38}. This means that if, starting with 1 mol of H_2O, there are x moles of H_2 at equilibrium, there will also be x/2 moles of O_2 and 1-x moles of H_2O. Since $K = 10^{-38} = P_{H2}(P_{O2})^{0.5}(P_{H2O})^{-1}$, x comes out to be of the order of 10^{-25}. Nevertheless, if electrical work is offered, H_2O is quantitatively decomposed to H_2 and O_2 at ambient conditions (electrolysis).

The second advantage of SSAS is that protons are the only species that can be transported from the anode to the cathode. In the H-B process, hydrogen is produced from steam reforming of natural gas which may contain compounds that can cause catalyst poisoning, even in trace amounts [5, 6]. In SSAS, only protons reach the cathode, and there is no reason for external purification. Moreover, in addition to gaseous H_2, the hydrogen source can be any hydrogen-containing compound, e.g., steam, hydrocarbons, or their mixture.

From 1998 and until 2013, a large number of investigators had studied SSAS in order to optimize the process. More than 30 solid electrolyte materials were tested, and at least 15 catalysts were used as working electrodes [6, 30]. In the past decade, research has expanded to include studies based on liquid electrolytes, operating at

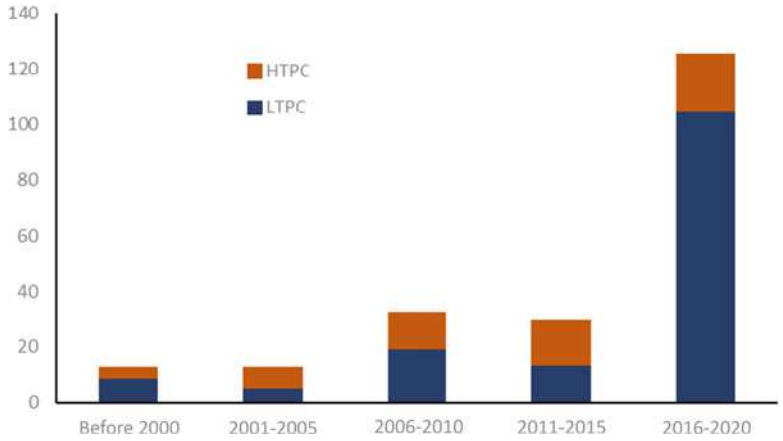

Fig. 8.2 Experimental works on the electrochemical synthesis of NH_3 up until 2020

near room temperature, and molten salt electrolytes, operating at 300–500 °C [7]. Figure 8.2 shows the number of experimental works on the electrochemical synthesis of NH_3 in the last 20 years. The orange part in each block represents the SSAS, high-temperature (T > 400 °C) studies, i.e., those in which the electrolyte was a solid-state proton conductor. The blue part represents aqueous or non-aqueous low-temperature (T < 100 °C) studies as well as those conducted in molten salt electrolytes. While very few papers were published before 2000, a gradual increase in publications is observed from 2000 to 2015 followed by an explosive increase in the past 5 years, as reviewed by several comprehensive studies [3, 6, 34, 35, 7, 8, 10, 16, 30–33].

In the past two decades, numerous studies on the electrochemical synthesis have been reported. The main findings from these works have been presented in several reviews [6–8, 30–34]. Also, the hurdles that need to be overcome in order to make the electrochemical synthesis competitive to the existing H-B process were identified therein and can be summarized as follows:

1. One of the reactants, hydrogen, is supplied electrochemically. Therefore, in order for the reaction rate not to be limited by the supply of protons, a high protonic conductivity of the electrolyte is required [6–8].
2. The working electrode (cathode) should exhibit high electronic conductivity. Unfortunately, several of the industrial catalysts, which have been developed and improved for many years, are poor conductors.
3. The cathodic electrode must be selective toward NH_3 synthesis. On most electrodes, the reaction between two protons to produce molecular H_2 competes favorably with the reaction of ammonia synthesis, and this results in a severe decrease in Faradaic efficiency (FE). In general, the FE values are lower than 10%. Worse is the picture in aqueous electrolyte systems (temperatures <100 °C), where most of the reported FE values are of the order of 1% [6–8].

4. An increase in the applied current results in an increase in the reaction rate up to a certain value above which the rate levels off or even decreases with current. This effect has been interpreted as "poisoning" of the electrode by protons which suppress the adsorption of nitrogen [16, 30].

8.3 Electrochemical Promotion in Ammonia Synthesis

Solid-state proton conductors can be used to electrochemically promote the rates of catalytic hydro- and dehydrogenation reactions. If the catalyst to be promoted is one of the electrodes, protons can be "pumped" to or away from the catalyst during reaction. The effect of electrochemical H^+ pumping can be quantitatively expressed by the use of two dimensionless parameters [36]:

$$\Lambda = \Delta r/(I/2F) \tag{8.5}$$

and

$$\rho = r/r_0 \tag{8.6}$$

where I is the imposed current, F is Faraday's constant, r is the catalytic reaction rate obtained at closed circuit, r_0 is the open-circuit catalytic rate, and $\Delta r = r - r_0$, with both r and r_0 expressed in mol/s of H_2 consumption (or production). Similarly, $I/2F$ is expressed in mol/s of H_2 transported through the electrolyte. If Δr, r, and r_0 are expressed in moles of NH_3 produced/s, instead of Eq. (8.5), Λ will be defined from the following equation:

$$\Lambda \quad = 1.5\ (\Delta r)/(I/2F) = (r - r_0)/(I/3F) \tag{8.7}$$

If $\Lambda = 1$, the effect is Faradaic, i.e., the increase in reaction rate equals the rate of proton transport through the electrolyte. If $\Lambda > 1$, the reaction system under study exhibits the phenomenon of non-Faradaic electrochemical modification of catalytic activity (NEMCA) or, equivalently, the phenomenon of electrochemical promotion (EPOC).

Despite the very large number of studies on the electrochemical synthesis of ammonia (Fig. 8.2), in only a few of them was hydrogen introduced together with nitrogen at the cathode. Consequently, there were very few studies that could report on the existence of EPOC effects. Table 8.1 contains these works regardless of the value of the Faradaic efficiency, i.e., even if $\Lambda < 1$. Also shown in this table are electrochemical promotion studies of the reverse reaction of ammonia decomposition. The first column on the left-hand side contains abbreviated symbols of the type of the electrolyte that was used. The exact formula of these electrolytes can be found below the table. The second column shows the catalyst used, which was also the working electrode (WE) of the cell. The next two columns show the operating

Table 8.1 Electrochemical promotion studies in ammonia synthesis

Electrolyte	Working electrode (WE)	Temperature (°C)	Reactor type	Reaction mixture – composition	Λ	ρ	References
Ammonia synthesis							
SCYb	Pd	570–750	SC	$H_2/N_2 = 1.0–5.0$	2.5	–	[37]
CIZ	Fe	440	SC	$H_2/N_2 = 0.3–3.0$	3	13.0	[38]
SZY	Fe	570–750	SC	$H_2/N_2 = 1.0–3.0$	<3	1.8	[39]
BCZY27	Rh	450–650	SC	$H_2/N_2 = 1.0$	<1	1.4	[40]
BCZY27	Ni-BZCY72	500–650	DC	$H_2/N_2 = 0.3–3.0$	<1	2.4	[41]
K-β”-Al_2O_3	Co_3Mo_3N-ag	400–550	SC	$H_2/N_2 = 1.0–6.0$	300	1.48	[42]
BCY	Fe-BCY	500–650	DC	$H_2/N_2 = 0.05–1.0$	<1	20.0	[43]
BCY	Fe, Fe-BCY, W-Fe-BCY	500–600	DC	$H_2/N_2 = 0.1–3.0$	<1	220.0	[44]
Ammonia decomposition							
CIZ	Fe	530–600	SC	11% NH_3/HE	120	3.6	[45]
KYZP	Fe	530–580	SC	11% NH_3/He	–	0.04	[45]
CIZ	Fe	500–600	SC	6.5% NH_3/He	100	4.5	[46]
SCYb	Pd	570–750	DC	13% NH_3–13.5% N_2/He	2.5	–	[37]
SCYb	Ru	350–650	SC	0.5–2.0% NH_3/He	4	5	[47]
SCYb	Ag	350–700	DC	0.5–2.0% NH_3/He	1	57	[48]
Na-βAl_2O_3	Ru	250–350	SC	1250 ppm NH_3/He	–	1.4	[49]
K-βAl_2O_3	Ru	250–350	SC	1250 ppm NH_3/He	–	3.3	[49]

BCY $BaCe_{0.9}Y_{0.1}O_{3-a}$, *CIZ* $CaIn_{0\cdot1}Zr_{0.9}O_{3-a}$, *SCYb* $SrCe_{0.95}Yb_{0\cdot05}O_3$, *SZY* $SrZr_{0.90}Y_{0\cdot1}O_{3-a}$, *BCZY27* $BaCe_{0.2}Zr_{0.7}Y_{0.1}O_{2.9}$, *KYZP* $K_2YZr(PO_4)_3$

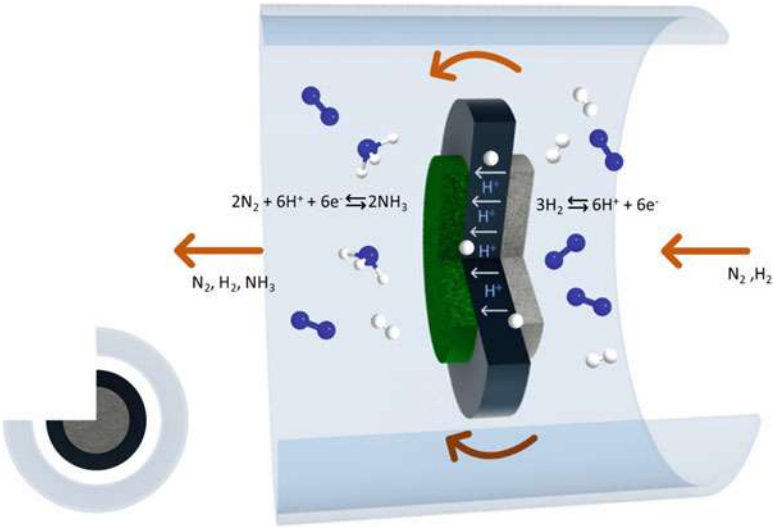

Fig. 8.3 Schematic diagram of a single-chamber (SC) H^+ cell, wherein NH_3 synthesis takes place, with or without NEMCA (side view in the bottom left)

temperature (°C) and the reactor type, respectively. Two main reactor types were used, the double-chamber (DC) reactor like that of Fig. 8.1 and the single-chamber (SC) reactor, schematically shown in Fig. 8.3. In the latter case, both electrodes (anode and cathode) are exposed to the reaction mixture. The next column shows the composition of the reactants, followed by two columns containing the values of Λ and ρ, respectively. The last column contains the reference of each work.

Equation (8.7) was used to calculate Λ if the electrolyte is a pure H^+ conductor. Otherwise, the following equation was used:

$$\Lambda = 1.5\ (r - r_0)/((I/2F)) \cdot t_{H+} \tag{8.8}$$

where t_{H+}, the proton transference number, is the fraction of the total current that is carried through the solid electrolyte in the form of H^+.

Using a perovskite of the form $SrCe_{0.95}Yb_{0.05}O_3$ (SCYb) as solid-state proton conductor and polycrystalline Pd as electrodes, the reaction of NH_3 synthesis was studied at temperatures between 570 and 750 °C and atmospheric total pressure [29, 37]. The reaction was studied in both DC and SC cells. The superficial surface area of each electrode was 1.3 cm^2 and 1.0 cm^2 for the DC and SC configurations, respectively. The experiments in the DC reactor were conducted at 570 °C. A mixture of 1.8% N_2 in He was introduced at the cathode, and a 100% H_2 stream was introduced at the anode. Upon pumping H^+ to the cathode, NH_3 was formed at a rate of up to $4{\cdot}10^{-9}$ moles/$cm^2{\cdot}s$. The FE, defined as the fraction of transported protons that react with nitrogen to produce ammonia, reached values as high as 78% [29].

The effect of electrochemical promotion was studied in the SC reactor at 750 °C [37]. A mixture of 2% N_2/6% H_2, balance helium, was introduced into the reactor.

Upon increasing the imposed current, both reaction rate and Λ increased. Although Λ exceeded unity, the values obtained were significantly lower than those typically reported in previous NEMCA studies [36, 50–52]. In a different set of experiments, the reactant gas composition was allowed to vary ($1 < P_{H2}/P_{N2} < 5$), while temperature and current were kept constant. It was found that Λ increased with P_{H2}/P_{N2}. Nevertheless, the Λ values remained very low ($\Lambda < 3$). Regarding the ρ values, at open circuit, r_o was extremely small (of the order of 10^{-13} moles/cm^2·s and sometimes even beyond the detection limit for NH_3). At closed circuit, the reaction rate attained values of the order of 10^{-9} mol/cm^2·s. Consequently, the calculated ρ values are as high as 10,000. This does not mean, however, that the system exhibited a huge NEMCA effect because Λ was close to unity, i.e., operation was nearly Faradaic. To avoid confusing the readers, there is no ρ value in Table 8.1 for this work.

The first demonstration of the NEMCA effect in the reaction of ammonia synthesis at high pressures (50 bar) was reported by Yiokari et al. [38]. An industrial Fe catalyst was used as working electrode. This work was also one step forward in moving from lab scale to industrial practice as a set of 24 catalyst pellets, connected in parallel, was used rather than 1 SC cell. The solid-state proton conductor was a perovskite of the form $CaIn_{0.1}Zr_{0.90}O_{3-a}$. Experiments were conducted at 440 °C. It was found that the rate enhancement was a strong function of the P_{H2}/P_{N2} ratio. Figure 8.4a shows the dependence of the rate enhancement on P_{H2}/P_{N2} at open circuit and upon imposition of a constant voltage of −1 V, i.e., upon transporting protons to the working electrode. The open-circuit rate goes through a maximum indicating competitive adsorption between nitrogen and hydrogen species on the catalyst surface. The maximum rate of $9.4 \cdot 10^{-8}$ g-atoms H/s occurs at a P_{H2}/P_{N2} close to 1. Under closed circuit (−1 V), the behavior is similar, but the maximum rate is shifted to a lower P_{H2}/P_{N2} value (about 0.67). At the same time, the peak reaction rate is more than double the open-circuit maximum ($23.3 \cdot 10^{-8}$ g-atoms H/s). Proton "pumping" to the catalyst surface has a positive effect on the reaction rate as long as $P_{H2}/P_{N2} < 1.5$. For $H_2/N_2 > 1.5$, the supply of protons causes a decrease in the reaction rate. This can also be seen in Fig. 8.4b where ρ and Λ are plotted vs P_{H2}/P_{N2}. Λ attains values as high as 3 for $0.33 < P_{H2}/P_{N2} < 0.67$ but becomes negative when this ratio exceeds 1. Similarly, $\rho = 12$ at $P_{H2}/P_{N2} = 0.5$ and decreases to zero above $P_{H2}/P_{N2} = 2$.

Application of positive potentials (removal of protons) resulted in a considerable poisoning of the catalytic activity. Moreover, prolonged application of positive potentials caused "permanent NEMCA" [53], i.e., the catalytic activity was lost permanently and could be restored only after passing hydrogen for at least 12 hours [38].

Using an industrial Fe-based catalyst, the catalytic and electrocatalytic synthesis of ammonia was studied by Ouzounidou et al. in DC and SC proton-conducting cells at 450–700 °C and at atmospheric total pressure [39]. The solid electrolyte was a strontia-zirconia-yttria (SZY) perovskite of the form $SrZr_{0.95}Y_{0.05}O_{3-a}$. A silver paste was used to prepare the anodic electrode. The superficial surface area of each electrode of either reactor (DC or SC) was about 2.0 cm^2. The DC reactor operated as a regular catalytic reactor and was used to obtain open-circuit kinetic results at temperatures between 450 and 650 °C. The reaction order was between

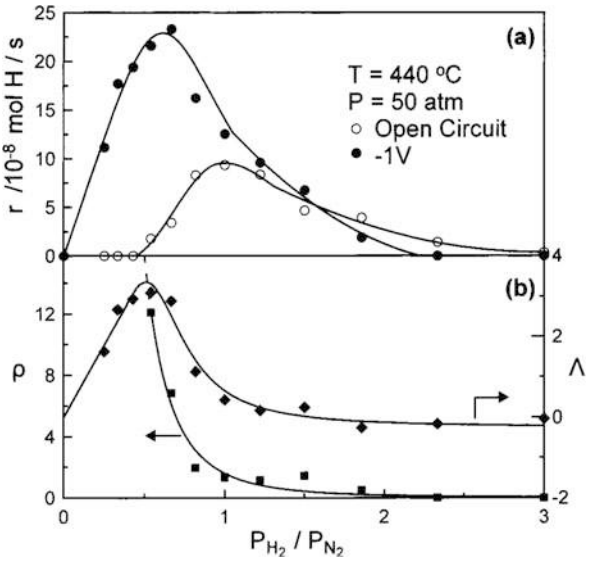

Fig. 8.4 Effect of P_{H2}/P_{N2} (**a**) on the reaction rate under open circuit (open symbols) and an applied bias of −1 V (full symbols) and (**b**) on the dimensionless parameters ρ (squares) and Λ (rhombi). (Reprinted with permission from Ref. [38])

0 and 1 for N_2 and between 1 and 2 for H_2. The reaction rate increased with temperature until about 550 °C, above which the reverse reaction of NH_3 decomposition started its negative effect. At each temperature, the maximum rate was attained when the reacting mixture was stoichiometric, i.e., $P_{H2}/P_{N2} = 3.0$ [39].

Closed-circuit experimental results were obtained using the SC cell. Figure 8.5 shows the effect of applied potential on the reaction rate. A stoichiometric reactant composition was used ($P_{H2} = 75$ kPa, $P_{N2} = 25$ kPa), and the temperature was kept at $T = 450$ °C. The cell operated potentiostatically, i.e., the applied potential was kept constant. The corresponding current is shown on the right-hand vertical axis. Both positive (top, Fig. 8.5) and negative (bottom, Fig. 8.5) potentials were imposed. At positive potentials, protons were transferred from the Fe to the Ag surface, i.e., hydrogen in the form of H^+ was removed from the Fe catalyst. At positive potentials, the cell current increases linearly with the applied potential, but there is no effect on the reaction rate. At negative potentials, however, an increase of the reaction rate was observed. The maximum rate ($r_{max} = 2.2 \cdot 10^{-9}$ mol/s) was obtained at −1.0 V. Compared to the open-circuit rate ($r_o = 1.2 \cdot 10^{-9}$ mol/s), this value corresponds to an 83% increase, i.e., $\rho = 1.8$. To calculate Λ and in order to keep its value positive when negative voltages or currents are applied, Eq. (8.7) was used. It was found that in all experiments, $\Lambda < 3.0$ and, moreover, at high temperatures, Λ attained values lower than 1.0, i.e., the effect was sub-Faradaic [39].

Vasileiou et al. [40] studied SSAS in a SC cell using a $BaCe_{0.2}Zr_{0.7}Y_{0.1}O_{2.9}$ (BCZY27) proton-conducting ceramic electrolyte at atmospheric pressure and at temperatures between 450 °C and 650 °C [40]. A polycrystalline Rh film and a Ni-BCZY27 cermet were the two electrodes. The highest open-circuit (catalytic) rate was attained at 600 °C and stoichiometric inlet H_2/N_2 ratio. Figure 8.6 shows the dependence of the rate of NH_3 formation vs the imposed voltage for 1.0 and 3.0 H_2/

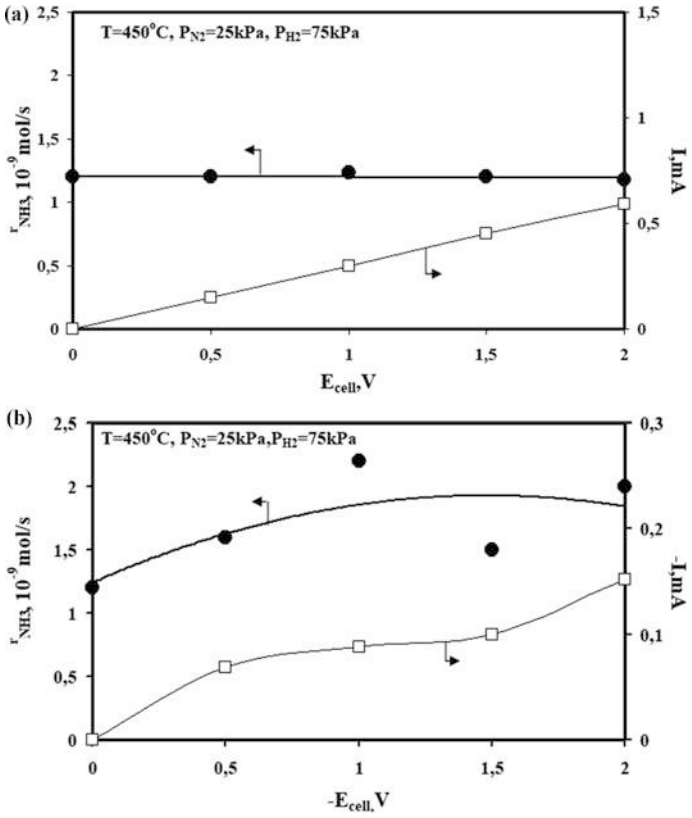

Fig. 8.5 Dependence of reaction rate and cell current on the applied positive (top) and negative (bottom) potentials. Data obtained in a SC reactor at $P_{H2} = 75$ kPa, $P_{N2} = 25$ kPa, and $T = 450$ °C. (Reprinted with permission from Ref. [39])

N_2 ratios. Upon imposing a negative potential, i.e., removing protons from Ni-BCZY27 and supplying them to the Rh electrode, a slight decrease in the rate was observed. On the other hand, at positive voltages, i.e., supplying protons to the Ni-BCZY27 surface, the reaction rate increased considerably. The highest enhancement of the reaction rate (about 40%) was obtained at 550 °C and for $P_{H2}/P_{N2} = 1.0$. The proton transport number, t_{H+}, of the BCZY27 electrolyte depended strongly on the partial pressure of water vapor in the reactor. Under the conditions of Fig. 8.6, it could vary from 0.2 to 1.0. [40].

The same BCZY27 electrolyte was used to construct a DC cell in which SSAS was studied in the presence and in the absence of H_2 at the cathode chamber [41]. A Ni-BZCY72 cermet and a porous Cu film were used as cathodic and anodic electrodes, respectively. The reaction was studied at 400–650 °C and atmospheric total pressure, both in the presence and in the absence of hydrogen at the cathode. With pure N_2 introduced over the cathode, the maximum synthesis rate of $1.7 \cdot 10^{-9}$ mol/s·cm^2 was observed at 620 °C. The highest FE (2.7%) was observed at 580 °C.

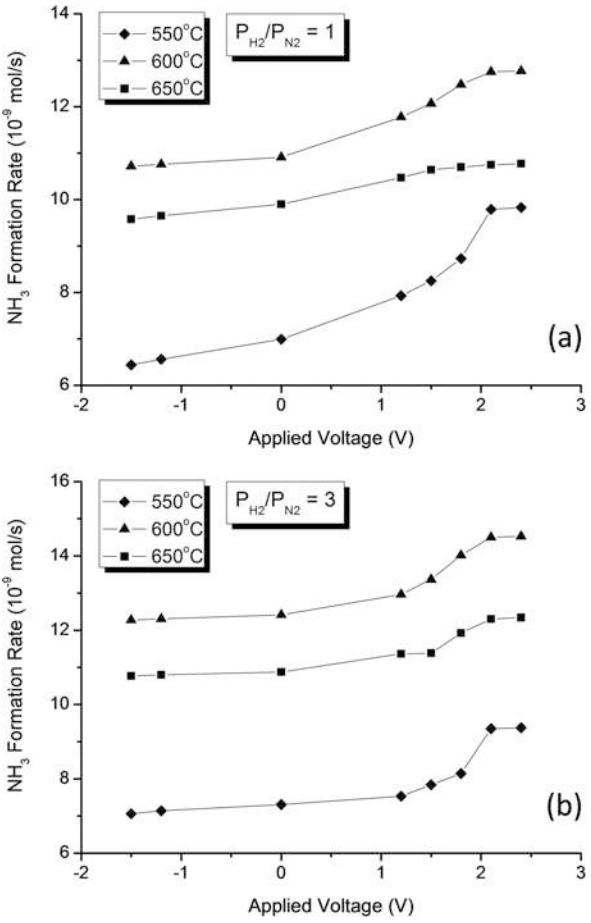

Fig. 8.6 Dependence of the reaction rate on the applied potential at $P_{H2}/P_{N2} = 1$ (**a**) and $P_{H2}/P_{N2} = 3$ (**b**). Data obtained in the Rh|BCZY27| Ni-BCZY27 SC cell. (Reprinted with permission from Ref. [40])

When H_2 was co-fed with N_2 over the cathode, NH_3 was produced under both open- and closed-circuit operations. In Fig. 8.7, the open-circuit rate is plotted vs temperature at various H_2/N_2 ratios. It can be seen that the rate increases with P_{H2}/P_{N2} and goes through a maximum at about $T = 500$ °C. Figure 8.8 contains closed-circuit results. The net electrochemical rate (NER), which is defined as the difference between closed- and open-circuit rate, is plotted vs the imposed voltage for H_2/N_2 feed ratios of 1 and 3 at 620 °C.

The highest NER was $4.1 \cdot 10^{-9}$ mol/s·cm^2 and was obtained at $H_2/N_2 = 1$, while the maximum NER for $H_2/N_2 = 3$ was about half that ($2.0 \cdot 10^{-9}$ mol/s·cm^2). Both rates were higher than the corresponding maximum rate observed when pure N_2 was introduced over the cathode. An enhancement of more than 140% over the open-circuit rate was achieved ($\rho = 2.4$). Also shown in the same figure is the corresponding FEs for each feed ratio (open symbols). It can be seen that the FE values were quite poor. Although increasing with the applied voltage, they did not exceed 10% ($\Lambda < 0.1$).

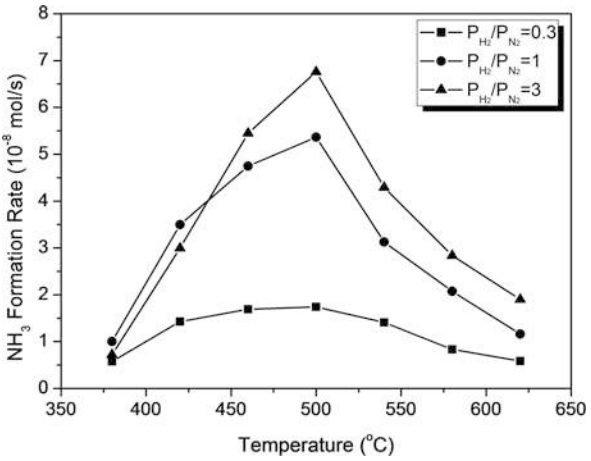

Fig. 8.7 Dependence of the open-circuit ammonia synthesis rate on the temperature for various feed ratios. The superficial area of the electrodes was 4 cm^2. (Reprinted with permission from Ref. [41])

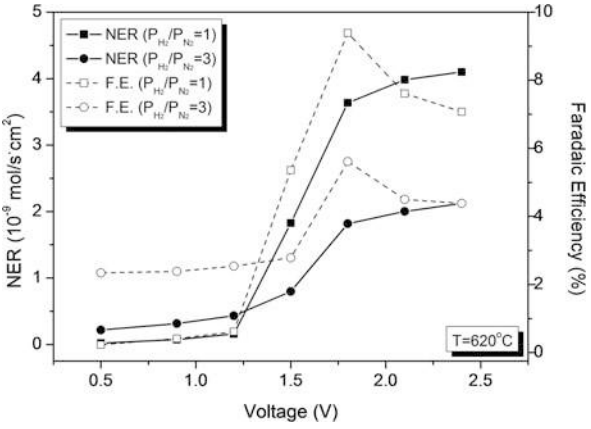

Fig. 8.8 Dependence of NER (full symbols) and FE (empty symbols) on the applied voltage for H_2/N_2 ratios of 1 and 3 at 620 °C. (Reprinted with permission from Ref. [41])

Díez-Ramírez et al. [42] studied the electrochemical promotion of NH_3 synthesis in a SC reactor using potassium ions (K^+). The solid electrolyte was K-β"-Al_2O_3, and the working electrode-catalyst was a Co_3Mo_3N nitride mixed with Ag in order to adhere properly to the solid electrolyte. The effects of the H_2/N_2 feed ratio, the operating temperature, and the applied potential were investigated. Figure 8.9 shows the effect of applied potential (U_{WR}) and potassium surface coverage (θ_{K^+}) on ρ, PI_{K^+}, and Λ_{NH3}, at various temperatures (400 °C < T < 500 °C). The promotion index (PI_{K+}) was calculated by the equation

$$PI_{K^+} = \left(\Delta r_{\text{catalytic}}/r_0\right)/\theta_{K^+} \tag{8.9}$$

where θ_{K^+} is the potassium to catalyst molar ratio [42]. Fig. 8.9 shows that all three parameters (ρ, PI_{K^+}, and Λ_{NH3}) increase with applied voltage until a maximum value

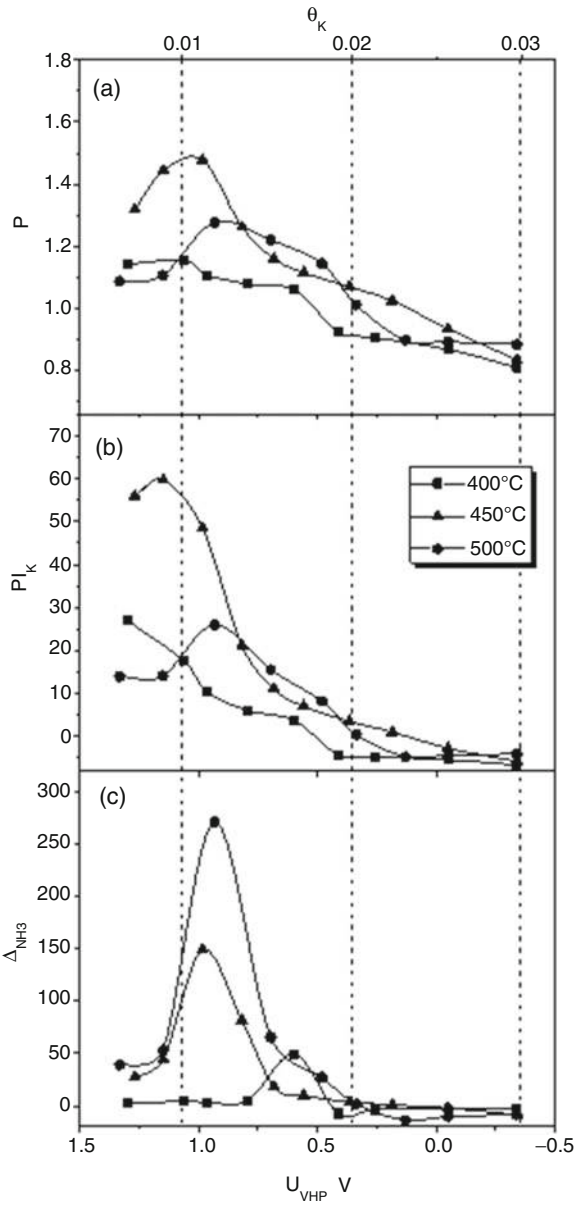

Fig. 8.9 Dependence of (**a**) the rate enhancement, ρ; (**b**) the promotion index, $PI_K{}^+$; and (**c**) the apparent Faradaic efficiency, Λ_{NH3}, on the applied voltage, U_{WR}, and potassium to catalyst ratio, $\theta_K{}^+$, for $H_2/N_2 = 3.0$ at $T = 400$, 450, and 500 °C. (Reprinted with permission from Ref. [42])

is reached above which (i.e., $\theta_K{}^+ > 0.01$) the effect is detrimental. The maximum value for ρ is 1.5 at 450 °C (for $P_{H2}/P_{N2} = 3.0$). The value of $PI_K{}^+$, under these conditions, is about 60. The maximum Λ_{NH3} for the conditions of Fig. 8.9 was about 250 but for a feed ratio of 1 (not shown in Fig. 8.9), while at 500 °C, a maximum Λ_{NH3} of 310 was achieved. The "volcano" behavior with voltage suggests that small

amounts of K^+ enhance the catalytic activity toward NH_3, but a too high surface concentration of K^+ has a poisoning effect probably because of the formation of K-N-H which blocks the active sites [42]. A full explanation of the physical meaning and calculation of this Λ can be found in the original published work.

Kosaka et al. [43] studied SSAS in a DC cell using a $BaCe_{0.9}Y_{0.1}O_{3-a}$ (BCY) proton conductor at temperatures between 500 °C and 650 °C in the presence and in the absence of gaseous H_2 in the cathode chamber [43]. The working electrode was a K, Al-modified Fe-BCY composite, while Pt was used as the counter electrode. The effects of (a) applied potential, (b) operating temperature, and (c) K addition were examined. Remarkably different results were obtained when H_2 was introduced together with N_2 in the feed stream over the cathode. Figure 8.10 shows the dependence of the rate of NH_3 synthesis on the applied potential at 650 °C. In Fig. 8.10a, a 100% N_2 stream was introduced over the working electrode, and a mixture of 2% H_2O, 20% H_2, and 78% Ar was introduced over the counter electrode. The reaction rate attained very low values, i.e., it varied from $5.5 \cdot 10^{-12}$ mol/s·cm^2 to $2.4 \cdot 10^{-11}$ mol/s·cm^2. When, however, a 15% H_2/85% N_2 mixture was fed in instead of pure N_2, as shown in Fig. 8.10b, a significant enhancement in NH_3 was observed upon cathodic polarization. Although the open-circuit reaction rate was quite low

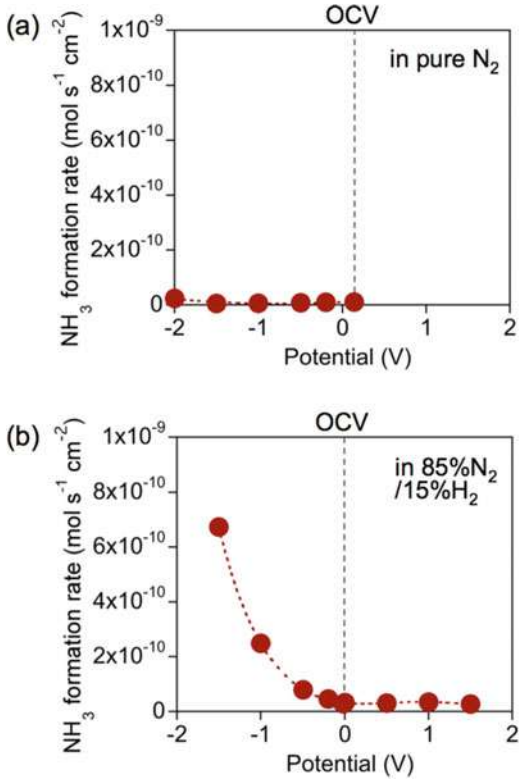

Fig. 8.10 Dependence of the NH_3 formation rate on the applied potential (**a**) without H_2 in the cathode chamber and (**b**) with H_2 in the cathode chamber. (Reprinted with permission from Ref. [43])

($2.8 \cdot 10^{-11}$ mol/s·cm^2), an exponential increase with the applied potential was observed resulting in ρ values as high as 20. The Λ values, however, were very low in both cases. Without H_2 at the cathode (when Λ could not exceed unity anyway), its values were of the order of 10^{-4}–10^{-3}, while with H_2 present at the cathode, despite increasing two orders of magnitude, Λ was still well below 1 [43].

More recently [44], in an effort to further clarify the promotion effect on Fe-based electrodes, the same group conducted experiments using three types of cathodes: (a) a porous pure Fe, (b) an Fe-BCY cermet electrode, and (c) a W-Fe-BCY cermet electrode. The anodic electrode (Pt) was exposed to a 3% H_2O-20% H_2–77% Ar, and the working electrode (cathode) was exposed to H_2-N_2 mixtures. Firstly, the performance in terms of ammonia synthesis and current density was tested as a function of the imposed potential with the three electrodes exposed to the same gaseous mixture, i.e., 10% H_2–90% N_2 at 550 °C and 650 °C. The porous pure Fe electrode gave the best performance: at 550 °C and at an electrode potential of -1.2 V, the NH_3 synthesis rate reached $1.3 \cdot 10^{-9}$ mol/s·cm^2 [44]. Secondly, the effect on NH_3 synthesis of the partial pressure of hydrogen at the cathode was examined. In Fig. 8.11, the dependence on the applied potential of the reaction rate (a), the current density

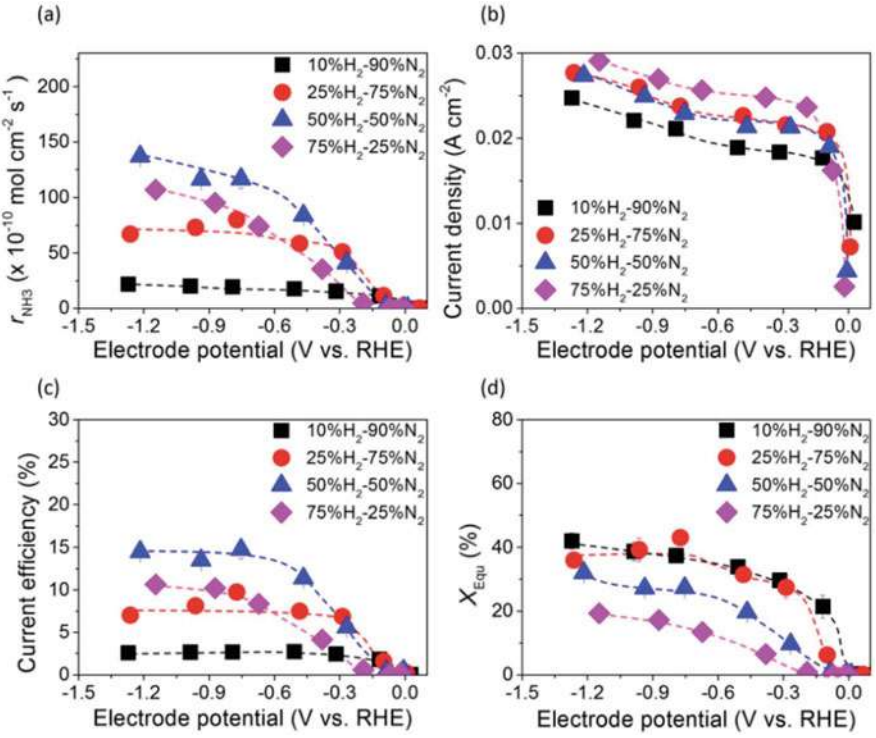

Fig. 8.11 Variation of (**a**) NH_3 synthesis rate, (**b**) current density, (**c**) current efficiency, and (**d**) percentage of equilibrium conversion achieved with the applied voltage at various H_2/N_2 feed ratios and 550 °C. (Reprinted with permission from Ref. [44])

(b), the current efficiency (c), and the fraction of produced NH_3 to that predicted at thermodynamic equilibrium (d) is presented for four different gaseous compositions at the cathode (10–75% H_2/25–90% N_2). The temperature was 550 °C, and the cathodic electrode was pure Fe. Figure 8.11a shows that, by increasing the partial pressure of hydrogen at the cathode, the reaction rate increased by 6 times from $2.2 \cdot 10^{-9}$ mol/s·cm^2 (10% H_2) to $1.4 \cdot 10^{-8}$ mol/s·cm^2 (50% H_2). Although not purely electrochemical but primarily catalytic, this rate of $1.4 \cdot 10^{-8}$ mol/s·cm^2 is one of the highest SSAS rates ever reported [6, 7, 16, 30]. The corresponding value of ρ was 220 [44]. On the other hand, the values of Λ were similar to those of their previous work [43], being of the order of 10^{-3} to 10^{-1}, either with or without H_2 at the cathode.

8.4 Post-electrochemical Open-Circuit Enhancement (PELOCE)

An interesting rate enhancement phenomenon was observed in the work of Vasileiou et al. [54]. The reaction was studied in a double-chamber proton-conducting cell at atmospheric pressure and at temperatures between 450 °C and 700 °C. The solid electrolyte was $BaZr_{0.7}Ce_{0.2}Y_{0.1}O_{2.9}$ (BZCY72), while a Ni-BZCY72 cermet and a polycrystalline Pt film served as cathodic and anodic electrodes, respectively. Figure 8.12 shows the basic characteristics of this phenomenon, named post-electrochemical open-circuit enhancement (PELOCE), with the reaction rate and the cell voltage plotted vs time.

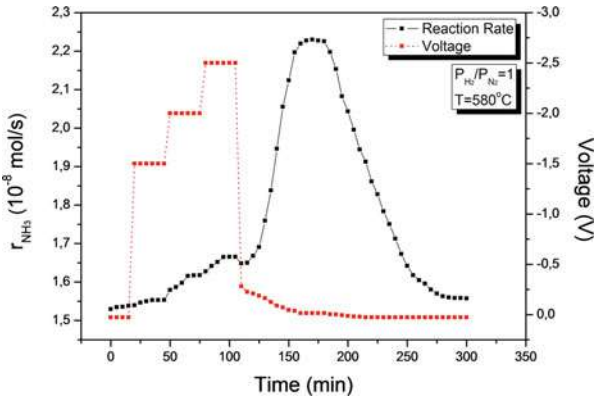

Fig. 8.12 Transient behavior of the NH_3 synthesis rate during PELOCE (black) in a DC H^+ reactor, at 580 °C with an equimolar feed ratio (Reprinted with permission from Ref. [54])

Up to $t = 20$ min, the cell operates at open circuit with a H_2-N_2 mixture ($P_{H2}/P_{N2} = 1.0$) and a 100% H_2 stream introduced over the Ni-BZCY72 and the Pt electrodes, respectively. At $t = 20$ min, the circuit is closed, imposing a voltage of -1.5 volt. A new steady state is established corresponding to a very small (2%) increase in the reaction rate. At $t = 50$ min and at $t = 80$ min, the cell voltage is changed to -2.0 volts and -2.5 volts, respectively, with the reaction rate gradually increasing to a value about 8% higher than its open-circuit value. At $t = 110$ min, the circuit is opened, and, instead of decreasing, the reaction rate increases up to a value corresponding to about 45% higher than the open-circuit rate. Finally, after a period of about 100 min, reaction rate and cell voltage slowly return to their open-circuit values. In Fig. 8.13, the PELOCE phenomenon is compared to those reported previously in solid-state electrochemical studies. The first case (Fig. 8.13a) is the "classic" NEMCA behavior, according to which the closed-circuit rate is significantly higher than its open-circuit value and, upon opening the circuit, the rate returns to its initial value [36, 47, 48]. Figure 8.13b is the case of "permanent NEMCA": the reaction rate increases upon closing the circuit, and it does not return to its initial value for a long (8–10 hours) period of time [55–58]. Figure 8.13c shows

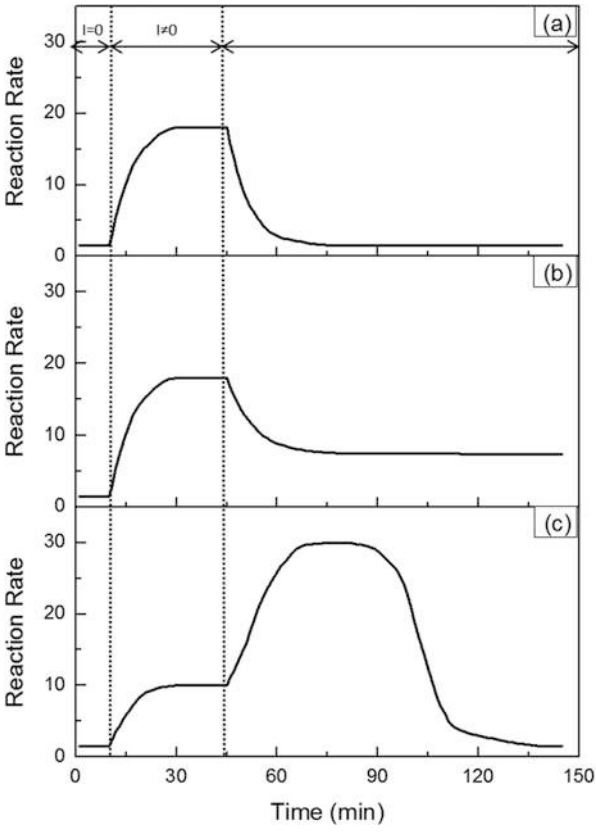

Fig. 8.13 Reaction rate transients during electrochemical ionic "pumping." (**a**) Classic NEMCA, (**b**) permanent NEMCA, and (**c**) post-electrochemical open-circuit enhancement. (Reprinted with permission from Ref. [54])

the PELOCE effect. It can be seen that, although of different nature, this phenomenon is related to the "memory" of the surface of the working electrode that has previously undergone ionic "pumping."

8.5 Electrochemical Promotion in Ammonia Decomposition

The electrochemical decomposition of ammonia has been studied extensively in recent years mainly because ammonia is a candidate fuel for storing hydrogen [48, 59]. The fact that ammonia contains no carbon is crucial for low-temperature fuel cell applications. Moreover, the electrochemical removal of ammonia compounds from wastewaters is an effective and advantageous method because of its simple operation, remote control, and minimal generation of secondary waste [60]. Similar to the electrochemical synthesis, however, very few studies have focused on the electrochemical promotion during the decomposition of NH_3. Table 8.1 contains these works.

Pitselis et al. [45] studied the electrochemical promotion of the decomposition of NH_3 on Fe electrode-catalysts using a H^+-conducting, $CaZr_{0.9}In_{0.1}O_{3-\alpha}$, and a K^+-conducting, $K_2YZr(PO_4)_3$, single-chamber solid electrolyte cell, respectively. The H^+ cell was studied at 530–600 °C. At 570 °C and upon application of +1 V (removal of protons from the catalyst surface), a 360% increase in the reaction rate ($\rho = 3.6$) was observed. The corresponding Λ value was 120. Figure 8.14 shows the dependence of the reaction rate on the partial pressure of NH_3 at 570 °C either at open circuit (open symbols) or at +2 V (closed symbols). The closed-circuit rate is almost double the open-circuit one and essentially independent of the partial pressure of NH_3.

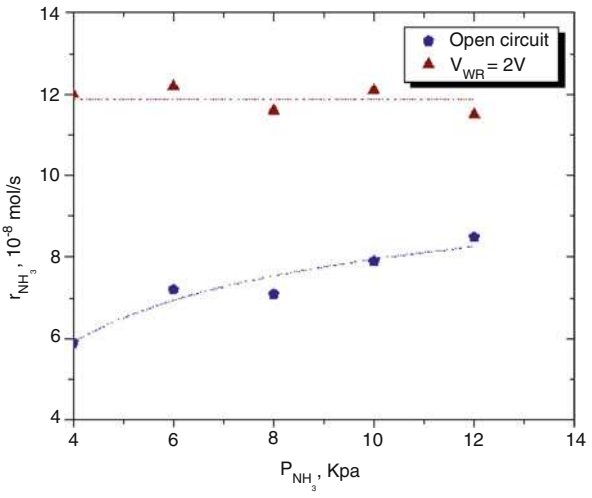

Fig. 8.14 Dependence of the NH_3 decomposition rate on the inlet partial pressure of the reactant, under open circuit (stars) and under an applied bias of 2 V (triangles). (Redrawn from Ref. [45])

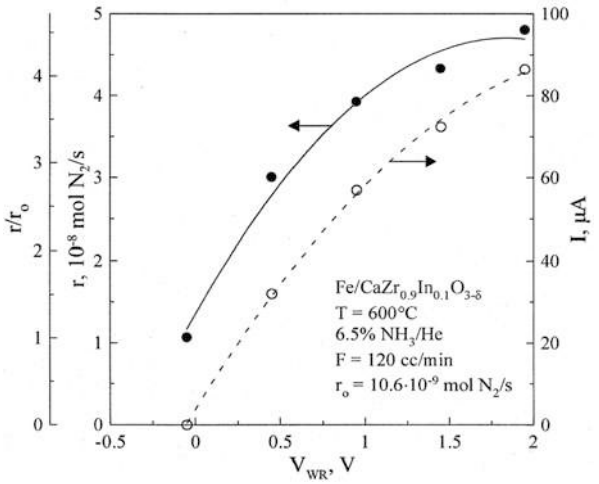

Fig. 8.15 Variations of NH_3 decomposition rate (and rate enhancement ratio – left axis) and obtained current with the applied cell voltage. (Reprinted with permission from Ref. [46])

Using the $K_2YZr(PO_4)_3$ cell, the electrochemical promotion of the Fe/K^+-catalyzed decomposition of NH3 was studied at 530–580 °C. At higher temperatures, a severe decrease in the reaction rate is observed upon pumping K^+ to the catalyst surface. An up to 30-fold decrease in the rate is observed at +2.8 V. At lower temperatures, e.g., 570 °C, pumping small amounts of K^+ to the Fe catalyst causes an increase in the reaction rate, while higher amounts inhibit the reaction [45].

The $CaZr_{0.9}In_{0.1}O_{3-\alpha}$ H^+ conductor was also used by Balomenou et al. [46] to investigate the electrochemical promotion of NH_3 decomposition on Fe. Figure 8.15 shows the effect of catalyst potential on the reaction rate (closed symbols) and on the generated current (open symbols) at 600 °C. By increasing the catalyst potential (pumping protons away from the catalyst), the rate increases reaching an enhancement ratio $\rho = 4.5$ at +1.95 V. The corresponding Λ values are up to 100.

Using the double-chamber Pd|$SrCe_{0.95}Yb_{0\cdot05}O_{3-a}$|Pd cell, Zisekas et al. studied the decomposition of NH_3 at 600 °C [37]. The anode was exposed to a 100% H_2 stream, while a 13% NH_3–13.5% N_2/He mixture was introduced over the cathode. A linear decrease in the reaction rate with the imposed current (protons pumped to the cathode) was observed. The effect was sub-Faradaic with Λs about 0.7 and the lowest ρ about 0.45.

The catalytic and electrocatalytic decomposition of ammonia on Ru was studied by Skodra et al. [47] in a single-chamber cell reactor at 350–650 °C and atmospheric total pressure. The solid-state proton conductor was a strontia-ceria-ytterbia perovskite of the form $SrCe_{0.95}Yb_{0.05}O_{3-a}$ (SCY), and Ag was used as the counter electrode. The inlet ammonia partial pressure varied between 0.5 kPa and 2 kPa (balance He). Figure 8.16 contains Arrhenius plots for open ($I = 0$)- and closed-circuit ($I = 0.4$ mA and $I = 1$ mA) operation. It can be seen that the closed-circuit

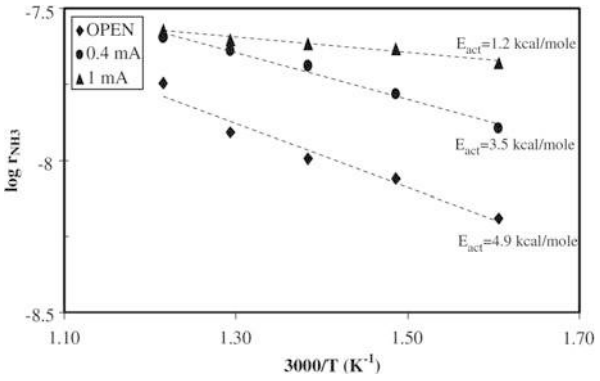

Fig. 8.16 Dependence of reaction rates on temperature under open circuit (rhombi) and under closed circuit (circles for I = 0.4 mA and triangles for I = 1.0 mA). $P_{NH3} = 1$ kPa. (Reprinted with permission from Ref. [47])

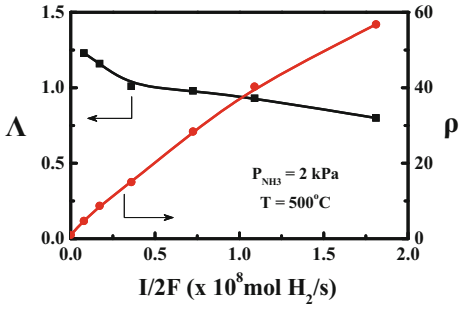

Fig. 8.17 Dependence of Faradaic efficiency (Λ) and reaction rate enhancement (ρ) on rate of proton removal from the catalyst surface. $P_{NH3} = 2$ kPa, $T = 500$ °C. (Reprinted with permission from Ref. [48])

operation is accompanied by a remarkable decrease in the apparent activation energy. The maximum Λ observed was about 4, and the corresponding maximum rate enhancement ρ was about 5.

Using the same H^+ conductor (SCY) and a double-chamber cell reactor, Zisekas et al. studied the electrochemical decomposition of NH_3 on Ag at 350–700 °C [48]. Figure 8.17 shows the effect of applied current on the Faradaic efficiency, Λ, and the corresponding enhancement ratio, ρ, at $T = 500$ °C and for $P_{NH3} = 2$ kPa. There is a moderate decrease in Λ with the applied current (protons moving away from the Ag surface), while there is an almost linear increase in ρ. The maximum value of ρ was 57, but Λ hardly exceeded unity at any current.

The latest work, to our knowledge, on NEMCA in ammonia decomposition was carried out by Pinzón et al. [49]. This research group used Na^+ and K^+ conductors to study the decomposition reaction at 250 to 350 °C on a Ru working electrode. They observed a general volcano-type behavior with applied potential/ion coverage of the Ru electrode. While they do not report FE values, they obtained rate enhancement ratios up to 1.4 with the Na^+ conductor and up to 3.3 (a 230% increase) with the K^+ conductor, both at 300 °C.

8.6 Discussion

Despite the large number of publications on the electrochemical synthesis of ammonia in the past two decades (Fig. 8.2), in only a few of them was hydrogen introduced together with nitrogen at the cathode. Consequently, very few studies report on the EPOC effect in either the forward reaction of NH_3 synthesis or the reverse reaction of NH_3 decomposition. The main findings from these EPOC studies are the following:

(a) In the studies of ammonia synthesis, the Faradaic efficiency, Λ, attains very low values, typically close to unity (Table 8.1). In fact, in certain cases [40, 43, 46, 61], $\Lambda < 1$, i.e., the phenomenon is "sub-Faradaic." An exception is the work of Díez-Ramírez et al. in which the maximum value of Λ attained was 300. The picture is much better with the reaction of NH_3 decomposition: in all cases, $\Lambda > 1$ and values of the order of 100 have been obtained [47, 48].
(b) Either for the forward or for the reverse reaction of ammonia decomposition, the ρ values are comparable to those reported in previous NEMCA studies. As shown in Table 8.1, a maximum $\rho = 220$ has been reported, while typically values vary between 2 and 10.
(c) Considerably higher values of Λ and ρ are observed when, instead of pure N_2, a H_2-N_2 mixture is introduced over the cathodic electrode [40, 46, 61].

There are several explanations for the very low Λ values observed in ammonia synthesis. First, at temperatures of industrial interest (400–500 °C), the reaction is of limited equilibrium conversion. On one hand, it appears that Λ can exceed unity only if the H^+ cell operates at conversions well below the equilibrium limit [62]. On the other hand, NEMCA refers to catalytic reaction kinetics, i.e., the enhancement of the catalytic reaction rate. Therefore, it is not clear why Λ could not exceed unity even when the reaction has reached equilibrium. In order to clarify the above, Garagounis et al. published [62] a thermodynamic analysis of NEMCA for reactions with limited equilibrium conversion. Their analysis used ammonia synthesis in a H^+ cell as a model system, and therefore, a brief summary is presented below as it is closely related to this review. According to the model, the H^+ double-chamber cell reactor operates first under open circuit with a stoichiometric H_2/N_2 mixture fed into the cathode chamber at a steady state. The reactor operates at constant temperature and at atmospheric total pressure. Assuming infinite reactor length and ideal gas behavior for reactants and products, the gas composition at the reactor exit can be calculated from the equilibrium constant K of reaction (Eq. 8.10):

$$K = (P_{NH3})^2/(P_{N2})(P_{H2})^3 \tag{8.10}$$

The "infinite length" assumption could be practically met either by using an extremely active catalyst or by keeping the inlet flow rate at extremely low levels (high residence time/low space velocity). Then, the circuit is closed, and a constant current (or, equivalently, a constant H^+ flux) is imposed. The minimum amount of

electric power that must be supplied to the reactor in order to attain a certain conversion can be calculated by solving simultaneously material and energy balances as well as an entropy balance assuming isentropic operation [62]. Figure 8.18 shows the dependence of Λ on the supplied electric power, W, at various temperatures for a constant proton flux $z = 50$ μg-atoms H^+/s and for a stoichiometric H_2/N_2 inlet flow rate. Clearly, Λ can take values greater than 1.0 at all temperatures. Nevertheless, regardless of the electric power input, Λ remains lower than 10, i.e., well below values of the order of 10^4 or even 10^5 reported in catalytic oxidation reactions [36, 53]. This can be explained by the fact that in the present case, the effect of proton pumping is both electrochemical and catalytic. The H^+ flux "conveys" the electrical energy required to attain conversions to ammonia higher than those predicted by Eq. 8.10. On the other hand, the properties of the catalytic surface are electrochemically promoted so that it is not necessary to supply in the form of H^+ all the required hydrogen.

In Fig. 8.19, experimental data from reference [37] are compared with the model predictions of reference [62]. The experiments were conducted at atmospheric pressure and $T = 1023$ K with a stoichiometric reactant mixture (6% H_2–2% N_2, balance He) introduced over the cathode. The Faradaic efficiency, Λ, is plotted vs z,

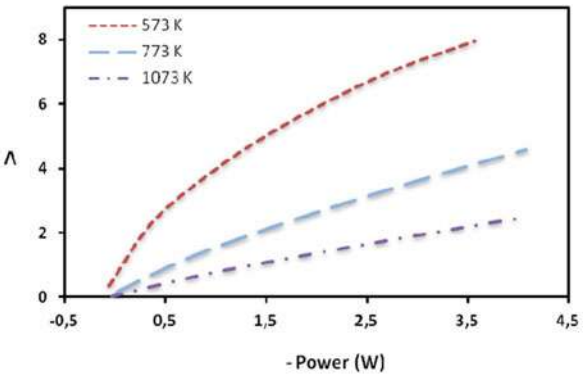

Fig. 8.18 Dependence of Λ on the supplied electric power, W, at various temperatures for a constant H^+ of 50 μg-atoms H^+/s. (Reprinted with permission from Ref. [62])

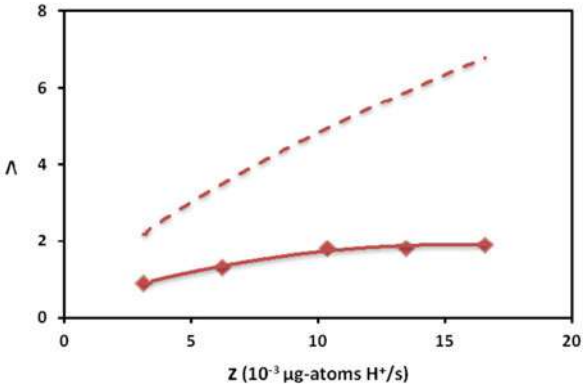

Fig. 8.19 Dependence of the theoretical and experimental values of Λ on z at 1023 K. (Reprinted with permission from Ref. [62])

the rate of H^+ pumping, with experimental Λ values lower than 2.0. The model predicts low Λ values (dotted curve in Fig. 8.19), although they can get to as high as 7. It should be noted that the dotted line is constructed assuming isentropic operation or, equivalently, supply of the minimum power (W_{min}) required to achieve a particular conversion. Obviously, the experiments were not run isentropically. Therefore, the continuous curve (experimental data) had to be below the dotted curve.

The above analysis makes it clear that in the case of ammonia synthesis, the Λ values are very low, close to, or below unity. In cases, however, where the reaction was far from equilibrium, as in the work of Yiokari et al. [38], Λ was allowed to attain higher values. Also, the explanation for the remarkably high Λ observed in the work of Díez-Ramírez et al. [42] can be found in the definition of the Faradaic efficiency: in that study, instead of H^+, the conducting ion was K^+ which was not consumed as a reactant. Moreover, the EPOC effect with the K^+ cation is expected be much stronger compared to that of H^+ as the latter is about 30 times smaller in size. Last but not least, an important factor with a negative effect on the Faradaic efficiency is the competing reaction of hydrogen evolution.

Table 8.1 shows that the Λs for the reverse reaction of NH_3 decomposition are relatively larger; there are no studies with $\Lambda < 1$. This is reasonable because (a) this reaction is not equilibrium limited under the studied conditions ($T > 350$ °C) and (b) there is no competing reaction (hydrogen evolution) that could cause a decrease in Λ. Similar to the reaction of NH_3 synthesis, the highest Λs are observed when a K^+ rather than a H^+ conductor is used [47, 48].

As opposed to the low Λs, the ρ values were comparable to previous NEMCA studies [52, 53] for either the forward or the reverse reaction of ammonia synthesis (Table 8.1). This is easily understood if one considers that ρ is defined by Eq. (8.6): $\rho = r/r_0$. In most studies, the open-circuit rate, r_0, was negligibly small, and, therefore, $r >> r_0$ and $\rho >> 1.0$ were easily achievable. This antithesis can also be seen in Table 8.1, where studies with the highest reported ρ values, e.g., 220 and 57 in references 44 and 48, respectively, had corresponding Λ values of <1 and 1.0.

The reaction rate enhancement observed upon introduction of a H_2-N_2 mixture rather than pure N_2 over the cathode is in agreement with the rules of electrochemical promotion developed by Vayenas and coworkers [36]. There are four basic categories of electrochemical promotion of catalytic reaction rates: (a) purely electrophobic, (b) purely electrophilic, (c) volcano type, and (d) inverted volcano. In the case of ammonia synthesis, the reaction exhibits electrophilic behavior because hydrogen, the electron donor, is much more strongly adsorbed than nitrogen, the electron acceptor. Consequently, the reaction rate increases with increasing the partial pressure of hydrogen. Additionally, the presence of hydrogen at the cathode protects the catalyst from poisoning by oxygen. It is well known that trace amounts of O_2 (even a few ppm) poison the catalyst [5]. If a H_2-N_2 mixture rather than pure N_2 is used, the catalyst surface will be cleaned from oxygen, and its activity will be maintained.

The PELOCE phenomenon (Figs. 8.12 and 8.13) exhibits similarities to the "permanent NEMCA" effect [36, 53, 55] although its origin is essentially the opposite: it appears upon interruption of the current. A reasonable interpretation of

PELOCE could be the formation of a hydride [54]. During H^+ pumping, part of the transported protons is "stored" at the Ni-BZCY72 interphase in the form of Ni_xH_y species. Upon current interruption, nitrogen reacts with the hydride to produce ammonia. Under closed-circuit operation, the phenomenon is not observed because the H^+ flux "floods" the cathode and hinders nitrogen chemisorption. Another, less likely, explanation could be the formation of a nickel nitride that is very stable under cathodic polarization and which reacts with the easily adsorbed H_2 when the circuit is closed.

As far as the outlook for the future of NEMCA in ammonia synthesis or decomposition, there are a few things that can be said. First of all, it should be pointed out that the electrical energy efficiency of a cell exhibiting NEMCA is generally higher than unity, which is a good incentive for practical applications. Specifically, for ammonia decomposition, NEMCA cells could be highly beneficial, since this is a spontaneous reaction, which means there is already an open-circuit reaction rate to be promoted, no matter whether the cell is in a double- or single-chamber configuration. For ammonia synthesis, a NEMCA cell reactor might be developed in the single-chamber configuration, which means that both reactants would be available at the catalyst-electrode regardless of the current density achievable in the cell. In such a setup, the role of the cell would simply be that of an in situ tunable catalyst and not that of a pure H_2 feed. This of course would require high-purity H_2 to be available before the ammonia reactor, in order to avoid poisoning the catalyst. In recent years, water electrolysis has been proposed and even begun to be introduced to partially replace reformers in H_2 production for Haber-Bosch plants [11], as a step toward the decarbonation and electrification of ammonia production. Unlike the reforming of fossil fuels, electrolysis produces high-purity H_2, which might be combined with the electrochemical ammonia synthesis under NEMCA operation for a highly efficient and fully electrified process.

8.7 Conclusions

Compared to most of the catalytic reaction systems examined thus far, a rather weak electrochemical promotion effect during ammonia synthesis has been observed. This is because, in this reaction, NEMCA is constrained by two factors: firstly, by the equilibrium-limited nature of the reaction at the operating conditions (>350 °C) and, secondly, by the competing hydrogen evolution reaction. However, it has been calculated that Λ values as high as 10 could be achieved in an ideal situation, wherein the electricity consumed both activates the catalyst-electrode and "pushes" the reaction past catalytic equilibrium. Part of this ideal setup would be the development of a selective electrocatalyst which effectively suppresses hydrogen evolution. This, of course, is a requirement for any study in electrochemical NH_3 synthesis. The rational design of catalysts with the help of DFT modeling to predict good candidate materials constitutes a promising step in this direction.

References

1. Smil V (2001) Enriching the earth. Fritz Haber, Carl Bosch and the transformation of world food production. The MIT Press, Cambridge, MA
2. Smil V (1999) Detonator of the population explosion. Nature 400:415–415. https://doi.org/10.1038/22672
3. Shipman MA, Symes MD (2017) Recent progress towards the electrosynthesis of ammonia from sustainable resources. Catal Today 286:57–68. https://doi.org/10.1016/j.cattod.2016.05.008
4. Erisman JW, Sutton MA, Galloway J, Klimont Z, Winiwarter W (2008) How a century of ammonia synthesis changed the world. Nat Geosci 1:636–639. https://doi.org/10.1038/ngeo325
5. Liu H (2013) Ammonia synthesis Catalysts. Innovation and practice. World Scientific Publishing Co. Pte. Ltd. and Chemical Industry Press, Singapore
6. Garagounis I, Kyriakou V, Skodra A, Vasileiou E, Stoukides M (2014) Electrochemical synthesis of ammonia in solid electrolyte cells. Front Energy Res 2:1–10. https://doi.org/10.3389/fenrg.2014.00001
7. Giddey S, Badwal SPS, Kulkarni A (2013) Review of electrochemical ammonia production technologies and materials. Int J Hydrog Energy 38:14576–14594. https://doi.org/10.1016/j.ijhydene.2013.09.054
8. Kyriakou V, Garagounis I, Vasileiou E, Vourros A, Stoukides M (2017) Progress in the electrochemical synthesis of ammonia. Catal Today 286. https://doi.org/10.1016/j.cattod.2016.06.014
9. Lan R, Irvine JTS, Tao S (2012) Ammonia and related chemicals as potential indirect hydrogen storage materials. Int J Hydrog Energy 37:1482–1494. https://doi.org/10.1016/j.ijhydene.2011.10.004
10. Stoukides M (2016) Proton conducting materials electrocatalyst in solid state ammonia synthesis. In: Marrony M (ed) Proton-conducting ceramics, from fundamentals to applied research. Pan Standford Publishing, Singapore, pp 377–405
11. MacFarlane DR, Cherepanov PV, Choi J, Suryanto BHR, Hodgetts RY, Bakker JM, Ferrero Vallana FM, Simonov AN (2020) A roadmap to the ammonia economy. Joule 4:1186–1205. https://doi.org/10.1016/j.joule.2020.04.004
12. Geng C, Li J, Weiske T, Schwarz H (2019) Complete cleavage of the N≡N triple bond by Ta 2 N + via degenerate ligand exchange at ambient temperature: a perfect catalytic cycle. Proc Natl Acad Sci 116:21416–21420. https://doi.org/10.1073/pnas.1913664116
13. Boudart M (1994) Ammonia synthesis: the bellwether reaction in heterogeneous catalysis. Top Catal 1:405–414. https://doi.org/10.1007/BF01492292
14. Rod TH, Logadottir A, Nørskov JK (2000) Ammonia synthesis at low temperatures. J Chem Phys 112:5343–5347. https://doi.org/10.1063/1.481103
15. Skúlason E, Bligaard T, Gudmundsdóttir S, Studt F, Rossmeisl J, Abild-Pedersen F, Vegge T, Jónsson H, Nørskov JK (2012) A theoretical evaluation of possible transition metal electro-catalysts for N_2 reduction. Phys Chem Chem Phys 14:1235–1245. https://doi.org/10.1039/c1cp22271f
16. Garagounis I, Vourros A, Stoukides D, Dasopoulos D, Stoukides M (2019) Electrochemical synthesis of ammonia: recent efforts and future outlook. Membranes (Basel) 9:1–17. https://doi.org/10.3390/membranes9090112
17. Van Der Ham CJM, Koper MTM, Hetterscheid DGH (2014) Challenges in reduction of dinitrogen by proton and electron transfer. Chem Soc Rev 43:5183–5191. https://doi.org/10.1039/c4cs00085d
18. Montoya JH, Tsai C, Vojvodic A, Nørskov JK (2015) The challenge of electrochemical ammonia synthesis: a new perspective on the role of nitrogen scaling relations. ChemSusChem 8:2180–2186. https://doi.org/10.1002/cssc.201500322
19. Van Tamelen EE, Akermark B (1968) Electrolytic reduction of molecular nitrogen. J Am Chem Soc 90:4492–4493. https://doi.org/10.1021/ja01018a074

20. Gorodyskii AV, Danilin VV, Efimov ON, Nechaeva NE, Tsarev VN (1979) Electrocatalytic properties of the Ti(OH)3−Mo(III) system in the reduction of molecular nitrogen. React Kinet Catal Lett 11:337–342. https://doi.org/10.1007/BF02079722
21. Sclafani A, Augugliaro V, Schiavello M (1983) Dinitrogen electrochemical reduction to ammonia over iron cathode in aqueous medium. J Electrochem Soc 130:734–736. https://doi.org/10.1149/1.2119794
22. Halmann M (1984) Electrochemical reduction of molecular nitrogen to ammonia in aqueous alkali: a re-examination. J Electroanal Chem Interfacial Electrochem 181:307–308. https://doi.org/10.1016/0368-1874(84)83639-4
23. Pickett CJ, Talarmin J (1985) Electrosynthesis of ammonia. Nature 317:652–653. https://doi.org/10.1038/317652a0
24. Furuya N, Yoshiba H (1989) Electroreduction of nitrogen to ammonia on gas-diffusion electrodes modified by metal phthalocyanines. J Electroanal Chem Interfacial Electrochem 272:263–266. https://doi.org/10.1016/0022-0728(89)87086-X
25. Tsuneto A, Kudo A, Sakata T (1993) Efficient electrochemical reduction of N_2 to NH_3 catalyzed by lithium. Chem Lett 22:851–854. https://doi.org/10.1246/cl.1993.851
26. Leigh GJ (1995) A fixation with fixation. Science (80-) 268:827–828. https://doi.org/10.1126/science.268.5212.827
27. Iwahara H, Esaka T, Uchida H, Maeda N (1981) Proton conduction in sintered oxides and its application to steam electrolysis for hydrogen production. Solid State Ionics 3–4:359–363. https://doi.org/10.1016/0167-2738(81)90113-2
28. Vourros A, Kyriakou V, Garagounis I, Vasileiou E, Stoukides M (2017) Chemical reactors with high temperature proton conductors as a main component: Progress in the past decade. Solid State Ionics 306:76–81. https://doi.org/10.1016/j.ssi.2017.02.019
29. Marnellos G, Stoukides M (1998) Ammonia synthesis at atmospheric pressure. Science (80-) 282:98–100. https://doi.org/10.1126/science.282.5386.98
30. Amar IA, Lan R, Petit CTG, Tao S (2011) Solid-state electrochemical synthesis of ammonia: a review. J Solid State Electrochem 15:1845–1860. https://doi.org/10.1007/s10008-011-1376-x
31. Gunduz S, Deka DJ, Ozkan US (2020) A review of the current trends in high-temperature electrocatalytic ammonia production using solid electrolytes. J Catal 387:207–216. https://doi.org/10.1016/j.jcat.2020.04.025
32. Choi J, Suryanto BHR, Wang D, Du H-L, Hodgetts RY, Ferrero Vallana FM, MacFarlane DR, Simonov AN (2020) Identification and elimination of false positives in electrochemical nitrogen reduction studies. Nat Commun 11:5546. https://doi.org/10.1038/s41467-020-19130-z
33. Andersen SZ, Čolić V, Yang S, Schwalbe JA, Nielander AC, McEnaney JM, Enemark-Rasmussen K, Baker JG, Singh AR, Rohr BA, Statt MJ, Blair SJ, Mezzavilla S, Kibsgaard J, Vesborg PCK, Cargnello M, Bent SF, Jaramillo TF, Stephens IEL, Nørskov JK, Chorkendorff I (2019) A rigorous electrochemical ammonia synthesis protocol with quantitative isotope measurements. Nature 570:504–508. https://doi.org/10.1038/s41586-019-1260-x
34. Qing G, Ghazfar R, Jackowski ST, Habibzadeh F, Ashtiani MM, Chen C-P, Smith MR, Hamann TW (2020) Recent advances and challenges of electrocatalytic N 2 reduction to ammonia. Chem Rev 120:5437–5516. https://doi.org/10.1021/acs.chemrev.9b00659
35. Zhu X, Mou S, Peng Q, Liu Q, Luo Y, Chen G, Gao S, Sun X (2020) Aqueous electrocatalytic N 2 reduction for ambient NH 3 synthesis: recent advances in catalyst development and performance improvement. J Mater Chem A 8:1545–1556. https://doi.org/10.1039/C9TA13044F
36. Vayenas CG, Bebelis S, Pliangos C, Brosda S, Tsiplakides D (2001) Electrochemical activation of catalysis: promotion, electrochemical promotion, and metal-support interaction. Kluwer Academic/Plenum, New York
37. Marnellos G, Zisekas S, Stoukides M (2000) Synthesis of ammonia at atmospheric pressure with the use of solid state proton conductors. J Catal 193:80–87. https://doi.org/10.1006/jcat.2000.2877

38. Yiokari CG, Pitselis GE, Polydoros DG, Katsaounis AD, Vayenas CG (2000) High-pressure electrochemical promotion of ammonia synthesis over an industrial iron catalyst. J Phys Chem A 104:10600–10602. https://doi.org/10.1021/jp002236v
39. Ouzounidou M, Skodra A, Kokkofitis C, Stoukides M (2007) Catalytic and electrocatalytic synthesis of NH_3 in a H^+ conducting cell by using an industrial Fe catalyst. Solid State Ionics 178:153–159. https://doi.org/10.1016/j.ssi.2006.11.019
40. Vasileiou E, Kyriakou V, Garagounis I, Vourros A, Stoukides M (2015) Ammonia synthesis at atmospheric pressure in a BaCe0.2Zr0.7Y0.1O2.9 solid electrolyte cell. Solid State Ionics 275: 110–116. https://doi.org/10.1016/j.ssi.2015.01.002
41. Vasileiou E, Kyriakou V, Garagounis I, Vourros A, Manerbino A, Coors WG, Stoukides M (2016) Electrochemical enhancement of ammonia synthesis in a BaZr0.7Ce0.2Y0.1O2.9 solid electrolyte cell. Solid State Ionics 288:357–362. https://doi.org/10.1016/j.ssi.2015.12.022
42. Díez-Ramírez J, Kyriakou V, Garagounis I, Vourros A, Vasileiou E, Sánchez P, Dorado F, Stoukides M (2017) Enhancement of ammonia synthesis on a Co 3 Mo 3 N-Ag electrocatalyst in a K-βAl 2 O 3 solid electrolyte cell. ACS Sustain Chem Eng 5:8844–8851. https://doi.org/10.1021/acssuschemeng.7b01618
43. Kosaka F, Nakamura T, Oikawa A, Otomo J (2017) Electrochemical acceleration of ammonia synthesis on Fe-based alkali-promoted electrocatalyst with proton conducting solid electrolyte. ACS Sustain Chem Eng 5:10439–10446. https://doi.org/10.1021/acssuschemeng.7b02469
44. Li CI, Matsuo H, Otomo J (2021) Effective electrode design and the reaction mechanism for electrochemical promotion of ammonia synthesis using Fe-based electrode catalysts. Sustain Energy Fuels 5:188–198. https://doi.org/10.1039/d0se01385d
45. Pitselis GE, Petrolekas PD, Vayenas CG (1997) Electrochemical promotion of ammonia decomposition over Fe catalyst films interfaced with K^+- & H^+- conductors. Ionics (Kiel) 3: 110–116. https://doi.org/10.1007/BF02375532
46. Balomenou S, Pitselis G, Polydoros D, Giannikos A, Vradis A, Frenzel A, Pliangos C, Pütter H, Vayenas CG (2000) Electrochemical promotion of Pd, Fe and distributed Pt catalyst-electrodes. Solid State Ionics 136–137:857–862. https://doi.org/10.1016/S0167-2738(00)00524-5
47. Skodra A, Ouzounidou M, Stoukides M (2006) NH_3 decomposition in a single-chamber proton conducting cell. Solid State Ionics 177:2217–2220. https://doi.org/10.1016/j.ssi.2006.03.051
48. Zisekas S, Karagiannakis G, Kokkofitis C, Stoukides M (2008) NH_3 decomposition in a proton conducting solid electrolyte cell. J Appl Electrochem 38:1143–1149. https://doi.org/10.1007/s10800-008-9551-1
49. Pinzón M, Ruiz-López E, Romero A, de la Osa AR, Sánchez P, de Lucas-Consuegra A (2021) Electrochemical activation of Ru catalyst with alkaline ion conductors for the catalytic decomposition of ammonia. Mol Catal 511:111721. https://doi.org/10.1016/j.mcat.2021.111721
50. Vayenas CG, Koutsodontis CG (2008) Non-faradaic electrochemical activation of catalysis. J Chem Phys 128. https://doi.org/10.1063/1.2824944
51. Vayenas CG (2011) Bridging electrochemistry and heterogeneous catalysis. J Solid State Electrochem 15:1425–1435. https://doi.org/10.1007/s10008-011-1336-5
52. Garagounis I, Kyriakou V, Anagnostou C, Bourganis V, Papachristou I, Stoukides M (2011) Solid electrolytes: applications in heterogeneous catalysis and chemical cogeneration. Ind Eng Chem Res 50:431–472. https://doi.org/10.1021/ie1001058
53. Nicole J, Tsiplakides D, Wodiunig S, Comninellis C (1997) Activation of catalyst for gas-phase combustion by electrochemical pretreatment. J Electrochem Soc 144:L312–L314. https://doi.org/10.1149/1.1838143
54. Vasileiou E, Kyriakou V, Garagounis I, Vourros A, Manerbino A, Coors WG, Stoukides M (2015) Reaction rate enhancement during the electrocatalytic synthesis of ammonia in a BaZr0.7Ce0.2Y0.1O2.9 solid electrolyte cell. Top Catal 58:1193–1201. https://doi.org/10.1007/s11244-015-0491-9
55. Nicole J, Comninellis C (1998) Electrochemical promotion of IrO_2 catalyst activity for the gas phase combustion of ethylene. J Appl Electrochem 28:223–226. https://doi.org/10.1023/A:1003295112211

56. Falgairette C, Jaccoud A, Fóti G, Comninellis C (2008) The phenomenon of "permanent" electrochemical promotion of catalysis (P-EPOC). J Appl Electrochem 38:1075–1082. https://doi.org/10.1007/s10800-008-9554-y
57. Fóti G, Jaccoud A, Falgairette C, Comninellis C (2009) Charge storage at the Pt/YSZ interface. J Electroceram 23:175–179. https://doi.org/10.1007/s10832-007-9352-7
58. Souentie S, Xia C, Falgairette C, Li YD, Comninellis C (2010) Investigation of the "permanent" electrochemical promotion of catalysis (P-EPOC) by electrochemical mass spectrometry (EMS) measurements. Electrochem Commun 12:323–326. https://doi.org/10.1016/j.elecom.2009.12.031
59. Metkemeijer R, Achard P (1994) Ammonia as a feedstock for a hydrogen fuel cell; reformer and fuel cell behaviour. J Power Sources 49:271–282. https://doi.org/10.1016/0378-7753(93)01822-Y
60. Kim K-W, Kim Y-J, Kim I-T, Park G-I, Lee E-H (2006) Electrochemical conversion characteristics of ammonia to nitrogen. Water Res 40:1431–1441. https://doi.org/10.1016/j.watres.2006.01.042
61. Marnellos G, Karagiannakis G, Zisekas S, Stoukides M (2000) Electrocatalytic synthesis of ammonia at atmospheric pressure. Stud Surf Sci Catal 130A:413–418. https://doi.org/10.1016/s0167-2991(00)80992-1
62. Garagounis I, Kyriakou V, Stoukides M (2013) Electrochemical promotion of catalytic reactions: thermodynamic analysis and calculation of the limits in faradaic efficiency. Solid State Ionics 231:58–62. https://doi.org/10.1016/j.ssi.2012.10.019

Part V
Prospects Towards the Application

Chapter 9
Challenges for Applications of the Electrochemical Promotion of Catalysis

J. González-Cobos, A. Caravaca, V. Kyriakou, and P. Vernoux

Abstract The phenomenon of the electrochemical promotion of catalysis (EPOC) has been exemplified at lab scale in numerous catalytic reactions, on several types of catalysts and solid electrolyte supports, as extensively described in previous chapters of this book. However, contrary to chemical promotion, there has been no commercial application of electrochemical promotion. This chapter discusses potential catalytic and electrocatalytic processes that could be appropriate for a potential EPOC commercial implementation, as well as for further required technological developments. The first part describes already explored promising reactions such as ethylene epoxidation, NO_x storage/reduction and H_2 production and storage. The second section deals with the innovative concept of EPOC applied to alcohol-assisted water electrolysis. The prospective final part discusses catalytic processes which are still in an early EPOC development stage but could attract increasing

J. González-Cobos (✉) · P. Vernoux
Université de Lyon, Institut de Recherches sur la Catalyse et l'Environnement de Lyon, UMR 5256, CNRS, Université Claude Bernard Lyon 1, Villeurbanne, France
e-mail: jesus.gonzalez-cobos@ircelyon.univ-lyon1.fr; philippe.vernoux@ircelyon.univ-lyon1.fr

A. Caravaca
Departamento de Ingeniería Mecánica, Universidad Politécnica de Madrid, Madrid, Spain
e-mail: angel.caravaca@upm.es

V. Kyriakou
Engineering and Technology Institute Groningen (ENTEG), University of Groningen, AG, Groningen, The Netherlands
e-mail: v.kyriakou@rug.nl

P. Vernoux, C. G. Vayenas (eds.), *Recent Advances in Electrochemical Promotion of Catalysis*, Modern Aspects of Electrochemistry 61,
https://doi.org/10.1007/978-3-031-13893-5_9

interest given their great relevance at industrial level. This is the case, for example, of selective CO_2 hydrogenation reactions and propylene epoxidation. We are discussing the state-of-the-art operation conditions for each catalytic process and the pioneering EPOC works which stand for a good starting point for future research efforts.

Keywords Electrochemical promotion · NEMCA · Prospective · Potential applications

9.1 Introduction

Electronic promoters are industrially used in heterogeneous catalysis to boost catalytic properties such as in the Haber-Bosch ammonia synthesis [1], in the Fischer-Tropsch process to synthesize fuels and lubrication oil from syngas [2] and in the epoxidation of ethylene to produce ethylene oxide [3]. Electronic promoters are either added into the catalysts during their synthesis, such as cationic promoters (e.g. K^+, Na^+ or Cs^+ [1, 2]), or mixed in the reaction mixture, as encountered for chlorine electronegative promoters in the epoxidation reaction [3]. The role of these promoters is to modify the electronic properties of the catalyst (usually a metal or a metal oxide) in order to tune its chemisorptive properties aiming to enhance its activity and/or selectivity. The non-faradaic electrochemical modification of catalytic activity (NEMCA) concept [4] or electrochemical promotion of catalysis (EPOC) [5] also involves electronic promoters, but utilizing electrolytes, either liquid or solid, as reservoir of these promoters. Ions contained in these electrolytes are electrochemically supplied via an electrical polarization to the catalyst surface and act as promoting agents to modify the electronic properties of the catalyst in order to achieve optimal catalytic performance. Many reviews have been published dealing with the main fundamental features of EPOC [6–11]. The comparison of this phenomenon with conventional promotion of catalysis and metal support interactions (MSI) [12–16] and its potential practical implementation [6, 17–19] are also fully documented. These reviews and studies concluded that EPOC mechanism is fundamentally similar to the conventional promotion of catalysts usually applied for industrial processes. However, contrary to chemical promotion, electrochemical promotion offers the possibility of in situ controlling the concentration of electronic promoters supplied on the catalyst via the applied current or potential. This underlines the EPOC potentiality to easily investigate the impact of various types of promoters, such as alkaline cations, on model catalysts aiming to upgrade conventional catalytic formulations. Moreover, the EPOC electrical energy consumption requirement is not a significant handicap, as noticed from some simple calculations found in literature on the energy savings [14, 15]. Therefore, several unique benefits of EPOC could make its industrial application competitive vs. conventional chemical promotion:

The activity/selectivity can be in operando controlled and optimized by tuning the applied potential/current. In addition, the electronic promoters can be fully removed from the catalyst surface with an opposite applied polarization. These dynamic modifications of the electronic properties could be valorized to activate/regenerate a catalyst, store/desorb a species, etc. This kind of transient operating conditions is not possible with conventional chemical promotion, where the concentration of promoters is generally fixed for a given catalytic process during the synthesis of the catalyst and is partially deposited on catalytically inactive support areas.

EPOC can supply electronegative promoters such as O^{2-} ions, which could substitute highly toxic and hazardous electronegative chemical promoters used in industrial catalysts such as chlorine species injected in the reaction feed of the ethylene epoxidation process.

Besides, EPOC can be implemented in state-of-the-art electrochemical reactors such as fuel cells and electrolysers. These currently available electrocatalytic devices could be a good starting point for the industrialization of EPOC. However, contrary to chemical promotion, there is no commercial application of electrochemical promotion. Several research groups [6, 11, 17–20] have identified the main limitations that hinder the practical application of the NEMCA effect:

- The use of low dispersion catalysts.
- A general use of expensive noble metal catalysts.
- The use of reactor designs with a low gas-catalyst or liquid-catalyst interface.

A recent research effort has been done by the scientific community to use non-expensive materials such as non-PGM (platinum group metal) catalysts, to implement electropromoted dispersed nanoparticles in EPOC processes and to scale up EPOC reactors. All these points are addressed and fully discussed in Chap. 3 of this book. On the other hand, the chemical processes that could be industrially improved by the concept of EPOC from an economical and/or environmental point of view have not been systematically considered in literature. This chapter will discuss potential catalytic and electrocatalytic processes that could be appropriate for a potential EPOC commercial implementation after a further technological development.

9.2 Potential Relevant Chemical Processes for EPOC Applications Already Explored in the Literature

9.2.1 Ethylene Epoxidation

Ethylene oxide (EO), an important building block for chemistry, is industrially produced by the epoxidation of ethylene (Eq. 9.1).

$$C_2H_4 + \tfrac{1}{2}\,O_2 \rightarrow C_2H_4O, \qquad \Delta H_{298} = -105\ \mathrm{kJ/mol} \qquad (9.1)$$

This process is catalysed by Ag supported on α-alumina (Ag/α-Al_2O_3) [21, 22] at intermediate temperatures (<300 °C) and pressures (10–30 bar). The reaction mechanism is still under debate. Nevertheless, electrophilic oxygen species, weakly adsorbed on Ag, are supposed to play a key role [23, 24]. Without any chemical promoters, the EO selectivity on Ag/α-Al_2O_3 catalysts is in the range of 35–50% [25]. The addition of promoters like Cs and chlorinated hydrocarbons (e.g. ethyl chloride or vinyl chloride introduced in the gas phase at the ppm level) strongly promotes the EO selectivity up to 90% [26, 27] at around 10% ethylene conversion. For example, 8% at. Cl on the Ag surface enhances the EO selectivity from 9 to nearly 60% [28]. These Cl^- anions are supposed to weaken the Ag-O bonds [29], leading to the production of reactive electrophilic oxygen species on Ag active sites. However, chlorinated precursors usually decrease the reaction yield by active site blocking, are not environmentally friendly and are highly hazardous. Therefore, the main challenge is to substitute these chlorinated promoters. As described in the introduction, EPOC can be a relevant alternative to provide electronegative promoters such as O^{2-} ions to Ag-based catalysts. This is especially evident as the first demonstration of the NEMCA effect was proven with the ethylene epoxidation reaction at 400 °C and atmospheric pressure on an Ag coating deposited on a YSZ (yttria-stabilized zirconia, an oxygen ionic conductor) dense membrane [30]. In this early study, it was observed that upon the application of positive polarizations on the Ag electrode (i.e. supply of O^{2-} ions from YSZ towards Ag), both the selectivity and the yield of EO increased, in contrast to conventional chemical promotion with Cl or Cs dopants [26, 27, 29]. The enhancement in the rate of EO production exceeded the rate of O^{2-} pumping (predicted by the Faraday's law) by a factor of 400, demonstrating the non-faradaic behaviour of the activation. The ethylene epoxidation reaction was also investigated in a similar electrochemical reactor on Ag coatings but at lower temperatures (<300 °C) and higher pressures (5 bar) and in the presence of chlorine promoters in the reaction mixture [31, 32]. The addition of chlorine caused qualitatively similar effects on the EO selectivity, and a constructive synergy exists between positive polarizations and the chlorine promoters. Both EO and CO_2 production rates can be enhanced either by the Cl doping or by increasing the applied potential, in a certain range, beyond the corresponding open circuit potential (i.e. −197 mV) [32]. A maximum EO selectivity of c.a. 78% was reached under optimal conditions, by combining 0.3 ppm $C_2H_4Cl_2$ in the gas phase and a catalyst potential of −156 mV (Fig. 9.1).

The ethylene epoxidation was also recently investigated in a solid oxide electrochemical cell based either on YSZ or GDC (gadolinia-doped ceria) dense membranes, two oxygen ionic conductors [33]. Ag-based cermets (Ag/YSZ and Ag/GDC) were used as electrocatalysts for ethylene epoxidation at atmospheric pressure in the temperature range 220–300 °C. The Ag/YSZ cermet film, prepared with a conventional chemical method from an Ag commercial paste mixed with a YSZ powder, exhibited a very specific behaviour in the reaction mixture. Indeed, the

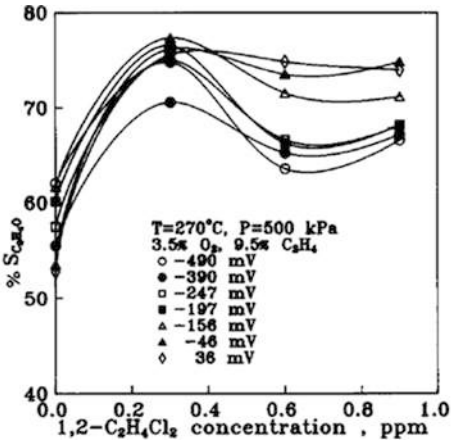

Fig. 9.1 Selectivity to ethylene oxide on an Ag/YSZ electrochemical catalyst tested for ethylene epoxidation reaction (3.5% O_2, 9.5% C_2H_4, 270 °C, 5 bar), with different $C_2H_4Cl_2$ gas-phase concentrations and applied catalyst potentials (V_{WR}). (Reprinted with permission from Ref. [32])

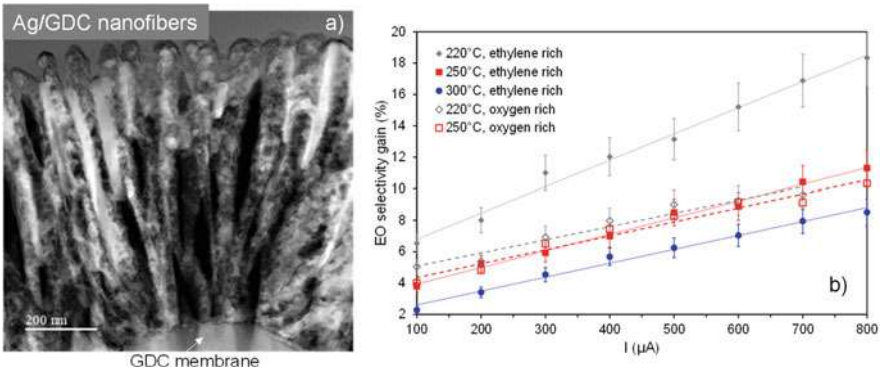

Fig. 9.2 Representative HAADF TEM image of the Ag/GDC cermet coatings deposited on GDC pellet after electrocatalytic tests (**a**). Linear relationship between the EO selectivity gain and the current intensity for the Ag/GDC cermet coating. Ethylene-rich reaction mixture: 3.8% C_2H_4/1.1% O_2. Oxygen-rich reaction mixture: 1% C_2H_4/2% O_2 (**b**). (Reprinted with permission from Ref. [33])

surface of micrometric Ag agglomerates of the cermet was oxidized during the calcination step at 600 °C, forming volatile AgOx species which were trapped on surface oxygen vacancies of YSZ to form very small Ag clusters. These latter, in strong interaction with YSZ, were found to be selective for the ethylene epoxidation, likely related with the phenomenon of self-sustained EPOC [11, 34], via the spontaneous thermal diffusion of oxygen ions from YSZ to Ag. Nevertheless, the sintering process of these small Ag clusters was very fast and the EO selectivity rapidly decayed [33]. On the other hand, Ag/GDC electrocatalysts deposited on a GDC membrane by reactive magnetron sputtering were composed of parallel GDC nanofibres partially covered by Ag nanoparticles (2–5 nm size) and by Ag agglomerates connecting the nanofibres to each other, ensuring a good electronic conductivity (Fig. 9.2a). In this case, the selectivity towards EO was found to linearly increase with the applied current (Fig. 9.2b), demonstrating for the first time the

direct electrooxidation of ethylene into EO by O^{2-} ions. Both the EO selectivity and the ethylene conversion could be significantly increased at 220 °C, by around 18%.

All these studies demonstrate that oxygen ions contained in a solid electrolyte can act as electronic promoters to boost the ethylene epoxidation on Ag-based catalysts in a similar way to hazardous chlorinated compounds. Oxygen anions behave as electronic "sacrificial promoters", modifying the electronic properties of Ag metal films and then their chemisorptive properties. Furthermore, direct electrochemical oxidation of ethylene into EO can also take place on Ag nanoparticles interfaced on a mixed ionic and electronic conductor (MIEC) material such as GDC. Contrary to the industrial catalysts doped with Cl^- anions, oxygen promoters enhance the selectivity without decreasing the overall activity. This discrepancy is probably due to different operating modes, including the method by which promoters are added on the catalyst. In the case of EPOC, the quantity of ionic promoters can be in situ controlled by the applied potential. Therefore, EPOC seems to be a promising technology for the ethylene epoxidation process. Nevertheless, some issues should be considered in view of its practical implementation. The nanostructure of the Ag-based coatings must be improved to combine a high metallic dispersion with a good electronic conductivity. The development of Ag/MIEC cermet as proposed in reference [33] could be a good option. The energy demand linked to the electrical polarization has to be also considered and compared with the cost of the chlorine chemical promotion.

A specific reactor has to be designed to manage temperature, pressure, contact time and polarization. The EPOC reactor already tested at high pressures for the NH_3 synthesis process [35] could be easily adapted.

9.2.2 NO_x Storage and Reduction (NSR)

The storage and reduction of nitrogen oxides (NO_x) emitted by light vehicles was developed in the mid-1990s by Toyota Laboratories [36–38] to reduce NO_x ($NO + NO_2$) into N_2 in the exhausts of internal combustion engines working under lean-burn conditions (i.e. air excess in the combustion chamber) such as diesel ones. The most commonly used NSR catalyst includes noble metals (Pt, Rh) for catalytic reactions and a NO_x sorbent/storage component (BaO) supported on γ-Al_2O_3 [39–41]. These catalysts operate in a cyclic mode with periodic switches between lean (the engine exhaust) and rich conditions. NO (the major NO_x species) contained in the exhaust is oxidized on Pt to NO_2, which is stored in the form of nitrite/nitrate species on Ba. When the NSR catalyst surface reaches the saturation, a short fuel post-injection (few seconds) is triggered to decompose nitrates, which are not stable in these reducing conditions, and released NO_x are reduced into N_2 on Rh. The NSR technology equips many diesel light vehicles in the world. However, periodic fuel post-injections lead to a significant fuel penalty and therefore to an economic impact. Solid oxide electrochemical cells based on K^+ or Ba^{2+} ionic conductors could be an alternative since these cations can act both as electronic promoters and sorbent

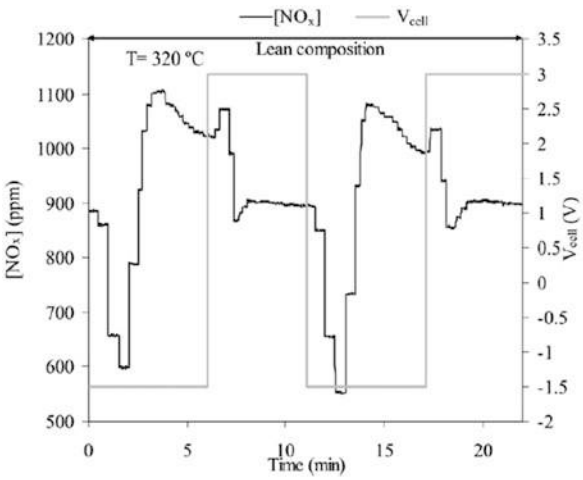

Fig. 9.3 Variation of the NO_x concentration as a function of time and the applied potential of a Pt/K^+-β"Al_2O_3/Au electrochemical cell under a fixed lean reaction composition ($NO/C_3H_6/O_2$, 1000 ppm/1000 ppm/5%, He balance) at 320 °C. (Reprinted with permission from [49])

components. The cell electrical polarization could control the flux of cations and then the NO_x storage capacity as well as the decomposition of nitrates.

The use of solid oxide electrochemical cells for the NO_x reduction into hazardless N_2 has been widely reported in the literature. The direct electrochemical reduction of NO_x (Eq. 9.2) on electrodes such as Pt, Ag or NiO interfaced on a O^{2-}-conducting solid electrolyte [42–44] is very attractive. However, the competition with the electrochemical reduction of oxygen is critical in lean conditions even if some studies have shown that adding a NO_x adsorbent such as Ba or K to the electrode formulation can significantly increase the selectivity to N_2 in an O_2-rich atmosphere through the formation of intermediate nitrate species [45–48].

$$NO_x + 2x\ e^- \rightarrow \tfrac{1}{2}\ N_2 + x\ O^{2-} \tag{9.2}$$

The implementation of the storage and reduction of NO_x in K^+-ion-conducting solid oxide cells was only investigated by two studies where K^+-β"Al_2O_3 was employed as solid electrolyte. The pioneer work has demonstrated the proof of concept using a Pt/K^+-β"Al_2O_3 electrochemical catalyst [49] in a single-chamber reactor configuration. The active Pt working electrode was prepared from the application and calcination of organometallic pastes, while a catalytically Au counter-electrode was deposited on the opposite side of the electrolyte. The K^+ coverage on the Pt coating can be controlled by the cell potential. Figure 9.3 displays the impact of the polarization on the catalytic properties of the Pt layer at 320 °C in a fixed lean reaction mixture. A negative potential (−1.5 V) triggered the migration of K^+ cations from the electrolyte towards Pt, resulting in a rapid drop of the NO_x concentration down to ca. 600 ppm followed by a fast increase to the inlet concentration value (around 1100 ppm). As widely reported in the literature on the basis of the EPOC phenomenon with K^+ promoters [9, 10, 13], K^+ ions on the Pt coating act as electronic promoters, as it was the case for O^{2-} anions above. The

electrochemically supplied K^+ ions behave in a similar way as conventional alkali promoters [13] and lead to the decrease of the Pt work function, enhancing the chemisorption of electron-acceptor species, such as NO and O_2, at the expense of the hydrocarbon, which results in the electrochemical promotion of NO oxidation. Once NO_2 was formed, K^+ ions also acted as NO_x trapping species, explaining the decrease of the NO_x concentration upon negative polarizations for a few minutes, until the saturation of these trapping sites takes place, leading to the increase of the NO_x concentration to a value close to the inlet one. Even if the storage step is chemical, EPOC is essential to promote the oxidation of NO. Very interestingly, when the potential was reversed (+3 V, still under lean conditions), the outlet concentration of NO_x temporally increased due to the release of NO_x species previously stored, but it was much less than expected. The mass-balance calculation clearly showed that a part of NO_x was reduced into N_2. This was explained by the removal of K^+ ions from the Pt surface during the positive polarization, which can promote the chemisorption of propene, enhancing the selective catalytic reduction of NO_x by propene (Eq. 9.3).

$$NO_x + x/9C_3H_6 \rightarrow 1/2\ N_2 + x/3\ CO_2 + x/3H_2O_{(g)} \tag{9.3}$$

In the second study [50], a similar tubular configuration was prepared with two symmetrical Pt coatings deposited on the K + -β"Al_2O_3 tube. Both Pt electrodes were exposed to the same simulated lean-burn reaction mixture. Upon polarization, one of the electrodes (negatively polarized) was promoted for NO oxidation and storage, while the other one (positively polarized) was boosted for the decomposition and the reduction of previously stored nitrates. Figure 9.4 shows that upon successive +3 V/−3 V polarization steps, the NO_x concentration can be continuously decreased in the range of 750–900 ppm (inlet concentration, 1000 ppm) during the polarization switching where the nitrates' decomposition is faster than their reduction into N_2. Very interestingly, part of the produced CO_2 was also stored on the catalyst, most likely as potassium carbonates, which can be formed and decomposed under negative and positive polarization, respectively.

These two studies demonstrate the proof of concept of the electrochemically assisted NSR process under constant lean-burn conditions. In this way, short fuel injections used in a conventional NSR process are no longer required, leading to a significant positive economic and environmental impact. K^+ ions behave, at the same time, as electronic promoters (EPOC) and as NO_x adsorption sites (electrocatalysis). Both phenomena are promoted by negative polarizations and can be easily in situ optimized by controlling the K^+ coverage via the intensity and the duration of the polarization. This operando control is not possible with conventional catalytic systems. Furthermore, contrary to oxide ions, K^+ cations do not behave as sacrificial promoters since they are not consumed during the chemical processes. Hence, after a short polarization period, once the necessary amount of K^+ species is supplied to or from the catalyst, the current and thus the electrical power become negligible, which makes the energy demand of this process low. However, this proof of concept is far

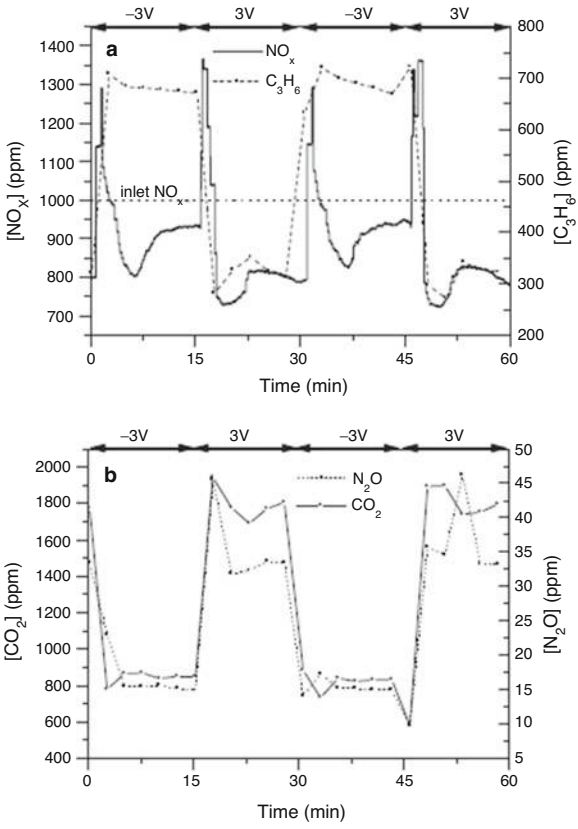

Fig. 9.4 NO_x and C_3H_6 (**a**) and N_2O and CO_2 (**b**) outlet concentration profiles vs. time during NO_x storage/reduction tests with a tubular Pt/K^+-β"Al_2O_3/Pt electrochemical reactor. Fixed lean reaction conditions, 1000 ppm NO, 1000 ppm C_3H_6, 5% O_2 (He balance), 320 °C. NO_x storage step, −3 V; NO_x reduction step, +3 V. (Reprinted with permission from Ref. [50])

from being optimized and competitive with current catalytic NSR systems. The following issues should be considered:

- The dispersion of the tested Pt layers is too small for a practical utilization.
- The catalytic reactor should be further improved and optimized, considering the limited space in vehicles exhaust.

Recent advances on electropromoted catalysts suggest that Pt nanoparticles supported on an electronic conductor such as perovskites, Co_3O_4 or TiO_2 [51–55] could be a good alternative to improve the Pt dispersion. Nanoporous electrodes can also be prepared to enhance the specific surface area [56, 57]. In addition, some monolithic reactors [58, 59] and, specially, the MEPR (monolithic electrochemically promoted reactor; see Fig. 2.18 in Chap. 2) [60, 61] could be used to scale up this EPOC application. Indeed, these reactors have been already tested in real exhausts of automotive engines and can overcome important technical constraints, including the space management together with the mechanical and thermal stability.

9.2.3 Hydrogen Production and Storage

H_2 is acquiring an increasing interest as energy carrier [62] and is expected to play a key role in the energy transition strategies, for instance, by means of fuel cell technology [63, 64]. These latter can convert the chemical energy of H_2 and oxygen into clean electrical energy at low temperature with a thermodynamic efficiency up to 83% [65], explaining their growing interest for dynamic and stationary applications [66, 67].

Hydrogen can be produced from a wide variety of catalytic processes such as steam reforming of different carbon feedstocks (e.g. methane, methanol, ethanol, acetic acid) [68–70], methane dry reforming [71, 72], partial oxidation of methane and other hydrocarbons [68, 73] or biomass gasification [74]. Steam reforming of natural gas (mainly composed of methane, CH_4) on Ni-based catalysts commonly supported on Al_2O_3 is still the main industrial production process of hydrogen [75, 76]. Methane steam reforming (MSR (Eq. 9.4)) is an endothermic process taking place at high temperatures (>700 °C) and producing a gas stream of H_2 mixed with CO and CO_2. This latter is generated by the water-gas shift (WGS) reaction (Eq. 9.5) and the CO oxidation (Eq. 9.6).

$$CH_4 + H_2O_{(g)} \rightarrow CO + 3H_2,\ \Delta H_{298} = +206.2\ \mathrm{kJ/mol} \tag{9.4}$$

$$CO + H_2O_{(g)} \rightarrow CO_2 + H_2,\ \Delta H_{298} = -41.2\ \mathrm{kJ/mol} \tag{9.5}$$

$$CO + 1/2O_2 \rightarrow CO_2,\ \Delta H_{298} = -283.0\ \mathrm{kJ/mol} \tag{9.6}$$

However, Ni-based MSR catalysts are prone to sintering at high temperature in the presence of steam. In addition, carbon deposition can occur on the active sites and deactivates the catalysts. To improve their coking resistance, these catalysts are promoted by alkalis (mainly potassium) [77–79] which can enhance the water chemisorption. However, the counterpart is a decrease of the Ni specific activity. EPOC could overcome this issue by electrochemically controlling and optimizing the potassium loading on the catalyst surface.

The electrochemical promotion of the H_2 production by using alkali ionically conducting electrolytes was recently reviewed [16]. Most of the studies investigate the impact of the electrochemical supply of alkali cations on the catalytic activity at steady-state and constant operating conditions. For instance, MSR (Eq. 9.4), along with methane partial oxidation (POX (Eq. 9.7)) and auto-thermal reforming (ATR (Eq. 9.8)), was performed on a Pt/YSZ composite layer deposited on a Na^+-βAl_2O_3 solid electrolyte membrane [80]. ATR is a commonly used alternative to steam reforming [81], as it partially counterbalances the endothermicity of MSR by the exothermicity of POX.

$$CH_4 + 1/2O_2 \rightarrow 2H_2 + CO,\ \Delta H_{298} = -35.7\ \mathrm{kJ/mol} \tag{9.7}$$

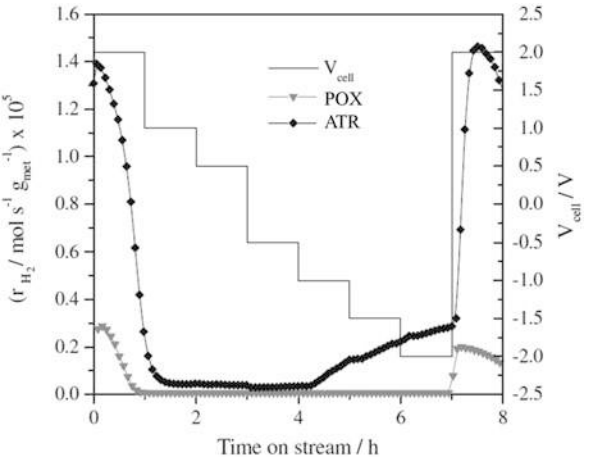

Fig. 9.5 Variation of the H_2 production rate as a function of time during different polarizations on a Pt-YSZ/Na^+-β"Al_2O_3 electrochemical catalyst. Methane partial oxidation (POX) conditions, 1% CH_4, 0.2% O_2 (N_2 balance); methane auto-thermal reforming (ATR) conditions, 1% CH_4, 4% H_2O, 0.2% O_2 (N_2 balance), 500 °C. (Reprinted with permission from Ref. [80])

$$2CH_4 + H_2O_{(g)} + 1/2O_2 \rightarrow 5H_2 + 2CO,\ \Delta H_{298} = +170.5\ \text{kJ/mol} \qquad (9.8)$$

Figure 9.5 displays the influence of the applied potential on the H_2 production rate under partial oxidation (1% CH_4, 0.2% O_2) and auto-thermal reforming (1% CH_4, 4% H_2O, 0.2% O_2) conditions at 500 °C. The Pt-based catalyst mainly produces H_2 and CO_2 and traces of CO in all cases [80].

Upon positive polarization (+2 V), a Pt surface free of Na^+ (unpromoted) was defined, and the catalyst showed a much higher activity under auto-thermal conditions with respect to partial oxidation conditions, which denotes that H_2 was predominantly produced by steam reforming. However, the carbon deposition rapidly deactivated the catalyst in both cases, as encountered in conventional unpromoted catalysts. Upon the application of negative polarizations below −0.5 V (i.e. supply of Na^+ onto the catalyst), the activity went up and became stable. Then, the second application of +2 V (i.e. the removal of Na^+ from the catalyst surface) strongly improved the catalytic rate of H_2, temporally reaching its initial value. Upon negative polarizations, Na^+ promoters on Pt/YSZ can enhance the chemisorption of electron-donor species, such as water and O_2, increasing the coking resistance. This results in a high stability but a low activity probably because Na^+ cations also block active Pt sites. However, upon positive polarizations, without any Na^+ cations on the catalyst, the catalytic activity strongly increases due to the release of active sites. Thus, the application of negative polarizations can in operando regenerate the catalyst since the enhanced chemisorption of water and O_2 boosts the oxidation of previously deposited carbon and allows to recover the initial activity. Then, by means of cyclic variations of the applied potential between +2 V (deactivation) and −1 V (regeneration), this study demonstrated that the issue of carbon deposition can be overcome by EPOC [80]. In other EPOC study on MSR, using a Ni/YSZ electrochemical cell [82], the group of Vayenas also achieved the in situ removal of the deposited carbon on the nickel, but, in this case, this regeneration step took place during the positive polarization, due to the

direct electrocatalytic oxidation of the carbon deposits by O^{2-} ions electrochemically transferred through the YSZ electrolyte. In any case, such dynamic cyclic operation mode with periodic in situ regeneration steps is not possible with conventional catalysts. However, the electrochemical catalysts described in these studies have to be improved in view of its further practical implementation:

- The Pt- and Ni-based composite layers exhibit a much higher cost and a much lower dispersion than conventional Ni-based catalysts.
- A specific reactor design should be developed to substitute the current methane reformers by EPOC technologies.

The first upgrade strategy could be to develop disperse catalysts based on transition metals (Fe, Ni, Cu). As suggested for NSR catalysts, other catalyst preparation methods, by using an electronic conductor matrix, could be used to increase the metallic dispersion. Regarding the reactor design, the MEPR could make possible the short−/mid-term scale-up of the EPOC approach for MSR.

EPOC studies were also focused on the catalytic decomposition (Eq. 9.9), partial oxidation (Eq. 9.10) and steam reforming (Eq. 9.11) of methanol for the production of H_2.

$$CH_3OH_{(g)} \rightarrow 2H_2 + CO,\ \Delta H_{298} = +90.8\ \text{kJ/mol} \tag{9.9}$$

$$CH_3OH_{(g)} + 1/2O_2 \rightarrow 2H_2 + CO_2,\ \Delta H_{298} = -192.2\ \text{kJ/mol} \tag{9.10}$$

$$CH_3OH_{(g)} + H_2O_{(g)} \rightarrow 3H_2 + CO_2,\ \Delta H_{298} = +49.6\ \text{kJ/mol} \tag{9.11}$$

For instance, we have reported the activity of Ni/K^+-$\beta''Al_2O_3$ electrochemical catalyst [57], with highly dispersed Ni nanocolumnar films of controlled microstructure prepared by oblique angle physical vapour deposition. This innovative study dealt with the simultaneous electrochemical promotion of the production and the storage of H_2 from methanol, as schematized in Fig. 9.6a. At 280 °C and atmospheric pressure, the production of H_2 was enhanced under the application of negative polarizations (spillover of potassium ions towards the Ni catalyst surface [83]), followed by a strong deactivation (Fig. 9.6b) probably linked to the blocking of Ni active sites. The most interesting point was the dynamic storage of H_2 at these negative potentials. Chemisorbed H atoms on Ni active sites could be stored on deposited carbonaceous compounds (Fig. 9.6a), while K^+ ions could stabilize the hydrogen adsorption, as already observed when alkali ions were intercalated into graphitic layers [84]. These results demonstrate that H_2 can be stored on the graphene oxide in the presence of potassium species. This explains why, upon positive polarizations, H_2 was desorbed and released under inert atmosphere (Fig. 9.6b). The graphitic nature of these carbonaceous deposits was proved by scanning electron microscopy (SEM), vibrational spectroscopic techniques (FTIR and Raman) and operando near-ambient pressure (NAP) X-ray photoelectron spectroscopy [57, 85, 86]. The latter spectroscopic studies performed under analogous methanol reaction conditions (280 °C, 1 mbar CH_3OH) by Espinós et al. [85, 86]

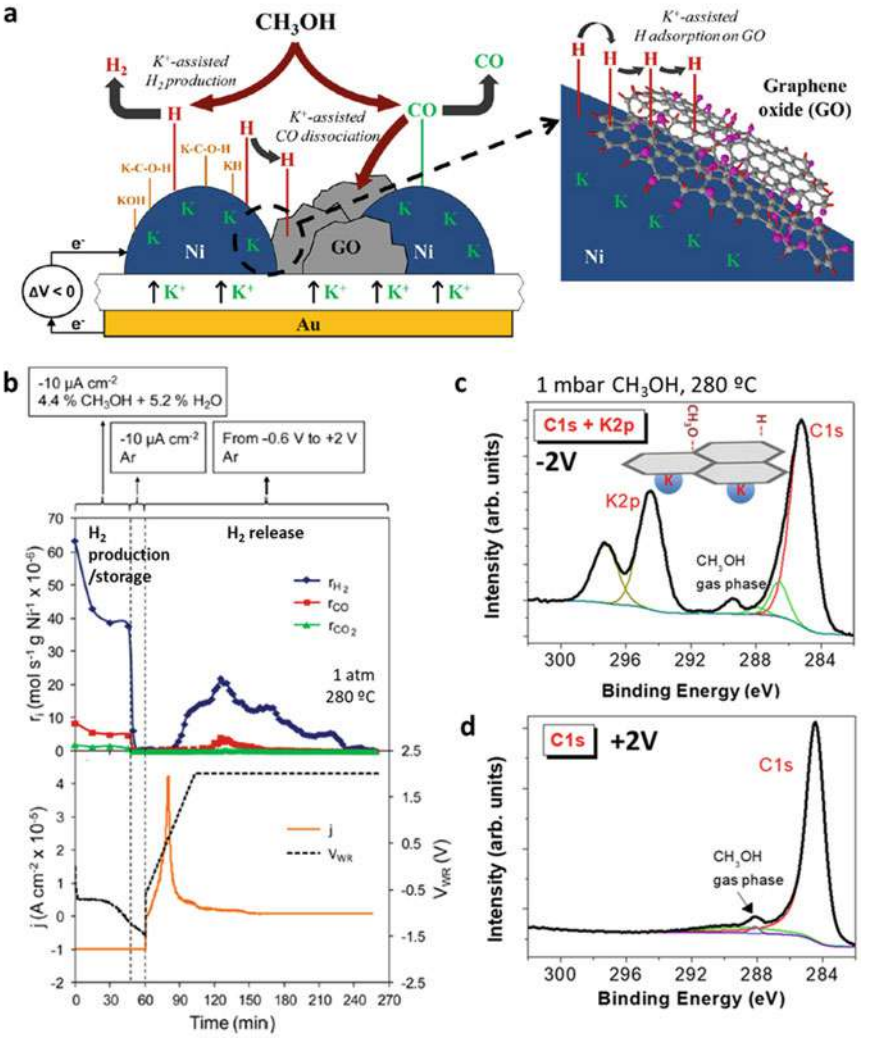

Fig. 9.6 Proposed mechanism of the K-promoted H_2 production and storage on a Ni/K^+-β"Al_2O_3 electrochemical catalyst (**a**). Evolution of current density (j), catalyst potential (V_{WR}) and H_2, CO and CO_2 production rates (r) during a H_2 storage experiment at 1 atm and 280 °C. H_2 production/storage step: CH_3OH/H_2O = 4.4%/5.2%, j = −10 μA. Cleaning step: 100% Ar, j = −10 μA. H_2 release step: 100% Ar, voltammetry from −0.6 V to +2 V (1 mV s^{-1}) (**b**). K2p and C1s spectra recorded by NAPP spectroscopy (1 mbar CH_3OH, 280 °C), at −2 V (**c**) and + 2 V (**d**). (Adapted with permission from Ref. [57, 86])

also showed that nickel and potassium remained in metallic form on the catalyst surface and in situ evidenced the totally reversible character of the potassium doping by EPOC, which seemed to affect both the Ni and the carbonaceous species, as observed, for example, in Fig. 9.6c, d.

To go further in this very innovative route for hydrogen production/storage, additional studies should be carried out to better understand the mechanism, for example, by using model catalysts containing controlled graphene-like deposits to directly focus on the H_2 storage and release stages. The main strengths of this electrocatalytic system are:

- A maximum hydrogen storage capacity as high as c.a. 19 wt.% H_2 with respect to catalyst loading [57], which outperforms the best metal hydrides used for H_2 storage (i.e. $LiBH_4$ with 18 wt.% H_2).
- The possibility to operate H_2 adsorption/desorption under fixed and mild conditions (280 °C and 1 atm) unlike all conventional storage methods [87, 88], under electric potential control.

From the technological point of view, the upgrade degree of the catalyst materials was high, but the electrochemical cell-like configuration still stands as a bottleneck for the scale-up of this EPOC application, and a proper reactor design (e.g. MEPR configuration) should be implemented.

9.3 EPOC-Assisted Electrolysers

Water electrolysis will play a major role in the energy transition. Water electrolysis consists of splitting the water molecule into pure H_2 and O_2 gases (Eq. 9.12 or 9.13, in liquid or steam phase, respectively) under the application of an electrical potential, and, when using only renewable electricity, green hydrogen is produced.

$$H_2O_{(l)} \rightarrow H_2 + 1/2O_2,\ \Delta H_{298} = +285.8\ \text{kJ/mol} \tag{9.12}$$

$$H_2O_{(g)} \rightarrow H_2 + 1/2O_2,\ \Delta H_{298} = +241.8\ \text{kJ/mol} \tag{9.13}$$

Except in alkaline water electrolysers (AWE), water electrolysis is operated in fuel cell-type reactors either at low temperature (<90 °C) in proton- or anion-exchange membrane (PEM or AEM) electrolysers [89, 90] or at high temperatures (500–1000 °C) in solid oxide electrolysers (SOE) [89, 91, 92]. However, the hydrogen production via electrolysis is not economically competitive compared to catalytic reforming processes. The water splitting is energy demanding leading to a high thermodynamic potential to electrolyse water (1.23 V at room temperature). Furthermore, the sluggish oxygen evolution reaction (OER) at the anode still increases the cell potentials up to around 1.8 V, which is demanding for the stability of materials and critical for the energy consumption. To overcome this issue, organic molecules like alcohols can be introduced at the anode, instead of H_2O, to depolarize the electrolysers for on-site pure H_2 production [52, 93–105]. Indeed, the electrooxidation of the organic molecules is thermodynamically much more favoured than the water electrolysis. For instance, the theoretical standard cell potential is 0.016 V for methanol, 0.084 V for ethanol and 0.003 V for glycerol

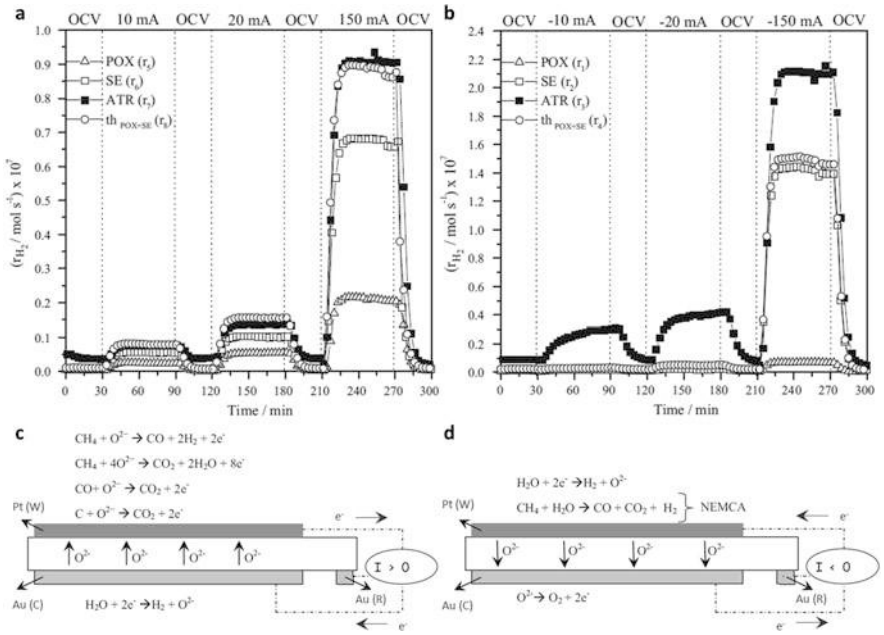

Fig. 9.7 Variation of the H_2 production rates as a function of time during different galvanostatic transitions on a Pt-YSZ/YSZ/Au electrochemical cell at 600 °C, under different reaction atmospheres: 1% CH_4/0.2% O_2 (POX), 1.5% H_2O/0.2% O_2 (SE) and 1% CH_4/1.5% H_2O/0.2% O_2 (ATR), upon positive (**a**) and negative (**b**) polarization. The joint contribution of POX and SE, $th_{POX + SE}$, is also depicted for comparison vs. ATR. Scheme of the electrocatalytic/EPOC reactions taking place at both electrodes, under ATR conditions, upon positive (**c**) and negative (**d**) polarization. Reprinted with permission from [107]

electrolysis. However, the kinetics of the electrooxidation of organic molecules below 90 °C remains slow even on Pt-based electrodes. Regarding SOE, high temperatures dramatically increase the kinetics for the electrochemical reactions [106] but require the development of stable and robust materials (due to the chemical compatibility between electrodes and electrolyte, sealing materials, etc.). One solution to lower the electrolysis cost could be to combine this technology with EPOC. PEM electrolysers and SOE technologies are mature and easy to scale up in stacks, allowing to polarize a catalyst-electrode and then to implement EPOC. The idea, recently proposed in the literature [107, 108], is to couple the electrolysis process with an electropromoted catalytic reaction at the cathode that can produce additional hydrogen, beyond the Faraday's law.

A pioneer study [107] has proposed to operate MSR in a single-chamber SOE reactor based on Pt-YSZ/YSZ/Au (cathode/solid electrolyte/anode). The reactor and the Pt-YSZ composite layer (cathode) were similar to those of the previously described study on MSR [80]. Three different reaction atmospheres were explored: steam electrolysis (SE), methane partial oxidation (POX) and auto-thermal reforming (ATR) (Fig. 9.7a, b). The steam electrolysis process for H_2 production

was coupled with the electrochemical promotion of catalytic methane conversion into H_2. In this particular configuration, the Pt-YSZ electrocatalyst and the Au electrode act as working and counter-electrode, respectively. Therefore, positive polarizations can trigger (i) the hydrogen evolution reaction (HER) on the Au electrode under steam electrolysis conditions, (ii) the electrocatalytic oxidation of methane on the Pt-YSZ by O^{2-} ions transferred through the electrolyte under POX conditions or (iii) both electrocatalytic processes simultaneously under auto-thermal conditions, i.e. in the presence of CH_4, H_2O and O_2 (Fig. 9.7c).

On the other hand, by applying negative polarizations and thus transferring O^{2-} ions from Pt-YSZ to Au, in the case of steam electrolysis, HER took place at the Pt-YSZ, with the subsequent production of H_2 and O^{2-} ions. In POX conditions, the H_2 production was negligible due to the absence of steam and the inertness of the Au electrode for methane electrooxidation. The most interesting results were obtained for ATR conditions (Fig. 9.7d), where the production of H_2 was negligible at open-circuit voltage (OCV) but drastically increased upon negative polarizations, even for low current intensities. The H_2 production was found to be much higher than that observed during SE, thus demonstrating that the steam electrolysis process (electrocatalysis) was coupled with a catalytic process via the electropromoted catalytic reforming of methane at Pt-YSZ (Fig. 9.7d). However, the H_2 production was lower than that predicted by the Faraday's law in all cases, due to partial recombination of H_2 with O_2 present in the reaction feed. Therefore, it could be very promising to validate this novel concept in a double-chamber SOE using Ni-based catalysts instead of Pt. For example, this EPOC approach could be investigated on nanoporous Ni/YSZ-based materials like those reported in literature prepared by physical vapour deposition (PVD) in oblique angle [109–111].

EPOC was also recently investigated in a low-temperature PEM electrolyser with Pt-C/(OH^--polymeric membrane)/Pd-C (anode/electrolyte/cathode). We introduced methanol, as a model alcohol molecule, in aqueous KOH electrolyte solution not only in the anode but also in the cathode [108]. Thus, in this case, the idea was to couple the electrolysis process with the catalytic methanol decomposition at the cathode.

Figure 9.8a shows the different cell configurations tested in this study. As expected, a steam electrolysis configuration (Conf. 1) showed no hydrogen production at cell voltages below 1.2 V. Then, in this voltage range, a conventional methanol/water electrolyser configuration (Conf. 2) showed a current-dependent hydrogen production that fitted well with that predicted by the Faraday's law. However, when performing the same electrochemical tests upon feeding methanol at both anode and cathode (Conf. 3), interestingly, the H_2 production values exceeded those expected, as can be observed in Fig. 9.8b. The overproduction of H_2 was attributed to the catalytic methanol decomposition on Pd. In addition, no H_2 production was observed under OCV, meaning that this catalytic reaction was electropromoted by K^+ cations. This electropromoted methanol decomposition was combined with the water electrolysis, which was not harmed by the presence of methanol in the cathode in these specific conditions (Fig. 9.8b). Therefore, the EPOC-assisted electrolysis concept could lower the cost of the H_2 produced in

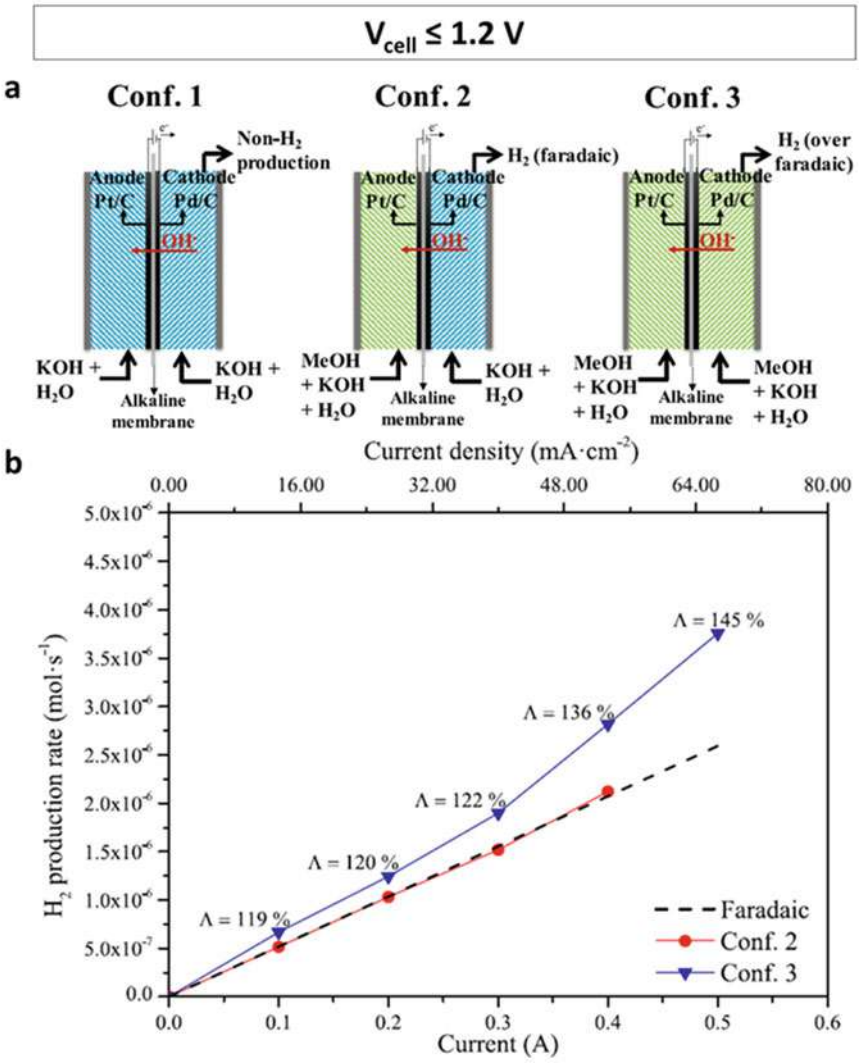

Fig. 9.8 Scheme of three different operation configurations with a Pt-C/(Fumapem FAA-3-50) membrane/Pd-C electrolysis cell: Conf. 1, water electrolysis, with no activity below 1.2 V cell voltage; Conf. 2, conventional methanol electrolysis, where methanol is fed to the anode and water to the cathode; and Conf. 3, EPOC-assisted methanol electrolysis where methanol is also added in the cathode feed stream leading to additional catalytic H_2 production via electrochemical promotion (**a**). Steady-state H_2 production rate under different chronopotentiometries with Conf. 2 and 3, along with predicted faradaic H_2 production rate (**b**). (Reprinted with permission from Ref. [108])

alcohol/water electrolysers. However, noble metal-based electrodes have to be replaced by Ni-based electrodes for a further possible practical application.

These recent studies have demonstrated the main advantage of these EPOC-electrolysis approaches which could improve the efficiency of high-temperature steam electrolysis in SOE and low-temperature electrolysis in PEM reactors. Both SOE and PEM water electrolysers are mature, and scale-up stack reactors can be acquired commercially for real applications. We believe that the EPOC-assisted electrolysis could constitute a breakthrough technology to enhance the "H_2 economy".

9.4 Prospective Catalytic Processes for EPOC

This section is a brainstorming on some potential catalytic reactions in which the unique properties of EPOC could be used as a tool to outgrow challenges in alluring processes. The prospective processes, as schematized in Fig. 9.9, were selected based on the pivotal role of promoting species in the upgrading of their reaction rate and selectivity towards the different products, as well as on their urgency for modern chemical industry and society. Regarding the ammonia synthesis, please refer to Chap. 8 in this book which describes in detail recent advances in the electrochemical synthesis of NH_3 for lowering the energy demand of the current

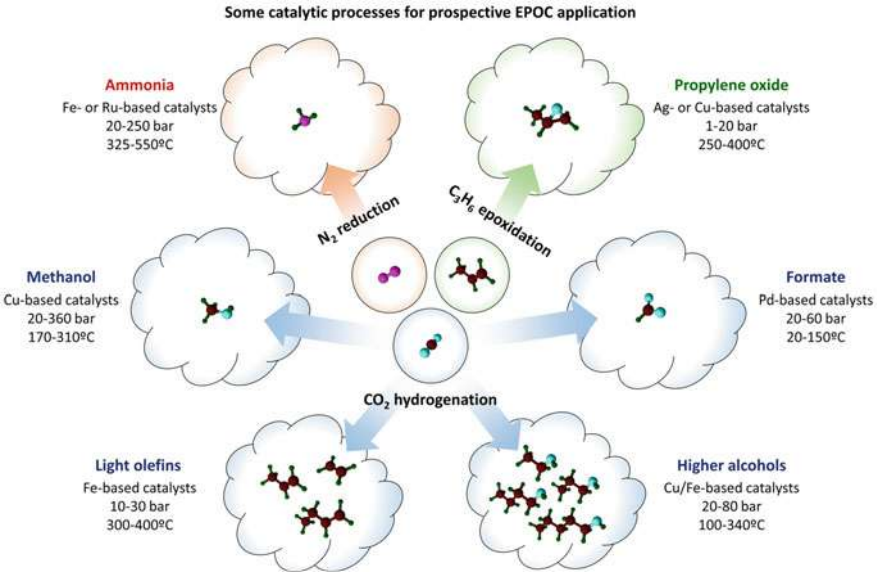

Fig. 9.9 Scheme of some relevant catalytic processes, along with reported operation conditions, that could be potentially improved by EPOC for the production of high-value chemicals

industrial Haber-Bosch process which is taking place at high pressure (100–300 bar) and temperature (400–500 °C).

9.4.1 CO_2 Valorization Through Catalytic Hydrogenation

One of the primary routes to mitigate the CO_2 emissions in large quantities is its capture and thermochemical conversion with hydrogen to value-added chemicals or fuels [112–115]. Since CO_2 is a thermally stable molecule, a heterogeneous catalyst is required to efficiently convert CO_2 into a variety of carbon-containing products or feedstocks. Among the hydrogenation products with considerable progress in the recent years are carbon monoxide, methane, methanol and formic acid [112]. This capability of producing different compounds from the same reactants by changing operating conditions and the employed catalyst offered a unique opportunity for applying EPOC to alter not only the reaction rates but also the product range [116–122]. In addition, the pioneering works performed on high-pressure systems for Fischer-Tropsch (FT) and NH_3 synthesis exemplified EPOC in reactions that necessitate high-pressure flow work due to thermodynamic limitations [35, 122]. Here, we will discuss such opportunities for CO_2 hydrogenation according to their current status, challenges and the critical role of promotion. The electrochemical promotion of CO_2 hydrogenation has been already deeply investigated, and the main findings are described in Chap. 6. Nonetheless, most of the studies dealt with the reverse water-gas shift (RWGS) and methanation reactions [117–119, 123, 124], while, here, we are exploring alternative routes for CO_2 hydrogenation.

9.4.1.1 Methanol Synthesis

Methanol is among the top 5 commodity chemicals due to its use as feedstock for the synthesis of a wide range of chemical products, including formaldehyde, acetic acid, methyl tert-butyl ether, hydrocarbons and aromatics [112, 125, 126]. Methanol may also be used as a fuel or a fuel supplement in combustion turbines [125, 127]. Nowadays, methanol is produced by synthesis gas that is derived from fossil fuels, raising serious environmental considerations. The direct conversion of captured CO_2 and renewable hydrogen from electrolysis to methanol has been proposed as a potentially profitable and carbon-neutral route for methanol production [112, 113].

The CO_2 hydrogenation towards methanol (Eq. 9.14) constitutes an exothermic reaction in which the volume is decreasing, and therefore as ethylene epoxidation, low temperature and high pressure are thermodynamically required to achieve appreciable reaction rates (170–310 °C, 20–360 bar) [112, 128, 129].

$$CO_2 + 3H_2 \leftrightarrow CH_3OH_{(g)} + H_2O_{(g)},\ \Delta H_{298} = -49.6\ \text{kJ/mol} \quad (9.14)$$

So far, different catalytic formulations have been explored to drive this reaction. Due to the similarity with the syngas-to-methanol process, Cu-based catalysts, particularly in combination with ZnO, have been extensively utilized [126, 130]. However, the CO_2-to-methanol conversion is more complicated compared with the syngas-to-methanol conversion. The research efforts have thus been focused on the fine tuning of the local surface chemistry of the catalysts through the use of different preparation techniques, supports and/or structural/surface promoters. Nevertheless, there is still debate on the reaction pathways and the exact active sites [125]. Cu catalysts display relatively poor activity at low temperatures (<250 °C). As a consequence, the operation temperature needs to be increased, thus decreasing the selectivity to methanol by favouring the endothermic side reaction of Reverse Water-Gas Shift (RWGS, Eq. 9.15):

$$CO_2 + H_2 \leftrightarrow CO + H_2O_{(g)},\ \Delta H_{298} = +41.2\ \text{kJ/mol} \quad (9.15)$$

The CO_2-to-methanol reaction is sensitive to metal dispersion, the structure of interface as well as the adsorption of reactant species. These properties are known to be tuned via promoters apart from the preparation methods. Among the different systems explored, alkali metals (e.g. K, Cs) are the most commonly employed due to their basicity. Their functionalities for methanol production involve, among others, the modification of the adsorption properties that affect the H/C ratios on the catalyst surface and the interaction of metal with the support for H_2 spillover [125, 131]. Bansode et al. [131] systematically examined Cu-based catalysts promoted with K and Ba. Although both promoters significantly enhance the CO_2 adsorption of the unpromoted Cu surface, the product selectivity was different. K was shown to boost the methanol yield by covering selectively the Al_2O_3 oxide support and facilitating Cu reducibility, which enhanced methanol production. On the other hand, Ba covered Cu surface besides Al_2O_3 support, resulting in the stabilization of intermediate species for RWGS.

There are, in the literature, some few preliminary studies on the electrochemical promotion of methanol synthesis by CO_2 hydrogenation, although leading to very low yields since they were performed at atmospheric pressure [132–135]. For instance, the methanol production rate showed to be slightly enhanced (in less than 10%), at temperatures up to 340 °C and H_2/CO_2 ratios up to 39, on a PdZn catalyst promoted with either Na^+ or K^+ ions, the latter showing a more stable effect [132]. The EPOC phenomenon was found to be electrophilic (i.e. at decreasing potentials), but, in all cases, CO selectivity was favoured. The electrochemical supply of alkaline ions to the catalyst surface and the expected strengthening of the CO_2 (electron acceptor vs. H_2) chemisorption led to the preferential enhancement of CO production even inhibiting methanol synthesis. The group of Ruiz also carried out several studies on CO_2 hydrogenation by EPOC where methanol was obtained, among other organic compounds [133–135]. There are some unclear issues in the

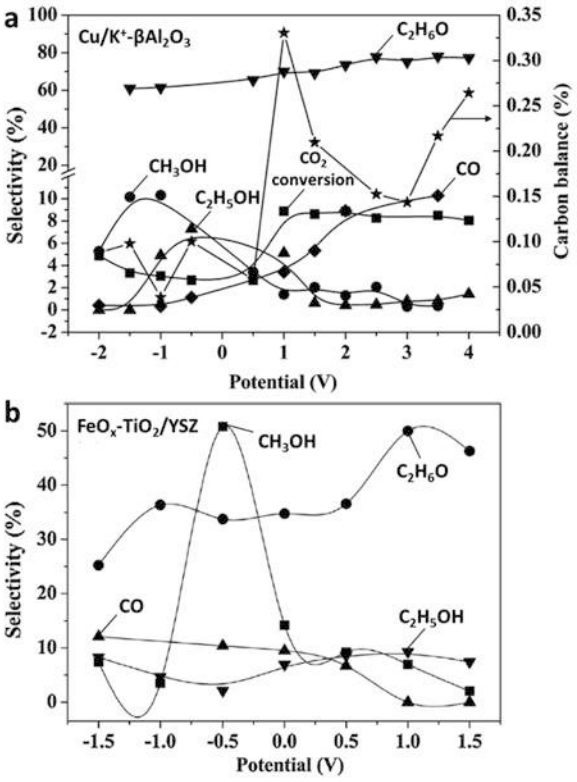

Fig. 9.10 Influence of the applied potential on the selectivity of the different CO_2 hydrogenation products (as marked on the maximum values obtained), at 325 °C and H_2/CO_2 ratio of 3, with Cu/K^+-β"Al_2O_3 (CO_2 conversion of 2–9%) (**a**) and FeO_x-TiO_2/YSZ (CO_2 conversion of 4–15%) (**b**). (Adapted with permission from Ref. [133, 134])

latter studies, such as the stability of the EPOC effect, since the time evolution of the reaction rates was not reported in any case, or the considered unpromoted reaction conditions, which were related to the application of 0 V in all cases, and this does not necessarily have to correspond to the promoter-free state. However, those studies show that the catalytic conversion of CO_2 and the selectivity of the hydrogenation products can be in situ modified by the application of an electric potential under given reaction conditions, even at atmospheric pressure, by using cationic (i.e. K^+) or anionic (i.e. O^{2-}) solid electrolyte supports. For example, by using a Cu/K^+-β"Al_2O_3 electrochemical catalyst [133], the methanol selectivity was enhanced up to 34 times to reach 10% at −1 V, at 325 °C with the stoichiometric H_2/CO_2 ratio (i.e. 3, reaction (9.14)), although the catalyst was specially selective for dimethyl ether production (c.a. 60%) under these conditions, as can be observed in Fig. 9.10a.

CH_3OH synthesis from CO_2 hydrogenation was also electrochemically promoted on Pt- [135] and Fe-based [134] catalysts supported on YSZ. For example, on Pt/YSZ, a methanol selectivity of 8% was obtained at +0.5 V, 400 °C with $H_2/CO_2 = 2$ and a CO_2 conversion of 24% [135], while, on a FeO_x-TiO_2/YSZ catalyst, the maximum methanol selectivity, c.a. 50%, was reached at −0.5 V, 325 °C, with $H_2/CO_2 = 3$ and a CO_2 conversion of c.a. 7% [134] (Fig. 9.10b). A potential advantage of using O^{2-} conductor solid electrolytes like YSZ for CO_2

hydrogenation, with respect to alkaline conductors, is the avoidance of the poisoning effect typically taking place in the latter case due to the formation of carbonate or hydride surface compounds which may block catalytic active sites. However, due to the still unclear electrochemical promotion mechanism for methanol synthesis by supplying/removing O^{2-} promoter ions to/from the catalyst surface, further investigations should be performed in this regard, and operating pressures higher than the atmospheric one should be explored to reach higher conversions, with a view to a possible competitive application.

9.4.1.2 Light Olefins (C_2–C_4) Production

The necessity to detach light olefins from fossil fuels has activated intense research efforts towards the single-step CO_2 valorization by renewable H_2 obtained from H_2O electrolysis [112, 115, 136].

$$n\,CO_2 + 3n\,H_2 \leftrightarrow C_nH_{2n} + 2n\,H_2O_{(g)},\ n = 2-4,\ \Delta H_{298} < 0 \tag{9.16}$$

The reaction (Eq. 9.16) is strongly exothermic, favoured by high pressures due to the volume decrease of the reactants. The process constitutes a catalysis benchmark and a complicated reaction system due to (i) multiple reaction pathways of CO_2 hydrogenation to various products (CO, CH_4, light olefins, higher hydrocarbons, methanol, etc.) and (ii) its sensitivity to numerous parameters involving, among others, the temperature and intra-catalytic temperature gradients, the dispersion and the interactions of active phases with the supports, the pore structure, the basicity/acidity of the catalyst surface and the limited CO_2 adsorption upon H_2 flooded surfaces. There are two main routes of CO_2 hydrogenation to olefins ($C_{2-4}^{=}$): (a) the methanol-mediated route (methanol to olefins, MTO), which proceeds through a complex reaction network involving CO_2 reduction to CO by RWGS (9.15), followed by the equilibrium-limited CO hydrogenation to CH_3OH and finally the conversion of methanol to olefins, and (b) the CO-mediated route, proceeding through the CO_2 activation to CO via the RWGS, followed by the selective CO conversion to $C_{2-4}^{=}$ (Fischer-Tropsch to olefins, FTO) [112, 115, 136, 137].

Both routes require high pressure (~30 bar) and suffer low CO_2 conversion (20–50%). MTO is conducted at relatively higher temperatures (370–400 °C), compared to FTO (300–320 °C), over acidic supports (for C-C coupling and methanol conversion to light olefins). On the other hand, FTO is driven by conventional alkali metal-promoted Fischer-Tropsch catalysts (i.e. Fe and Co) over alkaline supports [129, 138]. Due to increased temperatures and RWGS to CO, MTO displays high CO selectivity (~70%), which results in decreased olefin yield. These high rates of CO formation and the very low CO_2 conversions (20–30%) limit the overall $C_{2-4}^{=}$ yield to <7%. FTO, on the other hand, leads to low CO selectivity due to the lower temperatures that result in a leftwards shift of RWGS but increases CH_4 and, thus, lowers olefins selectivity (25–40%) within the HC fraction.

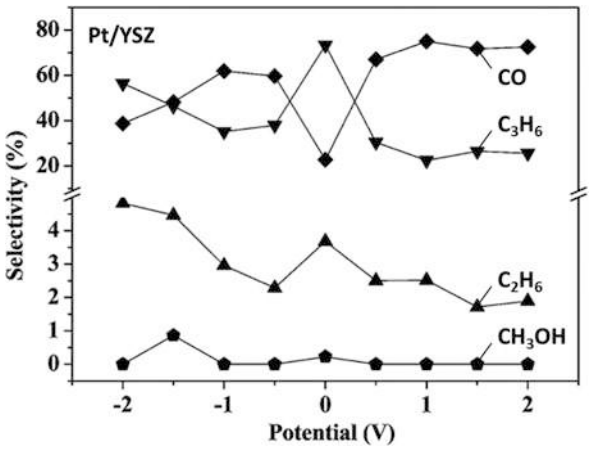

Fig. 9.11 Influence of the applied potential on the selectivity of the different CO_2 hydrogenation products, at 400 °C and H_2/CO_2 ratio of 4, with Pt/YSZ (CO_2 conversion of 1–10%). (Adapted with permission from Ref. [135])

Due to the relatively higher CO_2 conversions (40–60%) and CO minimization (<20%), FTO yield overpasses the values obtained with the MTO.

The most appropriate catalysts for the FTO route are Fe-based systems combined with the suitable supports and promoters in order to create the required active sites for driving the reaction. Typical supports for the process are metal oxides (e.g. Al_2O_3, ZrO_2) or carbon-based materials (e.g. carbon nanotubes), which are very important for the catalytic activity as well as selectivity to the different products. The alkali metal promoters, and specifically K and Na, are considered the most effective since they increase the selectivity as high as 57% to light olefins by simultaneously constraining the competitive methane formation [139]. This critical role of the alkali promoters has been investigated in several experimental studies [139–142]. For instance, Meiri et al. [140] could stabilize the texture of Fe-Al-O spinel and strengthen the CO_2 adsorption, whereas Martinelli et al. [142] reported that K promoter enhanced the alkene production at the expense of methane and other alkanes [141].

The electrochemical promotion of CO_2 hydrogenation to propylene was explored, at atmospheric pressure, by Ruiz et al. on different metal catalyst films (i.e. Pt, Pd, Ni) deposited on YSZ [135]. For instance, Fig. 9.11 shows that, under given reaction conditions, Pt/YSZ electrochemical catalysts reached a selectivity towards C_3H_6 above 70% at 0 V, along with significant selectivity towards ethane (maximum of c.a. 5% at −2 V). Both C_2 and C_3 selectivities follow an opposite trend as that of CO. This behaviour suggested that they were generated by hydrogenation of CO previously formed by RWGS (Eq. 9.15), i.e. via FTO mechanism rather than MTO, which opens new opportunities for EPOC application on CO_2 and CO hydrogenation.

The synthesis of light olefins can be also performed through the oxidative coupling of methane and the light alcohols dehydration. The former reaction leads to the production of ethylene as the main value-added product, and it has already been explored via electrocatalysis, in solid electrolyte membrane reactors using

catalysts mainly based on Ag and YSZ as electrolyte for the supply of O^{2-} ions [143–146], but it has not been studied from the EPOC perspective yet. On the other hand, an innovative and recent collaborative work between the Massachusetts Institute of Technology and the University of Patras [147] proved the electrochemical promotion of isopropanol and 2-butanol dehydration reactions to selectively produce propylene and butenes, respectively. Experiments were performed at 400 °C and near-ambient pressure, on a Mo film deposited on YSZ. The EPOC effect upon positive polarization (i.e. migration of O^{2-} ions onto the catalyst film) was explained on the basis of (i) the in situ generation of additional Brönsted acid sites at the three-phase boundary (tpb) between gas, catalyst and solid electrolyte, according to the observed Mo (V) fraction on the surface, and (ii) the strengthening of these acid sites due to the decrease of the electronic density on the oxide surface, thus decreasing the deprotonation energy and increasing the reactant dehydration rates. This study demonstrates that EPOC can also alter solid acid-catalysed reactions, opening new opportunities for further applications.

9.4.1.3 Higher Alcohol (C_2–C_5) Synthesis

While numerous studies have been carried out for the catalytic conversion of CO_2 with hydrogen to value-added chemicals, only a small number explored the production of higher alcohols (HAs) than methanol, i.e. C_2–C_5 [112, 114]. HAs have excellent energy density and can be employed as transportation fuels or as fuel additives. In addition, they may be used as solvents and precursors for chemical synthesis. Therefore, a direct conversion of CO_2 to HAs would be economically preferable, if high CO_2 conversion and HA selectivity were achieved in this vastly challenging process (Eq. 9.17).

$$n\,CO_2 + 3n\,H_2 \leftrightarrow C_nH_{2n+1}OH_{(g)} + (2n-1)\,H_2O_{(g)},\ n = 2-5,\ \Delta H_{298} < 0 \quad (9.17)$$

As the chemical processes previously discussed, HA production from CO_2 also requires high pressures (20–80 bar) and/or temperatures (100–340 °C) [112, 148]. Apart from the thermodynamic stability of CO_2, the path to HAs constitutes a complex set of competing reactions to hydrocarbons during Fischer-Tropsch (FT) that typically results in low yields. The minor control over C-C coupling and the need for different types of C-O bond adsorption in order to obtain C(H)O species are some of the reasons for this [149]. The resulting compounds are rather sensitive to the balance of the C-O bond activation (alkylation and alcohol formation) and the C-C coupling [150].

The critical steps in HA synthesis, such as the CH_x-CO coupling, are considered to take place at similar active sites as in the syngas-to-HA process [151], and thus, similar materials are expected to catalyse the reaction if RWGS would be also favoured. Therefore, the catalysts explored include noble metal (Rh, Ir, Au, Pt)-, Co-, Cu- and Mo-based materials. In all types of catalysts, the critical role of the

support and promoters towards the stabilization of key intermediate species for HA formation has been exemplified. Among the different types of catalysts, Cu-based materials are of particular interest due to their low cost and higher selectivity (79% in fixed-bed and 99% in tank reactors) to HA than Co and Rh. The surface of Cu favours the non-dissociative hydrogenation of $C(H_x)O$ bonds rather than the C-O bond cleavage which enables alcohol formation [150, 152]. The creation of HA is achieved by the addition of promoters in order to aid the creation of the required CH_x compounds in CH_x-$C(H_x)O$, which may be coupled to produce HAs [150, 152]. Hence, the emphasis in several studies on Cu catalysts was on their combination with FT catalysts, such as Co and Fe, which are promoted by alkali metals, such as K, Na and Cs. For these systems, promising HA fractions of up to 90% at 50–60 bar and 300–330 °C have been obtained [153, 154]. Nevertheless, the observed formation rates are still rather low (20–100 $mg \cdot g_{cat}^{-1} \cdot h^{-1}$) with selectivities which do not reach those obtained for methanol synthesis. Despite that the optimum catalytic systems are alkali promoted, the exact role of the alkali metal has not been elucidated, besides restraining catalyst reduction and hydrogenation capability.

Previously mentioned EPOC studies on CO_2 hydrogenation performed at room pressure report the production of ethanol enhanced by using either K^+ [133] or O^{2-} conductors [134] under specific reaction conditions. In the former case, on Cu catalyst, C_2H_5OH selectivity was enhanced up to c.a. 7% by electrochemical supply of K^+ ions at −0.5 V at 325 °C and $H_2/CO_2 = 3$ (see Fig. 9.10a). Interestingly, under the same temperature and composition conditions, the authors observed that a YSZ-supported FeO_x-TiO_2 catalyst polarized either at +0.5 V or at −1.5 V (i.e. upon supply or removal of O^{2-} ions to or from the catalyst film) reached a similar ethanol selectivity of c.a. 8% (Fig. 9.10b), and this value increased to c.a. 14% with a higher H_2/CO_2 ratio (i.e. 4) at both optimum applied potentials.

9.4.1.4 Formate Production in Aqueous Phase

Among the different carbon dioxide hydrogenation products, formate/formic acid is another one that requires special attention. Apart from its wide applications, in chemical, food and textile industries, it is acquiring increasing interest in energy applications, as a low-carbon energy vector or hydrogen carrier [155–157]. Direct liquid fuel cells are a potential alternative to conventional hydrogen fuel cells given the low volumetric energy density of H_2. Formic acid/formate can be easily and safely stored in the form of formic acid amine adducts or aqueous formate salt solution. Besides, direct formate fuel cells (DFFC) have a higher theoretical cell voltage (1.45 V using oxygen as oxidant), and thus a higher power density, than other kinds of fuel cells, e.g. using hydrogen (1.23 V), methanol (1.23 V) or ethanol (1.14 V) as fuels [158, 159]. Thus, DFFC is a renewable carbon-neutral energy technology as long as formate is produced using CO_2 as the carbon source and H_2 obtained from water splitting. CO_2 hydrogenation to formate (Eq. 9.18) has been

widely studied in the field of heterogeneous catalysis [157, 160], although big efforts are also made on the electrocatalytic [159] and photocatalytic [161] pathways.

$$CO_{2(\,g)} + H_{2(\,g)} \rightarrow HCOOH_{(l)},\ \Delta H_{298} = -31.6\ \mathrm{kJ/mol} \tag{9.18}$$

It should be noted that formic acid was only detected in trace amounts in some of the above-mentioned EPOC works on CO_2 hydrogenation by Ruiz et al. [133, 134]. Like all other catalytic reactions addressed in this chapter, this is an endergonic reaction ($\Delta G_{298} = +32.9$ kJ/mol). However, the solvation of the formic acid in a suitable solvent makes this reaction spontaneous [157, 160]. For instance, if CO_2 hydrogenation is conducted in aqueous solution (Eq. 9.19), formate formation becomes thermodynamically favoured ($\Delta G_{298} = -4.0$ kJ/mol).

$$CO_{2(aq)} + H_{2(\,g)} \rightarrow HCOO^{-}_{(aq)} + H^{+} \tag{9.19}$$

This reaction in aqueous solution is typically studied on Pd-based catalysts at 20–150 °C and 20–60 bar with either pure H_2 gas or a H_2/CO_2 ratio of 1, as very recently reviewed [160]. Two interesting studies [162, 163], using Pd/C catalysts (0.4–0.5 $mg_{Pd}\ cm^{-2}$), have demonstrated the potential of EPOC in this catalytic reaction. It should be noted that, apart from these studies, the EPOC phenomenon has been applied in very few cases at solid-liquid interfaces, for example, for the electrochemical promotion of H_2 oxidation reaction [164, 165], 1-butene isomerization [166], hydrazine oxidation [167], rearrangement of cis-stilbene oxide to diphenylacetaldehyde and diphenylethanone [168] or methanol decomposition reaction in EPOC-assisted water electrolysers [108] as described in Sect. 9.3. Herein, Cai et al. proved for the first time the electrochemical promotion of CO_2 hydrogenation in liquid phase by using a Pd/C electrode as the cathode, although in situ generated PdH_x was actually the active phase, Pt as the anode and H_2 (20%)/CO_2-saturated 1 M $KHCO_3$ as the electrolyte [162]. The authors found two different CO_2 hydrogenation pathways, i.e. catalytic and electrocatalytic, to compete with each other and with HER (hydrogen evolution reaction). Although faradaic efficiencies were not reported in this work, the transferred charges and the quantified formate production at different applied potentials, either with or without H_2 gas bubbling, showed evidence of electrochemical promotion of the catalytic production of formate under low applied potentials, i.e. −0.1 or −0.2 V vs. RHE. The authors proposed that the origin of the synergy between catalytic and electrocatalytic CO_2 hydrogenation reactions was the formation of $HCOO^{*}$ as a common intermediate.

In a more recent study on CO_2 hydrogenation to formate on Pd/C, Ryu and Surendranath rather attributed the EPOC effect to a local pH swing [163]. The authors observed that the formate production had a first-order dependence with respect to both CO_2 and OH^{-} concentrations, which are inversely correlated to each other by the carbon dioxide/bicarbonate equilibrium. Interestingly, the application of low potentials, up to −0.3 V vs. RHE, showed to locally increase the alkalinity, by electrocatalytic consumption of protons in the vicinity of the catalyst

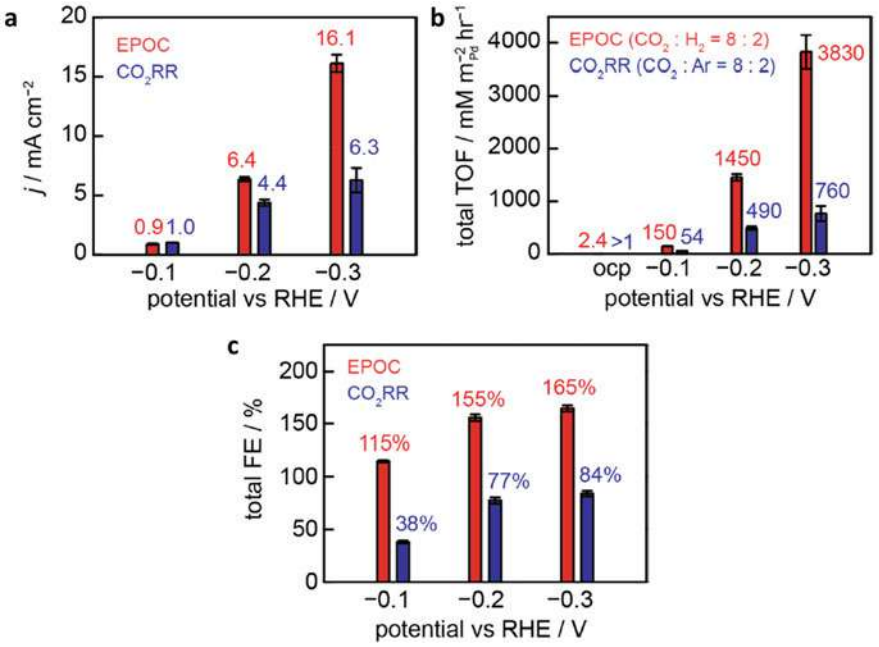

Fig. 9.12 Influence of the applied potential on the current density (**a**), total specific turnover frequencies (TOF) for formate production (**b**) and total faradaic efficiency (FE) for formate production (**c**), obtained with Pd/C catalyst (cathode), using Au as anode, in the presence of 50 mM $KHCO_3$/0.5 M $NaClO_4$ (pH 6.4) under EPOC conditions (20% H_2/80% CO_2) and CO_2 electroreduction (CO_2RR, 20% Ar/80% CO_2). (Reprinted with permission of the American Chemical Society from Ref. [163])

surface, while maintaining a high CO_2 concentration in the solution. Besides, the bubbling of H_2 gas in EPOC configuration (20% H_2/80% CO_2) likely inhibited the catalyst poisoning by adsorbed CO, which took place in CO_2 electroreduction (CO_2RR) configuration (bubbling 20% Ar/80% CO_2). Thus, both the obtained current densities (Fig. 9.12a) and the turnover frequencies (TOF) for formate production (Fig. 9.12b) increased under EPOC conditions, enhancing the latter up to 5 times at −0.3 V vs. RHE. Faradaic efficiencies over 100% were reached (Fig. 9.12c), which evidenced the non-faradaic CO_2 hydrogenation to formate.

9.4.2 Propylene Epoxidation to Propylene Oxide

Propylene is a commodity chemical of great importance derived from higher hydrocarbon cracking in oil refining industry. Among its different applications, propylene conversion to propylene oxide (PO, Eq. 9.20) is intriguing due to the use of the latter as raw material in the manufacturing of polyurethane foams [169].

$$C_3H_6 + 1/2O_2 \leftrightarrow C_3H_6O_{(g)}\ \Delta H_{298} = -114.9\ \text{kJ/mol} \tag{9.20}$$

The significance of this process becomes more pronounced by considering the environmental and economic considerations of the existing industrial methods for producing PO. Therefore, a successful outcome in propylene epoxidation reaction could have significant impact on a range of industrial processes [170, 171].

The concept of propylene epoxidation is not new; several types of reactors, energy input (thermal and light), catalysts and oxidizing agents have been already examined and summarized in recent reviews [172]. This reaction is commonly carried out at 1–20 bar and 250–400 °C, and the most common catalysts are Ag- (employed due to its use in ethylene epoxidation as described in Sect. 9.2.1) and Cu-based catalysts with high sensitivity to the shape and size of the catalyst. As for ethylene epoxidation, the primary challenge is the selectivity towards PO over the deep oxidation of propylene to carbon dioxide. Relatively low conversions of propylene deliver yields (~5%) that are far from commercialization targets [170, 171].

By examining the epoxidation reaction, an electrophilic insertion of an oxygen atom into the double C=C bond is required. At the same time, the side but undesired reaction is the allylic dehydrogenation of propylene that demands oxidizing species of nucleophilic nature, revealing how critical the nature of oxidizing species for the selectivity is. Moreover, the number of acidic sites, the geometry of the active sites and the electronic or dipole state of the surface of the catalysts (routinely caused by alkali metal promoters) play a key role in the resulting products.

The critical role of promoters towards increasing the formation rate and selectivity of PO has been demonstrated in both Ag and Cu catalytic systems. Routinely, alkali and alkaline earths are used, for instance, in the form of sodium and potassium salts [171, 173, 174]. In Ag-based materials, the unpromoted metallic Ag phase is expected to produce high flows of electrons to the adsorbed oxygen, thus increasing the nucleophilicity as well as the activity of oxygen for deep oxidation. However, when electron-donor promoters like Mo or W are added, this effect diminishes, and Ag remains in a cationic phase that considerably enhances PO selectivity by keeping adequate propylene conversion [175]. This effect was also apparent with highly dispersed Cu over SiO_2 materials [176]. Among the different alkali and alkali earth dopants, K displayed the strongest enhancement on PO selectivity. The authors exemplified a clear interaction between K^+ and CuO_x that decreased the strength and number of acid sites, thus limiting further oxidation to CO_2. Moreover, the existence of K^+ species aided the creation of lower-sized CuO_x clusters (i.e. higher surface area for catalysis) and the suppression of the lattice oxygen reactivity that facilitates deep oxidation [176, 177].

The spatial separation of propylene and oxygen reactants through a membrane reactor configuration has been also investigated, targeting at controlling the oxygen partial pressure in the reaction chamber which results in undesired deep oxidation at the gas phase. The authors also added steam to limit PO desorption and its deep oxidation over the catalyst surface. This configuration allowed up to 13 times (from

0.5 to 6.5%) higher PO yields than the conventional fixed bed [178]. These promising results with membrane systems were also reported in earlier studies by utilizing a tubular configuration reactor based on ZrO_2-Y_2O_3-TiO_2 which contained alkaline earth-promoted Ag catalysts with selectivity to PO larger than 30% [171].

Regarding EPOC studies on propylene reaction, the deep oxidation reaction has been widely studied [179–186] as well as the use of propylene as reducing agent for NO_x catalytic reduction [187–192]. However, to date, there is only one study exploring the EPOC application in the propylene epoxidation reaction, carried out by Stoukides and Vayenas by using an Ag/YSZ electrochemical catalyst at 395 °C and atmospheric pressure [193]. Given the excess of oxygen in the gas stream, the open-circuit reaction rate obtained for propylene combustion ($2.53 \cdot 10^{-7}$ mol s^{-1}) was much higher than that for epoxidation reaction ($0.05 \cdot 10^{-7}$ mol s^{-1}). Nevertheless, positive polarizations (supply of O^{2-} promoter ions to the Ag film) were found to enhance the propylene epoxidation rate and PO selectivity in a reversible manner. However, the rate enhancement ratios were below 2 under any reaction conditions.

9.4.3 Previous EPOC Studies as the Roadmap for the New Processes

The common denominator for all described processes is their sensitivity and reliance to promoters. On the other hand, EPOC studies have already shown remarkable progress in other numerous processes that display substantial similarities to the above in terms of reaction pathways, and therefore, they consolidate EPOC as a powerful tool to either enhance reaction rates or dramatically alter the selectivity to the desired products by controlling the work function of the catalyst. Moreover, the extensive research and results with the concurrent development in synthesis and characterization methods may facilitate the EPOC applications to such new intriguing processes [116]. For instance, the proposed CO_2 hydrogenation routes have all in common the high-pressure thermodynamic requirement. This is a major challenge due to the complexity of developing pressurized electrochemical reactors, but there are several examples of successful development of pressurized systems for electrochemical promotion in NH_3 synthesis and FT (CO hydrogenation) [35, 122].

FT process exhibits several similarities with CO_2 hydrogenation to hydrocarbons, HAs and methanol [114]. It is also highly complexed with still not clarified reaction mechanisms. Almost 20 years ago, the Lambert team in the UK exemplified EPOC on FT [120–122]. The group investigated initially CO hydrogenation over Ru catalyst deposited on β" alumina doped with Na. The study was performed at ~200 °C but at atmospheric pressure which does not favour the carbon chain growth [120]. The authors showed that by supplying Na^+ to a Ru surface, a considerable increase in the carbon chain growth probability and selectivity to olefins was observed but at the expense of CO conversion. Similar findings were also reported

when a Rh catalyst was used with K species as promoters, i.e. improved selectivity to C_2–C_4 hydrocarbons but lower reaction rates when K^+ was supplied to the catalyst [121]. Urquhart et al. [122] continued these studies by developing a high-pressure (14 bar) electrochemical reactor for EPOC. By employing the same Rh catalyst and K promoting species, they detected 43 products, comprising paraffins, olefins and HAs. Most notably, the electrochemical promotion by K influenced reversibly the product distribution, and specifically, negative polarization (K^+ supply to the catalyst) enhanced the olefin and HA formation rates and selectivity [122].

The studies of Lambert's group on promoted CO hydrogenation offer a starting point for exploring different CO_2-to-X (X: hydrocarbons, HA, methanol) schemes by employing EPOC for altering reaction rates and selectivity towards the desired products and by understanding the promoter role in the reaction mechanism. This is further corroborated by the recent works from the Vayenas and Katsaounis team (see Chap. 6) who demonstrated the high sensitivity of CO_2 hydrogenation to the electrochemical promoting species, which can dramatically alter the selectivity between CO and CH_4 [117–119, 123, 124].

From a promotional viewpoint, propylene epoxidation is an extremely intriguing and complex system, which requires the enhancement in the conversion of propylene by sustaining the selectivity towards PO, offering space for EPOC activities. Possible future works in the field could explore the possibility of promoting this reaction by using knowledge from the well-studied ethylene epoxidation for EPOC [30, 32, 33, 194]. For instance, the most common catalysts in both cases are Ag-based, and therefore, the studies on EPOC could initiate from this catalyst [171]. Ethylene epoxidation is also influenced by promoting species, such as O^{2-}, which may have both positive and negative effects on the catalyst performance. This offers an opportunity for studies that explore the potential promotion effect caused by different types of species, such as O^{2-}, Na^+ and K^+ (Na and K are typical promoters in propylene epoxidation) not only for altering selectivity and reaction rate, but also to operando optimize their desired coverage through voltage.

Besides promoting species, it is of particular interest that, when propylene epoxidation was performed in catalytic membrane reactors, a higher selectivity was achieved due to the shortening of residence time over the catalyst which, in turn, limited the side reaction of deep oxidation. Most likely, this effect could be even more pronounced by employing EPOC electrochemical membrane reactors, which can take advantage of the lesser catalytic surface of electrodes (lower residence time on the catalyst and, thus, lower chance for deep oxidation of PO), as well as the operando control of the catalyst work function [116]. EPOC may also offer some flexibility to the promotion of this reaction scheme by offering the capability to explore the effect of both electron donor, i.e. Na^+ and K^+ in β-Al_2O_3, and acceptor, i.e. O^{2-} in YSZ, as well as the self-sustained EPOC mentioned in Sect. 9.2.1, to modify the reported low yields for propylene epoxidation.

9.5 Conclusions

The main achievements in the field of electrochemical promotion of catalysis have been thoroughly reviewed from both scientific and technological aspects. However, in view of the potential future commercial application of the EPOC phenomenon, research efforts should concentrate on chemical processes with special industrial interest. In this chapter, we reviewed some of the most promising EPOC applications published to date, with some competitive advantages with respect to conventional thermal-catalysis-based processes, beyond the "in situ" character of the EPOC systems, i.e. providing interesting environmental, health or economic advantages. Recent promising studies highlight that EPOC could contribute in the substitution of platinum group metals by boosting the activity of transition metals.

EPOC is the only technology able to supply oxygen anionic promoters to a catalyst surface in an immediate and controlled manner, which is of particular interest in the case of the ethylene epoxidation reaction (to produce ethylene oxide) and CO_2 hydrogenation reactions. Besides, the supply/removal of alkaline promoters (e.g. Na^+, K^+) by EPOC, alternating negative and positive voltage pulses, can operate the NO_x storage and reduction, under fixed lean conditions, or the H_2 production/storage and release, under mild operation conditions. EPOC can also in situ regenerate a catalyst surface that has been poisoned by coke deposition during catalytic reforming reactions, and, what is most interesting, this phenomenon allows to unprecedentedly in situ promote methane or alcohol transformation catalytic reactions at the cathode of either high-temperature (SOE) or low-temperature (PEM) electrolysers in their current technological development level, thus increasing the hydrogen production in these systems and improving their energy efficiency.

There are other catalytic processes acquiring a growing interest, which should be also focused in depth for a prospective EPOC application. We refer, for instance, to CO_2 hydrogenation into high-value chemicals like olefins, formate, methanol or higher alcohols, to ammonia synthesis and to the propylene epoxidation reaction. Although the application of the EPOC approach is specially challenging in these cases, mainly due to harsh operation conditions and complex reaction mechanisms, there is still a significant know-how that can serve as starting point, obtained from other catalytic reactions, such as reverse water-gas shift, methanation, Fischer-Tropsch (FT) or ethylene epoxidation, as discussed herein. One of the main bottlenecks is the need for high-pressure electrochemical membrane reactors in most of these cases. For example, by operating the reactor at atmospheric pressure, CO_2 hydrogenation (as CO hydrogenation in FT) cannot lead to significant rates of C_2–C_4 hydrocarbons and higher alcohols due to thermodynamic limitations (decrease in reactants' volume). Hence, the development and validation of high-pressure reactors (> 10 bar) is essential for the proposed EPOC catalytic processes on CO_2 valorization. The EPOC reactor design is also crucial for the utilization of dispersed nanoparticles instead of continuous metal electrodes which required the development of new modes of current collection suitable with catalytic applications.

The centralized production of chemicals at large scale must also be considered. The prospective processes involve commodity products that are routinely produced at large quantities (kilo tonnes to million tonnes per year scales) in big centralized units. Unfortunately, the electrochemical ceramic membranes' production manufacturing has not yet demonstrated such production. However, the ceramic and energy industry have made huge steps, particularly with ZrO_2 materials used in solid oxide electrolysers, and therefore, it could compass the direction in case of outstanding outcomes with EPOC. In parallel, the development of more stable and efficient low-temperature O^{2-}-conducting ceramics and H^+/OH^--conducting polymers could be very useful for the upgrade of the EPOC technological development. This latter must be accompanied with the understanding of the reaction and electrochemical promotion mechanisms that will take place. In this sense, operando spectroscopy analysis such as X-ray absorption spectroscopy (XAS) and infrared spectroscopies should be systematically carried out along with the catalytic studies upon polarization**.** Despite recent EPOC studies that investigated catalyst modifications under voltage (e.g. in situ NAP-XPS) for elucidating the ion/metal diffusion processes under cathodic or anodic polarizations, these are still scarce due to the technical complexities on account of introducing electrical connections in the analysis chamber, and thus efforts should focus on this direction in order to elucidate the possible mechanistic pathways.

References

1. Nielsen A (1971) Review of ammonia catalysis. Catal Rev 4:1–26. https://doi.org/10.1080/01614947108075483
2. Jahangiri H, Bennett J, Mahjoubi P, Wilson K, Gu S (2014) A review of advanced catalyst development for Fischer-Tropsch synthesis of hydrocarbons from biomass derived syngas. Catalysis Science and Technology 4:2210–2229. https://doi.org/10.1039/c4cy00327f
3. Xu H, Zhu L, Nan Y, Xie Y, Cheng D (2019) Revisit the role of chlorine in selectivity enhancement of ethylene epoxidation. Ind Eng Chem Res 58:21403–21412. https://doi.org/10.1021/acs.iecr.9b04993
4. Vayenas CG, Bebelis S, Neophytides S (1988) Non-faradaic electrochemical modification of catalytic activity. J Phys Chem 92:5083–5085. https://doi.org/10.1021/j100329a007
5. Vayenas CG (2004) Thermodynamic analysis of the electrochemical promotion of catalysis. Solid State Ionics 168:321–326. https://doi.org/10.1016/j.ssi.2003.04.001
6. Tsiplakides D, Balomenou S, Katsaounis A, Archonta D, Koutsodontis C, Vayenas CG (2005) Electrochemical promotion of catalysis: mechanistic investigations and monolithic electropromoted reactors. Catal Today 100:133–144. https://doi.org/10.1016/J.CATTOD.2004.12.015
7. Lintz H-G, Vayenas CG (1989) Solid ion conductors in heterogeneous catalysis. Angew Chem Int Ed Engl 28:708–715. https://doi.org/10.1002/anie.198907081
8. Vayenas CG (2011) Bridging electrochemistry and heterogeneous catalysis. J Solid State Electrochem 15:1425–1435. https://doi.org/10.1007/s10008-011-1336-5
9. González-Cobos J, de Lucas-Consuegra A (2016) A review of surface analysis techniques for the investigation of the phenomenon of electrochemical promotion of catalysis with alkaline ionic conductors. Catalysts 6:15. https://doi.org/10.3390/catal6010015

10. de Lucas-Consuegra A (2015) New trends of alkali promotion in heterogeneous catalysis: electrochemical promotion with alkaline ionic conductors. Catal Surv Jpn 19:25–37. https://doi.org/10.1007/s10563-014-9179-6
11. Vernoux P (2017) Recent advances in electrochemical promotion of catalysis. In: Catalysis, Volumen 29. The Royal Society of Chemistry, pp. 9-59
12. Vayenas CG (2013) Promotion, electrochemical promotion and metal-support interactions: their common features. Catal Lett 143:1085–1097. https://doi.org/10.1007/s10562-013-1128-x
13. Yentekakis IV, Vernoux P, Goula G, Caravaca A (2019) Electropositive promotion by Alkalis or Alkaline earths of Pt-group metals in emissions control catalysis: a status report. Catalysts 9. https://doi.org/10.3390/catal9020157
14. Vayenas C, Bebeli S, Pliangos C, Brosda S, Tsiplakides D (2001) Electrochemical activation of catalysis: promotion, electrochemical promotion, and metal-support interactions. Springer
15. Vernoux P, Lizarraga L, Tsampas MN, Sapountzi FM, De Lucas-Consuegra A, Valverde J-L, Souentie S, Vayenas CG, Tsiplakides D, Balomenou S, Balomenou S, Baranova EA (2013) Ionically conducting ceramics as active catalyst supports. Chem Rev 113:8192–8260. https://doi.org/10.1021/cr4000336
16. González-Cobos J, Valverde JL, de Lucas-Consuegra A (2017) Electrochemical vs. chemical promotion in the H2 production catalytic reactions. Int J Hydrog Energy 42:13712–13723. https://doi.org/10.1016/j.ijhydene.2017.03.085
17. Anastasijevic NA (2009) NEMCA-from discovery to technology. Catal Today 146:308–311. https://doi.org/10.1016/j.cattod.2009.02.020
18. Tsiplakides D, Balomenou S (2009) Milestones and perspectives in electrochemically promoted catalysis. Catal Today 146:312–318. https://doi.org/10.1016/j.cattod.2009.05.015
19. Tsiplakides D, Balomenou S (2008) Electrochemical promoted catalysis: towards practical utilization. Chem Ind Chem Eng Q 14:97–105. https://doi.org/10.2298/CICEQ0802097T
20. Caravaca A, González-Cobos J, Vernoux P (2020) A discussion on the unique features of electrochemical promotion of catalysis (EPOC): are we in the right path towards commercial implementation? Catalysts 10:1276. https://doi.org/10.3390/catal10111276
21. TechNavio (2016) Global ethylene oxide and ethylene glycol market 2016–2020. TechNavio, London
22. Rebsdat S, Mayer D (2001) Ethylene Oxide. Ullmann's Encyclopedia of Industrial Chemistry
23. Van Santen RA, Kuipers HPCE (1987) The mechanism of ethylene epoxidation. In: Eley DD, Pines H, Weisz PBBT-A in C (eds). Academic Press, pp. 265–321
24. Kenge N, Pitale S, Joshi K (2019) The nature of electrophilic oxygen: insights from periodic density functional theory investigations. Surf Sci 679:188–195. https://doi.org/10.1016/j.susc.2018.09.009
25. Christopher P, Linic S (2008) Engineering selectivity in heterogeneous catalysis: Ag nanowires as selective ethylene epoxidation catalysts. J Am Chem Soc 130:11264–11265. https://doi.org/10.1021/ja803818k
26. Campbell CT, Paffett MT (1984) The role of chlorine promoters in catalytic ethylene epoxidation over the ag(110) surface. Applications of Surface Science 19:28–42. https://doi.org/10.1016/0378-5963(84)90051-5
27. Van Hoof AJF, Filot IAW, Friedrich H, Hensen EJM (2018) Reversible restructuring of silver particles during ethylene epoxidation. ACS Catal 8:11794–11800. https://doi.org/10.1021/acscatal.8b03331
28. Rocha TCR, Hävecker M, Knop-Gericke A, Schlögl R (2014) Promoters in heterogeneous catalysis: the role of Cl on ethylene epoxidation over Ag. J Catal 312:12–16. https://doi.org/10.1016/j.jcat.2014.01.002
29. Özbek MO, van Santen RA (2013) The mechanism of ethylene epoxidation catalysis. Catal Lett 143:131–141. https://doi.org/10.1007/s10562-012-0957-3

30. Stoukides M, Vayenas CG (1981) The effect of electrochemical oxygen pumping on the rate and selectivity of ethylene oxidation on polycrystalline silver. J Catal 70:137–146. https://doi.org/10.1016/0021-9517(81)90323-7
31. Karavasilis C, Bebelis S, Vayenas CG (1995) Selectivity maximization of ethylene epoxidation via NEMCA with zirconia and β″-Al2O3 solid electrolytes. Ionics 1:85–91. https://doi.org/10.1007/BF02426013
32. Karavasilis C, Bebelis S, Vayenas CG (1996) Non-faradaic electrochemical modification of catalytic activity: X. ethylene epoxidation on ag deposited on stabilized ZrO2 in the presence of chlorine moderators. J Catal 160:190–204. https://doi.org/10.1006/jcat.1996.0138
33. Gilbert B, Cavoue T, Aouine M, Burel L, Aires FJCS, Caravaca A, Rieu M, Viricelle JP, Bruyère S, Horwat D, Migot S, Vilasi P, Vernoux P (2021) Ag-based electrocatalysts for ethylene epoxidation. Electrochim Acta 394:139018. https://doi.org/10.1016/j.electacta.2021.139018
34. Nicole J, Tsiplakides D, Pliangos C, Verykios XE, Comninellis C, Vayenas CG (2001) Electrochemical promotion and metal–support interactions. J Catal 204:23–34. https://doi.org/10.1006/jcat.2001.3360
35. Yiokari CG, Pitselis GE, Polydoros DG, Katsaounis AD, Vayenas CG (2000) High-pressure electrochemical promotion of ammonia synthesis over an industrial iron catalyst. Chem A Eur J 104:10600–10602. https://doi.org/10.1021/jp002236v
36. Miyoshi N, Matsumoto S, Katoh K, Tanaka T, Harada J, Takahashi N, Yokota K, Sugiura M, Kasahara K (1995) Development of new concept three-way catalyst for automotive lean-burn engines. SAE Technical Papers. https://doi.org/10.4271/950809
37. Matsumoto S (1996) DeNOx catalyst for automotive lean-burn engine. Catal Today 29:43–45. https://doi.org/10.1016/0920-5861(95)00259-6
38. Takahashi N, Shinjoh H, Iijima T, Suzuki T, Yamazaki K, Yokota K, Suzuki H, Miyoshi N, Matsumoto S, Tanizawa T, Tanaka T, Tateishi S, Kasahara K (1996) The new concept 3-way catalyst for automotive lean-burn engine: NOx storage and reduction catalyst. Catal Today 27:63–69. https://doi.org/10.1016/0920-5861(95)00173-5
39. Epling WS, Campbell LE, Yezerets A, Currier NW, Parks JE II (2004) Overview of the fundamental reactions and degradation mechanisms of NOx storage/reduction catalysts. Catal Rev Sci Eng 46:163–245. https://doi.org/10.1081/CR-200031932
40. Liu G, Gao P-X (2011) A review of NOx storage/reduction catalysts: mechanism, materials and degradation studies. Catalysis Science and Technology 1:552–568. https://doi.org/10.1039/c1cy00007a
41. Kim DH (2014) Sulfation and Desulfation mechanisms on Pt–BaO/Al2O3 NOx storage-reduction (NSR) catalysts. Catal Surv Jpn 18:13–23. https://doi.org/10.1007/s10563-013-9160-9
42. Pancharatnam S (1975) Catalytic decomposition of nitric oxide on zirconia by electrolytic removal of oxygen. J Electrochem Soc 122:869. https://doi.org/10.1149/1.2134364
43. Bredikhin S, Maeda K, Awano M (2001) NO decomposition by an electrochemical cell with mixed oxide working electrode. Solid State Ionics 144:1–9. https://doi.org/10.1016/S0167-2738(01)00862-1
44. Awano M, Bredikhin S, Aronin A, Abrosimova G, Katayama S, Hiramatsu T (2004) NOx decomposition by electrochemical reactor with electrochemically assembled multilayer electrode. Solid State Ionics 175:605–608. https://doi.org/10.1016/J.SSI.2004.01.073
45. Hamamoto K, Fujishiro Y, Awano M (2008) Low-temperature NO[sub x] decomposition using an electrochemical reactor. J Electrochem Soc 155:E109. https://doi.org/10.1149/1.2936400
46. Hadjar A, Hernández WY, Princivalle A, Tardivat C, Guizard C, Vernoux P (2011) Electrochemical activation of Pt-Ba/YSZ NOxTRAP catalyst under lean-burn conditions. Electrochem Commun 13:924–927. https://doi.org/10.1016/j.elecom.2011.05.034

47. Wang X, Westermann A, Shi YX, Cai NS, Rieu M, Viricelle J-P, Vernoux P (2017) Electrochemical removal of NOx on ceria-based catalyst-electrodes. Catalysts 7:61. https://doi.org/10.3390/catal7020061
48. Shao J, Hansen KK (2013) NO_x reduction on Ag electrochemical cells with a K-Pt-Al_2O_3 adsorption layer. J Electrochem Soc 160:H294–H301. https://doi.org/10.1149/2.041306jes
49. de Lucas-Consuegra A, Caravaca Á, Sánchez P, Dorado F, Valverde JL (2008) A new improvement of catalysis by solid-state electrochemistry: An electrochemically assisted NOx storage/reduction catalyst. J Catal 259:54–65. https://doi.org/10.1016/j.jcat.2008.07.008
50. de Lucas-Consuegra A, Caravaca A, Martín de Vidales MJ, Dorado F, Balomenou S, Tsiplakides D, Vernoux P, Valverde JL (2009) An electrochemically assisted NOx storage/reduction catalyst operating under fixed lean burn conditions. Catal Commun 11:247–251. https://doi.org/10.1016/j.catcom.2009.10.004
51. Marwood M, Vayenas CG (1998) Electrochemical promotion of a dispersed platinum catalyst. J Catal 178:429–440. https://doi.org/10.1006/JCAT.1998.2156
52. de Lucas-Consuegra A, Princivalle A, Caravaca A, Dorado F, Marouf A, Guizard C, Valverde JL, Vernoux P (2009) Preparation and characterization of a low particle size Pt/C catalyst electrode for the simultaneous electrochemical promotion of CO and C3H6 oxidation. Appl Catal A Gen 365:274-280. https://doi.org/10.1016/j.apcata.2009.06.026
53. Jiménez V, Jiménez-Borja C, Sánchez P, Romero A, Papaioannou EI, Theleritis D, Souentie S, Brosda S, Valverde JL (2011) Electrochemical promotion of the CO2 hydrogenation reaction on composite Ni or Ru impregnated carbon nanofiber catalyst-electrodes deposited on YSZ. Appl Catal B Environ 107:210–220. https://doi.org/10.1016/j.apcatb.2011.07.016
54. de Lucas-Consuegra A, González-Cobos J, Carcelén V, Magén C, Endrino JL, Valverde JL (2013) Electrochemical promotion of Pt nanoparticles dispersed on a diamond-like carbon matrix: a novel electrocatalytic system for H2 production. J Catal 307:18–26. https://doi.org/10.1016/j.jcat.2013.06.012
55. González-Cobos J, Ruiz-López E, Valverde JL, de Lucas-Consuegra A (2016) Electrochemical promotion of a dispersed Ni catalyst for H2 production via partial oxidation of methanol. Int J Hydrog Energy 41:19418–19429. https://doi.org/10.1016/j.ijhydene.2016.06.027
56. González-Cobos J, Rico VJ, González-Elipe AR, Valverde JL, De Lucas-Consuegra A (2015) Electrochemical activation of an oblique angle deposited Cu catalyst film for H2 production. Catal Sci Technol 5:2203–2214. https://doi.org/10.1039/c4cy01524j
57. González-Cobos J, Rico VJ, González-Elipe AR, Valverde JL, de Lucas-Consuegra A (2016) Electrocatalytic system for the simultaneous hydrogen production and storage from methanol. ACS Catal 6:1942–1951. https://doi.org/10.1021/acscatal.5b02844
58. Christensen H, Dinesen J, Engell HH, Hansen KK (1999) Electrochemical reactor for exhaust gas purification. SAE Technical Papers. https://doi.org/10.4271/1999-01-0472
59. Christensen H, Dinesen J, Engell HH, Larsen LC, Hansen KK, Skou EM (2000) Electrochemical exhaust gas purification. SAE Technical Papers. https://doi.org/10.4271/2000-01-0478
60. Balomenou SP, Tsiplakides D, Vayenas CG, Poulston S, Houel V, Collier P, Konstandopoulos AG, Agrafiotis C (2007) Electrochemical promotion in a monolith electrochemical plate reactor applied to simulated and real automotive pollution control. Top Catal 44:481–486. https://doi.org/10.1007/s11244-006-0140-4
61. Souentie S, Hammad A, Brosda S, Foti G, Vayenas CG (2008) Electrochemical promotion of NO reduction by C2H4 in 10% O2 using a monolithic electropromoted reactor with Rh/YSZ/Pt elements. J Appl Electrochem 38:1159–1170. https://doi.org/10.1007/s10800-008-9548-9
62. Jena P (2011) Materials for hydrogen storage: past, present, and future. J Phys Chem Lett 2:206–211. https://doi.org/10.1021/jz1015372
63. Klingmann J, Andersson M (2020) Hydrogen and hydrogen-rich fuels: production and conversion to electricity BT innovations in sustainable energy and cleaner environment. In: Gupta AK, De A, Aggarwal SK, Kushari A, Runchal A (eds) . Springer, Singapore, pp 219–233

64. Dodds PE, Staffell I, Hawkes AD, Li F, Grünewald P, McDowall W, Ekins P (2015) Hydrogen and fuel cell technologies for heating: a review. Int J Hydrog Energy 40:2065–2083. https://doi.org/10.1016/j.ijhydene.2014.11.059
65. Khotseng L (2019) Fuel cell thermodynamics. Intech Open
66. Apostolou D, Xydis G (2019) A literature review on hydrogen refuelling stations and infrastructure. Current status and future prospects. Renew Sust Energ Rev:113:109292. https://doi.org/10.1016/j.rser.2019.109292
67. Cipriani G, Di Dio V, Genduso F, La Cascia D, Liga R, Miceli R, Ricco Galluzzo G (2014) Perspective on hydrogen energy carrier and its automotive applications. Int J Hydrog Energy 39:8482–8494. https://doi.org/10.1016/j.ijhydene.2014.03.174
68. Sengodan S, Lan R, Humphreys J, Du D, Xu W, Wang H, Tao S (2018) Advances in reforming and partial oxidation of hydrocarbons for hydrogen production and fuel cell applications. Renew Sust Energ Rev 82:761–780. https://doi.org/10.1016/j.rser.2017.09.071
69. Busca G, Costantino U, Montanari T, Ramis G, Resini C, Sisani M (2010) Nickel versus cobalt catalysts for hydrogen production by ethanol steam reforming: Ni-Co-Zn-Al catalysts from hydrotalcite-like precursors. Int J Hydrog Energy 35:5356–5366. https://doi.org/10.1016/j.ijhydene.2010.02.124
70. Megía PJ, Calles JA, Carrero A, Vizcaíno AJ (2020) Effect of the incorporation of reducibility promoters (Cu, Ce, Ag) in Co/CaSBA-15 catalysts for acetic acid steam reforming. Int J Energy Res 1:1–18. https://doi.org/10.1002/er.5832
71. Chen S, Zaffran J, Yang B (2020) Dry reforming of methane over the cobalt catalyst: theoretical insights into the reaction kinetics and mechanism for catalyst deactivation. Appl Catal B Environ 270:118859–118868. https://doi.org/10.1016/j.apcatb.2020.118859
72. Budiman AW, Song S-H, Chang T-S, Shin C-H, Choi M-J (2012) Dry reforming of methane over cobalt catalysts: a literature review of catalyst development. Catal Surv Jpn 16:183–197. https://doi.org/10.1007/s10563-012-9143-2
73. Osman AI (2020) Catalytic hydrogen production from methane partial oxidation: mechanism and kinetic study. Chem Eng Technol 43:641–648. https://doi.org/10.1002/ceat.201900339
74. Hossain MZ, Charpentier PA (2015) Hydrogen production by gasification of biomass and opportunity fuels. In: Subramani V, Basile A, Veziroglu TN (eds) Compendium of hydrogen energy. Woodhead Publishing, pp 137–175
75. Summa P, Samojeden B, Motak M (2019) Dry and steam reforming of methane. Comparison and analysis of recently investigated catalytic materials. A short review. Pol J Chem Technol 21:31–37. https://doi.org/10.2478/pjct-2019-0017
76. de Souza VP, Costa D, dos Santos D, Sato AG, Bueno JMC (2012) Pt-promoted α-Al2O3-supported Ni catalysts: effect of preparation conditions on oxi-reduction and catalytic properties for hydrogen production by steam reforming of methane. Int J Hydrog Energy 37:9985–9993. https://doi.org/10.1016/J.IJHYDENE.2012.03.141
77. Borowiecki T, Denis A, Rawski M, Gołębiowski A, Stołecki K, Dmytrzyk J, Kotarba A (2014) Studies of potassium-promoted nickel catalysts for methane steam reforming: effect of surface potassium location. Appl Surf Sci 300:191–200. https://doi.org/10.1016/j.apsusc.2014.02.053
78. Borowiecki T, Gołębiowski A, Ryczkowski J, Stasmska B (1998) The influence of promoters on the coking rate of nickel catalysts in the steam reforming of hydrocarbons. Stud Surf Sci Catal 119:711–716. https://doi.org/10.1016/S0167-2991(98)80515-6
79. Alstrup I, Clausen BS, Olsen C, Smits RHH, Rostrup-Nielsen JR (1998) Promotion of steam reforming catalysts. Stud Surf Sci Catal 119:5–14. https://doi.org/10.1016/S0167-2991(98)80402-3
80. de Lucas-Consuegra A, Caravaca A, Martínez PJ, Endrino JL, Dorado F, Valverde JL (2010) Development of a new electrochemical catalyst with an electrochemically assisted regeneration ability for H2 production at low temperatures. J Catal 274:251–258. https://doi.org/10.1016/J.JCAT.2010.07.007

81. Nurunnabi M, Mukainakano Y, Kado S, Miyazawa T, Okumura K, Miyao T, Naito S, Suzuki K, Fujimoto K-I, Kunimori K, Tomishige K (2006) Oxidative steam reforming of methane under atmospheric and pressurized conditions over Pd/NiO–MgO solid solution catalysts. Appl Catal A Gen 308:1–12. https://doi.org/10.1016/J.APCATA.2006.03.054
82. Yentekakis IV, Jiang Y, Neophytides S, Bebelis S, Vayenas CG (1995) Catalysis, electrocatalysis and electrochemical promotion of the steam reforming of methane over Ni film and Ni-YSZ cermet anodes. Ionics 1:91-498. https://doi.org/10.1007/BF02375296
83. González-Cobos J, López-Pedrajas D, Ruiz-López E, Valverde JL, de Lucas-Consuegra A (2015) Applications of the electrochemical promotion of catalysis in methanol conversion processes. Top Catal 58:1290–1302. https://doi.org/10.1007/s11244-015-0493-7
84. Deng W-Q, Xu X, Goddard WA (2004) New alkali doped pillared carbon materials designed to achieve practical reversible hydrogen storage for transportation. Phys Rev Lett 92:166103. https://doi.org/10.1103/PhysRevLett.92.166103
85. Espinós JP, Rico VJ, González-Cobos J, Sánchez-Valencia JR, Pérez-Dieste V, Escudero C, de Lucas-Consuegra A, González-Elipe AR (2018) In situ monitoring of the phenomenon of electrochemical promotion of catalysis. J Catal 358:27–34. https://doi.org/10.1016/j.jcat.2017.11.027
86. Espinós JP, Rico VJ, González-Cobos J, Sánchez-Valencia JR, Pérez-Dieste V, Escudero C, De Lucas-Consuegra A, González-Elipe AR (2019) Graphene formation mechanism by the electrochemical promotion of a Ni catalyst. ACS Catal 11447–11454. https://doi.org/10.1021/acscatal.9b03820
87. Van Den Berg AWC, Areán CO (2008) Materials for hydrogen storage: current research trends and perspectives. Chem Commun:668–681. https://doi.org/10.1039/B712576N
88. Dalebrook AF, Gan W, Grasemann M, Moret S, Laurenczy G (2013) Hydrogen storage: beyond conventional methods. Chem Commun 49:8735–8751. https://doi.org/10.1039/b000000x
89. Sapountzi FM, Gracia JM, Weststrate CJK-J, Fredriksson HOA, Niemantsverdriet JWH (2017) Electrocatalysts for the generation of hydrogen, oxygen and synthesis gas. Prog Energy Combust Sci 58:1–35. https://doi.org/10.1016/j.pecs.2016.09.001
90. Shiva Kumar S, Himabindu V (2019) Hydrogen production by PEM water electrolysis – a review. Mater Sci Energy Technol 2:442–454. https://doi.org/10.1016/j.mset.2019.03.002
91. Ni M, Leung MKH, Leung DYC (2008) Technological development of hydrogen production by solid oxide electrolyzer cell (SOEC). Int J Hydrog Energy 33:2337–2354. https://doi.org/10.1016/j.ijhydene.2008.02.048
92. Lei L, Zhang J, Yuan Z, Liu J, Ni M, Chen F (2019) Progress report on proton conducting solid oxide electrolysis cells. Adv Funct Mater. https://doi.org/10.1002/adfm.201903805
93. Sasikumar G, Muthumeenal A, Pethaiah SS, Nachiappan N, Balaji R (2008) Aqueous methanol electrolysis using proton conducting membrane for hydrogen production. Int J Hydrog Energy 33:5905–5910. https://doi.org/10.1016/j.ijhydene.2008.07.013
94. Caravaca A, Sapountzi FM, De Lucas-Consuegra A, Molina-Mora C, Dorado F, Valverde JL (2012) Electrochemical reforming of ethanol-water solutions for pure H2 production in a PEM electrolysis cell. Int J Hydrog Energy 37:9504–9513. https://doi.org/10.1016/j.ijhydene.2012.03.062
95. Caravaca A, De Lucas-Consuegra A, Calcerrada AB, Lobato J, Valverde JL, Dorado F (2013) From biomass to pure hydrogen: electrochemical reforming of bio-ethanol in a PEM electrolyser. Appl Catal B Environ 134–135:302–309. https://doi.org/10.1016/j.apcatb.2013.01.033
96. Calcerrada AB, de la Osa AR, Llanos J, Dorado F, de Lucas-Consuegra A (2018) Hydrogen from electrochemical reforming of ethanol assisted by sulfuric acid addition. Appl Catal B Environ 231:310–316. https://doi.org/10.1016/j.apcatb.2018.03.028
97. Calcerrada AB, de la Osa AR, Lopez-Fernandez E, Dorado F, de Lucas-Consuegra A (2019) Influence of the carbon support on the Pt–Sn anodic catalyst for the electrochemical reforming

of ethanol. Int J Hydrog Energy 44:10616–10626. https://doi.org/10.1016/j.ijhydene.2019.03.011
98. Calcerrada AB, de la Osa AR, Dole HAE, Dorado F, Baranova EA, de Lucas-Consuegra A (2018) Stability testing of PtxSn1 − x/C anodic catalyst for renewable hydrogen production via electrochemical reforming of ethanol. Electrocatalysis 9:293–301. https://doi.org/10.1007/s12678-017-0428-0
99. Gutiérrez-Guerra N, Jiménez-Vázquez M, Serrano-Ruiz JC, Valverde JL, de Lucas-Consuegra A (2015) Electrochemical reforming vs. catalytic reforming of ethanol: a process energy analysis for hydrogen production. Chem Eng Process Process Intensif 95:9–16. https://doi.org/10.1016/j.cep.2015.05.008
100. Ruiz-López E, Amores E, Raquel de la Osa A, Dorado F, de Lucas-Consuegra A (2020) Electrochemical reforming of ethanol in a membrane-less reactor configuration. Chem Eng J. 379:122289. https://doi.org/10.1016/j.cej.2019.122289
101. De Lucas-Consuegra A, De La Osa AR, Calcerrada AB, Linares JJ, Horwat D (2016) A novel sputtered Pd mesh architecture as an advanced electrocatalyst for highly efficient hydrogen production. J Power Sources 321:248–256. https://doi.org/10.1016/j.jpowsour.2016.05.004
102. Simões M, Baranton S, Coutanceau C (2012) Electrochemical valorisation of glycerol. ChemSusChem 5:2106–2124. https://doi.org/10.1002/cssc.201200335
103. Coutanceau C, Baranton S, Kouamé RSB (2019) Selective electrooxidation of glycerol into value-added chemicals: a short overview. Front Chem 7:100. https://doi.org/10.3389/fchem.2019.00100
104. Haisch T, Kubannek F, Baranton S, Coutanceau C, Krewer U (2019) The influence of adsorbed substances on alkaline methanol electro-oxidation. Electrochim Acta 295:278–285. https://doi.org/10.1016/j.electacta.2018.10.073
105. Coutanceau C, Baranton S (2016) Electrochemical conversion of alcohols for hydrogen production: a short overview. Wiley Interdisciplinary Reviews: Energy and Environment 5:388–400. https://doi.org/10.1002/wene.193
106. Ebbesen SD, Jensen SH, Hauch A, Mogensen MB (2014) High temperature electrolysis in alkaline cells, solid proton conducting cells, and solid oxide cells. Chem Rev 114:10697–10734. https://doi.org/10.1021/cr5000865
107. Caravaca A, De Lucas-Consuegra A, Molina-Mora C, Valverde JL, Dorado F (2011) Enhanced H2 formation by electrochemical promotion in a single chamber steam electrolysis cell. Appl Catal B Environ 106:54–62. https://doi.org/10.1016/j.apcatb.2011.05.004
108. Ruiz-López E, Caravaca A, Vernoux P, Dorado F, de Lucas-Consuegra A (2020) Over-faradaic hydrogen production in methanol electrolysis cells. Chem Eng J 396:125217. https://doi.org/10.1016/J.CEJ.2020.125217
109. Garcia-Garcia FJ, Yubero F, Espinós JP, González-Elipe AR, Lambert RM (2016) Synthesis, characterization and performance of robust poison-resistant ultrathin film yttria stabilized zirconia – nickel anodes for application in solid electrolyte fuel cells. J Power Sources 324:679–686. https://doi.org/10.1016/j.jpowsour.2016.05.124
110. Garcia-Garcia FJ, Beltrán AM, Yubero F, González-Elipe AR, Lambert RM (2017) High performance novel gadolinium doped ceria/yttria stabilized zirconia/nickel layered and hybrid thin film anodes for application in solid oxide fuel cells. J Power Sources 363:251–259. https://doi.org/10.1016/j.jpowsour.2017.07.085
111. Garcia-Garcia FJ, Yubero F, González-Elipe AR, Balomenou SP, Tsiplakides D, Petrakopoulou I, Lambert RM (2015) Porous, robust highly conducting Ni-YSZ thin film anodes prepared by magnetron sputtering at oblique angles for application as anodes and buffer layers in solid oxide fuel cells. Int J Hydrog Energy 40:7382–7387. https://doi.org/10.1016/j.ijhydene.2015.04.001
112. Ye R-P, Ding J, Gong W, Argyle MD, Zhong Q, Wang Y, Russell CK, Xu Z, Russell AG, Li Q, Fan M, Yao Y-G (2019) CO2 hydrogenation to high-value products via heterogeneous catalysis. Nat Commun 10:5698. https://doi.org/10.1038/s41467-019-13638-9

113. Jiang X, Nie X, Guo X, Song C, Chen JG (2020) Recent advances in carbon dioxide hydrogenation to methanol via heterogeneous catalysis. Chem Rev 120:7984–8034. https://doi.org/10.1021/acs.chemrev.9b00723
114. Xu D, Wang Y, Ding M, Hong X, Liu G, Tsang SCE (2021) Advances in higher alcohol synthesis from CO2 hydrogenation. Chem 7:849–881. https://doi.org/10.1016/j.chempr.2020.10.019
115. Ojelade OA, Zaman SF (2021) A review on CO2 hydrogenation to lower olefins: understanding the structure-property relationships in heterogeneous catalytic systems. Journal of CO2 Utilization 47(101506). https://doi.org/10.1016/j.jcou.2021.101506
116. Vernoux P, Lizarraga L, Tsampas MN, Sapountzi FM, De Lucas-Consuegra A, Valverde JL, Souentie S, Vayenas CG, Tsiplakides D, Balomenou S, Baranova EA (2013) Ionically conducting ceramics as active catalyst supports. Chem Rev 113:8192–8260. https://doi.org/10.1021/cr4000336
117. Zagoraios D, Panaritis C, Krassakopoulou A, Baranova EA, Katsaounis A, Vayenas CG (2020) Electrochemical promotion of Ru nanoparticles deposited on a proton conductor electrolyte during CO2 hydrogenation. Appl Catal B Environ 276:119148. https://doi.org/10.1016/j.apcatb.2020.119148
118. Zagoraios D, Tsatsos S, Kennou S, Vayenas CG, Kyriakou G, Katsaounis A (2020) Tuning the RWGS reaction via EPOC and in situ electro-oxidation of cobalt nanoparticles. ACS Catal 10:14916–14927. https://doi.org/10.1021/acscatal.0c04133
119. Chatzilias C, Martino E, Katsaounis A, Vayenas CG (2021) Electrochemical promotion of CO2 hydrogenation in a monolithic electrochemically promoted reactor (MEPR). Appl Catal B Environ 284:119695. https://doi.org/10.1016/j.apcatb.2020.119695
120. Williams FJ, Lambert RM (2000) A study of sodium promotion in Fischer-Tropsch synthesis: electrochemical control of a ruthenium model catalyst. Catal Lett 70:9–14. https://doi.org/10.1023/a:1019023418300
121. Urquhart AJ, Keel JM, Williams FJ, Lambert RM (2003) Electrochemical promotion by potassium of rhodium-catalyzed Fischer-Tropsch synthesis: XP spectroscopy and reaction studies. J Phys Chem B 107:10591–10597. https://doi.org/10.1021/jp035436q
122. Urquhart AJ, Williams FJ, Lambert RM (2005) Electrochemical promotion by potassium of Rh-catalysed Fischer-Tropsch synthesis at high pressure. Catal Lett 103:137–141. https://doi.org/10.1007/s10562-005-6519-1
123. Kotsiras A, Kalaitzidou I, Grigoriou D, Symillidis A, Makri M, Katsaounis A, Vayenas CG (2018) Electrochemical promotion of nanodispersed Ru-Co catalysts for the hydrogenation of CO2. Appl Catal B Environ 232:60–68. https://doi.org/10.1016/j.apcatb.2018.03.031
124. Kalaitzidou I, Makri M, Theleritis D, Katsaounis A, Vayenas CG (2016) Comparative study of the electrochemical promotion of CO2 hydrogenation on Ru using Na+, K+, H+ and O2− conducting solid electrolytes. Surf Sci 646:194–203. https://doi.org/10.1016/j.susc.2015.09.011
125. Jiang X, Nie X, Guo X, Song C, Chen JG (2020) Recent advances in carbon dioxide hydrogenation to methanol via heterogeneous catalysis. Chem Rev 120:7984. https://doi.org/10.1021/acs.chemrev.9b00723
126. Guil-López R, Mota N, Llorente J, Millán E, Pawelec B, Fierro JLG, Navarro RM (2019) Methanol synthesis from CO2: a review of the latest developments in heterogeneous catalysis. Materials 12:3902. https://doi.org/10.3390/ma12233902
127. Valera-Medina A, Xiao H, Owen-Jones M, David WIF, Bowen PJ (2018) Ammonia for power. Prog Energy Combust Sci 69:63–102. https://doi.org/10.1016/j.pecs.2018.07.001
128. Porosoff MD, Yan B, Chen JG (2016) Catalytic reduction of CO2 by H2 for synthesis of CO, methanol and hydrocarbons: challenges and opportunities. Energy Environ Sci 9:62–73. https://doi.org/10.1039/C5EE02657A
129. Saeidi S, Najari S, Hessel V, Wilson K, Keil FJ, Concepción P, Suib SL, Rodrigues AE (2021) Recent advances in CO2 hydrogenation to value-added products – Current challenges and

future directions. Prog Energy Combust Sci 85:100905. https://doi.org/10.1016/j.pecs.2021.100905
130. Niu J, Liu H, Jin Y, Fan B, Qi W, Ran J (2022) Comprehensive review of Cu-based CO2 hydrogenation to CH3OH: insights from experimental work and theoretical analysis. Int J Hydrog Energy 47:9183–9200. https://doi.org/10.1016/j.ijhydene.2022.01.021
131. Bansode A, Tidona B, von Rohr PR, Urakawa A (2013) Impact of K and Ba promoters on CO 2 hydrogenation over Cu/Al 2 O 3 catalysts at high pressure. Cat Sci Technol 3:767–778. https://doi.org/10.1039/C2CY20604H
132. Díez-Ramírez J, Sánchez P, Valverde JL, Dorado F (2016) Electrochemical promotion and characterization of PdZn alloy catalysts with K and Na ionic conductors for pure gaseous CO2 hydrogenation. Journal of CO2 Utilization 16:375–383. https://doi.org/10.1016/j.jcou.2016.09.007
133. Ruiz E, Cillero D, Martínez PJ, Morales Á, Vicente GS, de Diego G, Sánchez JM (2014) Electrochemical synthesis of fuels by CO2 hydrogenation on Cu in a potassium ion conducting membrane reactor at bench scale. Catal Today 236:108–120. https://doi.org/10.1016/j.cattod.2014.01.016
134. Ruiz E, Martínez PJ, Morales Á, San Vicente G, de Diego G, Sánchez JM (2016) Electrochemically assisted synthesis of fuels by CO2 hydrogenation over Fe in a bench scale solid electrolyte membrane reactor. Catal Today 268:46–59. https://doi.org/10.1016/j.cattod.2016.02.025
135. Ruiz E, Cillero D, Martínez PJ, Morales Á, Vicente GS, de Diego G, Sánchez JM (2014) Bench-scale study of electrochemically assisted catalytic CO2 hydrogenation to hydrocarbon fuels on Pt, Ni and Pd films deposited on YSZ. Journal of CO2 Utilization 8:1–20. https://doi.org/10.1016/j.jcou.2014.09.001
136. Do TN, Kim J (2020) Green C2-C4 hydrocarbon production through direct CO2 hydrogenation with renewable hydrogen: process development and techno-economic analysis. Energy Convers Manag 214:112866. https://doi.org/10.1016/j.enconman.2020.112866
137. Li W, Wang H, Jiang X, Zhu J, Liu Z, Guo X, Song C (2018) A short review of recent advances in CO2 hydrogenation to hydrocarbons over heterogeneous catalysts. RSC Adv 8:7651–7669. https://doi.org/10.1039/C7RA13546G
138. Gholami Z, Gholami F, Tišler Z, Hubáček J, Tomas M, Bačiak M, Vakili M (2022) Production of light olefins via Fischer-Tropsch process using iron-based catalysts: a review. Catalysts 12:174. https://doi.org/10.3390/catal12020174
139. Visconti CG, Martinelli M, Falbo L, Infantes-Molina A, Lietti L, Forzatti P, Iaquaniello G, Palo E, Picutti B, Brignoli F (2017) CO2 hydrogenation to lower olefins on a high surface area K-promoted bulk Fe-catalyst. Appl Catal B Environ 200:530–542. https://doi.org/10.1016/j.apcatb.2016.07.047
140. Meiri N, Dinburg Y, Amoyal M, Koukouliev V, Nehemya RV, Landau MV, Herskowitz M (2015) Novel process and catalytic materials for converting CO 2 and H 2 containing mixtures to liquid fuels and chemicals. Faraday Discuss 183:197–215. https://doi.org/10.1039/C5FD00039D
141. Ramirez A, Gevers L, Bavykina A, Ould-Chikh S, Gascon J (2018) Metal organic framework-derived iron catalysts for the direct hydrogenation of CO 2 to short chain olefins. ACS Catal 8:9174–9182. https://doi.org/10.1021/acscatal.8b02892
142. Martinelli M, Visconti CG, Lietti L, Forzatti P, Bassano C, Deiana P (2014) CO2 reactivity on Fe–Zn–Cu–K Fischer–Tropsch synthesis catalysts with different K-loadings. Catal Today 228:77–88. doi: https://doi.org/10.1016/j.cattod.2013.11.018
143. Tsiakaras P, Vayenas CG (1993) Oxidative coupling of CH4 on Ag catalyst-electrodes deposited on ZrO2 (8 mol% Y2O3). J Catal 144:333–347. https://doi.org/10.1006/jcat.1993.1334
144. Otsuka K, Yokoyama S, Morikawa A (1985) Catalytic activity- and selectivity-control for oxidative coupling of methane by oxygen-pumping through yttria-stabilized zirconia. Chem Lett 14:319–322. https://doi.org/10.1246/cl.1985.319

145. Caravaca A, de Lucas-Consuegra A, González-Cobos J, Valverde JL, Dorado F (2012) Simultaneous production of H2 and C2 hydrocarbons by gas phase electrocatalysis. Appl Catal B Environ 113–114:192–200. https://doi.org/10.1016/j.apcatb.2011.11.037
146. Caravaca A, de Lucas-Consuegra A, Ferreira VJ, Figueiredo JL, Faria JL, Valverde JL, Dorado F (2013) Coupling catalysis and gas phase electrocatalysis for the simultaneous production and separation of pure H2 and C2 hydrocarbons from methane and natural gas. Appl Catal B Environ 142–143:298–306. https://doi.org/10.1016/j.apcatb.2013.05.014
147. Khechfe AA, Sullivan MM, Zagoraios D, Katsaounis A, Vayenas CG, Román-Leshkov Y (2022) Non-faradaic electrochemical promotion of Brønsted acid-catalyzed dehydration reactions over molybdenum oxide. ACS Catal 12:906–912. https://doi.org/10.1021/acscatal.1c04885
148. Xi X, Zeng F, Zhang H, Wu X, Ren J, Bisswanger T, Stampfer C, Hofmann JP, Palkovits R, Heeres HJ (2021) CO2 hydrogenation to higher alcohols over K-promoted bimetallic Fe–In catalysts on a Ce–ZrO2 support. ACS Sustainable Chem. Eng. 9:6235–6249. https://doi.org/10.1021/acssuschemeng.0c08760
149. Aresta M, Dibenedetto A, Angelini A (2014) Catalysis for the valorization of exhaust carbon: from CO 2 to chemicals, materials, and fuels. Technological use of CO 2. Chem Rev 114:1709–1742. https://doi.org/10.1021/cr4002758
150. Luk HT, Mondelli C, Ferré DC, Stewart JA, Pérez-Ramírez J (2017) Status and prospects in higher alcohols synthesis from syngas. Chem Soc Rev 46:1358–1426. https://doi.org/10.1039/C6CS00324A
151. Wang L, Wang L, Zhang J, Liu X, Wang H, Zhang W, Yang Q, Ma J, Dong X, Yoo SJ, Kim J, Meng X, Xiao F (2018) Selective hydrogenation of CO 2 to ethanol over cobalt catalysts. Angew Chem Int Ed 57:6104–6108. https://doi.org/10.1002/anie.201800729
152. Gupta M, Smith ML, Spivey JJ (2011) Heterogeneous catalytic conversion of dry syngas to ethanol and higher alcohols on Cu-based catalysts. ACS Catal 1:641–656. https://doi.org/10.1021/cs2001048
153. Li S, Guo H, Luo C, Zhang H, Xiong L, Chen X, Ma L (2013) Effect of iron promoter on structure and performance of K/Cu–Zn catalyst for higher alcohols synthesis from CO2 hydrogenation. Catal Lett 143:345–355. https://doi.org/10.1007/s10562-013-0977-7
154. Guo H, Li S, Peng F, Zhang H, Xiong L, Huang C, Wang C, Chen X (2015) Roles investigation of promoters in K/Cu–Zn catalyst and higher alcohols synthesis from CO2 hydrogenation over a novel two-stage bed catalyst combination system. Catal Lett 145:620–630. https://doi.org/10.1007/s10562-014-1446-7
155. Mardini N, Bicer Y (2021) Direct synthesis of formic acid as hydrogen carrier from CO2 for cleaner power generation through direct formic acid fuel cell. Int J Hydrog Energy 46:13050–13060. https://doi.org/10.1016/j.ijhydene.2021.01.124
156. Eppinger J, Huang K-W (2017) Formic acid as a hydrogen energy carrier. ACS Energy Lett 2:188–195. https://doi.org/10.1021/acsenergylett.6b00574
157. Schaub T (2018) CO2-based hydrogen storage: CO2 hydrogenation to formic acid, formaldehyde and methanol. Physical Sciences Reviews 3:20170015. https://doi.org/10.1515/psr-2017-0015
158. An L, Chen R (2016) Direct formate fuel cells: a review. J Power Sources 320:127–139. https://doi.org/10.1016/j.jpowsour.2016.04.082
159. Ma Z, Legrand U, Pahija E, Tavares JR, Boffito DC (2021) From CO2 to formic acid fuel cells. Ind Eng Chem Res 60:803–815. https://doi.org/10.1021/acs.iecr.0c04711
160. Sun R, Liao Y, Bai S-T, Zheng M, Zhou C, Zhang T, Sels BF (2021) Heterogeneous catalysts for CO2 hydrogenation to formic acid/formate: from nanoscale to single atom. Energy Environ Sci 14:1247–1285. https://doi.org/10.1039/D0EE03575K
161. Pan H, Heagy MD (2020) Photons to formate: a review on photocatalytic reduction of CO2 to formic acid. Nano 10:2422. https://doi.org/10.3390/nano10122422

162. Cai F, Gao D, Zhou H, Wang G, He T, Gong H, Miao S, Yang F, Wang J, Bao X (2017) Electrochemical promotion of catalysis over Pd nanoparticles for CO2 reduction. Chem Sci 8: 2569–2573. https://doi.org/10.1039/C6SC04966D
163. Ryu J, Surendranath Y (2020) Polarization-induced local pH swing promotes Pd-catalyzed CO2 hydrogenation. J Am Chem Soc 142:13384–13390. https://doi.org/10.1021/jacs.0c01123
164. Neophytides SG, Tsiplakides D, Stonehart P, Jaksic MM, Vayenas CG (1994) Electrochemical enhancement of a catalytic reaction in aqueous solution. Nature 370:45–47. https://doi.org/10.1038/370045a0
165. Neophytides SG, Tsiplakides D, Stonehart P, Jaksic M, Vayenas CG (1996) Non-faradaic electrochemical modification of the catalytic activity of Pt for H2 oxidation in aqueous alkaline media. J Phys Chem 100:14803–14814. https://doi.org/10.1021/jp960971u
166. Ploense L, Salazar M, Gurau B, Smotkin ES (1997) Proton spillover promoted isomerization of n-butylenes on Pd-black cathodes/nafion 117. J Am Chem Soc 119:11550–11551. https://doi.org/10.1021/ja9728841
167. Sanabria-Chinchilla J, Asazawa K, Sakamoto T, Yamada K, Tanaka H, Strasser P (2011) Noble metal-free hydrazine fuel cell catalysts: EPOC effect in competing chemical and electrochemical reaction pathways. J Am Chem Soc 133:5425–5431. https://doi.org/10.1021/ja111160r
168. Gorin CF, Beh ES, Kanan MW (2012) An electric field–induced change in the selectivity of a metal oxide–catalyzed epoxide rearrangement. J Am Chem Soc 134:186–189. https://doi.org/10.1021/ja210365j
169. Sienel G, Rieth R, Rowbottom KT (2000) Epoxides. In: Ullmann's encyclopedia of industrial chemistry. Wiley-VCH Verlag GmbH & Co. KGaA, Weinheim
170. Khatib SJ, Oyama ST (2015) Direct oxidation of propylene to propylene oxide with molecular oxygen: a review. Catal Rev 57:306–344. https://doi.org/10.1080/01614940.2015.1041849
171. Teržan J, Huš M, Likozar B, Djinović P (2020) Propylene epoxidation using molecular oxygen over copper- and silver-based catalysts: a review. ACS Catal 10:13415–13436. https://doi.org/10.1021/acscatal.0c03340
172. Blanckenberg A, Malgas-Enus R (2019) Olefin epoxidation with metal-based nanocatalysts. Catal Rev 61:27–83. https://doi.org/10.1080/01614940.2018.1492503
173. Kalyoncu S, Düzenli D, Onal I, Seubsai A, Noon D, Senkan S, Say Z, Vovk EI, Ozensoy E (2015) NaCl-Promoted CuO–RuO2/SiO2 catalysts for propylene epoxidation with O2 at atmospheric pressures: a combinatorial micro-reactor study. Catal Lett 145:596–605. https://doi.org/10.1007/s10562-014-1454-7
174. Ren Y, Sun X, Huang J, Zhang L, Zhang B, Haruta M, Lu A-H (2020) Dual-component sodium and Cesium promoters for Au/TS-1: enhancement of propene epoxidation with hydrogen and oxygen. Ind Eng Chem Res 59:8155–8163. https://doi.org/10.1021/acs.iecr.9b07011
175. Lee EJ, Lee J, Seo Y-J, Lee JW, Ro Y, Yi J, Song IK (2017) Direct epoxidation of propylene to propylene oxide with molecular oxygen over Ag–Mo–W/ZrO2 catalysts. Catal Commun 89: 156–160. https://doi.org/10.1016/j.catcom.2016.11.001
176. Wang Y, Chu H, Zhu W, Zhang Q (2008) Copper-based efficient catalysts for propylene epoxidation by molecular oxygen. Catal Today 131:496–504. https://doi.org/10.1016/j.cattod.2007.10.022
177. Wang Q, Zhan C, Zhou L, Fu G, Xie Z (2020) Effects of Cl− on Cu2O nanocubes for direct epoxidation of propylene by molecular oxygen. Catal Commun 135:105897. https://doi.org/10.1016/j.catcom.2019.105897
178. Bere KE, Wakui Y, Niwa S, Shoji H, Sato K, Hamakawa S, Hanaoka T, Suzuki TM, Mizukami F (2007) Direct O 2 epoxidation of propylene by the membrane reactor loaded with Ag–Sr catalyst. Chem Lett 36:1170–1171. https://doi.org/10.1246/cl.2007.1170
179. Kaloyannis AC, Pliangos CA, Yentekakis IV, Vayenas CG (1995) In situ controlled promotion of catalyst surfaces via solid electrolytes: ethylene oxidation on Rh and propylene oxidation on Pt. Ionics 1:159–164. https://doi.org/10.1007/BF02388675

180. Kaloyannis A, Vayenas CG (1999) Non-faradaic electrochemical modification of catalytic activity: 12. Propylene oxidation on Pt. J Catal 182:37–47. https://doi.org/10.1006/jcat.1998.2311
181. Fóti G, Bolzonella I, Bachelin D, Comninellis CH (2004) Relation between potential and catalytic activity of rhodium in propylene combustion. J Appl Electrochem 34:9–17. https://doi.org/10.1023/B:JACH.0000005575.92134.60
182. Gaillard F, Li X, Uray M, Vernoux P (2004) Electrochemical promotion of propene combustion in air excess on perovskite catalyst. Catal Lett 96:177–183. https://doi.org/10.1023/B:CATL.0000030117.00142.3d
183. Vernoux P, Gaillard F, Lopez C, Siebert E (2004) In-situ electrochemical control of the catalytic activity of platinum for the propene oxidation. Solid State Ionics 175:609–613. https://doi.org/10.1016/j.ssi.2004.01.075
184. de Lucas-Consuegra A, Dorado F, Valverde JL, Karoum R, Vernoux P (2007) Low-temperature propene combustion over Pt/K-βAl2O3 electrochemical catalyst: characterization, catalytic activity measurements, and investigation of the NEMCA effect. J Catal 251:474–484. https://doi.org/10.1016/j.jcat.2007.06.031
185. Karoum R, Roche V, Pirovano C, Vannier R-N, Billard A, Vernoux P (2010) CGO-based electrochemical catalysts for low temperature combustion of propene. J Appl Electrochem 40:1867–1873. https://doi.org/10.1007/s10800-010-0156-0
186. Ippolito D, Andersen KB, Hansen KK (2012) Electrochemical oxidation of propene by use of LSM15/CGO10 electrochemical reactor. J Electrochem Soc 159:P57. https://doi.org/10.1149/2.084206jes
187. Fóti G, Lavanchy O, Comninellis C (2000) Electrochemical promotion of Rh catalyst in gas-phase reduction of NO by propylene. J Appl Electrochem 30:1223–1228. https://doi.org/10.1023/A:1026505829359
188. Raptis C, Badas T, Tsiplakides D, Pliangos C, Vayenas CG (2000) Electrochemical promotion of NO reduction by C3H6 on Rh/YSZ catalyst—electrodes and investigation of the origin of the promoting action using TPD and WF measurements. In: Corma A, Melo FV, Mendioroz S, Fierro JLG (eds) Studies in surface science and catalysis. Elsevier, pp 1283–1288
189. Williams FJ, Tikhov MS, Palermo A, Macleod N, Lambert RM (2001) Electrochemical promotion of rhodium-catalyzed NO reduction by CO and by propene in the presence of oxygen. J Phys Chem B 105:2800–2808. https://doi.org/10.1021/jp004131y
190. Vernoux P, Gaillard F, Karoum R, Billard A (2007) Reduction of nitrogen oxides over Ir/YSZ electrochemical catalysts. Appl Catal B Environ 73:73–83. https://doi.org/10.1016/j.apcatb.2006.06.009
191. Dorado F, de Lucas-Consuegra A, Vernoux P, Valverde JL (2007) Electrochemical promotion of platinum impregnated catalyst for the selective catalytic reduction of NO by propene in presence of oxygen. Appl Catal B Environ 73:42–50. https://doi.org/10.1016/j.apcatb.2006.12.001
192. Lintanf A, Djurado E, Vernoux P (2008) Pt/YSZ electrochemical catalysts prepared by electrostatic spray deposition for selective catalytic reduction of NO by C3H6. Solid State Ionics 178:1998–2008. https://doi.org/10.1016/j.ssi.2008.01.008
193. Stoukides M, Vayenas CG (1984) Electrocatalytic rate enhancement of propylene epoxidation on porous silver electrodes using a zirconia oxygen pump. J Electrochem Soc 131:839. https://doi.org/10.1149/1.2115710
194. Bebelis S, Vayenas C (1992) Non-faradaic electrochemical modification of catalytic activity 6. Ethylene epoxidation on Ag deposited on stabilized ZrO2. J Catal 138:588–610. https://doi.org/10.1016/0021-9517(92)90309-6

Index

P. Vernoux, C. G. Vayenas (eds.), *Recent Advances in Electrochemical Promotion of Catalysis*, Modern Aspects of Electrochemistry 61,
https://doi.org/10.1007/978-3-031-13893-5